APPENDIX 7-1

SCERIDE ROCKS OFFSHORE WINDFARM ENVIRONMENTAL EFFECTS - NUMERICAL MODELLING STUDY

Deltares

Sceirde Rocks offshore wind farm environmental effects

Numerical modelling study

Sceirde Rocks offshore wind farm environmental effects
Numerical modelling study

Author(s)
Antonios Emmanouil
Firmijn Zijl
Mostafa Saleh

Sceirde Rocks offshore wind farm environmental effects
Numerical modelling study

Client	Xodus Group
Contact	Ms A Chauffey
Reference	Deltares offer: 11210071-001-HYE-0001_v1.0-Sceirde Rocks wind farm effect modelling - signed.pdf PO: PO 26379 - signed.pdf (signed 18 January 2024).
Keywords	Metocean, offshore wind farm, flow modelling, wave modelling, Ireland, County Galway, Atlantic Ocean, environmental impacts, effects.

Document control	
Version	2.0
Date	02-05-2024
Project nr.	11210071-002
Document ID	11210071-002-HYE-0001
Pages	99
Classification	
Status	final

Author(s)		
	A. Emmanouil M. Saleh F. Zijl	

The allowed use of this table is limited to check the correct order-performance by Deltares. Any other client-internal-use and any external distribution is not allowed.

Doc. version	**Author**	**Reviewer**	**Approver**
2.0	A. Emmanouil	S. Caires	P. van Steeg
	M.M.E. Saleh		
	F. Zijl		

Summary

Xodus Group Ltd is supporting Corio Generation (Fuinneamh Sceirde Teoranta) in their consenting application for the Sceirde (or Skerd) Rocks Offshore Wind Farm (SROWF), envisioned to be built at the Atlantic coast of Ireland, approximately 10 km offshore southwest of Ard, County Galway. For this consenting application, an environmental impact assessment is required to describe the expected effects of the offshore wind farm. To that end, Deltares was requested by Xodus Group Ltd to provide them with hydrodynamic and wave information, based on numerical models developed by Deltares during the metocean study for SROWF (Deltares, 2022) for Corio Generation.

The present study is aimed at providing the client with the following information:

- Field plots and timeseries of flow conditions (including water levels and depth-averaged current magnitudes and directions) over a period of one month, namely January 2013 and residual flows over a period of two (2) Spring Neap tidal cycles within the same month.
- Field plots and timeseries of wave conditions (including significant wave heights, peak wave periods and mean wave directions) over events representative of 50th percentile, 90th percentile, 1-, 5-, 10- and 50-year conditions, for the two main approach directions (west and west-southwest), based on the data determined in Deltares (2022).

Aforementioned information is provided for two situations:

- Baseline, i.e., with no offshore wind farm in place and;
- Operational, i.e., with the Wind Turbine Generators (WTGs) in place.

For the operational situation, the effects of the WTGs are schematised in the employed numerical models, by local changes in the bathymetry due to the WTG foundations (for both hydrodynamic and wave model), by local addition of drag on ambient flow due to the WTG mast (hydrodynamic model) and finally through a wind speed reduction over the entire wind farm area due to the operation of the WTGs (for both hydrodynamic and wave model).

A single offshore wind farm layout (SRL069) and a single Gravity-Based Structure (GBS) foundation design (PDS revision 4, provided on 23 January 2024) was considered for the modelling of the operational conditions, as provided by Xodus Group.

The wave and hydrodynamic conditions are output at a large number of locations, spread across the greater area of interest, defined by a 15 km buffer around the offshore wind farm and the export cable corridor.

This report presents the results of the numerical study and describes the methodology behind the obtained information. The baseline flow and wave fields are deemed to be controlled by the complex topography of the area of interest and the steep bathymetric gradient just offshore from the Offshore Wind Farm (OWF) boundary. Overall, the wind farm effects in terms of differences observed in flow and wave fields between the baseline and operational situation are more pronounced near the direct vicinity of the WTG locations and diminish outside the offshore wind farm area.

More specifically, the presence of the WTGs leads to a very local increase of wave energy due to combined refraction and shoaling, developing only over a scale in the order of tens of meters, i.e., in the immediate vicinity of the foundations. This is followed by a reduction of wave energy in the lee side of each WTG relative to the incoming wave direction (mostly

towards the coast), which is noticeable up to a distance of roughly 1 km, due to a change in wave direction and breaking. Besides these relatively local wave effects, it is also observed that wave energy reduces over a relatively larger area directly downwave from the OWF towards the coast. This is, similarly to the local wave reduction in the vicinity of the foundations, predominantly due to dissipation and redistribution of wave energy to other directional sectors, but in this case as a cumulative result of the refraction occurring around several WTG locations spread over the OWF area. Finally, this larger-scale wave reduction is also due to wind extraction across the OWF area. This larger-scale effect does not reach the coast but is extending roughly up to 3 km from the OWF eastern boundary in the most extreme conditions considered. These larger-scale effects outside the OWF boundaries are barely noticeable in normal conditions and gradually increase with increasing severity of the sea conditions. They remain nevertheless for the most part of the area less than roughly 50 cm in terms of significant wave height difference, compared to the baseline. Compared to baseline slight changes in mean wave directions are noticeable predominantly in the direct vicinity of the foundations, whereas there is hardly any effect on peak wave periods.

The baseline flow field around the OWF is characterized by the presence of islands. These give rise to vortices that span a large part of the OWF area. In the operational situation, various WTGs are observed to influence the position of these vortices shed downstream from the islands. This is due to some WTGs being positioned directly downstream from the islands and hence interfering with the developing wakes. The development of these vortices is also affected by the presence of some WTGs directly upstream from the islands, and hence by their influence on approach flow conditions. Furthermore, the drag exerted by the WTG foundations is seen through a reduction of current speeds, which can extend depending on the location even for more than 1 km in a downstream direction. It is noted that effects on the flow fields in the simulated operational conditions are contained within the offshore wind farm area and do not extend (much) further than its boundaries, as opposed to the WTG foundation effects on wave fields. Finally, these generally local WTG influences have a relatively limited effect on residual flow patterns (changes less than 0.02 m/s in flow magnitudes) over the considered period of two spring neap cycles, as these are predominantly driven by larger-scale physical processes. Part of the influence of the operational scenario on the residual flow is due to the considered wind reduction across the wind farm area. However, the effect of such a local wind reduction is comparatively small with relation to the WTG effects, as the flows are not dominated by local winds.

Contents

1 Introduction

1.1 Background

Corio Generation (Fuinneamh Sceirde Teoranta) is planning the construction and operation of the Sceirde Rocks offshore wind farm (Sceirde Rocks OWF), hereafter referred to as SROWF. SROWF is located approximately 10 km offshore southwest of Ard, County Galway. This coastal region is an area of special environmental interest. Xodus Group Ltd (the Client) is supporting Corio Generation in their consenting application for the SROWF to the Irish authorities, with an Environmental Impact Assessment (EIA). Figure 1.1 shows an overview of the SROWF site next to the areas of special environmental interest.

According to the present Project Design Statement, the SROWF will include thirty (30) wind turbine generators (WTG) founded on Gravity Based Structures (GBS) and of an Offshore Substation (OSS) platform that will be installed within the OWF. Water depths at the WTG locations range roughly between 26 and 57 m below LAT, and the area is characterised by the presence of small islands (rock outcrops). The offshore export cable corridor (OECC), runs to the south east and will transport electricity generated in the OWF to the shore near Doonbeg.

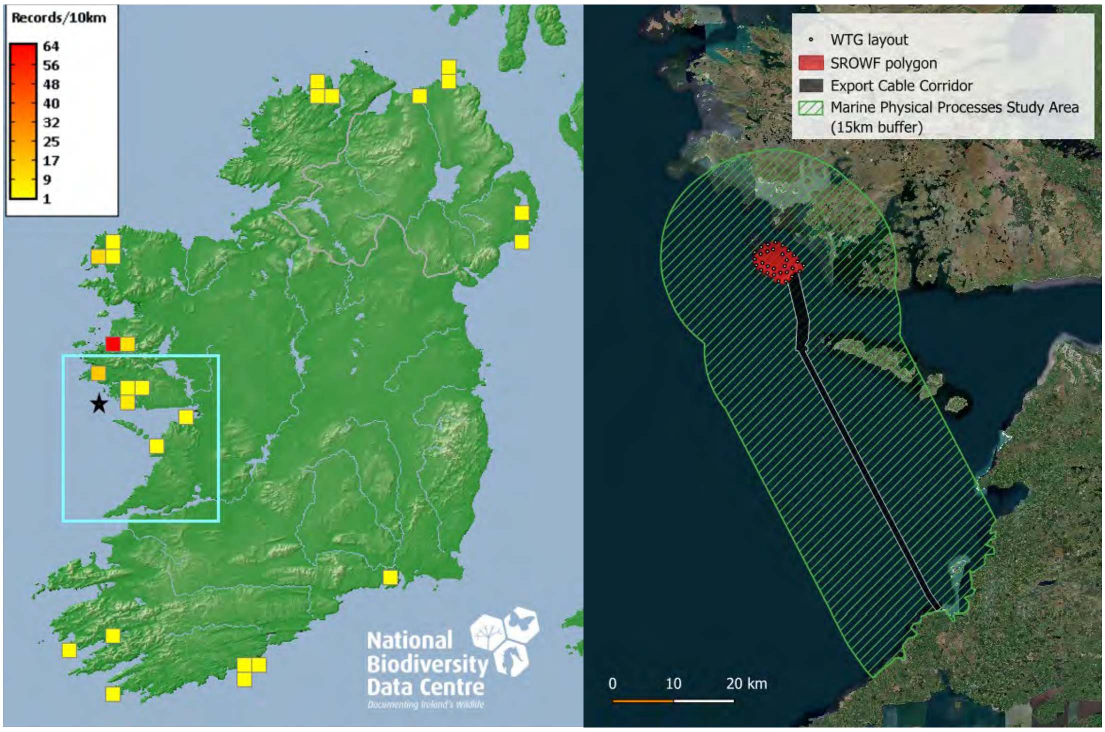

*Figure 1.1 **Left**: National Biodiversity Data Centre, Ireland, Records per 10km of Serpula vermicularis reefs, image, accessed 22 February 2024, (see link). **Right**: Overview Sceirde Rocks offshore wind farm project location.*

To describe the expected effects of the offshore wind farm, Deltares was requested by Xodus Group Ltd to provide hydrodynamic and wave information at multiple output locations spread across the entire, covering with a buffer of 15 km the OWF and the ECC, which is the study area used to inform the EIA. To that end, the numerical models developed by Deltares during the metocean study for SROWF (Deltares, 2022) for Corio Generation, are employed as a starting point for this study. This report presents the methodology behind the numerical study and the numerical modelling results. Next to this report, the results are also delivered in csv-datafiles containing the generated timeseries at the chosen reference locations.

1.2 Objectives

The objective of the study is to provide the Client with metocean conditions to support the environmental impact assessment of the SROWF. As requested by the Client, the main goal is to provide the following information:

- Field plots of instantaneous flows during Flood, Ebb, High Water and Low Water over both Spring and Neap conditions, timeseries of flow conditions (including water levels and depth-averaged current magnitudes and directions) over a period of one month, namely January 2013, and finally residual flows over a period of two (2) Spring Neap tidal cycles within January 2013.

- Field plots and timeseries of wave conditions (including significant wave heights, peak wave periods and mean wave directions) over events representative of 50th percentile, 90th percentile, 1-, 5-, 10- and 50-year conditions, for the two main approach directions (west and west-southwest), based on the data determined in Deltares (2022).

Abovementioned information is provided for two situations:
- Baseline, i.e., no offshore wind farm foundation is in place and;
- Operational, i.e., with the WTGs installed and in operation.

1.3 Approach

The determination of the required metocean timeseries and conditions is based on available hindcast, reanalysis and observation datasets and detailed numerical modelling.

1.3.1 Numerical modelling

Dedicated high-resolution numerical modelling was carried out to derive the hindcast timeseries of wave and hydrodynamic parameters for both baseline and operational conditions. To that end, the hydrodynamic and wave numerical models developed in Deltares (2022) metocean study, were used as a starting point. For the purposes of the present study, these models were further refined to capture changes in WTGs locations relative to the previously considered OWF layout in 2022, and to further increase the resolution, required for the set-up of the operational situation. The hydrodynamic and wave models were run with an one-way coupling between the hydrodynamic and the wave model. More precisely, the water levels and depth-averaged current velocities determined by the hydrodynamic model and applied in the wave model.

Hydrodynamics
The hydrodynamics (water levels and currents) were modelled using a refined version of Deltares’ extensively calibrated 2DH Flexible Mesh Dutch Continental Shelf Model (DCSM-FM). The DCSM-FM is the sixth-generation hydrodynamic model, developed by Deltares for the Dutch Government for the use in operational forecasting, water quality and ecology studies and covers the whole North Sea and part of the North Atlantic Ocean. Detailed background of the model setup, calibration and extensive validation is given in Deltares (2019). The application of the model in this study is further described in Section 2.2.

Waves
The third-generation shallow water wave model SWAN (Simulating WAves Nearshore; http://swanmodel.sourceforge.net/) has been used for the numerical modelling of waves in

combination with forcing by ERA5 wind data. The application of the wave model in this study is further described in Section 2.3.

Area of model interest

Both models cover a much larger area, but are locally refined to have the highest resolution (roughly in the order of the turbine foundation dimensions, see Figure 1.4) within the so-called model area of interest shown in Figure 1.2, along with the requested output locations, that encloses the greater Marine Physical Processes Study Area (hereafter MPPSA). This is the study area used to inform the EIA. The flow and wave timeseries at the output locations are acquired to inform the sediment analyses undertaken by the Client for the EIA.

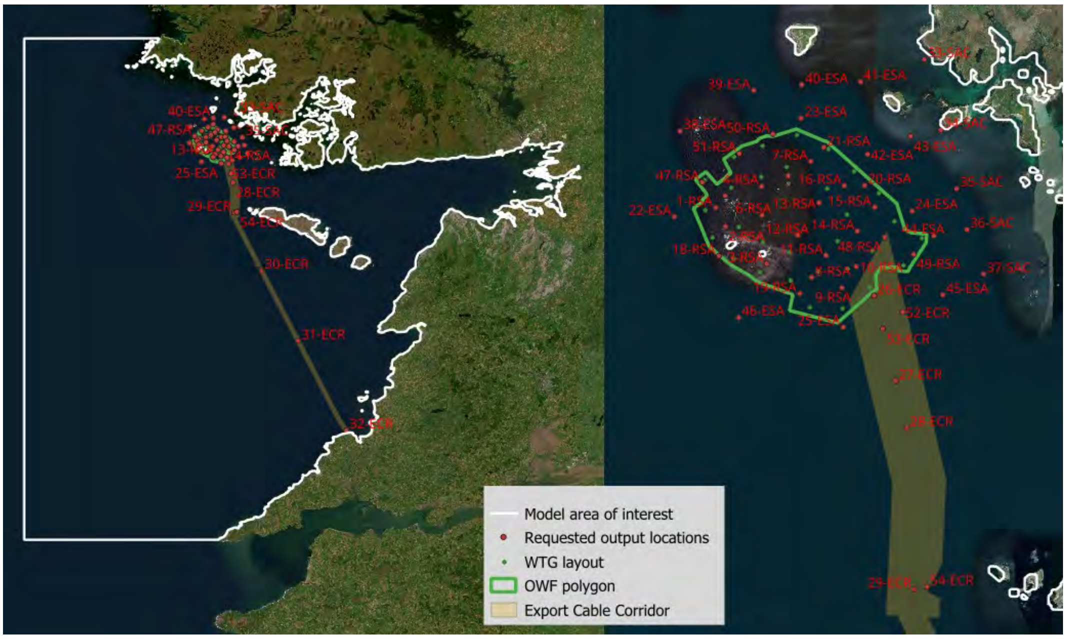

Figure 1.2 Model area of interest (left) and requested output locations by the Client.

1.3.2 Operational condition

For the operational condition, the presence of the WTGs is schematised in the employed hydrodynamic and wave models, by means of local changes in the applied bathymetry (for both hydrodynamic and wave model) and by local addition of drag on ambient flow (only relevant in the hydrodynamic model). In addition, a 10% wind speed reduction is applied over the entire wind farm area (for both hydrodynamic and wave model), aimed at capturing the effect of wind energy extraction from the lower atmospheric layers, due to the operation of the WTG. These effects are schematically presented in Figure 1.3.

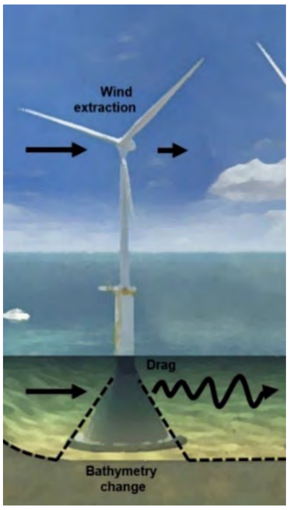

Figure 1.3 Impacts of wind turbines related to wave and flow conditions addressed in this study (source background figure: MARIN).

As opposed to the baseline model, obviously the validation of the model results on the operational situation is not possible due to lack of field measurements under these conditions at SROWF. Consequently, sensitivity analyses are done in the model set-up phase to understand the respective effects of the choices made in various parameters used in the OWF parameterization. Where relevant, conservative choices (i.e., leading to the largest impacts relative to the baseline) were made to address uncertainty in the selection of the numerical modelling parameters.

1.3.3 Data sources

The atmospheric data and boundary wave conditions needed to force the wave and hydrodynamic models, as well as the conditions for the wind and snow analyses were retrieved from the dataset of the most recent and accurate reanalysis of the European Centre for Medium-range Weather Forecast (ECMWF), ERA5. The ERA5 dataset currently covers the period from 1950 until now on a global model grid of about 0.25° x 0.25° (~30 km) at an hourly interval and has unprecedented accuracy in terms global atmospheric and wave data. The data from 1950 until 1978 are considered to be of lower quality than the data after that period given that more observations are available from 1979 for the applied data assimilation. In this study therefore the higher quality data from 01-01-1979 00:00 – 31-12-2021 23:00 are used.

Observations available in the Marine Institute database, from stations M1 (wave/meteorological buoy), Galway (tide gauge) and Inishmore (tide gauge), were used to revalidate and calibrate (where relevant, see Sections 2.2.5 and 2.3.6) the baseline models, following the additional refinements performed in this study compared to the metocean study of Deltares (2022).

The bathymetry data that were used as basis for the depth schematization of the hydrodynamic and wave models are from high-resolution bathymetrical survey datasets (INFOMAR https://www.infomar.ie/data as provided by Corio Generation during the metocean study of Deltares, 2022) and publicly available from EMODnet (https://portal.emodnet-bathymetry.eu/): European Marine Observation and Data Network) supplemented by the publicly available lower resolution (approximately 115x115 m) EMODnet dataset from 2020.

The WTG layout[3], OSS and output locations, as well as the OWF and OECC polygons were provided by the Client, see Figure 1.2 and Figure 1.5. The dimensions of the GBS foundations, and of the associated rock layers were also provided by Client[4], see Figure 1.4.

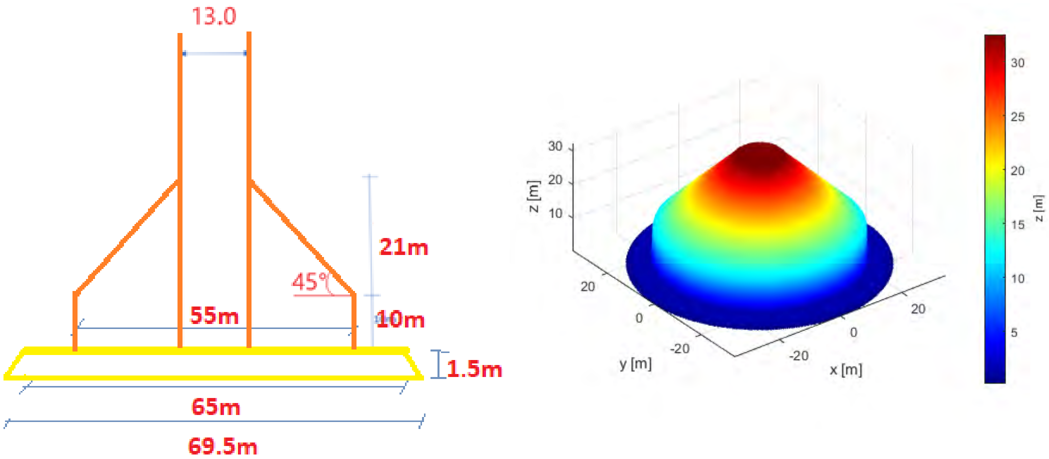

Figure 1.4 Left: The Gravity-based Structure (GBS) foundation as provided in PDS revision 4 (on the 23rd of January 2024) considered for the WTGs at SROWF, with a diameter of 55 m at the base and 13 m at the central column. The yellow polygon denotes the maximum dimensions of the anticipated rock layer. Right: The 3D model schematization of the GBS foundation base (conical part of the foundation together with the rock layer) reaching up to 33.3 m from the seabed, used in this study for extracting bathymetric samples at the locations of the WTGs.

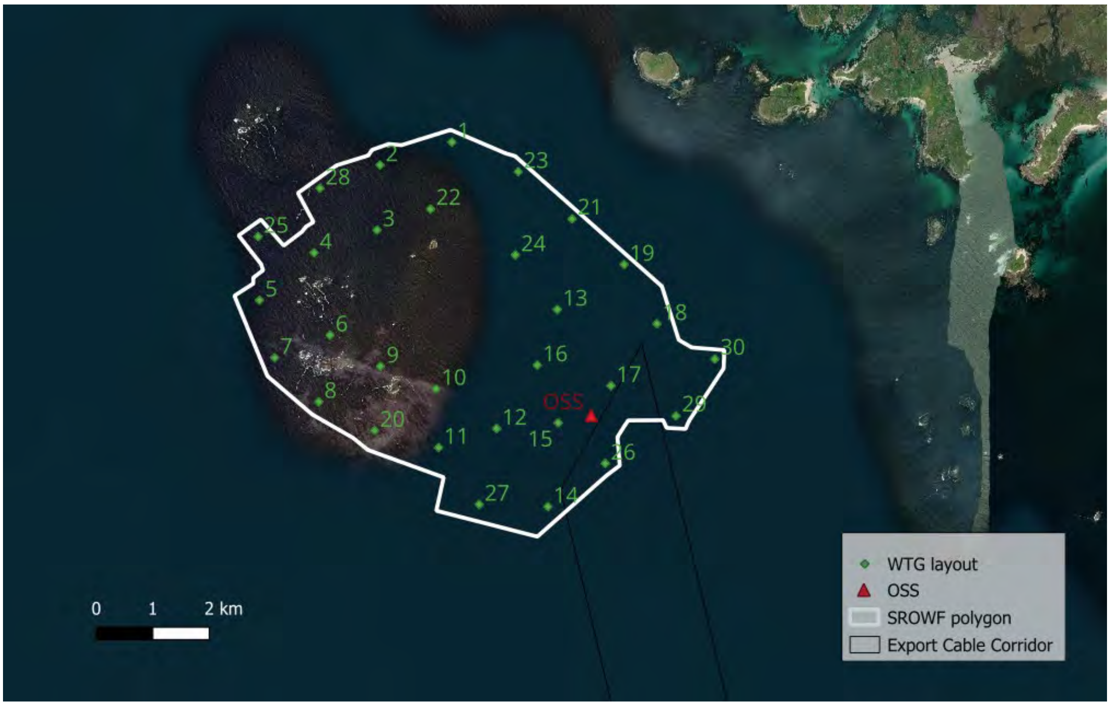

Figure 1.5 WTG layout (numbers denote WTG-ID), OWF polygon and OSS location (PDS layout SRL069).

1.3.4 Conventions

In this report all wind and wave directions follow the nautical convention: wind and wave directional values are defined as coming from in degrees clockwise from the geographical

[3] The WTG layout reference is SRL069.
[4] As provided in PDS revision 4, on 23rd January 2024.

North and referred to as °N (0°/360°N is coming from the North, 90°N is coming from the East, 180°N is coming from the South and 270°N is coming from the West). All current directions follow the oceanographic convention: current directional values are defined as going towards in degrees clockwise from the geographical North and referred to as °N (0°/360°N is going towards the North, 90°N is going towards the East, 180°N is going towards the South and 270°N is going towards the West).

All vertical levels in this report are referenced to the Lowest Astronomical Tide (LAT) level.

1.4 Outline of the report

The description, modelling and validation of the produced data are described first in the next chapter. The chapter can be skipped for those not wanting to look into the details of the data that have been used for the determination of the required flow and wave information. Chapter 3 describes the modelling results for the required conditions in separate sections per variable group (flow and waves). Certain methods and models referred to in Chapters 2 and 3 are described in more detail in Appendices. The entire set of wave and flow field plots over the considered conditions is also presented in the Appendix. Finally, the determined wave and hydrodynamic timeseries per assessment location are available digitally in Comma Separated Values (csv) file format.

2 Data and numerical modelling

2.1 Winds

2.1.1 Introduction

In this section the data sources for wind speed and wind direction used to force the hydrodynamic and wave models are described.

The wind data at 10 mMSL height used as basis for this study are from the ERA5 dataset. The hourly, 1-hour averaged wind velocity data from 1979 until 2021 (43 years, 01-01-1979 00:00 – 31-12-2021 23:00) were downloaded from the ERA5 repository in NetCDF format. For the forcing of the hydrodynamic model discussed in Section 2.2 and overall wave model (NWECS), ERA5 wind data at 10 m height and air pressure data were downloaded for the region going from 15°W to 31°E and from 41.5°N to 67°N with a resolution of 0.25° x 0.25°.

For forcing the (detailed) wave model discussed in Section 2.3, ERA5 wind data at 10 mMSL height were downloaded for the region going from -10.5°E to -9.6°E and from 53.0°N to 53.5°N with a resolution of 0.1° x 0.1°. For the ERA5 wind data validation and calibration discussed in this section, the ERA5 wind data at the coordinate (i.e. 53.3°N, -10°E) closest to the Doolickreef Rock metmast has been considered and additionally ERA5 data have been downloaded at the coordinate (i.e. 53.1°N, -11.2°E) closest to the location of the M1 buoy of the Marine institute (cf. Table 2.1). Pressure and temperature data for 10 m height were also obtained from the ERA5 dataset. The retrieved ERA5 wind velocity components have been converted to wind speed and direction[5].

The validation and calibration of the 10 mMSL ERA5 wind data are presented next in Section 2.1.2.

2.1.2 Data validation

The ERA5 10 m wind speed and direction data were validated against available wind speed and direction observations in the region of SROWF. Figure 2.1 shows the considered two observation stations and Table 2.1 shows the time periods covered by the data, the heights at which the data are measured (above MSL) and their provenience.

Table 2.1 Available wind observation datasets.

Station	Period	Origin	Heights above MSL (m)
M1 (buoy)	06-02-2001 – 09-07-2007	Marine Institute[6]	4 (assumed)
Doolickreef Rock (metmast)	18-12-2002 – 16-10-2004	Client	Cup anemometer (speeds): 20.1, 29.4, 30.4 Wind vane (directions): 30.0

Hourly 1-hour averaged wind speed and direction data at the M1 buoy location are available at approximately (assumed) 4 m height. At the Doolickreef Rock metmast location, 10-minute interval, 10-min averaged wind speeds are available at multiple heights and wind directions at

[5] Using the nautical convention, i.e. the direction the wind is coming from in degrees clockwise from the North and referred to as °N. The direction of wind blowing from the North is 0°N, from the East is 90°N, from the South is 180°N and from the West is 270°N.
[6] https://erddap.marine.ie/erddap/index.html

a single height. All wind observation data at the Doolickreef Rock metmast were converted to hourly-averaged data by averaging the 10-min averages from 30 minutes before to 30 minutes after the hour.

The observations are considered separately per instrument in the data validation.

Figure 2.1 Aerial overview of the wind observation stations. The SROWF area is outlined in red.

To be able to compare the observed wind speed data with the ERA5 data at 10 m height, the observed wind speeds at both locations were converted to the 10 m height assuming a vertical logarithmic wind profile (Komen et al., 1994), namely:

$$U(z) = \frac{u_*}{\kappa} \ln\left(\frac{z}{z_0}\right), \text{ with } z_0 = \alpha \frac{u_*^2}{g} \quad z_0 = \alpha \frac{u_*^2}{g}$$

where *z* is the height, u_x is the friction velocity in m/s, z_0 is the surface roughness in m, κ is the von Karman constant, g = 9.81 m/s^2 is the acceleration due to gravity and α is the Charnock 'constant'. An iterative algorithm or the approximation of Wu (1982) can be used to determine the friction velocity from the measurements. Hereafter, the corresponding wind velocity at 10 mMSL (U_{10}) can be computed. There are different estimates for α available in the literature varying from 0.004 to 0.032 (see e.g. Komen et al., 1994). In line with other projects and as is also done in the wave modelling, α is set equal to 0.018. Assuming again that the wind directions vary little over the lower levels of the vertical profile, the wind directions at 10 m have been assumed to be equal to the wind directions at the measurement levels.

For the comparison of the Doolickreef Rock observation data with the ERA5 data the measurements at the lowest level of the metmast were used: 20.1 m above the metmast base. Although the metmast was situated at a rock with an elevation of 3.9 m above mean sea level, on advice of Wind Pioneers, it is assumed that the wind streamlines followed the rock profile and that the reference height is not influenced by this. This means that the 20.1 m above the metmast base was considered as 20.1 m above MSL.

Figure 2.2 to Figure 2.5 show the density scatter and percentile comparisons and the main statistics of the data comparisons such as the correlation coefficient, root-mean-square errors, bias and standard deviation (check Appendix B for the error statistics definitions). For each station there is a figure with the omni-directional and directional wind speed comparisons (Figure 2.2 and Figure 2.4) and with the wind direction comparisons (Figure 2.3 and Figure 2.5).

The figures show a very high correlation between the observed wind speeds and directions and the ERA5 wind speeds and directions. The ERA5 wind fields are, therefore and in line with our experience in other locations, considered to be very reliable, due to the very high correlations with the observations and are considered to form a solid basis for the hydrodynamic and wave modelling.

As expected, given the relatively coarse resolution of the ERA5 atmospheric model, having considered all comparisons in detail (and some timeseries plots, not shown here) it has been concluded that in the considered area the ERA5 data shows some underestimation of the high wind speed percentiles. For the determination of the normal and extreme conditions at the SROWF turbines the ERA5 wind speeds need, therefore, to be corrected/calibrated. On the other hand, there is no need to correct/calibrate the ERA5 wind directions.

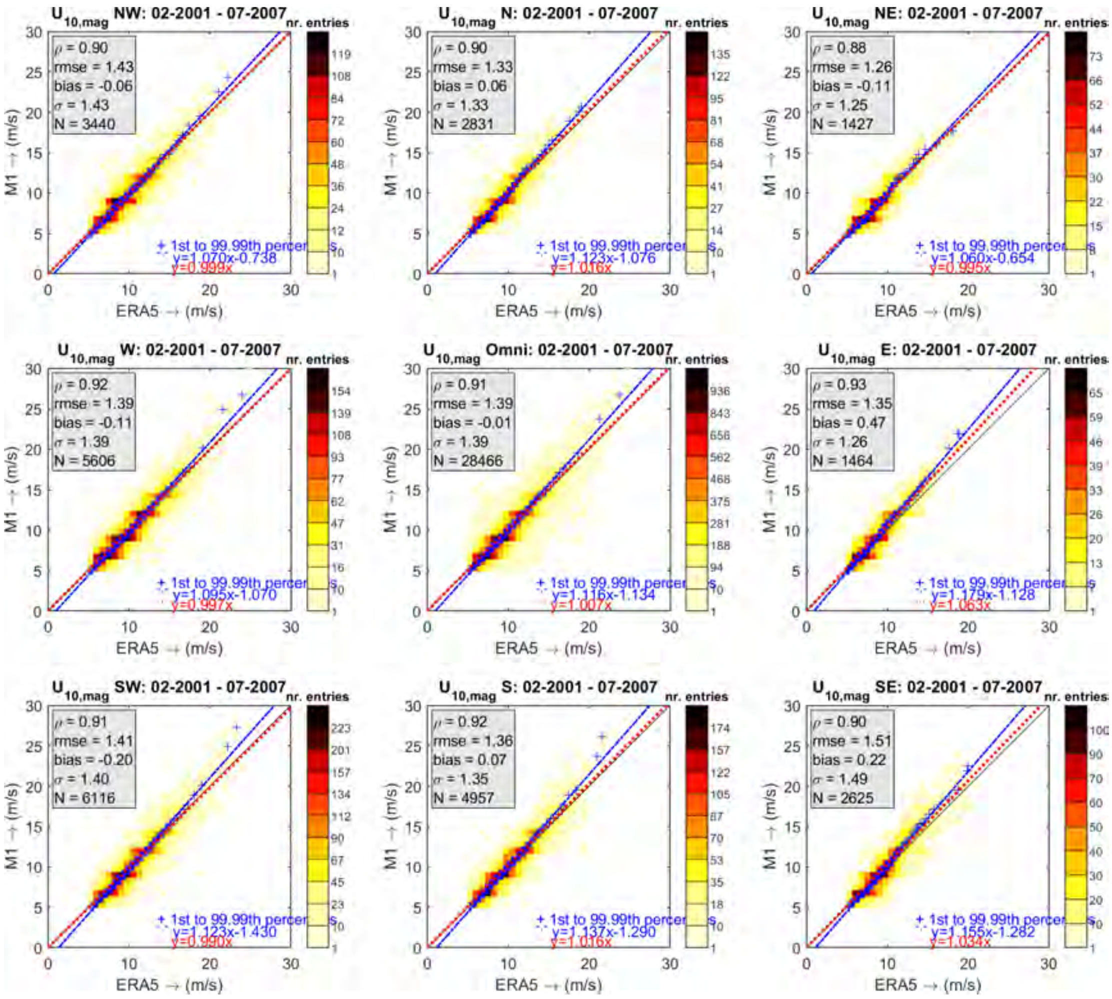

Figure 2.2 Wind speed density scatter comparisons between the M1 buoy observations and the ERA5 data at 10 mMSL height. The panel in the centre shows the omni-directional comparisons and the panels surrounding it show the comparisons for the corresponding directional sectors (from top left, clockwise: NW, N, NE, E, SE, S, SW and W). The symmetric fit to the data is given by the red dotted line and the linear fits through the data percentiles (blue pluses) is given by the dashed blue line. The statistics of the comparisons are printed in the panels.

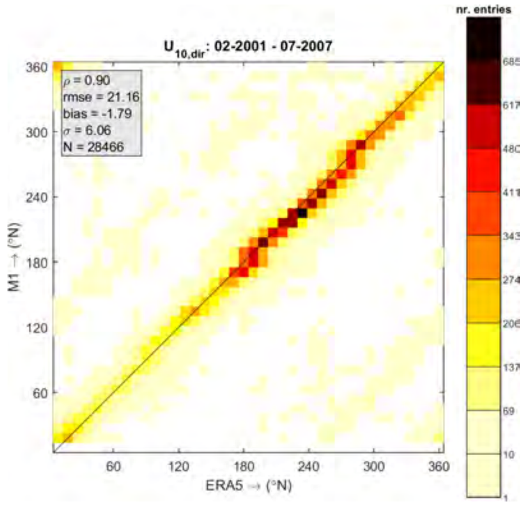

Figure 2.3 Wind direction density scatter comparisons between the M1 buoy observations and the ERA5 data at 10 mMSL height. The statistics of the comparisons are printed in the top left box.

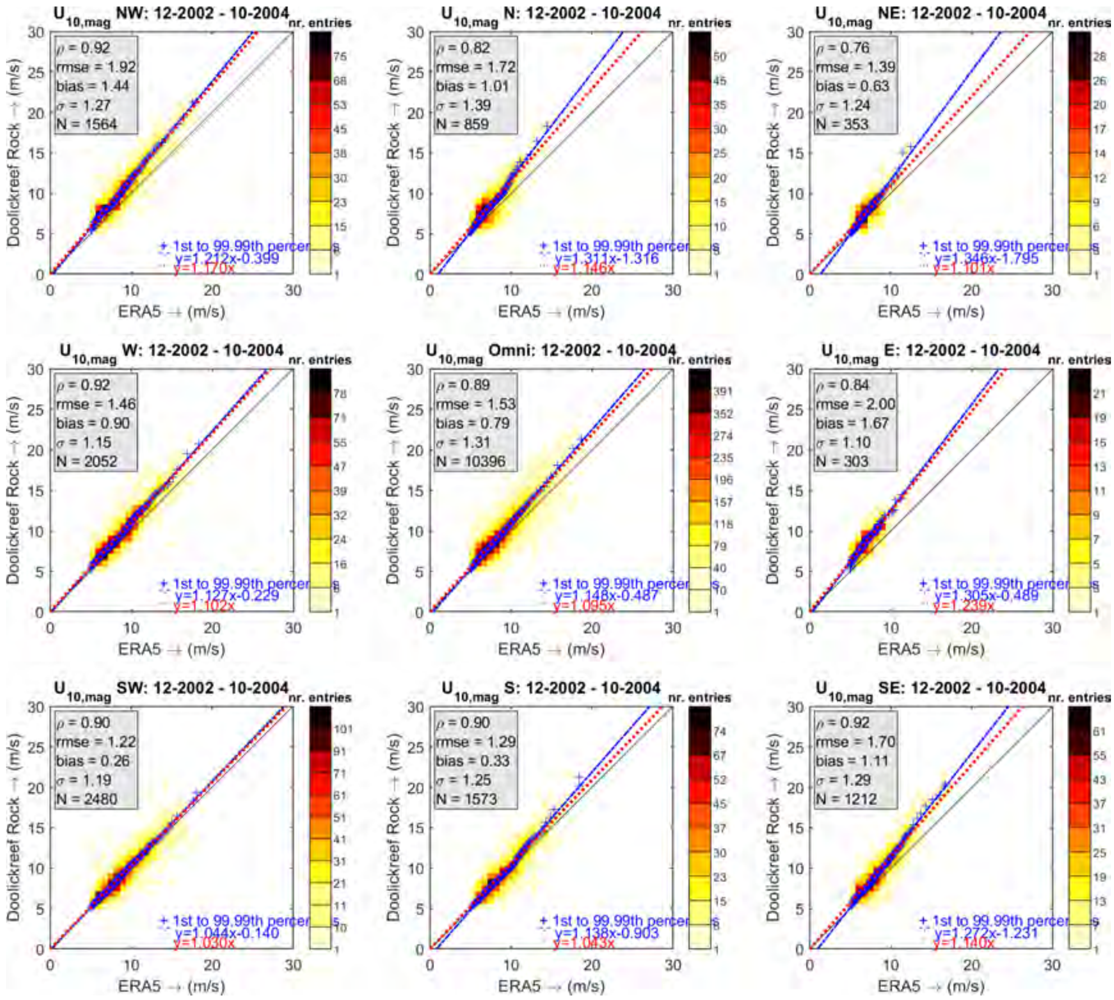

Figure 2.4 Wind speed density scatter comparisons between the Doolickreef Rock metmast observations and the ERA5 data at 10 mMSL height. The panel in the centre shows the omni-directional comparisons and the panels surrounding it show the comparisons for the corresponding directional sectors (from top left, clockwise: NW, N, NE, E, SE, S, SW and W).

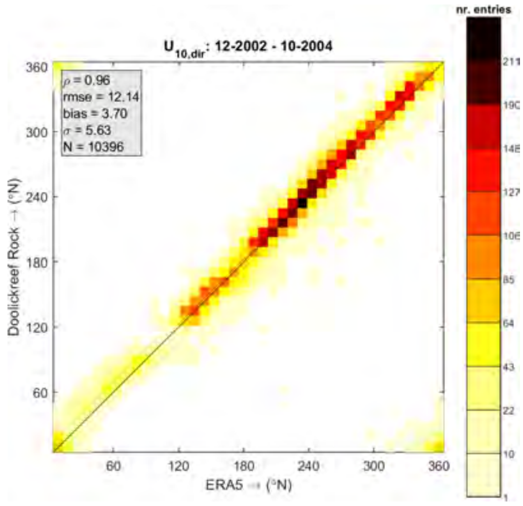

Figure 2.5 Wind direction density scatter comparisons between the Doolickreef Rock metmast observations and the ERA5 data at 10 mMSL height. The statistics of the comparisons are printed in the top left box.

2.1.3 Wind forcing

The models are forced with the raw ERA5 data, given the high correlation between the raw ERA5 data and the observation and that the quality of the model results does not depend only on the accuracy of the forcing winds. The effects of mismatches in the wind data and other model inaccuracies are considered jointly in the validation and calibration of the wave and hydrodynamic model results.

To account for the wind extraction by the turbines in the operational situation, wind speed magnitudes at 10 m were reduced within the entire OWF polygon (as presented in Figure 1.5) by 10%, while wind directions remained unchanged. This wind schematization and reduction factor for the operational condition reflect results from detailed numerical modelling (based on Large Eddy Simulation model, e.g., Wiegant, E., & Verzijlbergh, R. (2019), see also Figure 2.6 where this modelling is applied for a wind field around the Belgium Offshore Wind Farm zone) of the atmospheric layer through an operating offshore wind farm and has been applied to the Wind op Zee Ecologisch Programma (WoZEP).[7] research framework, when modelling the cumulative ecological impacts of large-scale offshore wind deployment in the North Sea, on commission from the Dutch Government (Van Duren, L. et al., 2021).

[7] Ecological Programme of Offshore wind (Synthesis report): https://www.noordzeeloket.nl/en/functions-and-use/offshore-wind-energy/ecology/offshore-wind-ecological-programme-wozep/reports-on-ecosystem-research/

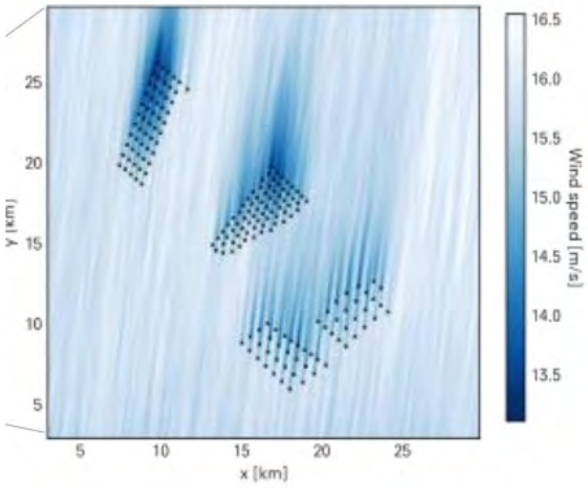

Figure 2.6 Snapshot of a 70 m wind field around the Belgium Offshore Wind Farm zone modeled by GRASP (GPU-Resident Atmospheric Simulation Platform) by Whiffle. Source: CHASM – Coupled High-resolution Atmosphere Sea Modelling.

2.2 Hydrodynamic modelling

2.2.1 Introduction

The hydrodynamic modelling performed in this study aimed at giving insight into the hydrodynamic conditions (water levels and currents) that are representative for the Sceirde Rocks OWF region for the baseline and operational conditions.

To allow for a direct comparison, for both baseline and operational conditions, the hydrodynamics are derived from a simulation for the period of one month chosen as representative of a typical tidal cycle, namely January 2013 (i.e., 01-01-2013 00:00 – 01-02-2013 00:00) based on a horizontally two-dimensional, and vertically depth-averaged modelling approach (2DH). The starting point was the previously employed hydrodynamic model for the metocean study of Sceirde Rocks (Deltares, 2022). The DCSM-FM 2DH model with additional gradual grid refinements towards the updated SROWF is applied.

In this section, first the model domain and bathymetry, forcing conditions, output definitions and validation of the baseline hydrodynamic model are presented in Sections 2.1.2, 2.2.3, 2.2.4, and 2.2.5 respectively. The changes applied to the baseline hydrodynamic model in order to reflect operational conditions are later discussed in Section 2.2.6. It is noted that the baseline model results were validated using available observation data (only water levels), as described in Section 2.2.5. For the operational schematization, in Section 2.2.6 we present the selection of relevant parameters and modelling choices made based on performed sensitivity analyses. Finally, the results for the two situations (baseline and operational) are presented in the next chapter.

2.2.2 Model domain and baseline bathymetry

In the hydrodynamic modelling, the gradual refinement of the 2DH (depth-averaged) Dutch Continental Shelf Model (DCSM-FM) is applied. The DCSM-FM is the sixth-generation hydrodynamic model, developed by Deltares for the Dutch government, which has been extensively calibrated. For detailed background information on the model including model setup, calibration and validation reference is made to report on the development of the sixth generation DCSM-FM (Deltares, 2019). In this report, only the main characteristics of the model and the additional model refinements and validation carried out proposedly for this study are discussed. For all other details, reference is made to Deltares (2019).

The model covers the northwest European continental shelf. The western boundary of the model is located at 15°W, and the northern and southern boundaries in the west of the model domain are located at 64°N to 43°N respectively. The original DCSM-FM grid was designed to have a resolution that increases with decreasing water depth. The starting point was a grid with a uniform cell size of 1/10° in east-west direction and 1/15° in north-south direction. This course gird was refined in three steps with a factor of 2 by 2. The areas of refinement were specified with smooth polygons that were approximately aligned with the 800 m, 200 m, 50 m and 12.5 m isobaths (i.e. lines with equal depth). Areas with different resolutions are connected with triangles. The choice of isobaths ensures that the cell size scales with the square root of the depth, resulting in relatively limited variations of wave Courant number within the model domain.

The original DCSM-FM grid had a resolution of 0.5 nautical mile (~900 m) in the region of interest. As this was too coarse for our goal, we have gradually refined it till we reached a horizontal resolution of ~25 m in the SROWF area. The refinement was implemented in five steps (from the ~900 m to the ~25 m) with a factor of 2 by 2. The ~25 m resolution was chosen after analysing and comparing the results of the ~25 m, ~50 m, and the ~100 m resolutions. The 25 m resolution was considered sufficient as it led to the modelling of trustworthy patterns of detailed flow patterns (vortices) around the rocks. The bathymetry and grid of the entire DCSM-FM model is shown in Figure 2.7. The final grid and bathymetry around the model area of interest (AOI as shown in Figure 1.2) are shown in Figure 2.8. This leads to a resolution of ~50 m along the coastline adjacent to the OWF (and across the region between the OWF and the coast) and a resolution of ~100 m along the largest part of the OECC (varying between 200 m and 1 nm towards the landfall). Figure 2.10 shows a clear flow vortex pattern in the OWF area resolved by the numerical model, induced by the complex topography and (submerged) islands.

Compared to the previous refinement employed in the metocean study by Deltares (2022), the area with the highest resolution was extended slightly to the east (by roughly 2 km), as shown in Figure 2.9. This was done in order to fully enclose a small part the updated OWF area, that was falling outside the previously employed 25m refinement area. Other than this change, the baseline model is identical to the hydrodynamic model employed for the generation of 43 years of hindcast timeseries in Deltares (2022) but for the purposes of the present study is only run for a period of 1 month (January 2013).

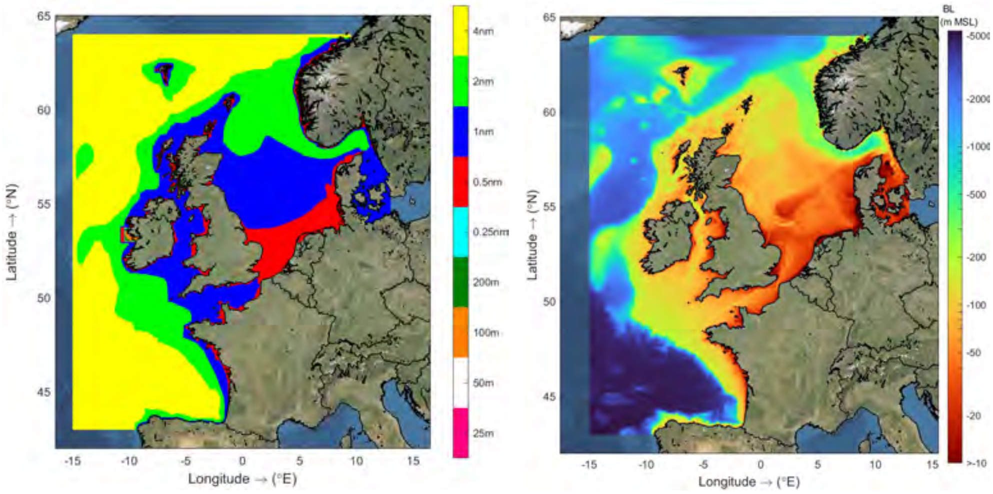

Figure 2.7 Grid (left panel, nm = nautical mile, m = meter) and bathymetry (right panel) of the entire DCSM-FM model.

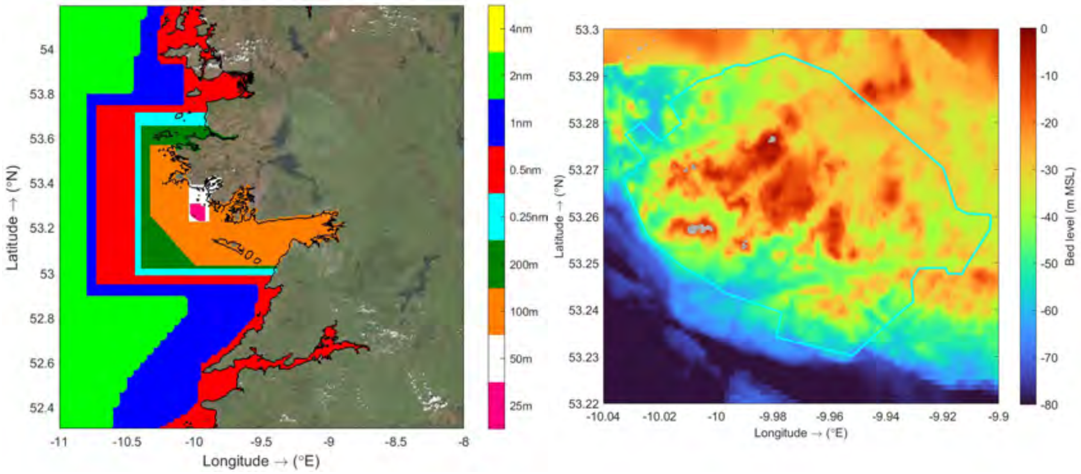

Figure 2.8 Local grid (left panel) and baseline bathymetry (right panel) in the area surroundings of the Sceirde Rocks OWF.

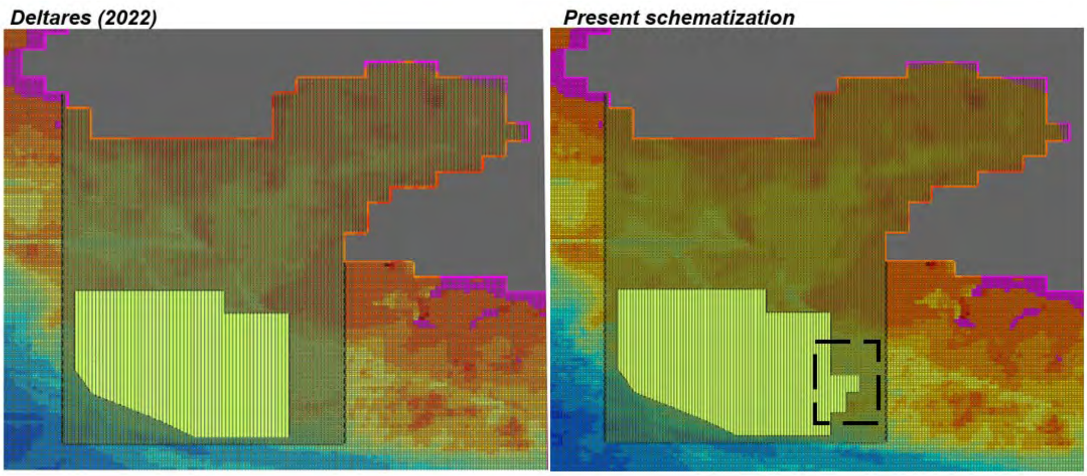

Figure 2.9 The area of the highest grid refinement was slightly extended to the south east (see dashed back polygon in right panel) in the present schematization (right panel) compared to the hydrodynamic model (left panel) employed in the metocean study of Deltares (2022) to fully enclose the updated OWF polygon.

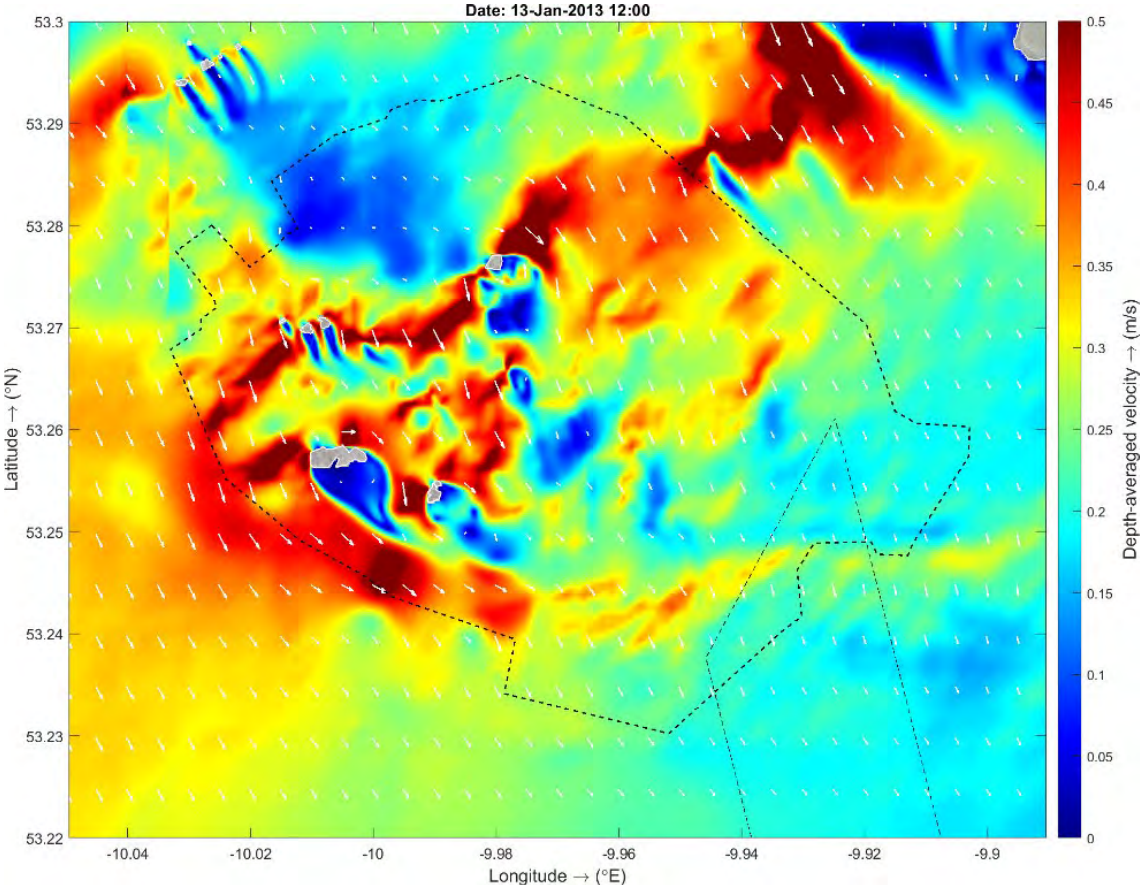

Figure 2.10 Flow pattern of the 13th of January 2013 at 12:00 (Low Water during Spring cycle) within the Sceirde Rocks OWF area for the baseline situation.

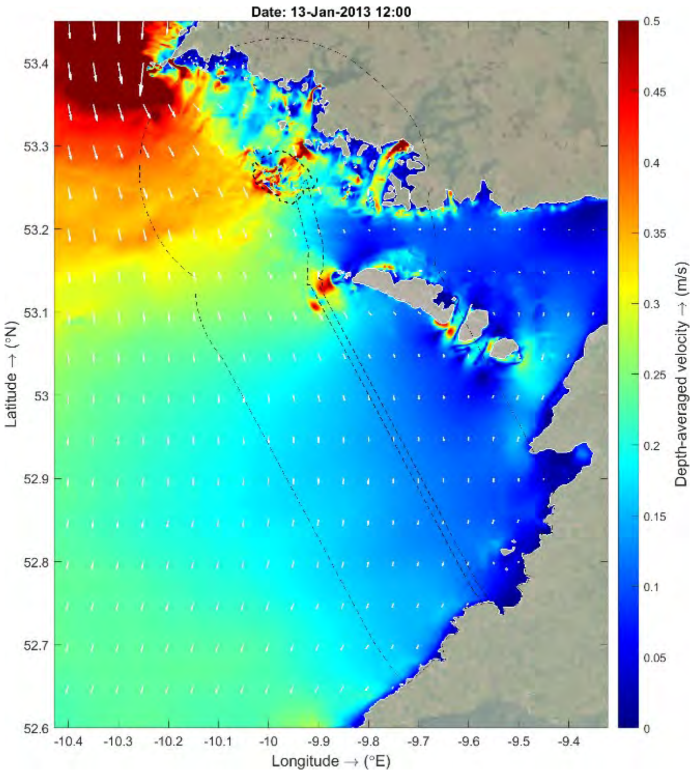

Figure 2.11 Flow pattern of the 13th of January 2013 at 12:00 (Low Water during Spring cycle) within the greater Marine Physical Processes Area for the baseline situation.

The resulting grid has more than 950,000 active cells with a variable resolution. The largest cells have a size of 1/10° in east-west direction and 1/15° in north-south direction, which corresponds to about 4 x 4 nautical miles (nm) or 4.9-8.1 km by 7.4 km, depending on the latitude. The smallest cells (shown in magenta) have a size of 25 m by 25 m in the SROWF.

The DCSM-FM model bathymetry in the AOI (see Figure 1.2) has been derived from the bathymetrical survey datasets (INFOMAR; https://www.infomar.ie/data) compiled and provided by Corio Generation in the study of Deltares (2022), supplemented by high and low resolution datasets of EMODnet (cf. Section 1.3) and in-house digitized nautical charts data in the Sceirde Rocks area. The EMODnet bathymetry data were converted to MSL using an in-house available conversion map for the North-West European coastal shelf.

2.2.3 Forcing conditions

The time- and space-varying hourly ERA5 10 mMSL wind and sea-level pressure data were used to force DCSM-FM. At the lateral open boundaries, water levels consisting of a tide and surge component were input. For the tide, 33 harmonic constituents from the global tide model FES2012[8] were used, while for the surge an Inverse Barometer Correction was applied. The effect of sea-level rise has not been considered in the hydrodynamic modelling.

The model was run from 01-01-2013 00:00 until 01-02-2013 00:00 (1 month) to hindcast total water levels and depth-averaged currents. This hindcast period is sufficient for the purposes of the present study, as it includes two full spring neap cycles, allowing for a proper calculation of residual flows. The computed total water level is the level that the sea surface (at a given point and time) would assume in the absence of waves and is also referred to as the still water level (SWL). It is comprised of the tide (astronomic) and surge (atmospheric or residual) water levels. Due to the large spatial extent of the model, the first 10 days of the model computations are always considered as a spin-up period; the results of that period are considered as not accurate enough for processing. These values are therefore excluded from the database. As these spin-up periods are chosen to fall in each previous years (i.e. modelling starts at 22 December 00:00 of the previous year), this has no effect on the resulting combined timeseries.

2.2.4 Output definitions

Spatial- and time-varying fields of SWL and depth-averaged current (magnitudes and direction) were output by the model with a time step of 30 minutes over a period of a full spring neap cycle. In addition, location-specific 10-minute timeseries of SWL were output at observation locations, to allow for a detailed validation of the model outcomes (see next section). Likewise, location-specific 10-minute timeseries of SWL and depth-averaged currents were output at the SROWF area (for each grid cell of the 30 wind turbine locations and at the location of the OSS). Residual flows were obtained as average water levels and flow components through statistical output from D-Flow FM[9] model over the prescribed period of two (2) spring neap cycles (determined based on the Standard list of Tidal Constituents prepared by the IHO Tidal Committee[10]), using a step equal to the dynamic computational step.

2.2.5 Baseline data validation

Figure 2.12 shows the water level observation stations and Table 2.2 shows the time periods of the data as well as their origin. Water level data are available from Galway Port and Inishmore stations. These two stations are the nearest to the location of SROWF. All water

[8] https://www.aviso.altimetry.fr/en/data/products/auxiliary-products/global-tide-fes/description-fes2012.html

[9] Using the Statistical output functionality of D-Flow (see D-Flow FM user manual – link).

[10] Determination of spring neap cycles as follows: M2 (speed)= 28.984104 deg/hr., S2 (speed)= 30.0 deg/hr. $\text{Difference}_{S2\text{-}M2}$=1.0158958 deg/hr, Period= 1.0158958/360 = 354.3670522 hours = 14.76529384 days

level data were obtained in the study of Deltares (2022) from the Marine Institute[11], the State agency responsible for marine research, technology development and innovation in Ireland. As previously discussed no current speed data is available to Deltares in the vicinity of the OWF or the OECC.

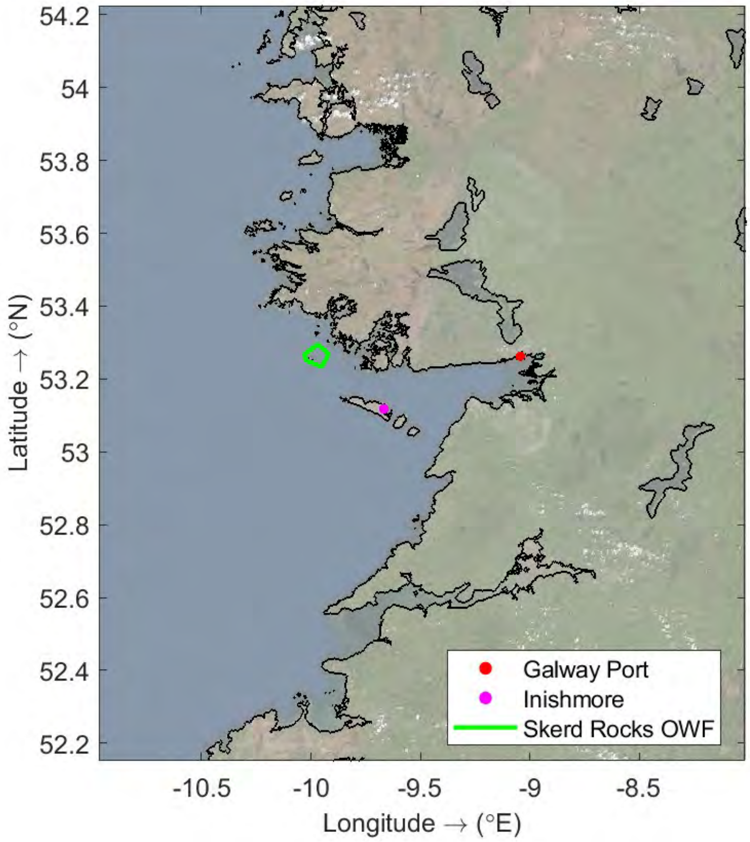

Figure 2.12 Aerial overview of the water level observation stations. The SROWF area is outlined in green.

Table 2.2 Periods of the available observation data per station.

Station	Period	Parameter	Origin
	Galway Port		
(a)	01-2008 – 01-2009	water level	Marine Institute
(b)	01-2010 – 01-2013	water level	Marine Institute
(c)	01-2014 – 01-2018	water level	Marine Institute
(d)	01-2019 – 01-2022	water level	Marine Institute
	Inishmore		
(a)	01-2014 – 01-2018	water level	Marine Institute
(b)	01-2019 – 01-2022	water level	Marine Institute

As discussed, the present hydrodynamic model is run for a period of only 1 month (January 2013) which is sufficient for the purposes of the present assessment, but falls outside of the measurement periods of the 2 stations near the study location (see Table 2.2). Nevertheless, the hydrodynamic model that forms the basis for the present model (which only introduces an extension of the 25m refinement area), has been run for a period of 43 years (1979-2022)

[11] http://www.marine.ie/Home/site-area/data-services/real-time-observations/tidal-observations

and covers very well the measurement periods of the two measurement stations. The water level model output of that model was already validated in Deltares (2022), and was considered to be very reliable, with high correlations with data observations and low root-mean-square-errors. For reference, the validation of the water levels is presented in the Appendix.

In general, it is expected that if any, the effect of extending the area of the highest resolution would improve the quality of the model, at least within the area of the extended refinement. A full hindcast run to cover the entire measurement period is deemed unnecessary and of course computationally inefficient, given the very limited change applied compared to the previous validated hydrodynamic model (Deltares, 2022). Nevertheless, to verify the quality of the present model, an additional validation simulation was submitted for the period of January of 2021 which falls within the periods of available measurements.

For this period, statistical comparisons are made of the observed and modelled data. Table 2.3 shows the main statistics of the water level data comparisons such as the correlation coefficient, bias and root-mean-square errors (RMSE) in January 2021 of available data for both stations considered (cf. Table 2.2). Additionally, Figure A.1 shows the density scatter plots that present the correlations and the best fit formula per each station/period. The reference level of the water level observations was corrected to the model reference level (MSL) similar to the validation of water levels in Deltares (2022), because mean differences may occur due to the different reference systems used by different observation locations. Next to the statistical comparisons, timeseries comparisons are also presented in Figure 2.14 to demonstrate how well the model captures individual events (peaks) in the observations. The observed water level peaks are typically only marginally lower (in absolute terms) than the modelled, as also indicated by the density scatter.

As expected, the statistical comparisons of the observed versus modelled water levels at all stations remains with a very high correlation ranging between 0.996 and 0.998, similar to Deltares (2022). The root-mean square error (RMSE) between the observed and modelled water levels is in the range of 0.06 m and 0.11 m. The bias is around 0 as the mean reference level of the observations have been corrected to the modelled reference level (MSL), the average bias-correction value is 0.075 m. Based on these results, it is concluded that no further calibration of the hydrodynamic model is needed with respect to water levels.

Table 2.3 Overview over all the statistics done by comparing the observed water level data with the modelled one over the periods mentioned in Table 2.2.

Station	Period	Correlation coefficient, ρ (-)	Bias correction value (m)	RMSE (m)
		Galway Port		
(d)	January 2021	0.996	-0.074	0.111
		Inishmore		
(b)	January 2021	0.998	-0.077	0.064

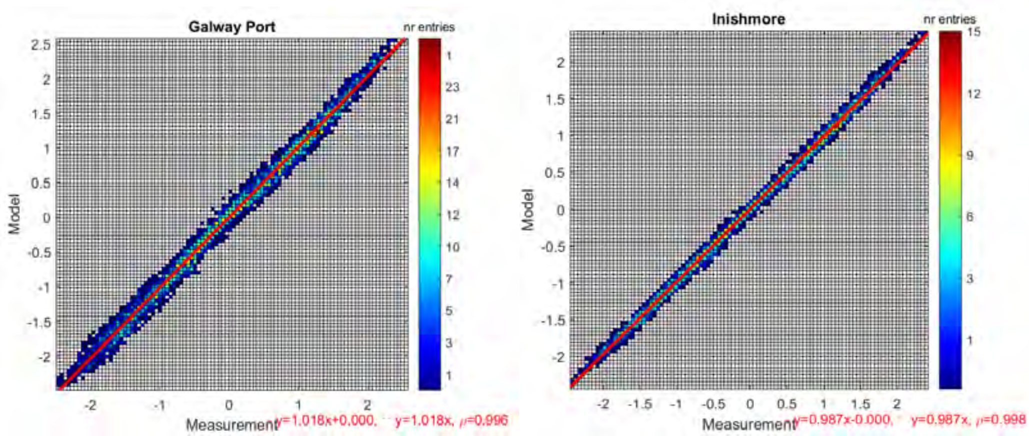

Figure 2.13 Water level density scatter comparisons for The Galway Port and Inishmore stations observation and the model data. The symmetric fit to the data is given by the red dotted line. Only the correlation coefficient and the best fit formulas of the comparisons are printed.

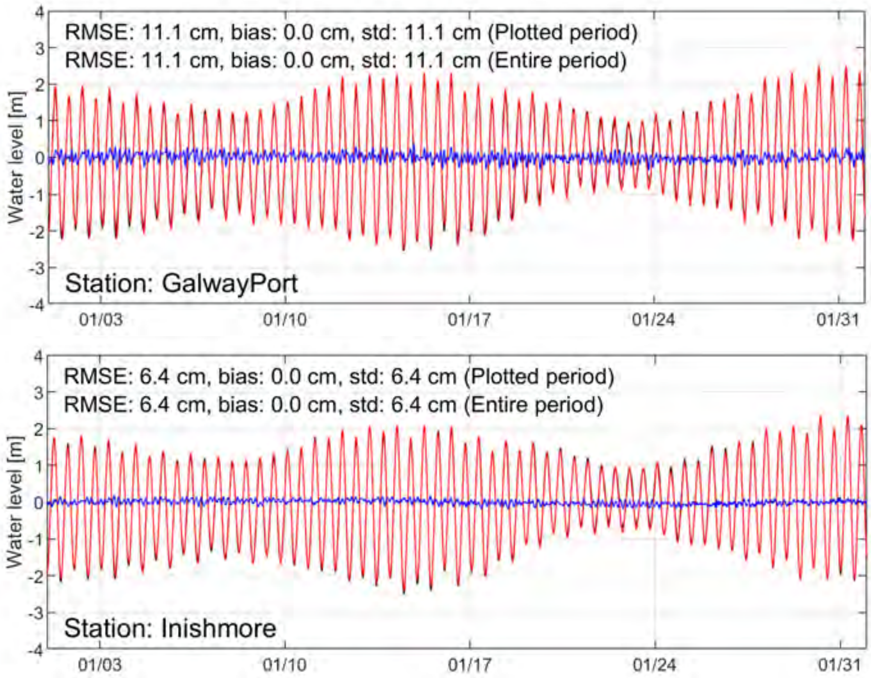

Figure 2.14 Timeseries comparison of the observed and modelled water levels data at Galway Port (top) and Inishmore station (bottom). Black lines (in the background) indicate the observed data, red lines (on top) the modelled data and blue lines the difference between the two, the latter being typically less 0.2 m in absolute terms. See also Table 2.2 and Table 2.3.

The current hydrodynamic model is concluded to be accurate overall for the purposes of the present assessment, based on the good agreement between observed and modelled water levels. The hydrodynamic model was already calibrated in Deltares (2022) to determine the necessary resolution for capturing flow patterns in the vicinity of the islands with sufficient accuracy. The resulting resolution of that calibration is also employed in the present schematization. For more information the reader is referred to Deltares (2022). Given the proper representation of these flow patterns, it is deemed that next to water levels, currents are also modelled with sufficient accuracy, also drawing confidence from the good performance of the 2D-DCSM, which is extensively calibrated and validated against a large number of observations across its domain. It would, nevertheless, be useful to further validate the model in case observations of flow velocities in proximity to the OWF and OECC become available.

2.2.6 Modelling of wind farm effects

2.2.6.1 Simulated conditions

To quantify the effects of the wind farm presence and operation on the flow fields around SROWF, a comparison is needed between the flow fields in two situations i.e., the baseline situation without any WTG present and the operational situation with WTG in place. The former situation is simply reproduced by running the validated hydrodynamic model described in the previous sections. For the operational situation, the presence of the WTGs and of the OSS platform is accounted for by using the baseline model as a starting point and further implementing (also summarized in Table 2.4):

- a local water depth decrease at all WTG locations, as a result of the presence of a large (55 m diameter) GBS foundation base on the seabed sitting on a rock layer (see Figure 1.4);
- a local drag force at all WTG locations exerted by the central column (diameter 13 m) extending upwards from the GBS base and finally;
- a wind speed reduction over the entire OWF area, due to wind extraction from the WTG operation.

All of these aspects are deemed to have a potential influence on the current speeds, directions and water levels around SROWF.

Table 2.4 Simulated conditions for the quantification of OWF effects.

Condition	Schematization	Simulation
Baseline	Pre-construction bathymetry (see Section 2.2.2) Raw ERA5 wind fields (see Section 2.1)	Hindcast January 2013
Operational	Local increase of seabed levels applied on pre-construction bathymetry, based on the GBS foundation base and rock layer geometry. Reduced raw ERA5 wind speeds by 10% within the OWF polygon. (see Section 2.1) Addition of local drag induced by the central column of the WTG foundation on ambient flow.	January 2013

It is noted that given the lack of information at the time of the study concerning the design of the OSS platform, it was decided to treat it as an additional WTG, meaning that a WTG founded on a GBS was considered at that location. This is a crude assumption that is nevertheless deemed plausible given level of detail with which hydrodynamics are modelled with the employed 2DH numerical model in this study.

In the remainder of this section, the implementation of the abovementioned schematizations is described in more detail.

2.2.6.2 Bathymetry treatment

The GBS foundation base (see Figure 1.4) is the part of the WTG foundation with a conical shape that extends downwards from the interface with the central column (of 13 m in diameter) and reaches a diameter of 55 m at the top of the rock layer. Together with the rock layer, the local decrease of depth extends within a diameter of roughly 70 m and at most approaches a vertical difference of 33.5 m. From a hydrodynamic perspective, local flow accelerations around such an obstacle are to be expected at the WTG locations. From continuity, it follows that this acceleration will be largest at shallower locations, where a large ratio of obstruction height to ambient water depth applies.

To capture this effect, first an area of obstruction was identified, by considering the sum of the GBS foundation base and the underlying rock layer. Consequently, this obstruction area was defined by drawing a polygon around each of the 31 locations (WTG and OSS), with a diameter determined based on the wider underlying rock layer. At these grid points, the average baseline seabed level foundation is calculated which is used as a level on top of which the obstruction levels are added. Considering the resolution of the grid at these locations (roughly 25 m), a seabed level change is applied in roughly 7 grid points, which obviously is not adequate to describe fully the geometry of the obstruction, but nevertheless is deemed adequate for the purposes of the present assessment. In line with the actual obstruction geometry, the average and maximum depth change over the treated grid points at each of the 31 obstruction locations varies around 10 and 30 m respectively.

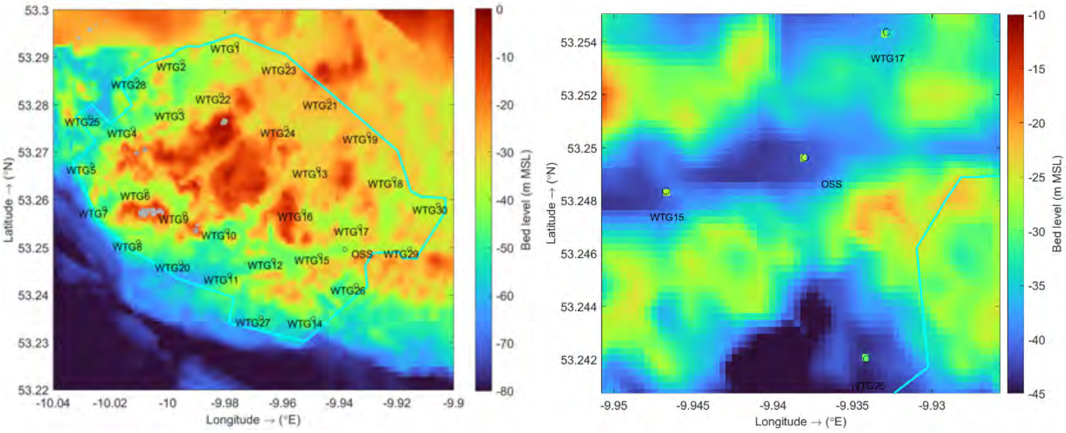

Figure 2.15 Bathymetry of the operational condition across the entire SROWF area (left panel) and at a zoomed area to the south east (right panel). The obstruction area is denoted by the black circle polygon plotted around each of the 31 obstruction locations.

A simulation was run where only this local bathymetry change was implemented to the baseline model to understand the effect of this schematization alone unobscured from the cumulative effect of all combined influences modelled in this study. Figure 2.16 below shows this effect during Low Water Spring conditions. At all locations, the decrease of water depth leads to accelerated flows around the obstacles and hence is seen as an increase of flow magnitudes. This effect is nevertheless at most locations only locally visible. Only for the shallowest locations to the east of the SROWF, i.e., WTG-23 -21 and -19, is the flow field influenced at a larger spatial scale. There, flow acceleration is largest due to the large ratio of obstruction height to total water depth, takes place especially around the foundation locations and is also followed by a deceleration downstream from the obstructions. This is most notable around WTG-21 where the obstruction height is even larger than the water depth, meaning that part of the GBS base remains above the water line.

Deltares

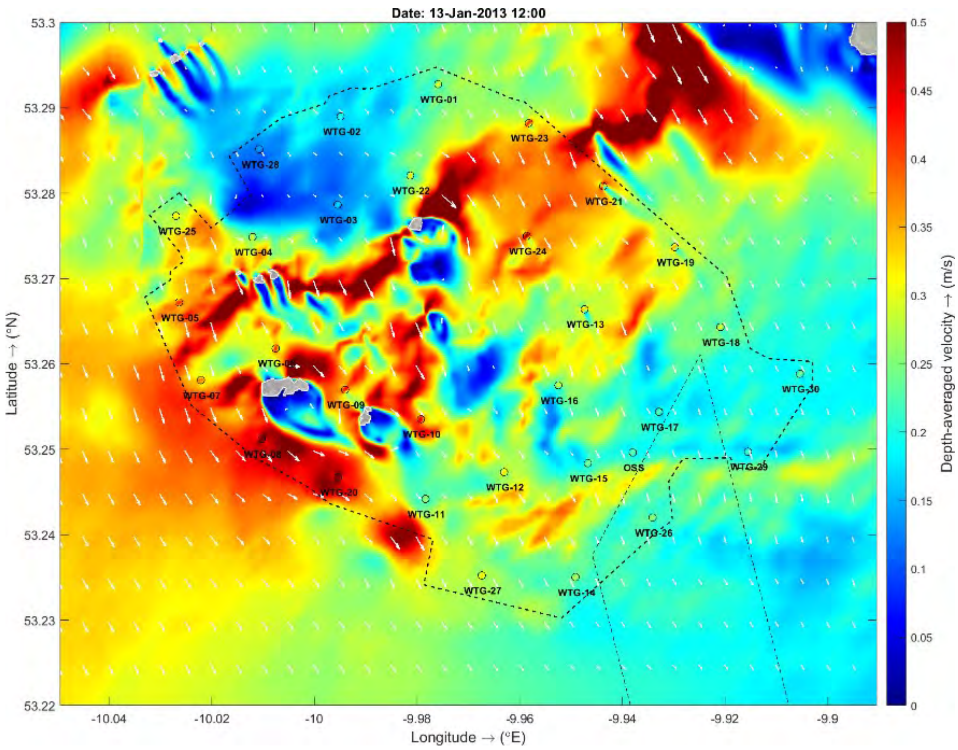

Figure 2.16 Flow field (depth-averaged flow magnitude and direction –going to-) during Low Water Spring conditions (LWS) with an operational situation where only a bathymetric change is applied to the hydrodynamic model (only with the schematization of GBS foundation).

Based on these results, it is deemed that the presence of the large GBS foundation base and associated rock layer is captured reasonably well by the schematization implemented in the hydrodynamic model via the bathymetric change. This is considering the resolution of the employed hydrodynamic model and the observed local flow fields that are in line with expectations.

2.2.6.3 Drag force

The presence of the GBS foundation base and associated rock layer are treated through the bathymetry as explained in the previous section. An additional effect stems from the central column that extends above the GBS foundation base all the way through the water column. The monopile with a diameter of 13 m, where submerged, will obstruct flow by inducing shear (turbulence) in its wake relative to the incoming flow direction, thereby locally extracting momentum.

With the DFM 2DH hydrodynamic model employed in this study, there are different ways in which this can be implemented but nevertheless follow similar principles in physics. The choice was made to schematize this effect by switching on the vegetation module of DFM, similar to the approach employed in WoZEP numerical modelling of cumulative impacts from large scale deployment of offshore wind in the North Sea, on commission of the Dutch government (Van Duren, L. et al. 2021). This is the state-of-the-art approach for including the effect of bottom-fixed monopile foundations on ambient flow fields and associated water quality.

By doing so, the extraction of momentum from the flow is introduced through a subgrid parameterization, in which the hydraulic resistance force through emerged rigid vegetation is calculated following the approach of Baptist et al. (2007). For submerged conditions, this approach accounts for the logarithmic profile of flow over the vegetation. Nevertheless, for emerged rigid vegetation, as in the present study (where stem diameter exceeds water depth) this reduces to a Chézy-type friction formula for uniform flow, employing a drag coefficient (Cd), stem diameter (diameter of the pile cylinder) and a stem density (ratio of blockage area over subgrid parameterization area).

More specifically, and according to Baptist et al. (2007), τ_v is the vegetation resistance force per unit horizontal area (together with τ_b bed resistance force result in the total resistance force), which is modelled as the drag force on an array of rigid cylinders with uniform properties:

$$\tau_{total} = \tau_b + \tau_v$$

$$\rho_0 ghi = \rho_0 g \frac{u^2}{C_b^{\,2}} + \frac{1}{2}\rho_0 C_d mDhu^2$$

$$u_{cb} = \sqrt{\frac{hi}{1/C_b^{\,2} + C_d mDh/2g}}$$

Where:

- ρ_0 denotes the Fluid density (kg/m^3)
- C_b Chézy coefficient of the bed (m$^{1/2}$/s)
- C_d denotes the Bulk drag coefficient (-)
- m denotes the Number of cylinders per m2 horizontal area (m^{-2})
- D denotes the Cylinder diameter (m)
- h denotes the Water depth (m)
- g denotes the gravitational acceleration (m/s^2)
- u_{cb} denotes the Uniform flow velocity (m/s)

In the hydrodynamic model, this subgrid parameterization is applied over a polygon surrounding a number of cells at each WTG location and at the OSS separately. In this parameterization, all parameters concerning the obstruction are known (e.g., pile diameter, area of pile over area of cells) except for the drag coefficient C_d for which a sensitivity analysis is done during set-up of the hydrodynamic model, with values in the range of 0.7 and 1.2, following from the drag coefficients of 2D circular shapes after Hoerner (1965), for Reynolds numbers between 10^4 and 10^6.

In addition, the area (in terms of number of grid cells) over which this subgrid parameterization is applied can also be varied within a reasonable range, from a single grid cell of ~25x25 m enclosing in this case the full 13 m diameter pile obstruction, to nine (9) grid cells around each location thus better reflecting uniform flow conditions. It is noted that with the latter schematization, in which the obstruction is extended to the neighbouring cell in all directions, a lower density is applied since the number of monopiles obviously remains unchanged (and equal to one).

The results over two (2) drag coefficient factors (C_d) and over two (2) areas of obstruction are summarized in Figure 2.17 for the reference instantaneous flow field during LWS (characterized by large ambient flow magnitudes) by means of difference plots relative to the ambient flow from the baseline condition. It is noted that as a starting point for this schematization, the model includes the local effect of bathymetry change, according to what was discussed in the previous section.

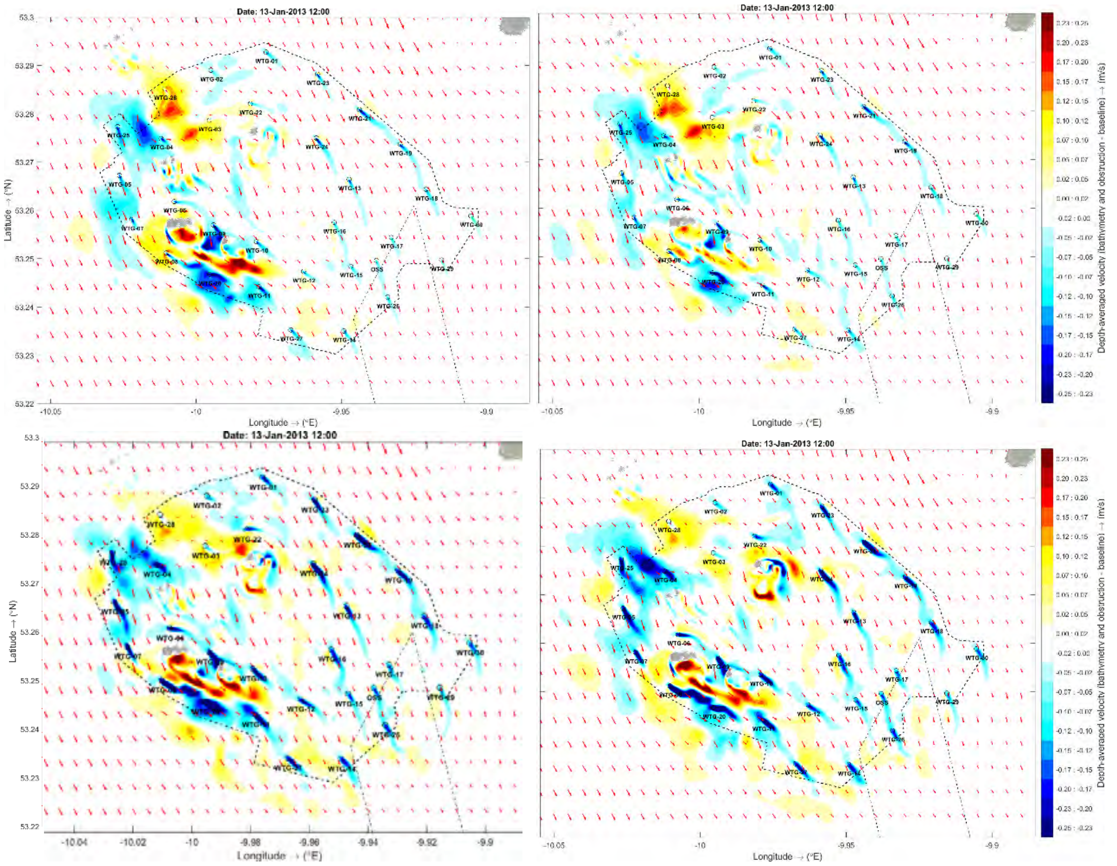

Figure 2.17 Difference plot of flow field (depth-averaged flow magnitude and direction –going to-) during Low Water Spring conditions (LWS) between an operational situation that includes the local bathymetric changes, and the drag force under various settings (Top / Bottom panels: subgrid parameterization area of 1 cell and 9 cells surrounding the obstruction locations respectively; Left / Right panels: Cd = 0.7 and Cd = 1.2 respectively) and the baseline condition. Background black arrows show flow directions in baseline conditions and red arrows plotted on top show directions in operational conditions.

From this sensitivity analysis, it follows that the extraction of momentum (decrease in ambient flow velocities) increases with:

- an increase of the area where the subgrid parameterization is applied, despite the fact that the overall blockage (i.e., ratio of pile area over the cell area) remains the same and;
- as expected an increasing drag coefficient, however for the tested range (0.7 – 1.2) the sensitivity is less pronounced compared to the effect of the tested subgrid parameterization area.

Considering the reasonable sensitivity ranges tested and given that it was not possible to validate this drag force schematization, it was chosen to proceed with the most conservative selection of parameters, meaning the one that results in the largest change in ambient flows compared to the baseline condition, which aligns with the focus of the present study. Subsequently, following this sensitivity study, we proceed in the schematization of the operational scenario with a drag coefficient (C_d) of 1.2, and a subgrid parameterization area of nine (9) cells surrounding each obstruction location.

2.2.6.4 Wind reduction

Finally, to capture the wind extraction from the operating WTG, the wind speeds at 10 m used to force the hydrodynamic model are reduced over the entire simulation period by 10%, with the directions remaining unaffected. Within D-Flow FM, the implementation is such that the reduction is applied on the wind forcing field that is interpolated to the actual high resolution of the grid cells within a provided polygon, being in this case the OWF polygon.

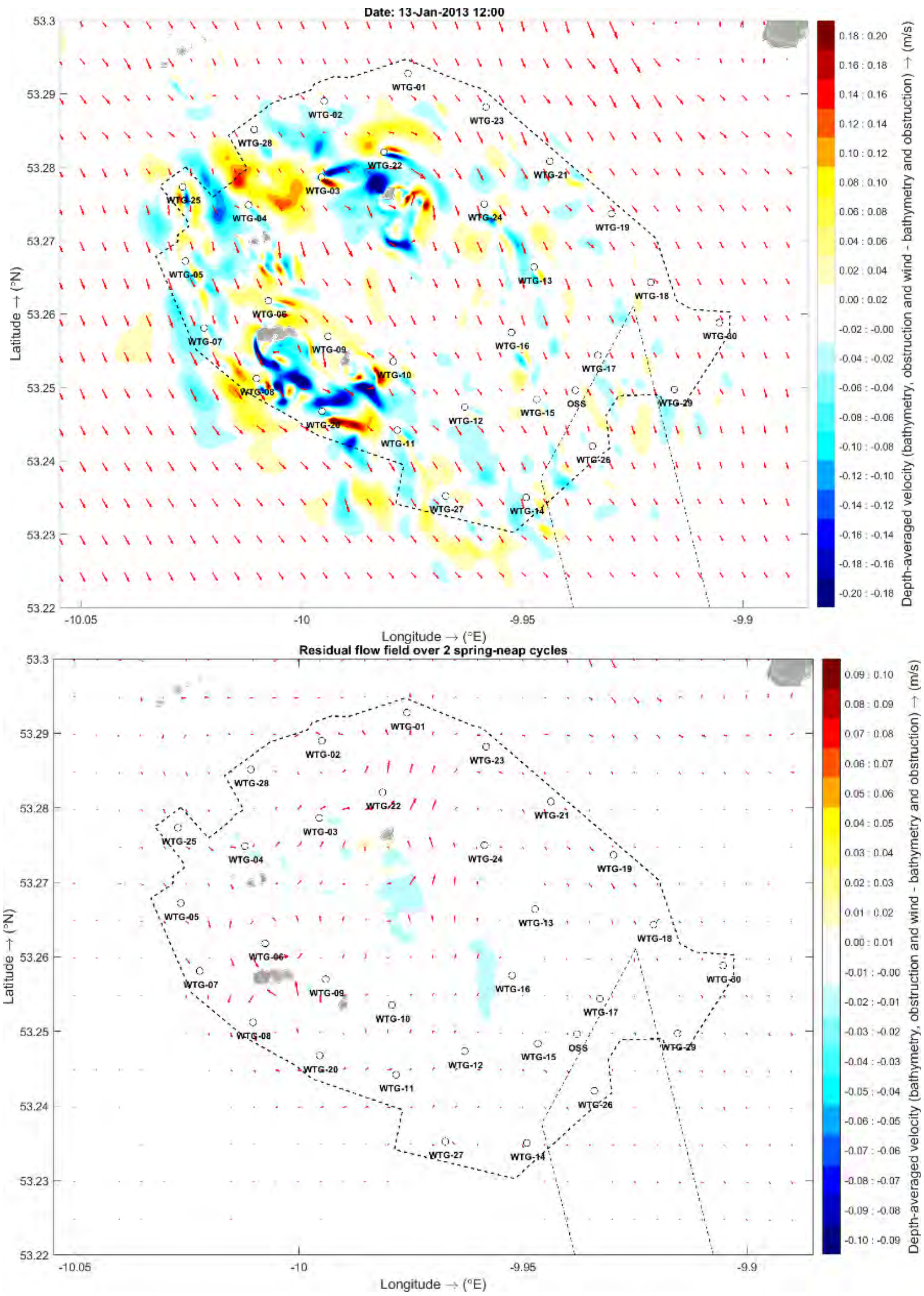

Figure 2.18 The isolated effect of the wind reduction on instantaneous and residual flow fields through a difference plot of flow field (depth-averaged flow magnitude and direction –going to-) during Low Water Spring conditions (LWS) and over two Spring-Neap cycles (residual flow) between an operational condition that includes the local bathymetric changes, the drag force and a wind speed reduction of 10% and an operational situation that includes only the local bathymetric changes and the drag force. Background black arrows show flow directions in former and red arrows plotted on top show directions in latter situations.

2.2.7 The SROWF water level and current timeseries dataset

The validation, calibration and post-processing of the 2DH DCSM-FM water level and current data led to the following 10-minute timeseries over January 2013 (01-01-2013 00:00 – 01-01-2013 00:00, 1 month) at all requested output locations:

- SWL (still water level, also referred to as total water level)
- total current speed and direction (depth-averaged)

The SWL corresponds to the raw model results as no calibration was deemed necessary based on the validation of the data at Galway Port and Inishmore stations. No local current observation data were available for performing further validation and/or calibration of the model results.

2.3 Wave modelling

2.3.1 Introduction

The wave data that were used to determine the SROWF wave fields under baseline and operational situations were derived by means of local wave modelling. To that end, multiple wave runs were performed representative of a number of various sea states, ranging from normal conditions all the way to extreme conditions with a return period of 50 years. The wave modelling is described in the next section and the validation of the baseline model results in Section 2.3.6. The determined SROWF wave fields are presented in the next chapter.

Numerical wave modelling was performed using SWAN to produce timeseries and fields of accurate wave conditions in this study. SWAN is widely used for nearshore wave modelling in the international coastal and offshore engineering communities and has been successfully validated under a large variety of field cases and conditions. The software is continually undergoing further development; see www.swan.tudelft.nl for more information. For this study we have used the latest operational version that includes the most recent insights and model developments (SWAN Version 41.31).

Two wave models were employed in this study to produce information across the entire model area of interest (see Figure 1.2) including the coastal area, the OWF and the entire OECC, namely:

1. a dedicated high resolution SROWF-SWAN that covers the extended area of the OWF and the adjacent coastal area and;
2. a large-scale lower resolution *North West European Continental Shelf* (NWECS)-SWAN which is in-house developed at Deltares, to produce information at the remaining parts of the entire model area of interest (see Figure 1.2) i.e., that fall outside the dedicated high resolution SROWF-SWAN, namely the part of the ECC that extends further to the south from the SROWF till landfall.

The dedicated SROWF-SWAN wave model is forced with the ERA5 hourly 10 mMSL wind fields, hourly depth-averaged current velocities and water levels from the 2DH DCSM-FM, and finally hourly 2D wave spectra at the open boundaries generated with the large scale NWECS-SWAN model. The two models have been run in the unstructured mode, which allows the generation of a boundary fitted grid and optimal solving of the bathymetric features. Please refer to Appendix A for more general information on the SWAN model.

2.3.2 Model domain and baseline bathymetry

SWAN requires the specification of three types of grids:

1. computational grid, which defines the 2D geographical locations of the nodes in the calculation grid;
2. directional grid, which defines the wave directional range (usually 360°) and resolution;
3. spectral grid, which defines the range and resolution of the computations in the wave frequency space.

2.3.2.1 Computational grid

<u>Dedicated high resolution SROWF-SWAN</u>
First, the dedicated high resolution SROWF-SWAN unstructured wave model was developed for this study with a spatial resolution varying between 25 m around the SROWF area (similar to the hydrodynamic model) and 250 m further away (see Figure 2.19). Similar to the hydrodynamic model, the starting point was the wave model employed in Deltares (2022) metocean study. Compared to its predecessor, the present wave numerical model was further refined in the area of the SROWF (highest resolution of 25 m as opposed to 50 m) and the refinement area was extended further to the east to fully enclose the updated OWF polygon, similar to the hydrodynamic model. This dedicated wave model fully encloses the area over which any effects of the wind farm operation are noticeable, as it will be shown in the results section.

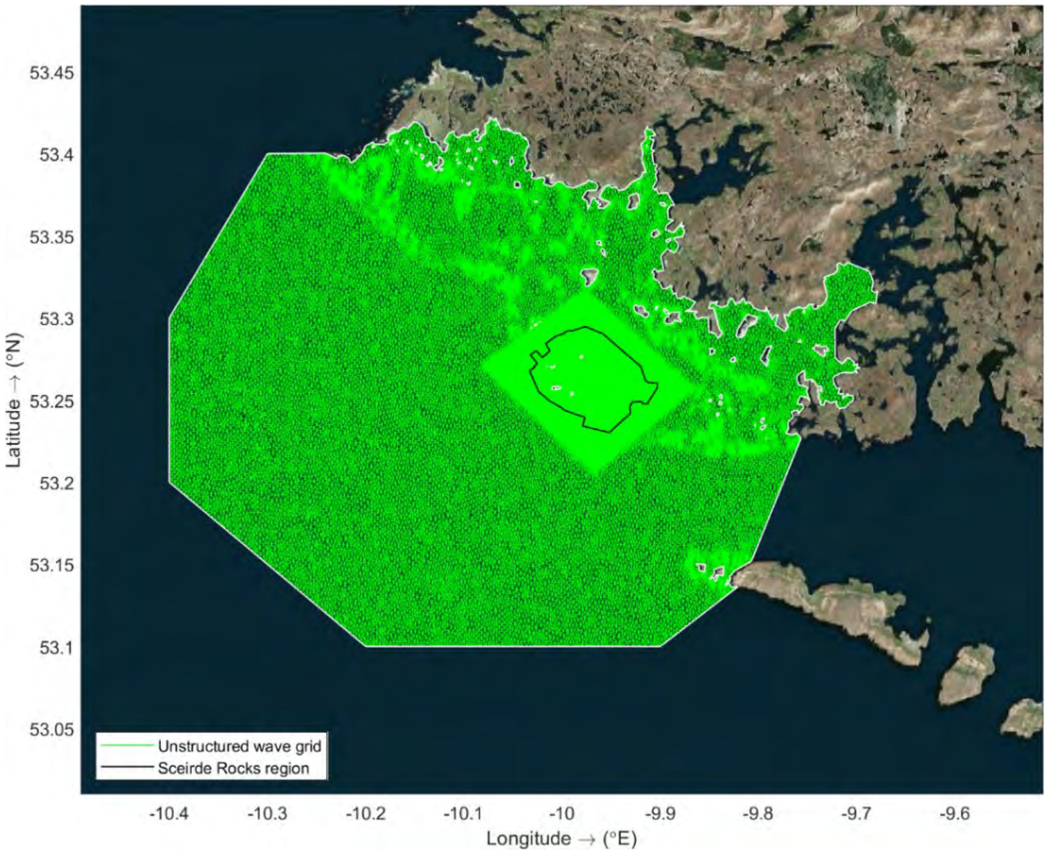

Figure 2.19 Computational <u>dedicated high-resolution SROWF-SWAN</u> wave model domain and grid (nested in NWECS-SWAN, see Figure 2.20 below).

Relatively larger islands within the area of the SROWF-SWAN that are expected to remain mostly dry based on observations from available satellite images, are excluded from the computational grid. For these islands, all incoming wave energy will be absorbed at the land boundaries which are visible in Figure 2.22. Instead, relatively smaller islands that might become wet during high water conditions are included in the computational grid. The influence of these islands on the propagation of wave energy at the area of interest will be accounted for by the locally implemented (shallower) water depths. Finally, for reasons of computational efficiency, not all enclosed bays along the coastline were considered in the model, as the conditions in those areas do not influence the wave conditions reaching the SROWF region. Such excluded bays are visible at the east and north of the dedicated SROWF wave model outline in Figure 2.19.

Large-scale coarse resolution NWECS-SWAN
Because information was requested by the Client also outside the area of the readily available SROWF-SWAN model, namely along the entire OECC up to landfall, a readily available and much larger scale wave unstructured SWAN model of the North Western European Continental Shelf (NWECSSWAN, see Figure 2.20) developed in-house at Deltares, was also employed in this study to produce information farther from the dedicated SROWF-SWAN wave model boundaries. This coarser wave model with a spatial resolution varying between 5 km and 300 m (around the model area of interest, see Figure 1.2) was not only used to generate wave fields and timeseries outside the area of the dedicated SROWF-SWAN domain, but also to force the open boundaries of the dedicated model with information concerning incoming waves, in the form of 2D wave spectra. This nesting approach ensures the best possible transition of wave fields between the two wave models.

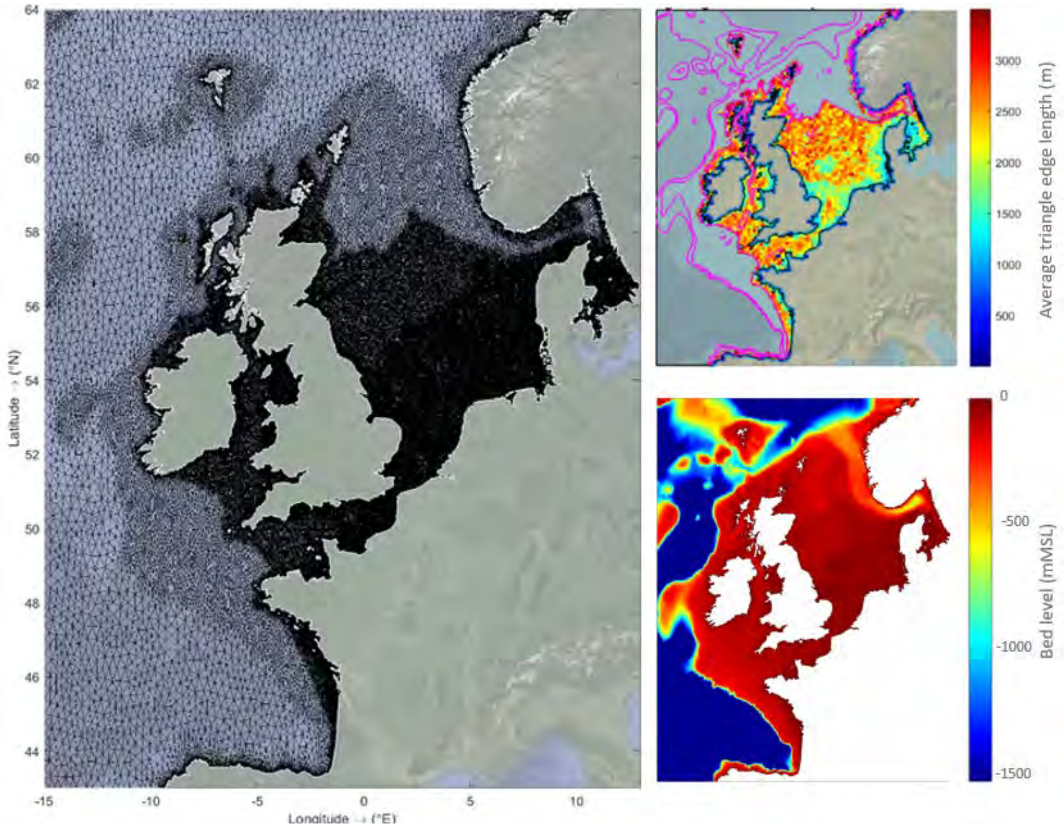

Figure 2.20 Left: Grid of the overall coarser resolution NWECS-SWAN wave model. Right: top - resolution of the NWECS wave model in the shallower areas of the domain, bottom – model bathymetry.

Summary
The OWF area is modelled with a resolution of ~25 m, the coastal area adjacent to the OWF with a resolution varying between ~25 m (closer to the OWF) and ~250 m (further towards the coast), and along the OECC wave conditions were modelled with a resolution varying between ~25 m (closest to the OWF), ~250 m (up to roughly the boundary of the SROWF-SWAN, as seen in Figure 2.19) and finally ~300-3000 m (from the SROWF-SWAN southeast boundary up to landfall, with the highest resolution at the coast).

2.3.2.2 Directional grid
For both wave models employed here, the defined directional grid covers the full circle (360°). The number of directional bins was set to 45, resulting in a directional resolution of 8°. This is a typical and often used directional resolution in such wave studies.

2.3.2.3 Spectral grid

The spectral grid of the numerical models covers a frequency range from 0.03 Hz to 2.5 Hz, allowing for representation of wave periods ranging from 0.40 s to 33.33 s. The distribution of the frequencies, f, is logarithmic with a constant relative resolution, $\Delta f/f$, close to 0.1. This results in a total number of frequency bins of 46. This way of distributing the modelled frequencies over the extent of the considered frequency range ensures that the resolution at lower frequencies is not as coarse as it would have been if an equidistant distribution of frequencies had been applied.

2.3.2.4 Bathymetry

As for the hydrodynamic model, the bathymetry information for the dedicated SROWF-SWAN wave model was based on a composite of various datasets with different resolutions as used in Deltares (2022). At the SROWF area, publicly available high resolution INFOMAR (provided by Corio Generation to Deltares for the metocean study of 2022) and EMODnet bathymetric data were combined with Deltares' in-house available data from historic navigational charts. The latter dataset was used to derive the complex topography at the very shallow areas of SROWF where information from high resolution INFOMAR and EMODnet was missing. Further away from the SROWF area, this composite bathymetry was supplemented by publicly available lower resolution bathymetry data from the EMODnet dataset from 2020, which also was the only bathymetric dataset used in the overall NWECS-SWAN model.

Already in Deltares (2022), special care was taken during processing of the bathymetry to allow for smooth transitions between different datasets and at the same time to ensure that higher resolution data were leading over lower resolution data. Finally, the input bathymetry was referenced relative to MSL, based on a spatially varying conversion from LAT which is available at the area from the large-scale 2DH DCSM-FM. The applied bathymetry of the wave model is shown in Figure 2.21 for the entire dedicated domain and in more detail within the SROWF region in Figure 2.22.

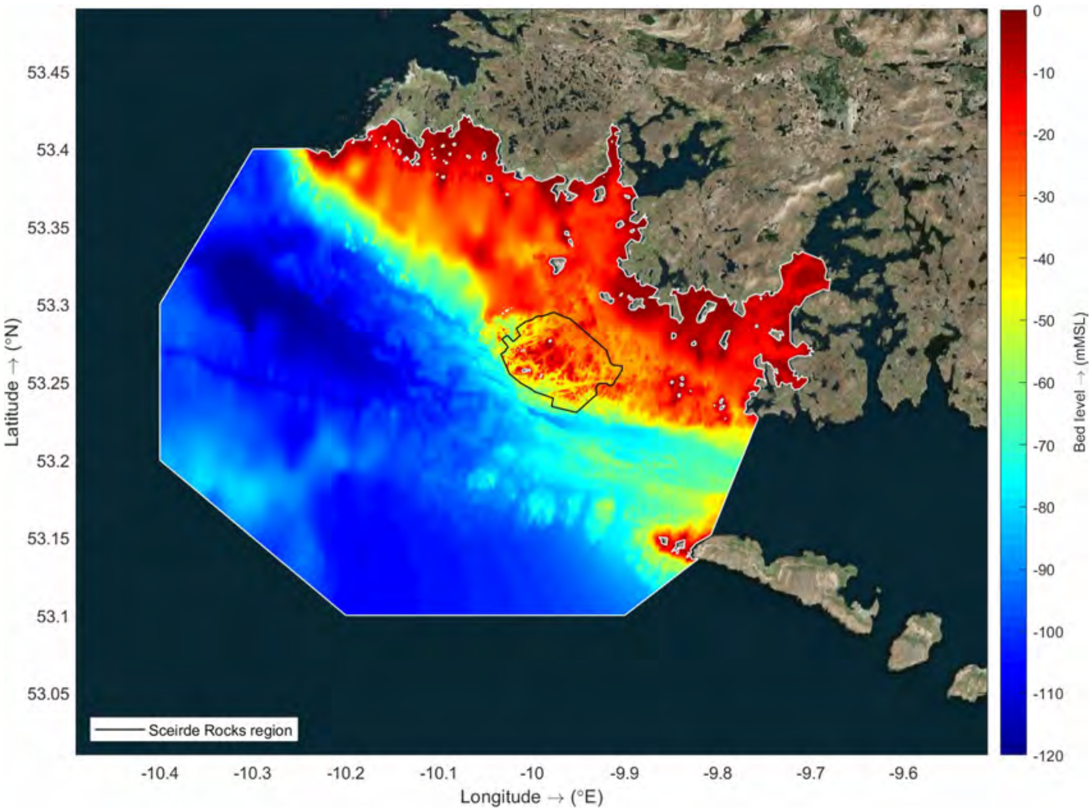

Figure 2.21 Bed levels relative to MSL as used in the computational grid of the baseline dedicated SROWF wave model.

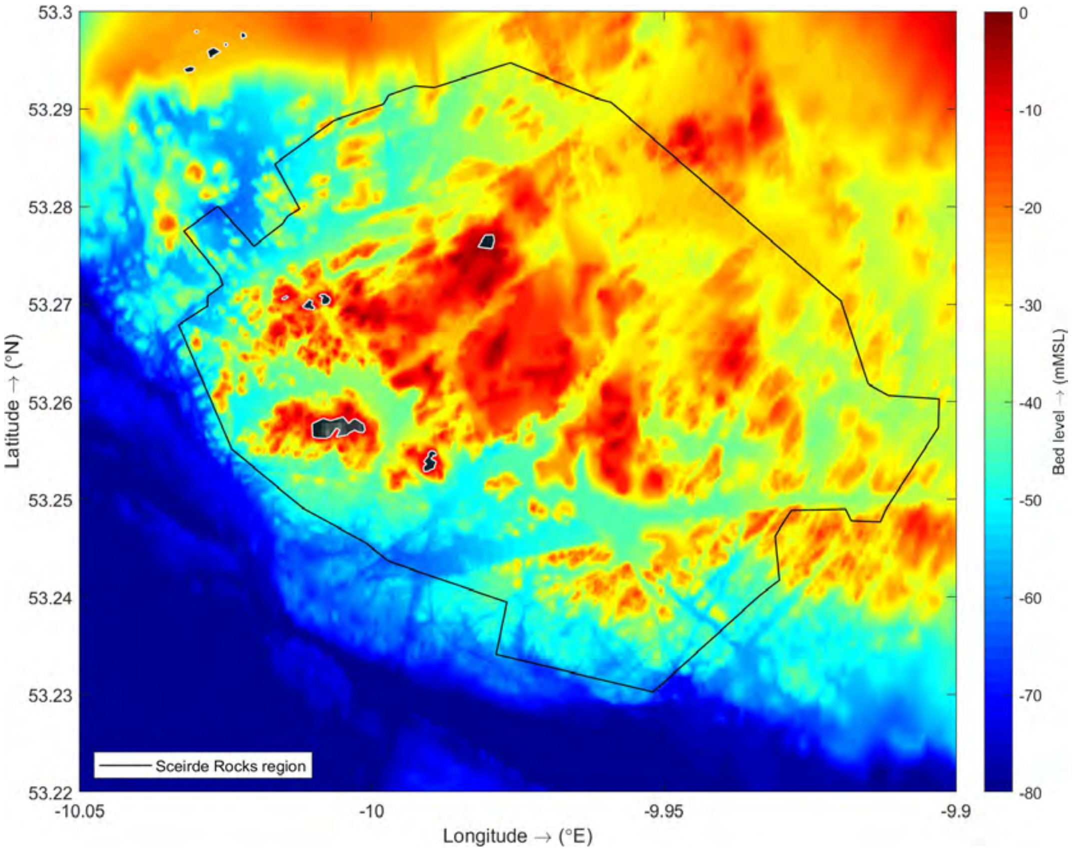

Figure 2.22 Bed levels relative to MSL as used in the surroundings of SROWF area in the baseline dedicated SROWF wave model. Zoom of Figure 2.21.

2.3.3 Boundary and input conditions

The wave models were run sequentially (first the overall NWECS model followed by the nested dedicated SROWF model using open boundary forcing produced by the former) in non-stationary mode i.e., taking evolution of the wave conditions in time into account. Several runs were submitted, each corresponding to a different sea state (with a duration of 4 days), representative (at the time instance half way the simulation) of reference normal (50th and 90th percentile) and extreme (return period of 1,-5,-10 and -50 years) conditions as requested by the Client, under two main approach directions at the offshore boundary of the SROWF, being waves coming from W (roughly 270°) and WSW (roughly 240°) directions (see Figure 2.23). These are also the predominant directions identified at the offshore reference location (WTG-15[12]) as per Deltares (2022), located nearest (at a horizontal distance of roughly 120 m) to WTG-08 of the latest layout used in this study.

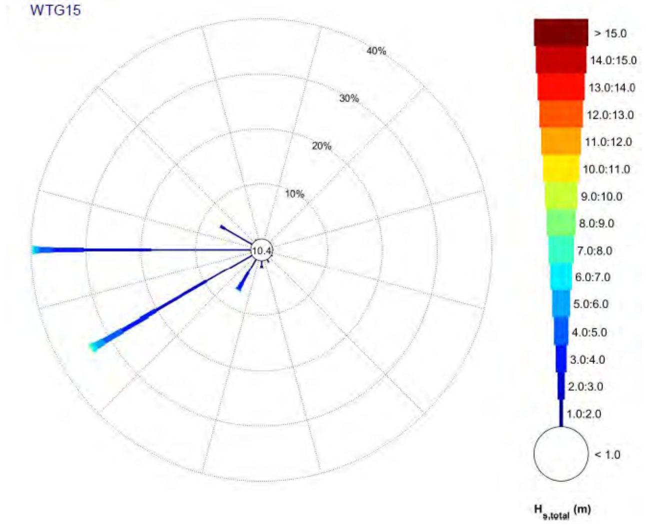

Figure 2.23 Wave rose at previously defined offshore exposed location (WTG-15) in Deltares (2022), positioned near present WTG-08, showing the predominant wave directions at the offshore boundary of the SROWF.

The model uses a timestep of one hour, which is equal to the time step of the (ERA5) input wind fields. The first 48 hours simulated time (of the 6 days total simulated period) are considered as the spin-up period of the model[13].

2.3.3.1 Selection of representative sea states

The dates of the representative conditions for these 12 simulations (2 directions x 6 sea states) from the various sea states were determined by identifying in the 43-year hindcast wave timeseries previously produced at the offshore reference location (WTG-15) used for the statistical analyses in Deltares (2022), the (peak) values of significant wave height (note that the associated peak wave periods are not considered here) more closely[14] corresponding to:

- the directional (W & WSW) percentile values extracted from the same timeseries (normal conditions) and;

[12] Not to be confused with the WTG-15 of the latest WTG layout considered in this study.

[13] The spin-up period is the modelling interval which is required for the model to start up and initialise. This includes allowing the wave energy from the boundary to distribute over the total modelling domain. A spin-up period of 48 hours (2 days) prior to the actual modelling period (in this case of 4 days) is typically used. Results for the spin-up period may not be reliable and are discarded.

[14] The reference values of extreme and normal conditions are statistically derived and hence theoretical. This implies that the identified sea states in the hindcast timeseries (and hence associated timings) closely approach but do not necessarily exactly match the reference values in terms H_s.

- the directional (W & WSW) extreme values of significant wave height determined in Deltares (2022) for the same location (WTG-15)

The respective target values, (associated) peak wave periods and timings of identified representative sea states are summarized per direction in Figure 2.24, Figure 2.25 and in Table 2.5 and Table 2.6.

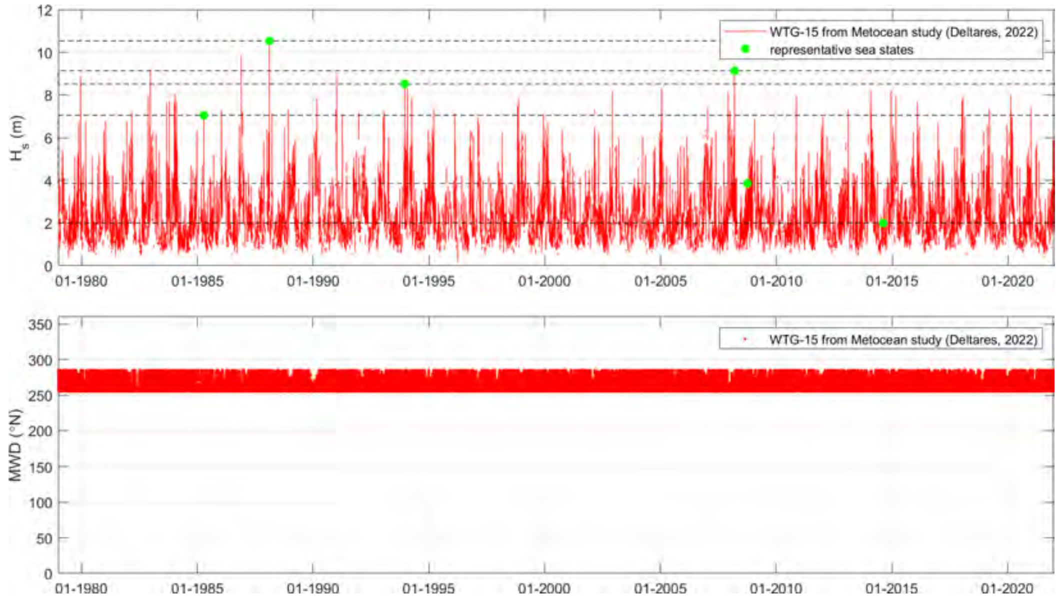

Figure 2.24 Hindcast timeseries (filtered around a MWD of 270° (255° – 285°)) produced in Deltares (2022) at the offshore reference location (WTG-15) for use in statistical analyses. The target values of significant wave height (corresponding to the various normal and extreme sea states) are denoted by the dashed horizontal lines. The identified corresponding representative sea states are denoted by the green markers, of which the dates are reported in Table 2.5 and Table 2.6.

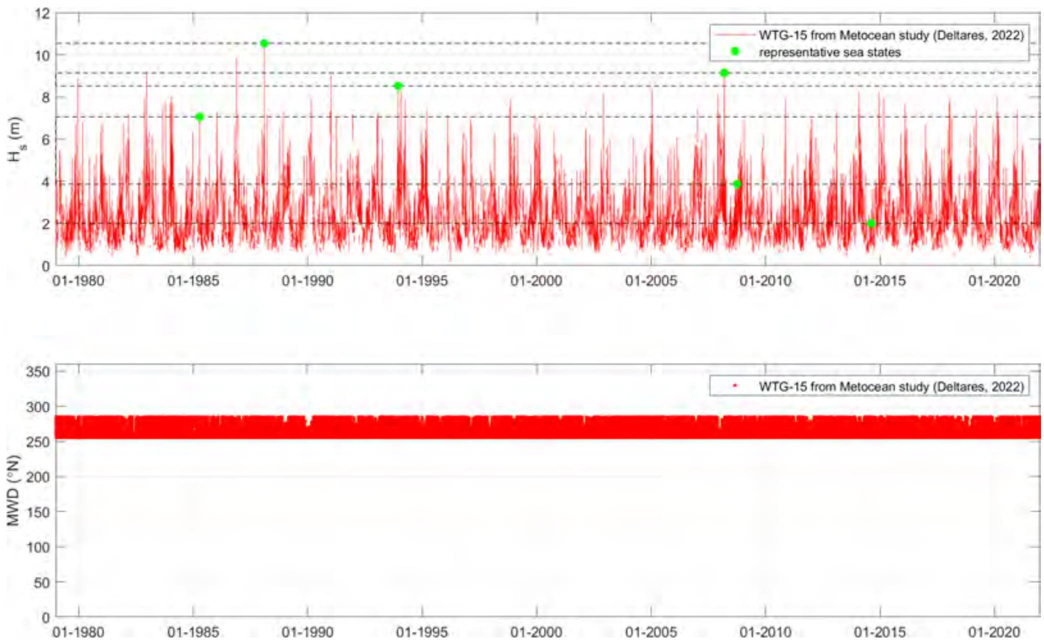

Figure 2.25 Hindcast timeseries (filtered around a MWD of 240° (225° – 255°)) produced in Deltares (2022) at the offshore reference location (WTG-15) for use in statistical analyses. The target values of significant wave height (corresponding to the various normal and extreme sea states) are denoted by the dashed horizontal lines. The identified corresponding representative sea states are denoted by the green markers, of which the dates are reported in Table 2.5 and Table 2.6.

.

Table 2.5 Normal target directional metocean conditions statistically determined based on wave hindcast timeseries at previously defined offshore exposed location (WTG-15) in Deltares (2022), positioned near present WTG-08 and timings of identified representative conditions in the same hindcast timeseries (based on H_s alone). Percentile values of peak wave periods (T_p) are presented for completeness but were not used in the identification of representative sea states.

Target sea state	MWD (240° ; 225° – 255°)			MWD (270° ;255° – 285°)		
	H_s (m)	T_p (s)	Rep. condition	H_s (m)	T_p (s)	Rep. condition
Normal–50th perc.	2.60	9.5	28-Aug-1984 16:00	2.00	9.1	10-Aug-2014 00:00
Normal–90th perc.	4.69	12.4	23-Mar-1981 21:00	3.86	11.8	01-Oct-2008 02:00

Table 2.6 Extreme target directional metocean conditions determined by means of extreme value analyses in the metocean study of Deltares (2022) at previously defined offshore exposed location (WTG-15), positioned near present WTG-08, and timings of identified representative conditions in the same hindcast timeseries (based on H_s alone). Associated values (to H_s) of peak wave periods (T_p) are presented for completeness but were not used in the identification of representative sea states.

Target sea state	MWD (240° ; 225° – 255°)			MWD (270° ;255° – 285°)		
	H_s (m)	ass. T_p (s)	Rep. condition	H_s (m)	ass. T_p (s)	Rep. condition
Extreme–RP1	8.02	14.9	08-Feb-2000 17:00	7.05	14.9	13-Apr-1985 23:00
Extreme–RP5	9.92	15.8	27-Dec-2013 05:00	8.52	15.8	15-Dec-1993 15:00
Extreme–RP10	10.72	16.1	19-Dec-1982 22:00	9.14	16.2	11-Mar-2008 23:00
Extreme–RP50	12.54	16.8	05-Jan-1991 14:00	10.54	16.9	09-Feb-1988 19:00

2.3.3.2 Incoming boundary conditions

The NWECS-SWAN model was forced at the open (offshore) boundaries with parameterized wave spectra described by ERA5 timeseries of five wave parameters (described in more detail below this list):

- Significant wave height, H_s
- Peak wave period, T_p
- Mean wave direction (coming from), MWD
- Directional spreading, DSpr
- Spectral shape, γ (an enhancement factor of the peak in the wave spectrum)

The spectral shape, γ, was at the boundary assumed constant and equal to the value of a standard JONSWAP (Hasselmann et al., 1973), γ = 3.3. The exact value of γ prescribed along the boundary is not critical, since the model will automatically properly redistribute the wave energy in the frequency domain and in balance with the wind forcing. The amount of directional spreading present at the incoming boundaries was derived from the ERA5 timeseries for “wave spectral directional width”. For numerical reasons, this value was capped at a maximum of DSpr = 37.5° (one-sided directional spreading level from the mean direction), which corresponds to a cosine-m power of m = 1 in SWAN[15]. Furthermore, for this parameter the exact value prescribed at the boundary is again not critical, since the model

[15] This power is used to describe directional distribution shape description according to $\cos^m(\theta)$, with θ representing the wave directions.

will automatically properly redistribute the wave energy over the different directions in the computational domain.

The dedicated SROWF-SWAN wave model was in turn forced at its open (offshore) boundaries with 2D wave spectra (i.e., describing the wave energy over prescribed directional and frequency computational grids) generated by the NWECS-SWAN model in the respective simulation periods. In the transitions between land and water occurring along the offshore boundary of the dedicated SROWF model (e.g., at the island to the southwest or near the coast, see Figure 2.19), the NWECS-generated 2D spectra were further processed before forcing SROWF-SWAN, to ensure that incoming wave energy from land is always zero. This was necessary considering the coarse resolution of the NWECS-SWAN model relative to the resolution of the SROWF-SWAN, especially near such land boundaries.

2.3.3.3 Reflecting/transmitting boundaries

No reflecting or transmitting boundaries were defined in both modelling domains. All wave energy reaching an outer boundary or land boundary is assumed in the model to be fully absorbed at that location. For sloping shorelines and beaches that is a fitting and often applied approach. At the sections bordering enclosed waters waves propagate out of the computational domain uninfluenced (as if they move into these areas).

2.3.3.4 Wind input

The wave model was forced spatially using the raw ERA5 wind fields with no corrections on the wind speeds or directions. This is mainly because the quality of the wind data is very high, the data are highly correlated with the observations, although showing some (order 10-13%) underestimation of the high wind speed peaks (cf. Section 2.1.2). Given that the quality of the wave model results does not depend only on the accuracy of the forcing winds we apply the raw ERA5 and shall correct for mismatches in the wind data and other model inaccuracies in the calibration of the modelled wave data.

2.3.3.5 Hydrodynamics input

The spatially varying hourly water level and depth-averaged current fields, from the hindcast 2D DCSM-FM model (covering the entire 43-year period between 1979 and 2022) have been used as input to the wave model. This means that the wave model accounts for the influence of the spatially distributed water levels and currents (speeds and directions) in the wave propagation and evolution.

2.3.4 Physics and numerical parameter settings

This section lists detailed settings for physics parameters and numerical aspects within the SWAN model. It is primarily included here for recording purposes, e.g. for possible future interpretation or reproduction of results. General readers may opt to skip this section.

2.3.4.1 Physics

The modelling was carried out using SWAN, version 41.31, in unstructured and non-stationary mode. The most relevant applied wave physics settings in the computations are:

- Dissipation of wave energy by bottom friction and wave breaking (wave steepness-induced and depth-induced) have both been applied in the SWAN computations.
  - For dissipation by bottom friction the JONSWAP formulation (Hasselmann et al., 1973) with a friction coefficient of 0.038 m^2s^{-3} (Zijlema et al., 2012) has been applied.
  - For dissipation by depth-induced wave breaking the Battjes-Janssen formulation (Battjes and Janssen, 1978) with a proportionality coefficient of 0.73 has been applied.

- For representing the effects of white-capping, the formulations by Rogers et al. (2003) have been applied, which is default setting since SWAN version 40.91 (see Appendix A for more details on the formulation).
- For the wind drag the default Wu (1982) approximation of the Charnock relation has been applied (see Appendix C.2 for more details on the formulation).

2.3.4.2 Numerics

The criteria for numerical accuracy thresholds were set as follows:

- the computation is finished in case of changes in the second derivative of the iteration curve of the significant wave height are less than 0.5% and the absolute (relative) change in significant wave height from one iteration to the next is less than 0.5 cm (or 1%) at 99% of the grid points, and
- a maximal number of 40 iterations is computed.

These settings mean that the computation will continue until a stable outcome has been reached for the modelled moment in time, with a maximum of 40 iterations to reach the result for that time step. Typically, 40 iteration steps will be sufficient, if not then often a setting in the model is incorrect or the computational grid is not optimal. In the computations performed for the present study, all timesteps after the two days spin-up period have been verified to have converged within 40 iterations (on average even within a much lower number), i.e. the computation has reached the proper numerical outcomes.

2.3.5 Output definitions

Spatial and time-varying fields of multiple wave (-related) parameters (H_s, T_p and MWD) were produced by the model as output at a time step of 1 hour (i.e. the computational time step). In addition, location-specific timeseries of the same parameters were generated from the numerical model at a number of output locations requested by the Client (see Figure 2.1).

2.3.6 Baseline validation

There are no local wave observations within the SROWF-SWAN model area available at the time of the study. M1 wave buoy (2001-2007) is the closest measurement station, located within the NWECS-SWAN domain, but approximately 50 km to the west of the detailed SROWF-SWAN model domain (cf. Figure 2.26). It is therefore not possible to directly validate the dedicated SROWF-SWAN domain’s modelling of the local bathymetric effect on the local wave fields. SWAN has on the other hand been validated in several other regions with complex bathymetries and been shown to properly model waves in such regions, provided that the quality of the bathymetric data are high.

Other variables affecting the accuracy of the wave results in this area are the boundary waves (generated from the overall NWECS-SWAN) and the (ERA5) wind forcing fields. A correction for the combined effect of the accuracy of these variables on the modelled results can be obtained by validating the NWECS wave timeseries generated at M1 (in previous hindcast wave modelling with NWECS that covers the measurement duration) against the M1 wave buoy observations available from the Marine Institute.

M1 is close enough for the bias of the NWECS simulated waves to be representative of the inaccuracies in the (ERA5) wind forcing and boundary wave conditions passed from NWECS to the detailed SWAN results in the SROWF area. All SWAN results across the greater MPPSA (and hence from both modelling domains) are therefore calibrated using the same calibration that is deemed necessary to be applied to the NWECS-generated waves at the M1 buoy location. This validation/calibration needs to be updated when future local wave observation data become available.

Table 2.7 presents the time periods covered by the data, the available variables and the provenience. It should be noted further that the observed mean wave directions at M1 only cover a very short period of less than 2 months in 2007. The quality of that data is also considered as low, given the rather large observed variance in the data, which is not expected for that location (see further below).

Figure 2.26 Location of M1 wave buoy relative to SROWF. The red outlines indicate the dedicated SROWF model boundaries and the green overlay polygon the SROWF area. M1 falls well within the NWECS domain.

Table 2.7 Observed variables and periods covered by the wave observations. Note that measurements are not continuous for any of the parameters during the survey period. While H_s, and $T_{m0.2}$ are measured with a good coverage, MWD timeseries are available only over a period of less than 2 months.

Station	Coordinates	Available variables	Period	Resolution	Origin
M1 (buoy)	53.1266°N, -11.2°E	H_s, $T_{m0.2}$, MWD*	02-2001 – 07-2007	hourly	Marine Institute[16]

Figure 2.27 and Figure 2.28 show the density scatter and percentile comparisons and the main statistics of respectively the significant wave height (H_s) and the zero-crossing wave period ($T_{m0,2}$) and mean wave direction comparisons between NWECS-SWAN model data and measurement data at the location of M1. The plots present the relevant statistics such as the correlation coefficient, root-mean-square errors, bias and standard deviation.

The figures show good to excellent correlations between the NWECS wave height (ρ=0.95, middle panel of Figure 2.27) and wave period (ρ=0.79, left panel of Figure 2.28) data and the observations, and only a minor underestimation of the significant wave height peaks.

As mentioned already, the quality of the observed mean wave directions is considered as low. It only covers a period of less than two months in 2007 and shows a relatively high variation in wave directions, whereas generally the main wave energy is coming from the West, from the North Atlantic (cf. right panel of Figure 2.28). The metadata also does not clearly describe over what frequency range the directions were observed, i.e. over the full frequency range or only covering shorter wind waves). The general trend in the mean wave direction is however captured correctly, giving confidence in the quality of the NWECS data.

Having considered all comparisons in detail (and also some timeseries plots, not shown), it has been concluded that the NWECS significant wave height data follow very well the high

[16] https://erddap.marine.ie/erddap/index.html

significant wave height percentiles (peaks in observations), and therefore require no correction.

From the consideration of the mean wave direction comparison, we have concluded that the SWAN mean wave directions already properly reflect the corresponding values in the considered calibration area (including SROWF, cf. Figure 2.22): i.e. there is no need for a correction of the SWAN wave directions.

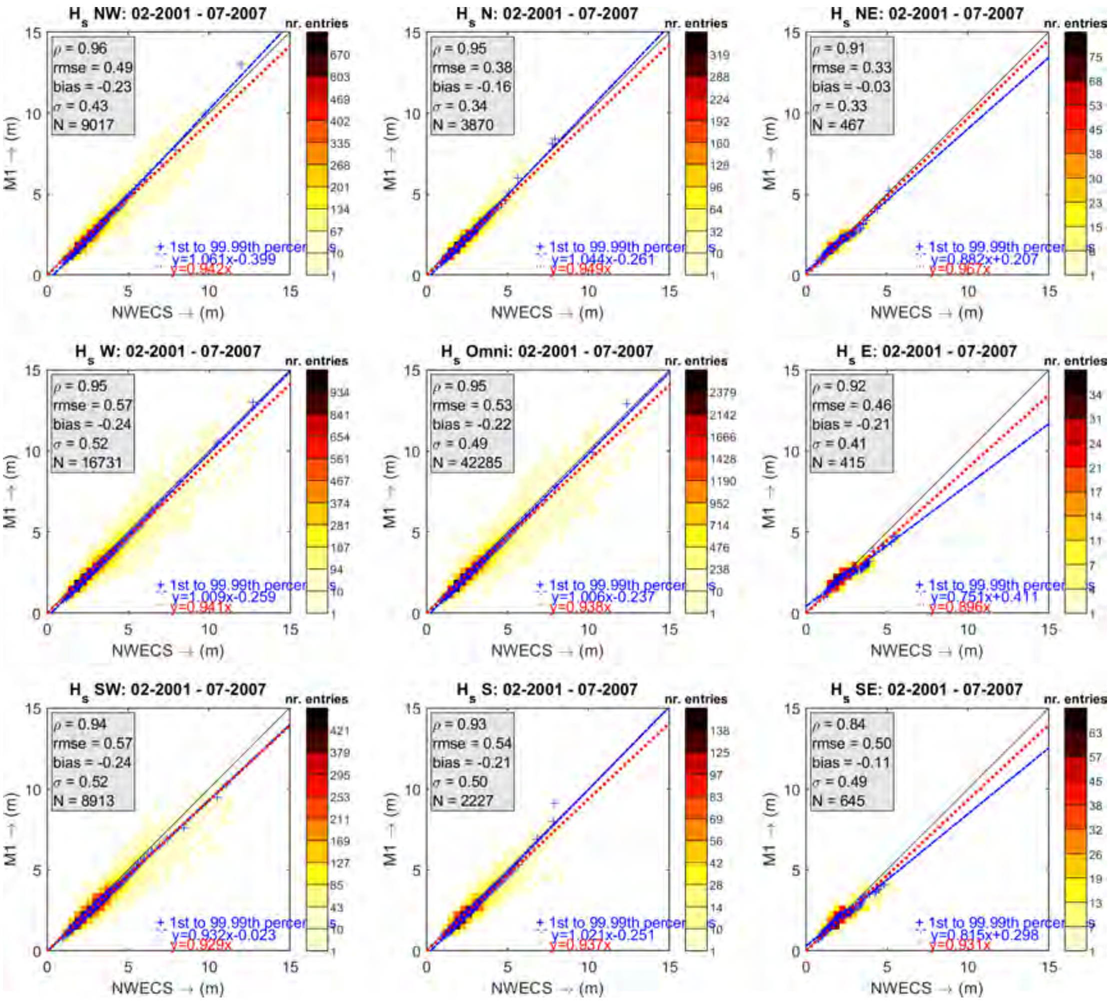

Figure 2.27 Significant wave height density scatter comparisons between the M1 observations and the uncalibrated NWECS (overall domain) timeseries at M1. The panel in the middle shows the omni-directional comparisons and the panels surrounding it show the comparisons for the corresponding directional sectors (from top left, clockwise: NW, N, NE, E, SE, S, SW and W). The symmetric fit to the data is given by the red dotted line and the linear fit through the data percentiles (blue pluses) is given by the dashed blue line. The statistics of the comparisons are printed in the panels.

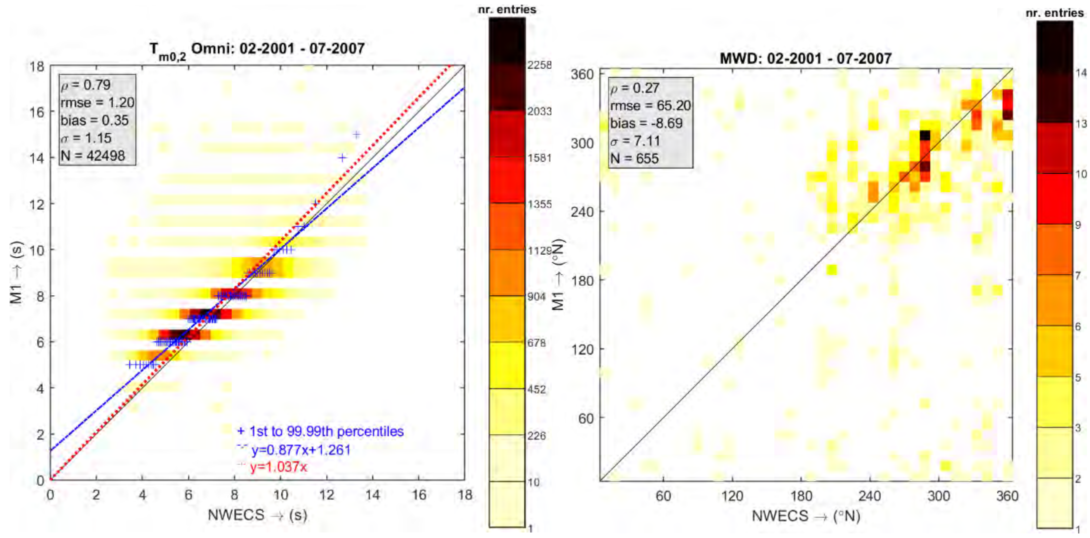

Figure 2.28 (Omni-directional) mean wave period $T_{m0,2}$ (left) and mean wave direction (right) density scatter comparisons between the M1 buoy observations and the NWECS data.

In conclusion of the NWECS data validation, adding to the fact that SWAN fully accounts for the effects of the complex bathymetry of the SROWF area, the wave conditions modelled using SWAN are considered to be very reliable, with very high correlations with the observations and considered to form a solid basis for the determination of the wave conditions in the SROWF area. The data produced across the MPPSA from the two (2) domains are deemed to require no further calibrations.

Last, although the quality of the offshore data is high, it is advised to perform an additional dedicated validation of the local modelled wave data as soon as local wave observation data become available. This is needed to ensure that local bathymetrical features and their effect on the wave propagation are indeed captured correctly.

2.3.7 Modelling of wind farm effects

2.3.7.1 Simulated situations

The same approach is followed for the quantification of the wind farm effects on wave fields as for the effects on flow fields described in Section 2.2.6.1 i.e., a comparison is made between the wave fields in two situations i.e., the baseline situation without any WTG present and the operational situation with WTG in place. The former situation is simply reproduced by running the validated wave model described in the previous sections over the periods reflecting representative conditions of normal and extreme sea states (see Section 2.3.3.1). For the operational scenario, the presence of the WTG and of the OSS platform is additionally accounted for by using the baseline model as a starting point and further implementing (also summarized in Table 2.4):

- a local water depth decrease at all WTG locations, as a result of the presence of a large (55m diameter) GBS foundation base on the seabed sitting on a rock layer;
- a wind speed reduction over the entire OWF area, due to wind extraction from the WTG operation.

Both aspects are deemed to have a potential influence on the significant wave heights, peak wave periods and mean wave directions around SROWF. To quantify operational influences, only the dedicated SROWF detailed wave domain was employed, which it will be shown that it fully encloses the area where OWF impacts are taking place. This means that the above mentioned schematizations were not relevant for the overall NWECS-SWAN model. The latter covers the greater MPPSA and was run only in hindcast mode (baseline situations) to force the open boundaries of the detailed model (in both baseline and operational situations) and to generate timeseries at output locations positioned far from the OWF polygon (e.g., along the OECC).

It is noted that contrary to the parameterization of the central column of the WTG foundation (with a diameter of 13 m, see Figure 1.4) by means of a drag force in the hydrodynamic model (see Section 2.2.6.3), there is no influence from this part of the foundation accounted for in the wave model OWF parameterization. Given the large difference between the length scales of the considered pile diameter (13 m) and the expected wave lengths (in the order of 100 m), a very limited (if any) effect to waves propagating past the turbine locations is expected. The waves will in fact propagate past those obstacles almost uninfluenced. In any case, it would not have been possible to capture such effects (if present and relevant for the environmental impacts of the OWF) by means of a phase averaged spectral wave model (such as SWAN). For such a study a phase resolving wave modelling approach would be required.

Table 2.8 Matrix of simulated situations for the quantification of OWF effects.

Situation	Schematization	Simulations
Baseline	Pre-construction bathymetry (see Section 2.2.2) Raw ERA5 wind fields (see Section 2.1)	twelve (12) 4-day <u>hindcast</u> simulations, each one representative of: - a normal (50th percentile, 90th percentile) or extreme condition (RP -1,-5,-10,-50 year) - over two (2) approach directions (W, WSW) denoted as: 1. Baseline W-N50th 2. Baseline W-N90th 3. Baseline W-RP1 4. Baseline W-RP5 5. Baseline W-RP10 6. Baseline W-RP50 7. Baseline WSW-N50th 8. Baseline WSW-N90th 9. Baseline WSW-RP1 10. Baseline WSW-RP5 11. Baseline WSW-RP10 12. Baseline WSW-RP50
Operational	Local increase of seabed levels applied on pre-construction bathymetry, based on the GBS foundation base and rock layer geometry. Reduced raw ERA5 wind speeds by 10% within the OWF polygon. (see Section 2.1)	twelve (12) 4-day simulations, each one representative of: - a normal (50th percentile, 90th percentile) or extreme condition (RP -1,-5,-10,-50 year) - over two (2) approach directions (W, WSW) denoted as: 1. Operational W-N50th 2. Operational W-N90th 3. Operational W-RP1 4. Operational W-RP5 5. Operational W-RP10 6. Operational W-RP50 7. Operational WSW-N50th 8. Operational WSW-N90th 9. Operational WSW-RP1 10. Operational WSW-RP5 11. Operational WSW-RP10 12. Operational WSW-RP50

Similar to the hydrodynamic model approach, the OSS was treated as an additional WTG also for the wave modelling, meaning that a WTG founded on a GBS was considered at that location. In the remainder of this section, the implementation of the abovementioned schematizations is described in larger detail.

2.3.7.2 Bathymetry treatment

The conical GBS foundation base supporting the WTGs (see Figure 1.4) together with the underlying rock layer, will lead to a local decrease of depth (reaching up to 33.5 m at the centre of the foundation) occurring within a diameter of roughly 70 m at the ambient seabed level. Wave propagation will be influenced from the seabed around such a significant obstruction even at the deepest WTG locations in SROWF. Locally, wave refraction, and possibly shoaling and wave breaking may occur as waves propagate past such an obstruction. For coastal waves, these effects will increase with an increasing seabed level (i.e., decreasing water depth), assuming the same ambient wave conditions.

To account for these effects, the GBS foundation base is schematized into the wave model bathymetry. This is done similarly as in the hydrodynamic model (see Section 2.2.6.2). The area of obstruction is determined by the sum of the GBS foundation base and the underlying rock layer (with a diameter of roughly 70 m). The GBS obstruction is added to the average baseline seabed level over that area. Considering the resolution of the grid at these locations (roughly 25 m), a seabed level change is applied to roughly 7 grid points, which obviously is not adequate to describe fully the geometry of the obstruction (as presented in Figure 1.4, right), but is nevertheless deemed sufficient for the purposes of the present assessment.

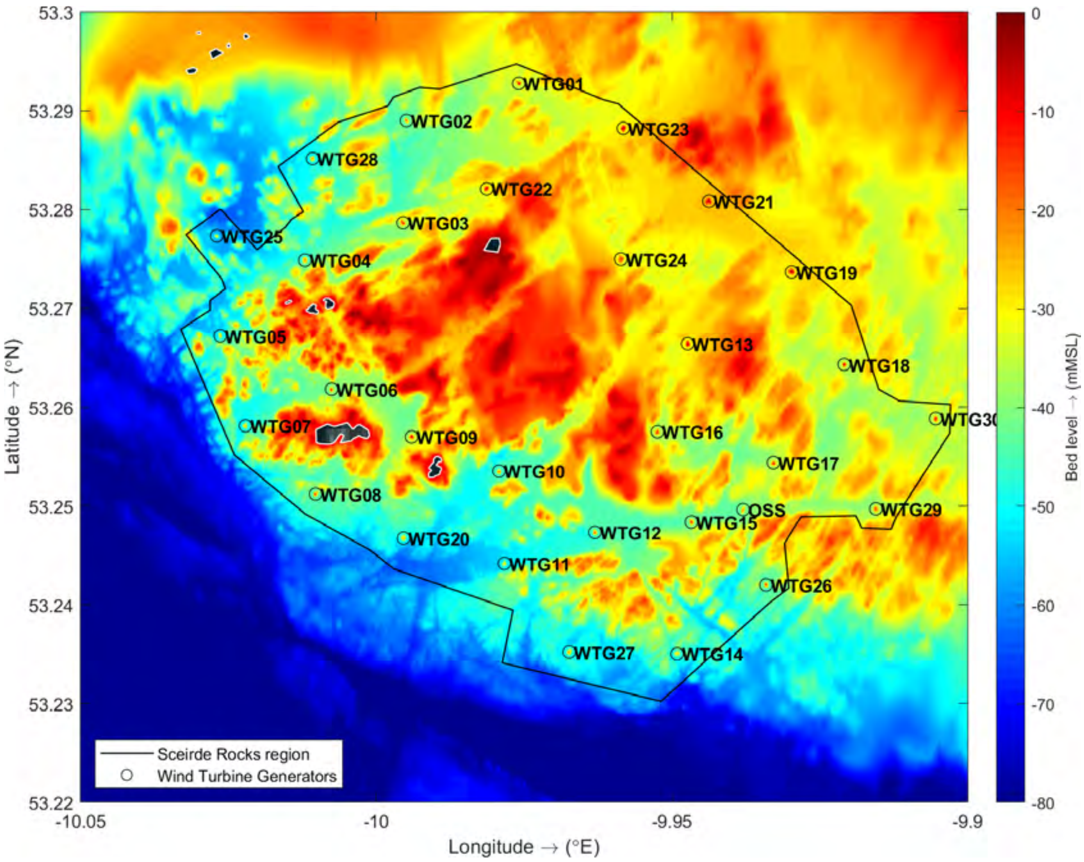

Figure 2.29 Bathymetry of the wave model for the operational situation. The obstruction area is denoted by the black circle polygon plotted around each of the 31 obstruction locations.

A simulation was run where only this local bathymetry change was implemented to the baseline model, to understand the effect of this schematization alone unobscured from the cumulative effect of all other influences (i.e., wind reduction) modelled in this study. Figure 2.30 to Figure 2.32 below show this effect during WSW-RP50 condition.

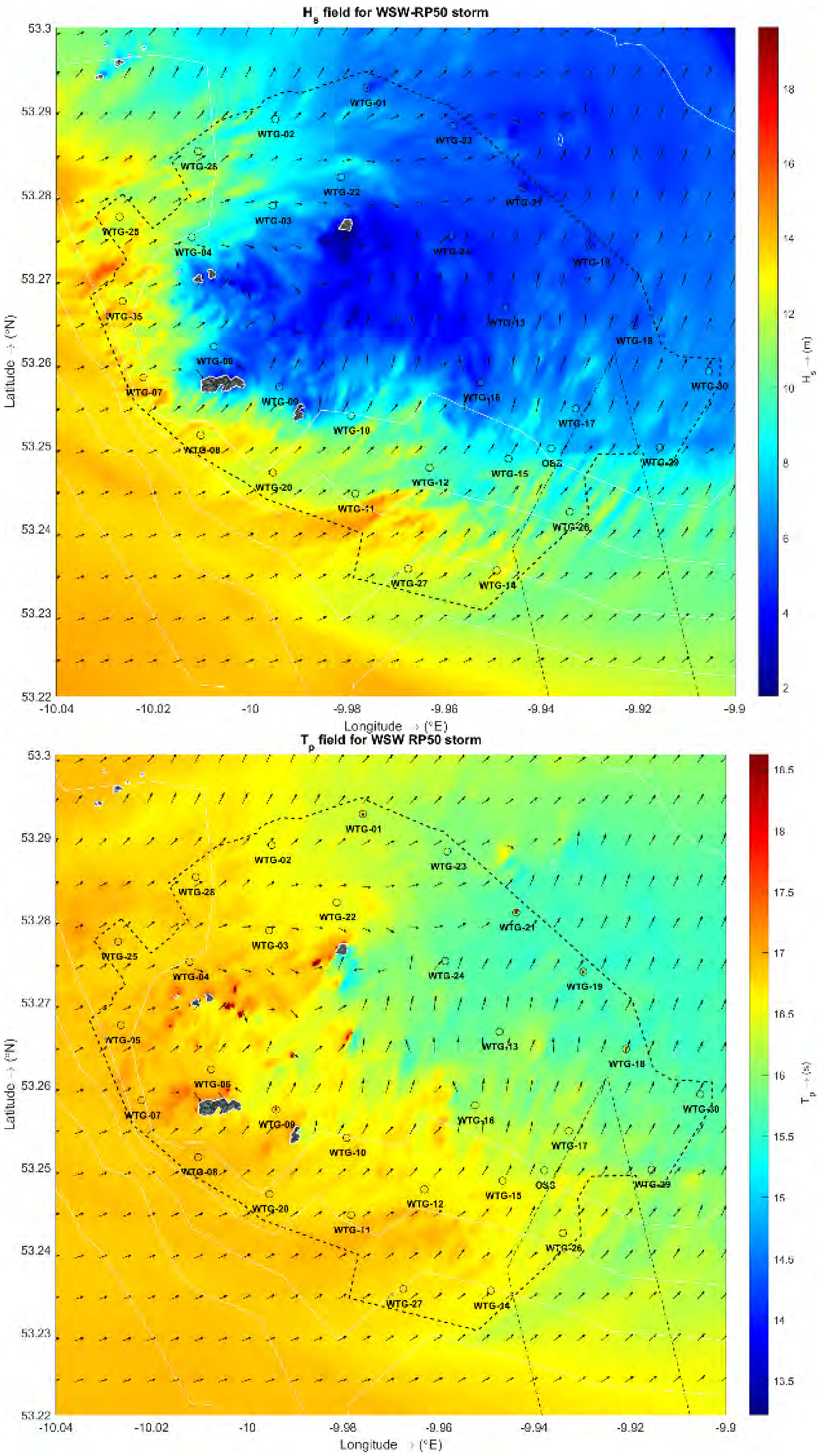

Figure 2.30 Wave field (top: significant wave height H_s, bottom: peak wave period and mean wave direction MWD) in WSW-RP50 conditions with an operational schematization where only a bathymetric change is applied to the detailed wave model.

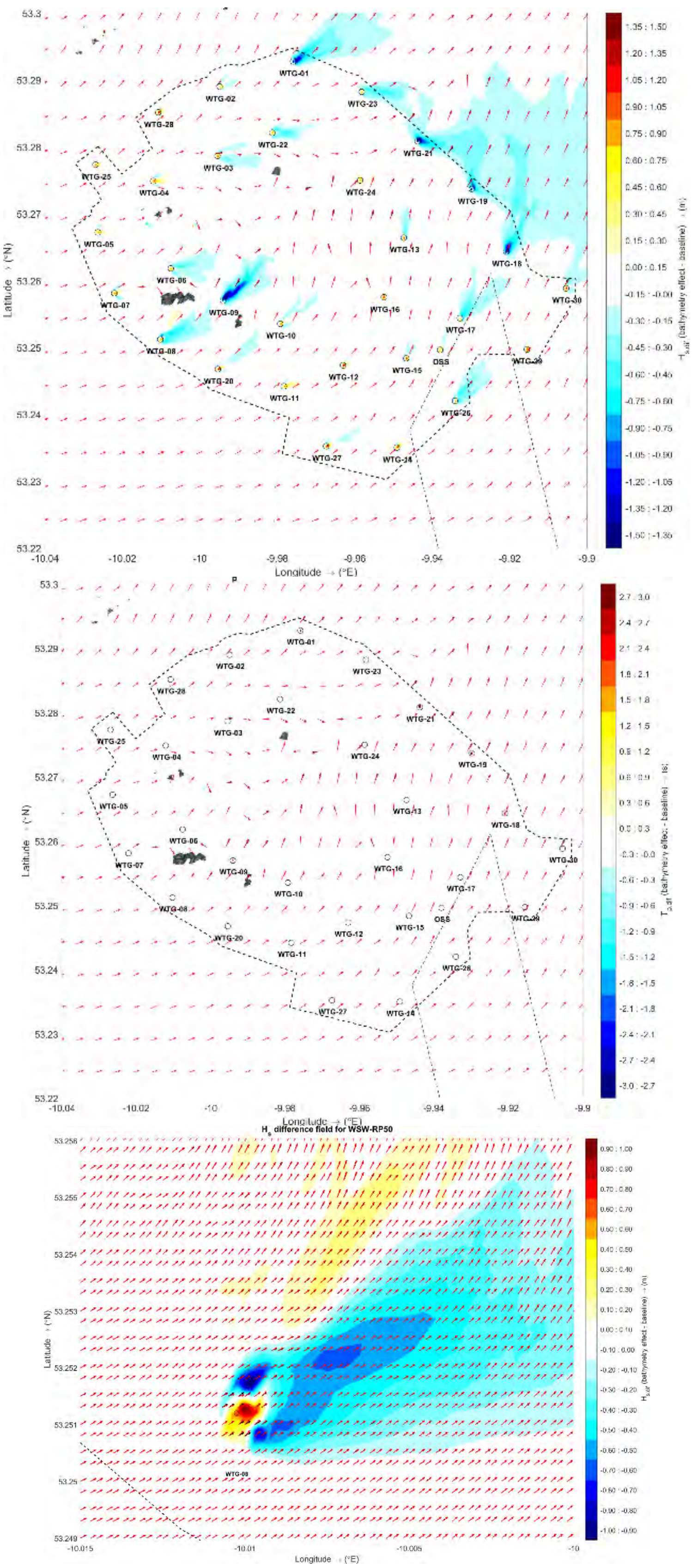

Figure 2.31 Wave field difference of an operational schematization where only a bathymetric change is applied relative to baseline situation (top and middle: H_s and T_p difference field around SROWF; bottom H_s difference field around the offshore WTG-08 location) in WSW-RP50. MWD directions of baseline and operational situation are plotted on top with black and overlaying red colours respectively.

Around all obstruction locations, the increased seabed level leads to a very local (comparable to the dimensions of the seabed obstruction) increase of wave energy followed by a wide-spread (evolving over a distance of multiple times the dimensions seabed obstruction) decrease of wave energy. These changes are expressed predominantly through changes in H_s, while peak wave periods remain for the most part unaffected, except for the direct vicinity of the foundations (at the shallower locations to the east), where a local effect is observed.

It is notable that wave energy is decreased over a relatively large area directly downwave and beyond the OWF boundary to the east (towards the coast). This is partly caused by a change in wave directions, as waves propagate past a field of obstructions. Around the foundations, MWD arrows indicate a local change of directions in operational situations, especially where waves are approaching the foundations (see Figure 2.31, bottom panel). Mean wave directions are nevertheless influenced also farther from the foundations in a downwave direction, especially around the locations to the east of the SROWF, closer to the coast (see Figure 2.32). It follows that next to wave energy lost due to dissipation, this northeast area of H_s decrease is also due to a rearrangement of wave energy in other directions, i.e., more wave energy propagates further to the north or south from that area where wave energy is seen to decrease.

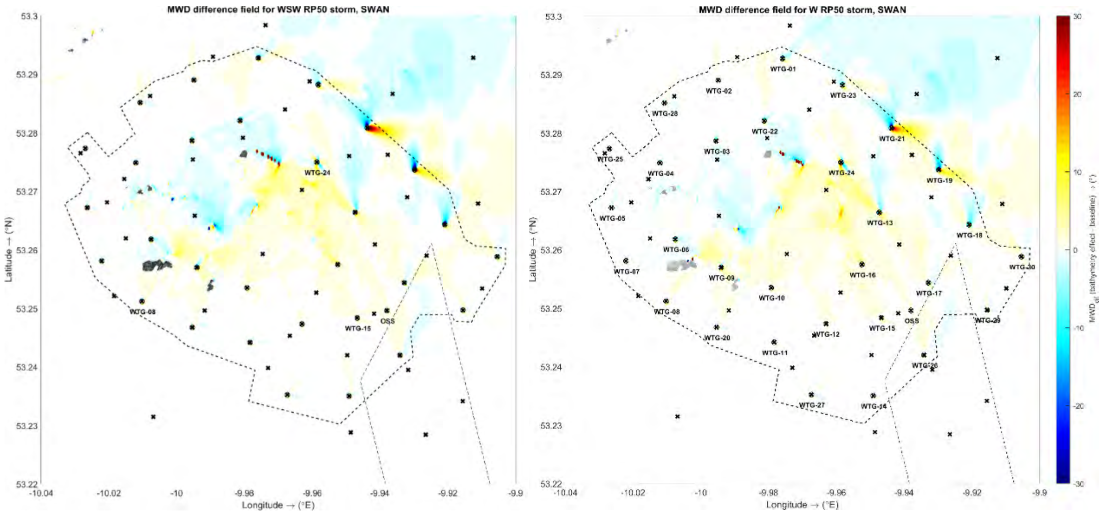

Figure 2.32 Difference field of MWD around SROWF between the operational schematization where only a bathymetric change is applied locally at the WTG and OSS locations relative to baseline situation. The MWD difference pattern is almost identical for WSW RP50 (left panel) and W RP50 (right panel).

The observed changes are according to expectations and due to a combination of depth-induced influences from physical phenomena that become relevant in the propagation of coastal waves through a field characterized by a complex topography and (local) seabed level features. These influences caused by refraction (change in propagation direction), shoaling (focusing of wave energy) and depth-induced breaking and bottom dissipation (dissipation of wave energy) are modelled well with SWAN, and evolve both due to large-scale bathymetric changes over the complex SROWF area as well as due to local bathymetric changes around the foundations. The observed (differences in) wave fields of the operational situation are a result of those cumulated effects. Based on these results, it is deemed that the presence of the large GBS foundation base and associated rock layer is well captured by the schematization implemented in the wave model via the local bathymetric change.

2.3.7.3 Wind reduction

To capture the wind extraction from the atmospheric layer due to the operating turbines, the wind speeds at 10 m used to force the wave model are reduced over the entire simulation period by 10%, with the directions remaining the same. As explained in Section 2.1.3, the raw ERA5 wind fields need to be downscaled to a much finer resolution compared to what is originally available (0.1 degrees), before it is possible to reduce the wind speeds adequately within the OWF polygon. This downscaling (by means of interpolation to a higher resolution forcing field) and subsequent reduction of wind speeds, as applied for the purposes of the wave modelling is presented in Figure 2.33. It is noted that SWAN performs a final interpolation on the actual computational grid of the modelling domain, in forcing the wave model with wind.

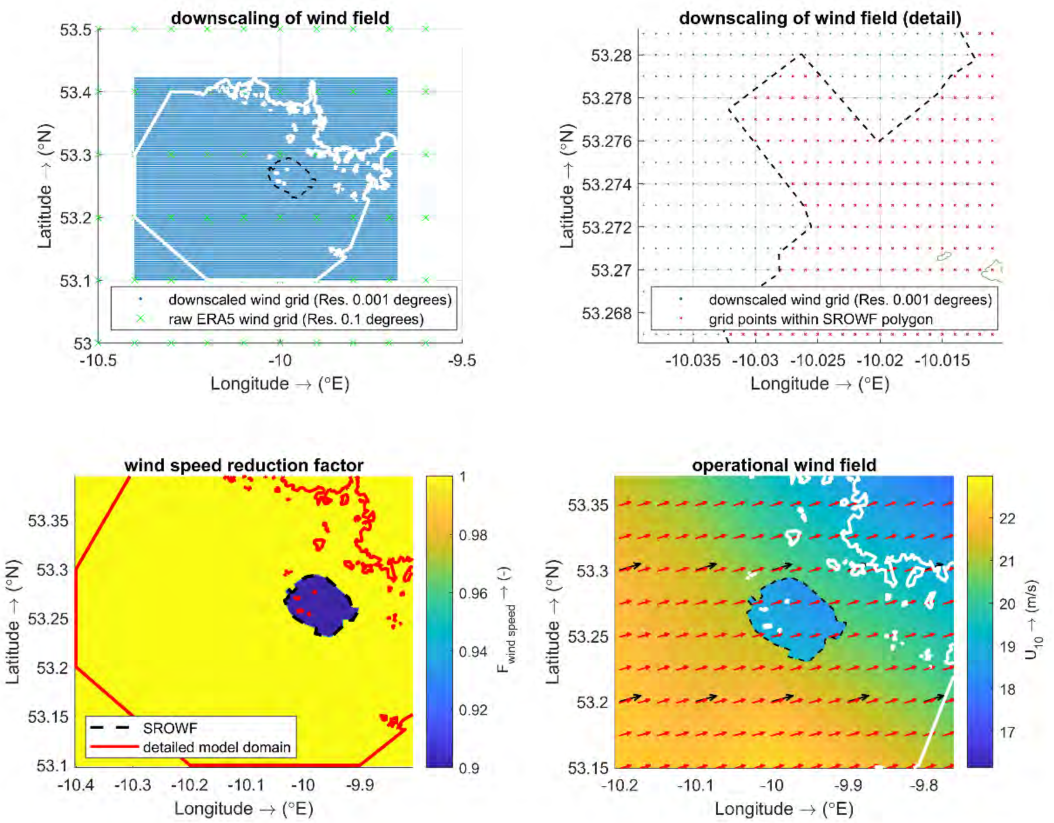

Figure 2.33 Downscaled resolution of wind field (top panels), subsequently applied wind magnitude factor (bottom left) and finally wind forcing field applied over the dedicated SROWF model domain at an example timestep of the simulation.

During extreme storm conditions wind farms are expected to stop their operation to ensure the technical safety of the turbine components (rotors). Typically reported cut-out wind speed (at hub height) is around 25 m/s (e.g., Jelavic et al. (2013), Markou et al. (2009)), which is exceeded even in RP1 storm conditions at SROWF, for which the $U_{10,1hr}$ and $U_{170,1hr}$ are assessed at 23.3 and 29.7 m/s respectively (at the offshore reference location WTG15) in Deltares (2022). Nevertheless, the actual cut-out speed varies per turbine design and could increase for newer and larger turbines, potentially employed in SROWF. Since information concerning the cut-out wind speed at SROWF is unavailable at the time of this study, it was selected to consider an operating wind farm during all considered sea states (normal and extreme), as this would theoretically lead to the larger (and hence most conservative) effects on wave fields in the area.

It is noted that both influences on the wave field from the operational condition are aligned and hence amplify each other when cumulated, given that a wind speed reduction (same as for the local bathymetry change as shown in Figure 2.31) is expected to lead to a decrease in wave energy over the SROWF area. This is confirmed in Figure 2.34, showing only the isolated effect of wind speed reduction over the wave field around SROWF in extreme conditions.

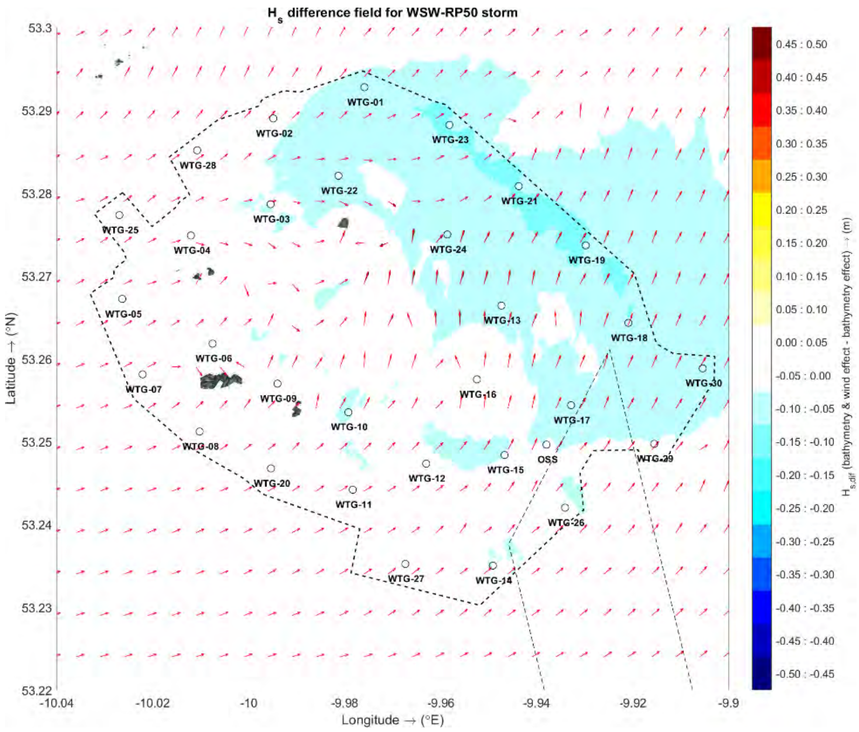

Figure 2.34 The isolated additional effect of wind energy reduction on the wave field around SROWF area.

2.3.8 The SROWF wave dataset

Having validated the SWAN wave models and concluded that wave modelling data forms a solid basis for the determination of the wave conditions at SROWF, timeseries are generated at a number of output locations (see Figure 2.1) for baseline and operational situations. It is noted that the timeseries for the output locations falling outside the SROWF dedicated wave model are identical between the two situations, since these originate from the overall NWECS model that was run only in hindcast mode (representative of the baseline situation). Nevertheless, all parameterized effects of the operational situation on the wave fields are well contained within the dedicated SROWF domain as will be shown later. The timeseries are hourly and cover the respective simulation periods of each considered sea state, with a total duration of 4 days around the occurrence of the reference condition (the significant wave height peak for storms and the reference significant wave height for normal conditions). Next to the timeseries, wave fields and (absolute and relative) difference plots between the operational and baseline situations are produced for each reference conditions for the significant wave height and peak wave period parameters. In these field plots, the mean wave direction is denoted with directional arrows.

3 Modelling results

3.1 Introduction

Flow and wave fields and timeseries are derived based on hydrodynamic and wave modelling where the baseline and operational situations are schematized in different sets of simulations. In the sections below, the respective fields are presented per metocean parameter. Water level and current results are presented in Section 3.2 and wave results are presented in Section 3.3. In each section, the results are first presented for the baseline situations.

3.2 Water levels and currents

3.2.1 Introduction

In this section the flow fields of the depth-averaged total current velocities and directions are presented at the area of interest and discussed for the baseline and operational situations (Sections 3.2.2 and 3.2.3). For both situations, the fields are presented at various tidal states through the simulation period of 1 month in January 2013 as well as over two (complete) Spring Neap cycles over the same simulation period. For operational situations (in all of which a wind speed reduction of 10% is implemented) in specific, the fields are presented in the form of absolute difference plots (of depth-averaged flow magnitude, water levels and directions) relative to the baseline situations. Corresponding relative difference plots are included in the Appendix[17]. Flow field plots are generated and presented over a number of selected tidal states (based on the reference offshore location WTG-08 in layout SRL069). The selection of those along with the respective timestamps are presented in larger detail in Table 3.1 and Figure 3.1.

Table 3.1 Selected instances and periods over which flow fields are presented.

Acronym	Definition	Timestamp / Duration[18]
FS	Peak flood during spring cycle (high flow magnitude during rising water levels)	`13-Jan-2013 13:30`
FN	Peak flood during neap cycle (high flow magnitude during rising water levels)	`06-Jan-2013 07:30`
ES	Peak ebb during spring cycle (high flow magnitude during falling water levels)	`13-Jan-2013 07:00`
EN	Peak ebb during neap cycle (high flow magnitude during falling water levels)	`06-Jan-2013 02:00`
HWS	High Water during Spring cycle	`13-Jan-2013 06:00`
LWS	Low Water during Spring cycle	`13-Jan-2013 12:00`
HWN	High Water during Neap cycle	`05-Jan-2013 23:00`
LWN	Low Water during Neap cycle	`06-Jan-2013 05:30`
Res	Residual flow over two (2) Spring Neap tidal cycles within January 2013	`02-Jan-2013 10:50 till 01-Feb-2013 00:00`

[17] To avoid misinterpretation of the results given the small baseline flow magnitudes, relative differences (given in percentages) are only presented where baseline flow magnitudes exceed a value of 0.1 m/s.
[18] Map output was generated on a 30-minute interval.

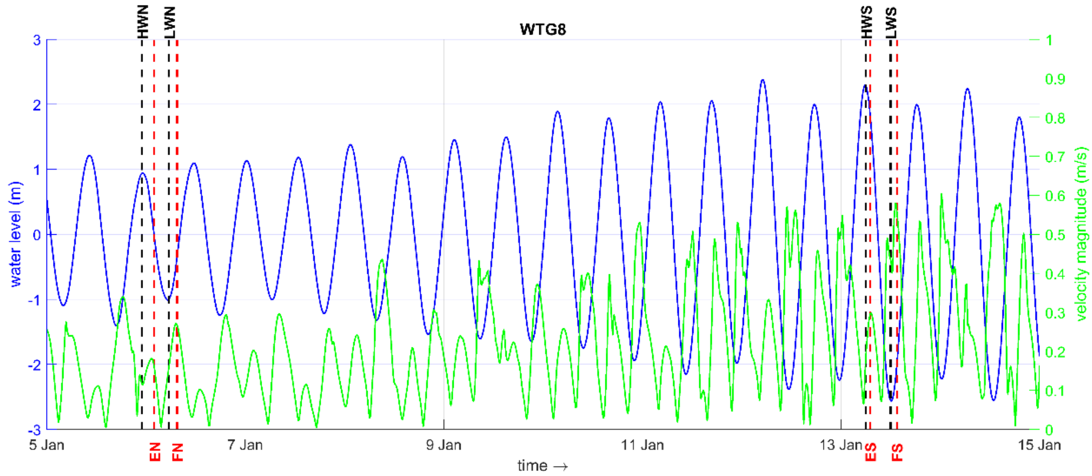

Figure 3.1 Timing of various instances selected for generating flow fields, plotted along with the water level and velocity magnitude at a reference offshore location WTG8.

3.2.2 Baseline

3.2.2.1 Instantaneous flow fields

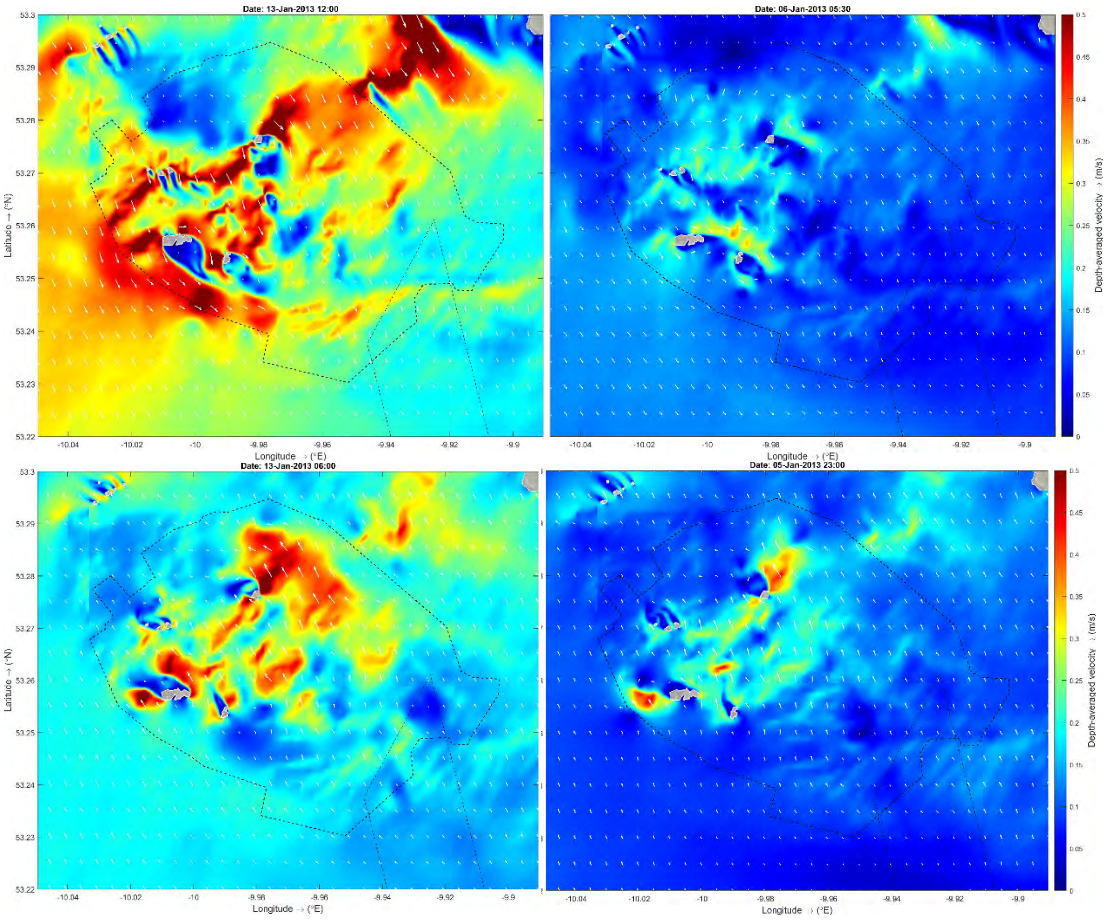

Figure 3.2 Field of depth-averaged flow magnitudes and directions (arrows going to) across the SROWF during LWS and LWN (left and right top panels respectively) and HWS and HWN (left and right bottom panels respectively), see also Table 3.1.

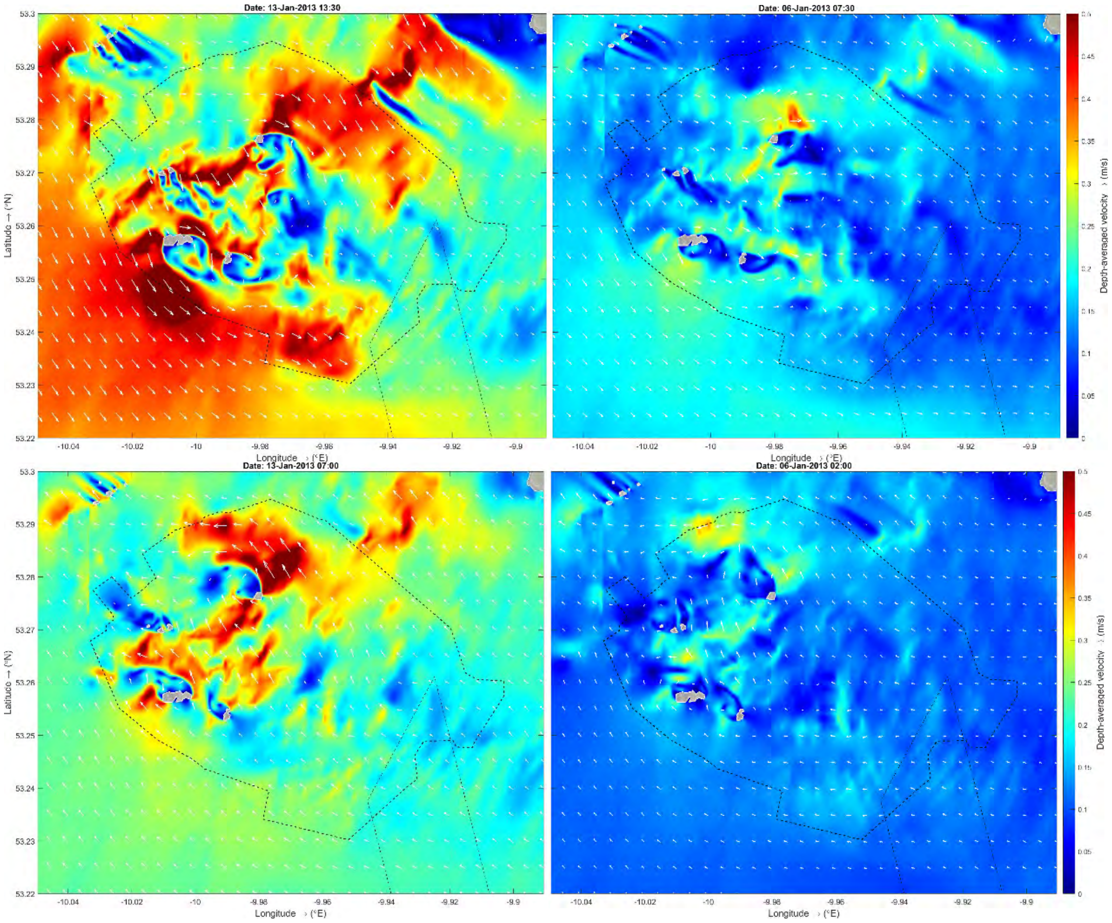

Figure 3.3 Field of depth-averaged flow magnitudes and directions (arrows going to) across the SROWF during FS and FN (left and right top panels respectively) and ES and EN (left and right bottom panels respectively), see also Table 3.1.

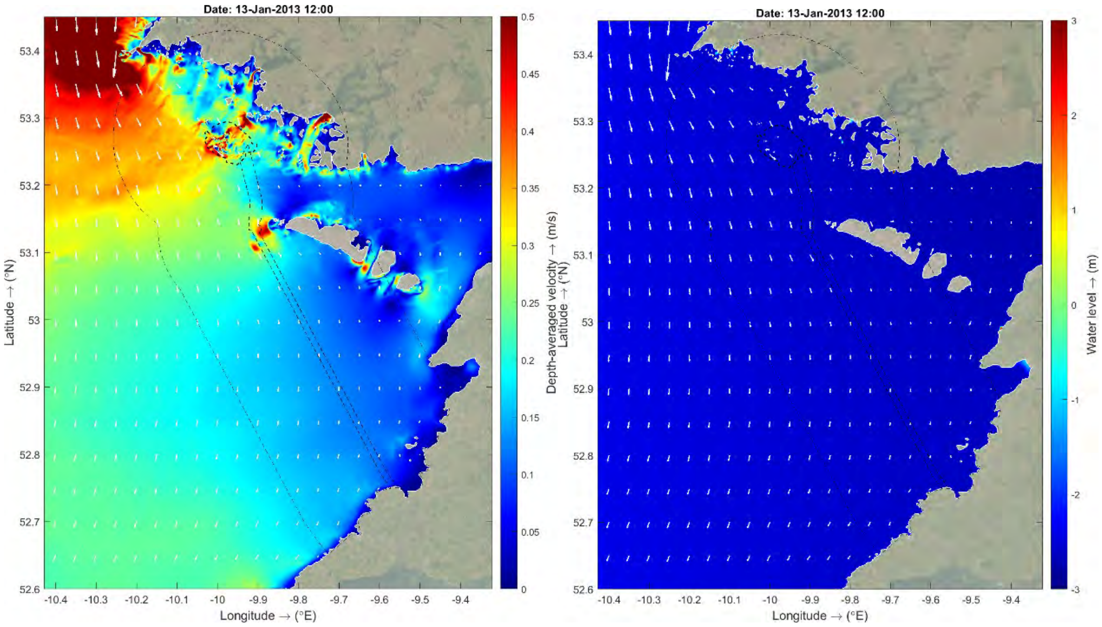

Figure 3.4 Field of depth-averaged flow magnitudes (left panel) and associated water levels (right panel) plotted next to directions (arrows going to) across the MPPSA during LWS, see also Table 3.1.

3.2.2.2 Residual flow fields

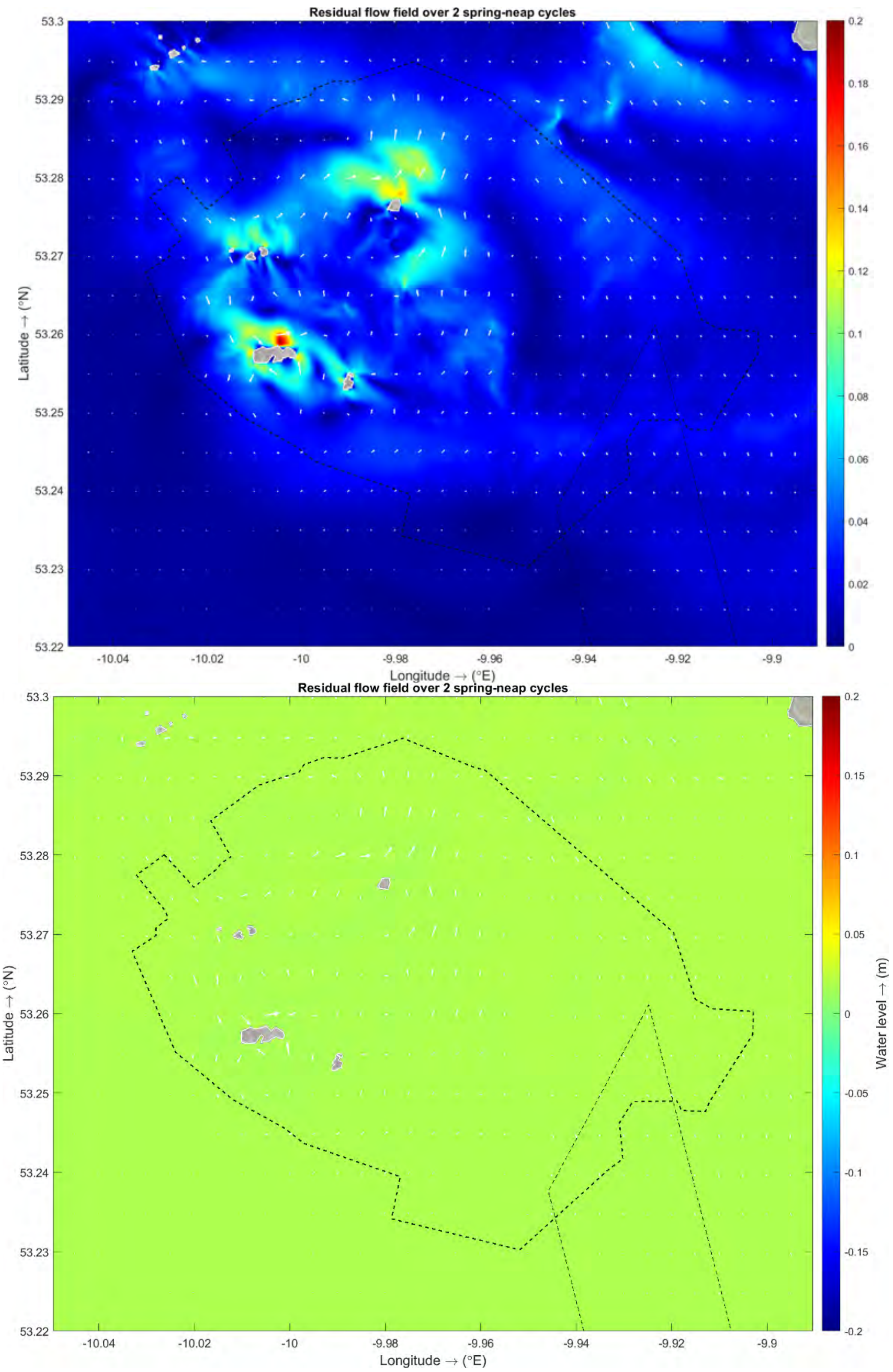

Figure 3.5 Field of residual flow magnitudes (top panel) and associated residual water levels (bottom panel) plotted along with residual directions (arrows going to) across the SROWF over 2 spring neap cycles in January 2013, see also Table 3.1.

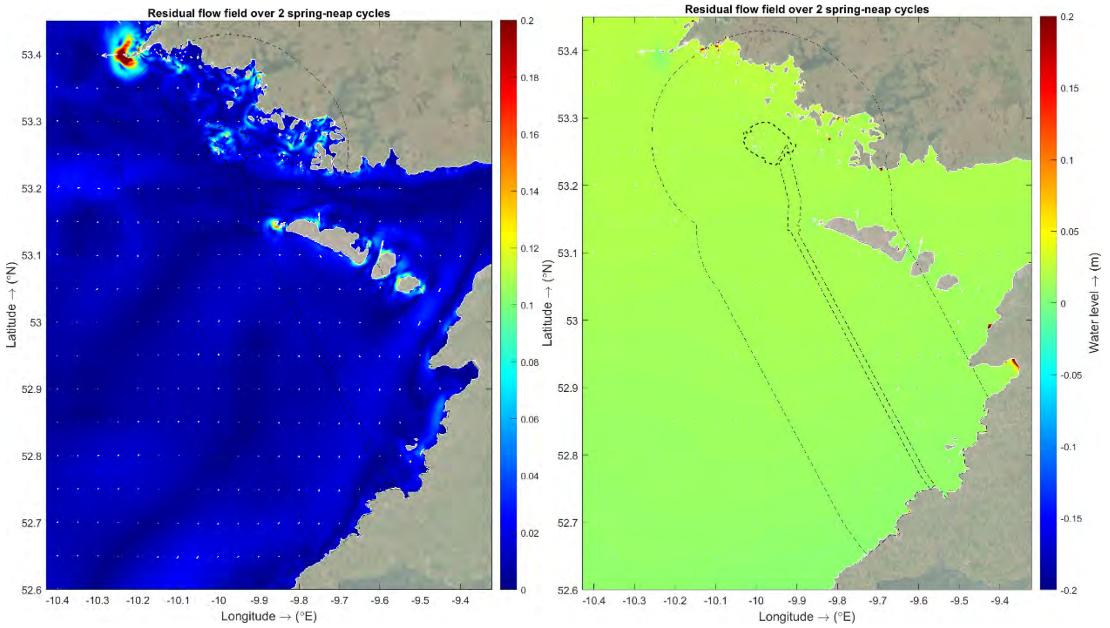

Figure 3.6 Field of residual flow magnitudes (left panel) and associated residual water levels (right panel) plotted along with residual directions (arrows going to) across the entire MPPSA over 2 spring neap cycles in January 2013, see also Table 3.1.

3.2.2.3 Observations

The following observations are made with respect to the various instantaneous and residual flow fields presented in Figure 3.2 to Figure 3.6 in the previous sections:

- The baseline flow patterns within the SROWF area are largely dictated for all considered conditions (spring and neap) and tidal phases (flood and ebb) by the local complex topography, which involves several islands and rocks.
- The observed flow pattern in the vicinity of those islands is characterized by: a) *flow acceleration* at the sides of the several islands relative to the incoming flow, that is initiated somewhat upstream but persists over a distance of a few times the obstruction horizontal dimension in a downstream direction combined with b) *horizontal vortex shedding* in a downstream direction. The wakes associated with the latter are expressed as a decrease in flow magnitudes and alternating flow directions in a downstream direction, and also extend over a distance of a few times the obstruction dimension.
- The area with the lowest flow magnitudes is observed to the south (east) of the SROWF area, where the local bathymetry (see also right panel in Figure 2.8) is relatively less complex compared to north (west) and central areas of the SROWF, that are characterized by the presence of islands and steep slopes in bed topography.
- As expected, the largest flow magnitudes over SROWF occur during Spring tide conditions, namely during FS and LWS.
- Residual flows over the two (2) spring neap cycles in January 2013 remain well below 0.1 m/s in magnitude (and 1 cm in water level) over the greater part of the SROWF area as well as for the vast majority of the greater MPPSA, and only exceed those values near steep seabed transitions, evolving for example in the vicinity of islands.
- Water levels are nearly uniform across not only the SROWF but also across the greater MPPSA.
- An area to the north and just outside of the MPPSA shows relatively high magnitudes due to the headland and presence of the islands, leading to local flow accelerations.

Within the marine area covering the OWF and immediately surrounding it, as illustrated in e.g. Figure 3.2 and bounded by coordinates -10.04 and -9.9 degrees longitude and 53.22 and 53.3 degrees latitude, the calculated, the maximum baseline local current speeds simulated are presented in Table 3.2

Table 3.2 Maximum calculated local current speeds within extended OWF area in baseline conditions.

Tidal state / condition	Maximum local current speed (m/s)
LWS	0.80
LWN	0.37
HWS	0.64
HWN	0.45
FS	0.72
FN	0.43
ES	0.64
EN	0.36
residual	0.19

3.2.3 Operational

3.2.3.1 Instantaneous flow fields

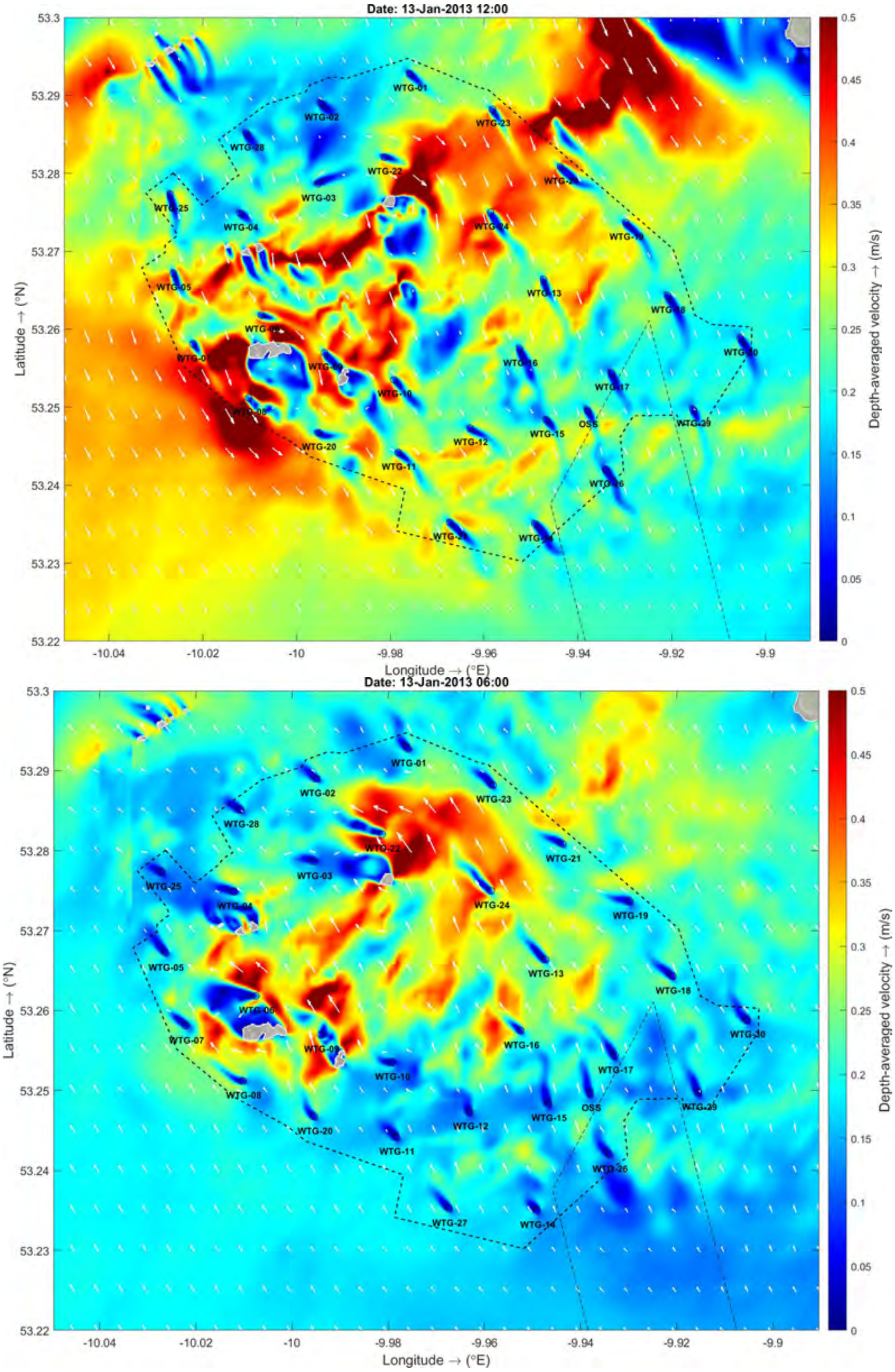

Figure 3.7 Field plot of depth-averaged flow magnitudes and directions (arrows going to) across the SROWF during LWS and HWS (top and bottom panels respectively), see also Table 3.1.

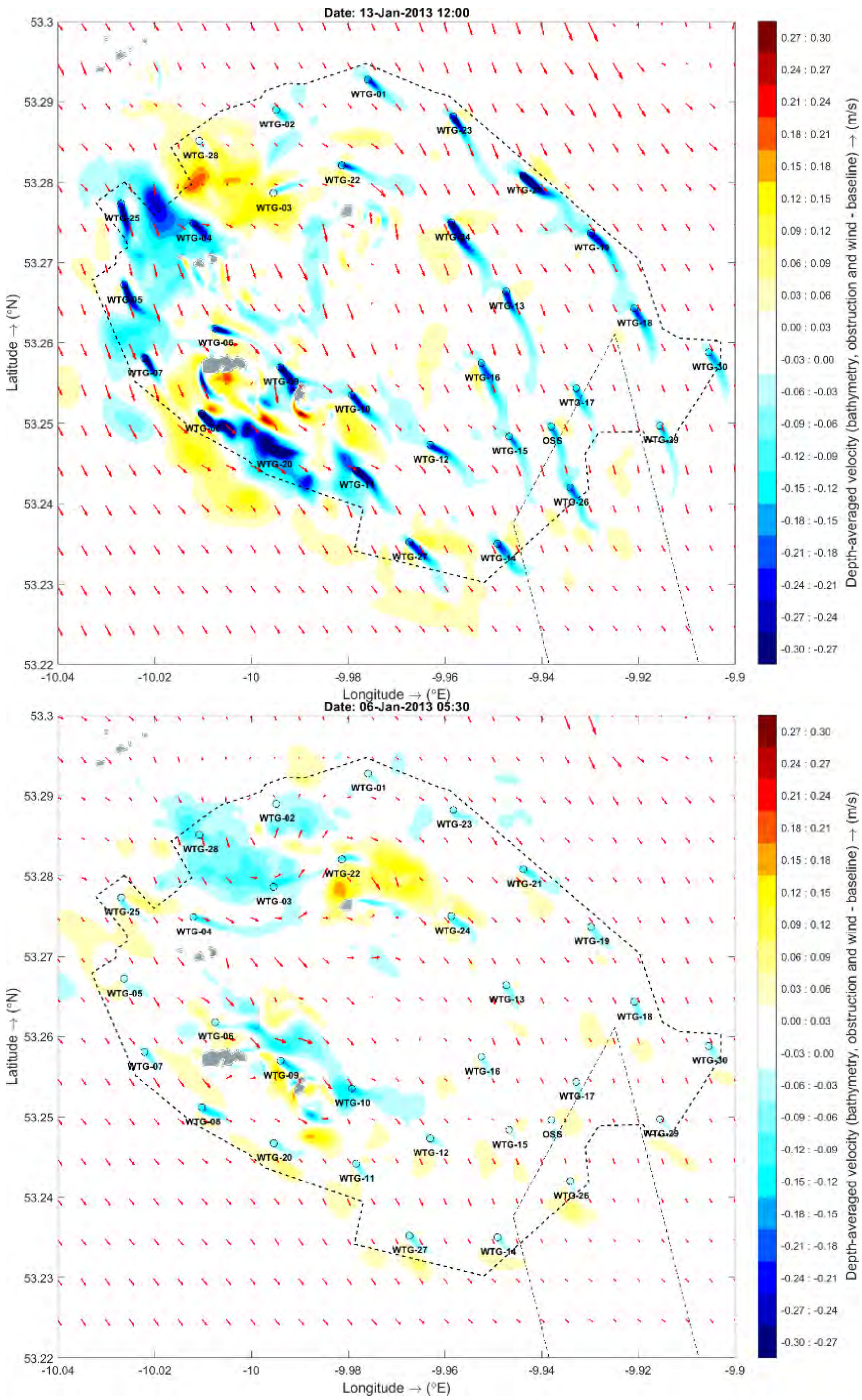

Figure 3.8 Difference field (relative to baseline) of depth-averaged flow magnitudes and directions (arrows going to) across the SROWF during LWS and LWN (top and bottom panels respectively), see also Table 3.1. Background black arrows show flow directions in baseline situations and red arrows plotted on top show directions in operational situations.

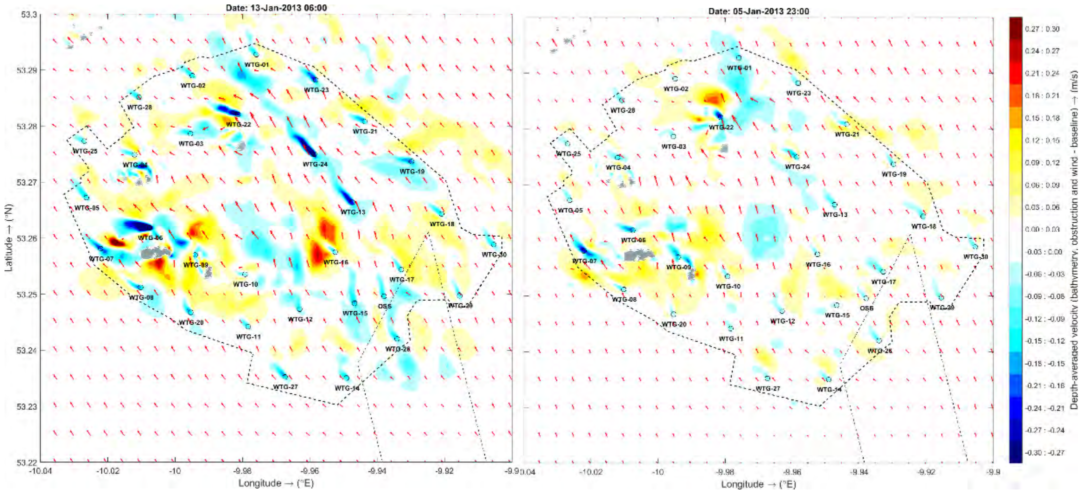

Figure 3.9 Difference field (relative to baseline) of depth-averaged flow magnitudes and directions (arrows going to) across the SROWF HWS and HWN (left and right panels respectively), see also Table 3.1. Background black arrows show flow directions in baseline situations and red arrows plotted on top show directions in operational situations.

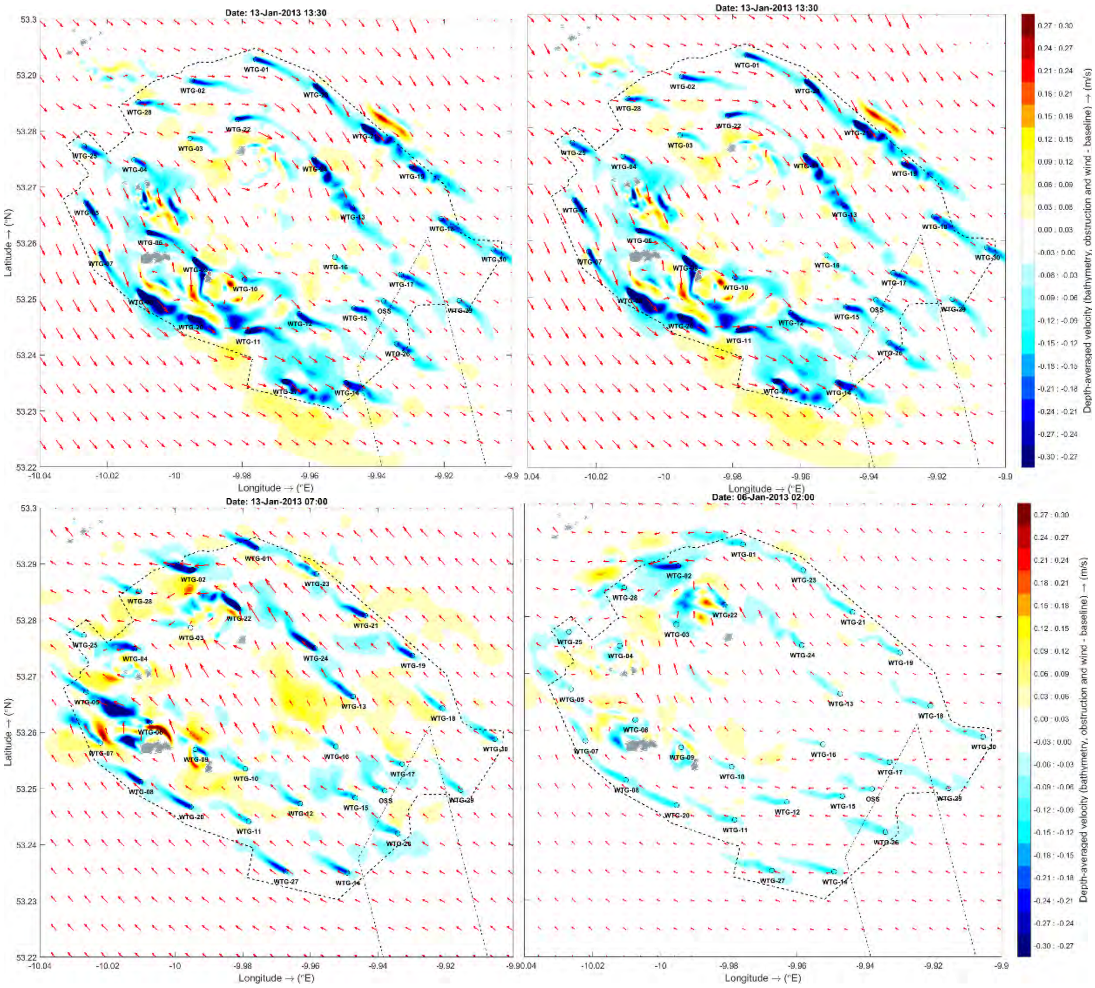

Figure 3.10 Difference field (relative to baseline) of depth-averaged flow magnitudes and directions (arrows going to) across the SROWF during FS and FN (left and right top panels respectively) and ES and EN (left and right bottom panels respectively), see also Table 3.1. Background black arrows show flow directions in baseline situations and red arrows plotted on top show directions in operational situations.

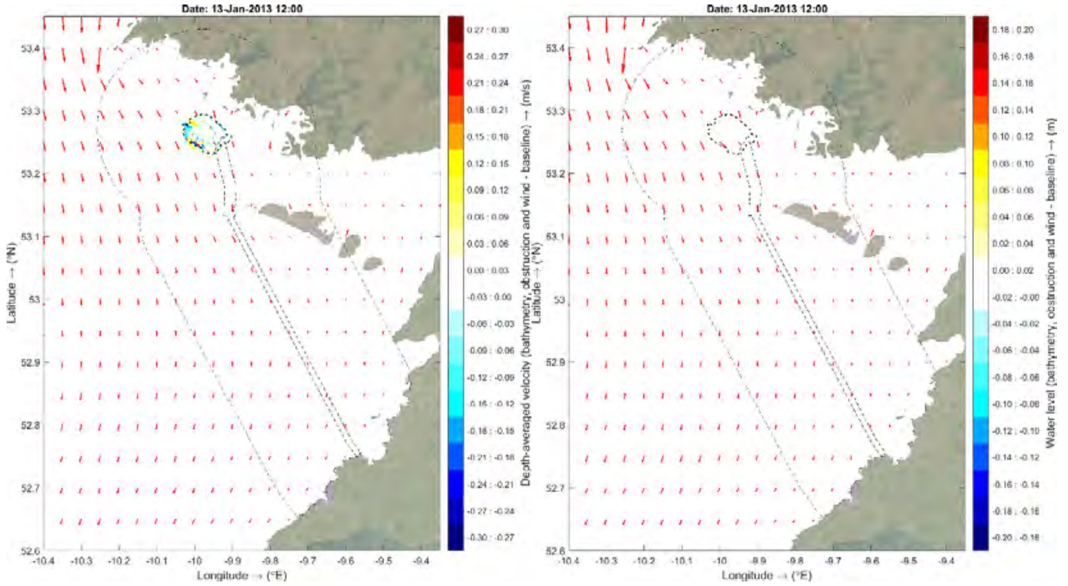

Figure 3.11 Difference field (relative to baseline) of depth-averaged flow magnitudes (left panel) and associated water levels (right panel) plotted next to directions (arrows going to) across the MPPSA during LWS, see also Table 3.1. Background black arrows show flow directions in baseline situations and red arrows plotted on top show directions in operational situations.

3.2.3.2 Residual flow fields

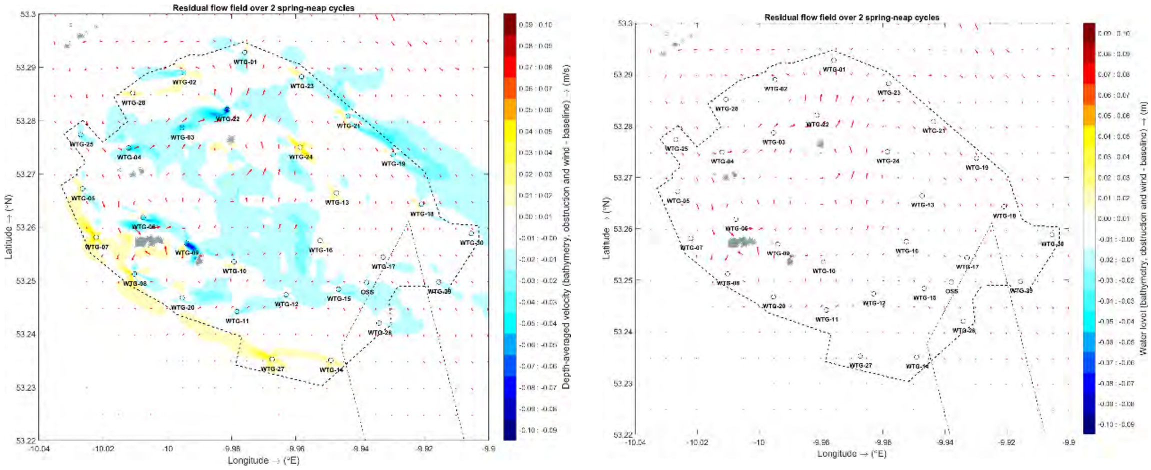

Figure 3.12 Difference field (relative to baseline) of residual flow magnitudes (top panel) and associated residual water levels (bottom panel) plotted along with residual directions (arrows going to) across the SROWF over 2 spring neap cycles in January 2013, see also Table 3.1. Background black arrows show flow directions in baseline situations and red arrows plotted on top show directions in operational situations.

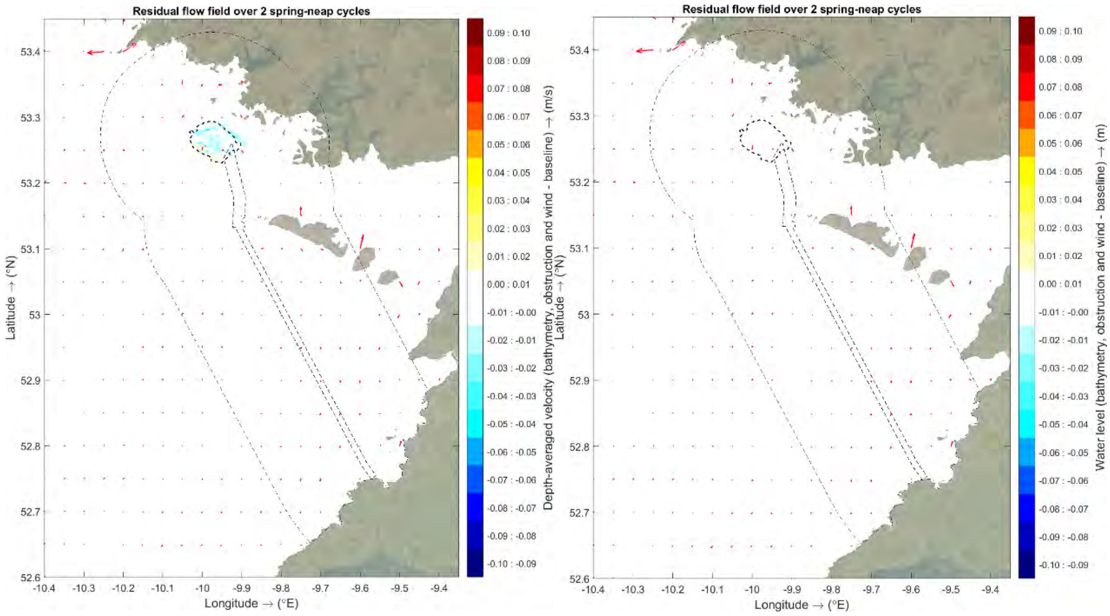

Figure 3.13 Difference field (relative to baseline) of residual flow magnitudes (left panel) and associated residual water levels (right panel) plotted along with residual directions (arrows going to) across the entire MPPSA over 2 spring neap cycles in January 2013, see also Table 3.1. Background black arrows show flow directions in baseline situations and red arrows plotted on top show directions in operational situations.

3.2.3.3 Observations

The following observations are made with respect to the various instantaneous and residual flow fields presented in Figure 3.7 to Figure 3.13 in the previous sections:

- The overall flow patterns within the SROWF remain dictated by the complex topography as in the baseline situation. The turbines affect these flow patterns predominantly by influencing the development and position of the wakes downstream from islands. This is the case especially for turbines positioned within these wakes (as observed in the baseline situation, e.g., see Figure 3.2), or even right upstream the islands interfering with approach flow conditions.
- The turbines also introduce a significant drag force in the flow, leading to clearly noticeable wakes, developing in a downstream direction. This is observed around all WTG locations, but is slightly more pronounced around the turbines closer to the perimeter of the OWF polygon, compared to the ones positioned more centrally. Similar to the wakes developing downstream from islands, the wake position obviously reverses between flood and ebb conditions.
- The effect of the drag force is predominant on the flow fields developing in the vicinity of the foundations, over the effect of the local bathymetry change. Where the local water depth decrease would introduce local accelerations (very locally around the WTG locations as observed in Figure 2.16), this is overruled by strong deceleration introduced by drag when the cumulative effect is plotted (e.g., see Figure 3.7).
- There is an increase in flow speeds along the western and offshore most boundary of the OWF. There is, however, no change in flow directions. This increase in flow magnitudes is demonstrated predominantly in LWS conditions and residuals and only extends slightly beyond the OWF boundary (up to less than 1 km).
- Especially since tidal forcing dominates SROWF flow fields, the wind speed reduction over the OWF polygon in specific has only a secondary effect on the flow fields observed in the area, meaning that differences compared to the baseline situation are overall dominated by drag exerted from the turbines and shifts in the wake development downstream from islands due to interfacing with the turbine locations.

- As expected, there is hardly any effect from the turbines on the observed water levels.
- Residual flows are affected by the sum of local influences from the turbines (over reversing tidal conditions), however differences in residual flows are somewhat limited, i.e., for the most part remaining below 0.02 m/s across the SROWF area.
- Overall, the effects of the operational situation are limited within the SROWF area, and for the most part in the vicinity of the turbine locations and do not extend further than a couple of kilometres from the considered OWF polygon.

Within the marine area covering the OWF and immediately surrounding it, as illustrated in e.g. Figure 3.7 and bounded by coordinates -10.04 and -9.9 degrees longitude and 53.22 and 53.3 degrees latitude, the calculated, the calculated maximum operational local current speeds and associated maximum local differences in current speed compared to baseline are presented in Table 3.3.

Table 3.3 Maximum calculated local current speeds within extended OWF area in baseline conditions. It is noted that the locations where maximum reported local current speeds and differences are not necessarily coincident.

Tidal state / condition	**Maximum local current speed (m/s)**	**Maximum local current speed increase between operational and baseline (m/s)**	**Maximum local current speed decrease between operational and baseline (m/s)**
LWS	0.81	0.31	-0.47
LWN	0.37	0.21	-0.17
HWS	0.66	0.35	-0.48
HWN	0.41	0.20	-0.27
FS	0.72	0.31	-0.55
FN	0.38	0.17	-0.27
ES	0.58	0.38	-0.48
EN	0.35	0.22	-0.28
residual	0.19	0.05	-0.08

3.3 Waves

3.3.1 Introduction

In this section the wave fields of the significant wave height, peak wave period and associated mean wave direction are presented at the area of interest and discussed for the baseline and operational situations[19] (sections 3.3.2 and 3.3.3 respectively). For both situations, the fields are presented for various sea states representative of normal (50th, 90th percentile) and extreme (RP 1-,5-, 10-, 50-yr) conditions. As already discussed in Section 2.3.3.1, the selection of the associated time instances (and hence relevant simulation periods) was based on hindcast timeseries at the previously offshore reference location used for the determination of metocean conditions in Deltares (2022). For reference, the "reference", (i.e., the values at the WTG-15 reference location computed in Deltares (2022)) and the now computed wave heights along with concurrent peak wave periods at the nearest WTG location[20] of the updated OWF layout (being WTG-08 in SRL069) are presented in Table 3.4 for the baseline situation.

Table 3.4 Computed conditions in the modelling performed in the present study at WTG-8 compared to "reference" conditions computed at offshore exposed location (WTG-15, old layout) in Deltares (2022). It is noted that the identified representative sea states were based only on H_s. Values of peak wave periods (T_p) are presented for completeness but were not used in the identification of representative sea states. In addition, it is noted that the comparison between peak wave periods is between associated (to H_s) values from the metocean study (extreme conditions) and concurrent values in the hindcast timeseries computed in this study.

Computed conditions in this study		**MWD (240°** ; 225° – 255°) **"WSW"**			**MWD (270°** ;255° – 285°**) "W"**		
		H_s (m)	**T_p (s)**	**Rep. condition**	**H_s (m)**	**T_p (s)**	**Rep. condition**
Normal–50th perc.	WTG15 Deltares (2022)	2.60	9,5	28-Aug-1984 16:00	2.00	9.1	10-Aug-2014 00:00
	WTG8	2.83	10.6		1.52	8.8	
	%	**109**	**112**		**76**	**97**	
Normal–90th perc.	WTG15 Deltares (2022)	4.69	12.4	23-Mar-1981 21:00	3.86	11.8	01-Oct-2008 02:00
	WTG8	5.18	11.9		4.11	10.4	
	%	**110**	**96**		**106**	**88**	
Extreme–RP1	WTG15 Deltares (2022)	8.02	14.9	08-Feb-2000 17:00	7.05	14.9	13-Apr-1985 23:00
	WTG8	8.21	14.0		6.29	14.8	
	%	**102**	**94**		**89**	**99**	
Extreme–RP5	WTG15 Deltares (2022)	9.92	15/8	27-Dec-2013 05:00	8.52	15.8	15-Dec-1993 15:00
	WTG8	10.45	14.8		8.66	16.4	
	%	**110**	**96**		**106**	**88**	
Extreme–RP10	WTG15 Deltares (2022)	10.72	16.1	19-Dec-1982 22:00	9.14	16.2	11-Mar-2008 23:00
	WTG8	11.18	16.9		9.50	14.9	
	%	**104**	**105**		**104**	**92**	
Extreme–RP50	WTG15 Deltares (2022)	12.54	16.8	05-Jan-1991 14:00	10.54	16.9	09-Feb-1988 19:00
	WTG8	12.91	16.9		10.83	16.8	
	%	**103**	**101**		**103**	**99**	

[19] All operational conditions are simulated with a 10% wind speed decrease within SROWF area.
[20] WTG-08 (SRL069) is roughly 120 m to the northwest of the WTG-15 (Deltares, 2022), and two locations have roughly the same water depth.

Reported deviations in H_s (typically below 10%) relative to "reference" conditions are within expectations and deemed acceptable for the purposes of the present study. These are explained predominantly by the fact that reference values of extreme and normal conditions are statistically derived and hence theoretical. This implies that the identified sea states in the hindcast timeseries (and hence associated timings) approximate but do not necessarily exactly match the reference values in H_s. Secondary influences for the reported deviations stem from the slight offset between the two considered output locations (about 120 m) as well as potential differences in the forcing of the detailed SROWF domain between the present study and Deltares (2022), see also Section 2.3.3.2 related to incoming wave conditions. Overall, the simulated conditions and hence ambient wave fields are deemed well representative of normal and extreme sea states in the SROWF area.

A selection of wave fields is presented in the following section, to allow for a discussion of wave field (difference) characteristics. The entire produced output is given in the Appendix. Finally, specifically for operational situations the wave fields are presented in the form of absolute difference plots (of significant wave height, peak wave period along with the associated mean wave directions) relative to the baseline situations. Corresponding relative difference plots (given in percentages) are included in the Appendix.

3.3.2 Baseline

3.3.2.1 Wave fields in normal conditions

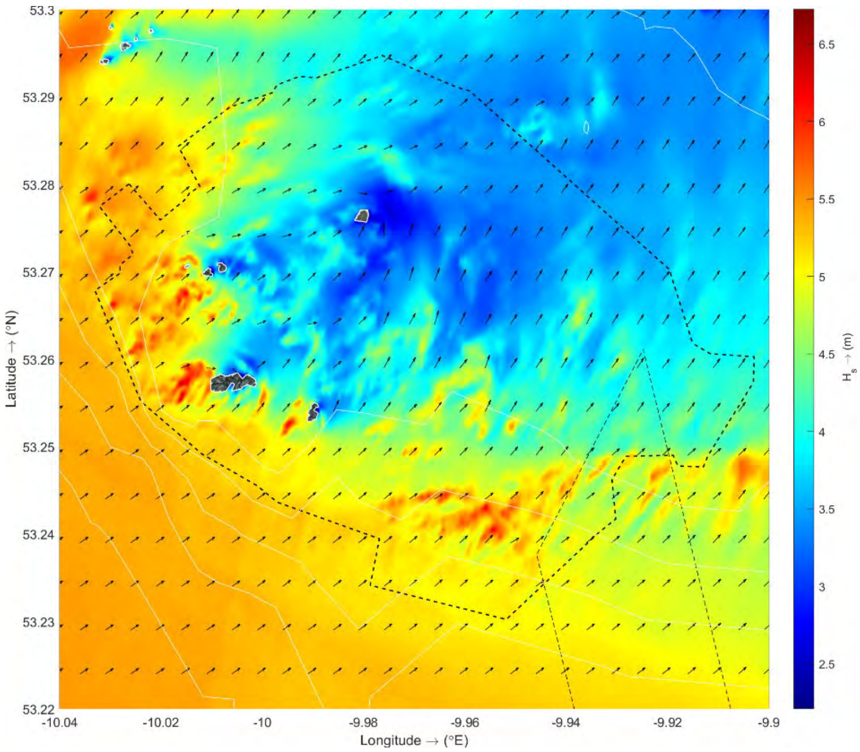

Figure 3.14 Field of H_s and associated mean wave directions (by means of directional arrows) across the SROWF during normal (WSW 90th percentile) baseline situations, see also Table 3.4.

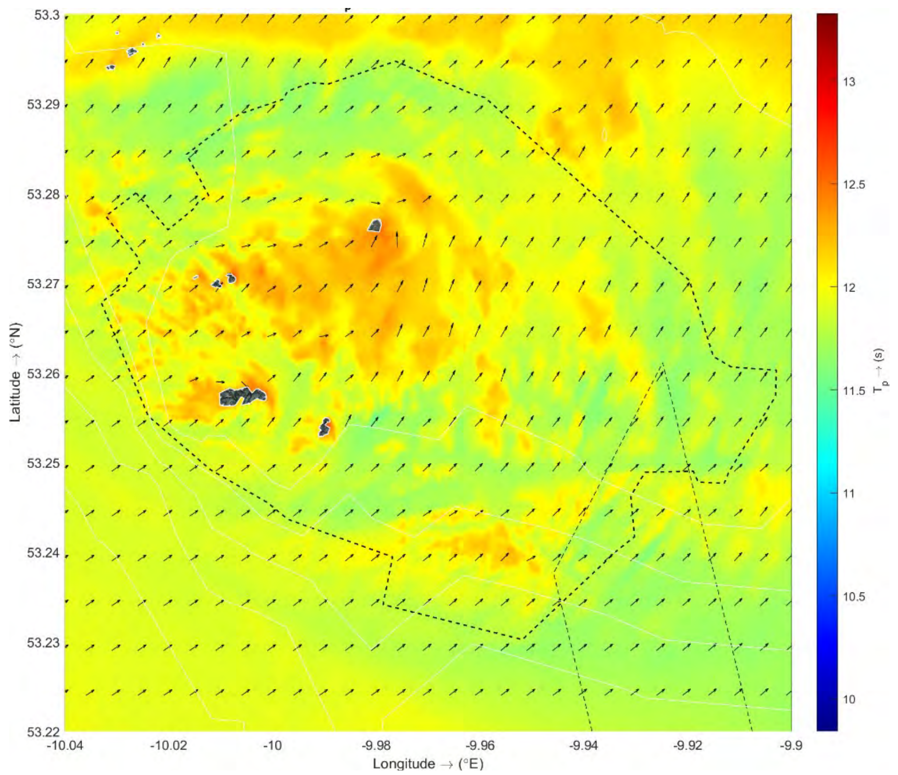

Figure 3.15 Field of T_p and associated mean wave directions (by means of directional arrows) across the SROWF during normal (WSW 90th percentile) baseline situations, see also Table 3.4.

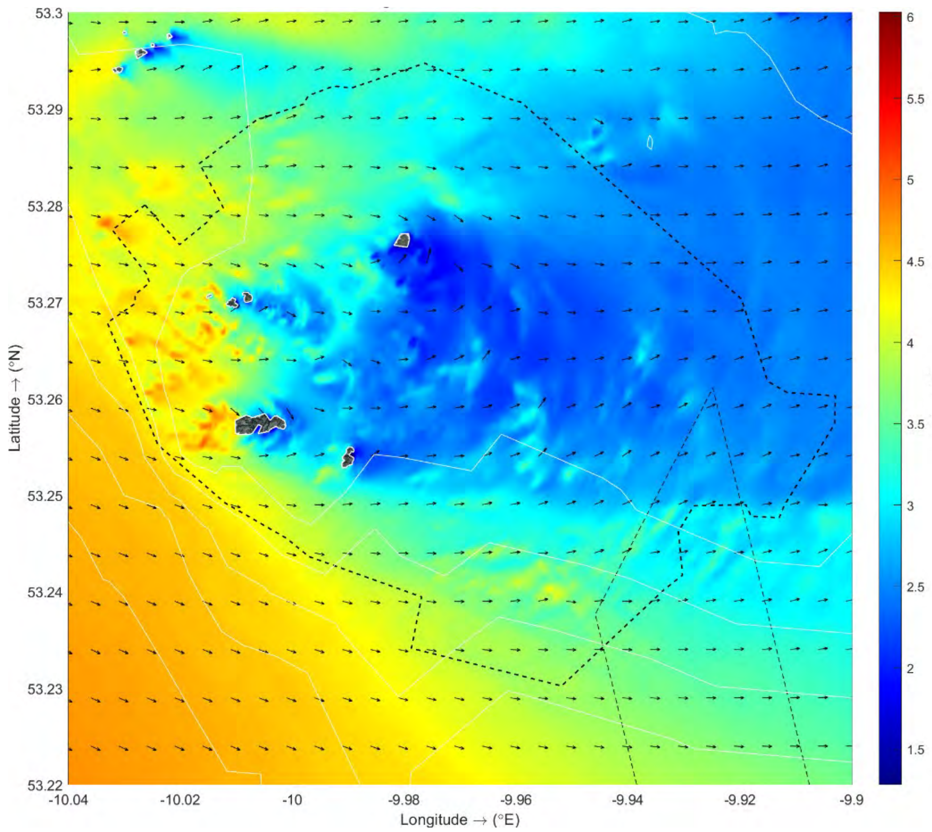

Figure 3.16 Field of H_s and associated mean wave directions (by means of directional arrows) across the SROWF during normal (W 90th percentile) baseline situations, see also Table 3.4.

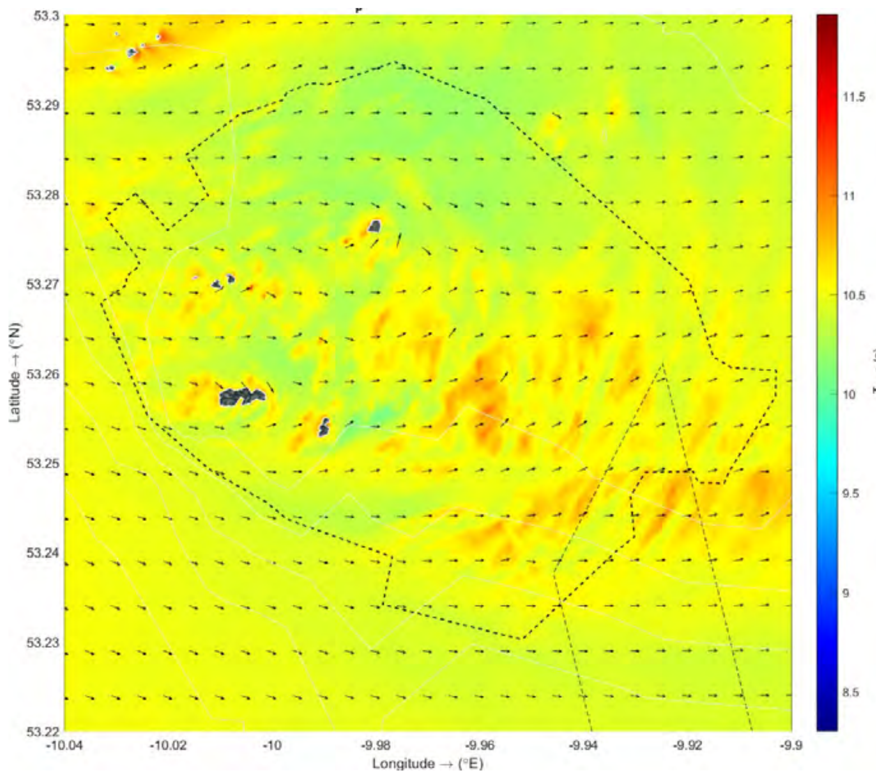

Figure 3.17 Field of T_p and associated mean wave directions (by means of directional arrows) across the SROWF during normal (W 90th percentile) baseline situations, see also Table 3.4.

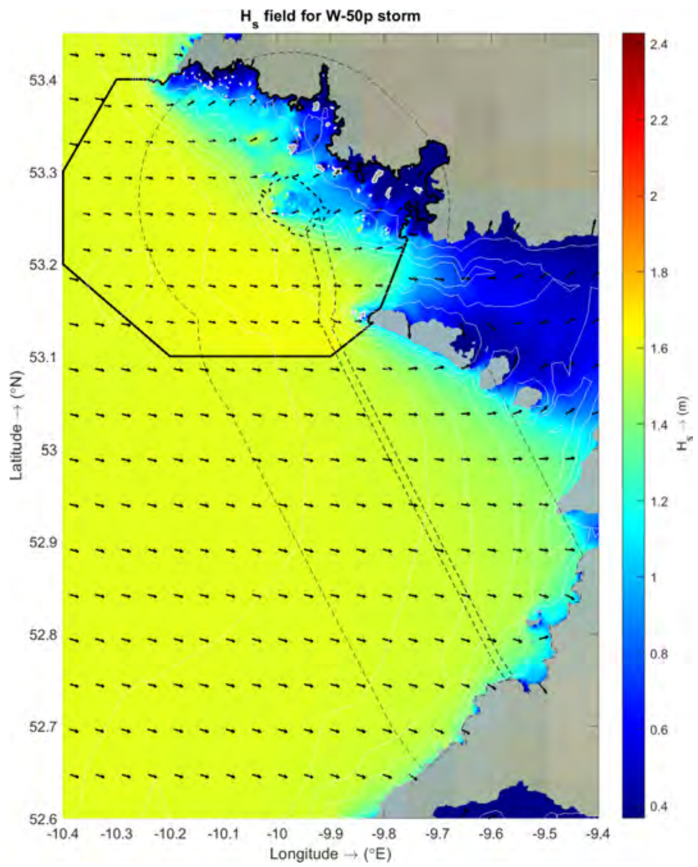

Figure 3.18 Field of H_s and associated mean wave directions (by means of directional arrows) across the entire MPPSA during normal (W 50th percentile) baseline situations, see also Table 3.4.

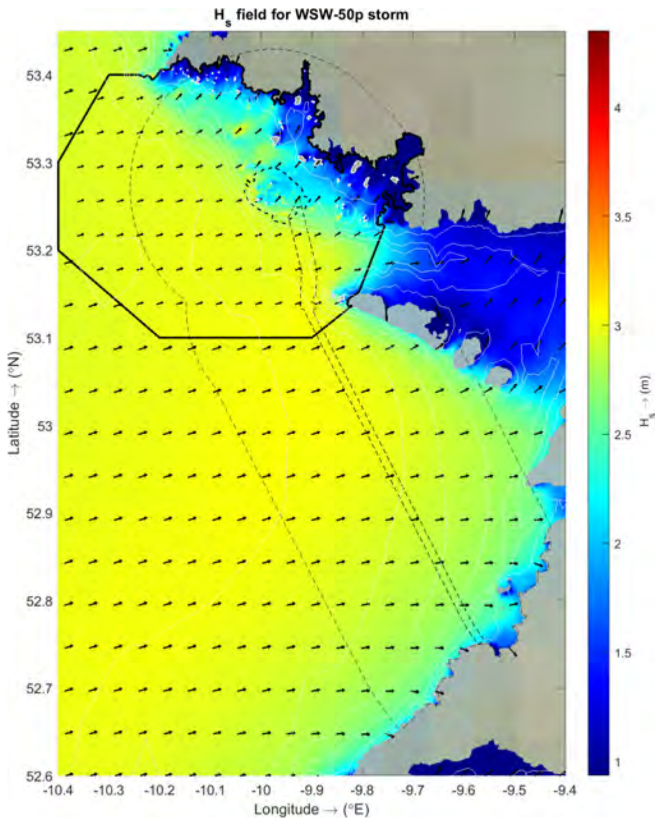

Figure 3.19 Field of H_s and associated mean wave directions (by means of directional arrows) across the entire MPPSA during normal (WSW 50th percentile) baseline situations, see also Table 3.4.

3.3.2.2 Wave fields in extreme conditions

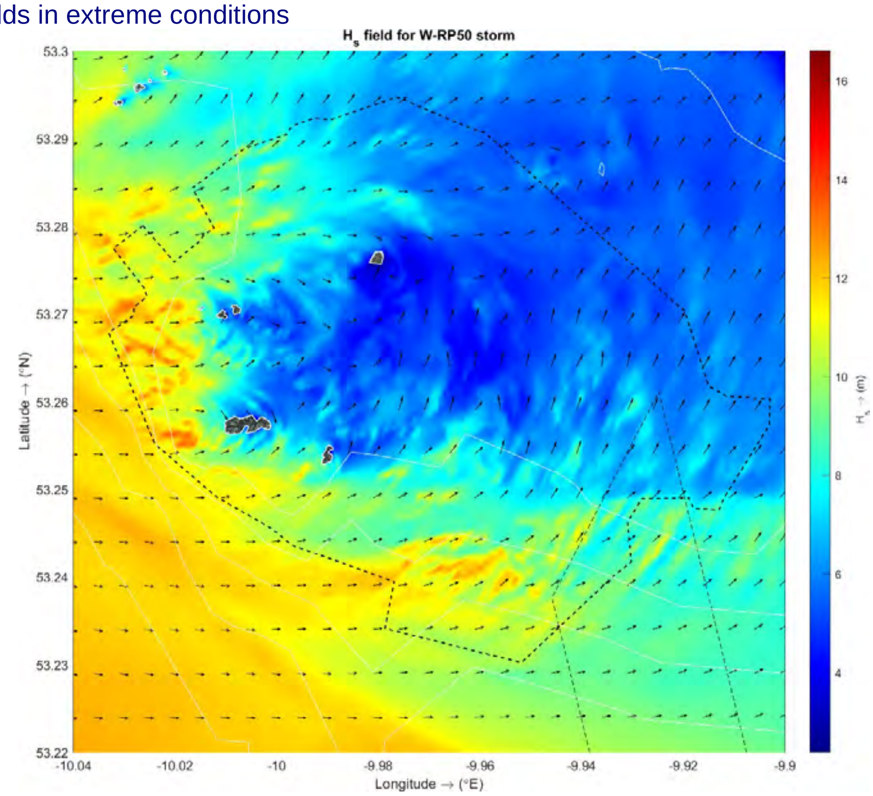

Figure 3.20 Field of H_s and associated mean wave directions (by means of directional arrows) across the SROWF during normal (W RP50) baseline situations, see also Table 3.4.

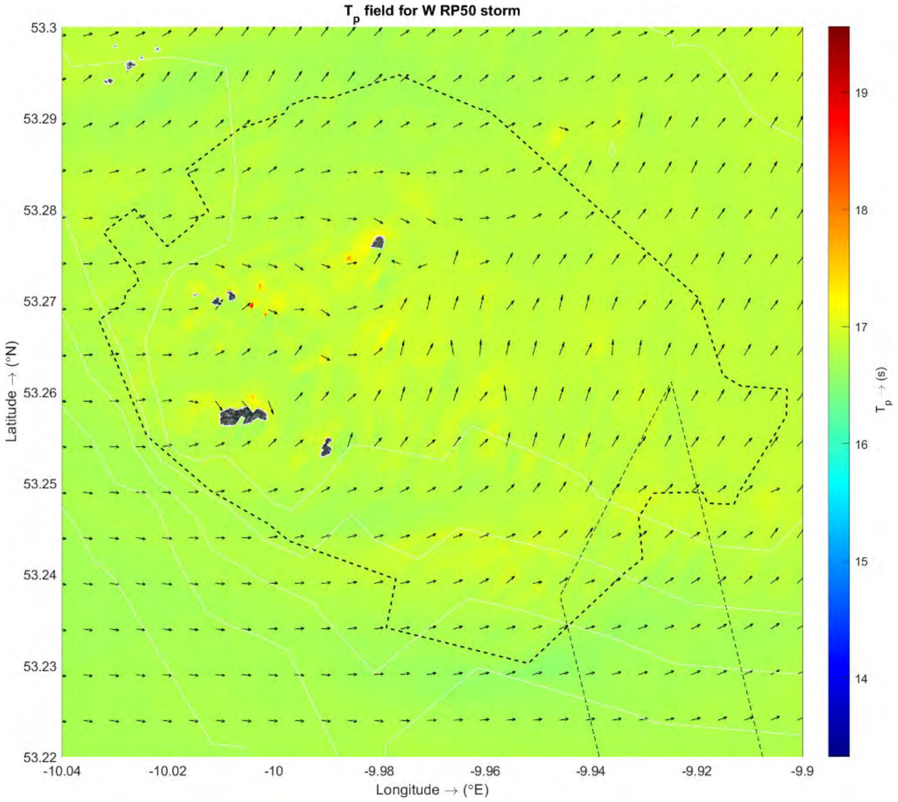

Figure 3.21 Field of T_p and associated mean wave directions (by means of directional arrows) across the SROWF during normal (W RP50) baseline situations, see also Table 3.4.

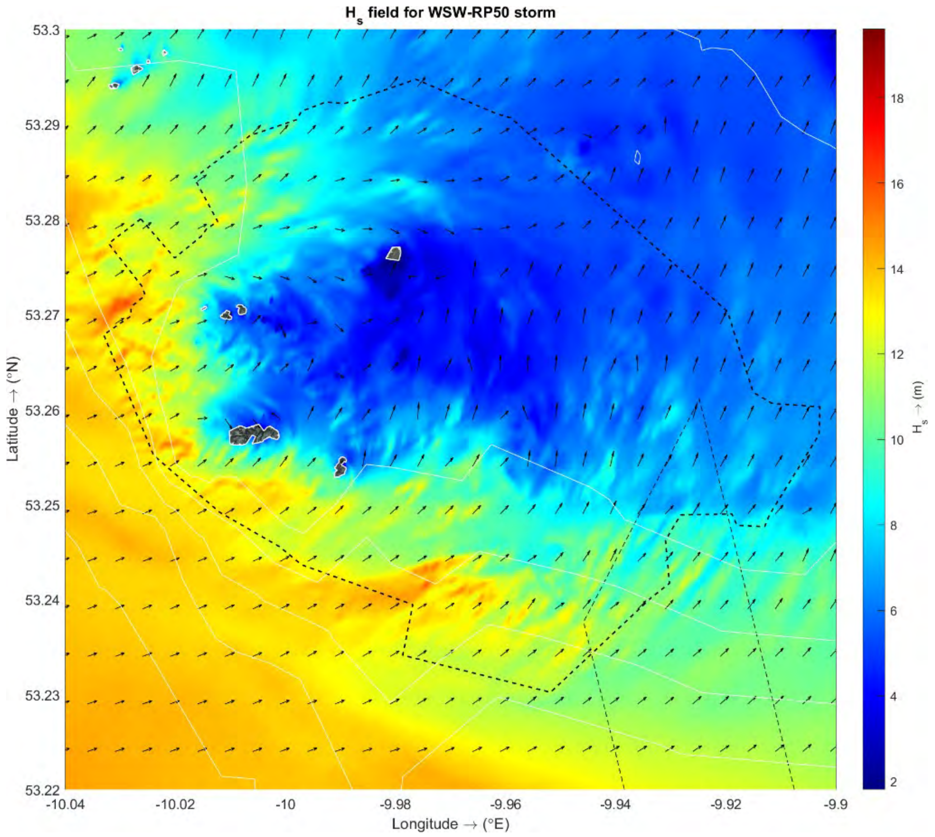

Figure 3.22 Field of H_s and associated mean wave directions (by means of directional arrows) across the SROWF during normal (WSW RP50) baseline situations, see also Table 3.4.

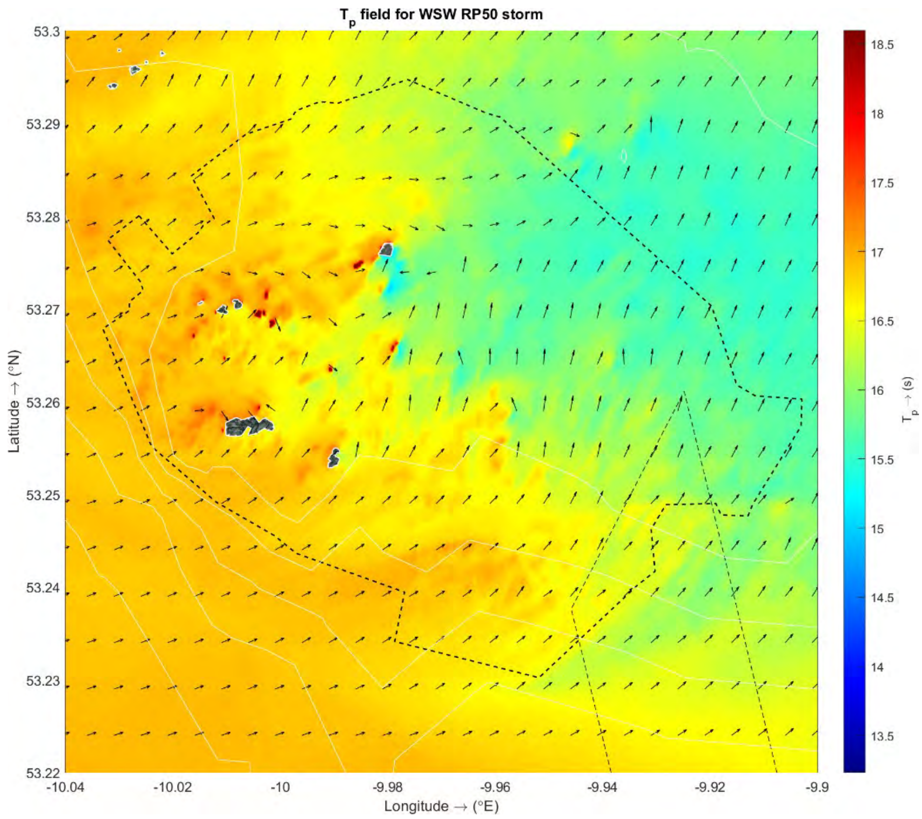

Figure 3.23 Field of T_p and associated mean wave directions (by means of directional arrows) across the SROWF during normal (WSW RP50) baseline situations, see also Table 3.4.

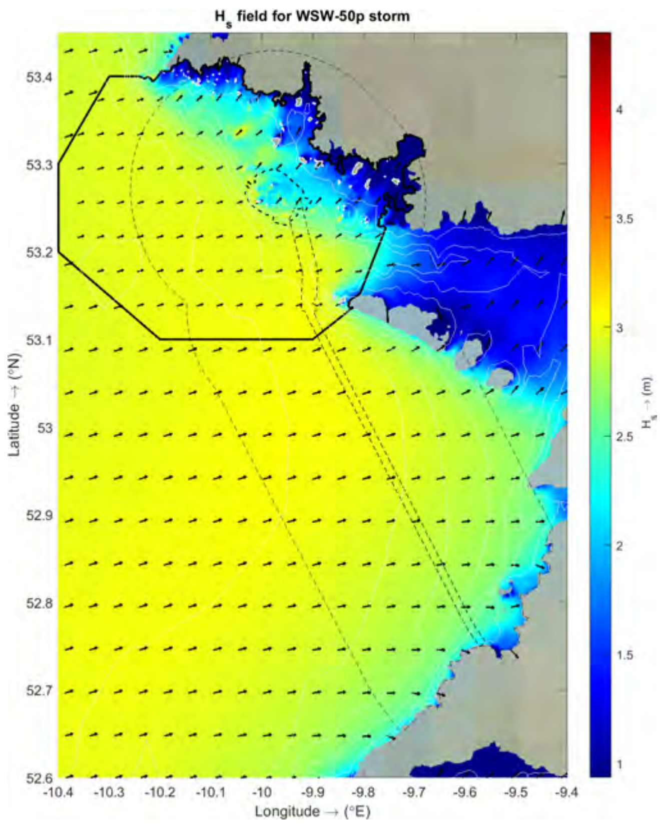

Figure 3.24 Field of H_s and associated mean wave directions (by means of directional arrows) across the entire MPPSA during normal (W RP10 percentile) baseline situations, see also Table 3.4.

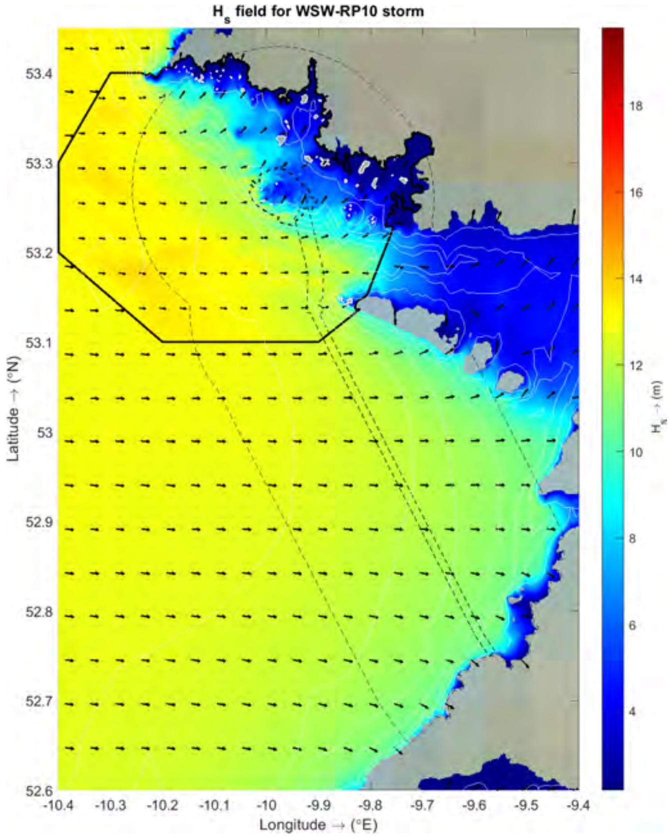

Figure 3.25 Field of H_s and associated mean wave directions (by means of directional arrows) across the entire MPPSA during normal (WSW RP10 percentile) baseline situations, see also Table 3.4.

3.3.2.3 Observations

The following observations are made with respect to the various wave fields presented in Figure 3.14 to Figure 3.25 in the previous sections:

- The waves further offshore from the SROWF area (in terms of H_s, T_p and MWD) and for the most part of the export cable corridor are nearly uniform in magnitude of significant wave height and direction, as they propagate uninfluenced from the seabed (deep water conditions).
- The steep seabed gradient evolving landwards from the isobath that is nearly aligned with the offshore-most boundary of the OWF polygon (to the west), see also Figure 2.21, leads to a abrupt change in the overall wave field pattern. Roughly from that point, waves start being influenced by the seabed topography, with refraction (evolving towards northward directions), and bottom dissipation becoming predominant as waves are passing through the SROWF area. In that sense, the offshore boundary of the SROWF aligns well for both considered approach directions, with the onset of coastal wave propagation around SROWF. This is obviously positioned slightly further offshore in the case of extreme conditions (when waves are generally higher and longer) and hence become influenced at deeper waters compared to normal conditions.
- More specifically, within the SROWF area, wave propagation is controlled by the complex topography, i.e., the presence of various submerged rocks and islands. These features lead to stronger wave refraction in their vicinity (compared to the larger scale refraction of waves in that same area), dissipation expressed through shoaling and subsequent breaking, and finally to shadow areas in a downwave direction. Wave focusing followed by dissipation is more prominent in normal

conditions, since for extreme conditions, wave dissipation is occurring somewhat further offshore.

- Not only wave heights and directions but also peak wave periods change in a wave propagation direction. This change is nevertheless less than 1 s across the OWF and adjacent coastal region, but a different pattern is observed depending the wave approach direction (W vs. WSW). As waves are propagating through the OWF towards the coast, the peak wave period somewhat increases in W conditions and decreases in WSW conditions. The reason for this difference is twofold and originates by the difference in wave energy and propagation direction between the two conditions. WSW conditions are characterized by higher waves at approximately similar periods compared to W, leading to an earlier and stronger dissipation of wave energy. Because the longer waves break first, a reduction of T_p is observed in the propagation direction. On the other hand, lower waves approaching from W, need to refract more while propagating through the OWF and coastal region and dissipate later (during their propagation path) compared to waves in WSW conditions. Due to this difference and also their refraction being further influenced by the complex topography in the OWF, waves coming from the West exhibit a different focusing pattern (observed as an increase in Tp) compared to waves in WSW conditions.

3.3.3 Operational

3.3.3.1 Wave fields in normal conditions

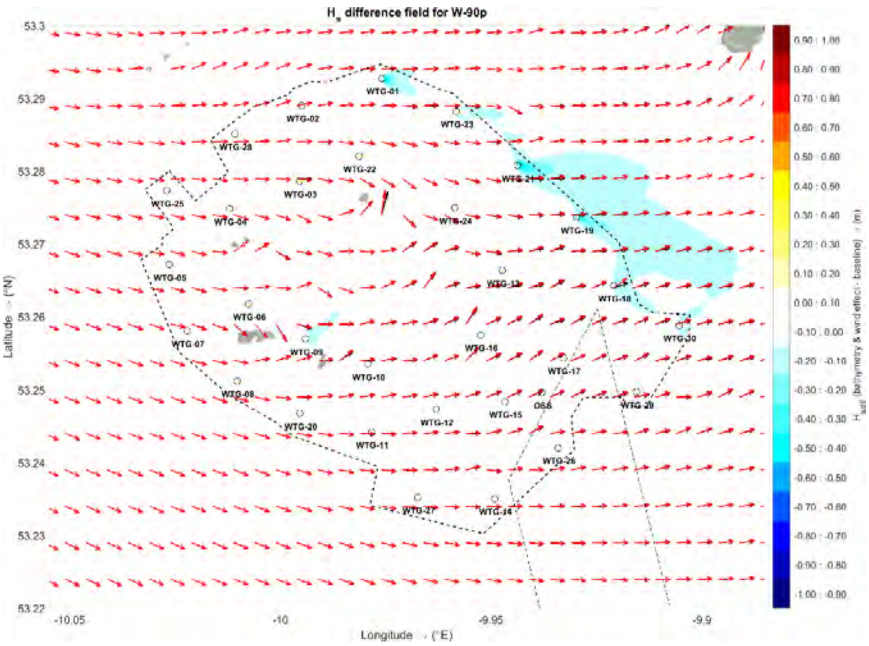

Figure 3.26 Field of absolute H_s difference and associated mean wave directions (by means of directional arrows) across the SROWF during normal (W 90th percentile) between operational and baseline situations, see also Table 3.4. Background black arrows show flow directions in baseline situations and red arrows plotted on top show directions in operational situations.

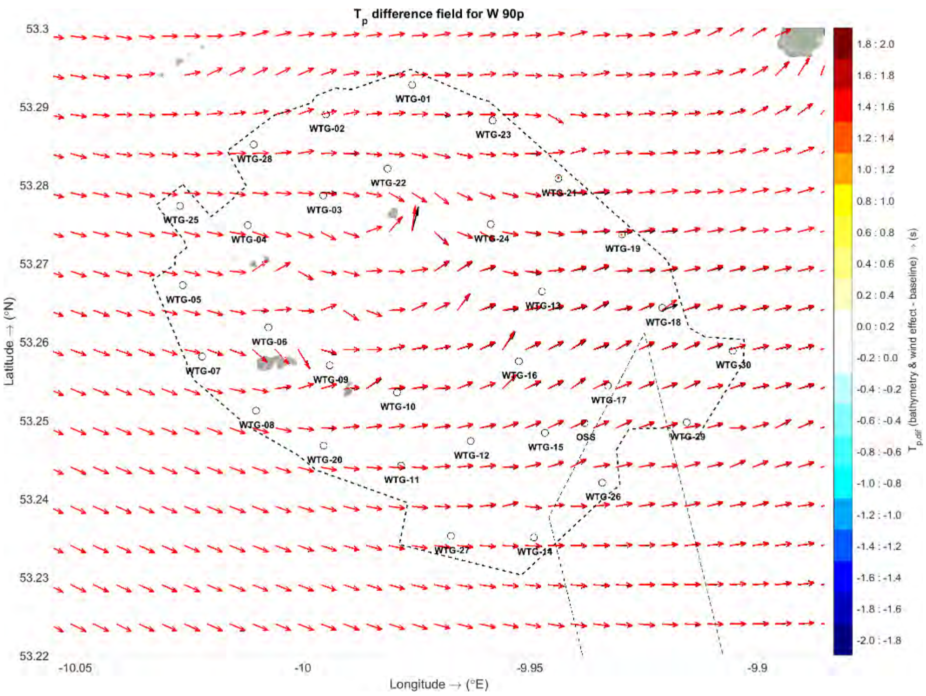

Figure 3.27 Field of absolute T_s difference and associated mean wave directions (by means of directional arrows) across the SROWF during normal (W 90th percentile) between operational and baseline situations, see also Table 3.4. Background black arrows show flow directions in baseline situations and red arrows plotted on top show directions in operational situations.

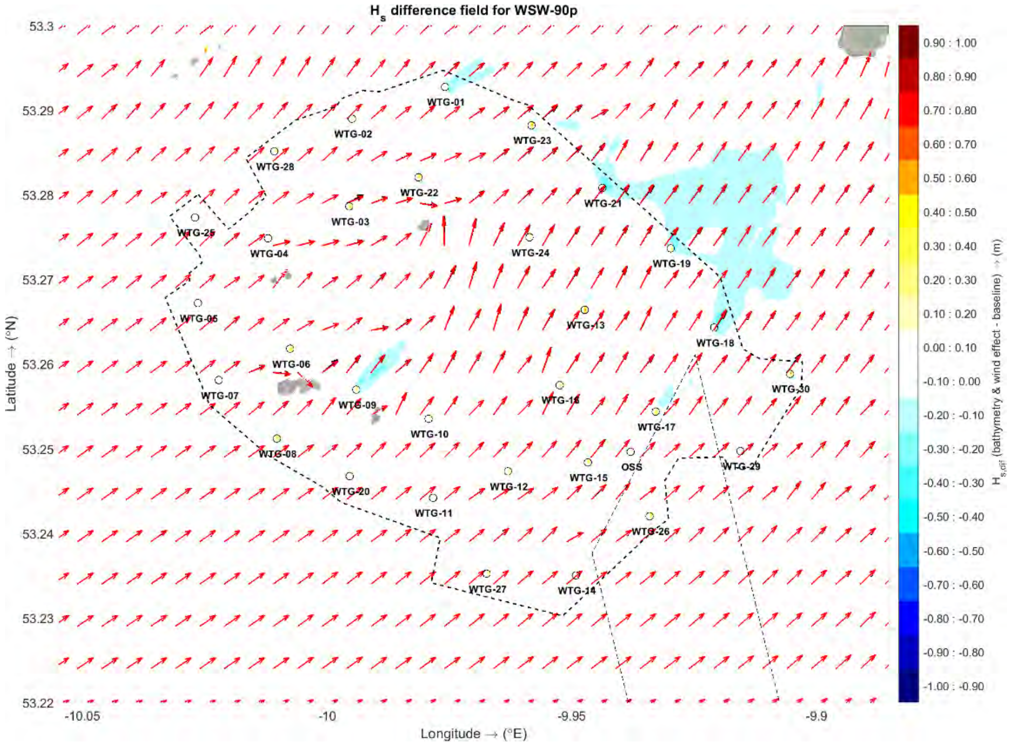

Figure 3.28 Field of absolute H_s difference and associated mean wave directions (by means of directional arrows) across the SROWF during normal (WSW 90th percentile) between operational and baseline situations, see also Table 3.4. Background black arrows show flow directions in baseline situations and red arrows plotted on top show directions in operational situations.

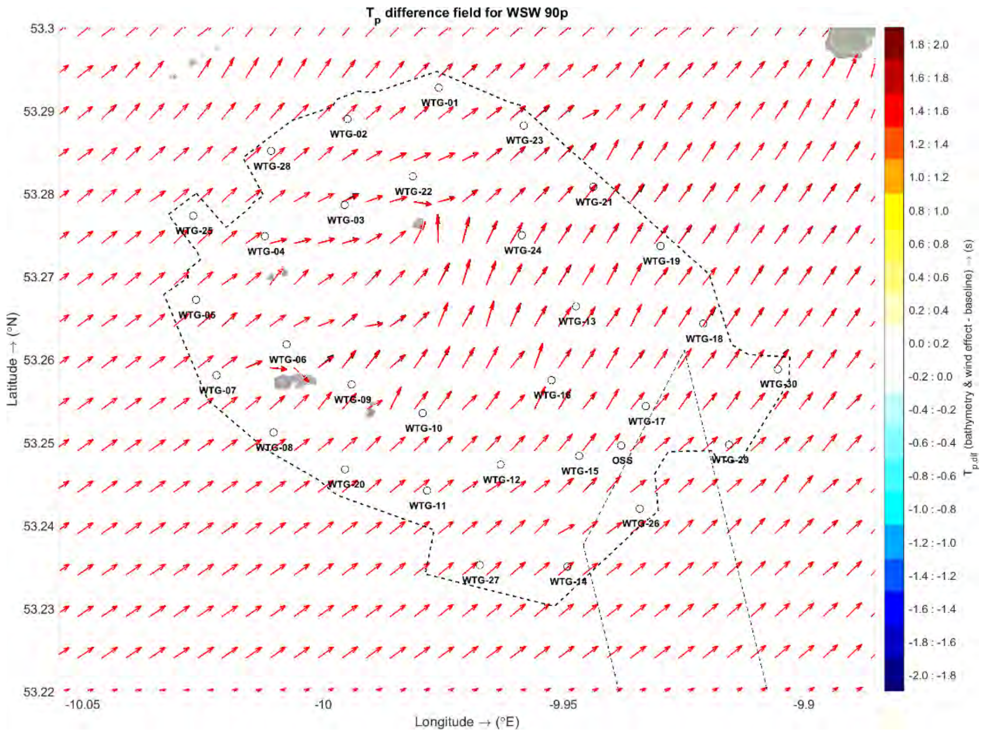

Figure 3.29 Field of absolute T_s difference and associated mean wave directions (by means of directional arrows) across the SROWF during normal (WSW 90th percentile) between operational and baseline situations, see also Table 3.4. Background black arrows show flow directions in baseline situations and red arrows plotted on top show directions in operational situations.

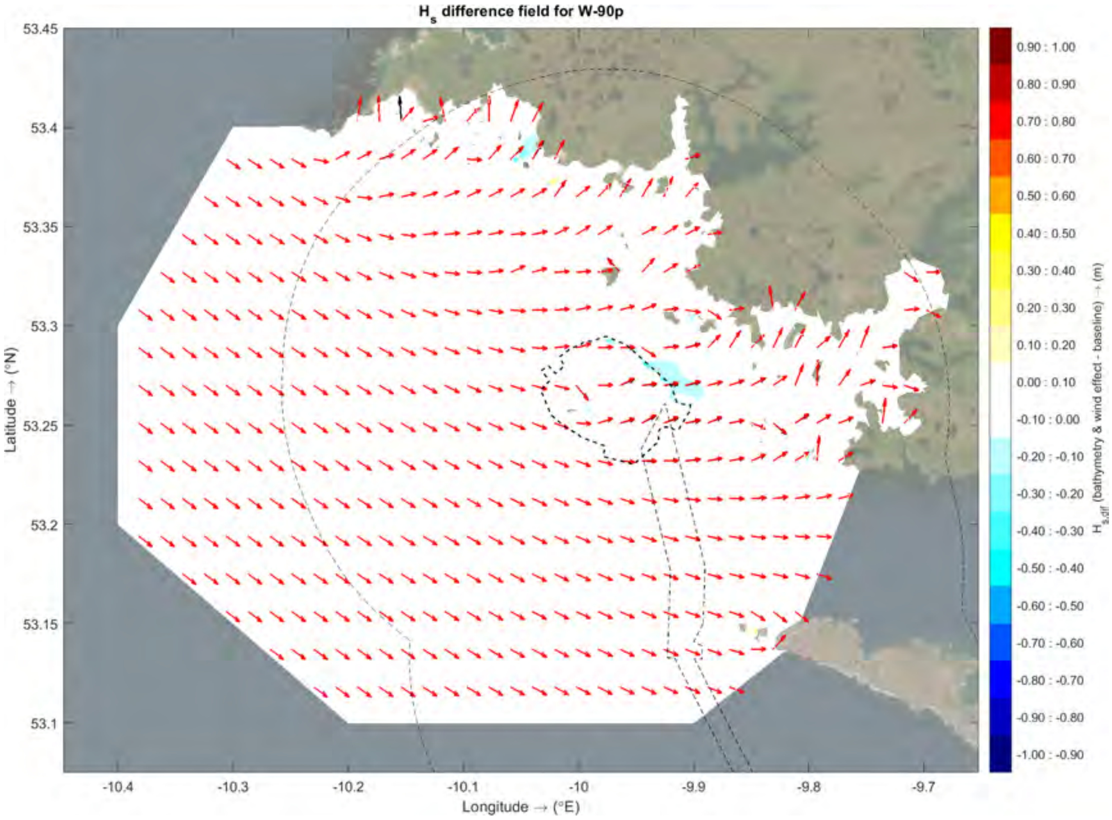

Figure 3.30 Field of absolute H_s differences and associated mean wave directions (by means of directional arrows) across the greater MPPSA during normal (W 90th percentile) baseline situations, see also Table 3.4.

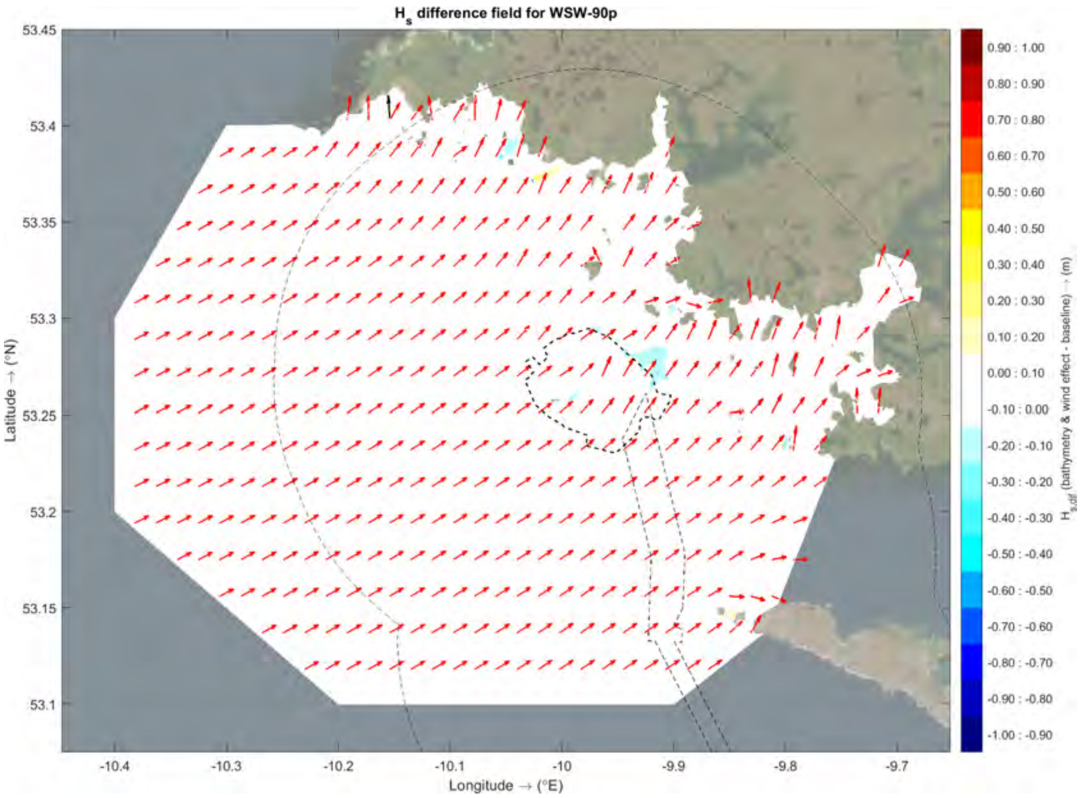

Figure 3.31 Field of absolute H_s differences and associated mean wave directions (by means of directional arrows) across the greater MPPSA during normal (WSW 90th percentile) baseline situations, see also Table 3.4.

3.3.3.2 Wave fields in extreme conditions

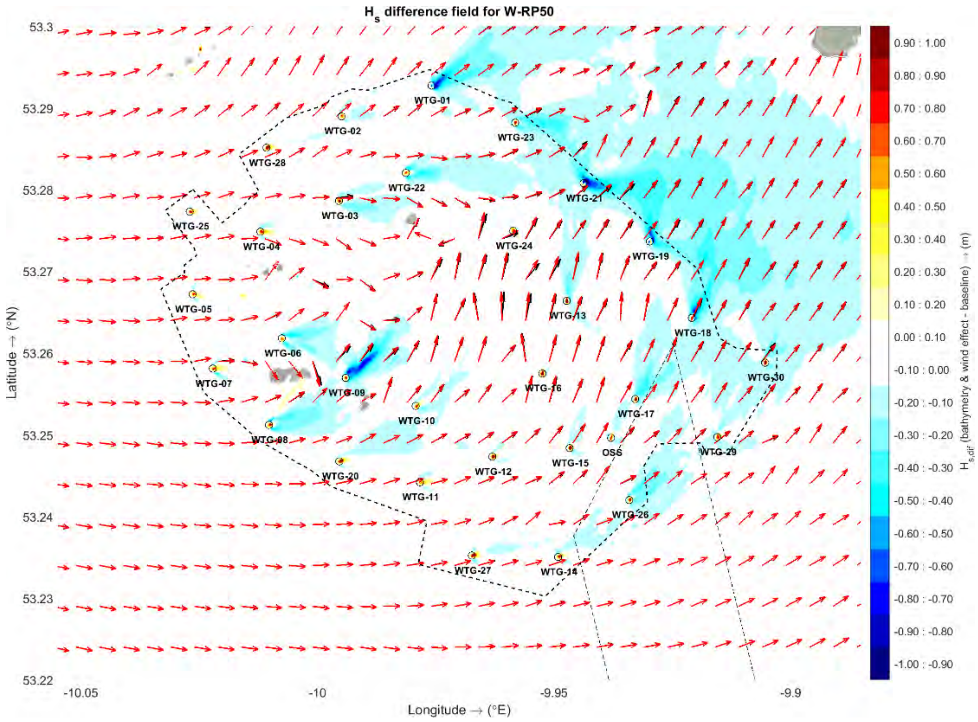

Figure 3.32 Field of absolute H_s difference and associated mean wave directions (by means of directional arrows) across the SROWF during normal (W RP50 year) between operational and baseline situations, see also Table 3.4. Background black arrows show flow directions in baseline situations and red arrows plotted on top show directions in operational situations.

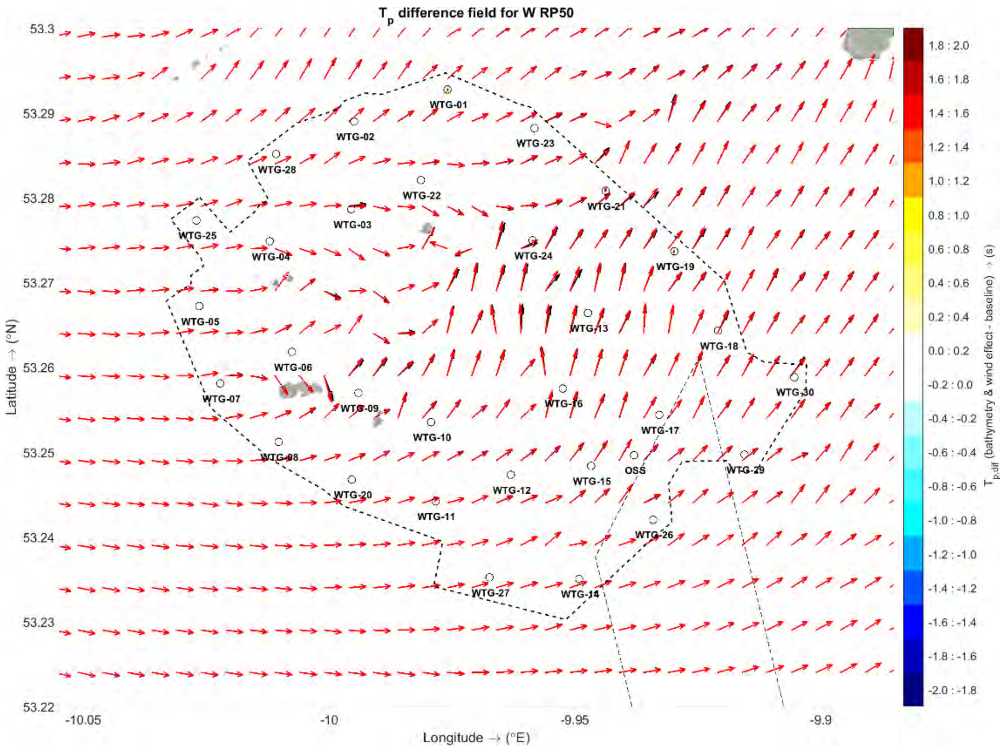

Figure 3.33 Field of absolute T_s difference and associated mean wave directions (by means of directional arrows) across the SROWF during normal (W RP50 year) between operational and baseline situations, see also Table 3.4. Background black arrows show flow directions in baseline situations and red arrows plotted on top show directions in operational situations.

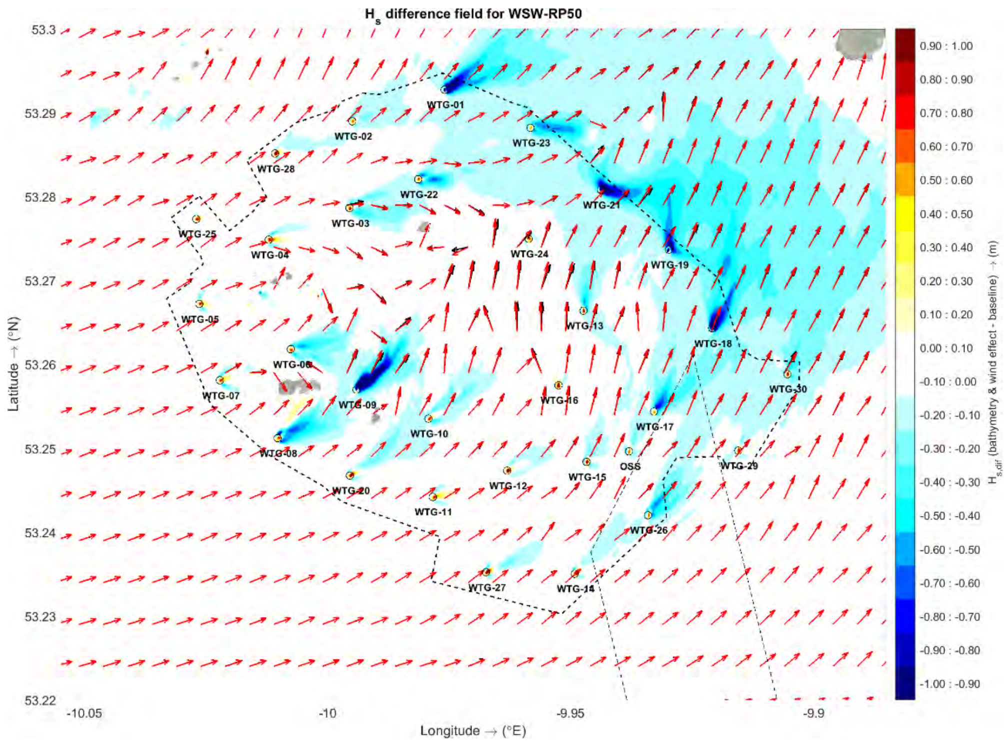

Figure 3.34 Field of absolute H_s difference and associated mean wave directions (by means of directional arrows) across the SROWF during normal (WSW RP50 year) between operational and baseline situations, see also Table 3.4. Background black arrows show flow directions in baseline situations and red arrows plotted on top show directions in operational situations.

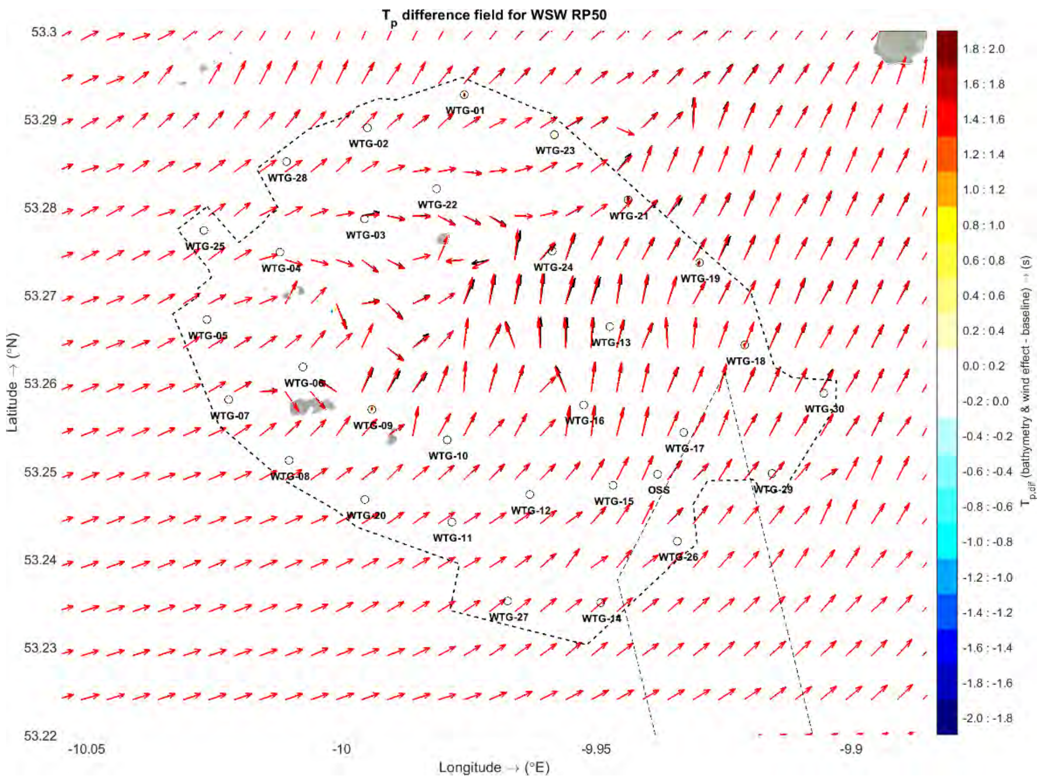

Figure 3.35 Field of absolute T_p difference and associated mean wave directions (by means of directional arrows) across the SROWF during normal (WSW RP50 year) between operational and baseline situations, see also Table 3.4. Background black arrows show flow directions in baseline situations and red arrows plotted on top show directions in operational situations.

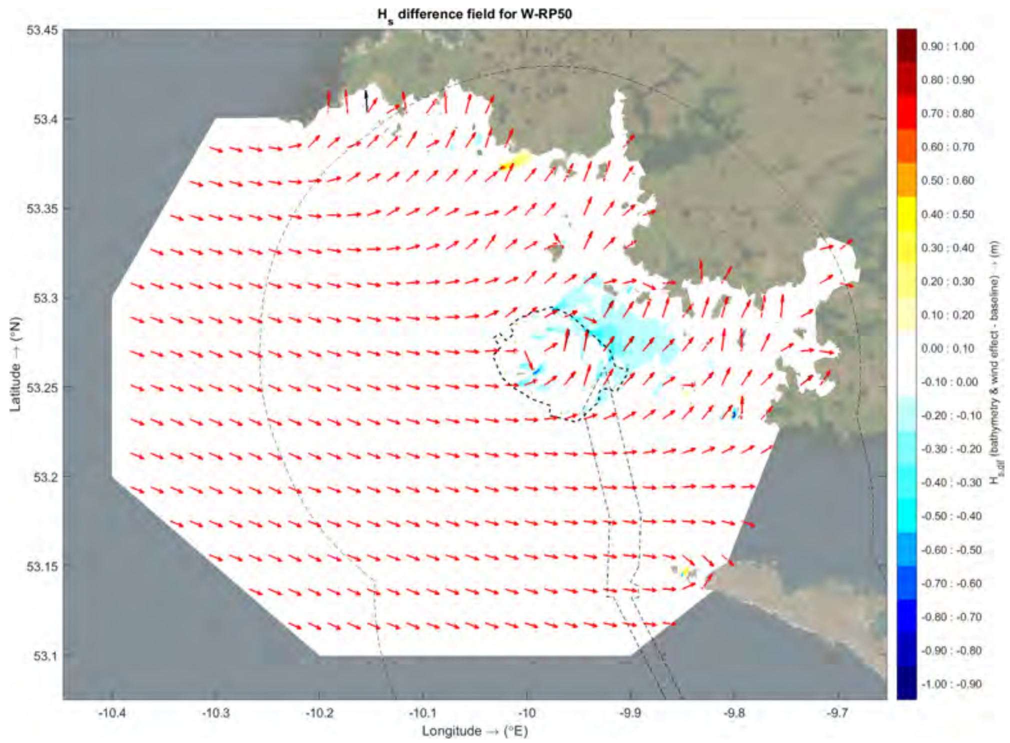

Figure 3.36 Field of absolute H_s differences and associated mean wave directions (by means of directional arrows) across the greater MPPSA during normal (W RP50 year) baseline situations, see also Table 3.4.Background black arrows show flow directions in baseline situations and red arrows plotted on top show directions in operational situations.

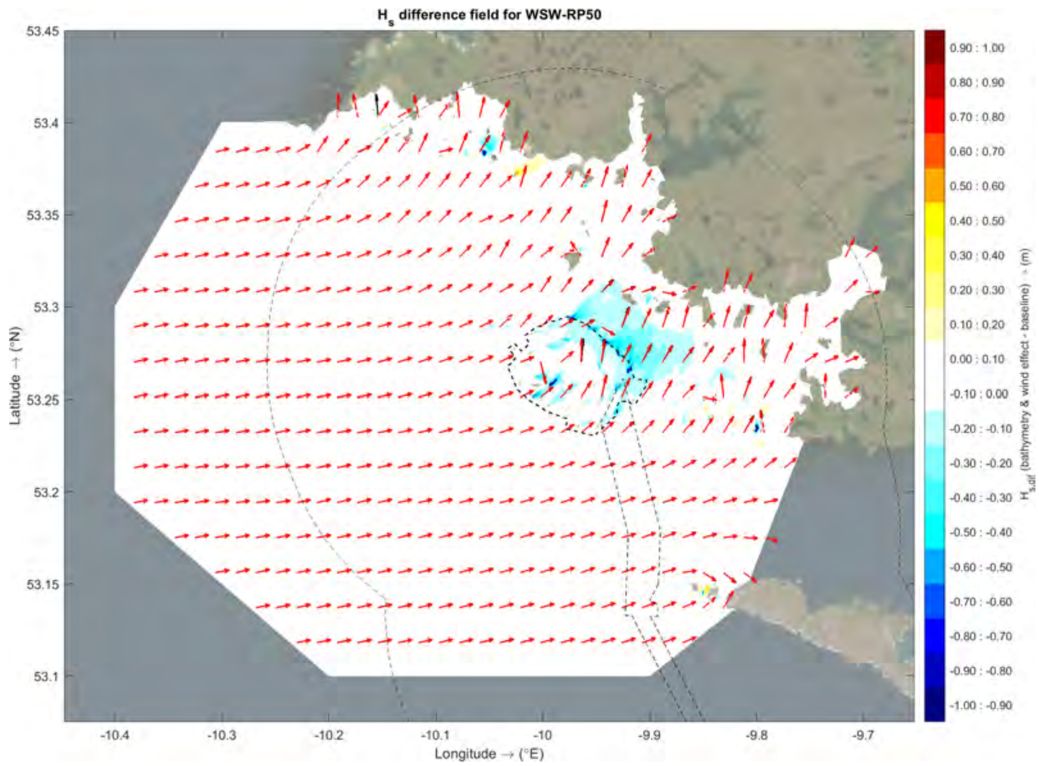

Figure 3.37 Field of absolute H_s differences and associated mean wave directions (by means of directional arrows) across the greater MPPSA during normal (WSW RP50 year) baseline situations, see also Table 3.4.Background black arrows show flow directions in baseline situations and red arrows plotted on top show directions in operational situations.

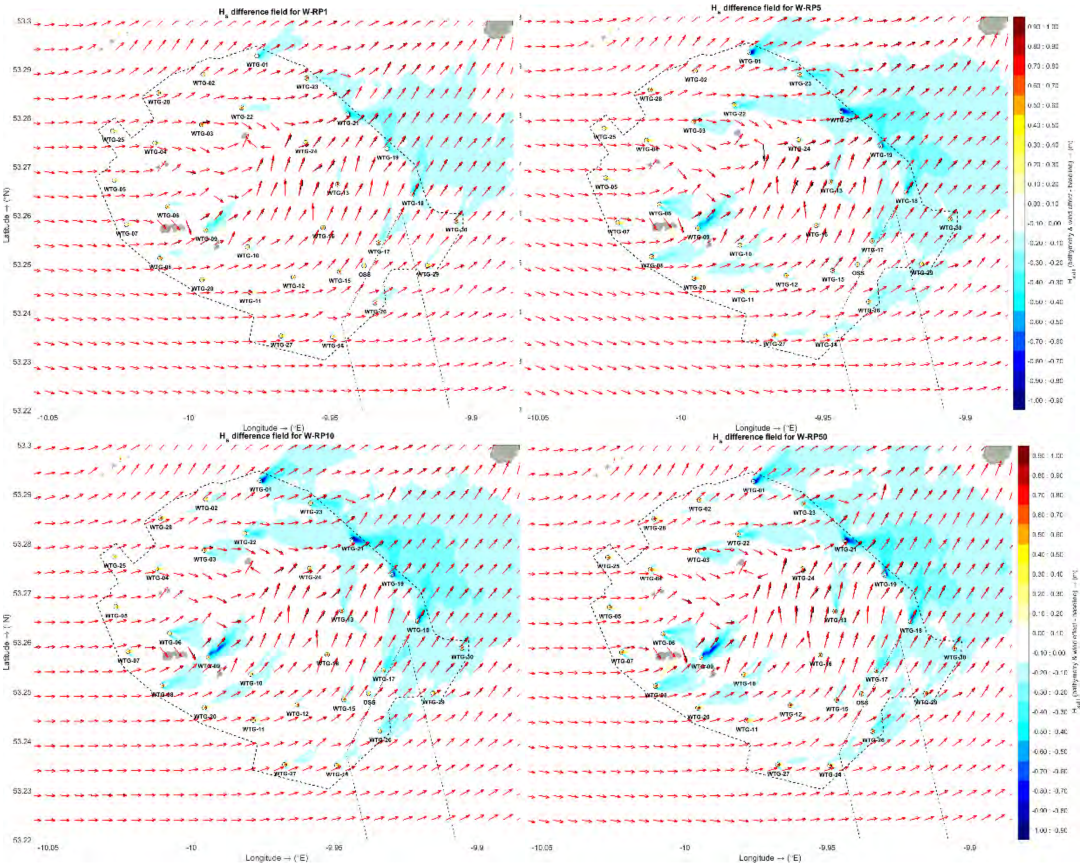

Figure 3.38 Overview of fields of absolute H_s difference and associated mean wave directions (by means of directional arrows) across the SROWF during all considered extreme conditions (ordered with increased severity from top left to bottom right) under W approach wave condition, between operational and baseline situations, see also Table 3.4. Background black arrows show flow directions in baseline situations and red arrows plotted on top show directions in operational situations.

3.3.3.3 Observations

The following observations are made with respect to the various wave fields presented in Figure 3.26 to Figure 3.38 in the previous sections:

- In operational conditions, similar to baseline conditions, wave propagation is controlled by the steep gradient in bathymetry directly offshore from the western most boundary of the OWF as well as by the complex topography within the SROWF, characterized by the presence of islands and rocky outcrops.
- Operational conditions, parameterized in the wave model through the presence of WTG foundations in the bathymetry and wind speed reduction over the entire OWF polygon, influence the wave fields predominantly in the vicinity of the WTG and OSS locations and directly downwave from the OWF, over a relatively large area towards the coast.
- In the vicinity of the WTGs and OSS, refraction and shoaling lead to a very local (characterized by a spatial scale in the order of tens of meters) increase of wave energy. This is followed by dissipation through wave breaking which leads to an overall decrease of wave energy to a downstream direction that is noticeable over a distance equal to the spacing of the WTGs (roughly 1 km). This decrease of wave energy is expressed through a change in MWD (both up and downwave from the WTG locations) combined with a reduction of H_s, while T_p remains almost uninfluenced.
- These local effects in the vicinity of the WTGs, are most pronounced (in terms of H_s magnitude change and in terms of the spatial extent downwave from the foundations) at the shallower locations along the eastern OWF boundary. Secondary these effects

are also noticeable for most considered conditions around the 4 WTG locations closest to the island near the western OWF boundary (namely WTG-6, -8, -9, -20).

- The wave energy decrease at the area beyond the OWF boundary (and downwave relative to wave propagation), is due to the combined effect of wind speed reduction (affecting the local wave energy generation), and depth-induced wave dissipation around the shallowest foundations. Based on the differences in mean wave directions observed (see also Figure 2.32), it is concluded that this observation is also partly due to a rearrangement of wave energy over different directions (further to the north or south relative to the main propagation direction) induced by the wave propagation over a field of local obstructions (i.e., refraction over several localized seabed features that are nevertheless spread over the entire OWF area).
- The effects are hardly noticeable in normal conditions (due to the relative mild conditions for the seabed at) and appear gradually increasing, with increasing severity of considered conditions (i.e., from RP1 to RP50).
- Storms generating waves that approach the OWF from a nearly WSW direction, lead to more severe effects on the wave fields compared to the respective storms with the same frequency approaching from a W direction, as expected from the associated reference extreme values of H_s.
- The observed effects (decrease of wave energy), extend (downwave) into the direction of the coastline for the most severe conditions considered (i.e., RP50), but in all cases the effects are fully contained not more beyond than roughly 3 km from the OWF boundaries (in all directions). This also means that the dedicated domain fully encloses all wave field influences from the operational condition. In other words, areas or output locations that fall within the MPPSA but outside the detailed domain (e.g., along the export cable corridor) are by no means subjected to influences from the OWF operation.
- Slight differences observed far from the OWF and near the coast towards the northern boundary of the MSSP, are more likely due to model artefacts (e.g., potentially driven by small differences between the two compared simulations in wet and drying near the coastal boundaries) rather than actual effects from OWF operation.

4 Conclusions

Xodus Group Ltd is supporting Corio Generation (Fuinneamh Sceirde Teoranta) in their consenting application for the Sceirde (or Skerd) Rocks Offshore Wind Farm (SROWF), envisioned to be built at the Atlantic coast of Ireland, approximately 10 km offshore southwest of Ard, County Galway. For this consenting application, an environmental impact assessment is required to describe the expected effects of the offshore wind farm. To that end, Deltares was requested by Xodus Group Ltd to provide them with hydrodynamic and wave information, based on numerical models developed by Deltares during the metocean study for SROWF (Deltares, 2022) for Corio Generation.

The present study aimed at providing the client with the following information:

- Field plots and timeseries of flow conditions (including water levels and depth-averaged current magnitudes and directions) over a period of one month, namely January 2013 and residual flows over a period of two (2) Spring Neap tidal cycles within the same month.
- Field plots and timeseries of wave conditions (including significant wave heights, peak wave periods and mean wave directions) over events representative of 50th percentile, 90th percentile, 1-, 5-, 10- and 50-year conditions, for the two main approach directions (west and west-southwest), based on the data determined in Deltares (2022).

Abovementioned information is provided for two situations:

- Baseline, i.e., with no offshore wind farm in place and;
- Operational, i.e., with the WTGs in place.

A single offshore wind farm layout (SRL069) and a single GBS foundation design (PDS revision 4, provided on 23 January 2024) was considered for the modelling of the operational conditions, as provided by Xodus Group. The wave and hydrodynamic wave models were validated for the baseline conditions against available observations at the area, and the choices concerning the OWF parameterization were selected based on sensitivity analysis where relevant. It is recommended to revalidate the results of both wave and hydrodynamic numerical models (if possible also for the operational conditions) when additional relevant observations become available in the future.

For the operational situation, the effects of the WTGs are schematised in the employed numerical models, by local changes in the bathymetry due to the WTG foundations (for both hydrodynamic and wave model), by local addition of drag on ambient flow due to the WTG mast (hydrodynamic model) and finally through a wind speed (10%) reduction over the entire wind farm area due to the operation of the WTGs (for both hydrodynamic and wave model).

The wave and hydrodynamic conditions are output at a large number of locations, spread across the greater area of interest, defined by a 15 km buffer (applied as the MPPSA) around the offshore wind farm and the export cable corridor.

Overall, the wind farm effects in terms of differences observed in flow and wave fields between the baseline and operational situation are more pronounced near the direct vicinity of the WTG locations and diminish outside the offshore wind farm area.

In general, wave propagation through the SROWF area is controlled by the steep gradient in bathymetry at the offshore-most boundary of the OWF, and by the complex bathymetry throughout the OWF area. Consequently, the location of the OWF coincides with the onset of

coastal wave propagation (waves influenced by the seabed topography) in baseline conditions.
With respect to influences from the OWF operation on wave fields in the area, the presence of the WTGs leads first to a very local increase of wave energy. This is due to combined refraction and shoaling induced by the large GBS foundation base. This effect is local, i.e., it appears only over a spatial scale in the order of tens of meters and is followed by a reduction of wave energy in a downwave direction. The latter is noticeable up to a distance of roughly 1 km from the WTG locations, and is explained by a change in wave directions (from the wake area of the foundation) and depth-induced wave breaking (dissipation).

Most notably, it is also observed that wave energy reduces over a relatively larger area directly downwave from the offshore wind farm, predominantly due dissipation and a redistribution of wave energy to other directional sectors. This as a cumulative result of refraction occurring around the several WTG locations spread over the OWF area, amplified by wind speed reduction (affecting local wave energy generation) and depth induced wave breaking at the shallowest WTG locations to the east. This effect does not reach the coast, but extends outside the OWF eastern boundary in extreme (storm) conditions. Such effects are barely noticeable in normal conditions and gradually increase with increasing severity of the sea conditions, but remain for the most part of the affected area less than roughly 50 cm in terms of significant wave height difference, compared to the baseline.

Similar to waves, the ambient flow fields are also dictated by the complex local topography within the SROWF area, and especially from the presence of islands and (temporarily) submerged rocky outcrops. Wakes are observed to develop downstream from such features that extend over several times the horizontal dimensions of the respective obstructions.

Concerning effects of the OWF on the flow field, significant changes are observed in the position of the vortices shed downstream from the islands located within the wind farm area. This is due to some WTGs being positioned directly downstream from the islands and hence interfering with the developing wakes. The development of these vortices is also affected by the presence of some WTGs directly upstream from the islands, and hence by their influence on approach flow conditions. Second, the drag exerted by the WTG foundations is clearly noticeable through a reduction of current speeds, which can extend - depending on the location - even to more than 1 km in a downstream direction. It is noted that effects on the flow fields in the simulated conditions are contained within the offshore wind farm area and do not extend (much) further than its boundaries, as opposed to effects on wave fields. Finally, these generally local influences have a relatively limited effect on residual flow patterns (changes less than 0.02 m/s in flow magnitudes) over the considered period of two spring neap cycles, as these are predominantly driven by larger-scale physical processes.

References

Aijaz, S., W.E. Rogers and A. V. Babanin, 2016: Wave spectral response to sudden changes in wind direction in finite-depth waters, Ocean Modelling, 103, 98-117.

Baptist, M. J., Babovic, V., Rodríguez Uthurburu, J., Keijzer, M., Uittenbogaard, R. E., Mynett, A., & Verwey, A. (2007). On inducing equations for vegetation resistance. Journal of Hydraulic Research, 45(4), 435-450.

Battjes, J.A. and H.W. Groenendijk, 2000: Wave height distributions on shallow foreshores, Coastal Engineering. 40, 161-182.

Battjes, J. A., and J. P. F. M. Janssen, 1978: Energy loss and set-up due to breaking of random waves, Coastal Engineering 1978 (pp. 569–588), Am. Soc. of Civ. Eng., New York.

Charnock, H., 1955: Wind stress on a water surface. Q. J. R. Meteorol. Soc., 81, 639-640.

Deltares, 2019: Development of a sixth-generation model for the NW European Shelf (DCSM-FM 0.5nm), https://publications.deltares.nl/11203715_004.pdf.

Deltares, 2022: Skerd Rocks offshore wind farm metocean study; Final report: 11208193-002-HYE-0001_v3-Skerd Rocks offshore wind farm metocean study.pdf.

Hasselmann, K., T.P. Barnett, E. Bouws, H. Carlson, D.E. Cartwright, K. Enke, J.A. Ewing, H. Gienapp, D.E. Hasselmann, P. Kruseman, A. Meerburg, P. Mller, D.J. Olbers, K. Richter, W. Sell, and H. Walden, 1973: Measurements of wind-wave growth and swell decay during the Joint North Sea Wave Project (JONSWAP). Ergnzungsheft zur Deutschen Hydrographischen Zeitschrift Reihe, A(8), Nr. 12, p.95.

Hoerner, S. F. (1965). Fluid-Dynamic Drag. Theoretical, experimental and statistical information. Copyright by: SF Hoerner Fluid Dynamics, Vancouver, printed in the USA, Card Number 64-19666.

Jelavic, M., Petrovic, V., Barišic, M., & Ivanovic, I. (2013, February). Wind turbine control beyond the cut-out wind speed. In Annual Conference and Exhibition of European Wind Energy Association (EWEA2013).

Komen, G. J., L. Cavaleri, M. Donelan, K. Hasselmann, S. Hasselmann and P. A. E. M. Janssen, 1994: Dynamics and Modelling of Ocean Waves. Academic Press.

Markou, H., & Larsen, T. J. (2009). Control strategies for operation of pitch regulated turbines above cut-out wind speeds. In 2009 European Wind Energy Conference and Exhibition, EWEC (pp. 16-19).

Rogers, W.E., P.A. Hwang, and D.W. Wang. 2003: Investigation of wave growth and decay in the SWAN model: three regional-scale applications, J. Phys. Oceanogr., 33, 366-389.

Rogers, W.E., A.V. Babanin, and D.W. Wang, 2012: Observation-consistent input and whitecapping-dissipation in a model for wind-generated surface waves: Description and simple calculations. J. Atmos. Ocean. Technol. 29, 1329- 1346.

Van der Westhuysen, A. J., M. Zijlema and J.A. Battjes, 2007: Nonlinear saturation-based whitecapping dissipation in SWAN for deep and shallow water. Coastal Engineering, 54, 151–170.

Van Duren, L. A., F. Zijl, T. Van Kessel, V. T. M. van Zelst, L. M. Vilmin, J. Van der Meer, G. M. Aarts, J. van der Molen, K. Soetaert, and A. W. Minns. "Ecosystem effects of large upscaling of offshore wind on the North Sea-Synthesis report." (2021).

Van Os, J. and S. Caires, 2011: How to Carry out metocean studies. Proc. 30th Int. Conf. on Offshore Mechanics and Arctic Eng. (OMAE2011-49066).

WAMDI group, 1988: The WAM model - a third generation ocean wave prediction model, J. Phys. Oceanogr., 18, 1775-1810.

Wiegant, E., & Verzijlbergh, R. (2019). GRASP model description & validation report.

Wu, J., 1982: Wind-stress coefficients over sea surface from breeze to hurricane, J. Geophys. Res., 87 (C12), 9704-9706.

Zijlema, M., G.Ph. van Vledder and L.H. Holthuijsen, 2012: Bottom friction and wind drag for wave models. Coastal Engineering, 65, 19-26.

Appendices

A Validation of water levels in Deltares (2022)

For reference, the validation of water levels over the entire measurement period based on the 43-year hydrodynamic hindcast timeseries generated in Deltares (2022) is presented here, in support of the validation performed in the present study, employing essentially the same hydrodynamic model but over a shorter period of 1 month.

Table A.1 Overview over all the statistics done by comparing the observed water level data with the modelled one over the periods mentioned in Table 2.2

Station	Period	Correlation coefficient, ρ (-)	Bias correction value (m)	RMSE (m)
		Galway Port		
(a)	Jan/2008 – Jan/2009	0.995	-0.033	0.114
(b)	Jan/2010 - Jan/2013	0.996	-0.052	0.114
(c)	Jan/2014 - Jan/2018	0.994	-0.053	0.137
(d)	Jan/2019 - Jan/2022	0.995	-0.039	0.127
		Inishmore		
(a)	Jan/2008 – Jan/-2010	0.997	0.070	0.089
(b)	Jan/2019 - Jan/2022	0.997	-0.041	0.084

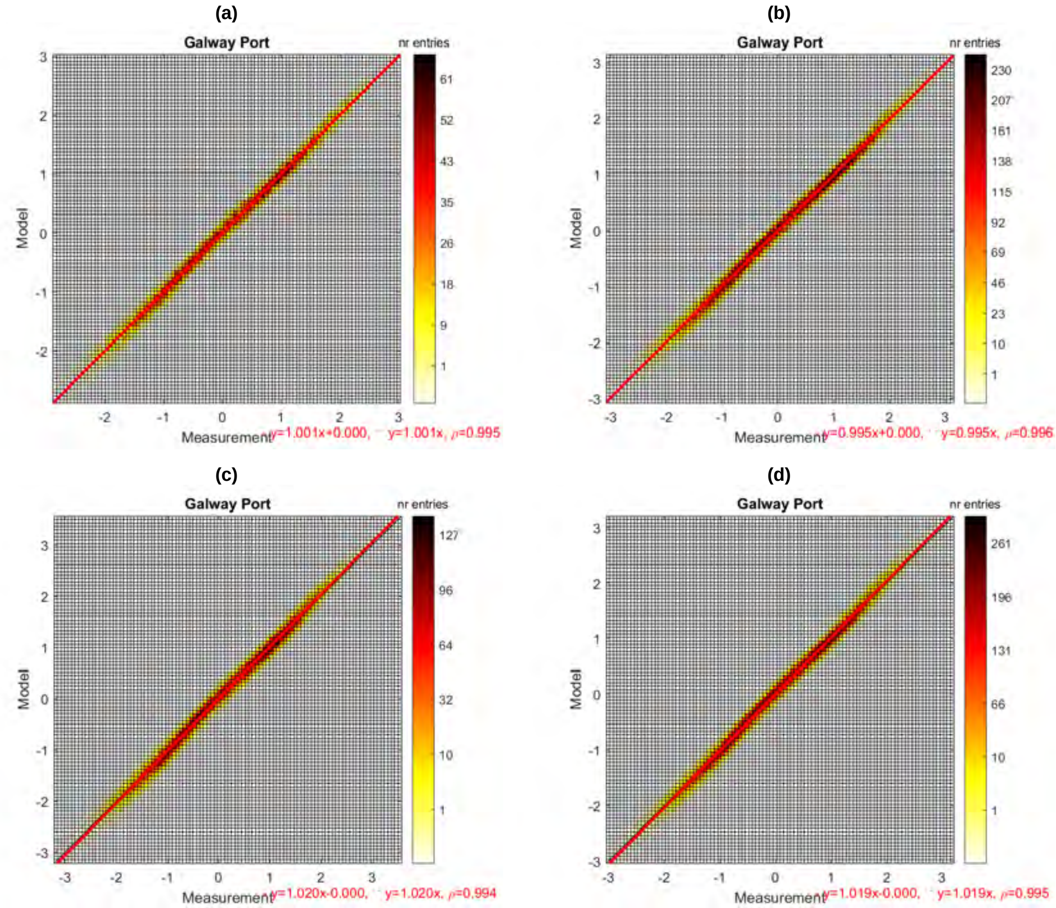

Figure A.1 Water level density scatter comparisons for The Galway Port station observation and the model data. The symmetric fit to the data is given by the red dotted line. Only the correlation coefficient and the best fit formulas of the comparisons are printed. Letters a, b, c, and d corresponds to the letters in Table A.1.

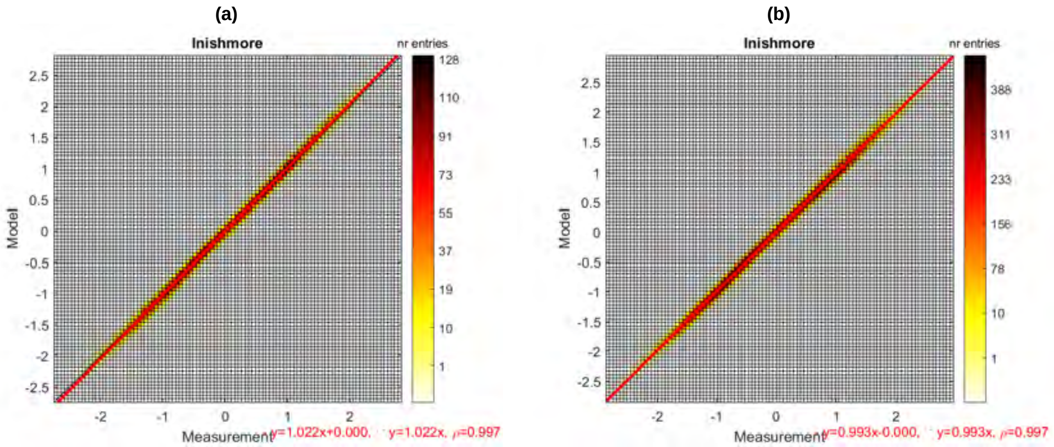

Figure A.2 Water level density scatter comparisons for The Inishmore station observation and the model data. The symmetric fit to the data is given by the red dotted line. Only the correlation coefficient and the best fit formulas of the comparisons are printed. Letters a and b corresponds to the letters in Table A.1.

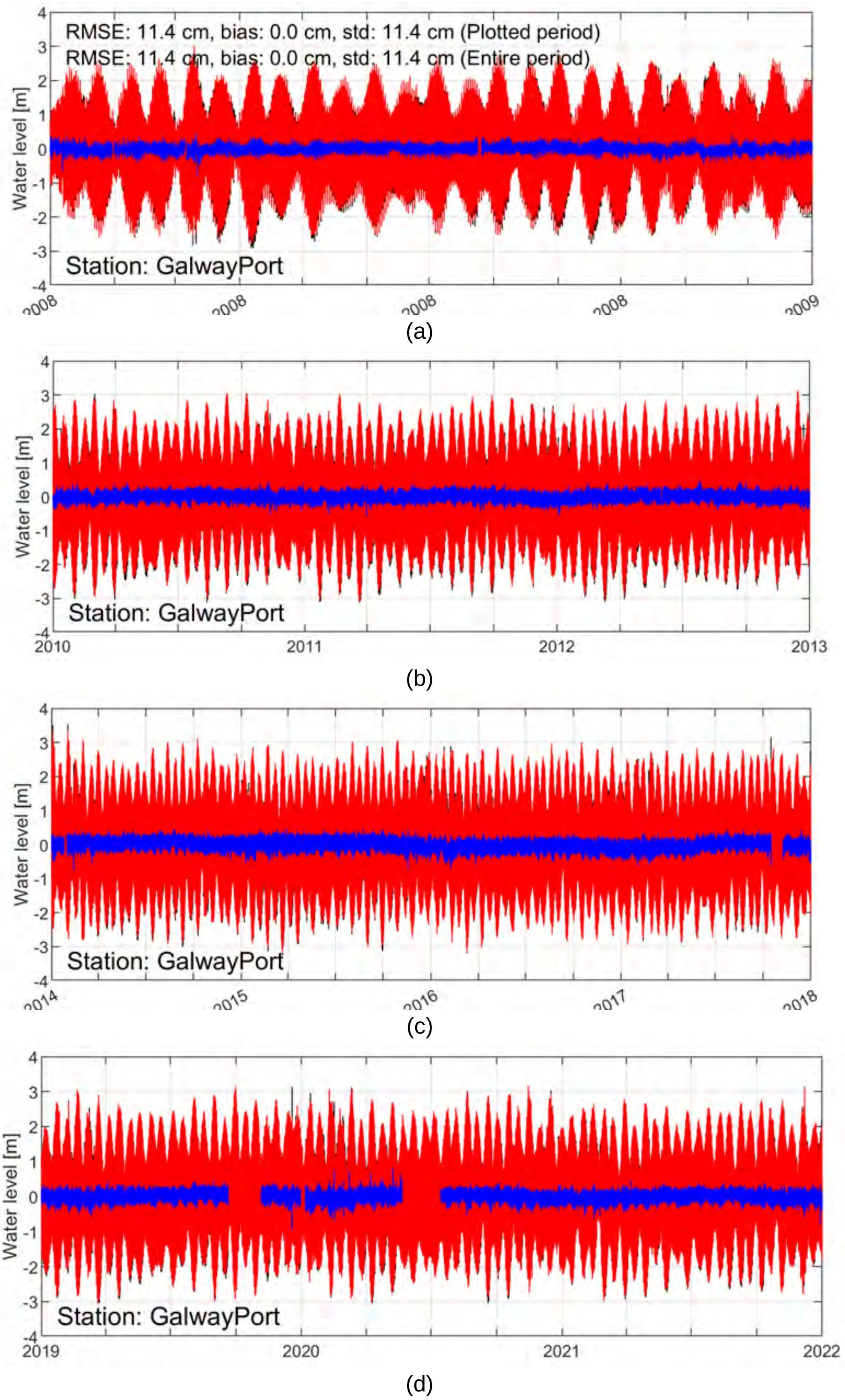

Figure A.3 Timeseries comparison of the observed and modelled water levels data at Galway Port. Black lines (in the background) indicate the observed data, red lines (on top) the modelled data and blue lines the difference between the two, the latter being typically less 0.2 m in absolute terms. See also Table 2.2 and Table A.1. The observed water level peaks are typically only marginally lower (in absolute terms) than the modelled, as also indicated by the density scatter plots.

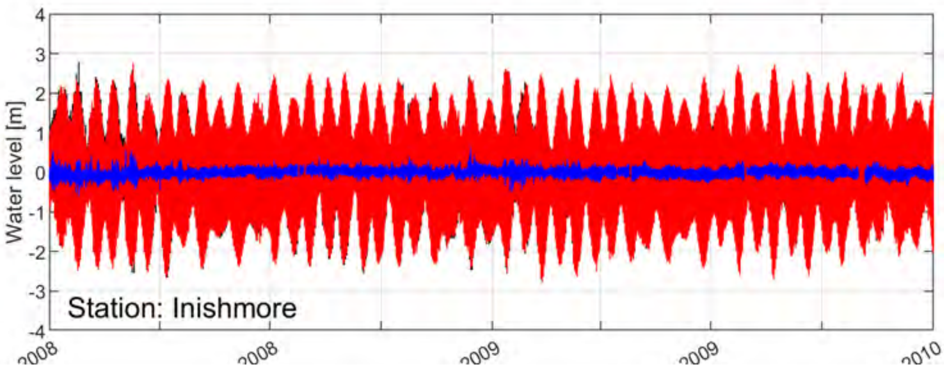

(a)

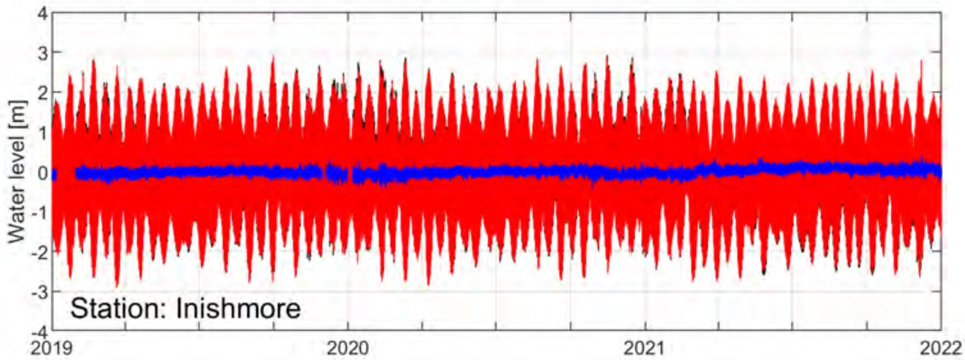

(b)

Figure A.4 Timeseries comparison of the observed and modelled water levels data at Inishmore station. Black lines (in the background) indicate the observed data, red lines (on top) the modelled data and blue lines the difference between the two, the latter being typically less 0.2 m in absolute terms. See also Table 2.2 and Table A.1. The observed water level peaks are typically only marginally lower (in absolute terms) than the modelled, as also indicated by the density scatter plots.

B Error statistics

B.1 Introduction

A particularity of certain environmental data (e.g. wave data) is that they can be classified into *linear data* (*e.g.* mean wave period and significant wave height) and *circular data* (*e.g.* mean wave direction and directional spread), and this distinction must be taken into consideration when carrying out error analysis (Van Os and Caires, 2011). The statistical techniques for dealing with these two types of data are different – circular (or directional) data require a special approach. Basic concepts of statistical analysis of circular data are given in the books of Mardia (1972) and Fisher (1993).

B.2 Linear variables

Differences between linear variables are often quantified using the following standard statistics:

- the bias: $\bar{y}-\bar{x}$;
- the root-mean-square error: $RMSE=\sqrt{n^{-1}\sum(y_i-x_i)^2}$;
- the scatter index: $SI=\sqrt{n^{-1}\sum\left[(y_i-\bar{y})-(x_i-\bar{x})\right]^2}\Big/\bar{x}$;
- the standard deviation: $\sigma=\sqrt{n^{-1}\sum[(y_i-\bar{y})(x_i-\bar{x})]^2}$
- the correlation coefficient: $\rho=\frac{\sum[(x_i-\bar{x})(y_i-\bar{y})]}{\sqrt{\sum(x_i-\bar{x})^2\sum(y_i-\bar{y})^2}}$;
- the symmetric slope: $r=\sqrt{\sum x_i^2/\sum y_i^2}$.

In all these formulae x_i usually represents observations (or the dataset which is considered less uncertain or baseline), y_i represents the model results (or the dataset which is considered more uncertain or with a certain deviation from the baseline results) and n the number of observations. Is this study, when trying to derive calibration expressions, x_i corresponds to the model results.

B.3 Circular variables

If we compute an average of angles as their arithmetic mean, we may find that the result is of little use as a statistical location measure. Consider for instance the case of two angles of 359º and 1º; their arithmetic mean is 180º, when in reality 359º is only two degrees away from 1º and the mid direction between the two is 0º. This phenomenon is typical for circular data and illustrates the need for special definitions of statistical measures in general.

When dealing with circular data, each observation is considered as unit vector, and it requires vector addition rather than ordinary (or scalar) addition to compute the average of angles, the so-called mean direction.

Writing

$$C_n = \sum_{i=1}^{n} cos\, x_i \quad \text{and} \quad S_n = \sum_{i=1}^{n} sin\, x_i, \qquad (1)$$

the *sample resultant vector* R_n of a sample $\boldsymbol{x}$ ={$x_i, i = 1, \ldots, n$} is defined as

$$R_n = \sqrt{C_n^2 + S_n^2},$$

and its *sample mean direction* $\bar{x} \equiv \bar{x}_n$ as the direction of R_n:

$$\bar{x} = TAN^{-1}(S_n/C_n) \qquad (2)$$

where $TAN^{-1}(S_n/C_n)$ is the inverse of the tangent of (S_n/C_n) in the range [0,2π[, *i.e.*,

$$TAN^{-1}(\frac{S_n}{C_n}) := \begin{cases} tan^{-1}(\frac{S_n}{C_n}), & S_n > 0, \quad C_n > 0 \\ tan^{-1}(\frac{S_n}{C_n}) + \pi, & C_n < 0 \\ tan^{-1}(\frac{S_n}{C_n}) + 2\pi, & S_n < 0, \quad C_n > 0 \end{cases}$$

The *sample mean resultant length* of $\boldsymbol{x}$ ={$x_i, i = 1, \ldots, n$} is defined by

$$\bar{R}_n = R_n/n, \; 0 < \bar{R}_n < 1$$

If $\bar{R}_n = 1$, then all angles coincide.

Eq. (2) can be used to compute the bias between two circular variables by substituting x_i by $y_i - x_i$ in Eq. (1). In a similar way, the root-mean-square error and standard deviation between two circular variables can be computed.

Since circular data are concentrated on [0°, 360°], and in spite of the analogies with the linear case, it makes no sense to consider a symmetric slope for circular data other than one.

There are several circular analogues of the correlation coefficient, but the most widely used is the one proposed by Fisher and Lee (1983), the so-called *T*-linear correlation coefficient. Given two sets x ={$x_i, i = 1, \ldots, n$}, $\boldsymbol{y}$ ={$y_i, i = 1, \ldots, n$} of circular data, the *T-linear correlation coefficient* between x and $\boldsymbol{y}$ is defined by

$$\rho_T = \frac{\sum_{1 \le i < j \le n} sin(x_i - x_j)\, sin(y_i - y_j)}{\sqrt{\sum_{1 \le i < j \le n} sin^2(x_i - x_j) \sum_{1 \le i < j \le n} sin^2(y_i - y_j)}}.$$

This statistic satisfies $-1 \le \rho_T \le 1$, and its population counterpart (which is not given here but can be seen in Fisher and Lee, 1983) satisfies properties analogous to those of the usual population correlation coefficient for linear data: that is, the population counterpart achieves the extreme values -1 and 1 if and only if the two population variables involved are exactly '*T*-linear associated', with the sign indicating discordant or concordant rotation, respectively (see Fisher (1993), p. 146, for these concepts).

For computational ease, we use an equivalent formula for ρ_T, given by Fisher (1993):

$$\rho_T = \frac{4(AB - CD)}{\sqrt{(n^2 - E^2 - F^2)}\sqrt{(n^2 - G^2 - H^2)}},$$

where

$A = \sum_{i=1}^{n} cos\, x_i\, cos\, y_i$, $B = \sum_{i=1}^{n} sin\, x_i\, sin\, y_i$,

$C = \sum_{i=1}^{n} cos\, x_i\, sin\, y_i$, $D = \sum_{i=1}^{n} sin\, x_i\, cos\, y_i$,

$E = \sum_{i=1}^{n} cos(\,2x_i)$, $\quad F = \sum_{i=1}^{n} sin(\,2x_i)$,

$G = \sum_{i=1}^{n} cos(\,2y_i)$, $\quad H = \sum_{i=1}^{n} sin(\,2y_i)$.

B.4 References

Fisher, N.I., 1993. Statistical analysis of circular data. Cambridge Univ. Press, 277 pp.

Fisher, N.I. and A.J. Lee, 1983. A correlation coefficient for circular data. Biometrika, 70, pp. 327-32.

Mardia, K.V., 1972. Statistics of directional data. Academic Press, (London and New York).

Van Os, J. and S. Caires, 2011: How to Carry out metocean studies. Proc. 30th Int. Conf. on Offshore Mechanics and Arctic Eng. (OMAE2011-49066).

C Description of SWAN

C.1 General

SWAN is the state-of-the-art third generation shallow water phase-averaging wave model (Booij et al, 1999) SWAN has been developed at the Delft University of Technology (e.g., Van der Westhuysen, 2010 and Zijlema, 2010) with contributions by Deltares. It computes wave propagation and wave energy evolution efficiently and accurately and it describes several non-linear effects via parameterised formulations. More specifically, SWAN can account for several wave propagation phenomena, including (only the most relevant for the present project mentioned):

- Wave propagation in time and space, shoaling[21], refraction[22] due to current and depth, frequency shifting due to currents and non-uniform depth;
- Wave generation by wind;
- Three- and four-wave interactions[23];
- Energy dissipation by: white-capping, bottom friction and depth-induced breaking.

Whitecapping is the phenomenon that waves show foam effects at the wave crests due to dissipation of wave energy. It is sometimes called deep-water wave breaking, as opposite to shallow-water wave breaking that can be observed at the beach (depth-induced breaking). Bottom friction causes dissipation of wave energy when the waves are long enough to be influenced by the roughness of the sea bed while propagating. At shallow depths and for longer wave periods bed friction has the largest influence.

Furthermore, SWAN computations can be made on a regular, a curvi-linear grid and a triangular mesh in a Cartesian or spherical co-ordinate system. Nested runs, using input, namely two-dimensional wave spectra, from other (larger scale) models can be made with SWAN.

The SWAN model has been validated and verified successfully under a variety of field cases and is continually undergoing further development. It sets today's standard for nearshore wave modelling.

For more information on SWAN, reference is made to http://swanmodel.sourceforge.net/online_doc/online_doc.htm from where the SWAN scientific/technical documentation and used manual can be downloaded.

In short, the model solves the action balance equation, in Cartesian or spherical coordinates, without any ad hoc assumption on the shape of the wave spectrum. In Cartesian coordinates the equation is

$$\frac{\partial N}{\partial t}+\frac{\partial}{\partial x}\left(c_x N\right)+\frac{\partial}{\partial y}\left(c_y N\right)+\frac{\partial}{\partial \sigma}\left(c_\sigma N\right)+\frac{\partial}{\partial \theta}\left(c_\theta N\right)=\frac{S_{tot}}{\sigma}, \qquad (3)$$

---

[21] Shoaling is the steepening of waves as they approach the coast and reach shallower water. This increases the energy density of the waves, leading to an increase in wave height.

[22] Refraction is the effect that (non-uniform) bed levels have on the propagation direction of waves.

[23] Multiple wave components at different frequencies can interact (in deeper water 4 components, in shallow water 3), leading to a redistribution of wave energy over different wave frequencies. Since it causes energy transfer between components/frequencies these are non-linear processes.

where N is the action density, *t* is the time, σ is the relative angular frequency, and θ the wave direction. The first term on the left-hand side of Eq. (3) represents the local rate of change of action density in time. The second and third terms represent propagation of action in geographical space. The fourth term represents shifting of the relative frequency due to variation in depth and currents. The fifth term represents depth-induced and current-induced refractions. The quantities c_x, c_y, c_θ and c_σ are the propagation speeds in the geographical x- and y-space, and in the θ- and the σ-space, respectively. The expressions of these propagation speeds are taken from linear wave theory. In Eq. (3) S_{tot} is the energy source term. This source term is the sum of separate source terms representing different types of processes: wave energy growth by wind input, wave energy transfer due to non-linear wave-wave interactions (both quadruplets and triads), and the decay of wave energy due to whitecapping, bottom friction, and depth induced wave breaking. For some source terms more than one formulation is implemented in SWAN, see http://swanmodel.sourceforge.net/online_doc/online_doc.htm.

C.2 Drag coefficient

In SWAN the input 10-m wind speeds are converted to surface stress using the drag coefficient. There are two options in SWAN for the drag coefficient parameterization,

1. the drag coefficient from Wu (1982), which corresponds to a roughness of a standard Charnock relation (1955) Charnock with a Charnock parameter of 0.0185 and which is given by the dashed red line in Figure C.1.
2. an approximation of Zijlema et al. (2012) which accounts for a decrease of the drag for wind speeds above 31.5 m/s and which is given by the full red line in Figure C.1.

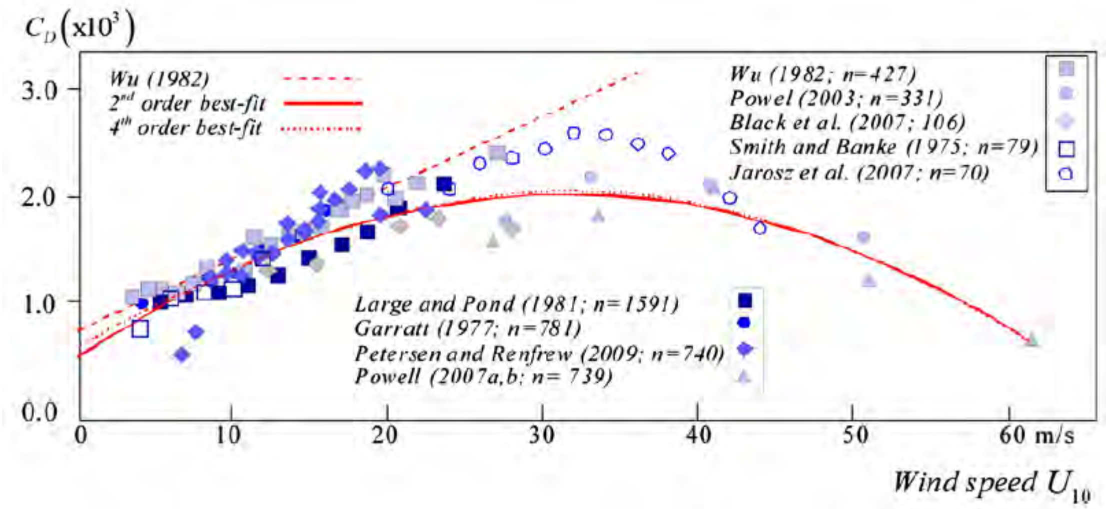

Figure C.1 Observed values of the wind drag coefficient (Cd) from various studies and the weighted best-fit 2nd and 4th-order polynomial (n is the number of independent data points per study). Figure taken from of Zijlema et al. (2012).

In this study the approximation of Wu (1982) is applied.

C.3 Whitecapping

Because it is relevant for the settings that have been chosen for the model, a more detail description of the available options for the modelling of wave growth and whitecapping is given.

SWAN's original formulation of dissipation by whitecapping is based on the pulse-based model of Hasselmann (1974), as adapted by the WAMDI group (1988):

$$S_{wcap}(\sigma,\theta) = -\Gamma\,\bar{\sigma}\frac{k}{\bar{k}}E(\sigma,\theta)\ ,$$

where

$$\Gamma = C_{ds}\left((1-\delta)+\delta\frac{k}{\bar{k}}\right)\left(\frac{\bar{s}}{\bar{s}_{PM}}\right)^4 ,$$

and which can also be written as

$$S_{wcap}(\sigma,\theta) = C_{ds}\left(\frac{\bar{s}}{\bar{s}_{PM}}\right)^4 \bar{\sigma}\left(\frac{k}{\bar{k}}\right)^n E(\sigma,\theta)\ , \qquad (4)$$

a bar over a variable denotes its mean, *k* is the wavenumber, and *s* the wave steepness. The remaining parameters in Γ depend on the wind input formulation that is used and are determined by closing the energy balance of the waves in fully developed conditions.

In SWAN the following options are available:

- For situations in which the formulation recommended Komen et al. (1984) is used,
- δ=0, n=1 (default until SWAN version 40.85).
- For situations in which the formulation recommended by Rogers et al. (2003) is used:
- δ=1, n=2 (default since SWAN version 40.91).
- For situations in which the formulation recommended by Janssen (1991) is used
- δ=0.5, n≈1.5.

For *n*=1 the right hand side of Eq. (4) is proportional to $\frac{k}{\bar{k}}$. Increasing the parameter *n* above 1 has the effect of reducing dissipation at lower frequencies while increasing dissipation at higher frequencies, resulting in relatively more low frequency wave energy and larger wave periods. In this study the formulation recommended by Rogers et al. (2003), δ=1 and n=2, is applied.

In addition to these formulations based on Eq. (4), two extra formulations have been implemented in SWAN:

- the one suggested by Van der Westhuysen et al., 2007 and referred to as the Westhuysen formulation; and the
- the one suggested by Rogers et al. (2012) and referred to as the ST6 (as it is referred to in Source Term package of the WAVEWATCH III® model) formulation.

The Westhuysen formulation is not based as those described using Eq. B.4 on the average wave number $\bar{k}$ and does, therefore, not lead to an overestimation of dissipation of wind sea when just a little swell is present.

In the ST6 formulation models the wave breaking in two phases and with waves not breaking unless the spectral density, $E(f)$, exceeds a threshold spectral density, $E_T(f)$, calculated from the spectral saturation spectrum (Rogers et al., 2012, Eq. (5)), with

$$S_{wcap}(\sigma,\theta) = -\left[T_1(\sigma,\theta) + T_2(\sigma,\theta)\right] E(\sigma,\theta)$$

where

$T_1(k) = a_1 \gamma_1^{p_1}$ is the inherent term,

$T_2(k) = a_2 \int_{f'}^{f} \gamma_2^{p_2} df'$ accounts for the cumulative effect of (shorter) wave dissipation due to the breaking of longer waves,

$$\gamma_1 = \frac{\Delta(f)}{\tilde{E}(f)}, \ \gamma_2 = \frac{\Delta(f')}{\tilde{E}(f')}, \Delta(f) = E(f) - E_T(f),$$

$\tilde{E}$ is a normalizing generic spectral density and a_1, a_2, p_1 and p_2 are tuneable coefficients (Aijaz et al., 2016).

C.4 Numerics

As to SWAN's numerical approach, the integration of the propagation and of the source terms of Eq. (3) has been implemented with finite difference schemes in all four dimensions (geographical space and spectral space). A constant time increment is used for the time integration. The model propagates the wave action density of all components of the spectrum across the computational area using implicit schemes in geographical and spectral space, supplemented with a central approximation in spectral space. In geographical space the scheme is upwind and applied to each of the four directional quadrants of wave propagation in sequence. Three of such schemes are available in SWAN: a first-order backward space, backward time (BSBT) scheme, a second-order upwind scheme with second order diffusion (the SORDUP scheme) and a second order upwind scheme with third order diffusion (the S&L scheme). The numerical schemes used for the source term integration are essentially implicit. In order to match physical scales at relatively high frequencies and to ensure numerical stability at relatively large time steps, a limiter controlling the maximum total change of action density per iteration at each discrete wave component is imposed. The BSBT scheme is applied in this study.

D Current velocity and water level fields

It is noted that for baseline water level and current speed values less than 0.1 m and m/s respectively, no relative differences are computed. These locations are included within the white band of the colormap applied in the relative difference plots.

D.1 EN currents

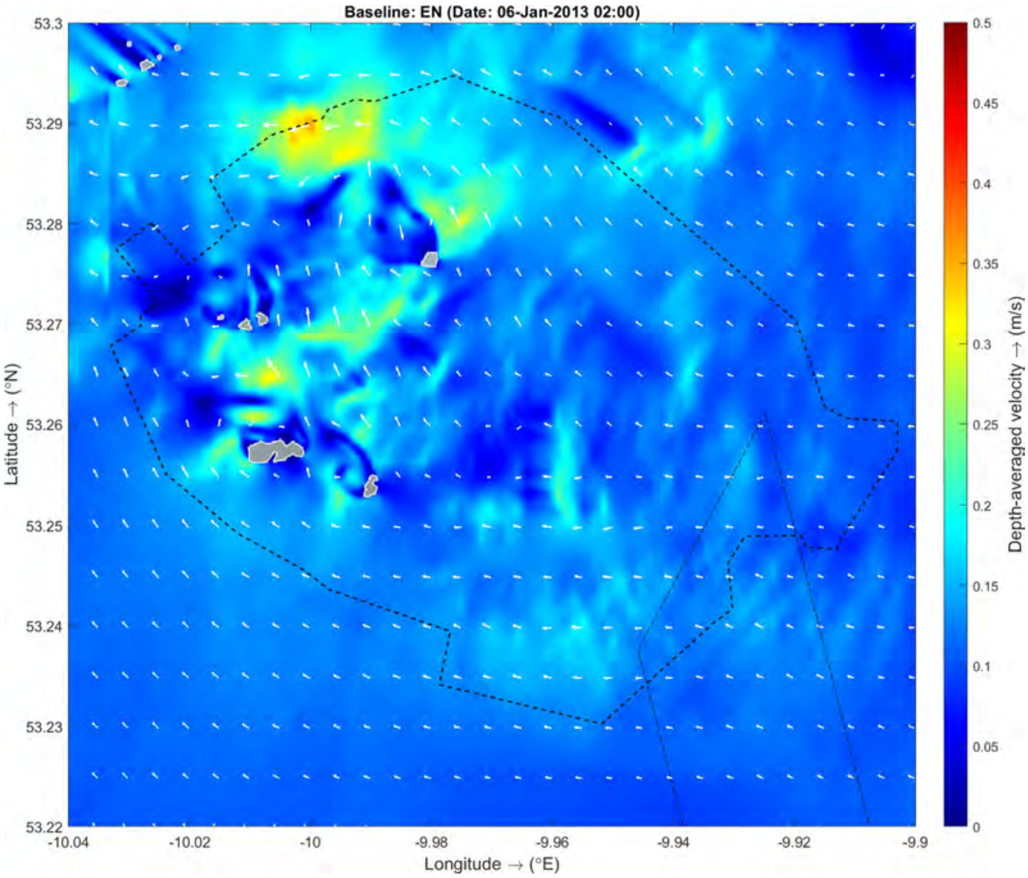

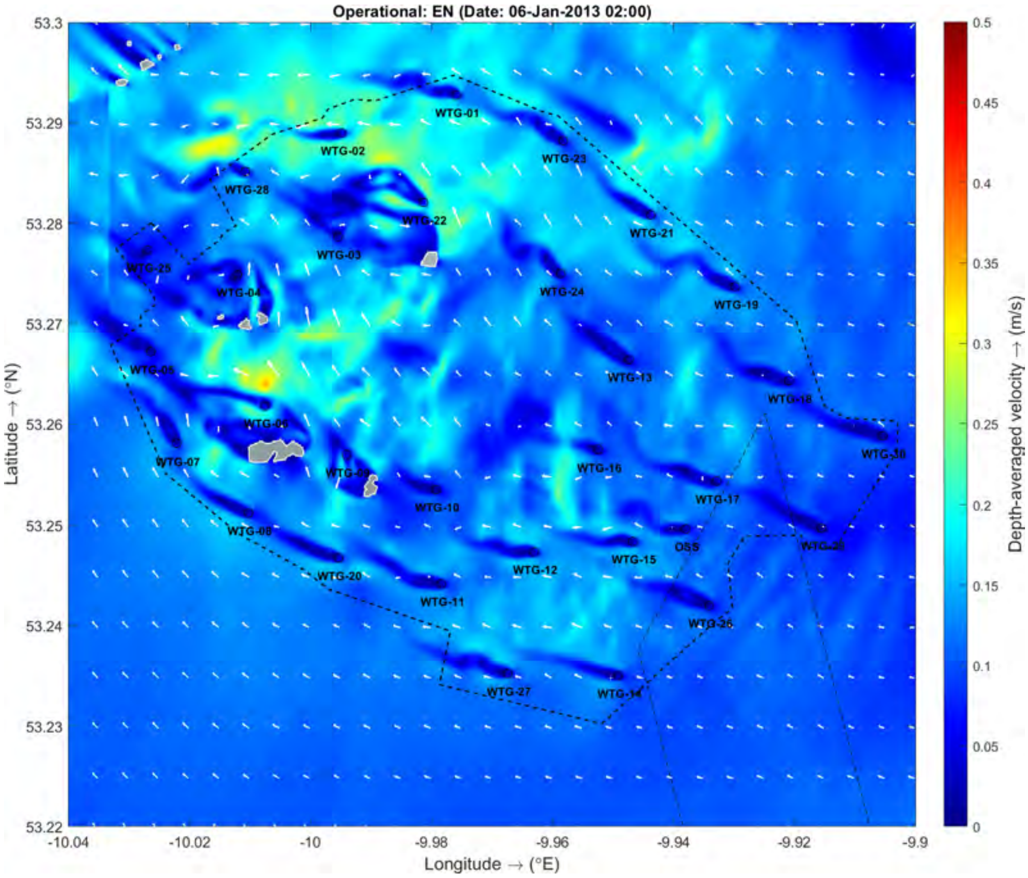

Operational: EN (Date: 06-Jan-2013 02:00)
Latitude → (°N)
Longitude → (°E)
Depth-averaged velocity → (m/s)
53.3
53.29
53.28
53.27
53.26
53.25
53.24
53.23
53.22
-10.04
-10.02
-10
-9.98
-9.96
-9.94
-9.92
-9.9
0
0.05
0.1
0.15
0.2
0.25
0.3
0.35
0.4
0.45
0.5
WTG-01
WTG-02
WTG-28
WTG-22
WTG-03
WTG-23
WTG-21
WTG-24
WTG-19
WTG-04
WTG-13
WTG-18
WTG-07
WTG-16
WTG-17
WTG-10
WTG-08
WTG-15
OSS
WTG-12
WTG-20
WTG-11
WTG-27

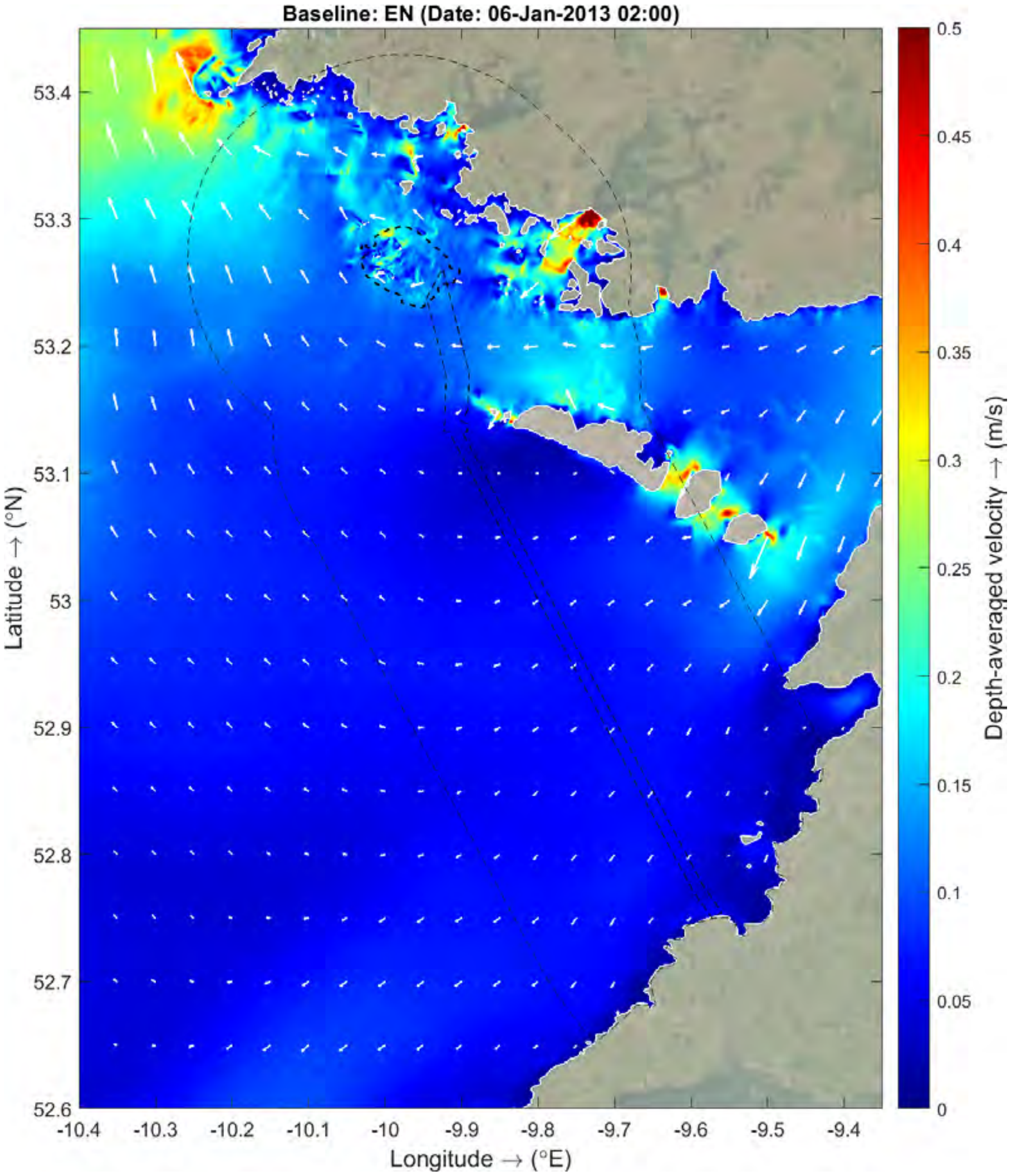
Baseline: EN (Date: 06-Jan-2013 02:00)
53.4
53.3
53.2
53.1
53
52.9
52.8
52.7
52.6
Latitude → (°N)
-10.4
-10.3
-10.2
-10.1
-10
-9.9
-9.8
-9.7
-9.6
-9.5
-9.4
Longitude → (°E)
0.5
0.45
0.4
0.35
0.3
0.25
0.2
0.15
0.1
0.05
0
Depth-averaged velocity → (m/s)

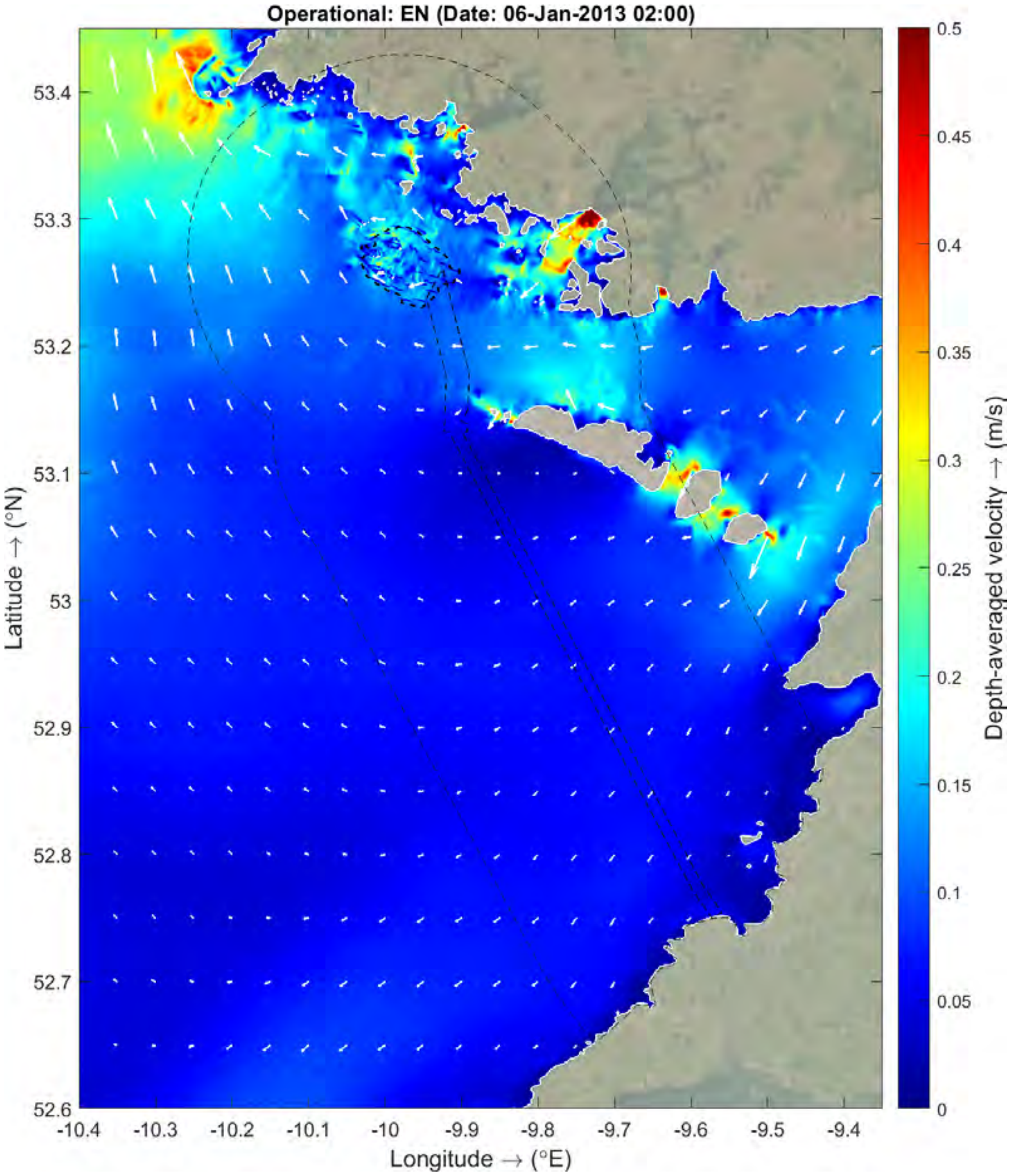
Operational: EN (Date: 06-Jan-2013 02:00)
Latitude → (°N)
Longitude → (°E)
Depth-averaged velocity → (m/s)
53.4
53.3
53.2
53.1
53
52.9
52.8
52.7
52.6
-10.4
-10.3
-10.2
-10.1
-10
-9.9
-9.8
-9.7
-9.6
-9.5
-9.4
0.5
0.45
0.4
0.35
0.3
0.25
0.2
0.15
0.1
0.05
0

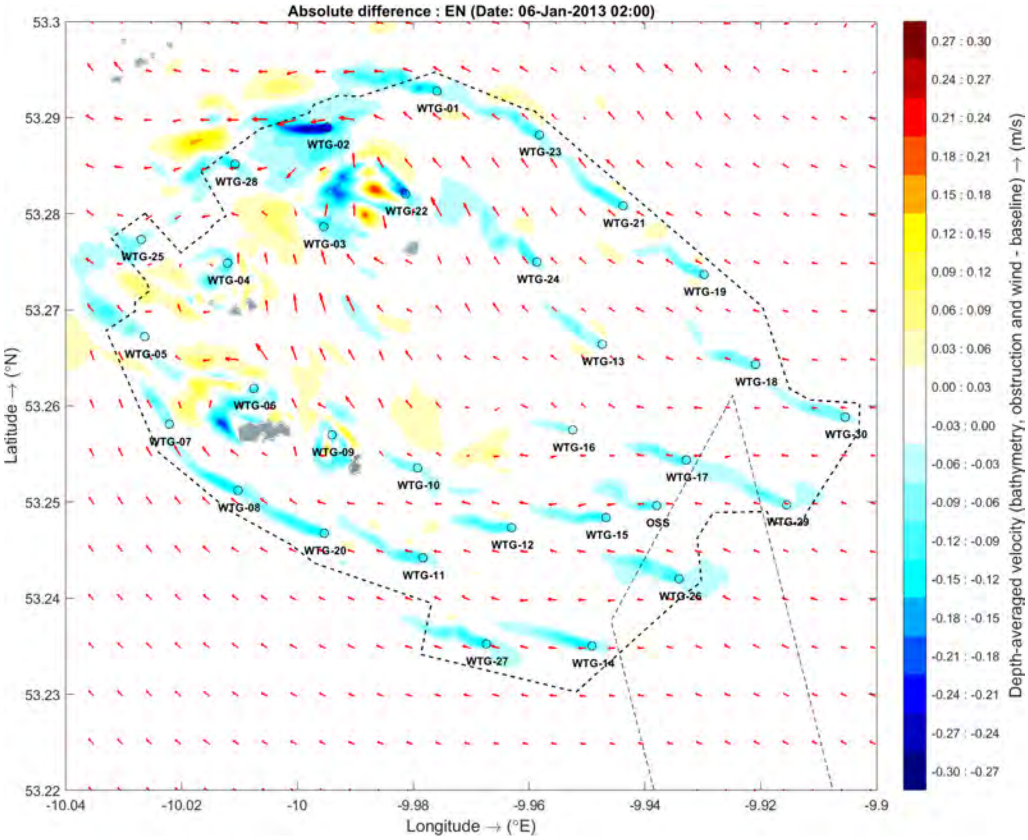
Absolute difference : EN (Date: 06-Jan-2013 02:00)
Latitude → (°N)
Longitude → (°E)
Depth-averaged velocity (bathymetry, obstruction and wind - baseline) → (m/s)
WTG-01
WTG-02
WTG-03
WTG-04
WTG-05
WTG-06
WTG-07
WTG-08
WTG-09
WTG-10
WTG-11
WTG-12
WTG-13
WTG-14
WTG-15
WTG-16
WTG-17
WTG-18
WTG-19
WTG-20
WTG-21
WTG-22
WTG-23
WTG-24
WTG-25
WTG-26
WTG-27
WTG-28
WTG-29
WTG-30
OSS
0.27 : 0.30
0.24 : 0.27
0.21 : 0.24
0.18 : 0.21
0.15 : 0.18
0.12 : 0.15
0.09 : 0.12
0.06 : 0.09
0.03 : 0.06
0.00 : 0.03
-0.03 : 0.00
-0.06 : -0.03
-0.09 : -0.06
-0.12 : -0.09
-0.15 : -0.12
-0.18 : -0.15
-0.21 : -0.18
-0.24 : -0.21
-0.27 : -0.24
-0.30 : -0.27

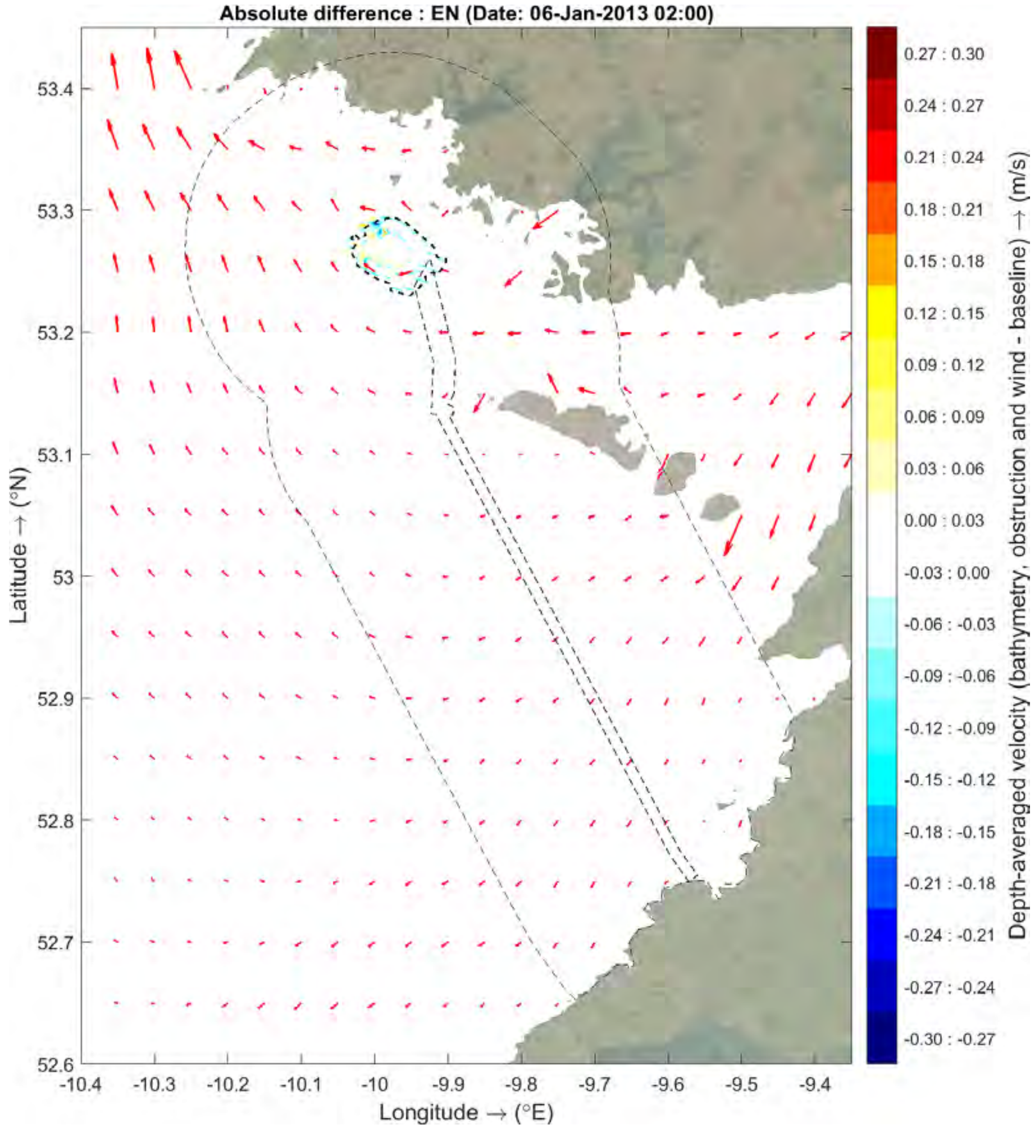
Absolute difference : EN (Date: 06-Jan-2013 02:00)
53.4
53.3
53.2
53.1
53
52.9
52.8
52.7
52.6
Latitude → (°N)
-10.4
-10.3
-10.2
-10.1
-10
-9.9
-9.8
-9.7
-9.6
-9.5
-9.4
Longitude → (°E)
0.27 : 0.30
0.24 : 0.27
0.21 : 0.24
0.18 : 0.21
0.15 : 0.18
0.12 : 0.15
0.09 : 0.12
0.06 : 0.09
0.03 : 0.06
0.00 : 0.03
-0.03 : 0.00
-0.06 : -0.03
-0.09 : -0.06
-0.12 : -0.09
-0.15 : -0.12
-0.18 : -0.15
-0.21 : -0.18
-0.24 : -0.21
-0.27 : -0.24
-0.30 : -0.27
Depth-averaged velocity (bathymetry, obstruction and wind - baseline) → (m/s)

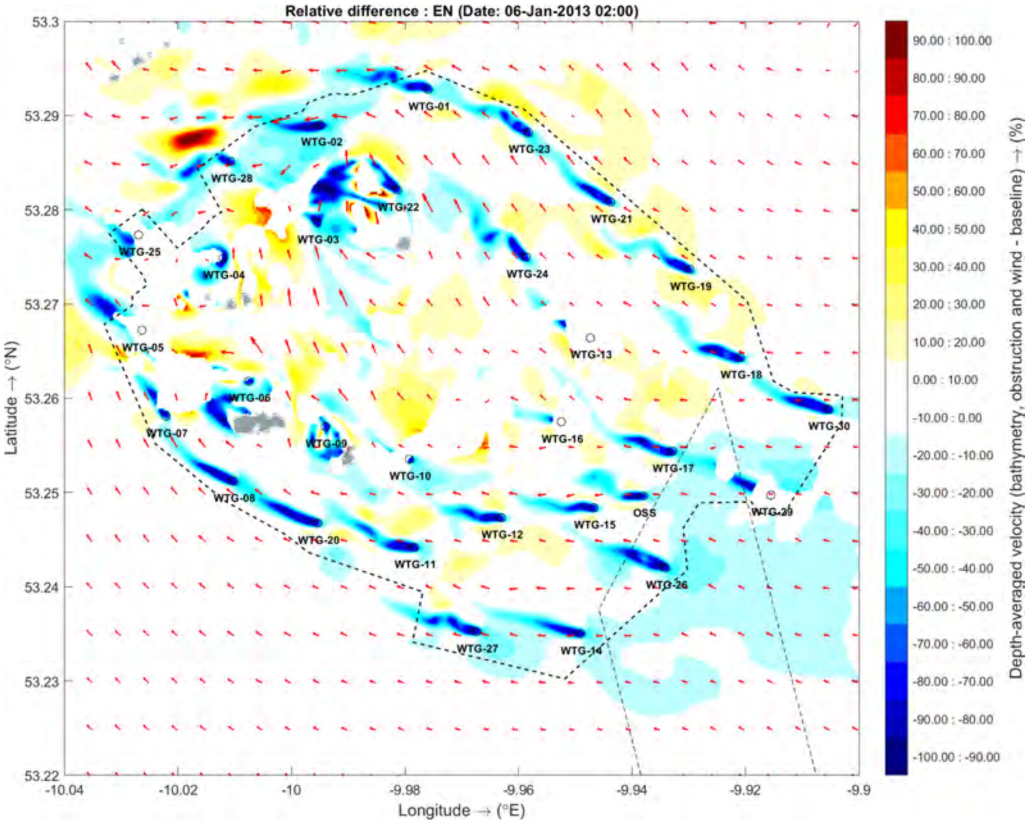
Relative difference : EN (Date: 06-Jan-2013 02:00)
Latitude → (°N)
Longitude → (°E)
Depth-averaged velocity (bathymetry, obstruction and wind - baseline) → (%)
90.00 : 100.00
80.00 : 90.00
70.00 : 80.00
60.00 : 70.00
50.00 : 60.00
40.00 : 50.00
30.00 : 40.00
20.00 : 30.00
10.00 : 20.00
0.00 : 10.00
-10.00 : 0.00
-20.00 : -10.00
-30.00 : -20.00
-40.00 : -30.00
-50.00 : -40.00
-60.00 : -50.00
-70.00 : -60.00
-80.00 : -70.00
-90.00 : -80.00
-100.00 : -90.00
WTG-01
WTG-02
WTG-03
WTG-04
WTG-05
WTG-06
WTG-07
WTG-08
WTG-09
WTG-10
WTG-11
WTG-12
WTG-13
WTG-14
WTG-15
WTG-16
WTG-17
WTG-18
WTG-19
WTG-20
WTG-21
WTG-22
WTG-23
WTG-24
WTG-25
WTG-26
WTG-27
WTG-28
WTG-29
WTG-30
OSS

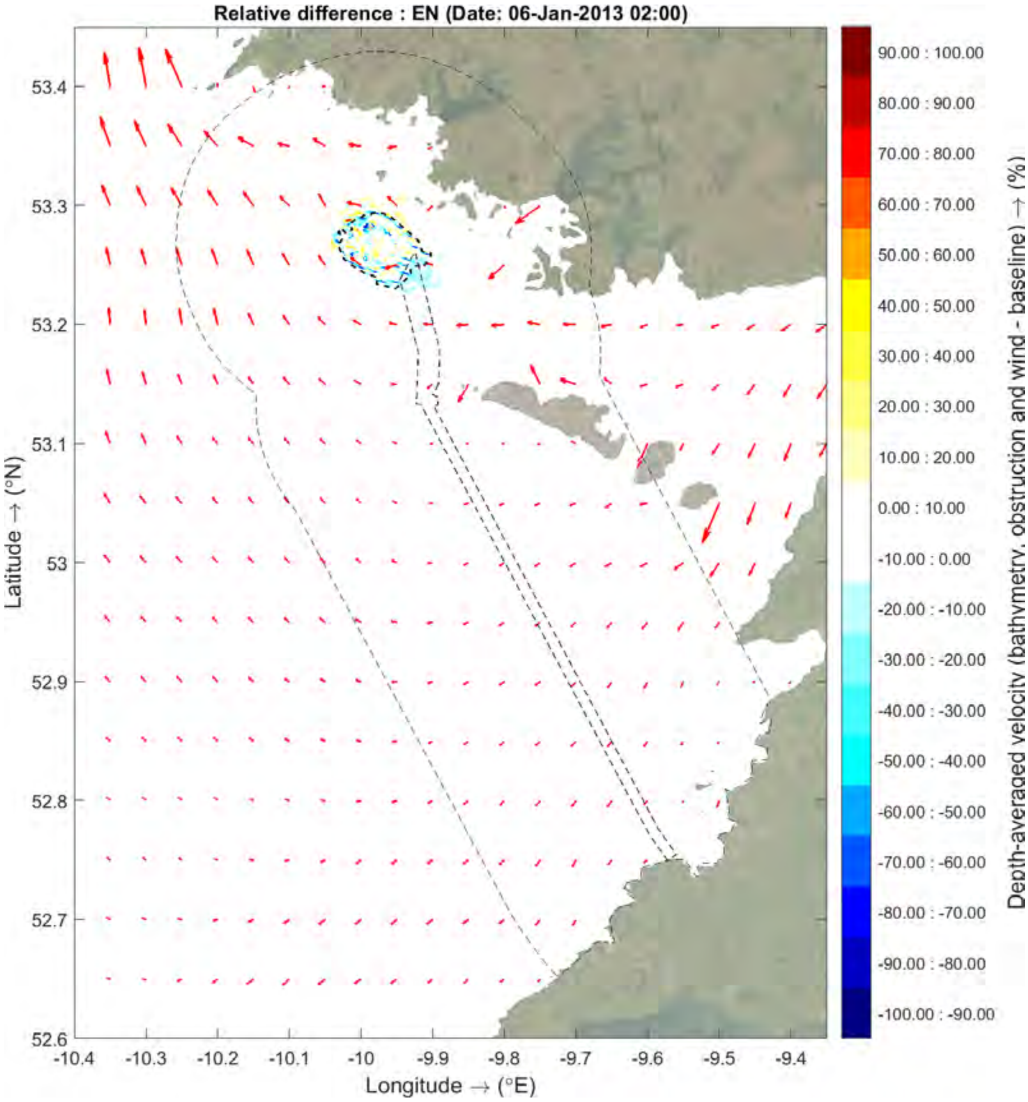
Relative difference : EN (Date: 06-Jan-2013 02:00)
Latitude → (°N)
Longitude → (°E)
53.4
53.3
53.2
53.1
53
52.9
52.8
52.7
52.6
-10.4
-10.3
-10.2
-10.1
-10
-9.9
-9.8
-9.7
-9.6
-9.5
-9.4
90.00 : 100.00
80.00 : 90.00
70.00 : 80.00
60.00 : 70.00
50.00 : 60.00
40.00 : 50.00
30.00 : 40.00
20.00 : 30.00
10.00 : 20.00
0.00 : 10.00
-10.00 : 0.00
-20.00 : -10.00
-30.00 : -20.00
-40.00 : -30.00
-50.00 : -40.00
-60.00 : -50.00
-70.00 : -60.00
-80.00 : -70.00
-90.00 : -80.00
-100.00 : -90.00
Depth-averaged velocity (bathymetry, obstruction and wind - baseline) → (%)

D.2 EN water levels

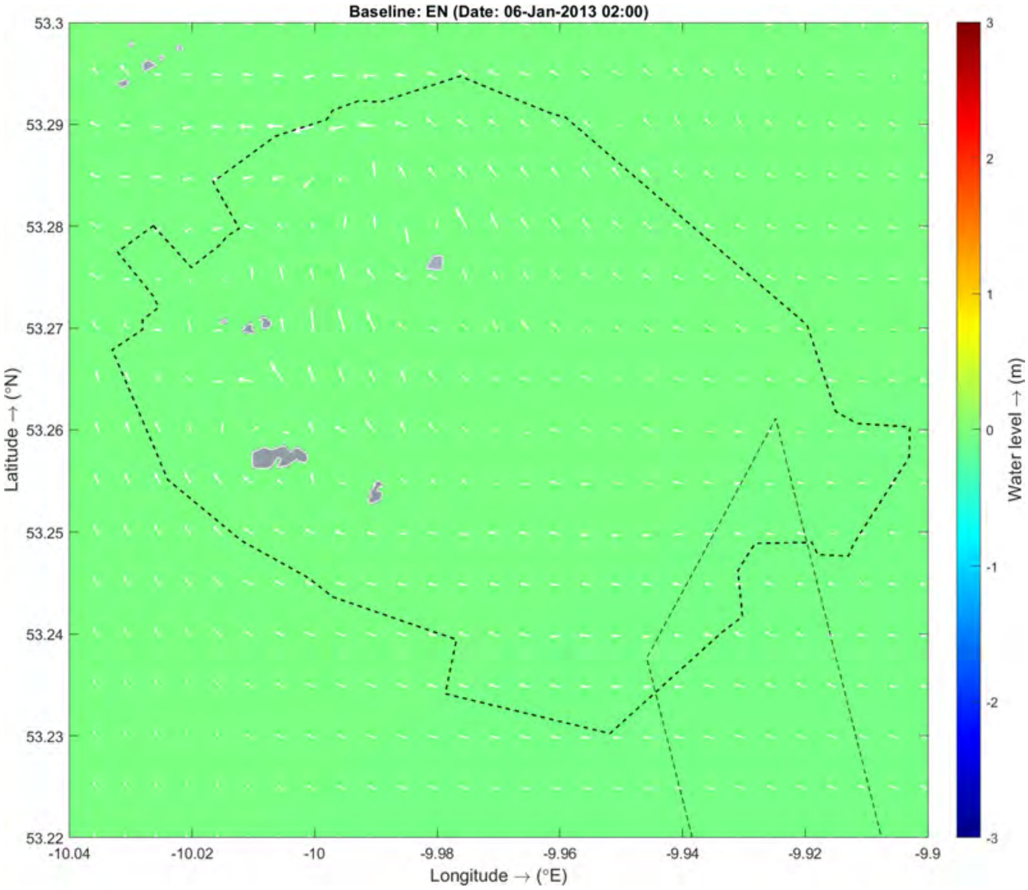

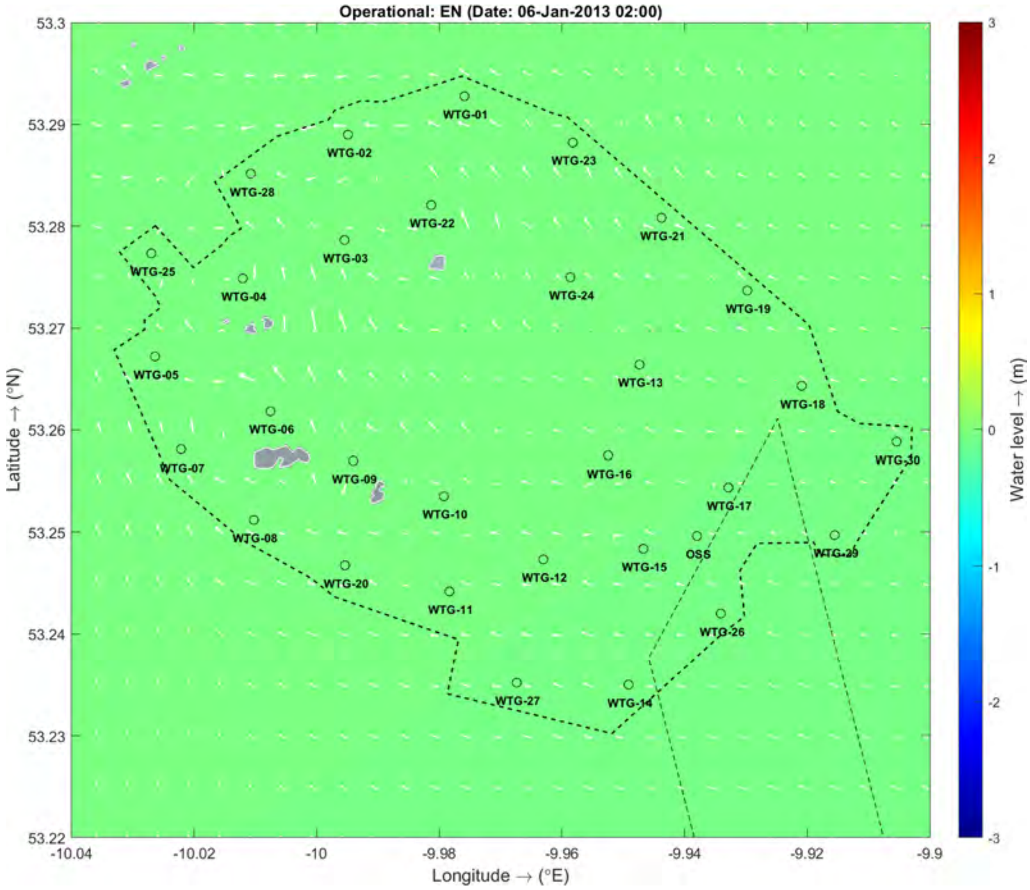
Operational: EN (Date: 06-Jan-2013 02:00)
Latitude → (°N)
Longitude → (°E)
Water level → (m)
WTG-01
WTG-02
WTG-03
WTG-04
WTG-05
WTG-06
WTG-07
WTG-08
WTG-09
WTG-10
WTG-11
WTG-12
WTG-13
WTG-14
WTG-15
WTG-16
WTG-17
WTG-18
WTG-19
WTG-20
WTG-21
WTG-22
WTG-23
WTG-24
WTG-25
WTG-26
WTG-27
WTG-28
WTG-29
WTG-30
OSS

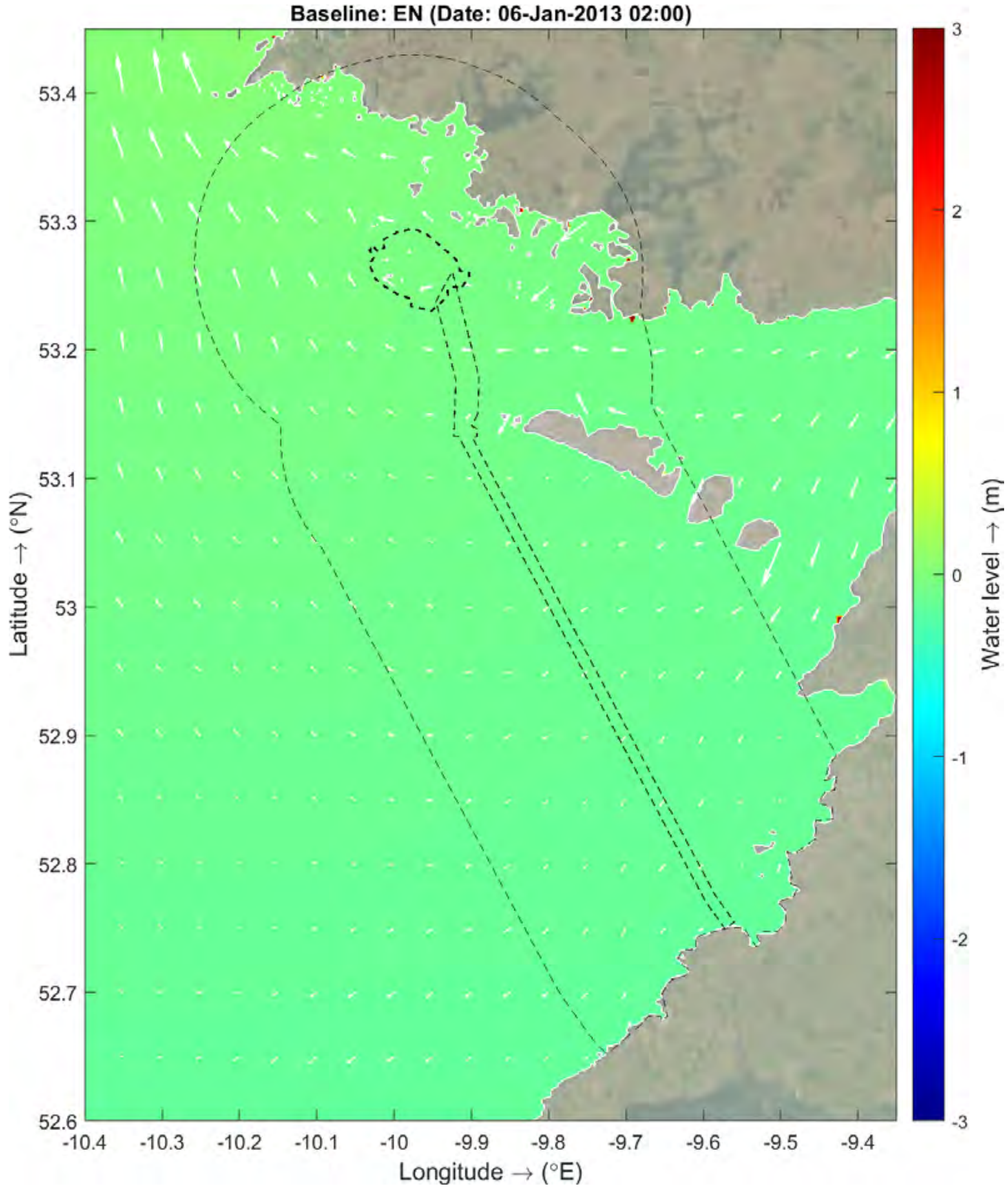
Baseline: EN (Date: 06-Jan-2013 02:00)
53.4
53.3
53.2
53.1
53
52.9
52.8
52.7
52.6
Latitude → (°N)
-10.4
-10.3
-10.2
-10.1
-10
-9.9
-9.8
-9.7
-9.6
-9.5
-9.4
Longitude → (°E)
3
2
1
0
-1
-2
-3
Water level → (m)

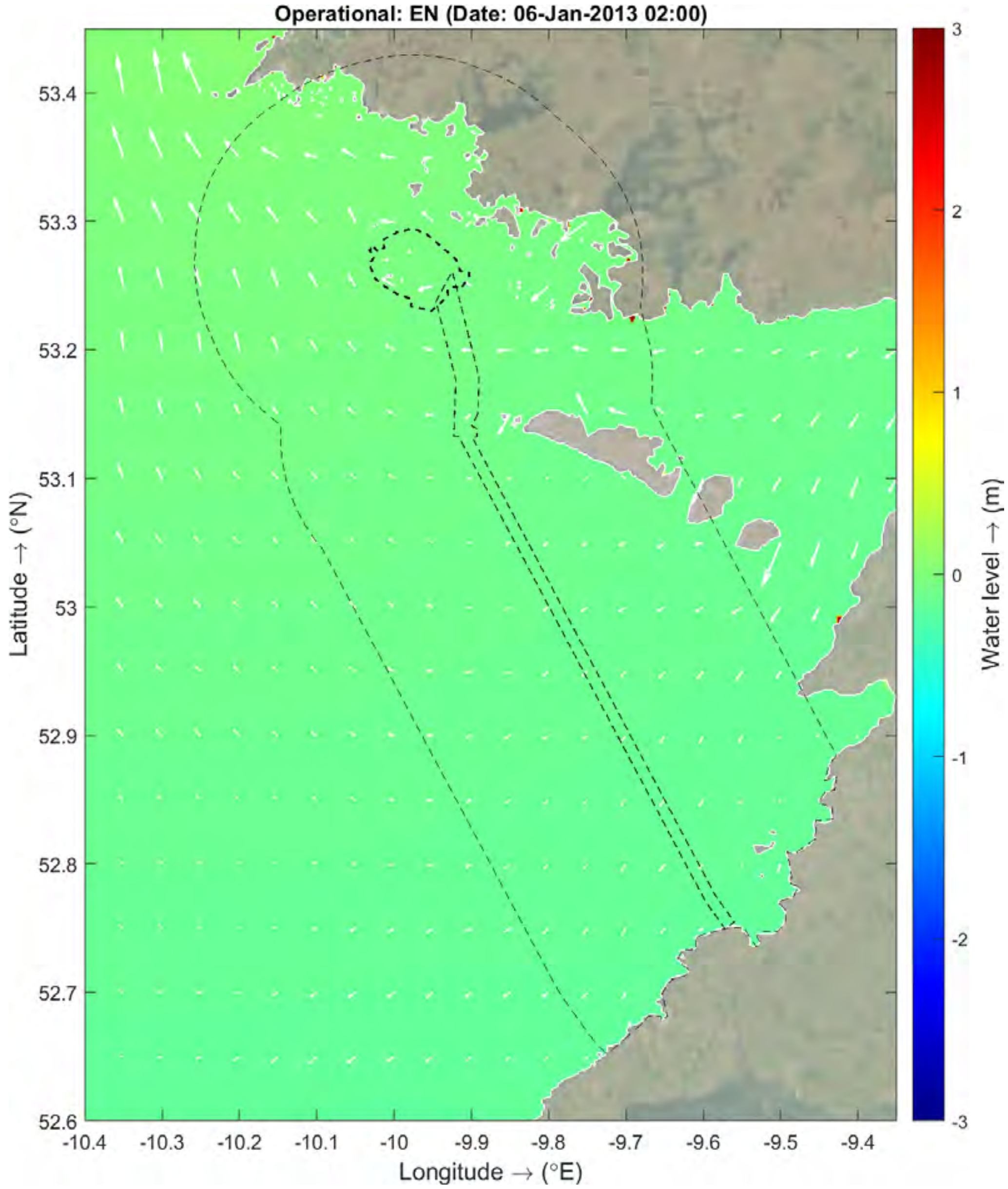

Operational: EN (Date: 06-Jan-2013 02:00)
Latitude → (°N)
Longitude → (°E)
Water level → (m)
53.4
53.3
53.2
53.1
53
52.9
52.8
52.7
52.6
-10.4
-10.3
-10.2
-10.1
-10
-9.9
-9.8
-9.7
-9.6
-9.5
-9.4
3
2
1
0
-1
-2
-3

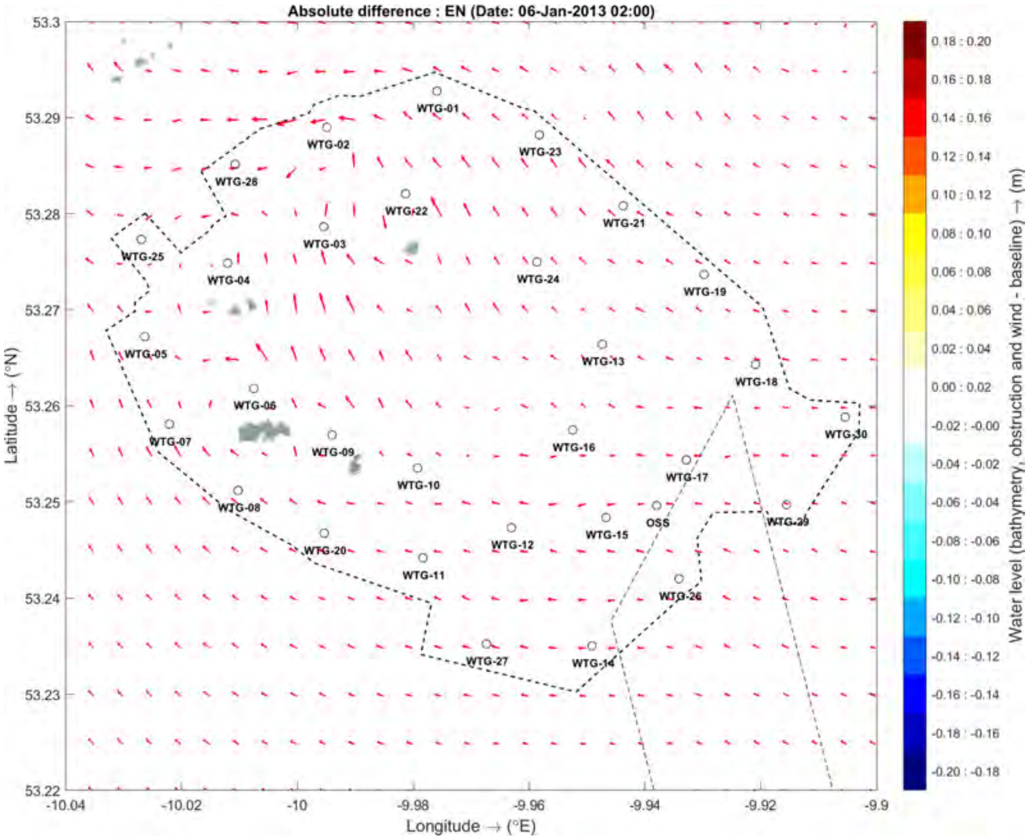
Absolute difference : EN (Date: 06-Jan-2013 02:00)
Latitude → (°N)
Longitude → (°E)
Water level (bathymetry, obstruction and wind - baseline) → (m)
WTG-01
WTG-02
WTG-03
WTG-04
WTG-05
WTG-06
WTG-07
WTG-08
WTG-09
WTG-10
WTG-11
WTG-12
WTG-13
WTG-14
WTG-15
WTG-16
WTG-17
WTG-18
WTG-19
WTG-20
WTG-21
WTG-22
WTG-23
WTG-24
WTG-25
WTG-26
WTG-27
WTG-28
WTG-29
WTG-30
OSS

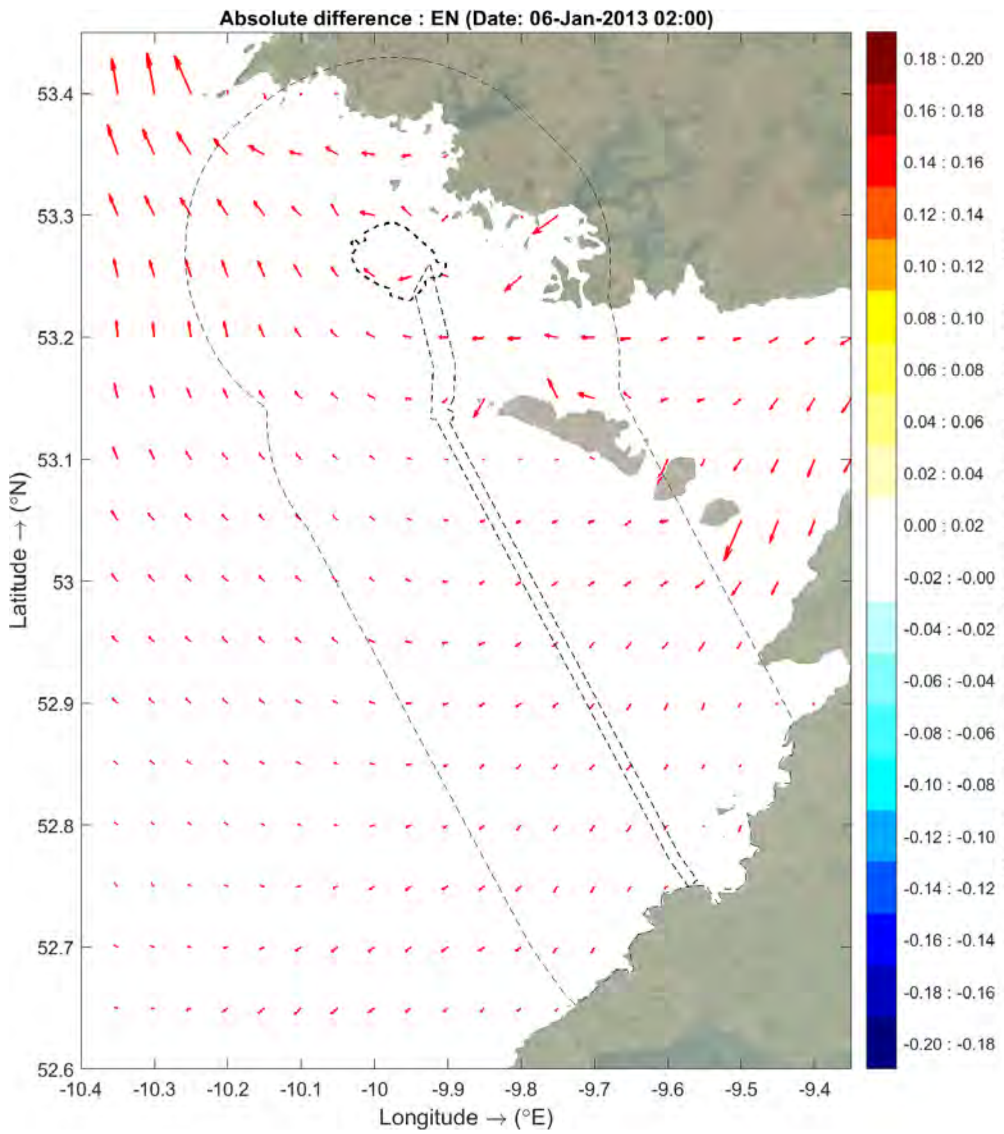
Absolute difference : EN (Date: 06-Jan-2013 02:00)
Latitude → (°N)
Longitude → (°E)
Water level (bathymetry, obstruction and wind - baseline) → (m)
53.4
53.3
53.2
53.1
53
52.9
52.8
52.7
52.6
-10.4
-10.3
-10.2
-10.1
-10
-9.9
-9.8
-9.7
-9.6
-9.5
-9.4
0.18 : 0.20
0.16 : 0.18
0.14 : 0.16
0.12 : 0.14
0.10 : 0.12
0.08 : 0.10
0.06 : 0.08
0.04 : 0.06
0.02 : 0.04
0.00 : 0.02
-0.02 : -0.00
-0.04 : -0.02
-0.06 : -0.04
-0.08 : -0.06
-0.10 : -0.08
-0.12 : -0.10
-0.14 : -0.12
-0.16 : -0.14
-0.18 : -0.16
-0.20 : -0.18

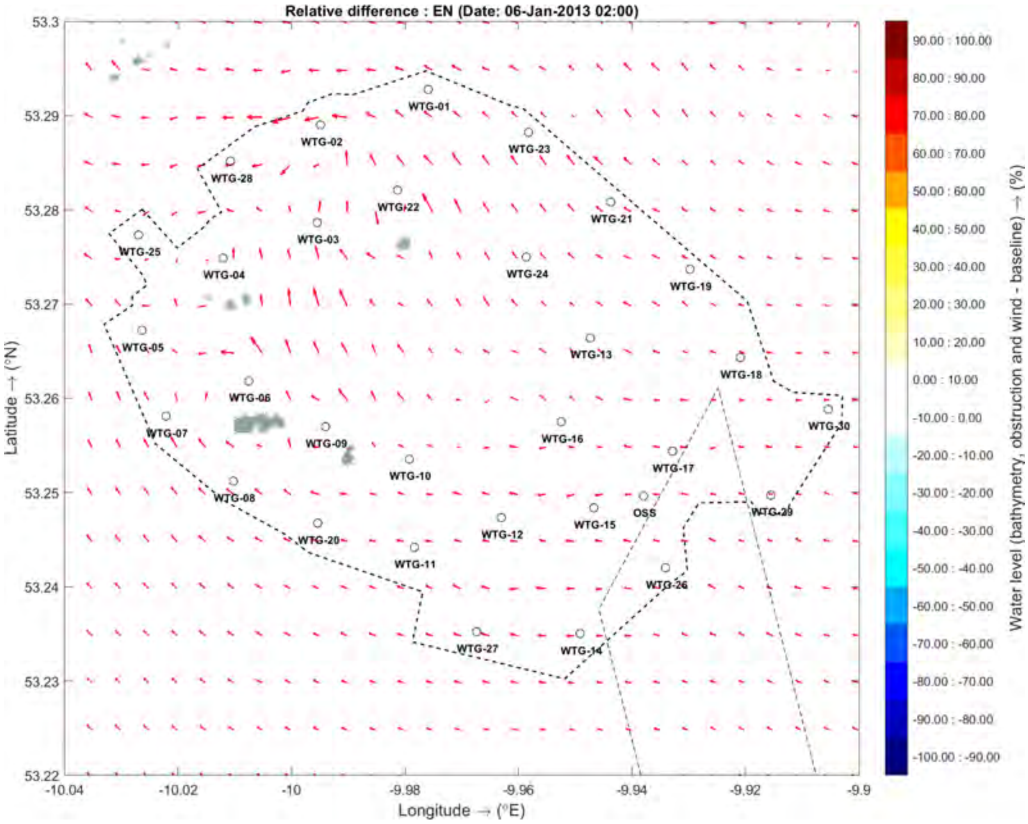
Relative difference : EN (Date: 06-Jan-2013 02:00)
Latitude → (°N)
Longitude → (°E)
Water level (bathymetry, obstruction and wind - baseline) → (%)
WTG-01
WTG-02
WTG-03
WTG-04
WTG-05
WTG-06
WTG-07
WTG-08
WTG-09
WTG-10
WTG-11
WTG-12
WTG-13
WTG-14
WTG-15
WTG-16
WTG-17
WTG-18
WTG-19
WTG-20
WTG-21
WTG-22
WTG-23
WTG-24
WTG-25
WTG-26
WTG-27
WTG-28
WTG-29
WTG-30
OSS
90.00 : 100.00
80.00 : 90.00
70.00 : 80.00
60.00 : 70.00
50.00 : 60.00
40.00 : 50.00
30.00 : 40.00
20.00 : 30.00
10.00 : 20.00
0.00 : 10.00
-10.00 : 0.00
-20.00 : -10.00
-30.00 : -20.00
-40.00 : -30.00
-50.00 : -40.00
-60.00 : -50.00
-70.00 : -60.00
-80.00 : -70.00
-90.00 : -80.00
-100.00 : -90.00

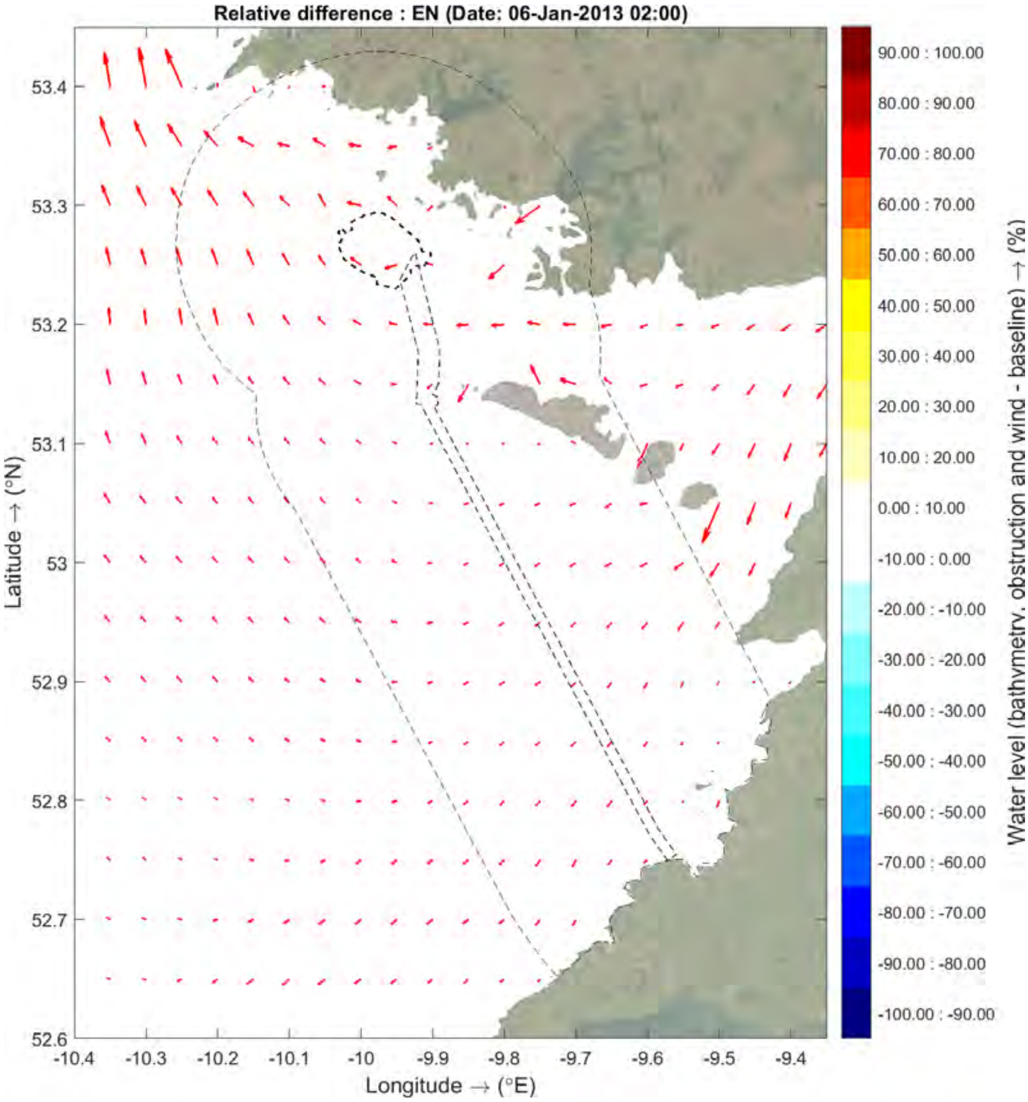
Relative difference : EN (Date: 06-Jan-2013 02:00)
Latitude → (°N)
Longitude → (°E)
53.4
53.3
53.2
53.1
53
52.9
52.8
52.7
52.6
-10.4
-10.3
-10.2
-10.1
-10
-9.9
-9.8
-9.7
-9.6
-9.5
-9.4
90.00 : 100.00
80.00 : 90.00
70.00 : 80.00
60.00 : 70.00
50.00 : 60.00
40.00 : 50.00
30.00 : 40.00
20.00 : 30.00
10.00 : 20.00
0.00 : 10.00
-10.00 : 0.00
-20.00 : -10.00
-30.00 : -20.00
-40.00 : -30.00
-50.00 : -40.00
-60.00 : -50.00
-70.00 : -60.00
-80.00 : -70.00
-90.00 : -80.00
-100.00 : -90.00
Water level (bathymetry, obstruction and wind - baseline) → (%)

D.3 ES currents

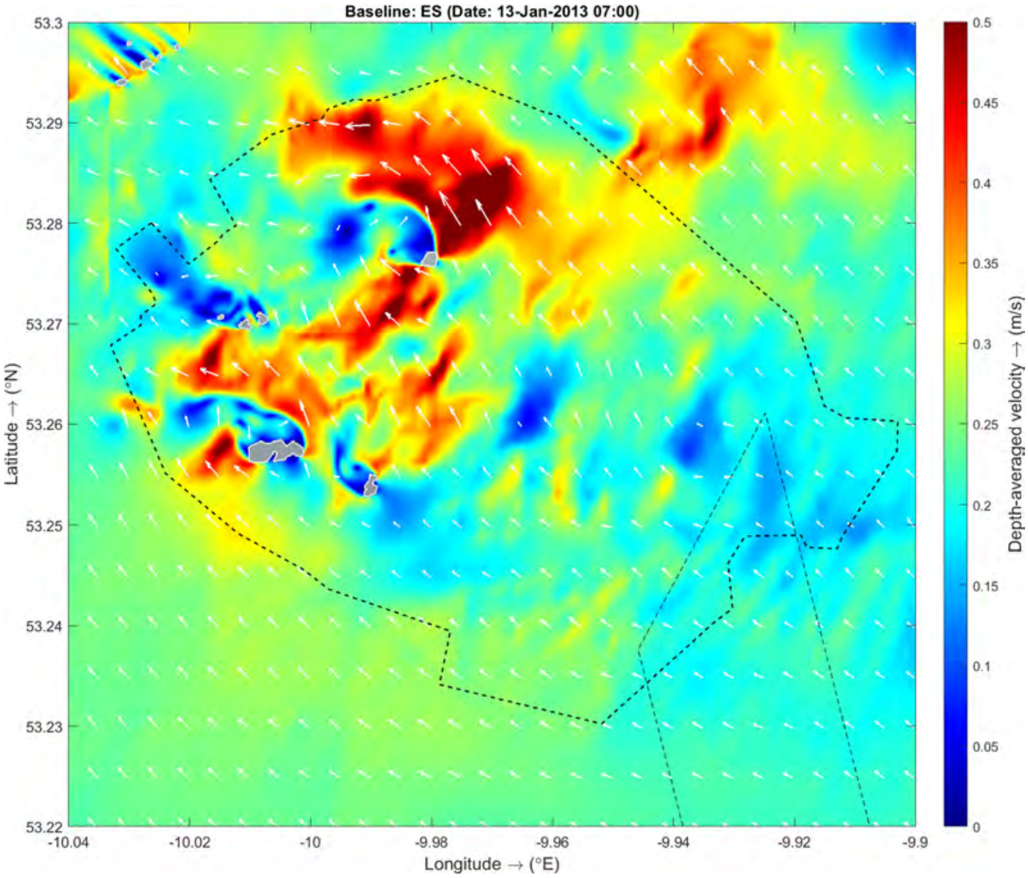

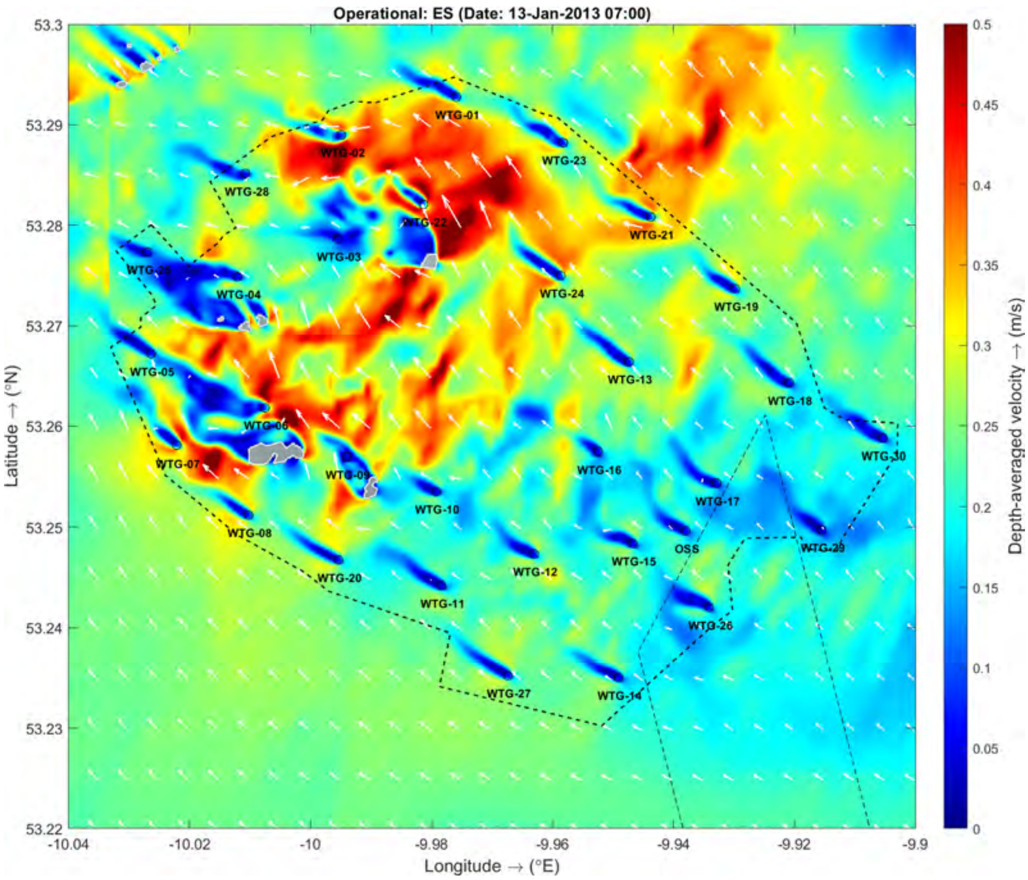

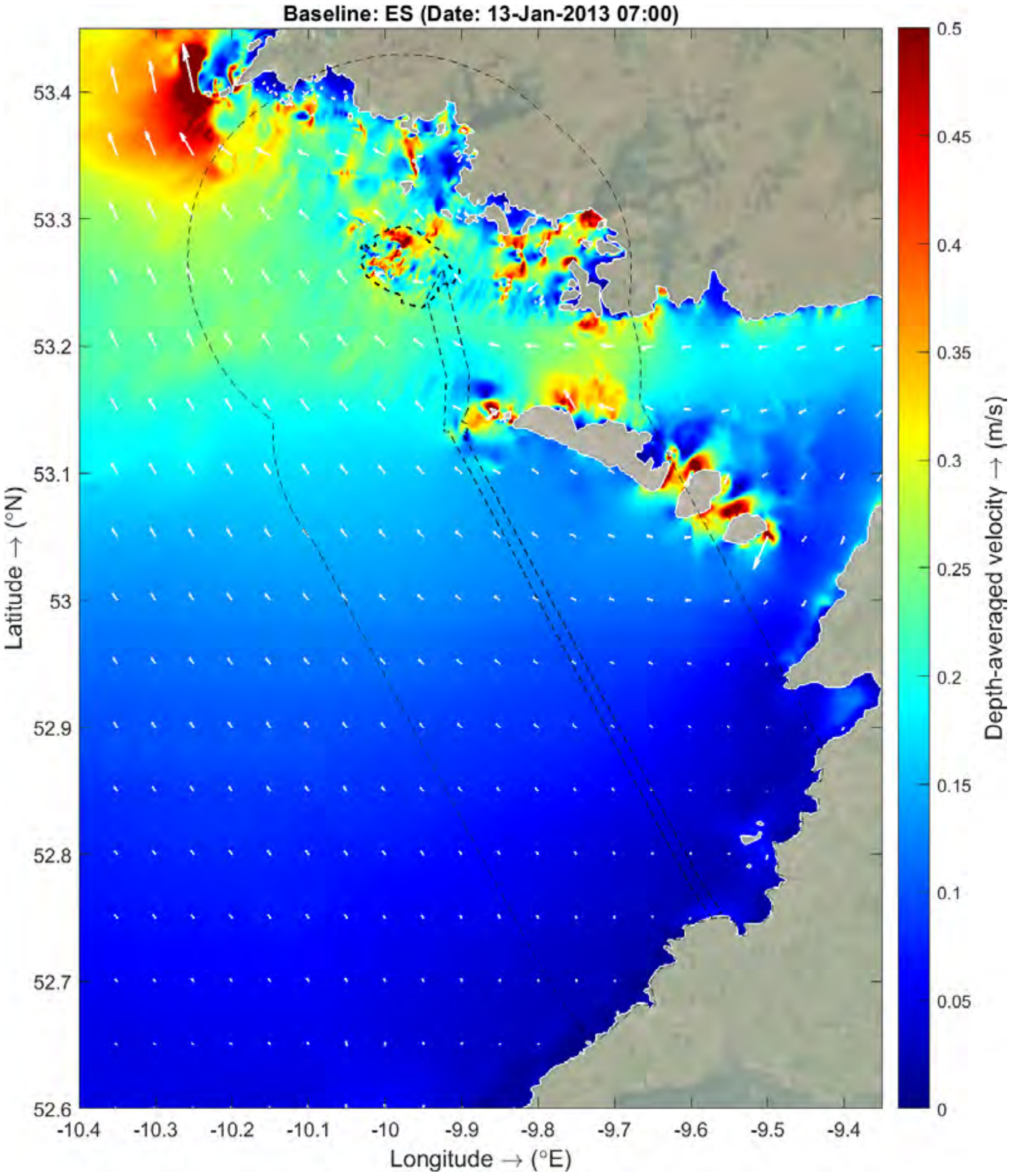
Baseline: ES (Date: 13-Jan-2013 07:00)
53.4
53.3
53.2
53.1
53
52.9
52.8
52.7
52.6
Latitude → (°N)
-10.4
-10.3
-10.2
-10.1
-10
-9.9
-9.8
-9.7
-9.6
-9.5
-9.4
Longitude → (°E)
0.5
0.45
0.4
0.35
0.3
0.25
0.2
0.15
0.1
0.05
0
Depth-averaged velocity → (m/s)

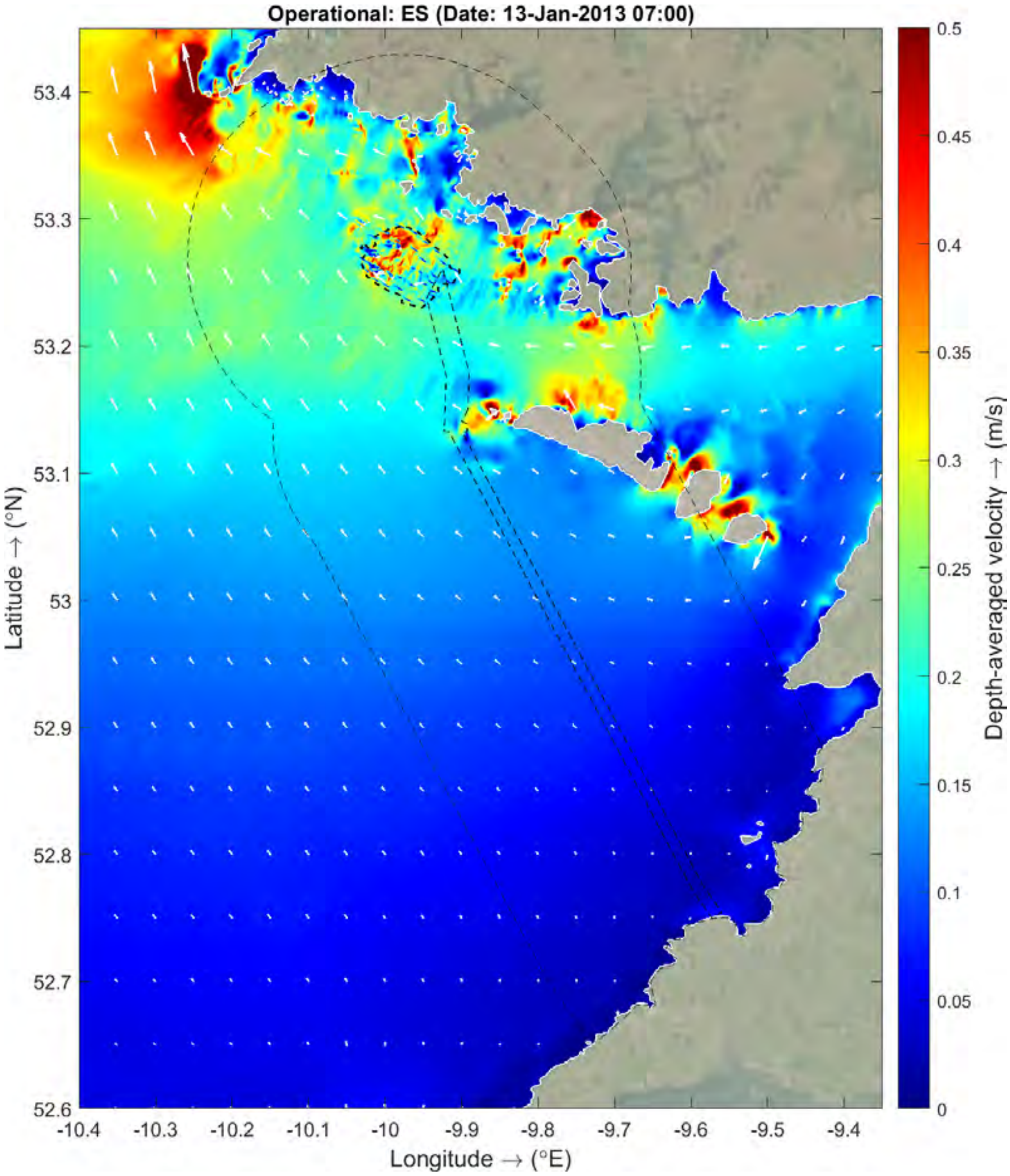
Operational: ES (Date: 13-Jan-2013 07:00)
53.4
53.3
53.2
53.1
53
52.9
52.8
52.7
52.6
Latitude → (°N)
-10.4
-10.3
-10.2
-10.1
-10
-9.9
-9.8
-9.7
-9.6
-9.5
-9.4
Longitude → (°E)
0.5
0.45
0.4
0.35
0.3
0.25
0.2
0.15
0.1
0.05
0
Depth-averaged velocity → (m/s)

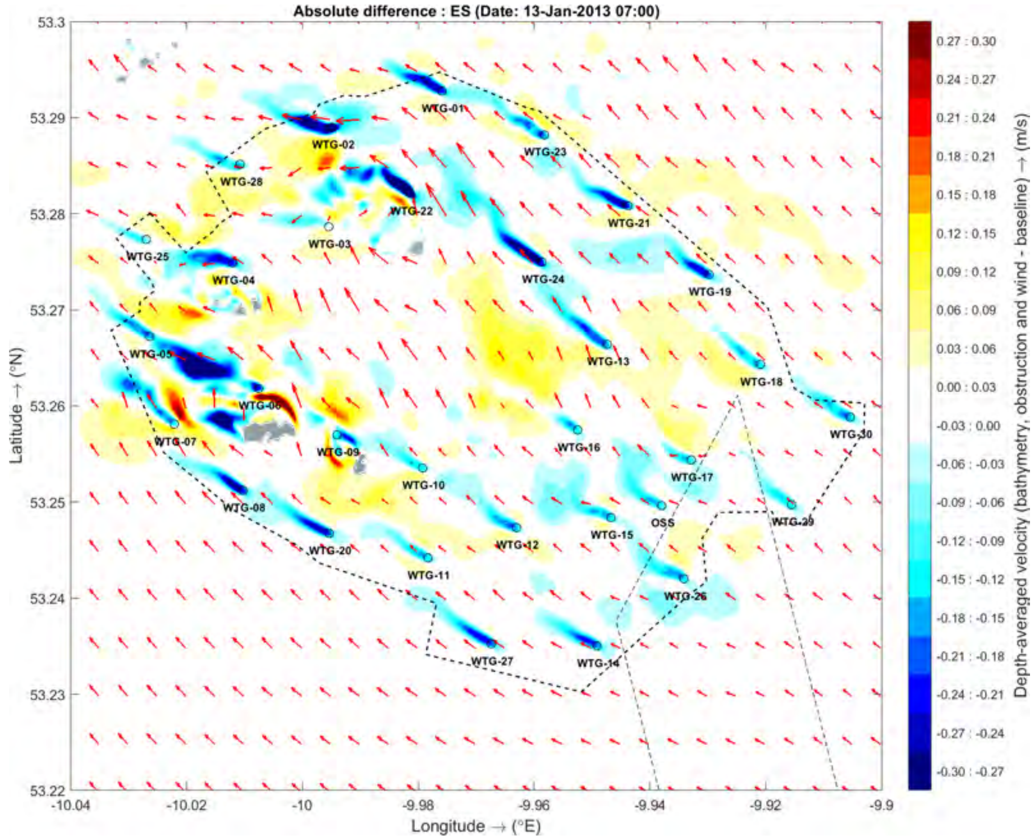
Absolute difference : ES (Date: 13-Jan-2013 07:00)
Latitude → (°N)
Longitude → (°E)
Depth-averaged velocity (bathymetry, obstruction and wind - baseline) → (m/s)
0.27 : 0.30
0.24 : 0.27
0.21 : 0.24
0.18 : 0.21
0.15 : 0.18
0.12 : 0.15
0.09 : 0.12
0.06 : 0.09
0.03 : 0.06
0.00 : 0.03
-0.03 : 0.00
-0.06 : -0.03
-0.09 : -0.06
-0.12 : -0.09
-0.15 : -0.12
-0.18 : -0.15
-0.21 : -0.18
-0.24 : -0.21
-0.27 : -0.24
-0.30 : -0.27
WTG-01
WTG-02
WTG-03
WTG-04
WTG-05
WTG-06
WTG-07
WTG-08
WTG-09
WTG-10
WTG-11
WTG-12
WTG-13
WTG-14
WTG-15
WTG-16
WTG-17
WTG-18
WTG-19
WTG-20
WTG-21
WTG-22
WTG-23
WTG-24
WTG-25
WTG-26
WTG-27
WTG-28
WTG-29
WTG-30
OSS

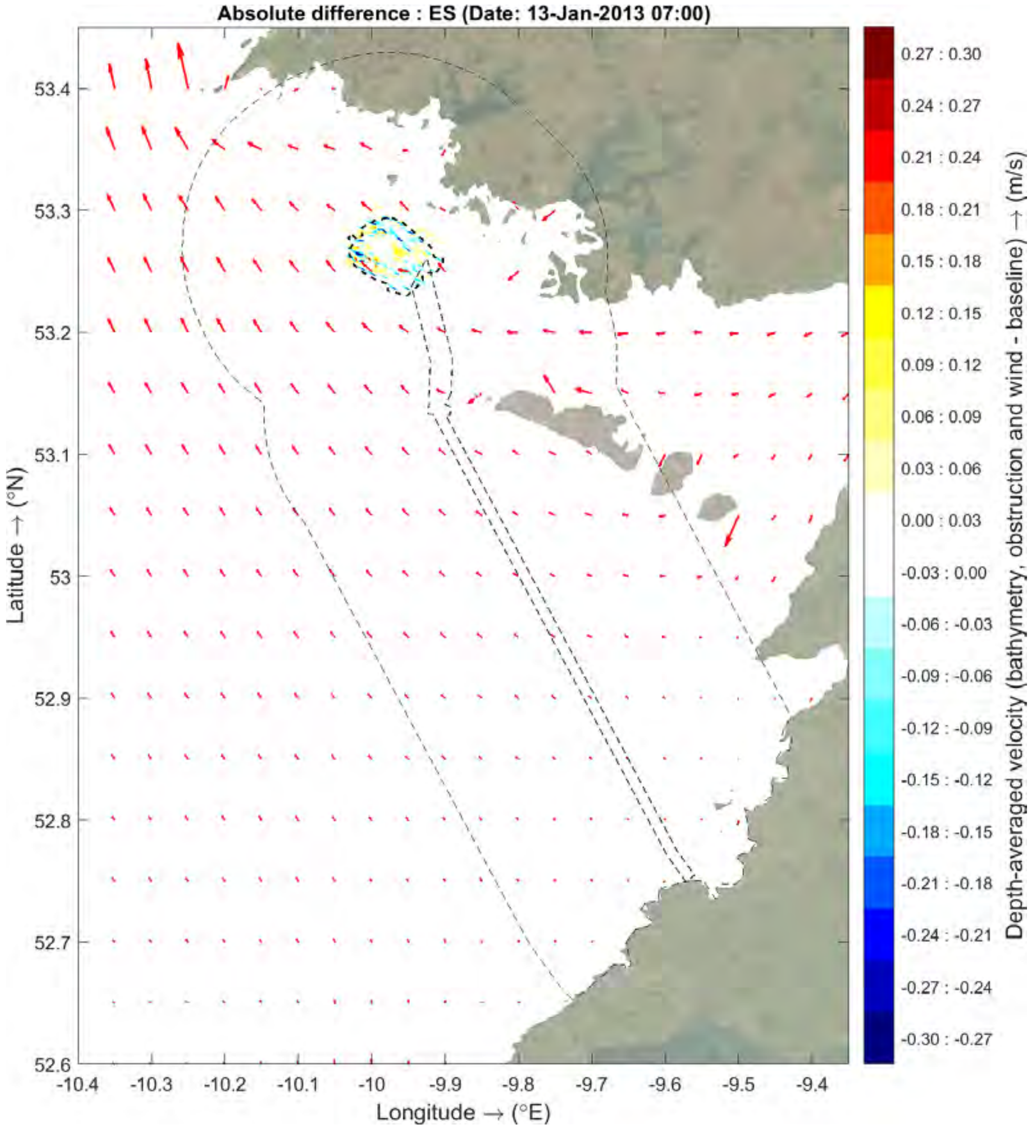
Absolute difference : ES (Date: 13-Jan-2013 07:00)
Latitude → (°N)
Longitude → (°E)
53.4
53.3
53.2
53.1
53
52.9
52.8
52.7
52.6
-10.4
-10.3
-10.2
-10.1
-10
-9.9
-9.8
-9.7
-9.6
-9.5
-9.4
0.27 : 0.30
0.24 : 0.27
0.21 : 0.24
0.18 : 0.21
0.15 : 0.18
0.12 : 0.15
0.09 : 0.12
0.06 : 0.09
0.03 : 0.06
0.00 : 0.03
-0.03 : 0.00
-0.06 : -0.03
-0.09 : -0.06
-0.12 : -0.09
-0.15 : -0.12
-0.18 : -0.15
-0.21 : -0.18
-0.24 : -0.21
-0.27 : -0.24
-0.30 : -0.27
Depth-averaged velocity (bathymetry, obstruction and wind - baseline) → (m/s)

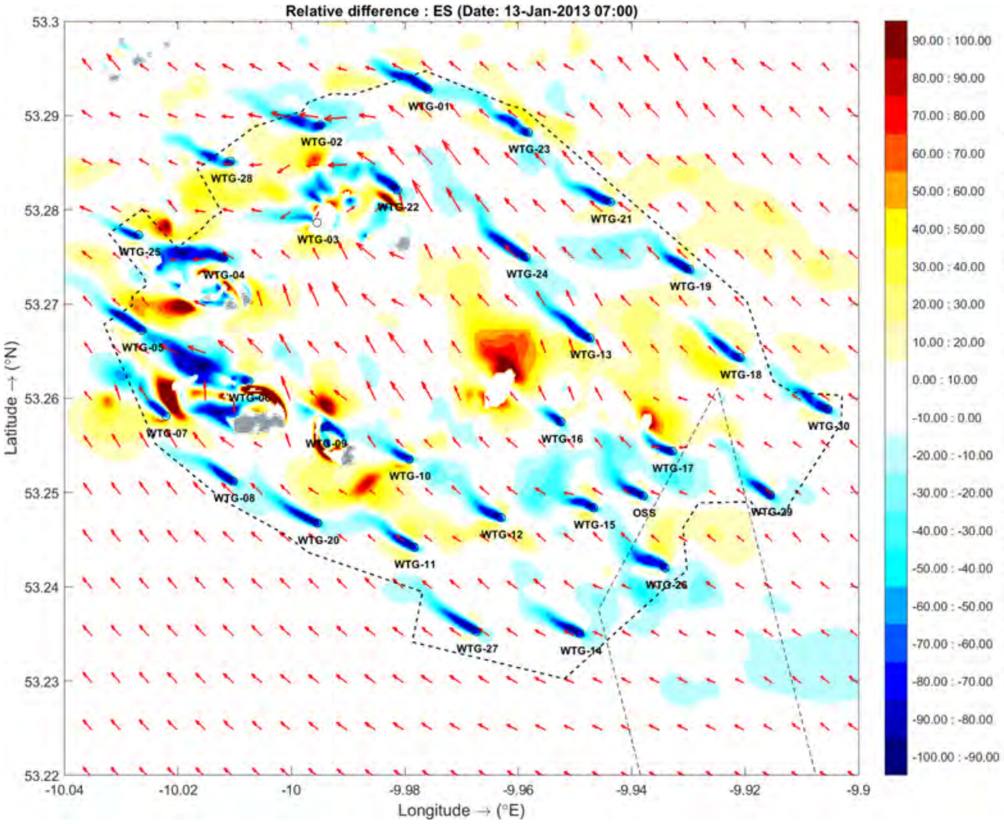
Relative difference : ES (Date: 13-Jan-2013 07:00)
Latitude → (°N)
Longitude → (°E)
Depth-averaged velocity (bathymetry, obstruction and wind - baseline) → (%)
90.00 : 100.00
80.00 : 90.00
70.00 : 80.00
60.00 : 70.00
50.00 : 60.00
40.00 : 50.00
30.00 : 40.00
20.00 : 30.00
10.00 : 20.00
0.00 : 10.00
-10.00 : 0.00
-20.00 : -10.00
-30.00 : -20.00
-40.00 : -30.00
-50.00 : -40.00
-60.00 : -50.00
-70.00 : -60.00
-80.00 : -70.00
-90.00 : -80.00
-100.00 : -90.00
WTG-01
WTG-02
WTG-03
WTG-04
WTG-05
WTG-07
WTG-08
WTG-09
WTG-10
WTG-11
WTG-12
WTG-13
WTG-14
WTG-15
WTG-16
WTG-17
WTG-18
WTG-19
WTG-20
WTG-21
WTG-22
WTG-23
WTG-24
WTG-25
WTG-26
WTG-27
WTG-28
WTG-29
WTG-30
OSS

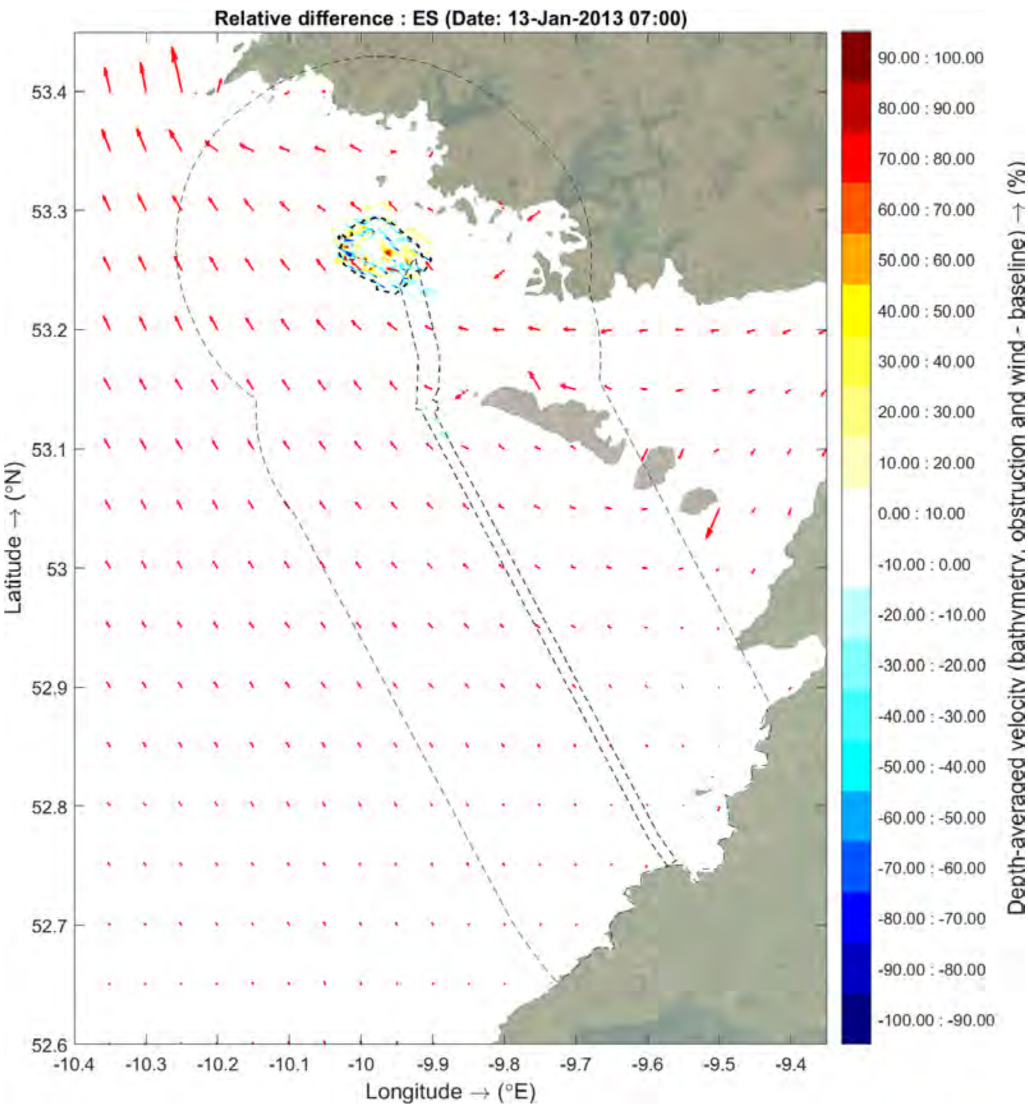
Relative difference : ES (Date: 13-Jan-2013 07:00)
Latitude → (°N)
Longitude → (°E)
Depth-averaged velocity (bathymetry, obstruction and wind - baseline) → (%)
90.00 : 100.00
80.00 : 90.00
70.00 : 80.00
60.00 : 70.00
50.00 : 60.00
40.00 : 50.00
30.00 : 40.00
20.00 : 30.00
10.00 : 20.00
0.00 : 10.00
-10.00 : 0.00
-20.00 : -10.00
-30.00 : -20.00
-40.00 : -30.00
-50.00 : -40.00
-60.00 : -50.00
-70.00 : -60.00
-80.00 : -70.00
-90.00 : -80.00
-100.00 : -90.00

D.4 ES water levels

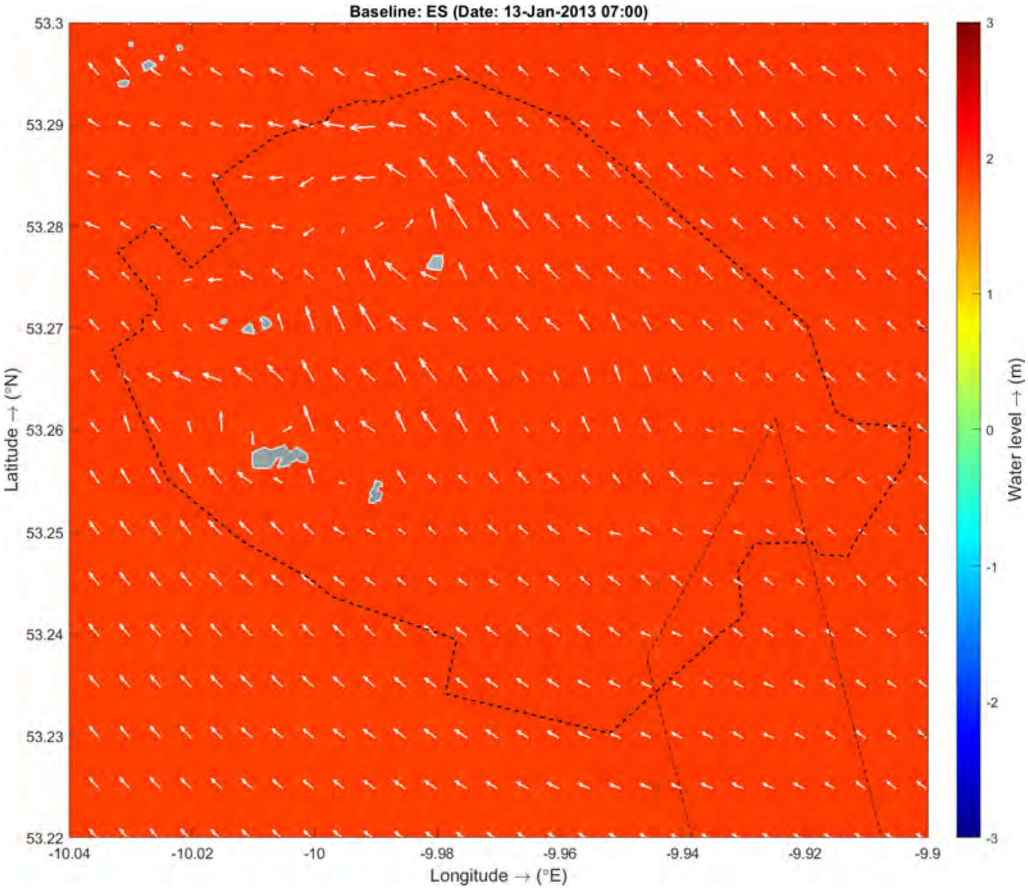

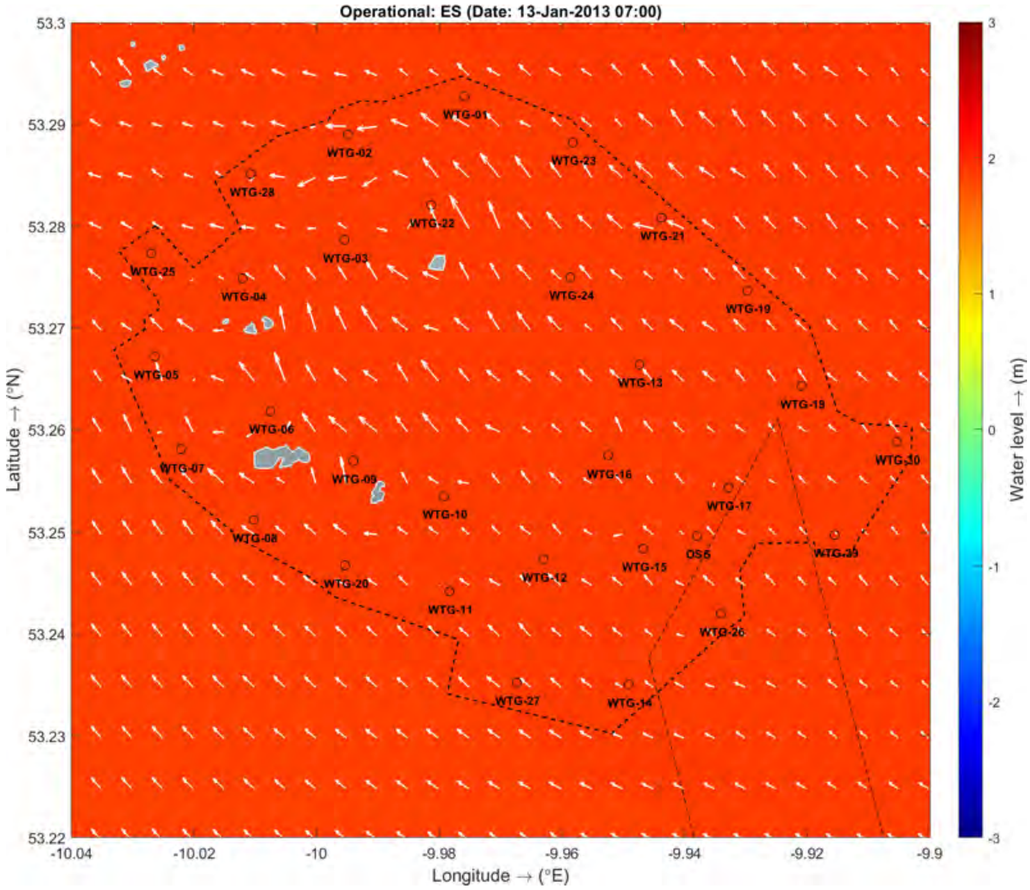
Operational: ES (Date: 13-Jan-2013 07:00)
Latitude → (°N)
Longitude → (°E)
Water level → (m)
WTG-01
WTG-02
WTG-03
WTG-04
WTG-05
WTG-06
WTG-07
WTG-08
WTG-09
WTG-10
WTG-11
WTG-12
WTG-13
WTG-14
WTG-15
WTG-16
WTG-17
WTG-18
WTG-19
WTG-20
WTG-21
WTG-22
WTG-23
WTG-24
WTG-25
WTG-26
WTG-27
WTG-28
WTG-29
WTG-30
OSS

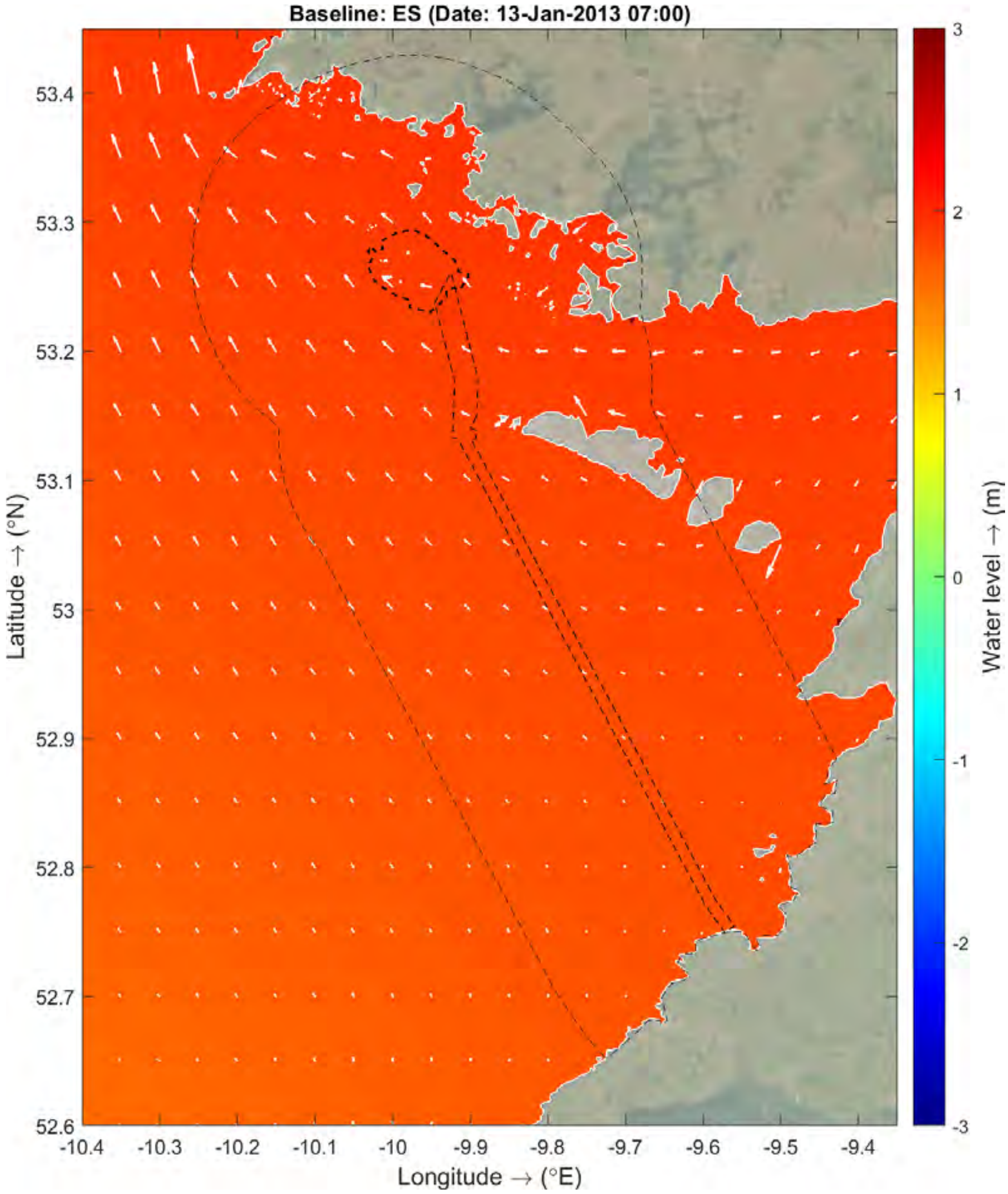

Baseline: ES (Date: 13-Jan-2013 07:00)
Latitude → (°N)
Longitude → (°E)
Water level → (m)
53.4
53.3
53.2
53.1
53
52.9
52.8
52.7
52.6
-10.4
-10.3
-10.2
-10.1
-10
-9.9
-9.8
-9.7
-9.6
-9.5
-9.4
3
2
1
0
-1
-2
-3

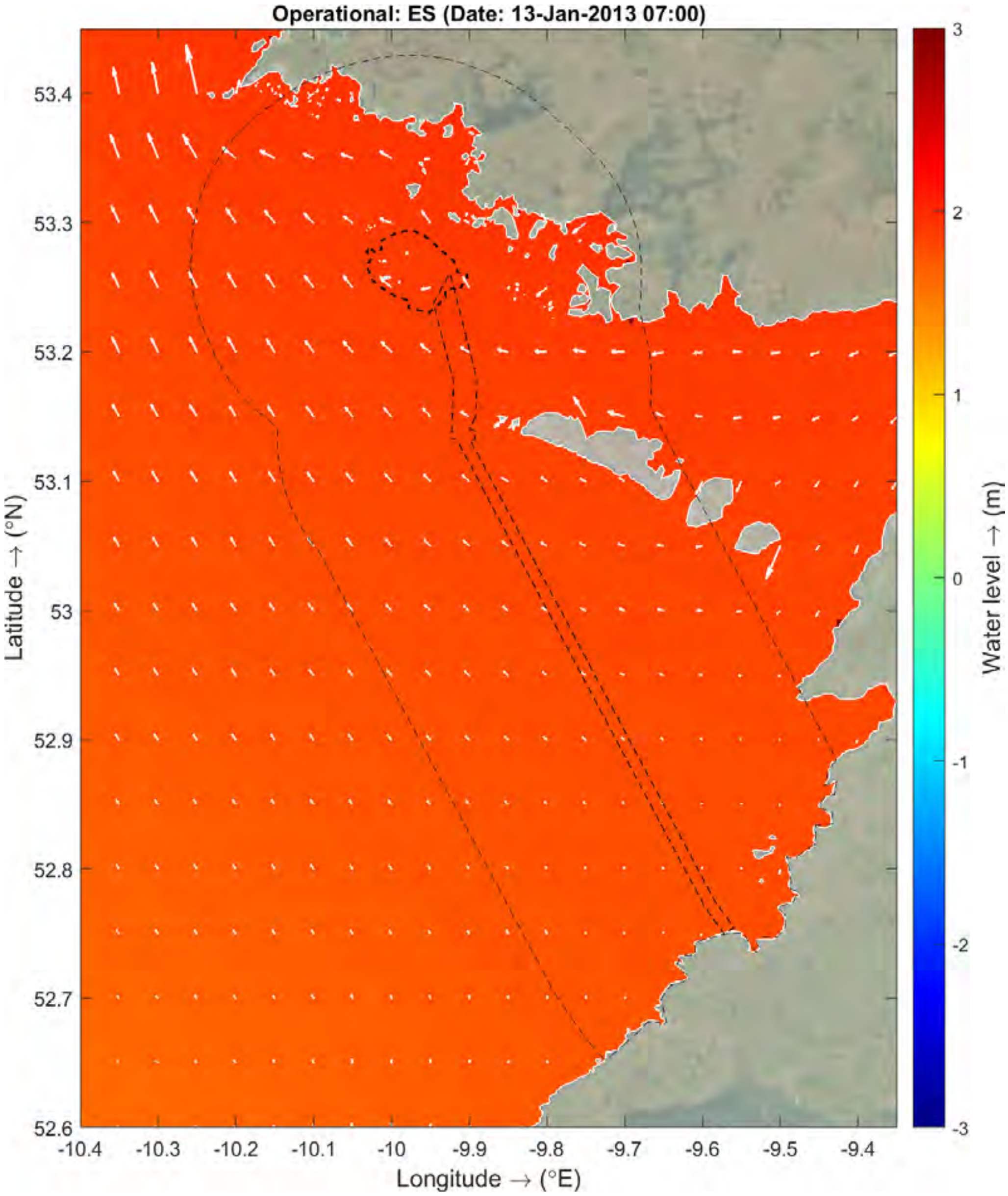
Operational: ES (Date: 13-Jan-2013 07:00)
Latitude → (°N)
Longitude → (°E)
Water level → (m)
53.4
53.3
53.2
53.1
53
52.9
52.8
52.7
52.6
-10.4
-10.3
-10.2
-10.1
-10
-9.9
-9.8
-9.7
-9.6
-9.5
-9.4
3
2
1
0
-1
-2
-3

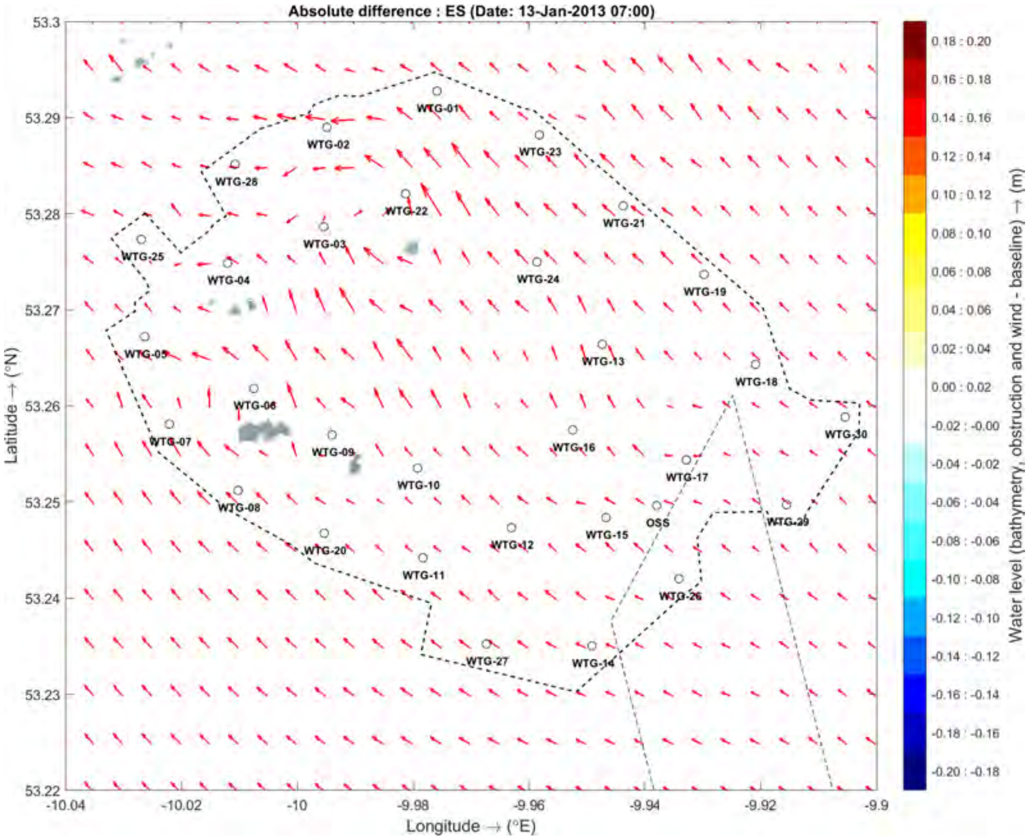
Absolute difference : ES (Date: 13-Jan-2013 07:00)
Latitude → (°N)
Longitude → (°E)
Water level (bathymetry, obstruction and wind - baseline) → (m)
53.3
53.29
53.28
53.27
53.26
53.25
53.24
53.23
53.22
-10.04
-10.02
-10
-9.98
-9.96
-9.94
-9.92
-9.9
0.18 : 0.20
0.16 : 0.18
0.14 : 0.16
0.12 : 0.14
0.10 : 0.12
0.08 : 0.10
0.06 : 0.08
0.04 : 0.06
0.02 : 0.04
0.00 : 0.02
-0.02 : -0.00
-0.04 : -0.02
-0.06 : -0.04
-0.08 : -0.06
-0.10 : -0.08
-0.12 : -0.10
-0.14 : -0.12
-0.16 : -0.14
-0.18 : -0.16
-0.20 : -0.18
WTG-01
WTG-02
WTG-03
WTG-04
WTG-05
WTG-06
WTG-07
WTG-08
WTG-09
WTG-10
WTG-11
WTG-12
WTG-13
WTG-14
WTG-15
WTG-16
WTG-17
WTG-18
WTG-19
WTG-20
WTG-21
WTG-22
WTG-23
WTG-24
WTG-25
WTG-26
WTG-27
WTG-28
WTG-29
WTG-30
OSS

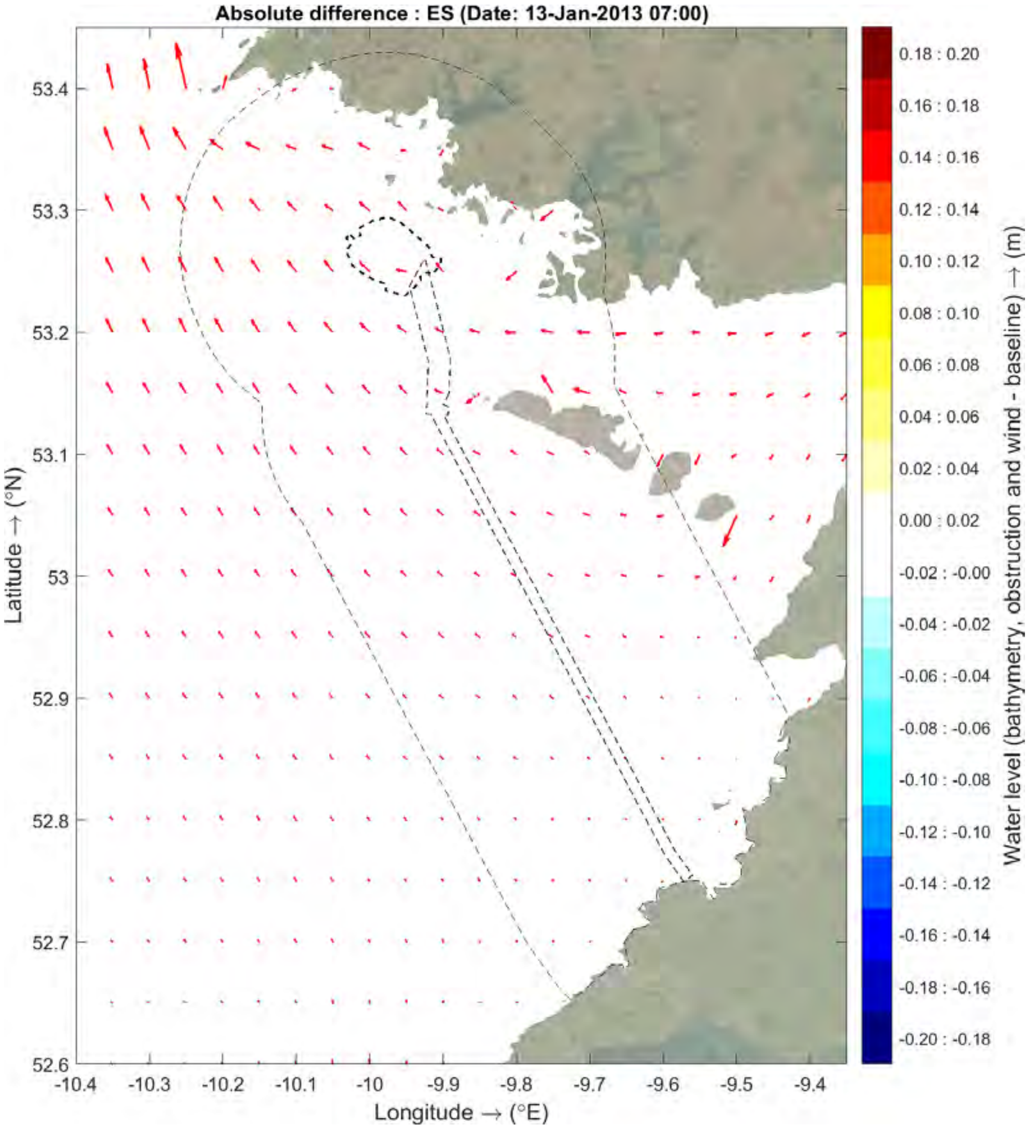
Absolute difference : ES (Date: 13-Jan-2013 07:00)
53.4
53.3
53.2
53.1
53
52.9
52.8
52.7
52.6
Latitude → (°N)
-10.4
-10.3
-10.2
-10.1
-10
-9.9
-9.8
-9.7
-9.6
-9.5
-9.4
Longitude → (°E)
0.18 : 0.20
0.16 : 0.18
0.14 : 0.16
0.12 : 0.14
0.10 : 0.12
0.08 : 0.10
0.06 : 0.08
0.04 : 0.06
0.02 : 0.04
0.00 : 0.02
-0.02 : -0.00
-0.04 : -0.02
-0.06 : -0.04
-0.08 : -0.06
-0.10 : -0.08
-0.12 : -0.10
-0.14 : -0.12
-0.16 : -0.14
-0.18 : -0.16
-0.20 : -0.18
Water level (bathymetry, obstruction and wind - baseline) → (m)

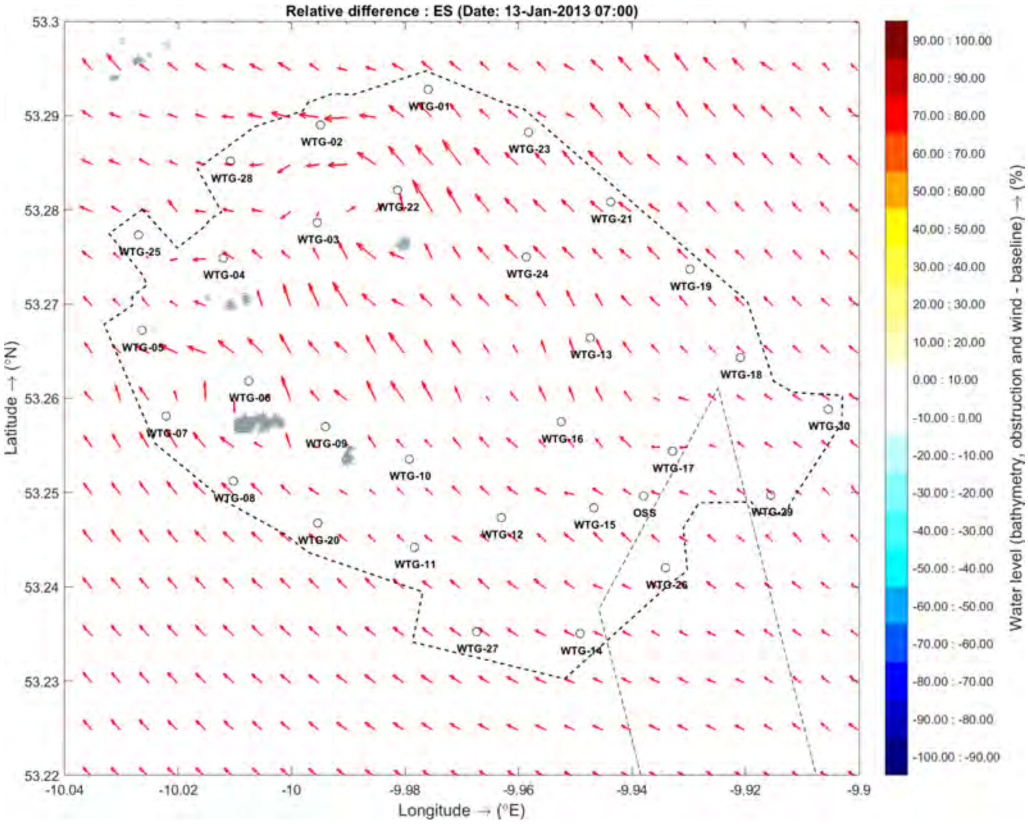
Relative difference : ES (Date: 13-Jan-2013 07:00)
Latitude → (°N)
Longitude → (°E)
Water level (bathymetry, obstruction and wind - baseline) → (%)
WTG-01
WTG-02
WTG-03
WTG-04
WTG-05
WTG-06
WTG-07
WTG-08
WTG-09
WTG-10
WTG-11
WTG-12
WTG-13
WTG-14
WTG-15
WTG-16
WTG-17
WTG-18
WTG-19
WTG-20
WTG-21
WTG-22
WTG-23
WTG-24
WTG-25
WTG-26
WTG-27
WTG-28
WTG-29
WTG-30
OSS
90.00 : 100.00
80.00 : 90.00
70.00 : 80.00
60.00 : 70.00
50.00 : 60.00
40.00 : 50.00
30.00 : 40.00
20.00 : 30.00
10.00 : 20.00
0.00 : 10.00
-10.00 : 0.00
-20.00 : -10.00
-30.00 : -20.00
-40.00 : -30.00
-50.00 : -40.00
-60.00 : -50.00
-70.00 : -60.00
-80.00 : -70.00
-90.00 : -80.00
-100.00 : -90.00

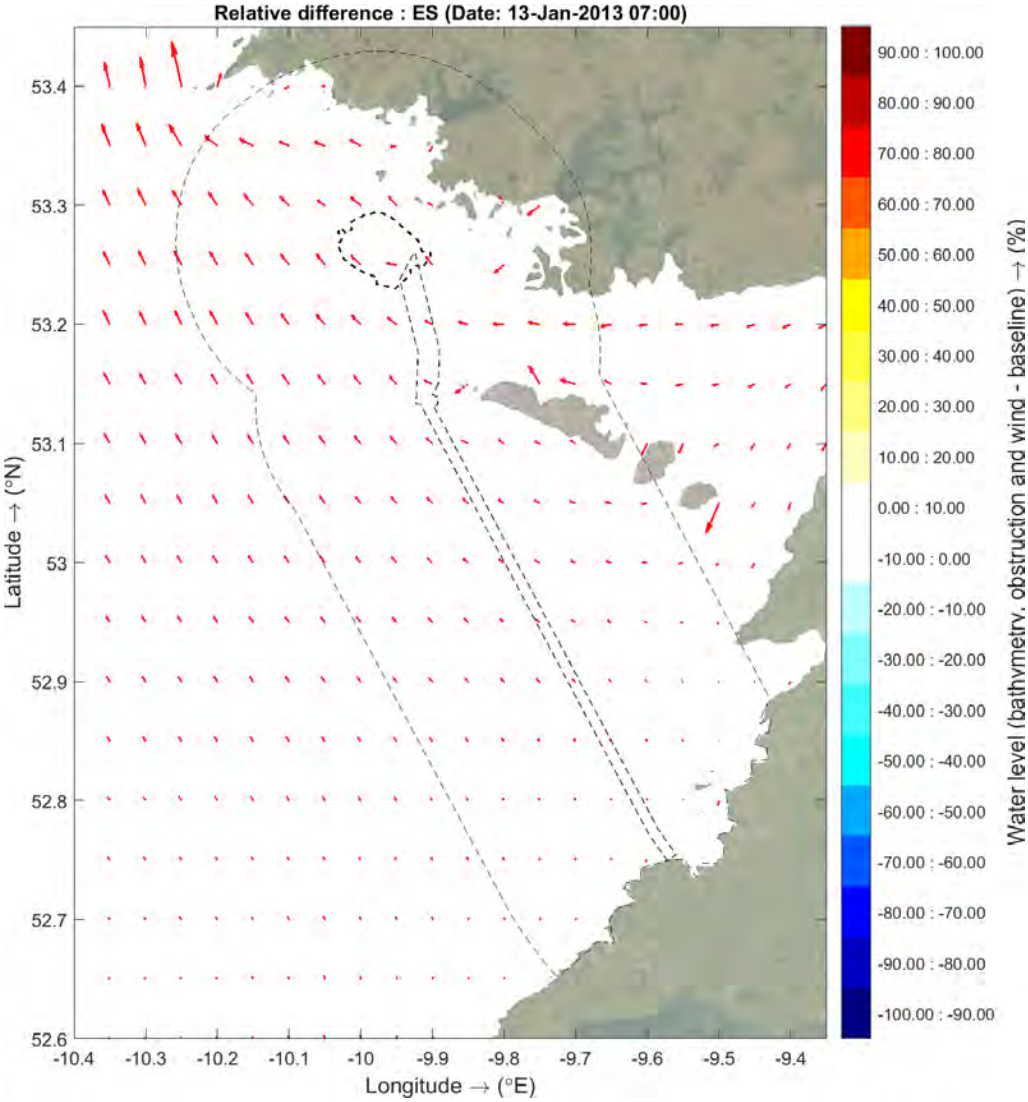
Relative difference : ES (Date: 13-Jan-2013 07:00)
Latitude → (°N)
Longitude → (°E)
Water level (bathymetry, obstruction and wind - baseline) → (%)
90.00 : 100.00
80.00 : 90.00
70.00 : 80.00
60.00 : 70.00
50.00 : 60.00
40.00 : 50.00
30.00 : 40.00
20.00 : 30.00
10.00 : 20.00
0.00 : 10.00
-10.00 : 0.00
-20.00 : -10.00
-30.00 : -20.00
-40.00 : -30.00
-50.00 : -40.00
-60.00 : -50.00
-70.00 : -60.00
-80.00 : -70.00
-90.00 : -80.00
-100.00 : -90.00

D.5 FN currents

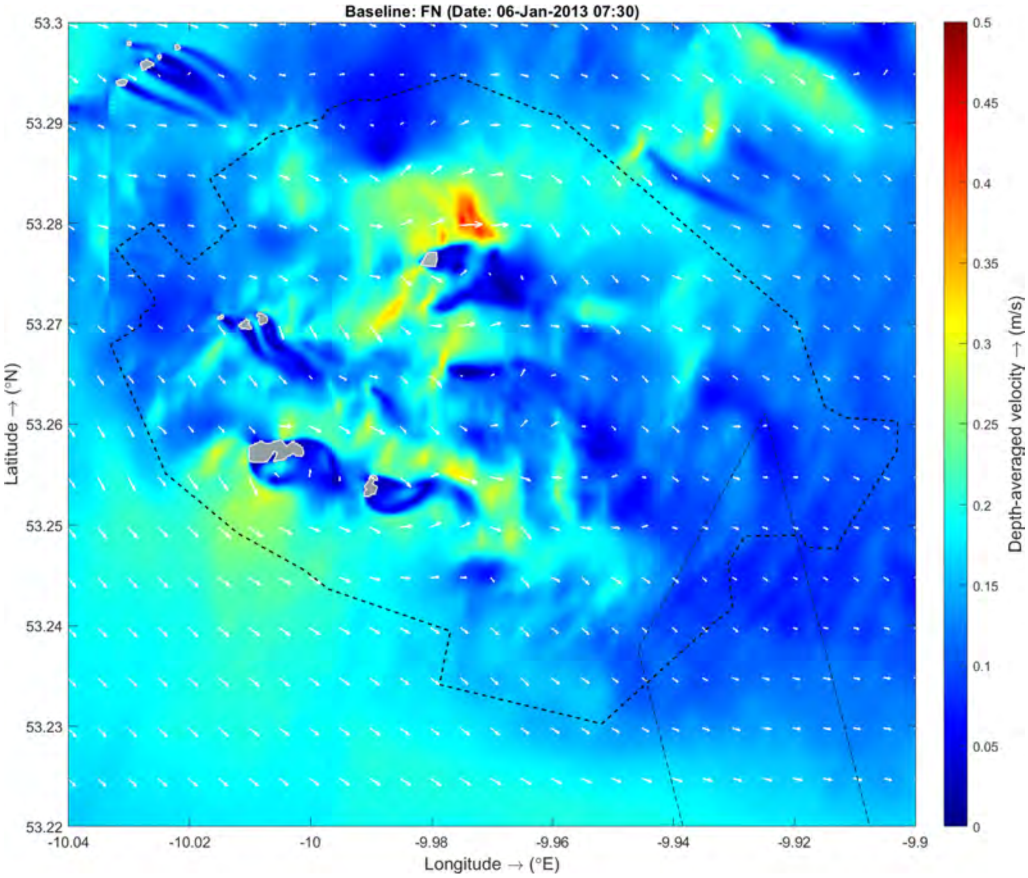

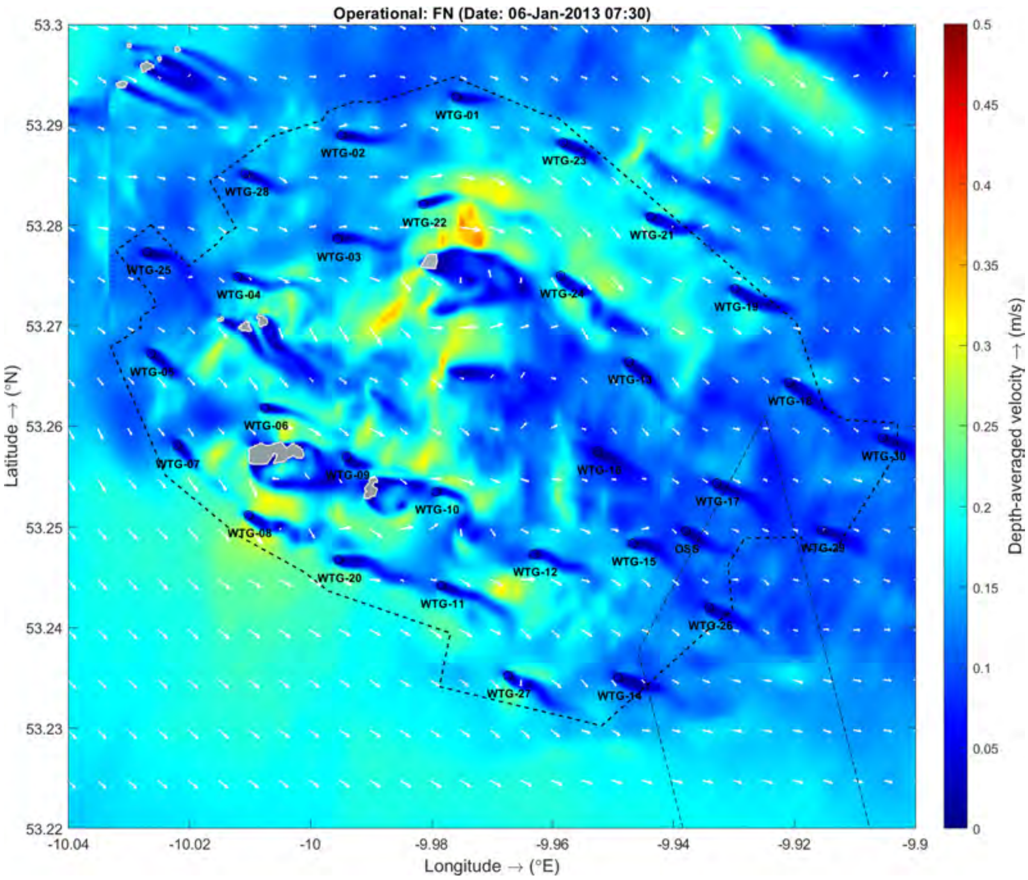

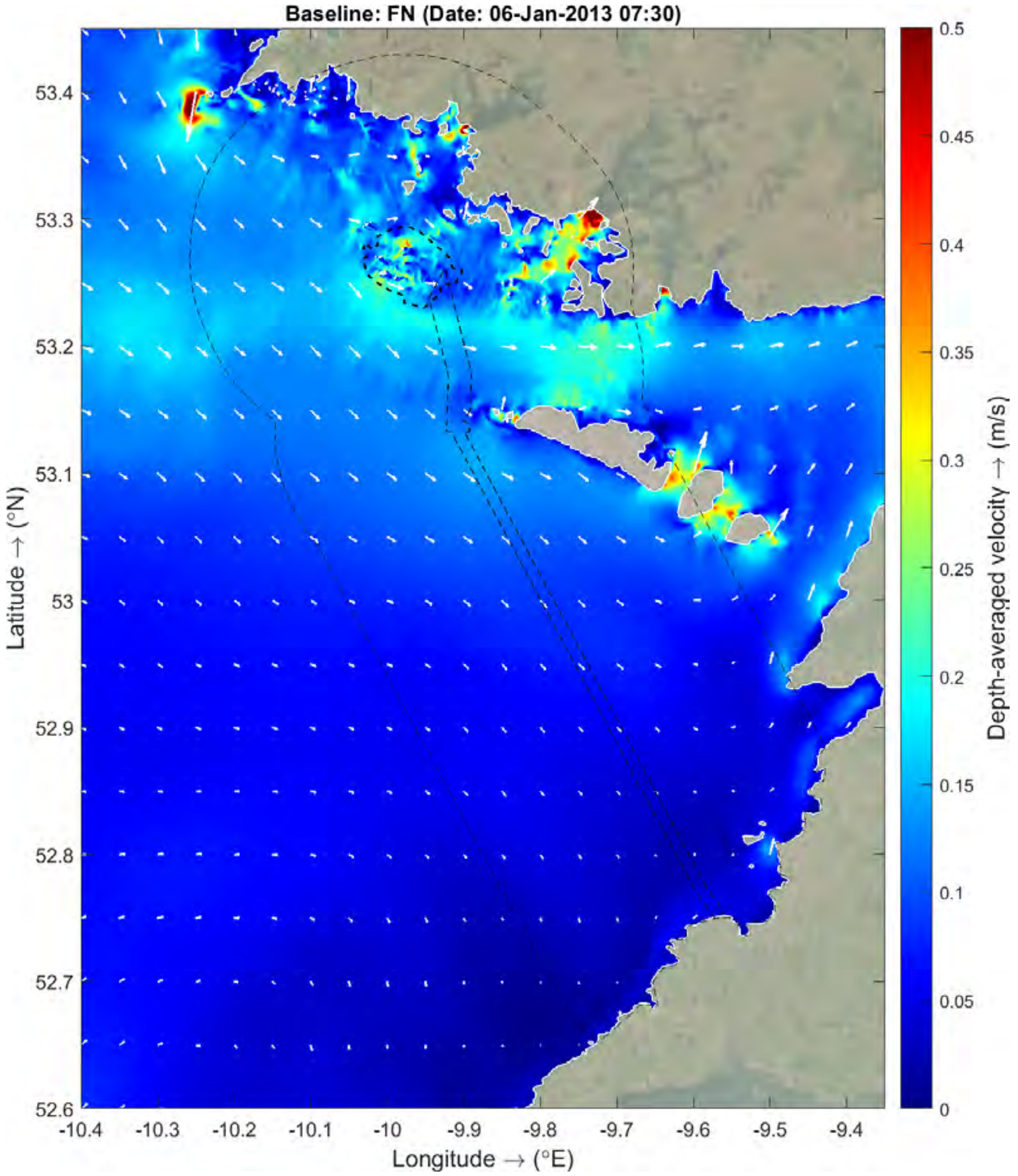
Baseline: FN (Date: 06-Jan-2013 07:30)
53.4
53.3
53.2
53.1
53
52.9
52.8
52.7
52.6
Latitude → (°N)
-10.4
-10.3
-10.2
-10.1
-10
-9.9
-9.8
-9.7
-9.6
-9.5
-9.4
Longitude → (°E)
0.5
0.45
0.4
0.35
0.3
0.25
0.2
0.15
0.1
0.05
0
Depth-averaged velocity → (m/s)

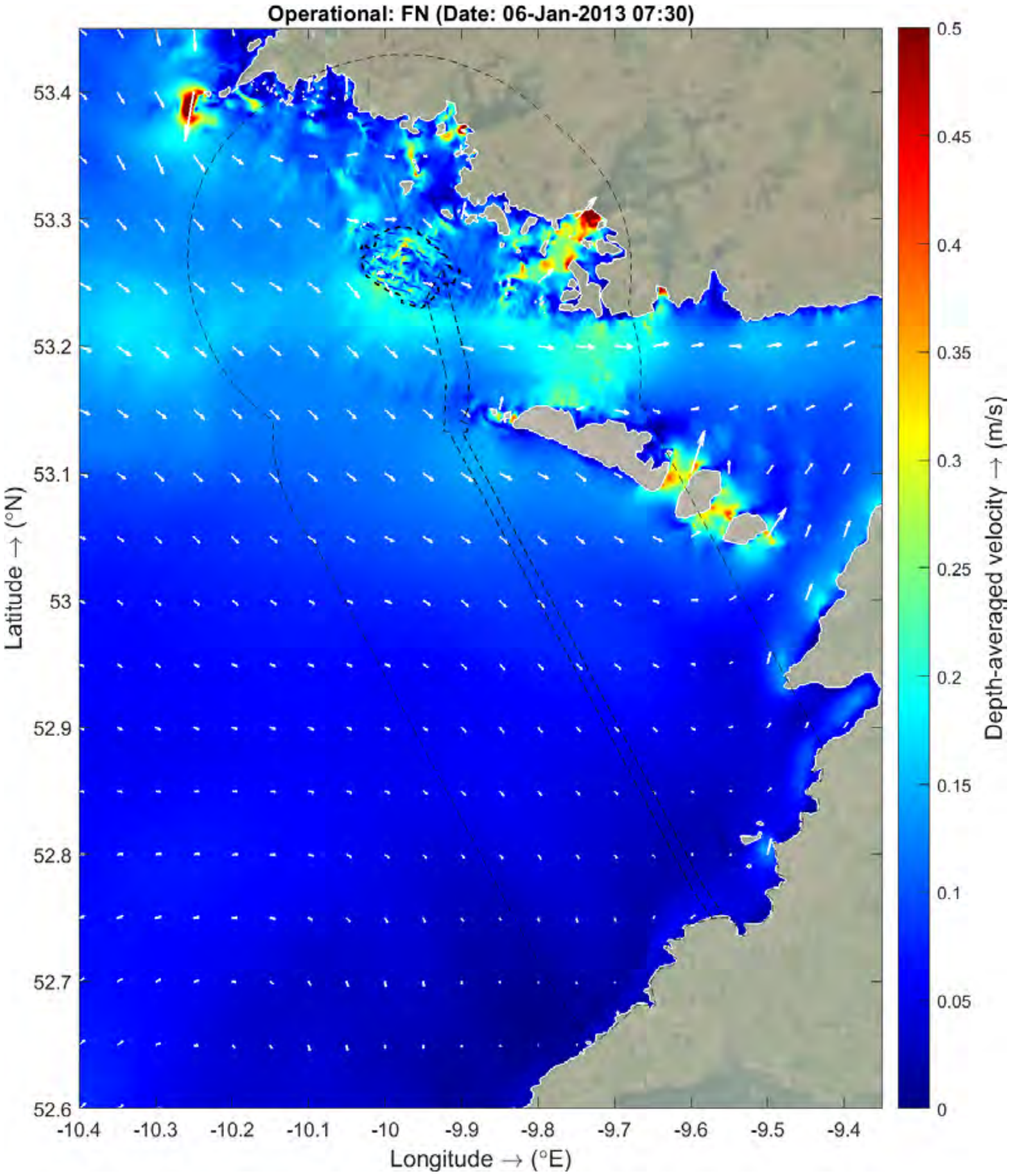
Operational: FN (Date: 06-Jan-2013 07:30)
53.4
53.3
53.2
53.1
53
52.9
52.8
52.7
52.6
Latitude → (°N)
-10.4
-10.3
-10.2
-10.1
-10
-9.9
-9.8
-9.7
-9.6
-9.5
-9.4
Longitude → (°E)
0.5
0.45
0.4
0.35
0.3
0.25
0.2
0.15
0.1
0.05
0
Depth-averaged velocity → (m/s)

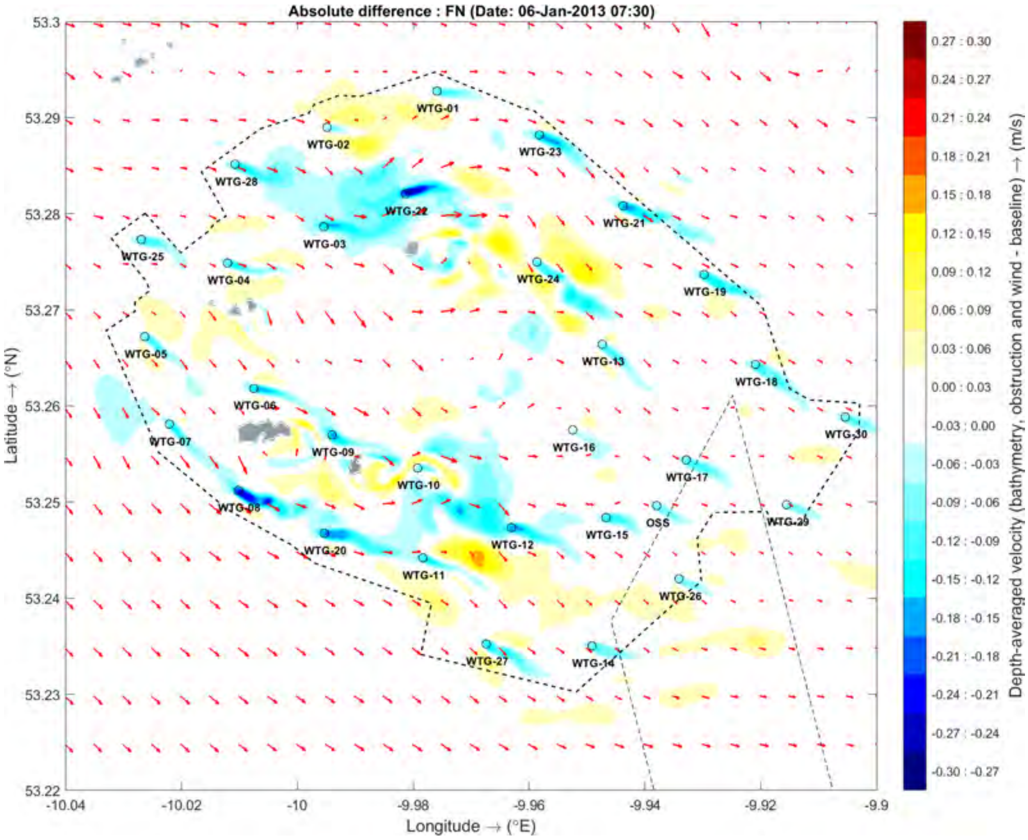
Absolute difference : FN (Date: 06-Jan-2013 07:30)
Latitude → (°N)
Longitude → (°E)
Depth-averaged velocity (bathymetry, obstruction and wind - baseline) → (m/s)
0.27 : 0.30
0.24 : 0.27
0.21 : 0.24
0.18 : 0.21
0.15 : 0.18
0.12 : 0.15
0.09 : 0.12
0.06 : 0.09
0.03 : 0.06
0.00 : 0.03
-0.03 : 0.00
-0.06 : -0.03
-0.09 : -0.06
-0.12 : -0.09
-0.15 : -0.12
-0.18 : -0.15
-0.21 : -0.18
-0.24 : -0.21
-0.27 : -0.24
-0.30 : -0.27
WTG-01
WTG-02
WTG-03
WTG-04
WTG-05
WTG-06
WTG-07
WTG-08
WTG-09
WTG-10
WTG-11
WTG-12
WTG-13
WTG-14
WTG-15
WTG-16
WTG-17
WTG-18
WTG-19
WTG-20
WTG-21
WTG-22
WTG-23
WTG-24
WTG-25
WTG-26
WTG-27
WTG-28
WTG-29
WTG-30
OSS

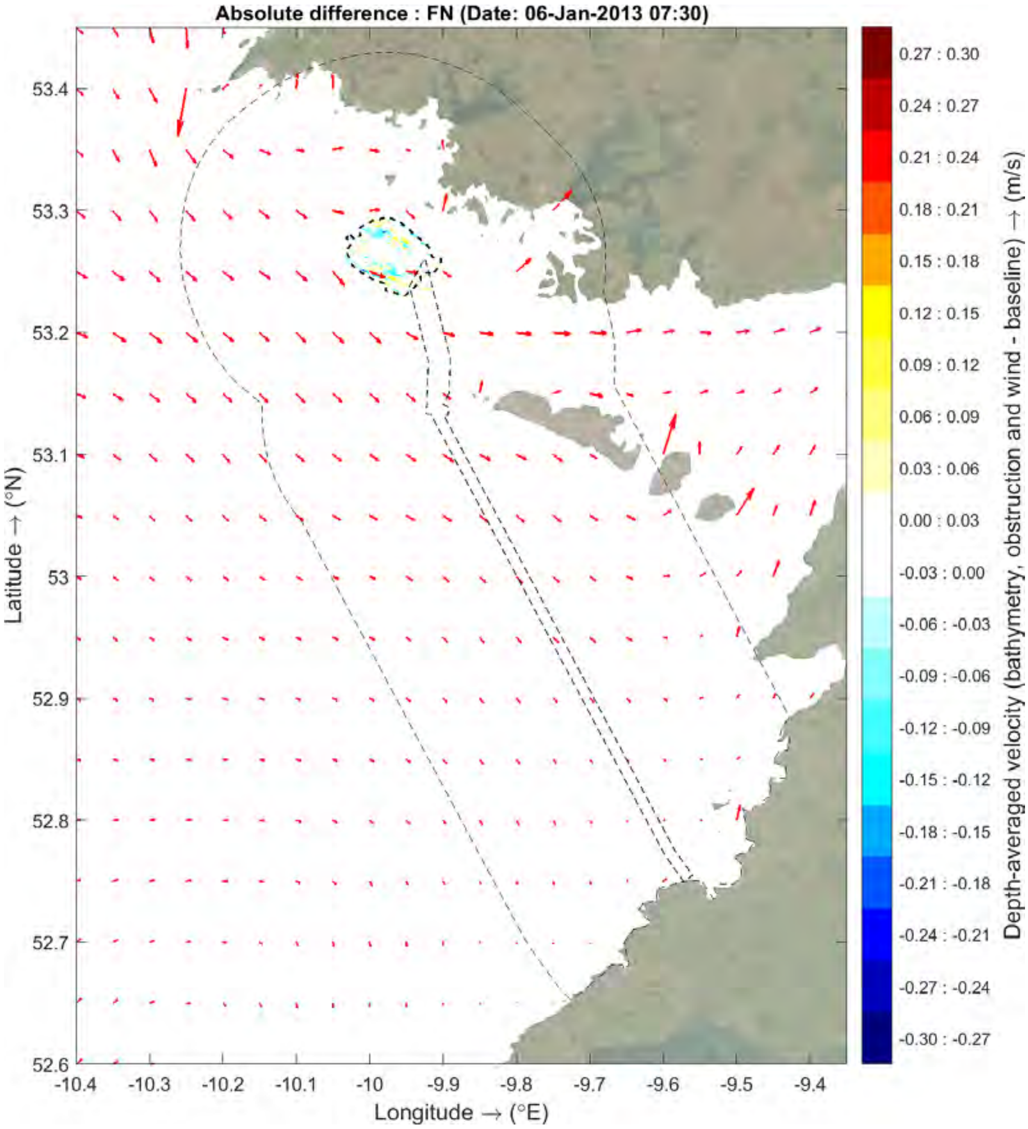
Absolute difference : FN (Date: 06-Jan-2013 07:30)
53.4
53.3
53.2
53.1
53
52.9
52.8
52.7
52.6
Latitude → (°N)
-10.4
-10.3
-10.2
-10.1
-10
-9.9
-9.8
-9.7
-9.6
-9.5
-9.4
Longitude → (°E)
0.27 : 0.30
0.24 : 0.27
0.21 : 0.24
0.18 : 0.21
0.15 : 0.18
0.12 : 0.15
0.09 : 0.12
0.06 : 0.09
0.03 : 0.06
0.00 : 0.03
-0.03 : 0.00
-0.06 : -0.03
-0.09 : -0.06
-0.12 : -0.09
-0.15 : -0.12
-0.18 : -0.15
-0.21 : -0.18
-0.24 : -0.21
-0.27 : -0.24
-0.30 : -0.27
Depth-averaged velocity (bathymetry, obstruction and wind - baseline) → (m/s)

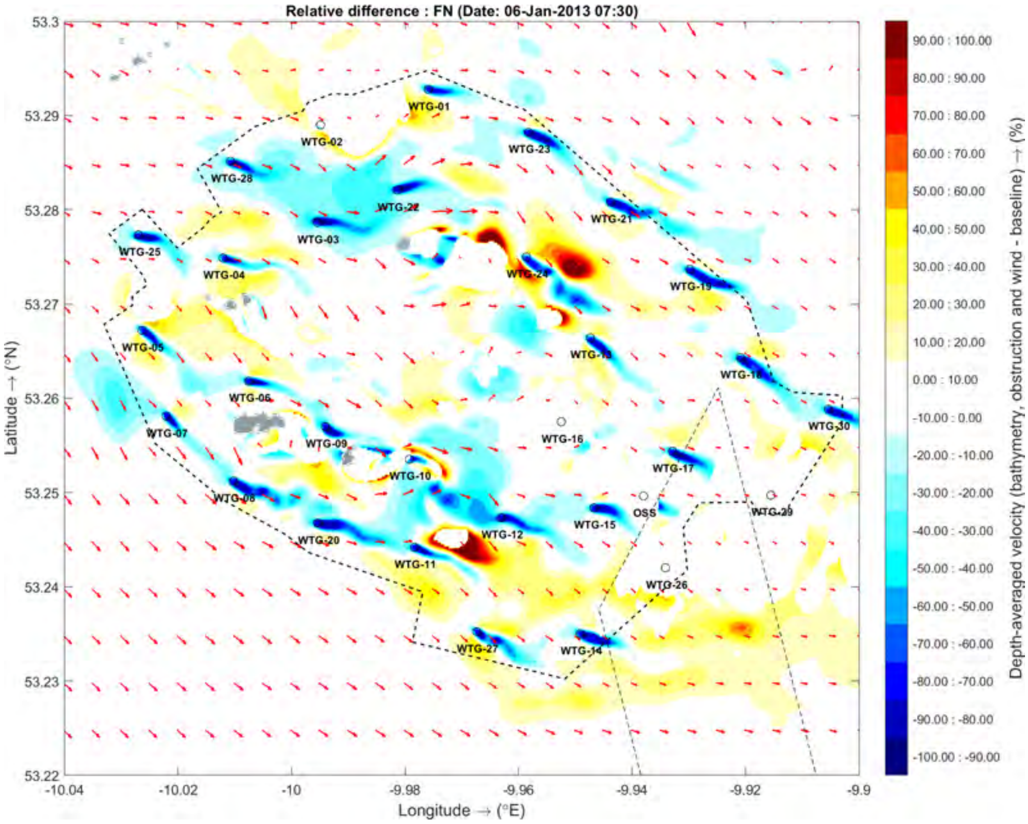
Relative difference : FN (Date: 06-Jan-2013 07:30)
Latitude → (°N)
Longitude → (°E)
Depth-averaged velocity (bathymetry, obstruction and wind - baseline) → (%)
90.00 : 100.00
80.00 : 90.00
70.00 : 80.00
60.00 : 70.00
50.00 : 60.00
40.00 : 50.00
30.00 : 40.00
20.00 : 30.00
10.00 : 20.00
0.00 : 10.00
-10.00 : 0.00
-20.00 : -10.00
-30.00 : -20.00
-40.00 : -30.00
-50.00 : -40.00
-60.00 : -50.00
-70.00 : -60.00
-80.00 : -70.00
-90.00 : -80.00
-100.00 : -90.00
OSS

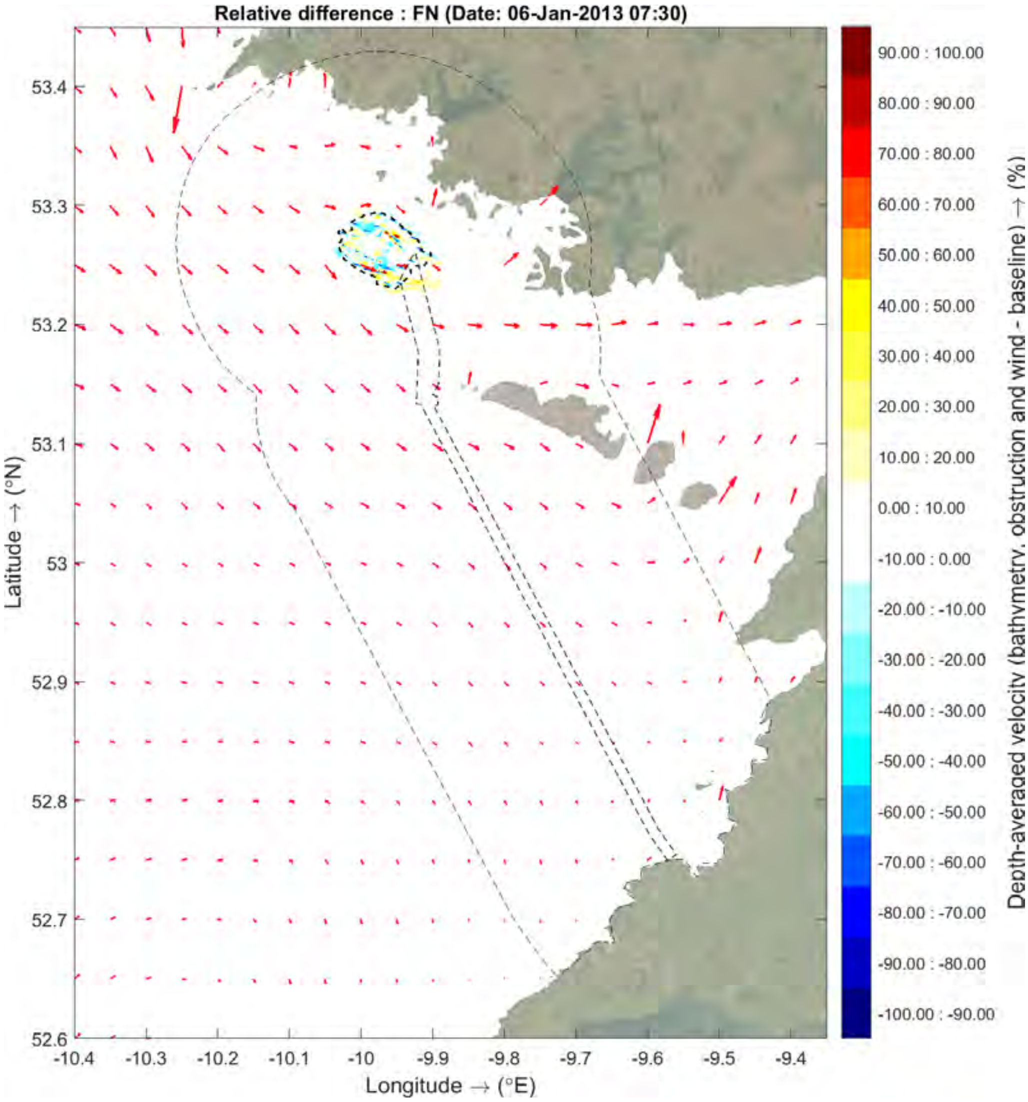
Relative difference : FN (Date: 06-Jan-2013 07:30)
Latitude → (°N)
Longitude → (°E)
Depth-averaged velocity (bathymetry, obstruction and wind - baseline) → (%)
90.00 : 100.00
80.00 : 90.00
70.00 : 80.00
60.00 : 70.00
50.00 : 60.00
40.00 : 50.00
30.00 : 40.00
20.00 : 30.00
10.00 : 20.00
0.00 : 10.00
-10.00 : 0.00
-20.00 : -10.00
-30.00 : -20.00
-40.00 : -30.00
-50.00 : -40.00
-60.00 : -50.00
-70.00 : -60.00
-80.00 : -70.00
-90.00 : -80.00
-100.00 : -90.00

D.6 FN water levels

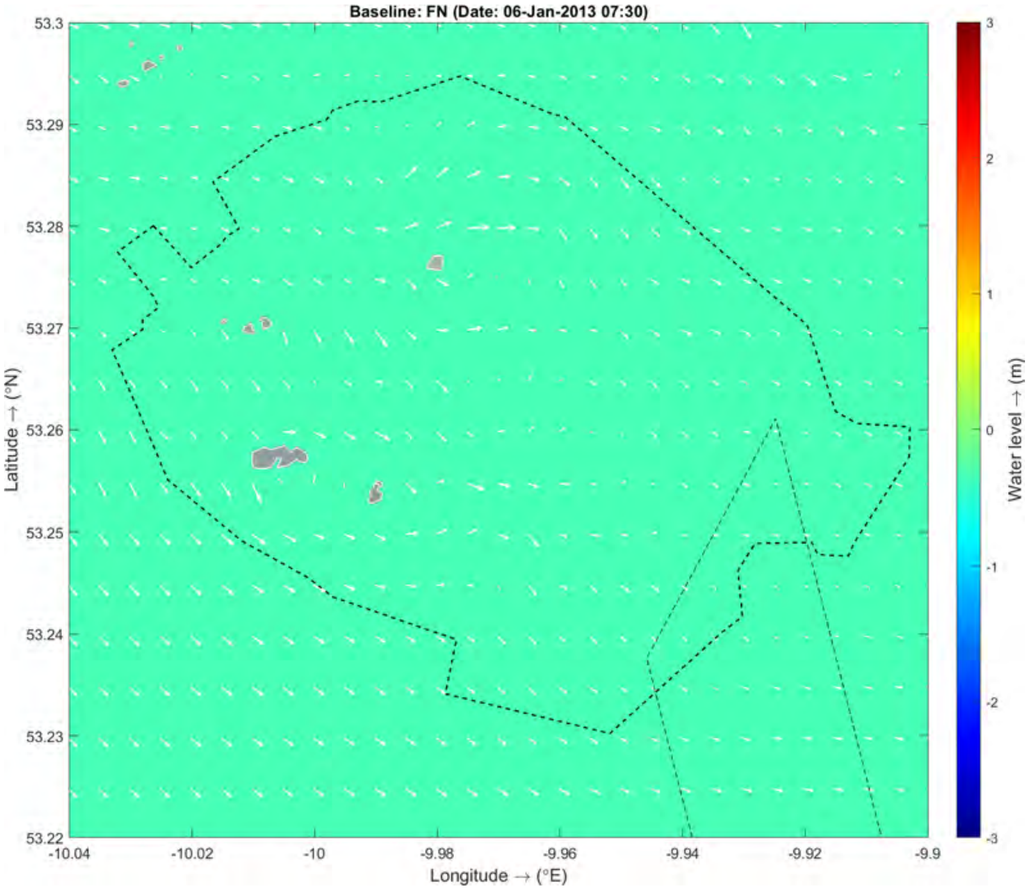

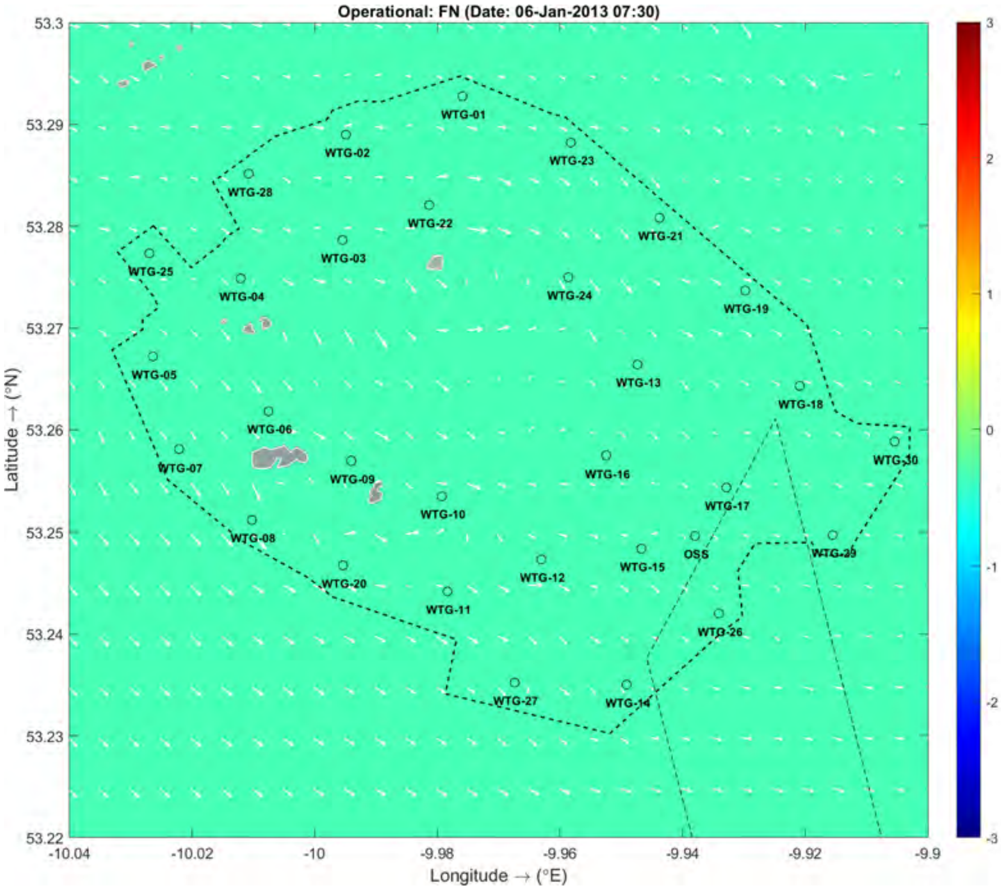
Operational: FN (Date: 06-Jan-2013 07:30)
Latitude → (°N)
Longitude → (°E)
Water level → (m)
WTG-01
WTG-02
WTG-03
WTG-04
WTG-05
WTG-06
WTG-07
WTG-08
WTG-09
WTG-10
WTG-11
WTG-12
WTG-13
WTG-14
WTG-15
WTG-16
WTG-17
WTG-18
WTG-19
WTG-20
WTG-21
WTG-22
WTG-23
WTG-24
WTG-25
WTG-26
WTG-27
WTG-28
WTG-29
WTG-30
OSS

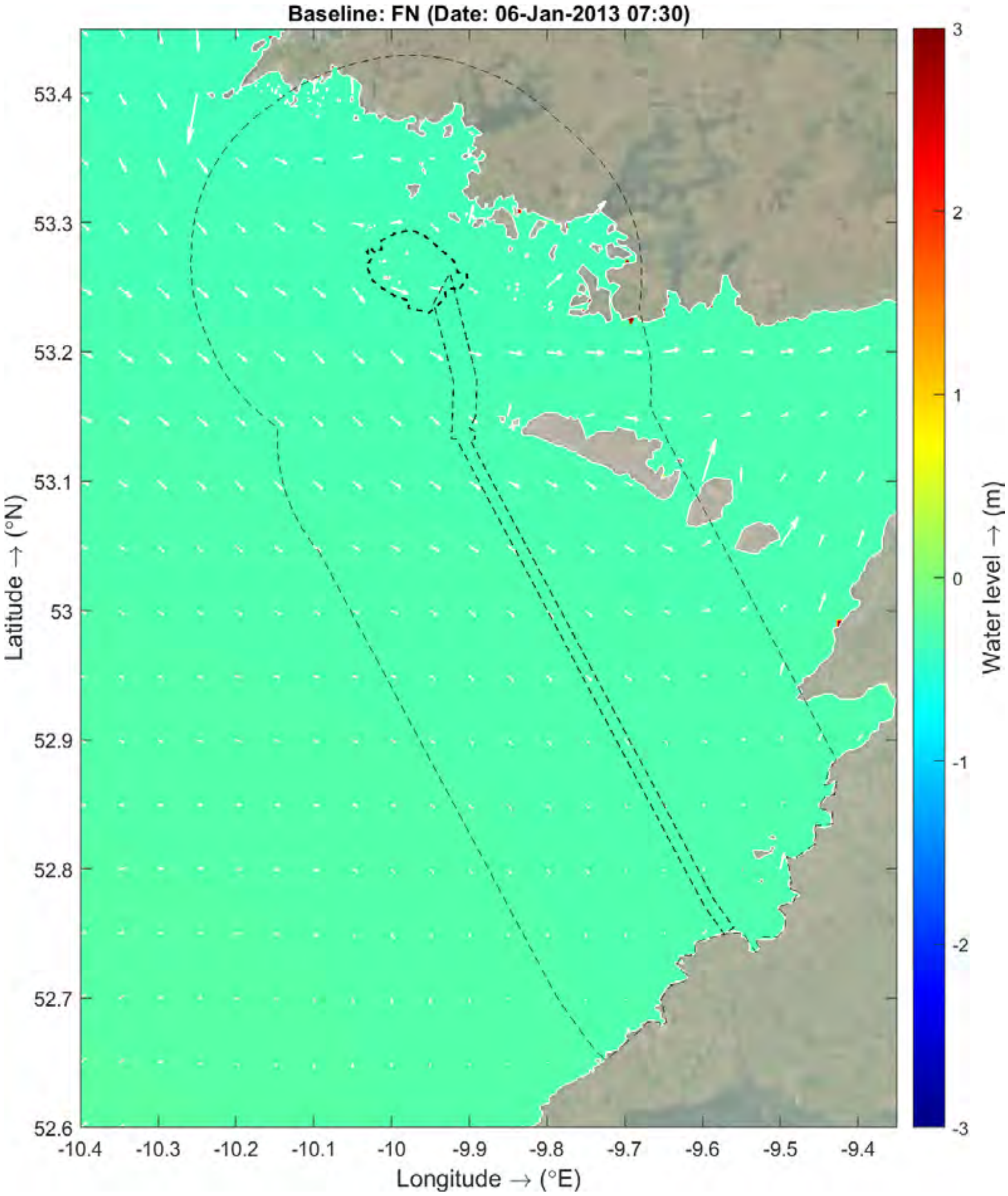
Baseline: FN (Date: 06-Jan-2013 07:30)
Latitude → (°N)
Longitude → (°E)
Water level → (m)
53.4
53.3
53.2
53.1
53
52.9
52.8
52.7
52.6
-10.4
-10.3
-10.2
-10.1
-10
-9.9
-9.8
-9.7
-9.6
-9.5
-9.4
3
2
1
0
-1
-2
-3

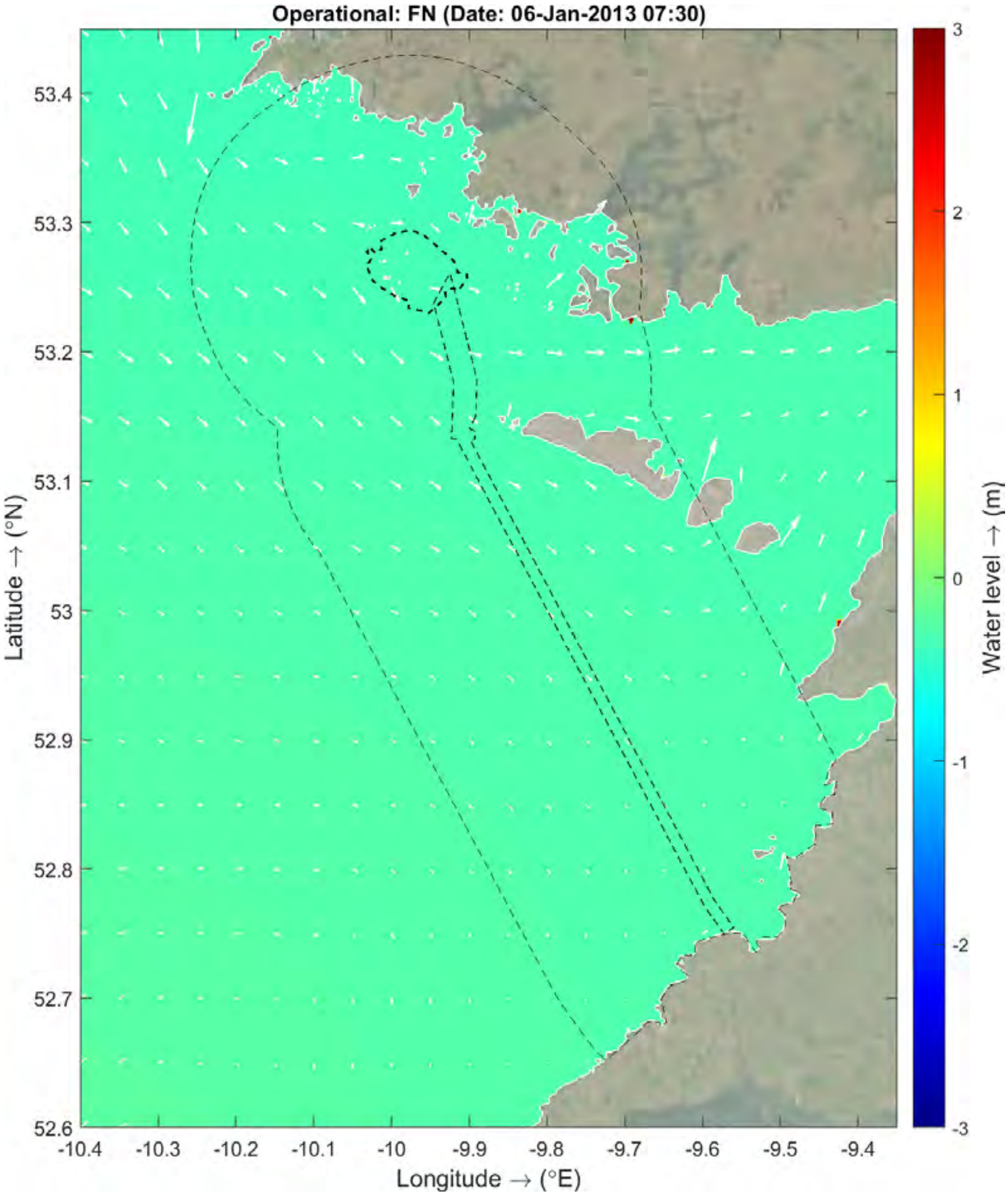
Operational: FN (Date: 06-Jan-2013 07:30)
Latitude → (°N)
Longitude → (°E)
Water level → (m)
53.4
53.3
53.2
53.1
53
52.9
52.8
52.7
52.6
-10.4
-10.3
-10.2
-10.1
-10
-9.9
-9.8
-9.7
-9.6
-9.5
-9.4
3
2
1
0
-1
-2
-3

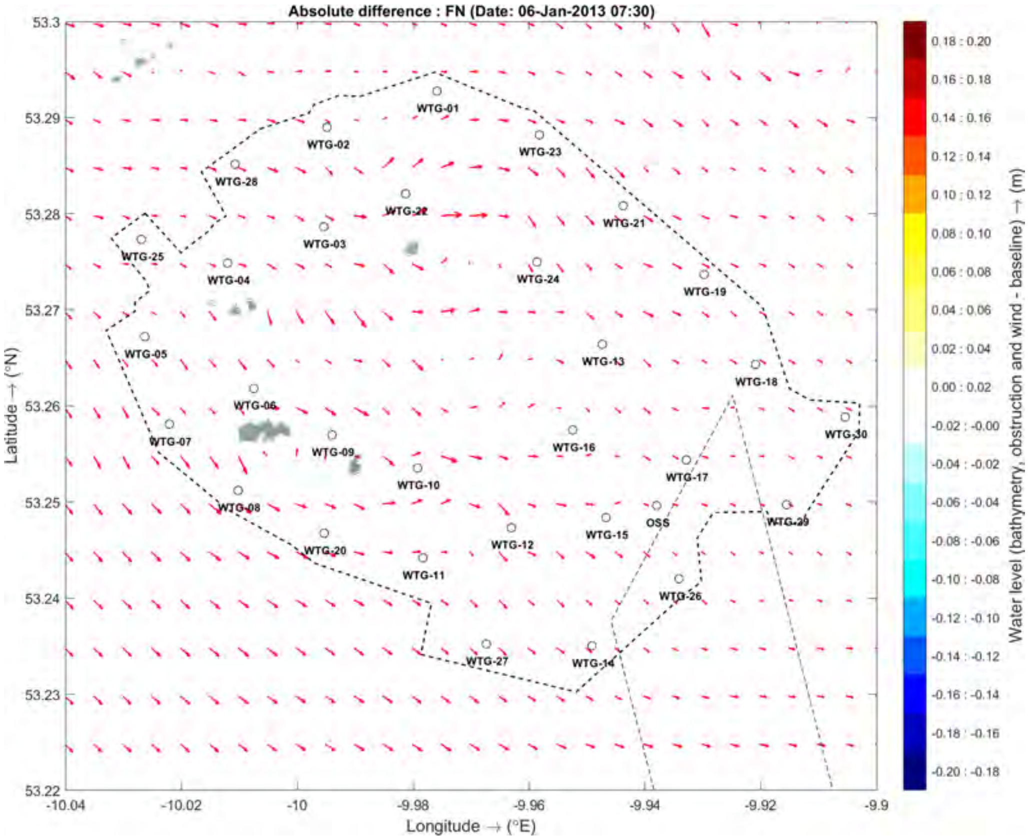
Absolute difference : FN (Date: 06-Jan-2013 07:30)
Latitude → (°N)
Longitude → (°E)
Water level (bathymetry, obstruction and wind - baseline) → (m)
WTG-01
WTG-02
WTG-03
WTG-04
WTG-05
WTG-06
WTG-07
WTG-08
WTG-09
WTG-10
WTG-11
WTG-12
WTG-13
WTG-14
WTG-15
WTG-16
WTG-17
WTG-18
WTG-19
WTG-20
WTG-21
WTG-22
WTG-23
WTG-24
WTG-25
WTG-26
WTG-27
WTG-28
WTG-29
WTG-30
OSS
0.18 : 0.20
0.16 : 0.18
0.14 : 0.16
0.12 : 0.14
0.10 : 0.12
0.08 : 0.10
0.06 : 0.08
0.04 : 0.06
0.02 : 0.04
0.00 : 0.02
-0.02 : -0.00
-0.04 : -0.02
-0.06 : -0.04
-0.08 : -0.06
-0.10 : -0.08
-0.12 : -0.10
-0.14 : -0.12
-0.16 : -0.14
-0.18 : -0.16
-0.20 : -0.18

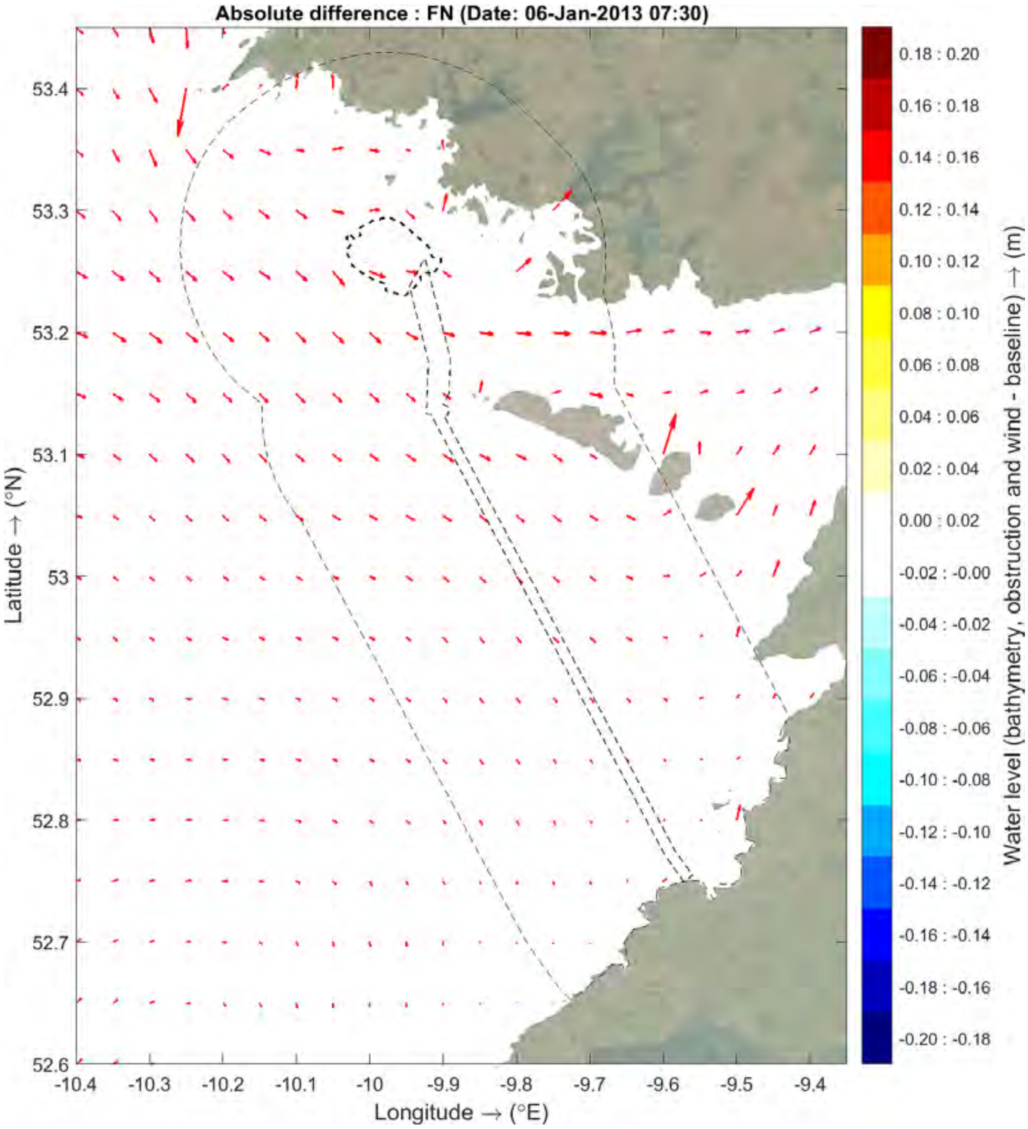
Absolute difference : FN (Date: 06-Jan-2013 07:30)
53.4
53.3
53.2
53.1
53
52.9
52.8
52.7
52.6
Latitude → (°N)
-10.4
-10.3
-10.2
-10.1
-10
-9.9
-9.8
-9.7
-9.6
-9.5
-9.4
Longitude → (°E)
0.18 : 0.20
0.16 : 0.18
0.14 : 0.16
0.12 : 0.14
0.10 : 0.12
0.08 : 0.10
0.06 : 0.08
0.04 : 0.06
0.02 : 0.04
0.00 : 0.02
-0.02 : -0.00
-0.04 : -0.02
-0.06 : -0.04
-0.08 : -0.06
-0.10 : -0.08
-0.12 : -0.10
-0.14 : -0.12
-0.16 : -0.14
-0.18 : -0.16
-0.20 : -0.18
Water level (bathymetry, obstruction and wind - baseline) → (m)

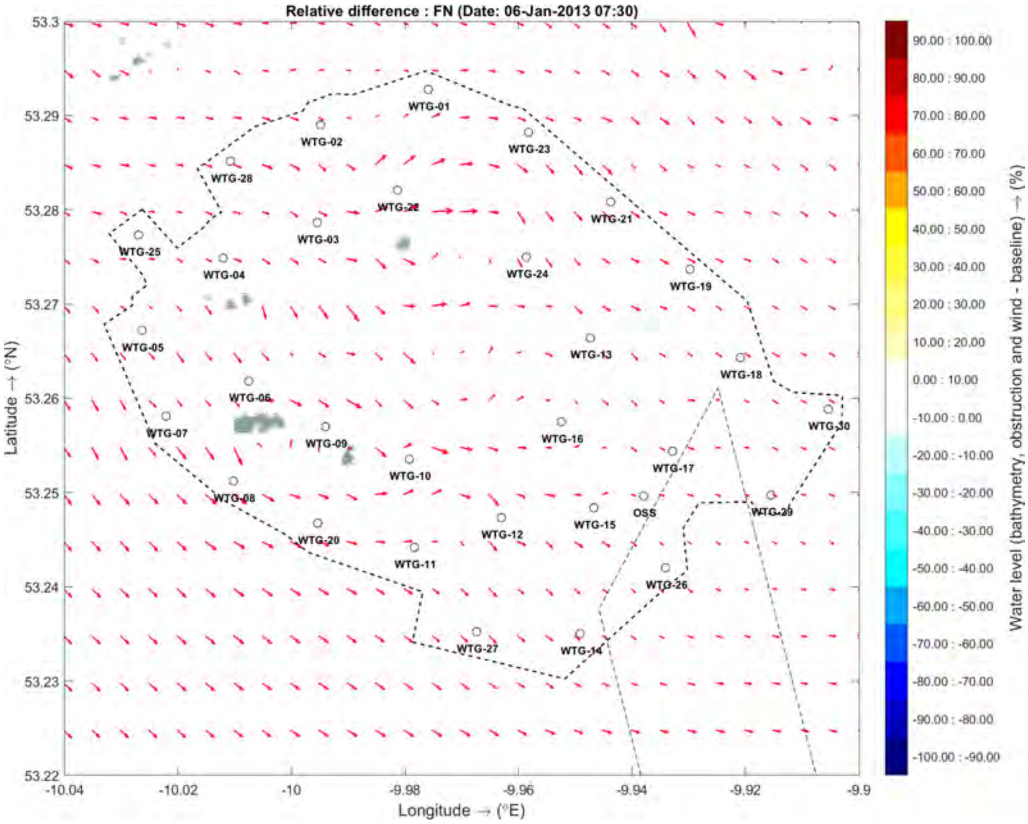
Relative difference : FN (Date: 06-Jan-2013 07:30)
Latitude → (°N)
Longitude → (°E)
Water level (bathymetry, obstruction and wind - baseline) → (%)
WTG-01
WTG-02
WTG-03
WTG-04
WTG-05
WTG-06
WTG-07
WTG-08
WTG-09
WTG-10
WTG-11
WTG-12
WTG-13
WTG-14
WTG-15
WTG-16
WTG-17
WTG-18
WTG-19
WTG-20
WTG-21
WTG-22
WTG-23
WTG-24
WTG-25
WTG-26
WTG-27
WTG-28
WTG-29
WTG-30
OSS
90.00 : 100.00
80.00 : 90.00
70.00 : 80.00
60.00 : 70.00
50.00 : 60.00
40.00 : 50.00
30.00 : 40.00
20.00 : 30.00
10.00 : 20.00
0.00 : 10.00
-10.00 : 0.00
-20.00 : -10.00
-30.00 : -20.00
-40.00 : -30.00
-50.00 : -40.00
-60.00 : -50.00
-70.00 : -60.00
-80.00 : -70.00
-90.00 : -80.00
-100.00 : -90.00

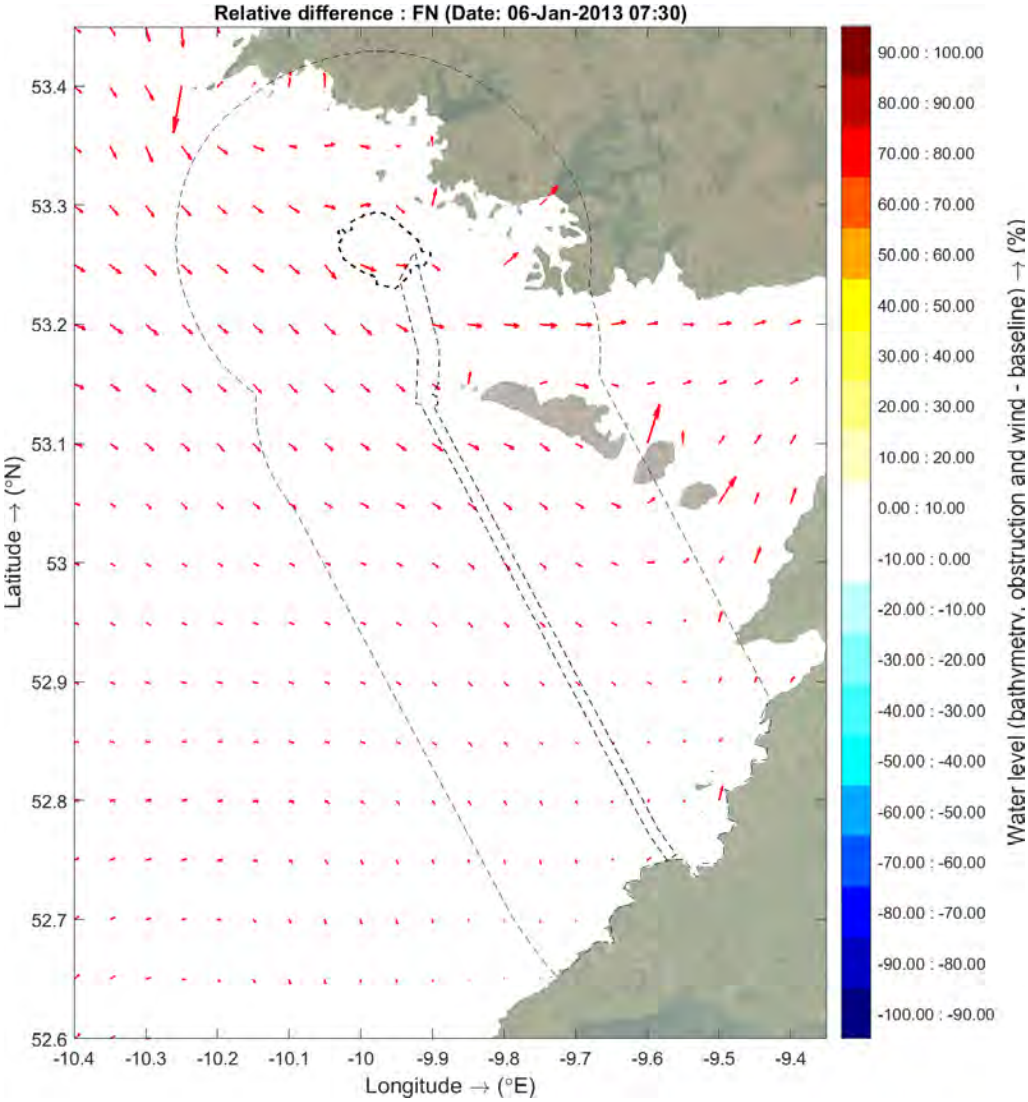
Relative difference : FN (Date: 06-Jan-2013 07:30)
53.4
53.3
53.2
53.1
53
52.9
52.8
52.7
52.6
Latitude → (°N)
-10.4
-10.3
-10.2
-10.1
-10
-9.9
-9.8
-9.7
-9.6
-9.5
-9.4
Longitude → (°E)
90.00 : 100.00
80.00 : 90.00
70.00 : 80.00
60.00 : 70.00
50.00 : 60.00
40.00 : 50.00
30.00 : 40.00
20.00 : 30.00
10.00 : 20.00
0.00 : 10.00
-10.00 : 0.00
-20.00 : -10.00
-30.00 : -20.00
-40.00 : -30.00
-50.00 : -40.00
-60.00 : -50.00
-70.00 : -60.00
-80.00 : -70.00
-90.00 : -80.00
-100.00 : -90.00
Water level (bathymetry, obstruction and wind - baseline) → (%)

D.7 FS currents

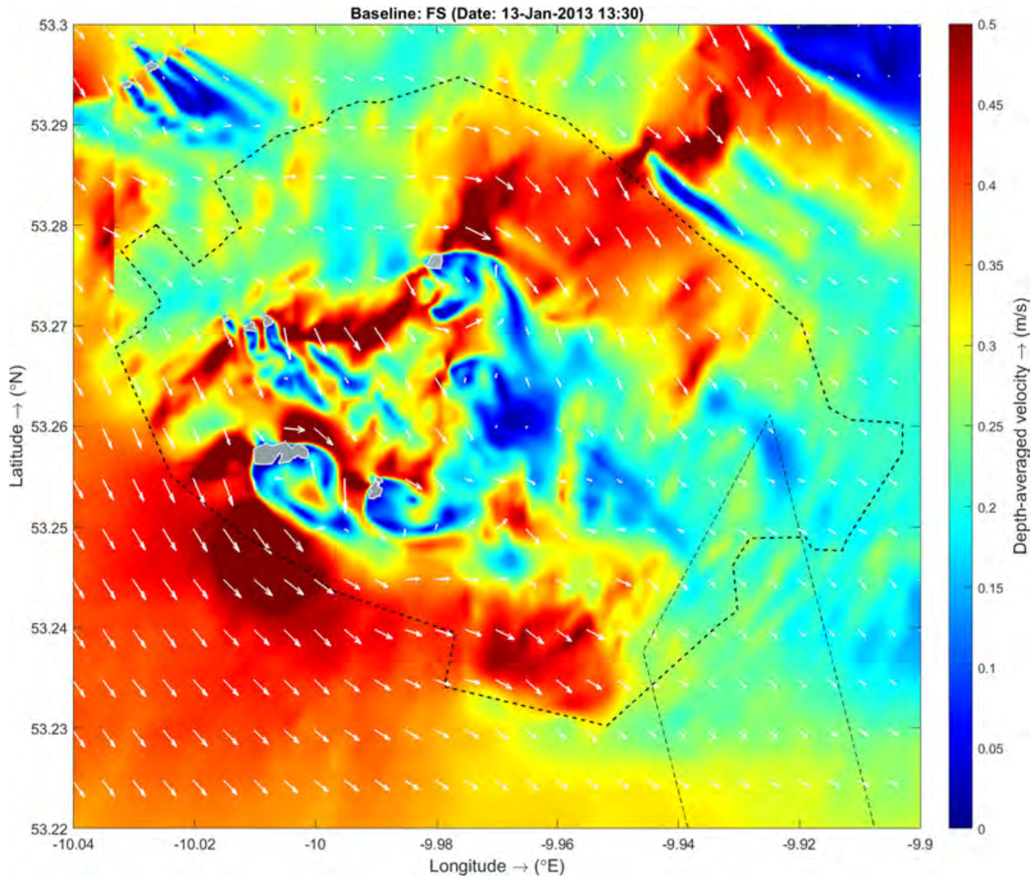

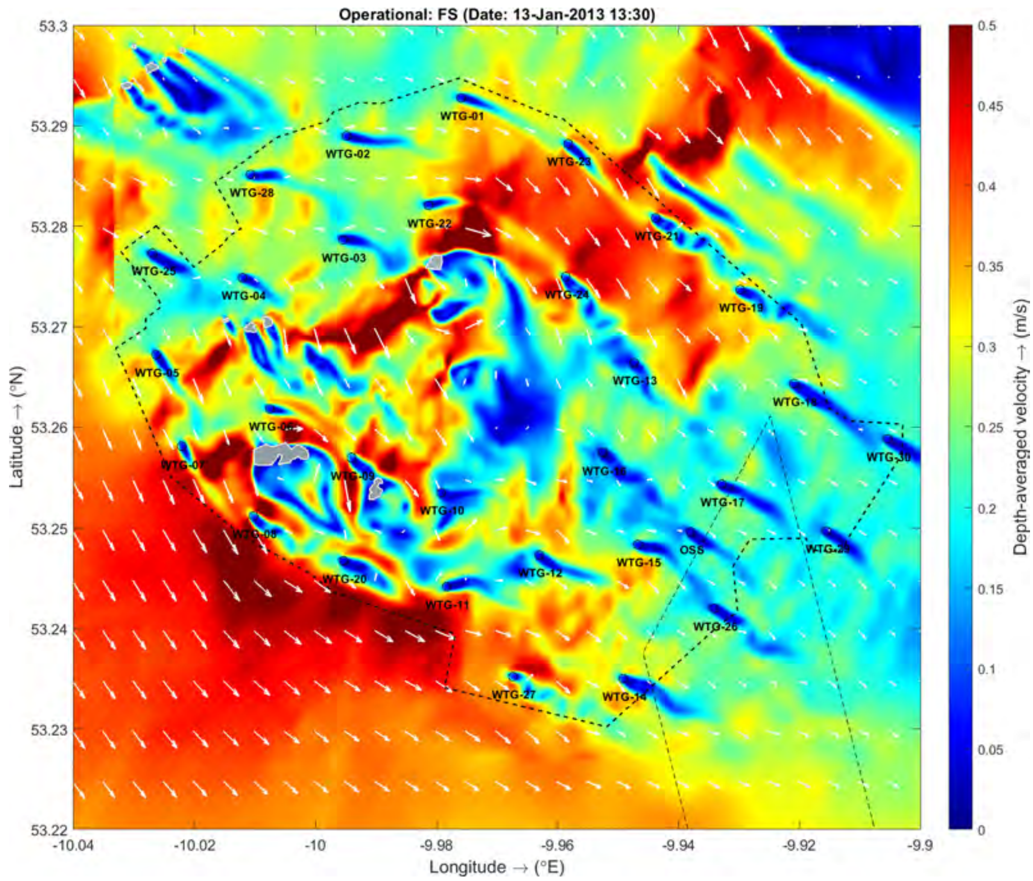

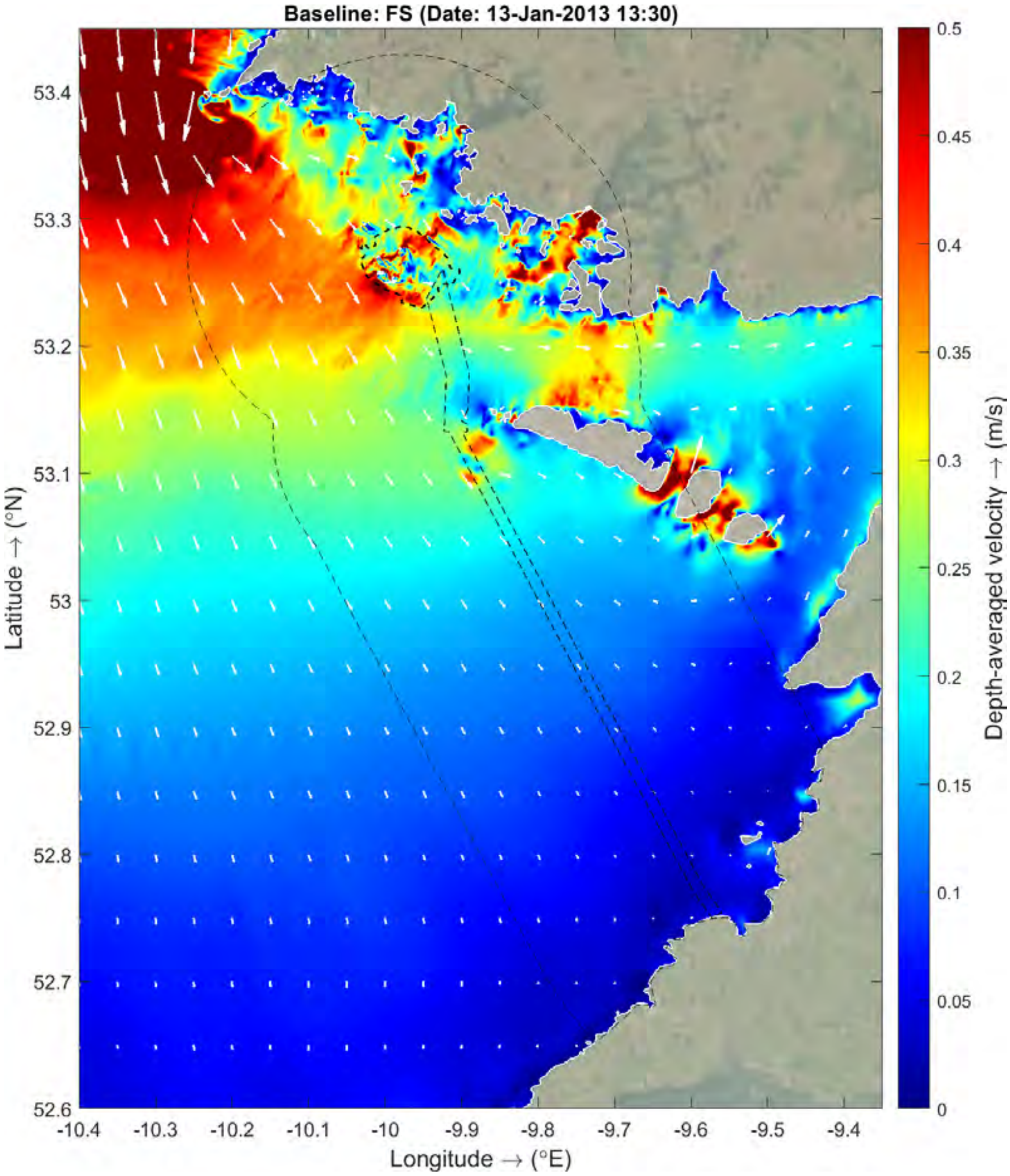
Baseline: FS (Date: 13-Jan-2013 13:30)
53.4
53.3
53.2
53.1
53
52.9
52.8
52.7
52.6
Latitude → (°N)
-10.4
-10.3
-10.2
-10.1
-10
-9.9
-9.8
-9.7
-9.6
-9.5
-9.4
Longitude → (°E)
0.5
0.45
0.4
0.35
0.3
0.25
0.2
0.15
0.1
0.05
0
Depth-averaged velocity → (m/s)

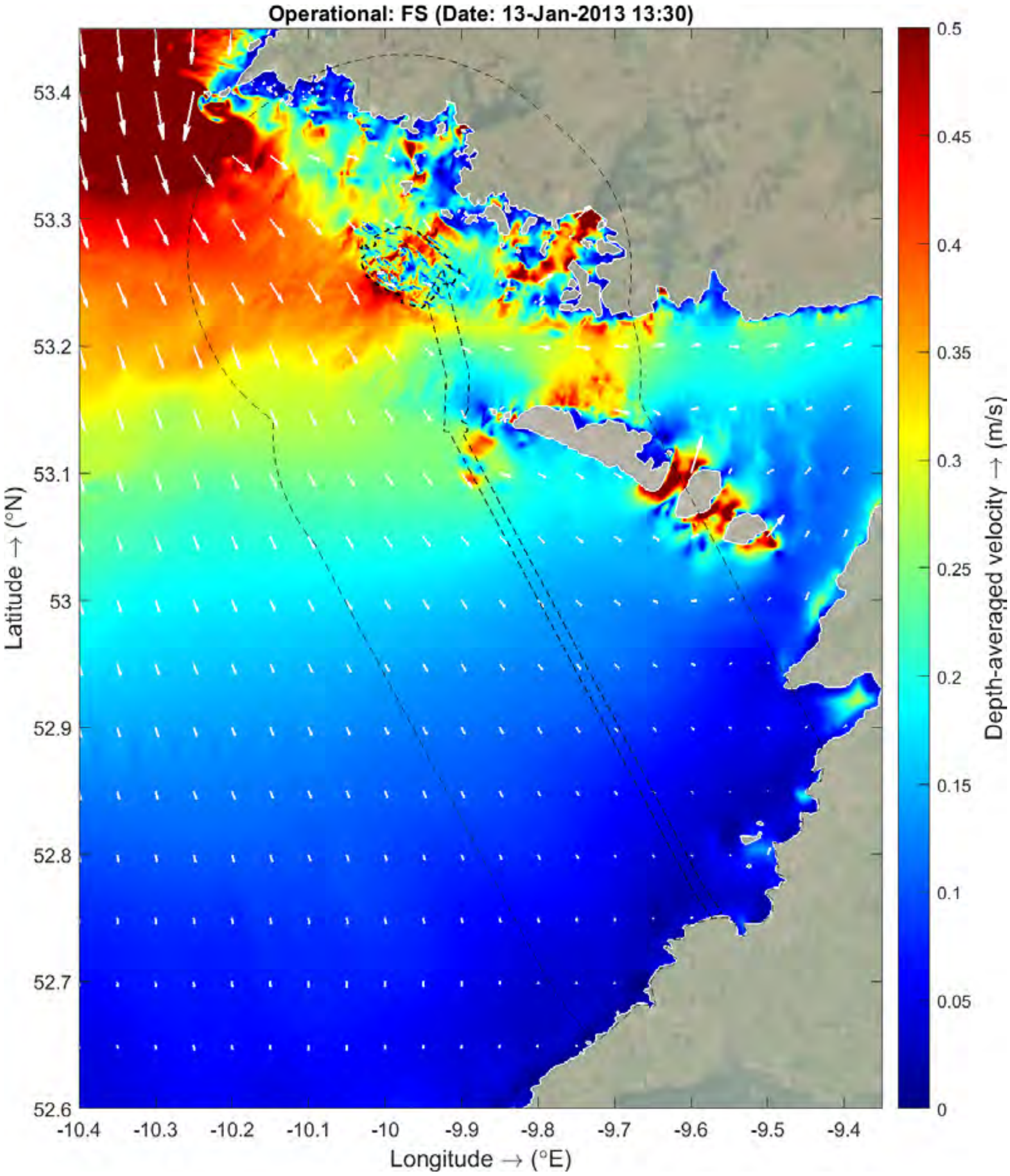
Operational: FS (Date: 13-Jan-2013 13:30)
Latitude → (°N)
Longitude → (°E)
Depth-averaged velocity → (m/s)
53.4
53.3
53.2
53.1
53
52.9
52.8
52.7
52.6
-10.4
-10.3
-10.2
-10.1
-10
-9.9
-9.8
-9.7
-9.6
-9.5
-9.4
0.5
0.45
0.4
0.35
0.3
0.25
0.2
0.15
0.1
0.05
0

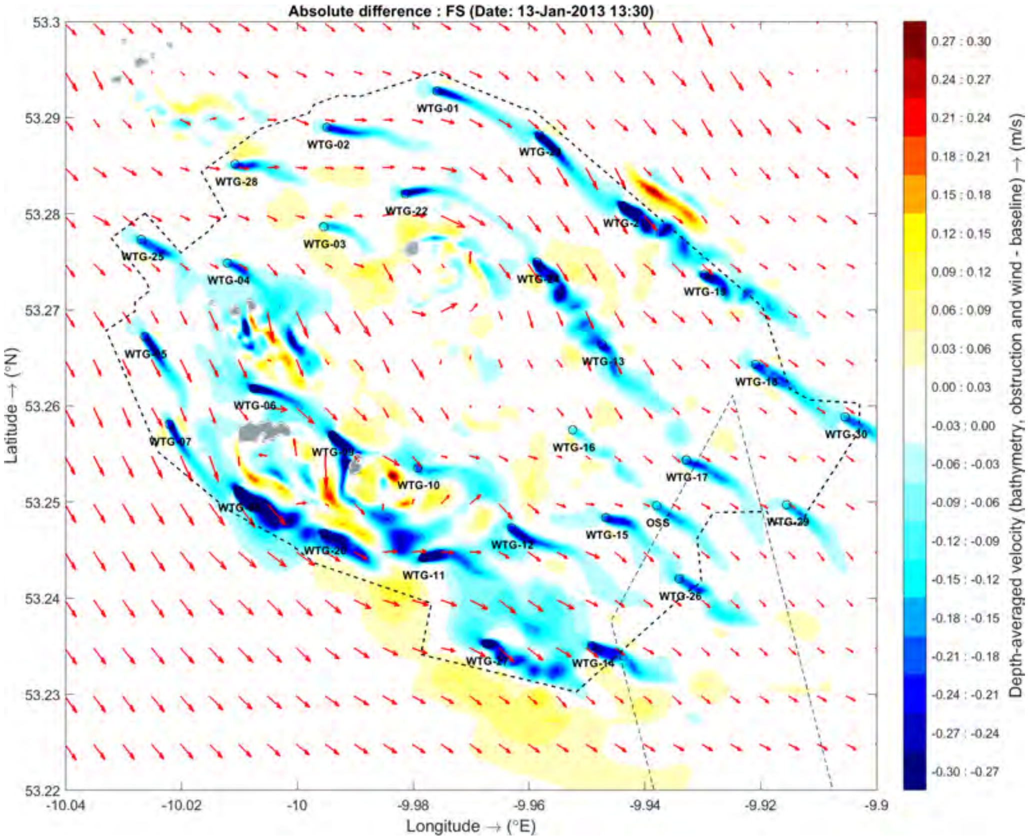
Absolute difference : FS (Date: 13-Jan-2013 13:30)
Latitude → (°N)
Longitude → (°E)
Depth-averaged velocity (bathymetry, obstruction and wind - baseline) → (m/s)
WTG-01
WTG-02
WTG-28
WTG-22
WTG-03
WTG-25
WTG-04
WTG-06
WTG-07
WTG-10
WTG-11
WTG-12
WTG-13
WTG-15
WTG-16
WTG-17
WTG-18
WTG-19
WTG-20
WTG-26
WTG-27
WTG-29
WTG-30
WTG-14
OSS
0.27 : 0.30
0.24 : 0.27
0.21 : 0.24
0.18 : 0.21
0.15 : 0.18
0.12 : 0.15
0.09 : 0.12
0.06 : 0.09
0.03 : 0.06
0.00 : 0.03
-0.03 : 0.00
-0.06 : -0.03
-0.09 : -0.06
-0.12 : -0.09
-0.15 : -0.12
-0.18 : -0.15
-0.21 : -0.18
-0.24 : -0.21
-0.27 : -0.24
-0.30 : -0.27

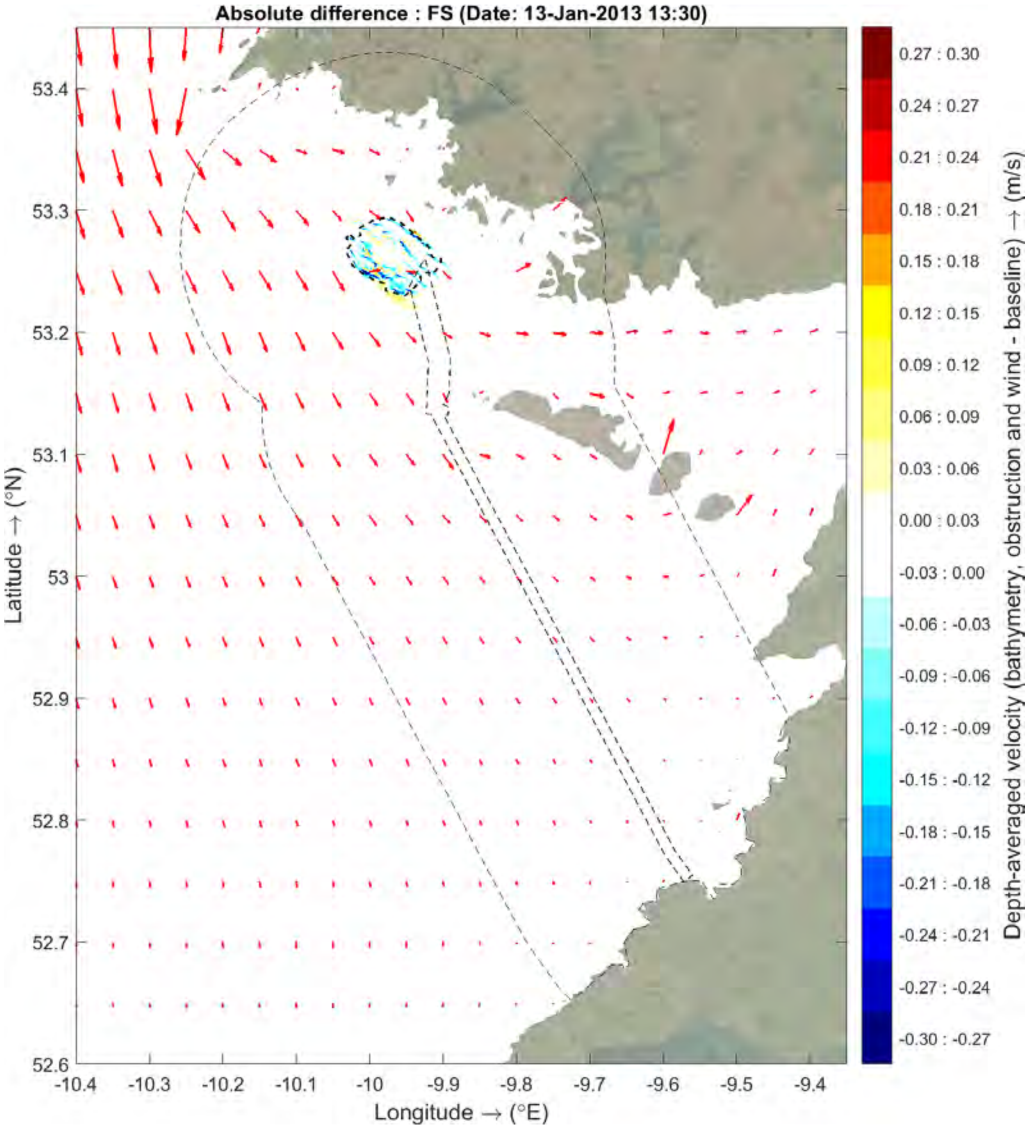
Absolute difference : FS (Date: 13-Jan-2013 13:30)
Latitude → (°N)
Longitude → (°E)
Depth-averaged velocity (bathymetry, obstruction and wind - baseline) → (m/s)
0.27 : 0.30
0.24 : 0.27
0.21 : 0.24
0.18 : 0.21
0.15 : 0.18
0.12 : 0.15
0.09 : 0.12
0.06 : 0.09
0.03 : 0.06
0.00 : 0.03
-0.03 : 0.00
-0.06 : -0.03
-0.09 : -0.06
-0.12 : -0.09
-0.15 : -0.12
-0.18 : -0.15
-0.21 : -0.18
-0.24 : -0.21
-0.27 : -0.24
-0.30 : -0.27

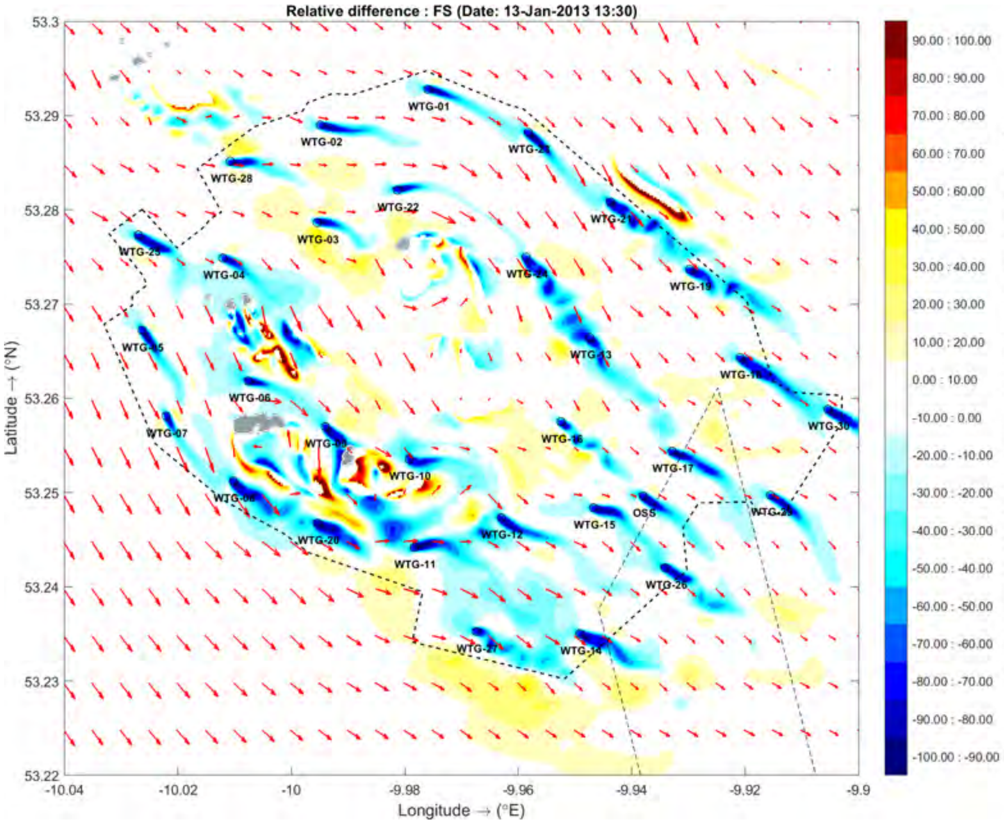
Relative difference : FS (Date: 13-Jan-2013 13:30)
Latitude → (°N)
Longitude → (°E)
Depth-averaged velocity (bathymetry, obstruction and wind - baseline) → (%)
90.00 : 100.00
80.00 : 90.00
70.00 : 80.00
60.00 : 70.00
50.00 : 60.00
40.00 : 50.00
30.00 : 40.00
20.00 : 30.00
10.00 : 20.00
0.00 : 10.00
-10.00 : 0.00
-20.00 : -10.00
-30.00 : -20.00
-40.00 : -30.00
-50.00 : -40.00
-60.00 : -50.00
-70.00 : -60.00
-80.00 : -70.00
-90.00 : -80.00
-100.00 : -90.00
WTG-01
WTG-02
WTG-28
WTG-22
WTG-03
WTG-04
WTG-06
WTG-07
WTG-10
WTG-11
WTG-12
WTG-13
WTG-15
WTG-17
WTG-19
WTG-20
WTG-27
WTG-14
OSS
WTG-30

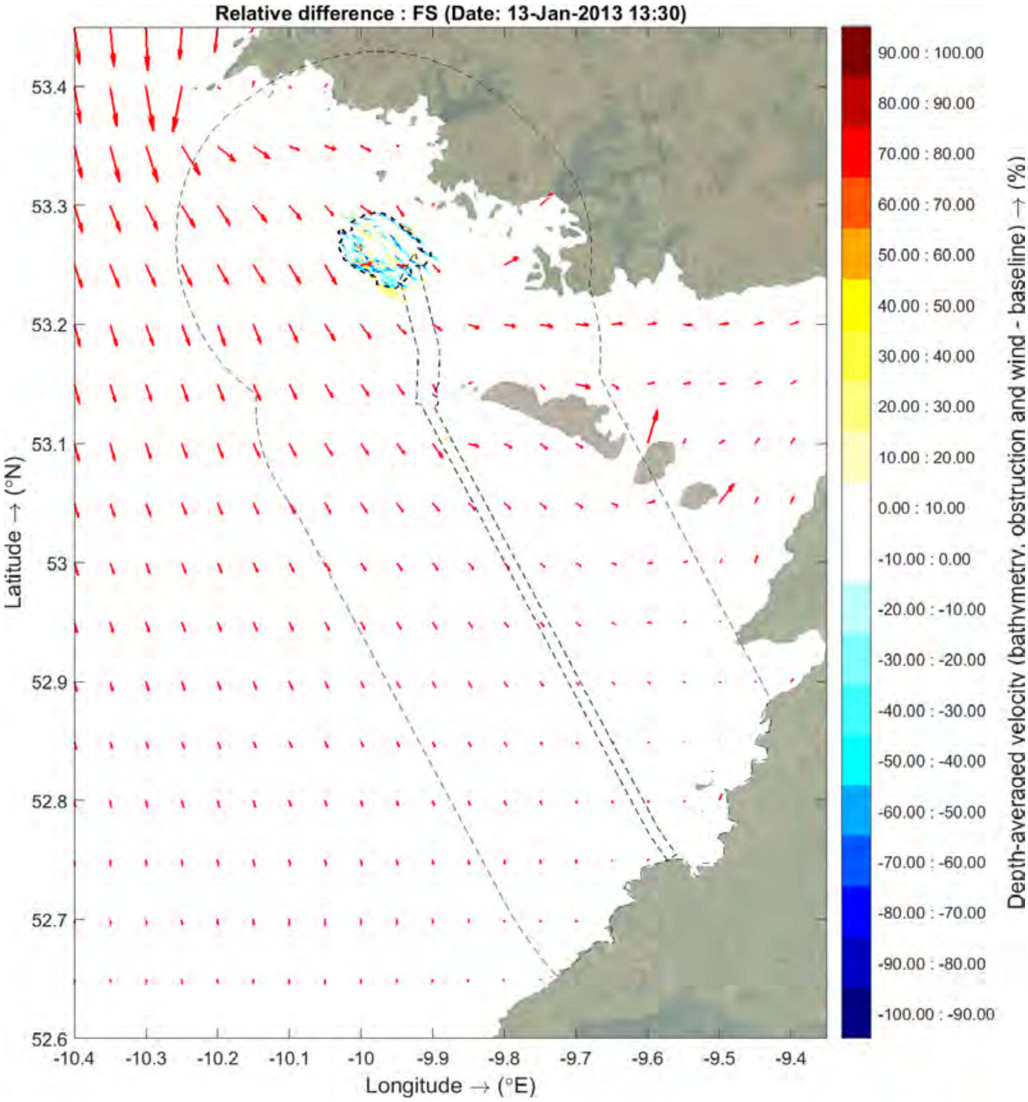
Relative difference : FS (Date: 13-Jan-2013 13:30)
53.4
53.3
53.2
53.1
53
52.9
52.8
52.7
52.6
Latitude → (°N)
-10.4
-10.3
-10.2
-10.1
-10
-9.9
-9.8
-9.7
-9.6
-9.5
-9.4
Longitude → (°E)
90.00 : 100.00
80.00 : 90.00
70.00 : 80.00
60.00 : 70.00
50.00 : 60.00
40.00 : 50.00
30.00 : 40.00
20.00 : 30.00
10.00 : 20.00
0.00 : 10.00
-10.00 : 0.00
-20.00 : -10.00
-30.00 : -20.00
-40.00 : -30.00
-50.00 : -40.00
-60.00 : -50.00
-70.00 : -60.00
-80.00 : -70.00
-90.00 : -80.00
-100.00 : -90.00
Depth-averaged velocity (bathymetry, obstruction and wind - baseline) → (%)

D.8 FS water levels

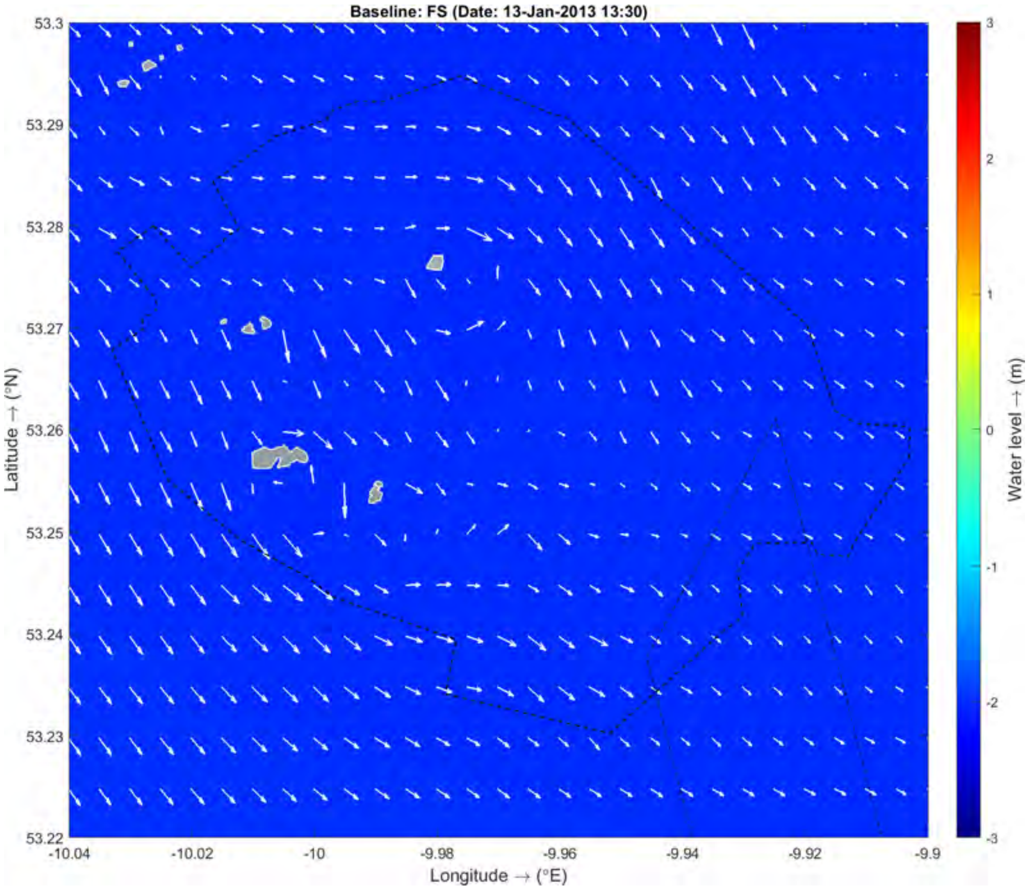

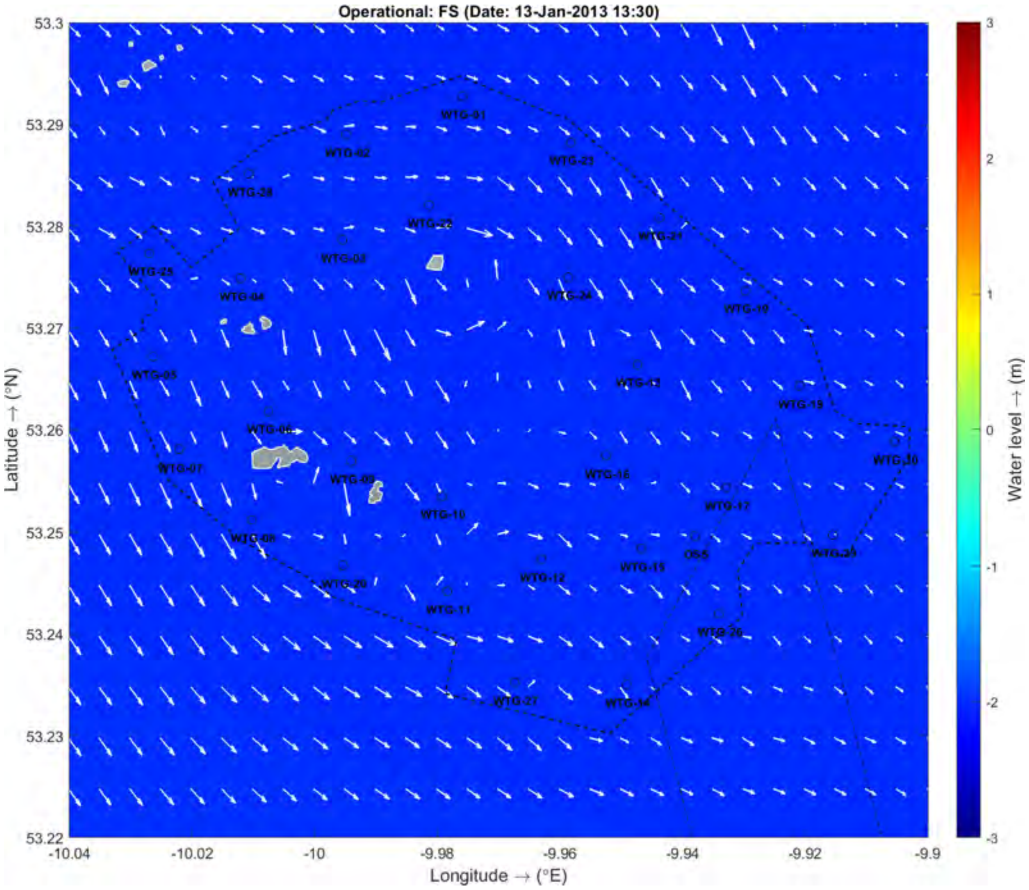
Operational: FS (Date: 13-Jan-2013 13:30)
Latitude → (°N)
Longitude → (°E)
Water level → (m)

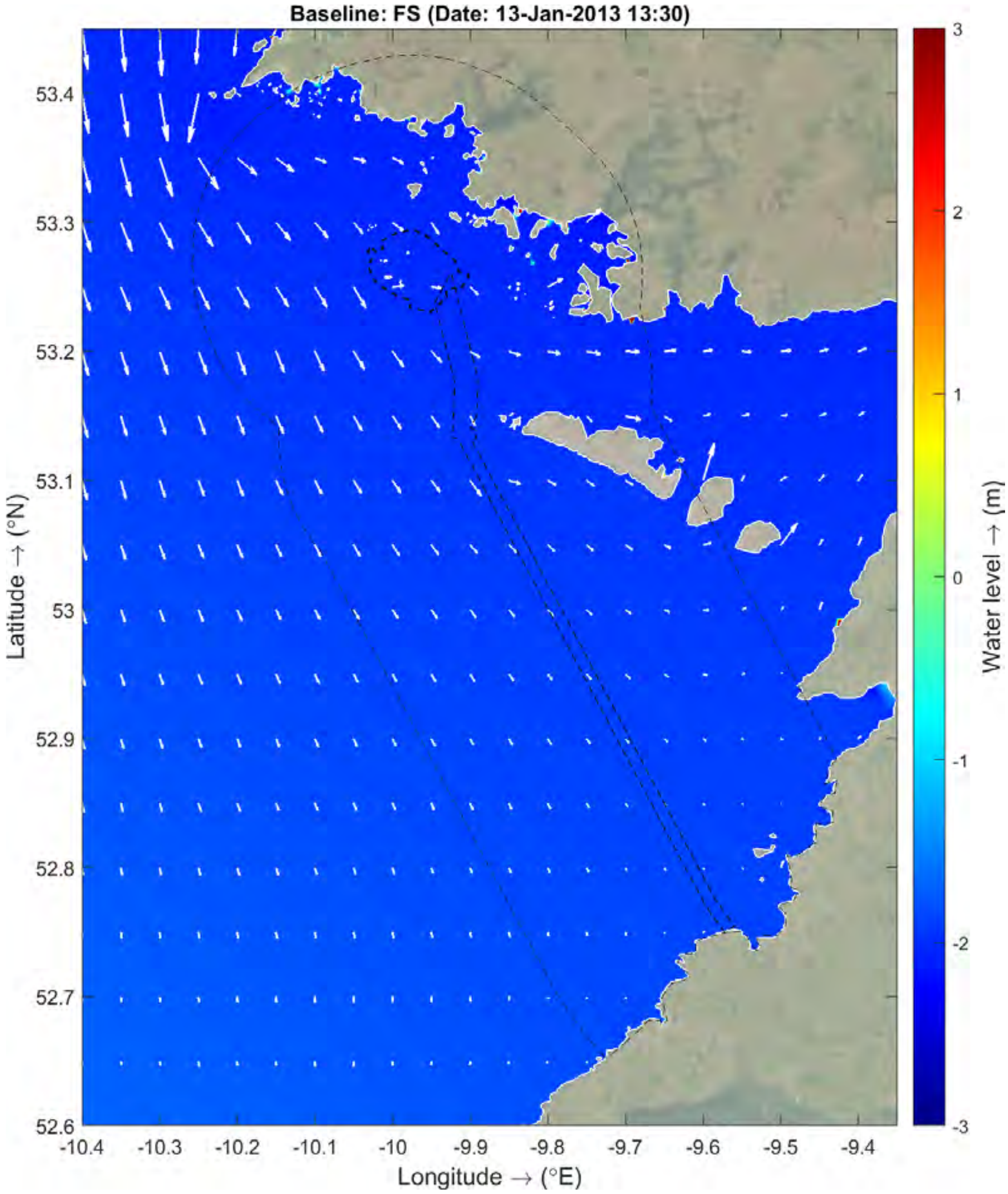
Baseline: FS (Date: 13-Jan-2013 13:30)
Latitude → (°N)
Longitude → (°E)
Water level → (m)
53.4
53.3
53.2
53.1
53
52.9
52.8
52.7
52.6
-10.4
-10.3
-10.2
-10.1
-10
-9.9
-9.8
-9.7
-9.6
-9.5
-9.4
3
2
1
0
-1
-2
-3

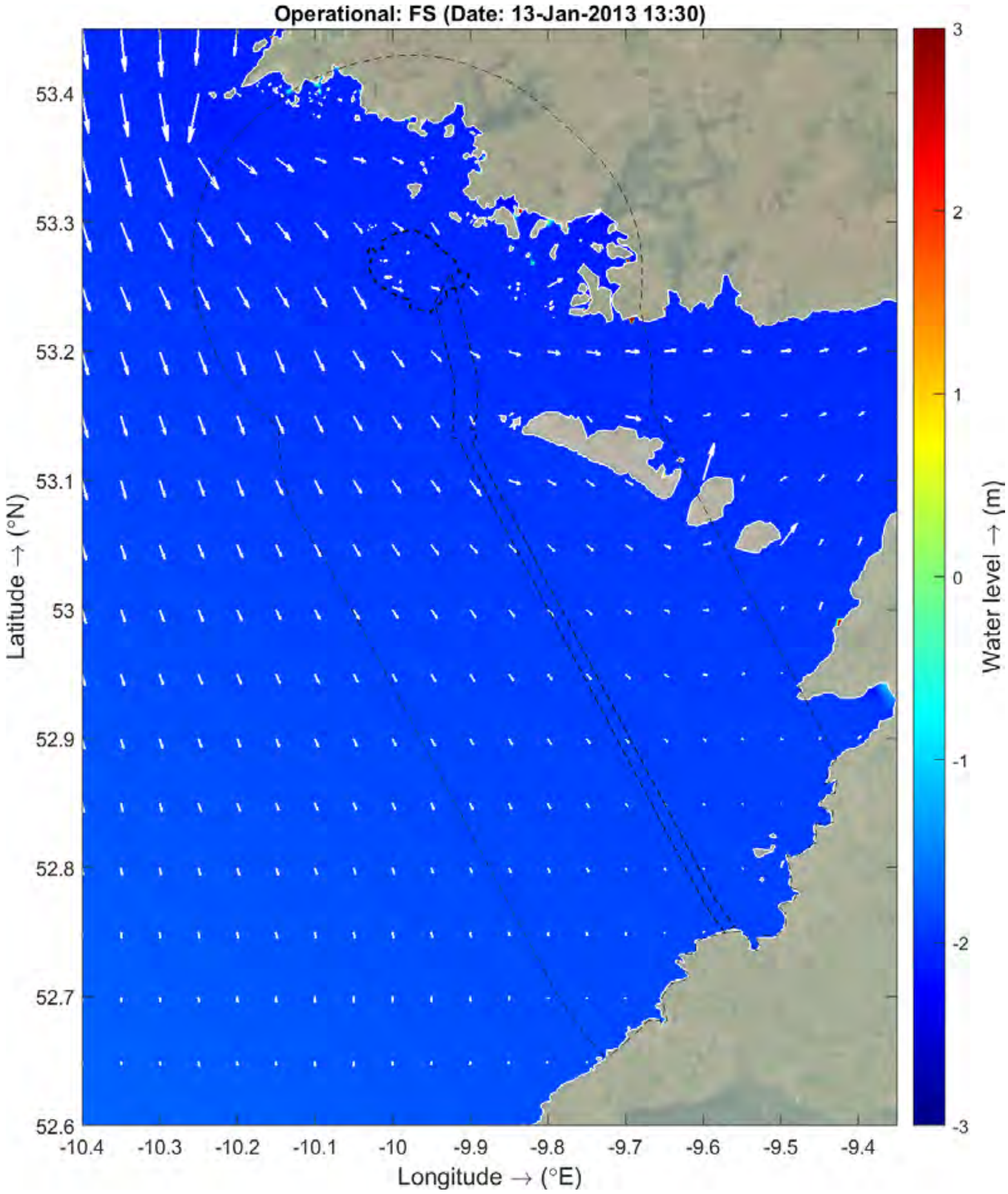
Operational: FS (Date: 13-Jan-2013 13:30)
Latitude → (°N)
Longitude → (°E)
Water level → (m)
53.4
53.3
53.2
53.1
53
52.9
52.8
52.7
52.6
-10.4
-10.3
-10.2
-10.1
-10
-9.9
-9.8
-9.7
-9.6
-9.5
-9.4
3
2
1
0
-1
-2
-3

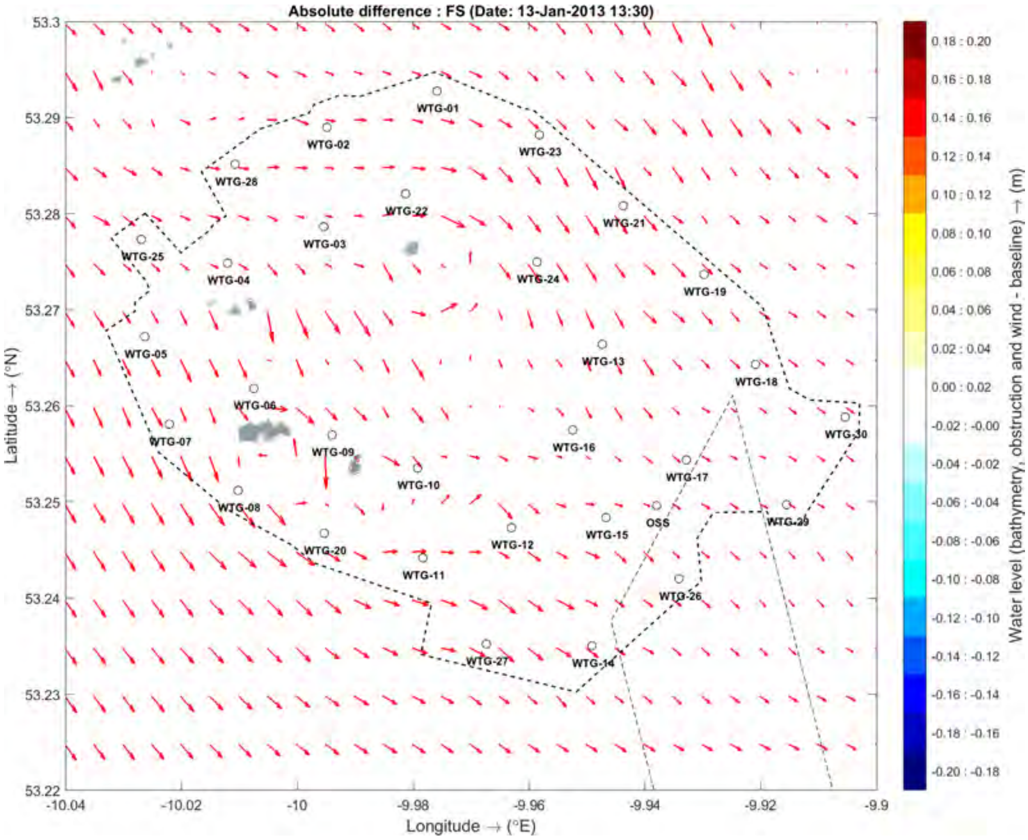
Absolute difference : FS (Date: 13-Jan-2013 13:30)
Latitude → (°N)
Longitude → (°E)
Water level (bathymetry, obstruction and wind - baseline) → (m)
WTG-01
WTG-02
WTG-03
WTG-04
WTG-05
WTG-06
WTG-07
WTG-08
WTG-09
WTG-10
WTG-11
WTG-12
WTG-13
WTG-14
WTG-15
WTG-16
WTG-17
WTG-18
WTG-19
WTG-20
WTG-21
WTG-22
WTG-23
WTG-24
WTG-25
WTG-26
WTG-27
WTG-28
WTG-29
WTG-30
OSS

Deltares

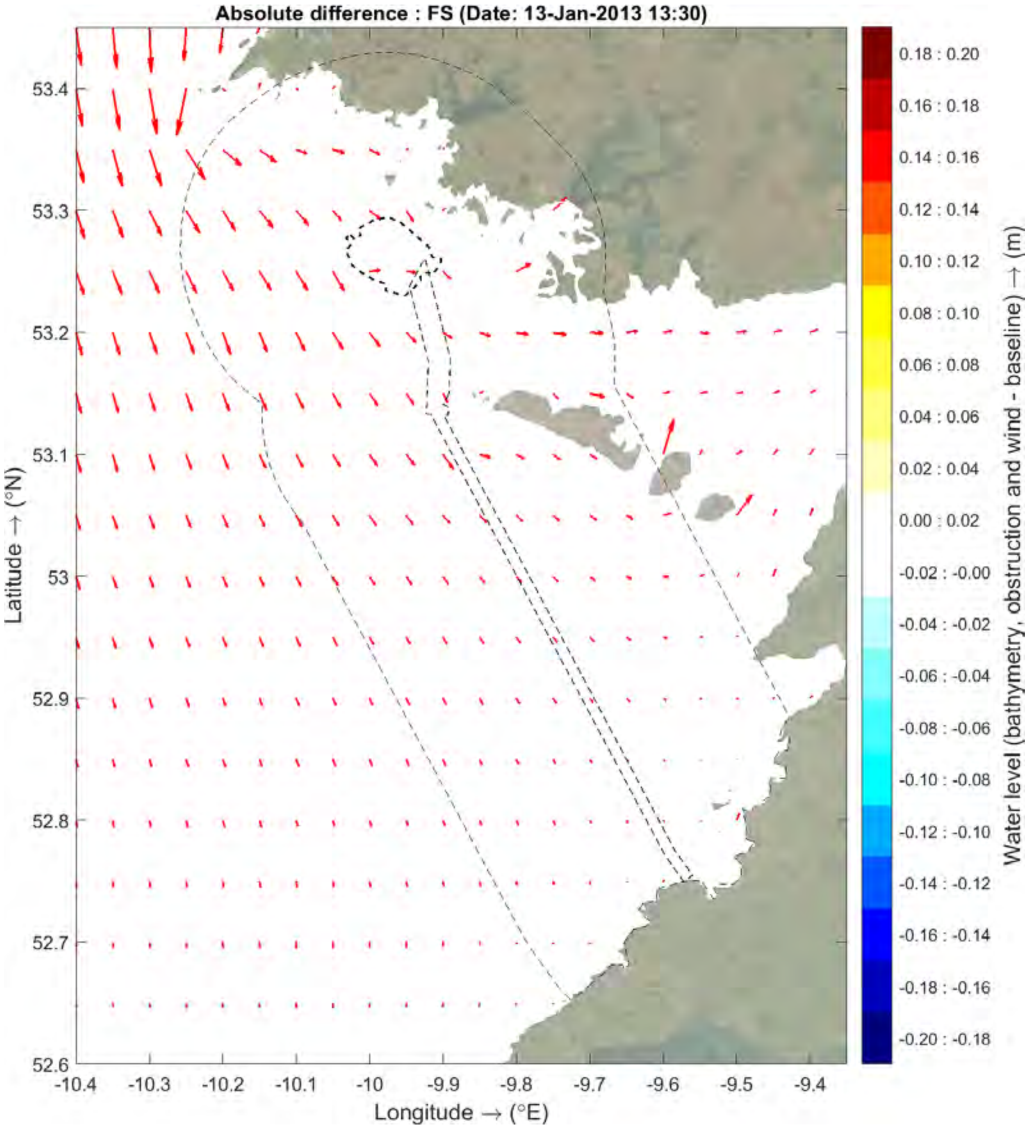

Absolute difference : FS (Date: 13-Jan-2013 13:30)
53.4
53.3
53.2
53.1
53
52.9
52.8
52.7
52.6
Latitude → (°N)
-10.4
-10.3
-10.2
-10.1
-10
-9.9
-9.8
-9.7
-9.6
-9.5
-9.4
Longitude → (°E)
0.18 : 0.20
0.16 : 0.18
0.14 : 0.16
0.12 : 0.14
0.10 : 0.12
0.08 : 0.10
0.06 : 0.08
0.04 : 0.06
0.02 : 0.04
0.00 : 0.02
-0.02 : -0.00
-0.04 : -0.02
-0.06 : -0.04
-0.08 : -0.06
-0.10 : -0.08
-0.12 : -0.10
-0.14 : -0.12
-0.16 : -0.14
-0.18 : -0.16
-0.20 : -0.18
Water level (bathymetry, obstruction and wind - baseline) → (m)

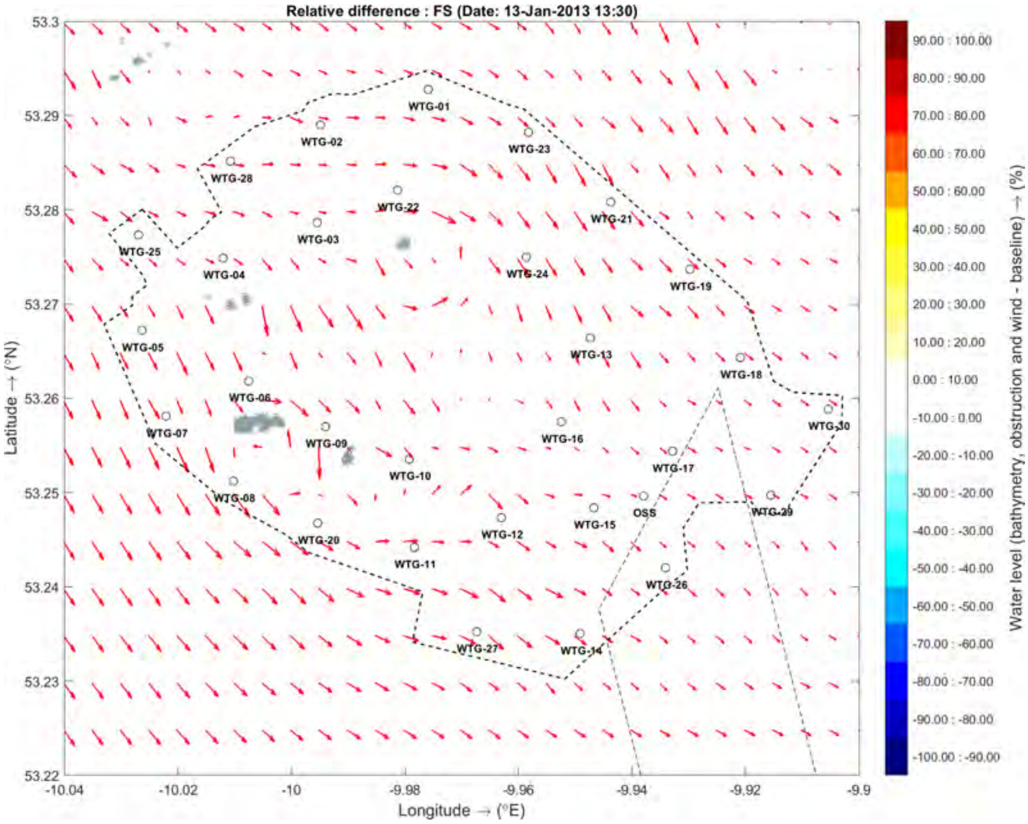
Relative difference : FS (Date: 13-Jan-2013 13:30)
Latitude → (°N)
Longitude → (°E)
Water level (bathymetry, obstruction and wind - baseline) → (%)
WTG-01
WTG-02
WTG-03
WTG-04
WTG-05
WTG-06
WTG-07
WTG-08
WTG-09
WTG-10
WTG-11
WTG-12
WTG-13
WTG-14
WTG-15
WTG-16
WTG-17
WTG-18
WTG-19
WTG-20
WTG-21
WTG-22
WTG-23
WTG-24
WTG-25
WTG-26
WTG-27
WTG-28
WTG-29
WTG-30
OSS
90.00 : 100.00
80.00 : 90.00
70.00 : 80.00
60.00 : 70.00
50.00 : 60.00
40.00 : 50.00
30.00 : 40.00
20.00 : 30.00
10.00 : 20.00
0.00 : 10.00
-10.00 : 0.00
-20.00 : -10.00
-30.00 : -20.00
-40.00 : -30.00
-50.00 : -40.00
-60.00 : -50.00
-70.00 : -60.00
-80.00 : -70.00
-90.00 : -80.00
-100.00 : -90.00

Deltares

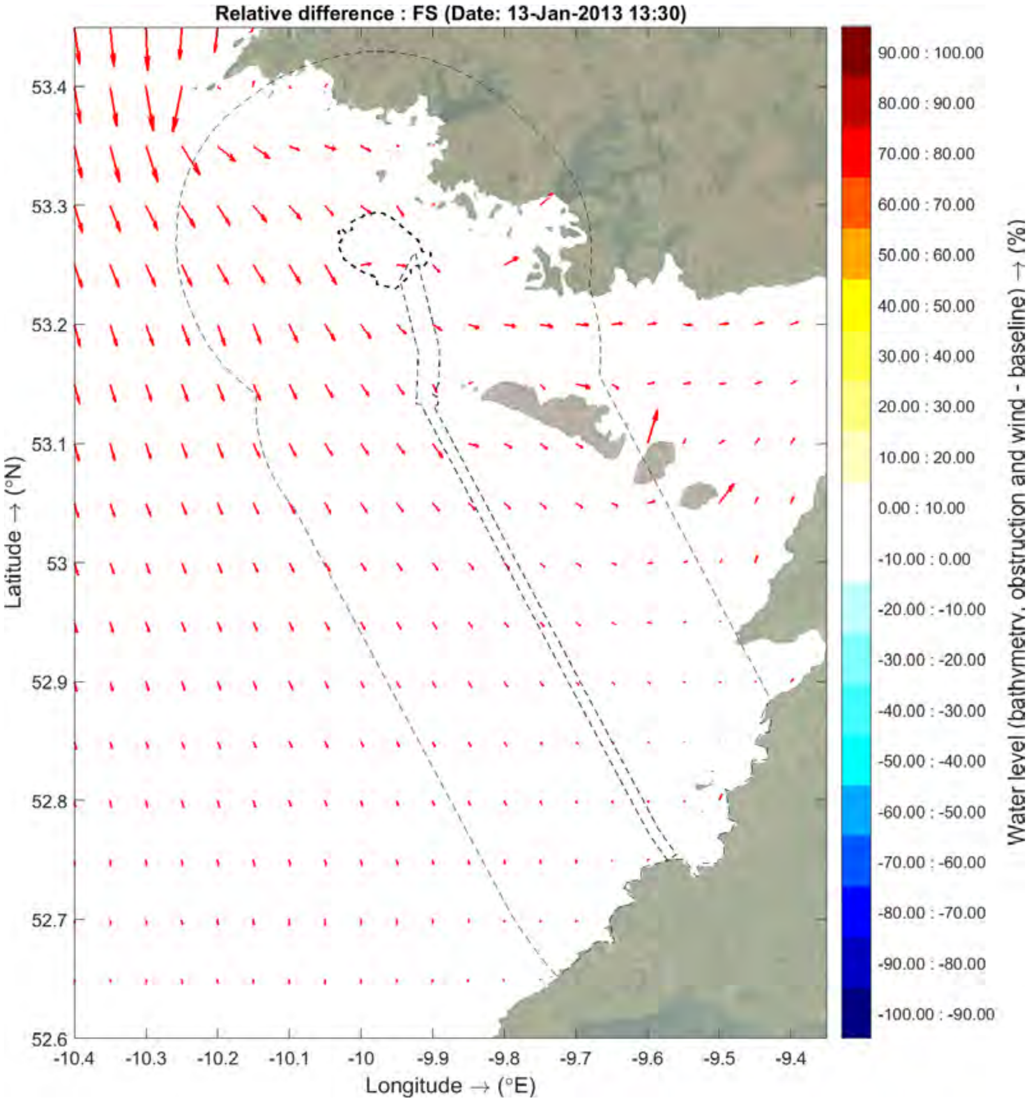
Relative difference : FS (Date: 13-Jan-2013 13:30)
53.4
53.3
53.2
53.1
53
52.9
52.8
52.7
52.6
Latitude → (°N)
-10.4
-10.3
-10.2
-10.1
-10
-9.9
-9.8
-9.7
-9.6
-9.5
-9.4
Longitude → (°E)
90.00 : 100.00
80.00 : 90.00
70.00 : 80.00
60.00 : 70.00
50.00 : 60.00
40.00 : 50.00
30.00 : 40.00
20.00 : 30.00
10.00 : 20.00
0.00 : 10.00
-10.00 : 0.00
-20.00 : -10.00
-30.00 : -20.00
-40.00 : -30.00
-50.00 : -40.00
-60.00 : -50.00
-70.00 : -60.00
-80.00 : -70.00
-90.00 : -80.00
-100.00 : -90.00
Water level (bathymetry, obstruction and wind - baseline) → (%)

D.9 HWN currents

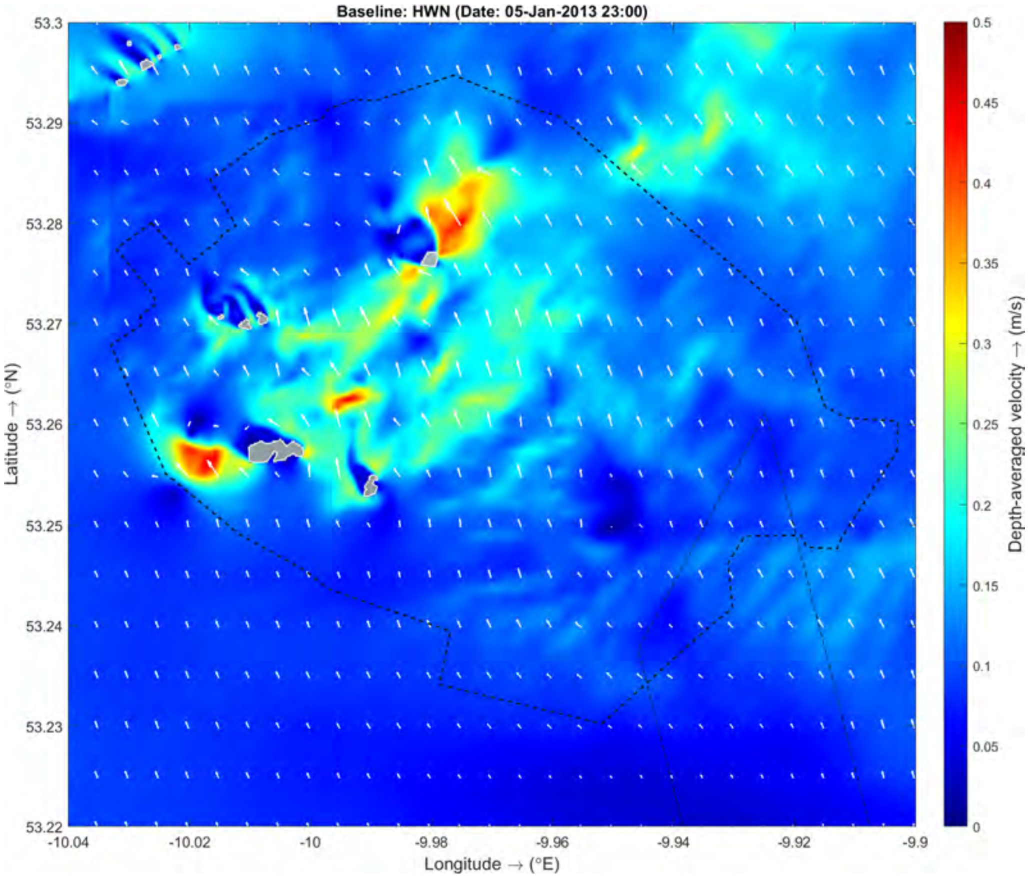

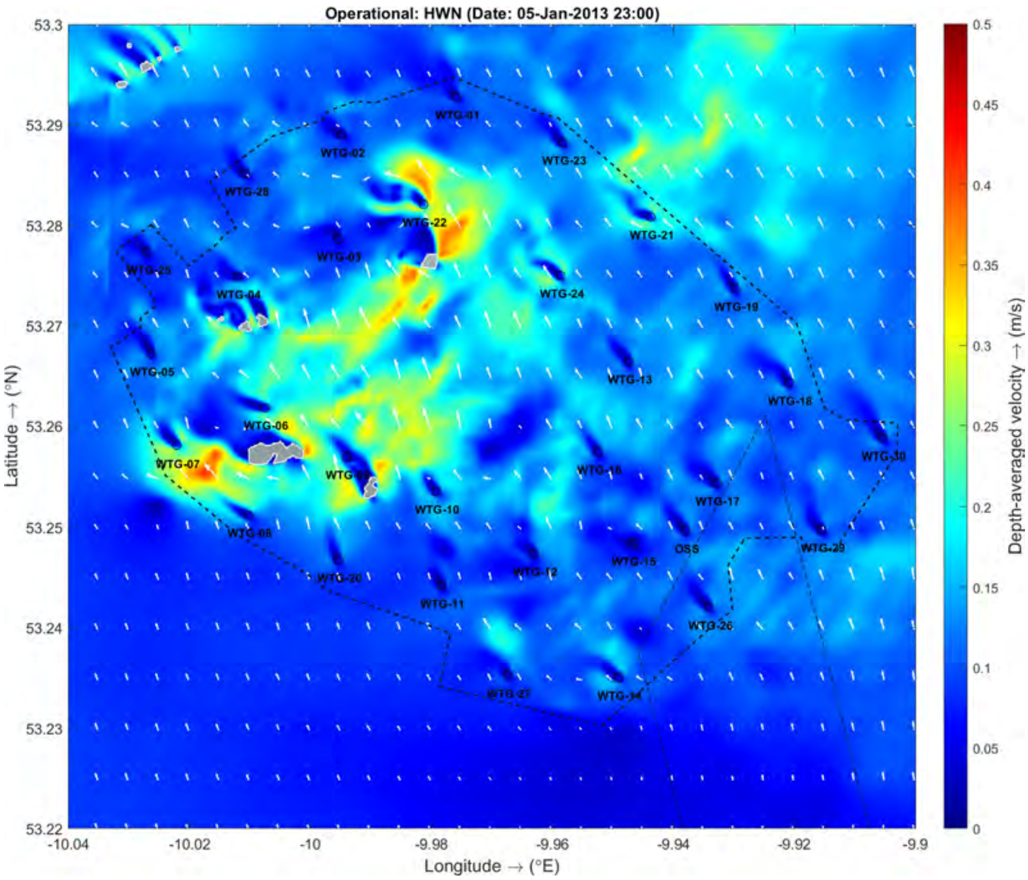

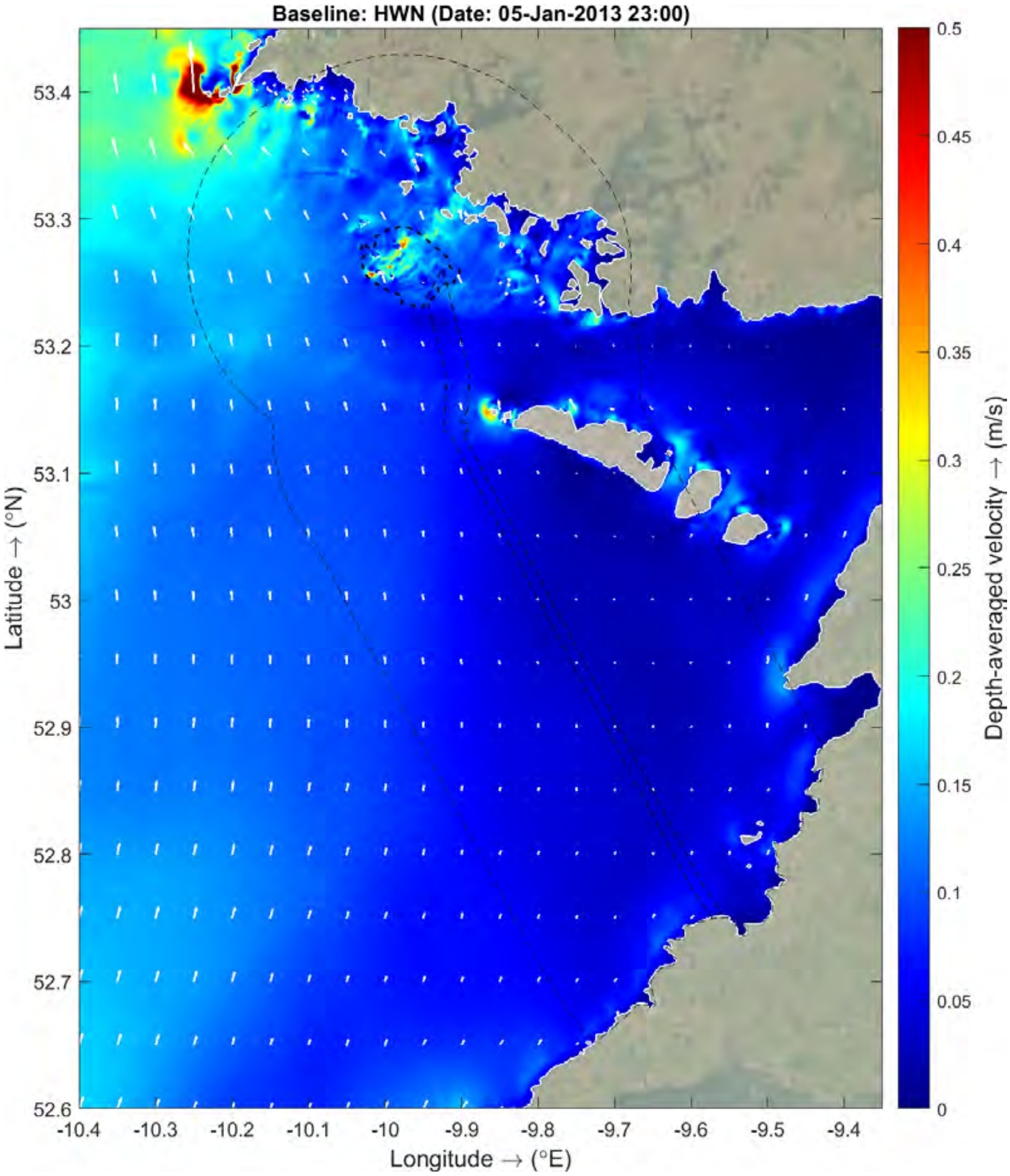
Baseline: HWN (Date: 05-Jan-2013 23:00)
53.4
53.3
53.2
53.1
53
52.9
52.8
52.7
52.6
Latitude → (°N)
-10.4
-10.3
-10.2
-10.1
-10
-9.9
-9.8
-9.7
-9.6
-9.5
-9.4
Longitude → (°E)
0.5
0.45
0.4
0.35
0.3
0.25
0.2
0.15
0.1
0.05
0
Depth-averaged velocity → (m/s)

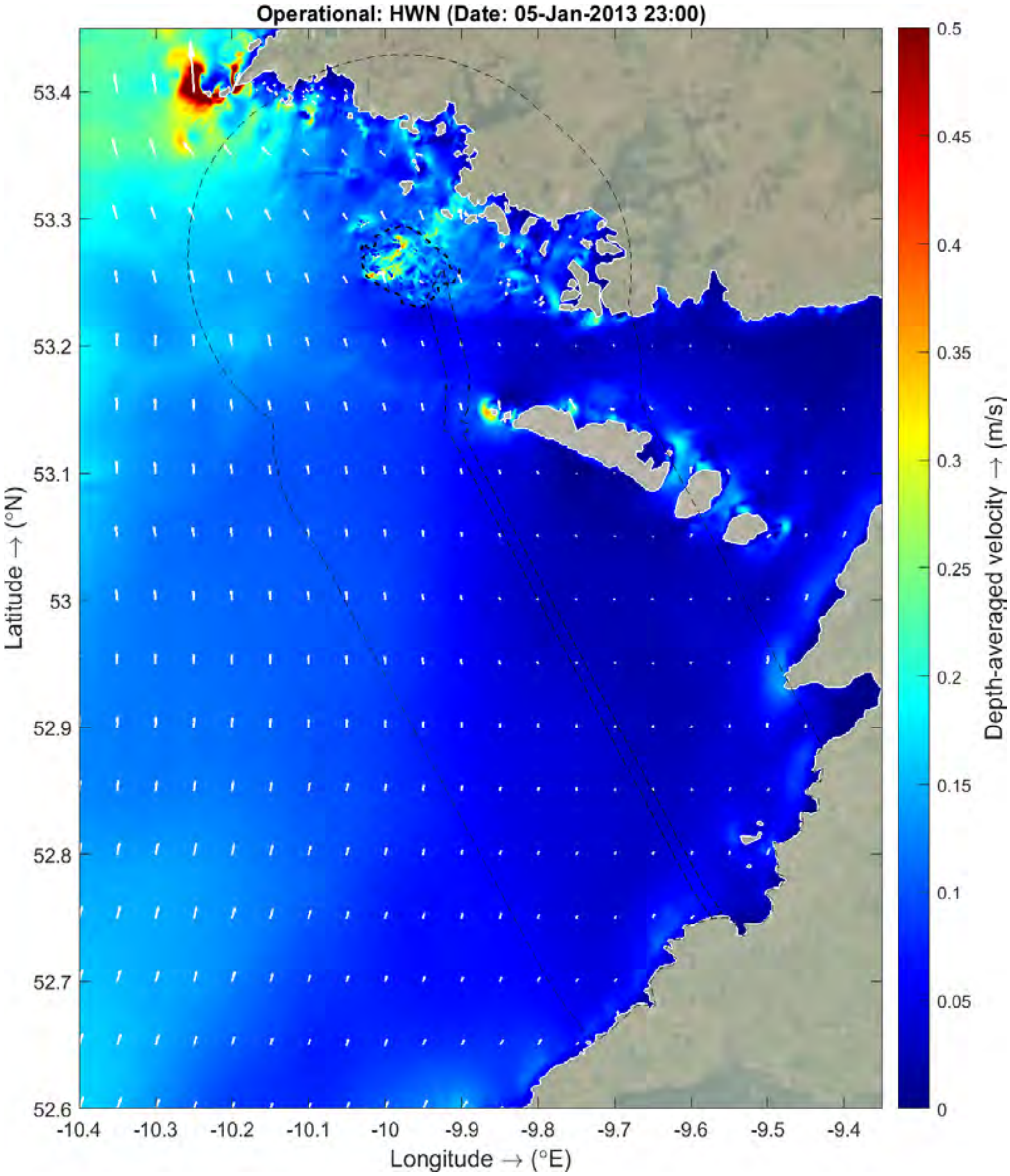
Operational: HWN (Date: 05-Jan-2013 23:00)
Latitude → (°N)
Longitude → (°E)
Depth-averaged velocity → (m/s)
53.4
53.3
53.2
53.1
53
52.9
52.8
52.7
52.6
-10.4
-10.3
-10.2
-10.1
-10
-9.9
-9.8
-9.7
-9.6
-9.5
-9.4
0.5
0.45
0.4
0.35
0.3
0.25
0.2
0.15
0.1
0.05
0

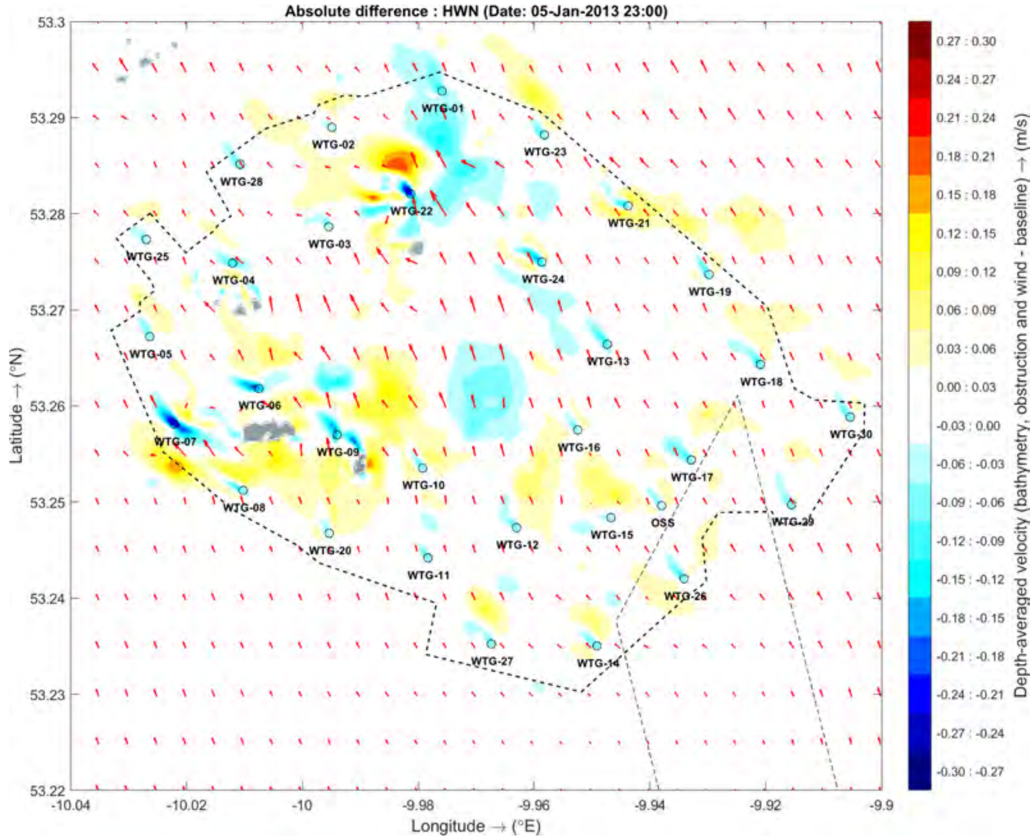

Absolute difference : HWN (Date: 05-Jan-2013 23:00)
Latitude → (°N)
Longitude → (°E)
Depth-averaged velocity (bathymetry, obstruction and wind - baseline) → (m/s)
WTG-01
WTG-02
WTG-03
WTG-04
WTG-05
WTG-06
WTG-07
WTG-08
WTG-09
WTG-10
WTG-11
WTG-12
WTG-13
WTG-14
WTG-15
WTG-16
WTG-17
WTG-18
WTG-19
WTG-20
WTG-21
WTG-22
WTG-23
WTG-24
WTG-25
WTG-26
WTG-27
WTG-28
WTG-29
WTG-30
OSS

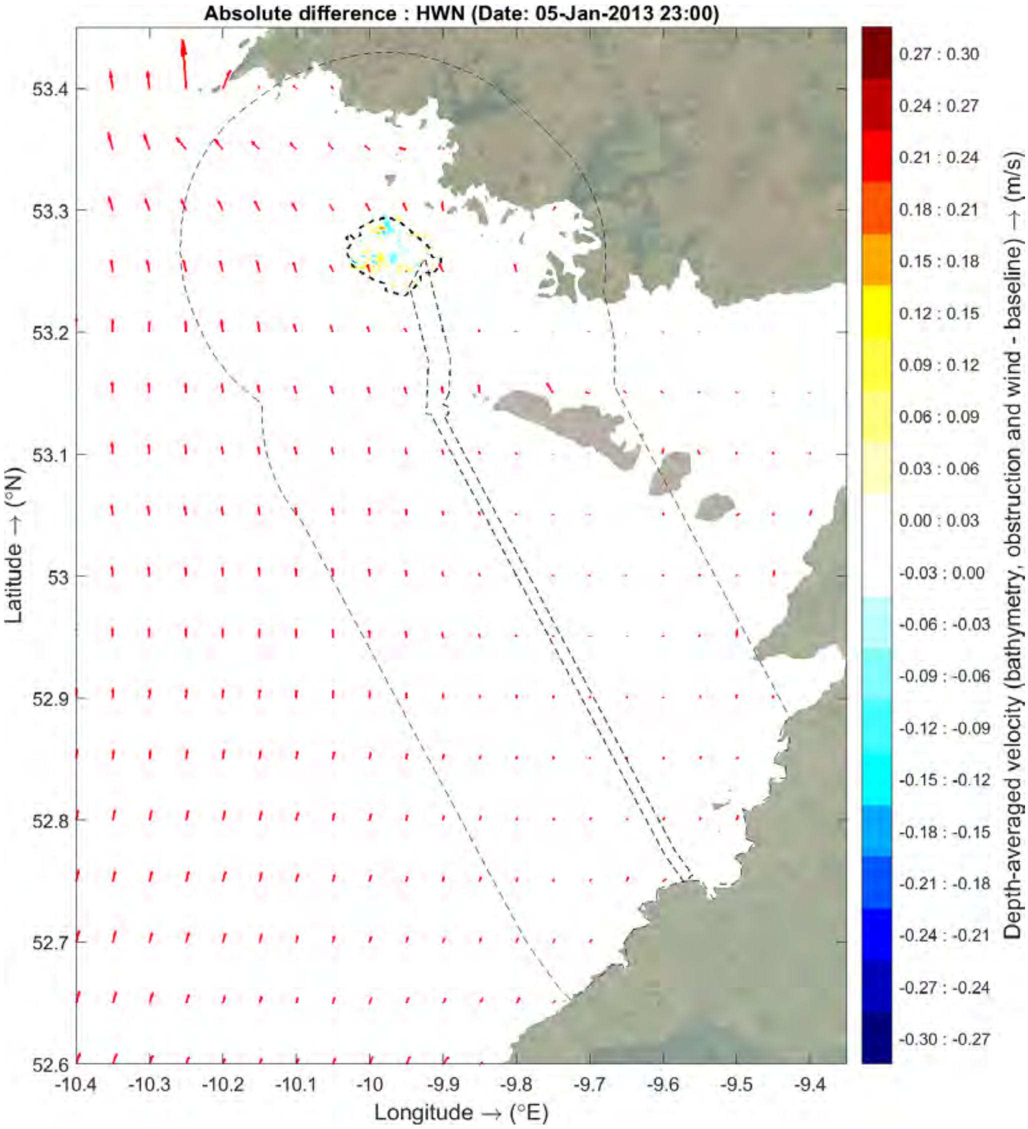
Absolute difference : HWN (Date: 05-Jan-2013 23:00)
Latitude → (°N)
Longitude → (°E)
Depth-averaged velocity (bathymetry, obstruction and wind - baseline) → (m/s)
0.27 : 0.30
0.24 : 0.27
0.21 : 0.24
0.18 : 0.21
0.15 : 0.18
0.12 : 0.15
0.09 : 0.12
0.06 : 0.09
0.03 : 0.06
0.00 : 0.03
-0.03 : 0.00
-0.06 : -0.03
-0.09 : -0.06
-0.12 : -0.09
-0.15 : -0.12
-0.18 : -0.15
-0.21 : -0.18
-0.24 : -0.21
-0.27 : -0.24
-0.30 : -0.27

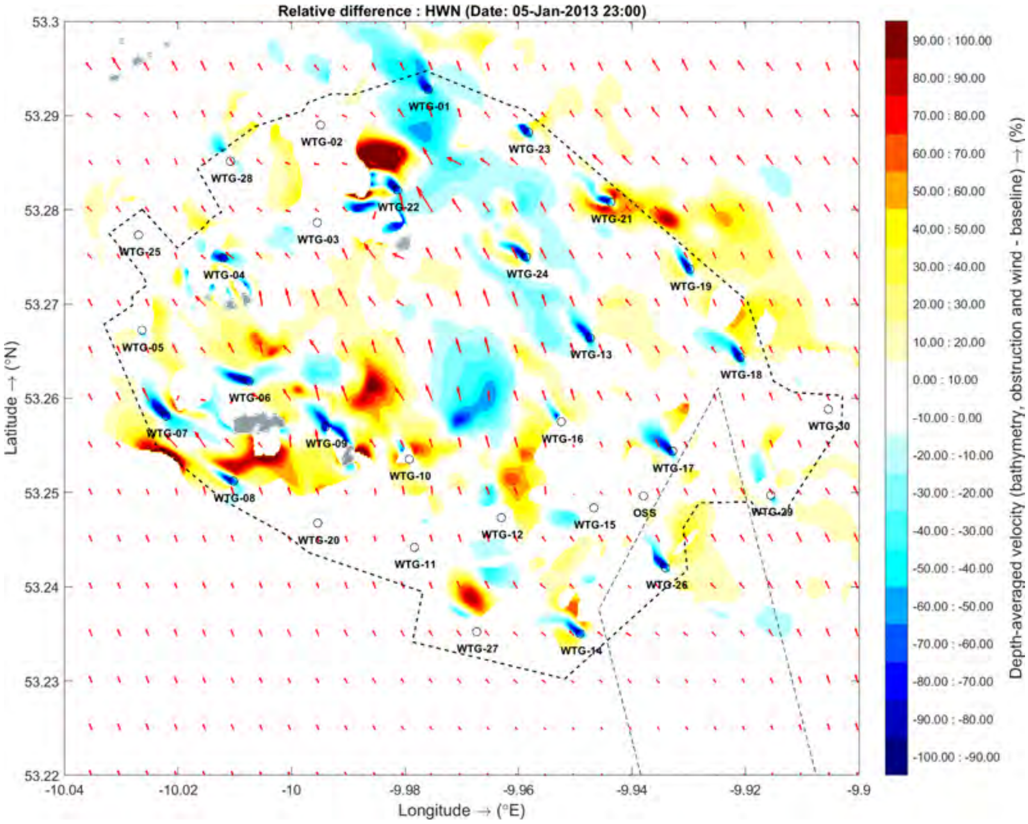
Relative difference : HWN (Date: 05-Jan-2013 23:00)
Latitude → (°N)
Longitude → (°E)
Depth-averaged velocity (bathymetry, obstruction and wind - baseline) → (%)
WTG-01
WTG-02
WTG-03
WTG-04
WTG-05
WTG-06
WTG-07
WTG-08
WTG-09
WTG-10
WTG-11
WTG-12
WTG-13
WTG-14
WTG-15
WTG-16
WTG-17
WTG-18
WTG-19
WTG-20
WTG-21
WTG-22
WTG-23
WTG-24
WTG-25
WTG-26
WTG-27
WTG-28
WTG-29
WTG-30
OSS
90.00 : 100.00
80.00 : 90.00
70.00 : 80.00
60.00 : 70.00
50.00 : 60.00
40.00 : 50.00
30.00 : 40.00
20.00 : 30.00
10.00 : 20.00
0.00 : 10.00
-10.00 : 0.00
-20.00 : -10.00
-30.00 : -20.00
-40.00 : -30.00
-50.00 : -40.00
-60.00 : -50.00
-70.00 : -60.00
-80.00 : -70.00
-90.00 : -80.00
-100.00 : -90.00

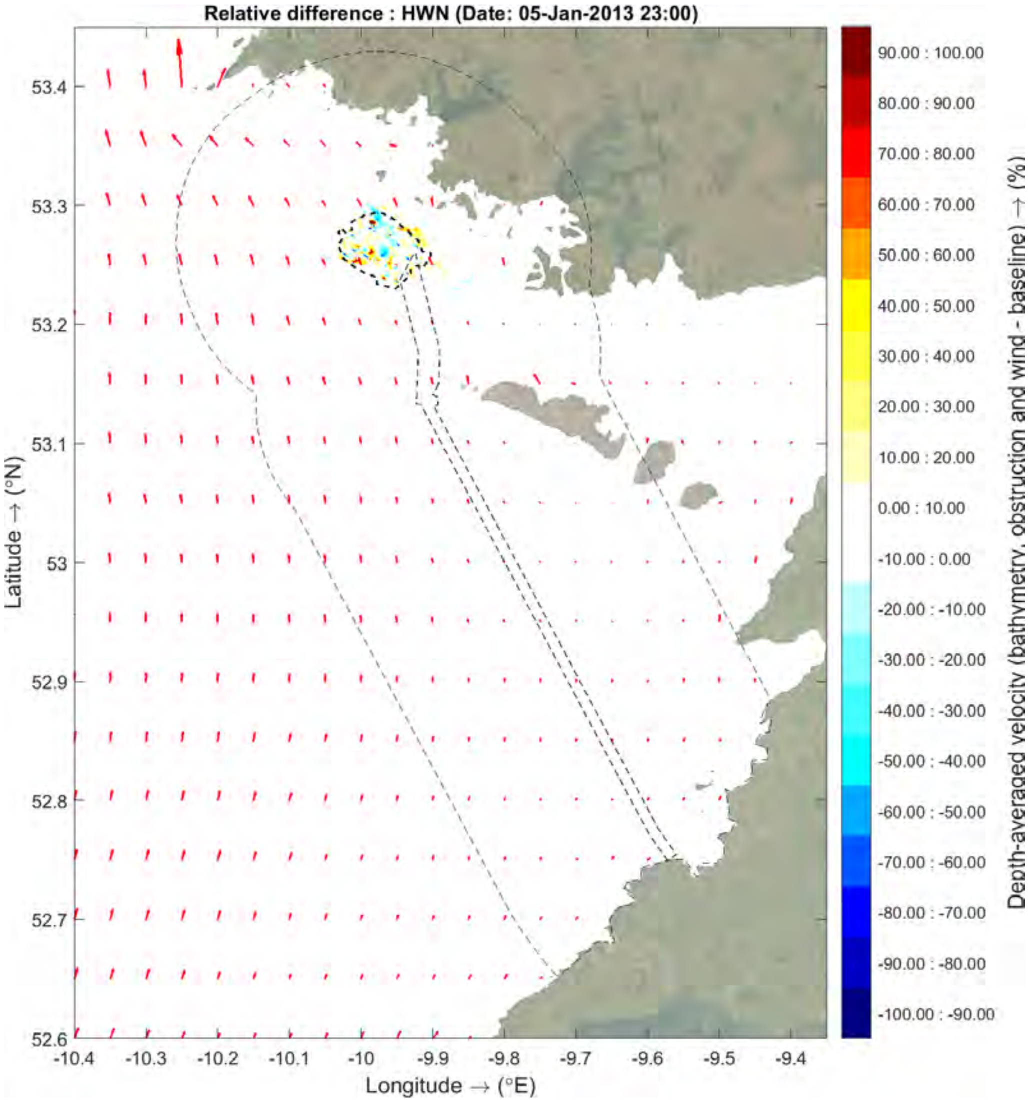
Relative difference : HWN (Date: 05-Jan-2013 23:00)
Latitude → (°N)
Longitude → (°E)
53.4
53.3
53.2
53.1
53
52.9
52.8
52.7
52.6
-10.4
-10.3
-10.2
-10.1
-10
-9.9
-9.8
-9.7
-9.6
-9.5
-9.4
90.00 : 100.00
80.00 : 90.00
70.00 : 80.00
60.00 : 70.00
50.00 : 60.00
40.00 : 50.00
30.00 : 40.00
20.00 : 30.00
10.00 : 20.00
0.00 : 10.00
-10.00 : 0.00
-20.00 : -10.00
-30.00 : -20.00
-40.00 : -30.00
-50.00 : -40.00
-60.00 : -50.00
-70.00 : -60.00
-80.00 : -70.00
-90.00 : -80.00
-100.00 : -90.00
Depth-averaged velocity (bathymetry, obstruction and wind - baseline) → (%)

D.10 HWN water levels

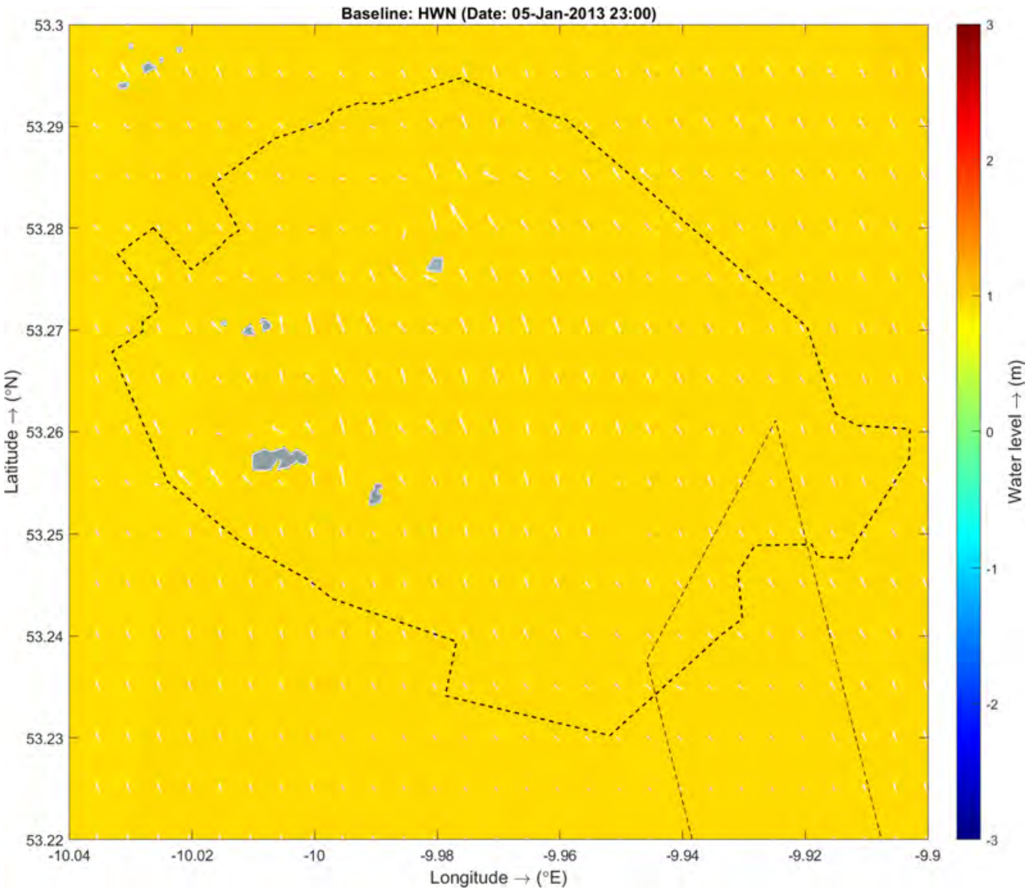

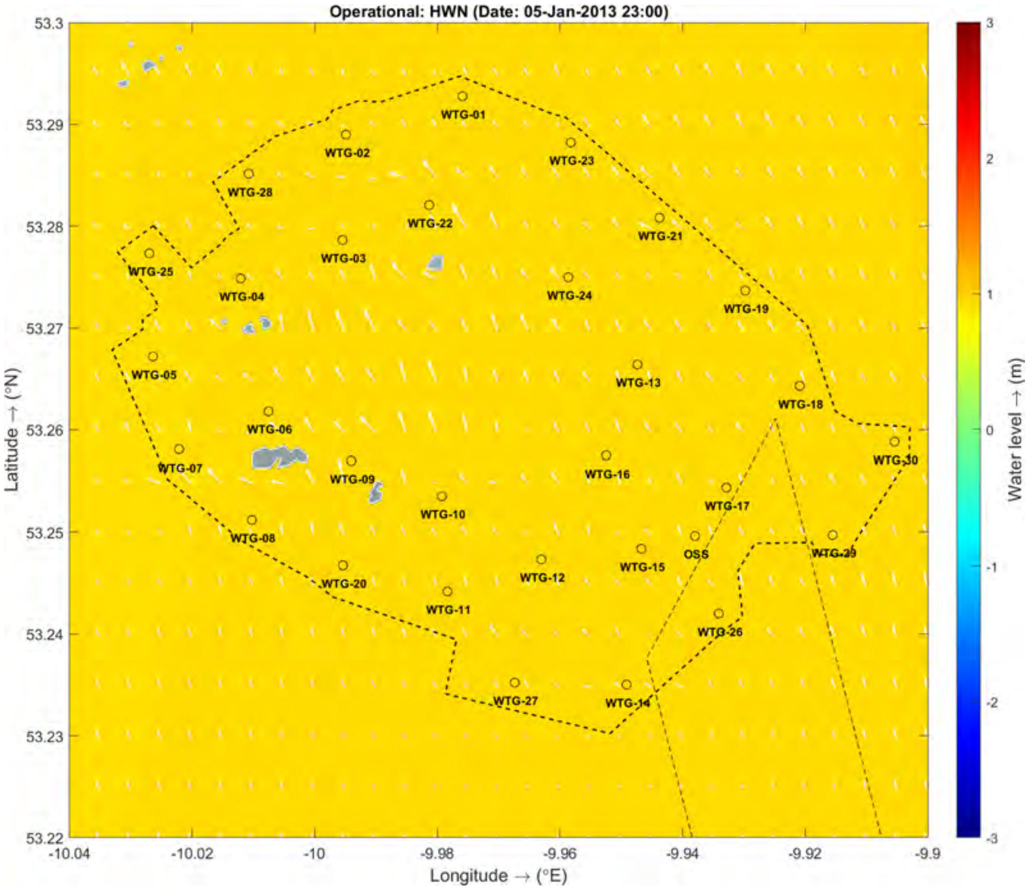

Operational: HWN (Date: 05-Jan-2013 23:00)
WTG-01
WTG-02
WTG-03
WTG-04
WTG-05
WTG-06
WTG-07
WTG-08
WTG-09
WTG-10
WTG-11
WTG-12
WTG-13
WTG-14
WTG-15
WTG-16
WTG-17
WTG-18
WTG-19
WTG-20
WTG-21
WTG-22
WTG-23
WTG-24
WTG-25
WTG-26
WTG-27
WTG-28
WTG-29
WTG-30
OSS
Latitude → (°N)
Longitude → (°E)
Water level → (m)

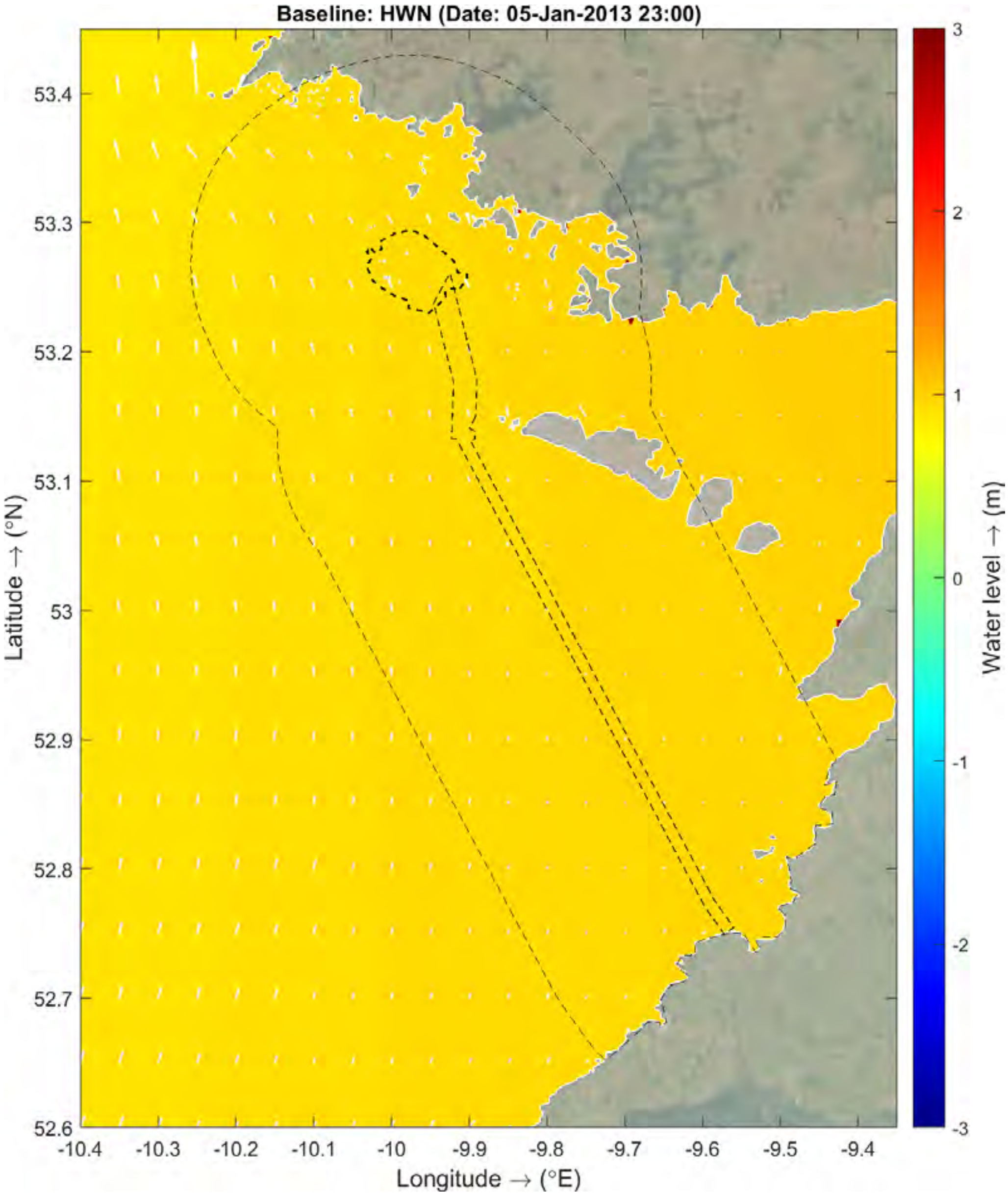
Baseline: HWN (Date: 05-Jan-2013 23:00)
Latitude → (°N)
53.4
53.3
53.2
53.1
53
52.9
52.8
52.7
52.6
-10.4
-10.3
-10.2
-10.1
-10
-9.9
-9.8
-9.7
-9.6
-9.5
-9.4
Longitude → (°E)
Water level → (m)
3
2
1
0
-1
-2
-3

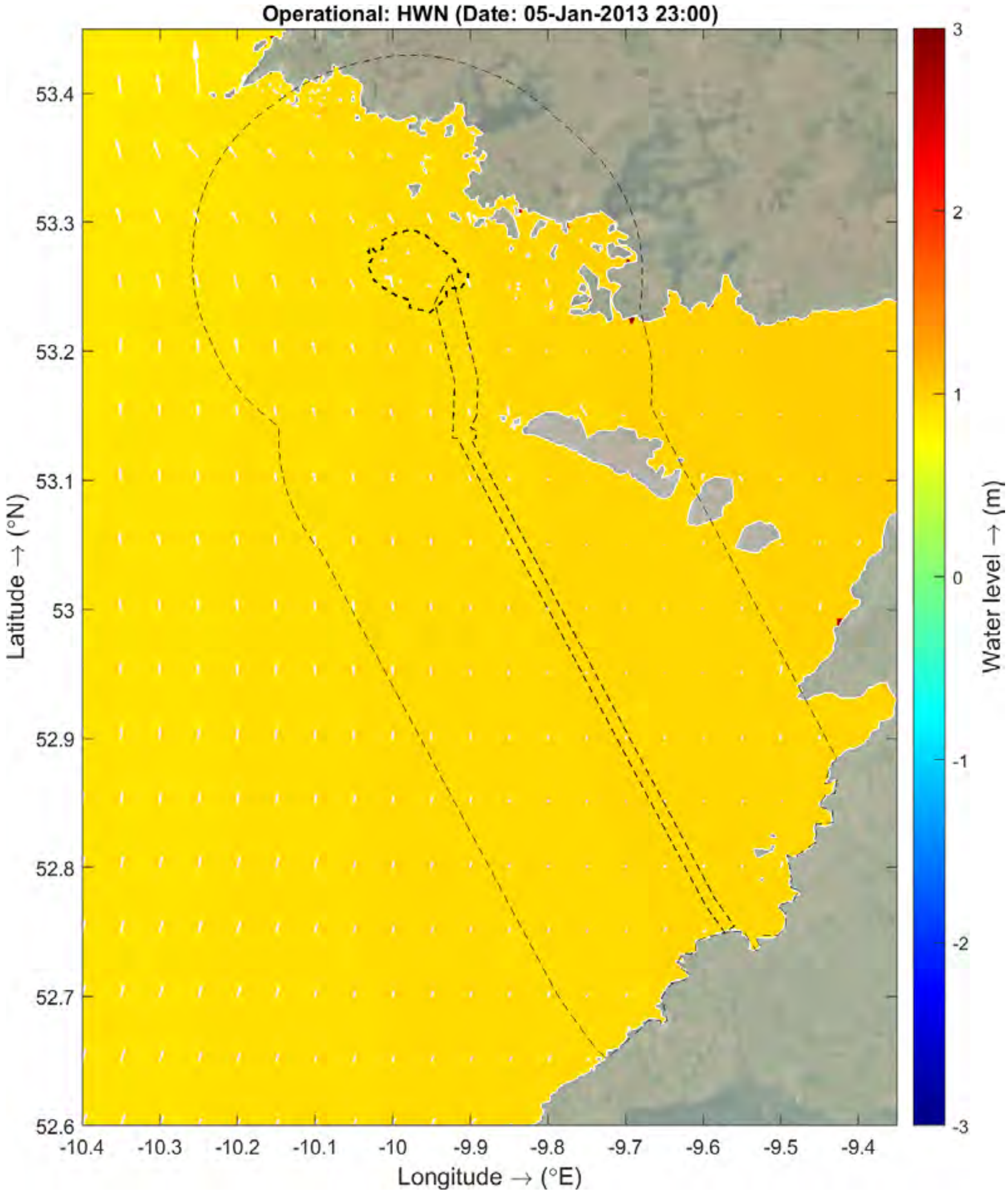

Operational: HWN (Date: 05-Jan-2013 23:00)
53.4
53.3
53.2
53.1
53
52.9
52.8
52.7
52.6
Latitude → (°N)
-10.4
-10.3
-10.2
-10.1
-10
-9.9
-9.8
-9.7
-9.6
-9.5
-9.4
Longitude → (°E)
3
2
1
0
-1
-2
-3
Water level → (m)

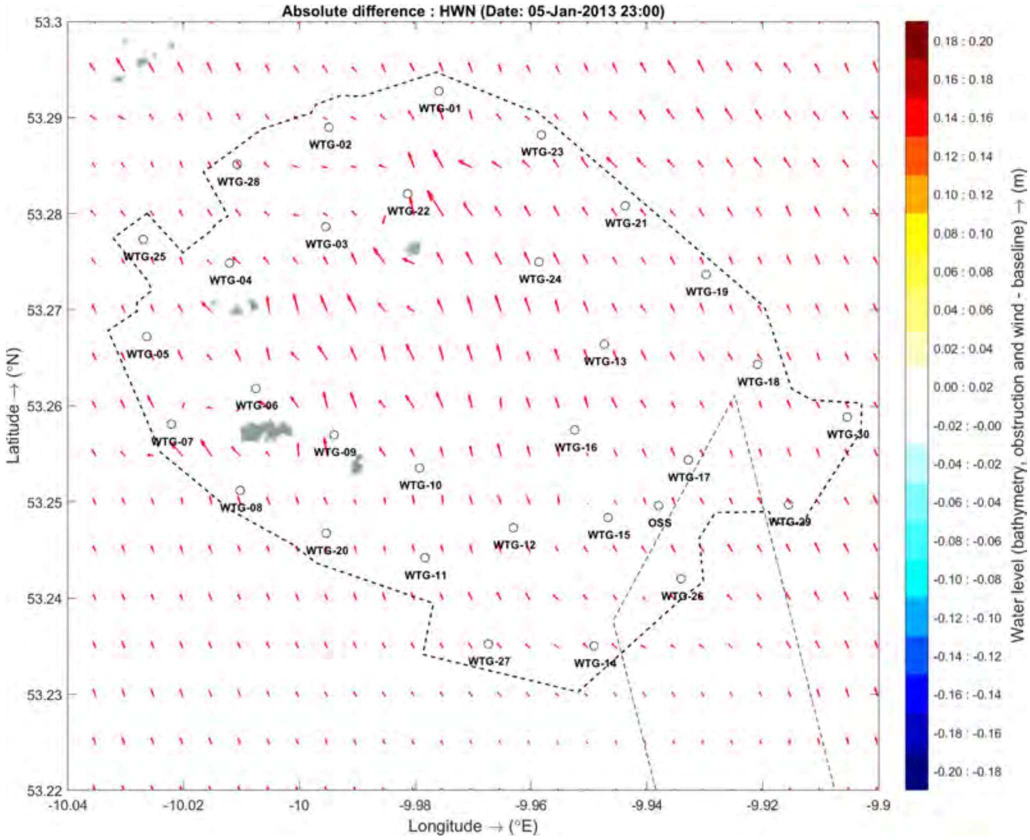
Absolute difference : HWN (Date: 05-Jan-2013 23:00)
Latitude → (°N)
Longitude → (°E)
Water level (bathymetry, obstruction and wind - baseline) → (m)
WTG-01
WTG-02
WTG-03
WTG-04
WTG-05
WTG-06
WTG-07
WTG-08
WTG-09
WTG-10
WTG-11
WTG-12
WTG-13
WTG-14
WTG-15
WTG-16
WTG-17
WTG-18
WTG-19
WTG-20
WTG-21
WTG-22
WTG-23
WTG-24
WTG-25
WTG-26
WTG-27
WTG-28
WTG-29
WTG-30
OSS
0.18 : 0.20
0.16 : 0.18
0.14 : 0.16
0.12 : 0.14
0.10 : 0.12
0.08 : 0.10
0.06 : 0.08
0.04 : 0.06
0.02 : 0.04
0.00 : 0.02
-0.02 : -0.00
-0.04 : -0.02
-0.06 : -0.04
-0.08 : -0.06
-0.10 : -0.08
-0.12 : -0.10
-0.14 : -0.12
-0.16 : -0.14
-0.18 : -0.16
-0.20 : -0.18

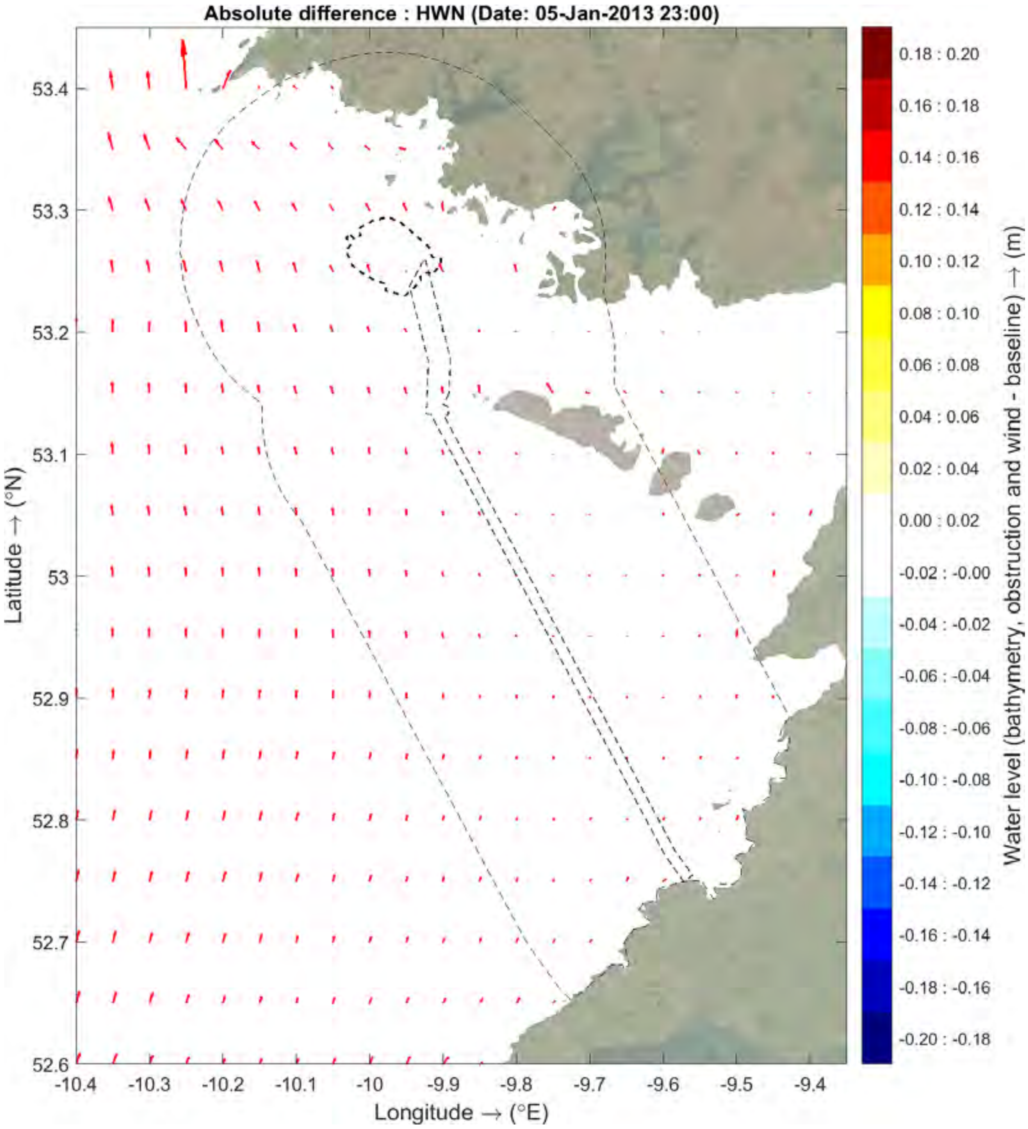

Absolute difference : HWN (Date: 05-Jan-2013 23:00)
53.4
53.3
53.2
53.1
53
52.9
52.8
52.7
52.6
-10.4
-10.3
-10.2
-10.1
-10
-9.9
-9.8
-9.7
-9.6
-9.5
-9.4
Latitude → (°N)
Longitude → (°E)
0.18 : 0.20
0.16 : 0.18
0.14 : 0.16
0.12 : 0.14
0.10 : 0.12
0.08 : 0.10
0.06 : 0.08
0.04 : 0.06
0.02 : 0.04
0.00 : 0.02
-0.02 : -0.00
-0.04 : -0.02
-0.06 : -0.04
-0.08 : -0.06
-0.10 : -0.08
-0.12 : -0.10
-0.14 : -0.12
-0.16 : -0.14
-0.18 : -0.16
-0.20 : -0.18
Water level (bathymetry, obstruction and wind - baseline) → (m)

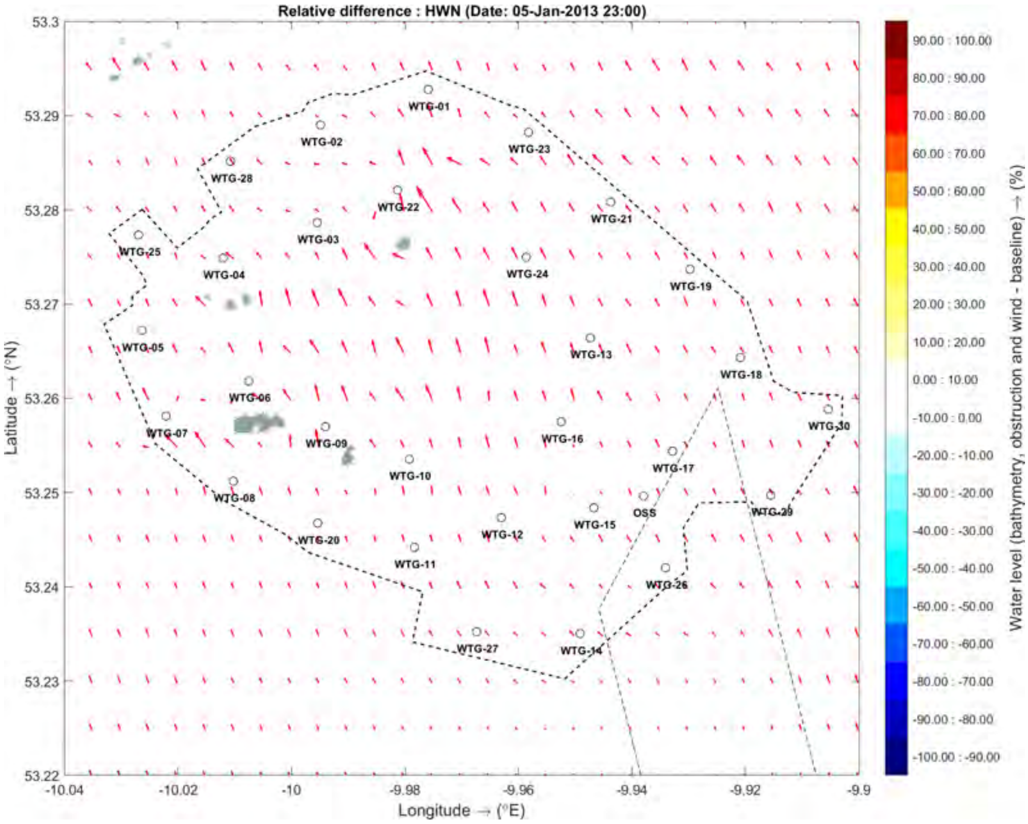

Relative difference : HWN (Date: 05-Jan-2013 23:00)
Latitude → (°N)
Longitude → (°E)
Water level (bathymetry, obstruction and wind - baseline) → (%)
90.00 : 100.00
80.00 : 90.00
70.00 : 80.00
60.00 : 70.00
50.00 : 60.00
40.00 : 50.00
30.00 : 40.00
20.00 : 30.00
10.00 : 20.00
0.00 : 10.00
-10.00 : 0.00
-20.00 : -10.00
-30.00 : -20.00
-40.00 : -30.00
-50.00 : -40.00
-60.00 : -50.00
-70.00 : -60.00
-80.00 : -70.00
-90.00 : -80.00
-100.00 : -90.00
WTG-01
WTG-02
WTG-03
WTG-04
WTG-05
WTG-06
WTG-07
WTG-08
WTG-09
WTG-10
WTG-11
WTG-12
WTG-13
WTG-14
WTG-15
WTG-16
WTG-17
WTG-18
WTG-19
WTG-20
WTG-21
WTG-22
WTG-23
WTG-24
WTG-25
WTG-26
WTG-27
WTG-28
WTG-29
WTG-30
OSS

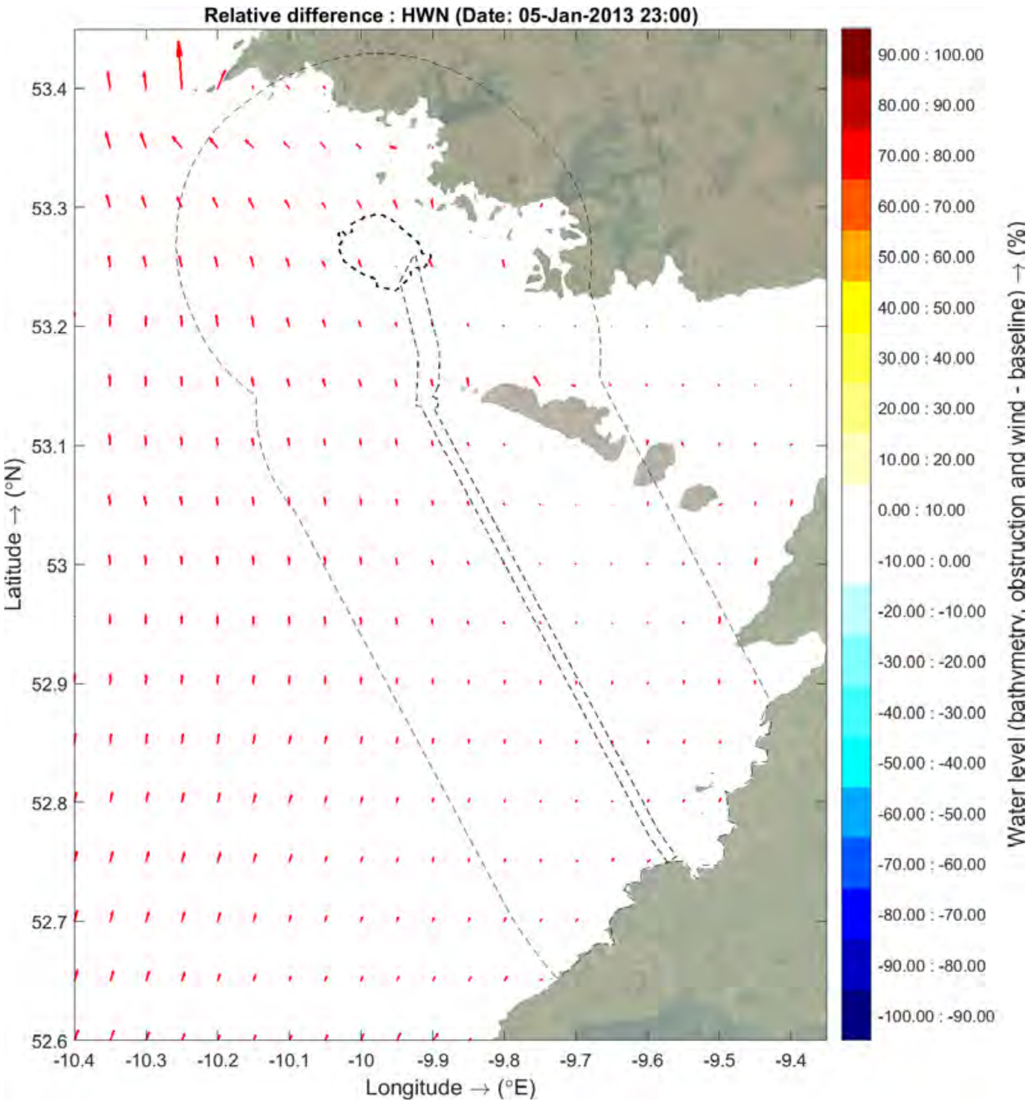
Relative difference : HWN (Date: 05-Jan-2013 23:00)
Latitude → (°N)
Longitude → (°E)
53.4
53.3
53.2
53.1
53
52.9
52.8
52.7
52.6
-10.4
-10.3
-10.2
-10.1
-10
-9.9
-9.8
-9.7
-9.6
-9.5
-9.4
90.00 : 100.00
80.00 : 90.00
70.00 : 80.00
60.00 : 70.00
50.00 : 60.00
40.00 : 50.00
30.00 : 40.00
20.00 : 30.00
10.00 : 20.00
0.00 : 10.00
-10.00 : 0.00
-20.00 : -10.00
-30.00 : -20.00
-40.00 : -30.00
-50.00 : -40.00
-60.00 : -50.00
-70.00 : -60.00
-80.00 : -70.00
-90.00 : -80.00
-100.00 : -90.00
Water level (bathymetry, obstruction and wind - baseline) → (%)

D.11 HWS currents

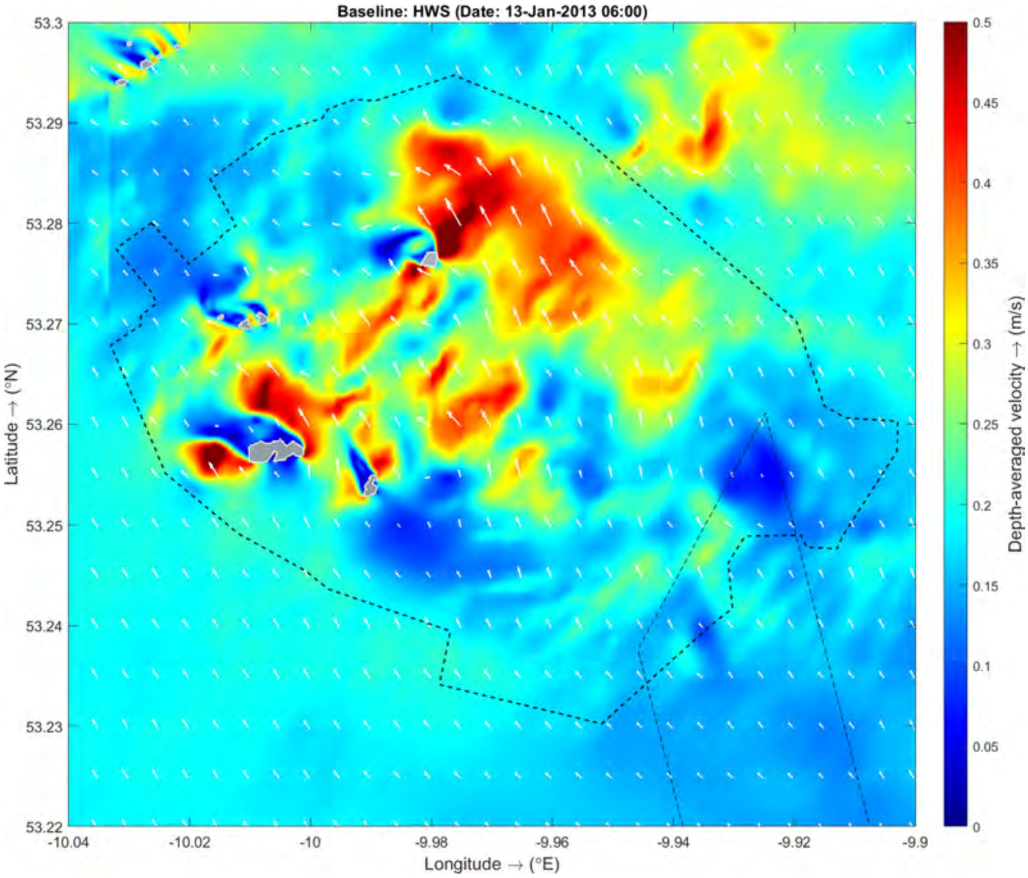

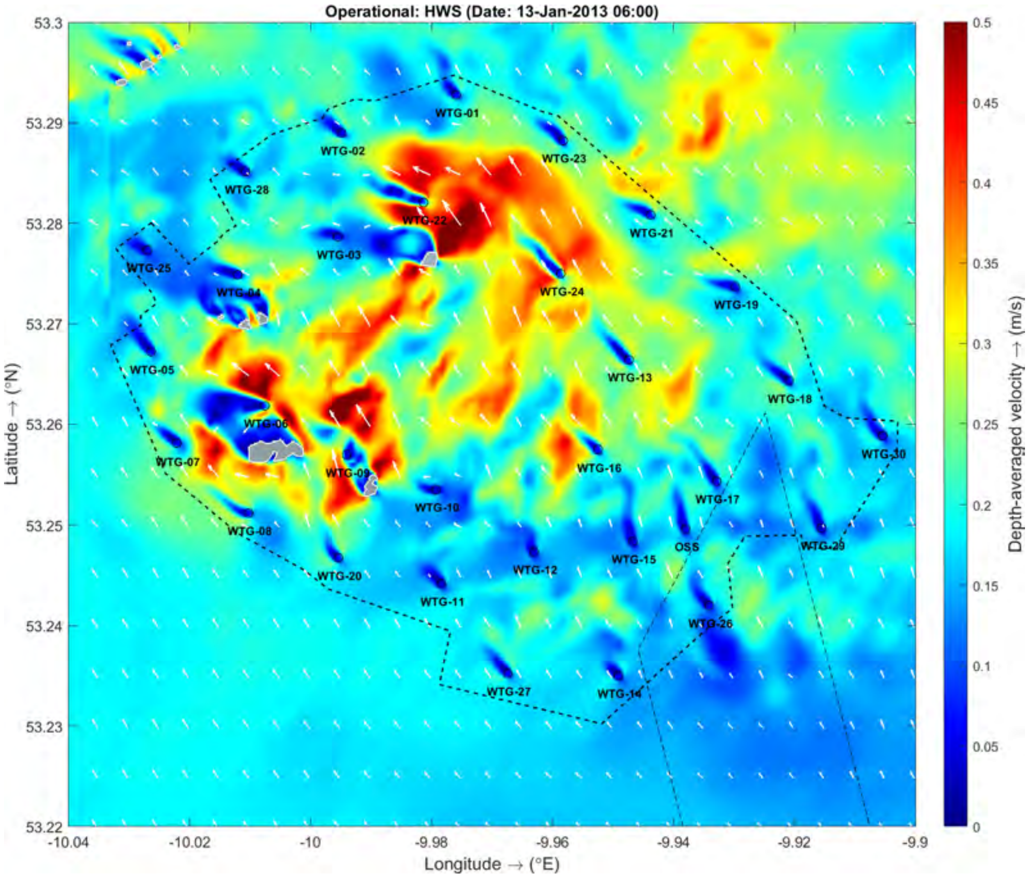

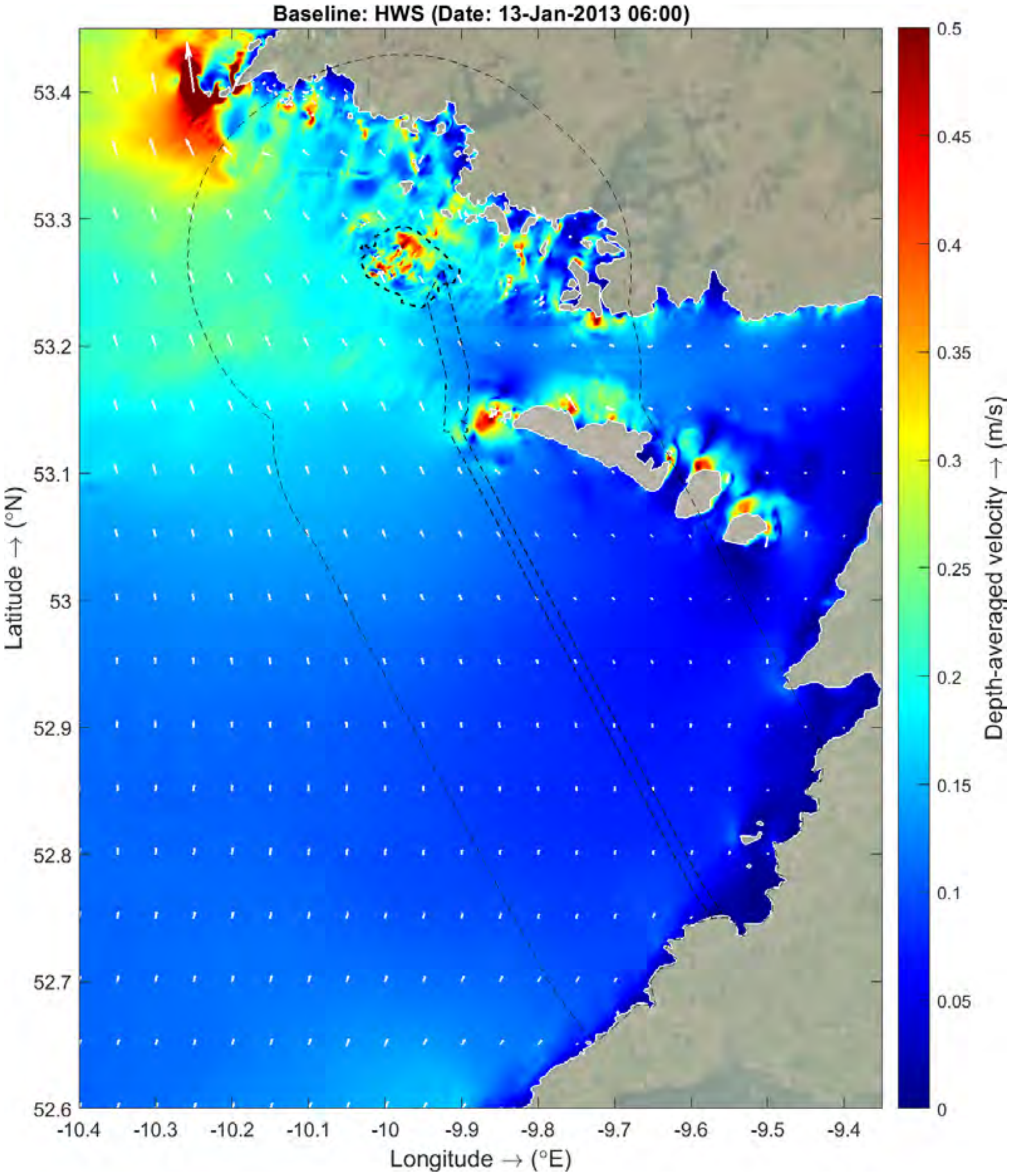

Baseline: HWS (Date: 13-Jan-2013 06:00)
53.4
53.3
53.2
53.1
53
52.9
52.8
52.7
52.6
Latitude → (°N)
-10.4
-10.3
-10.2
-10.1
-10
-9.9
-9.8
-9.7
-9.6
-9.5
-9.4
Longitude → (°E)
0.5
0.45
0.4
0.35
0.3
0.25
0.2
0.15
0.1
0.05
0
Depth-averaged velocity → (m/s)

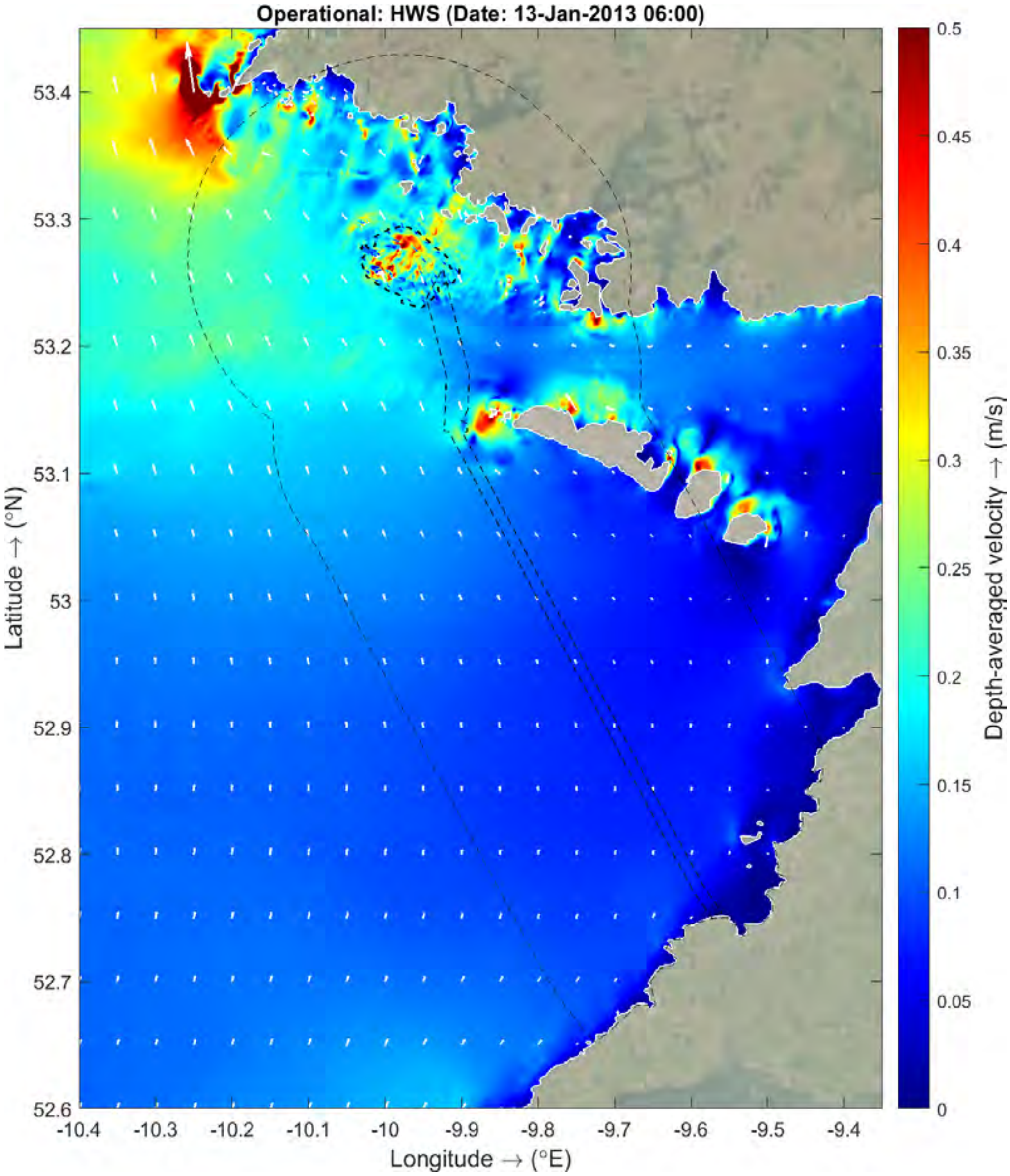

Operational: HWS (Date: 13-Jan-2013 06:00)
Latitude → (°N)
Longitude → (°E)
Depth-averaged velocity → (m/s)
53.4
53.3
53.2
53.1
53
52.9
52.8
52.7
52.6
-10.4
-10.3
-10.2
-10.1
-10
-9.9
-9.8
-9.7
-9.6
-9.5
-9.4
0.5
0.45
0.4
0.35
0.3
0.25
0.2
0.15
0.1
0.05
0

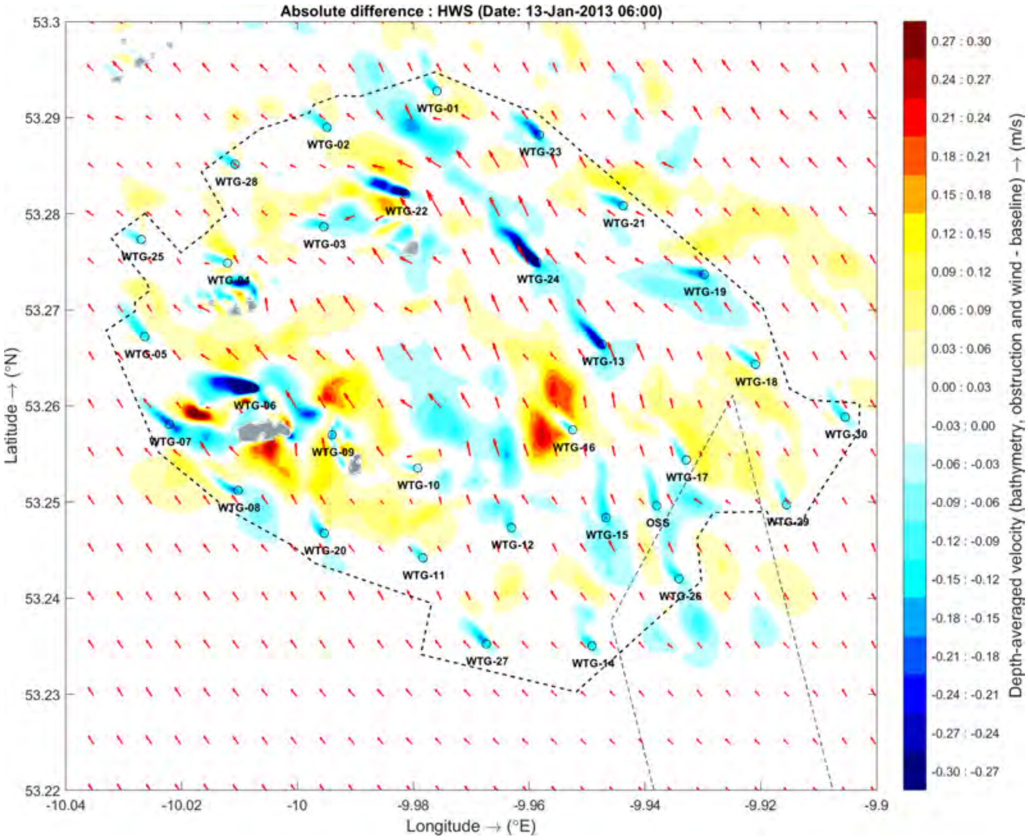
Absolute difference : HWS (Date: 13-Jan-2013 06:00)
Latitude → (°N)
Longitude → (°E)
Depth-averaged velocity (bathymetry, obstruction and wind - baseline) → (m/s)
0.27 : 0.30
0.24 : 0.27
0.21 : 0.24
0.18 : 0.21
0.15 : 0.18
0.12 : 0.15
0.09 : 0.12
0.06 : 0.09
0.03 : 0.06
0.00 : 0.03
-0.03 : 0.00
-0.06 : -0.03
-0.09 : -0.06
-0.12 : -0.09
-0.15 : -0.12
-0.18 : -0.15
-0.21 : -0.18
-0.24 : -0.21
-0.27 : -0.24
-0.30 : -0.27
WTG-01
WTG-02
WTG-03
WTG-04
WTG-05
WTG-06
WTG-07
WTG-08
WTG-09
WTG-10
WTG-11
WTG-12
WTG-13
WTG-14
WTG-15
WTG-16
WTG-17
WTG-18
WTG-19
WTG-20
WTG-21
WTG-22
WTG-23
WTG-24
WTG-25
WTG-26
WTG-27
WTG-28
WTG-29
WTG-30
OSS

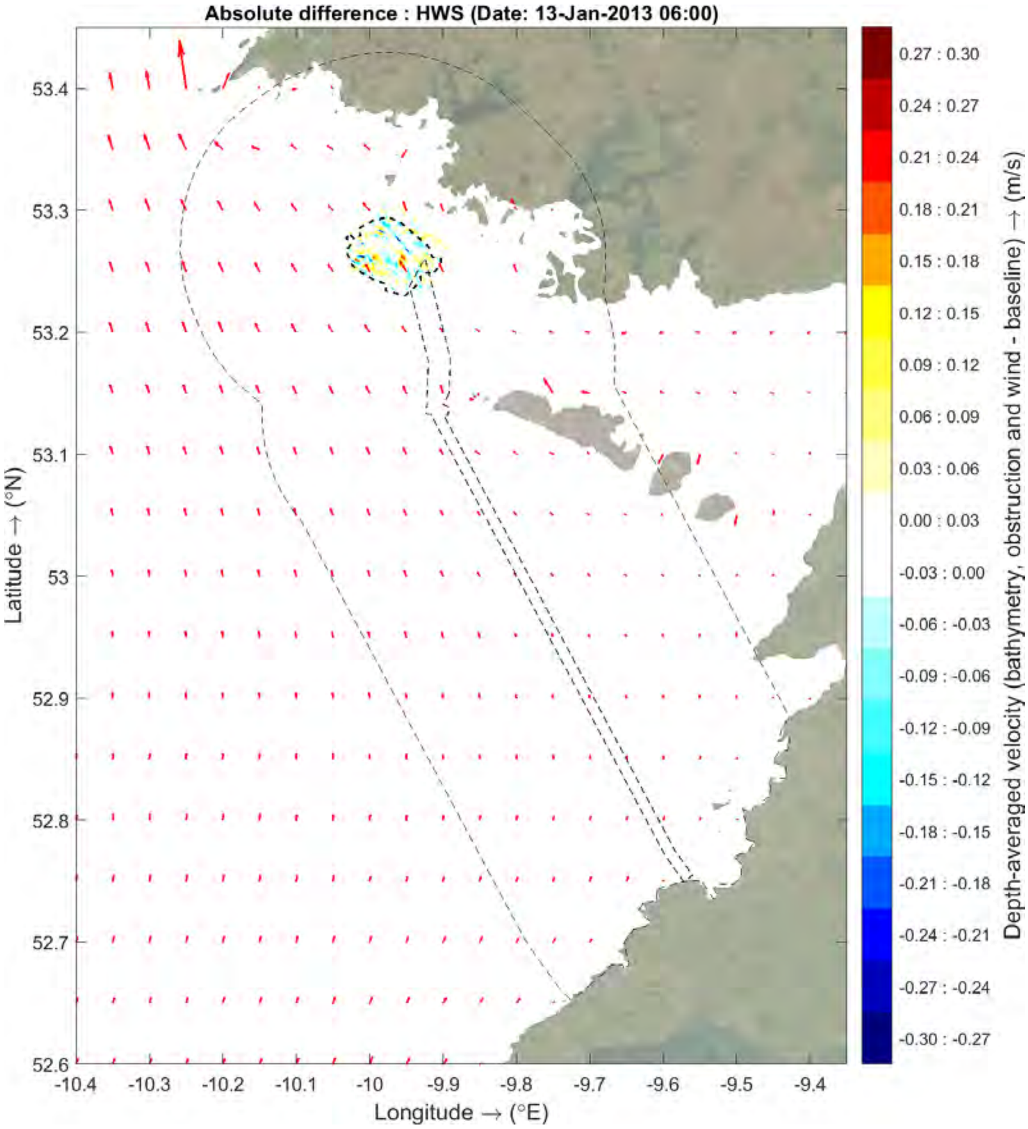
Absolute difference : HWS (Date: 13-Jan-2013 06:00)
Latitude → (°N)
Longitude → (°E)
Depth-averaged velocity (bathymetry, obstruction and wind - baseline) → (m/s)
53.4
53.3
53.2
53.1
53
52.9
52.8
52.7
52.6
-10.4
-10.3
-10.2
-10.1
-10
-9.9
-9.8
-9.7
-9.6
-9.5
-9.4
0.27 : 0.30
0.24 : 0.27
0.21 : 0.24
0.18 : 0.21
0.15 : 0.18
0.12 : 0.15
0.09 : 0.12
0.06 : 0.09
0.03 : 0.06
0.00 : 0.03
-0.03 : 0.00
-0.06 : -0.03
-0.09 : -0.06
-0.12 : -0.09
-0.15 : -0.12
-0.18 : -0.15
-0.21 : -0.18
-0.24 : -0.21
-0.27 : -0.24
-0.30 : -0.27

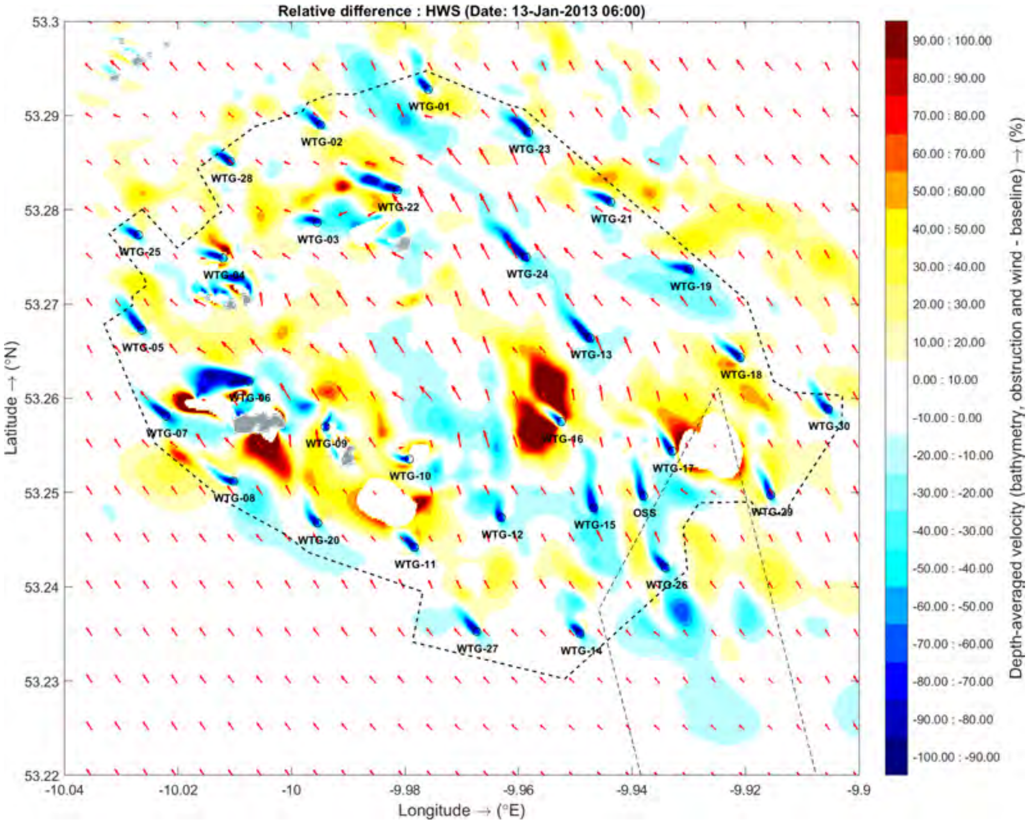
Relative difference : HWS (Date: 13-Jan-2013 06:00)
Latitude → (°N)
Longitude → (°E)
Depth-averaged velocity (bathymetry, obstruction and wind - baseline) → (%)
WTG-01
WTG-02
WTG-03
WTG-04
WTG-05
WTG-06
WTG-07
WTG-08
WTG-09
WTG-10
WTG-11
WTG-12
WTG-13
WTG-14
WTG-15
WTG-16
WTG-17
WTG-18
WTG-19
WTG-20
WTG-21
WTG-22
WTG-23
WTG-24
WTG-25
WTG-26
WTG-27
WTG-28
WTG-29
WTG-30
OSS
90.00 : 100.00
80.00 : 90.00
70.00 : 80.00
60.00 : 70.00
50.00 : 60.00
40.00 : 50.00
30.00 : 40.00
20.00 : 30.00
10.00 : 20.00
0.00 : 10.00
-10.00 : 0.00
-20.00 : -10.00
-30.00 : -20.00
-40.00 : -30.00
-50.00 : -40.00
-60.00 : -50.00
-70.00 : -60.00
-80.00 : -70.00
-90.00 : -80.00
-100.00 : -90.00

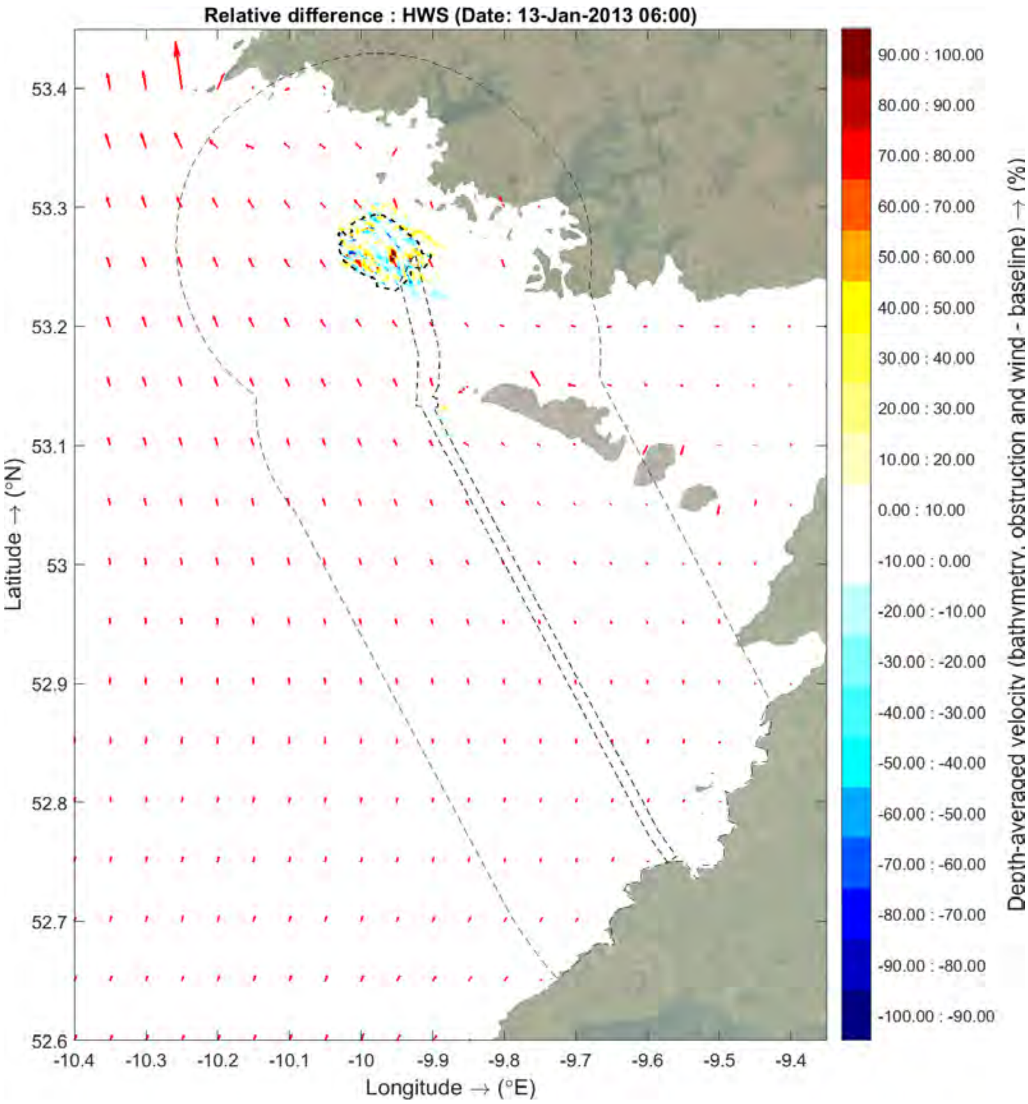

Relative difference : HWS (Date: 13-Jan-2013 06:00)
53.4
53.3
53.2
53.1
53
52.9
52.8
52.7
52.6
Latitude → (°N)
-10.4
-10.3
-10.2
-10.1
-10
-9.9
-9.8
-9.7
-9.6
-9.5
-9.4
Longitude → (°E)
90.00 : 100.00
80.00 : 90.00
70.00 : 80.00
60.00 : 70.00
50.00 : 60.00
40.00 : 50.00
30.00 : 40.00
20.00 : 30.00
10.00 : 20.00
0.00 : 10.00
-10.00 : 0.00
-20.00 : -10.00
-30.00 : -20.00
-40.00 : -30.00
-50.00 : -40.00
-60.00 : -50.00
-70.00 : -60.00
-80.00 : -70.00
-90.00 : -80.00
-100.00 : -90.00
Depth-averaged velocity (bathymetry, obstruction and wind - baseline) → (%)

D.12 HWS water levels

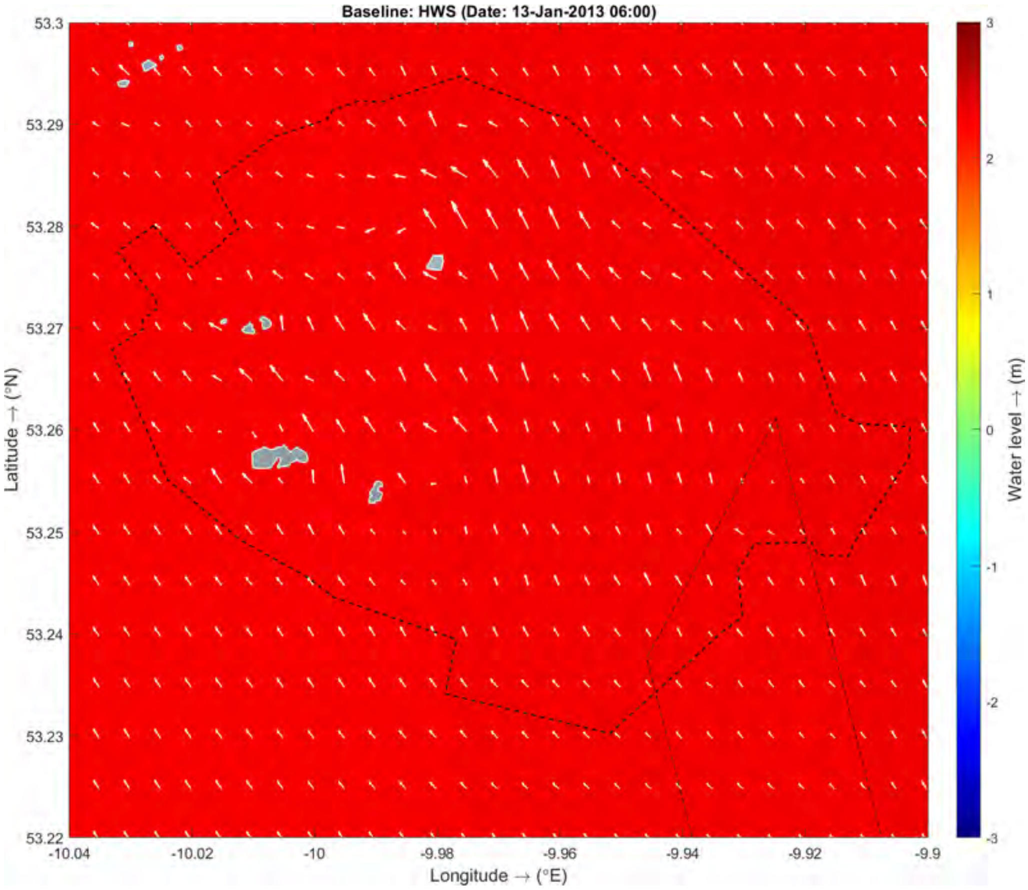

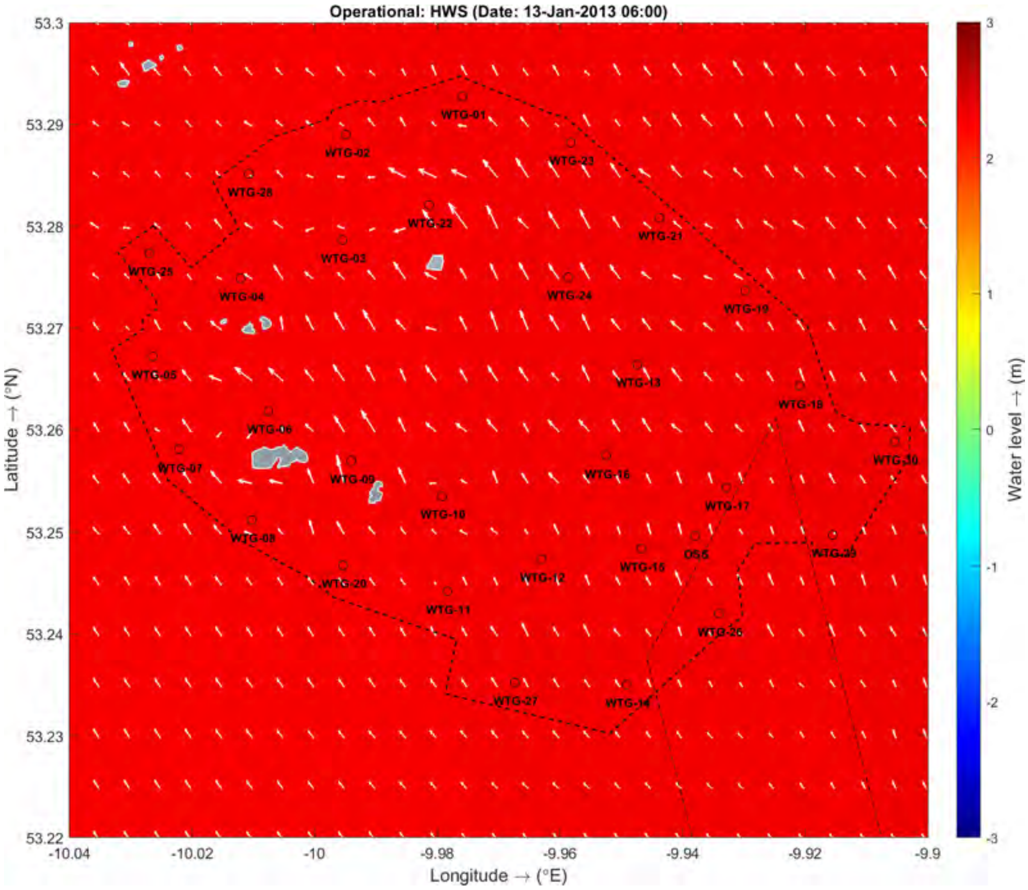
Operational: HWS (Date: 13-Jan-2013 06:00)
Latitude → (°N)
Longitude → (°E)
Water level → (m)
WTG-01
WTG-02
WTG-03
WTG-04
WTG-05
WTG-06
WTG-07
WTG-08
WTG-09
WTG-10
WTG-11
WTG-12
WTG-13
WTG-14
WTG-15
WTG-16
WTG-17
WTG-18
WTG-19
WTG-20
WTG-21
WTG-22
WTG-23
WTG-24
WTG-25
WTG-26
WTG-27
WTG-28
WTG-29
WTG-30
OSS

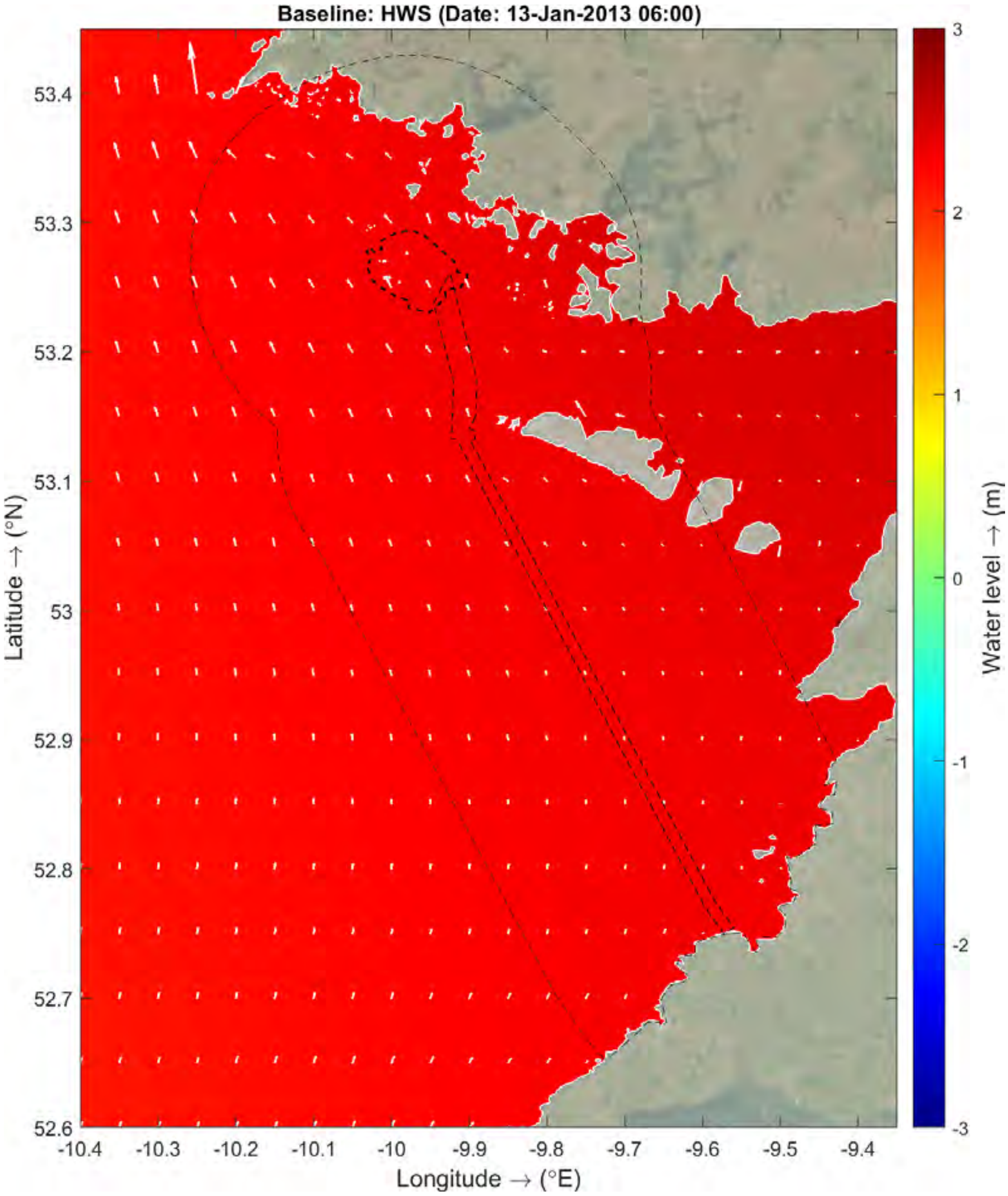
Baseline: HWS (Date: 13-Jan-2013 06:00)
Latitude → (°N)
Longitude → (°E)
Water level → (m)
53.4
53.3
53.2
53.1
53
52.9
52.8
52.7
52.6
-10.4
-10.3
-10.2
-10.1
-10
-9.9
-9.8
-9.7
-9.6
-9.5
-9.4
3
2
1
0
-1
-2
-3

Deltares

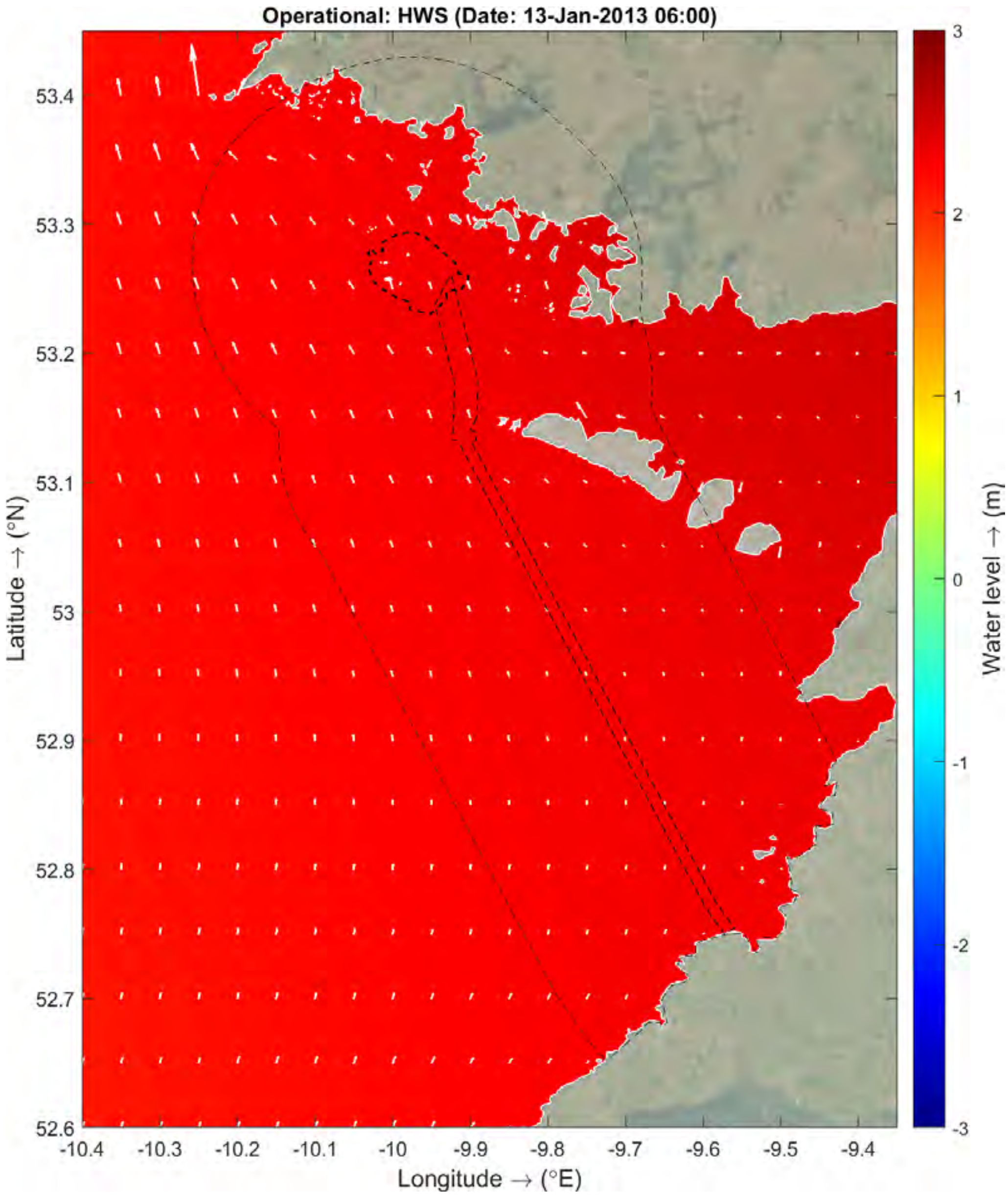

Operational: HWS (Date: 13-Jan-2013 06:00)
53.4
53.3
53.2
53.1
53
52.9
52.8
52.7
52.6
Latitude → (°N)
-10.4
-10.3
-10.2
-10.1
-10
-9.9
-9.8
-9.7
-9.6
-9.5
-9.4
Longitude → (°E)
3
2
1
0
-1
-2
-3
Water level → (m)

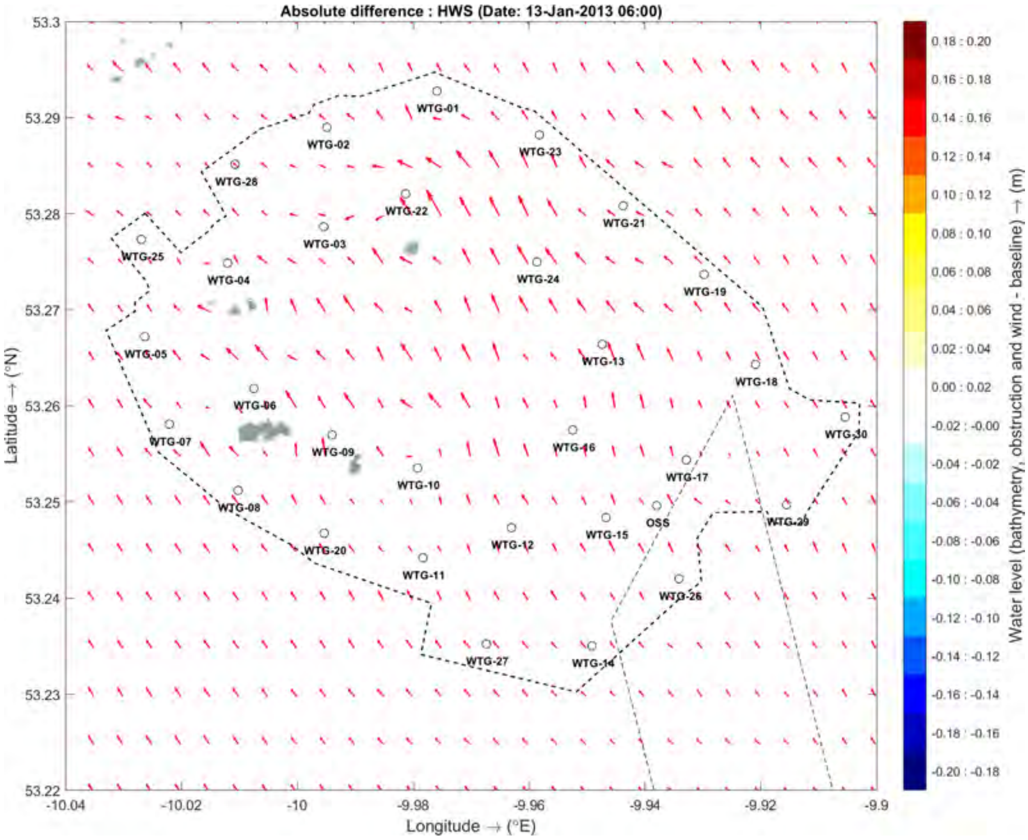

Absolute difference : HWS (Date: 13-Jan-2013 06:00)
Latitude → (°N)
Longitude → (°E)
Water level (bathymetry, obstruction and wind - baseline) → (m)
WTG-01
WTG-02
WTG-03
WTG-04
WTG-05
WTG-06
WTG-07
WTG-08
WTG-09
WTG-10
WTG-11
WTG-12
WTG-13
WTG-14
WTG-15
WTG-16
WTG-17
WTG-18
WTG-19
WTG-20
WTG-21
WTG-22
WTG-23
WTG-24
WTG-25
WTG-26
WTG-27
WTG-28
WTG-29
WTG-30
OSS

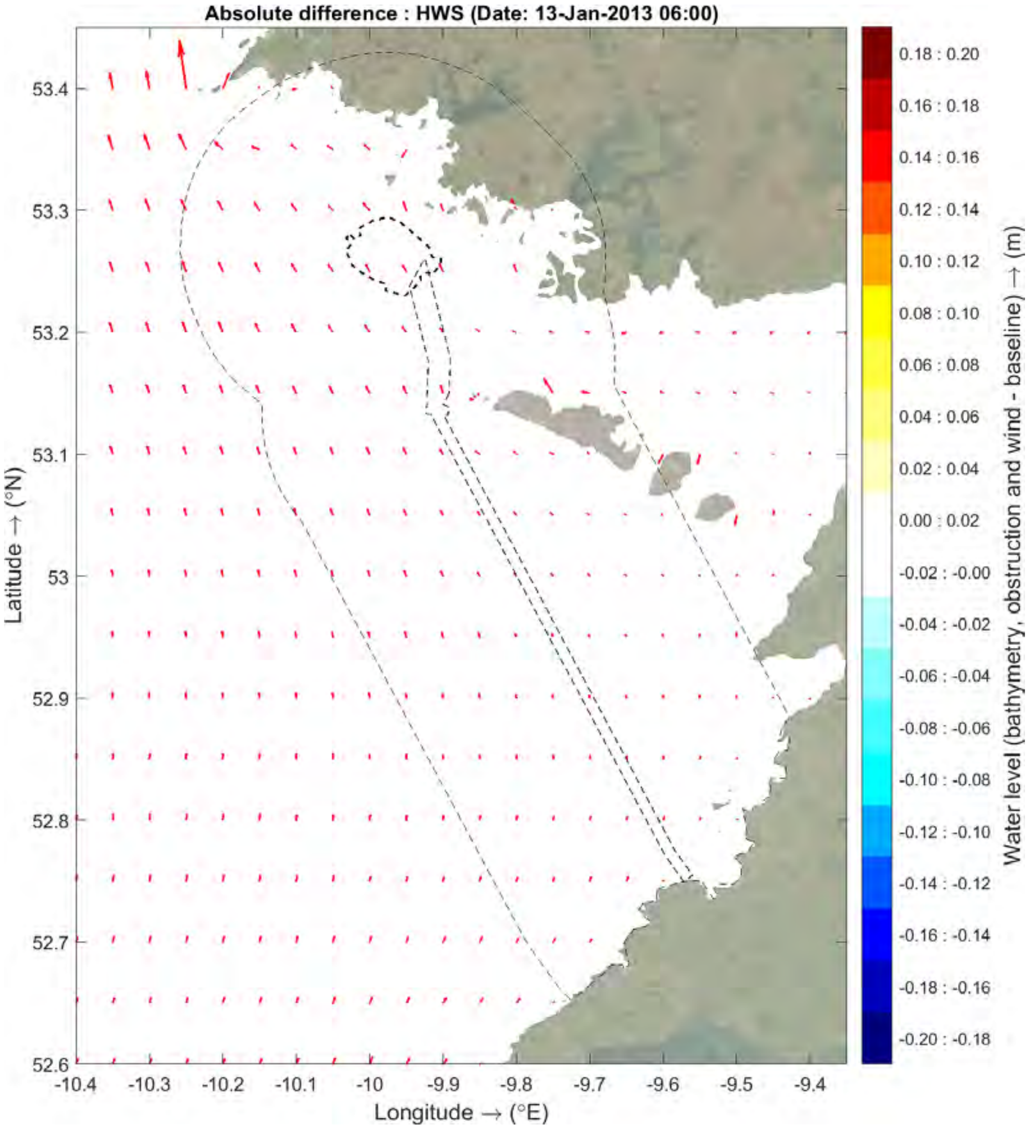
Absolute difference : HWS (Date: 13-Jan-2013 06:00)
Latitude → (°N)
Longitude → (°E)
53.4
53.3
53.2
53.1
53
52.9
52.8
52.7
52.6
-10.4
-10.3
-10.2
-10.1
-10
-9.9
-9.8
-9.7
-9.6
-9.5
-9.4
0.18 : 0.20
0.16 : 0.18
0.14 : 0.16
0.12 : 0.14
0.10 : 0.12
0.08 : 0.10
0.06 : 0.08
0.04 : 0.06
0.02 : 0.04
0.00 : 0.02
-0.02 : -0.00
-0.04 : -0.02
-0.06 : -0.04
-0.08 : -0.06
-0.10 : -0.08
-0.12 : -0.10
-0.14 : -0.12
-0.16 : -0.14
-0.18 : -0.16
-0.20 : -0.18
Water level (bathymetry, obstruction and wind - baseline) → (m)

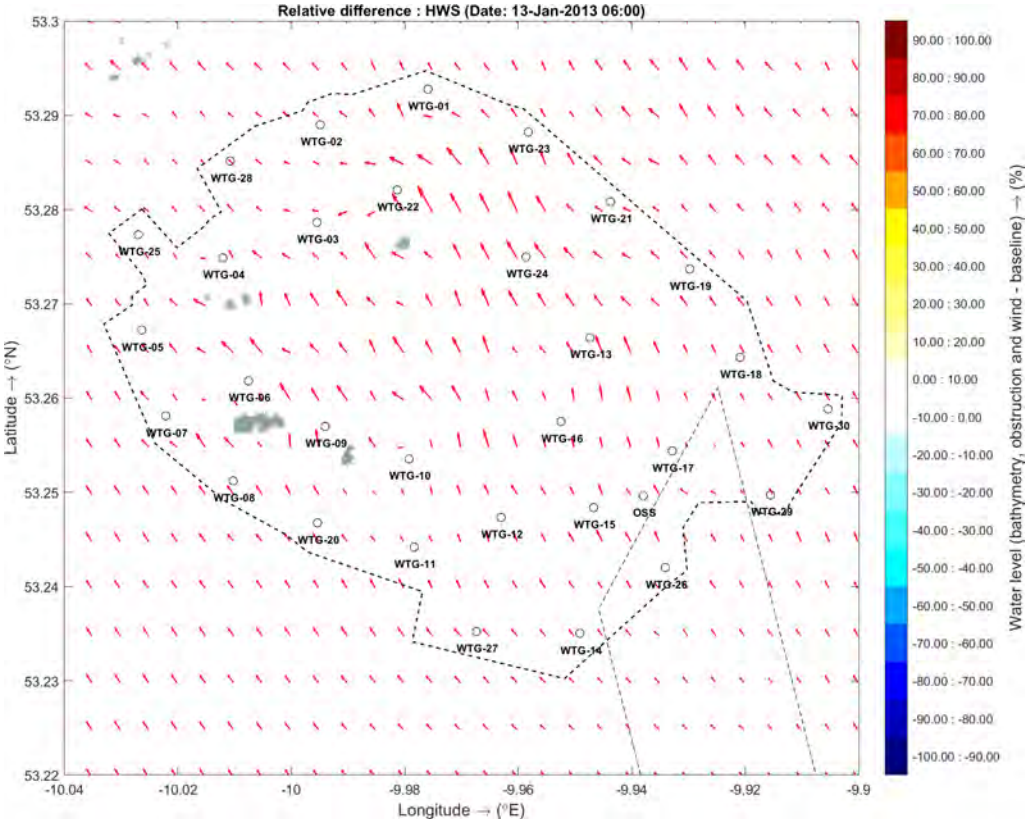
Relative difference : HWS (Date: 13-Jan-2013 06:00)
Latitude → (°N)
Longitude → (°E)
Water level (bathymetry, obstruction and wind - baseline) → (%)
90.00 : 100.00
80.00 : 90.00
70.00 : 80.00
60.00 : 70.00
50.00 : 60.00
40.00 : 50.00
30.00 : 40.00
20.00 : 30.00
10.00 : 20.00
0.00 : 10.00
-10.00 : 0.00
-20.00 : -10.00
-30.00 : -20.00
-40.00 : -30.00
-50.00 : -40.00
-60.00 : -50.00
-70.00 : -60.00
-80.00 : -70.00
-90.00 : -80.00
-100.00 : -90.00
WTG-01
WTG-02
WTG-03
WTG-04
WTG-05
WTG-06
WTG-07
WTG-08
WTG-09
WTG-10
WTG-11
WTG-12
WTG-13
WTG-14
WTG-15
WTG-16
WTG-17
WTG-18
WTG-19
WTG-20
WTG-21
WTG-22
WTG-23
WTG-24
WTG-25
WTG-26
WTG-27
WTG-28
WTG-29
WTG-30
OSS

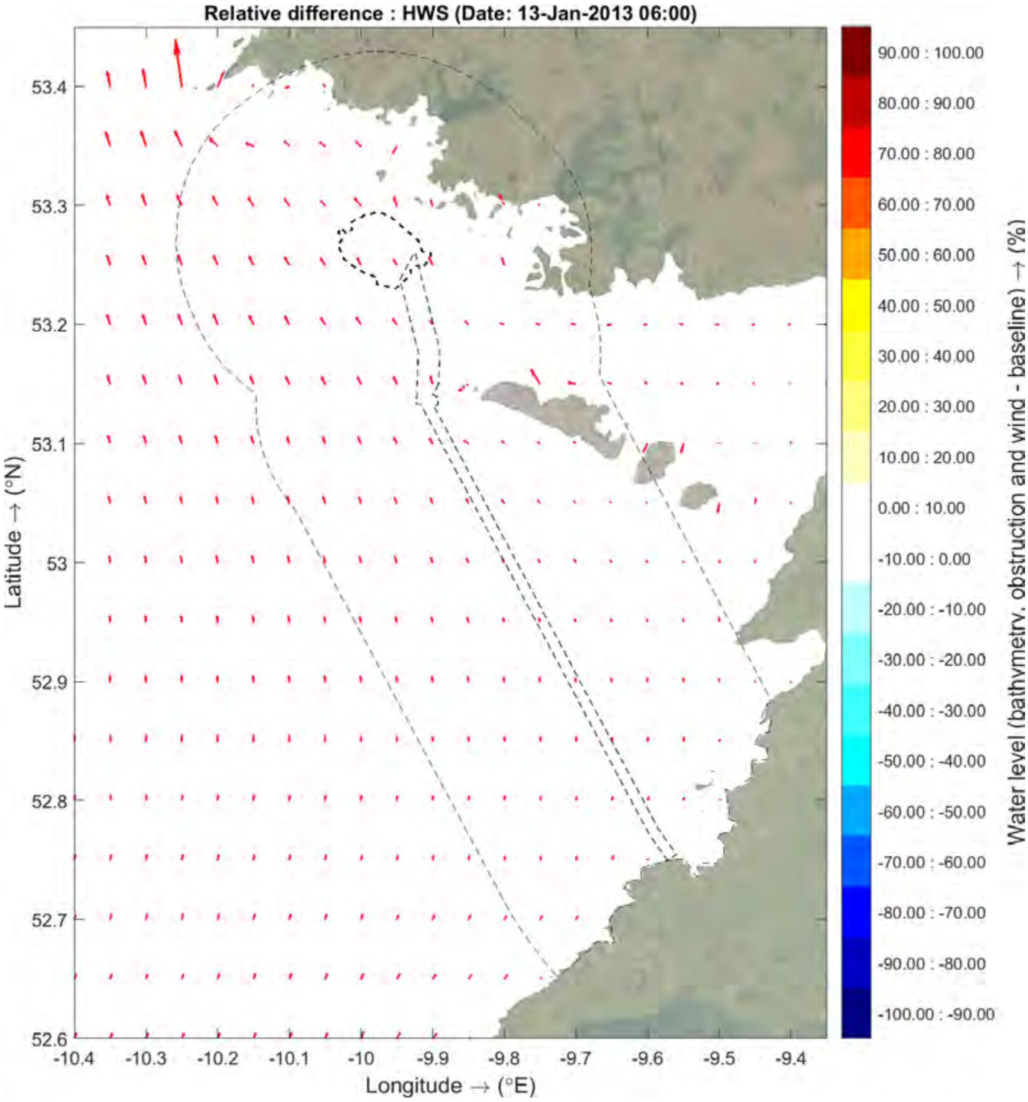

Relative difference : HWS (Date: 13-Jan-2013 06:00)
53.4
53.3
53.2
53.1
53
52.9
52.8
52.7
52.6
Latitude → (°N)
-10.4
-10.3
-10.2
-10.1
-10
-9.9
-9.8
-9.7
-9.6
-9.5
-9.4
Longitude → (°E)
90.00 : 100.00
80.00 : 90.00
70.00 : 80.00
60.00 : 70.00
50.00 : 60.00
40.00 : 50.00
30.00 : 40.00
20.00 : 30.00
10.00 : 20.00
0.00 : 10.00
-10.00 : 0.00
-20.00 : -10.00
-30.00 : -20.00
-40.00 : -30.00
-50.00 : -40.00
-60.00 : -50.00
-70.00 : -60.00
-80.00 : -70.00
-90.00 : -80.00
-100.00 : -90.00
Water level (bathymetry, obstruction and wind - baseline) → (%)

D.13 LWN currents

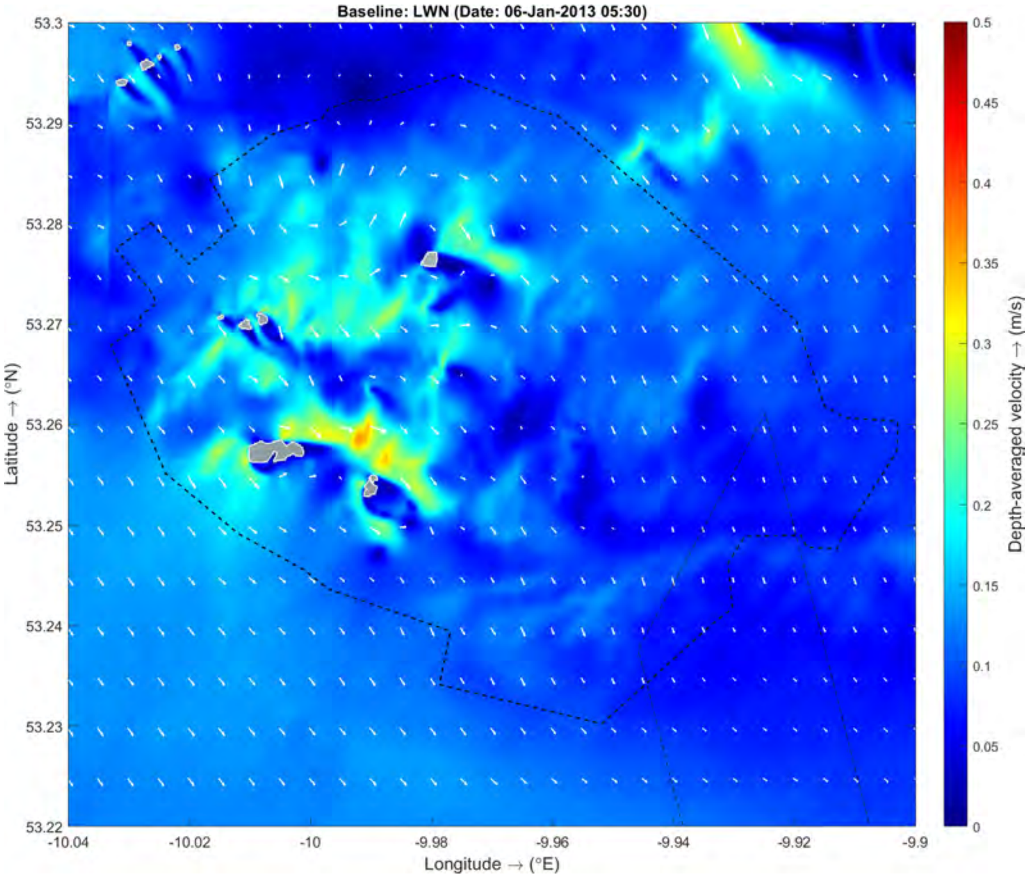

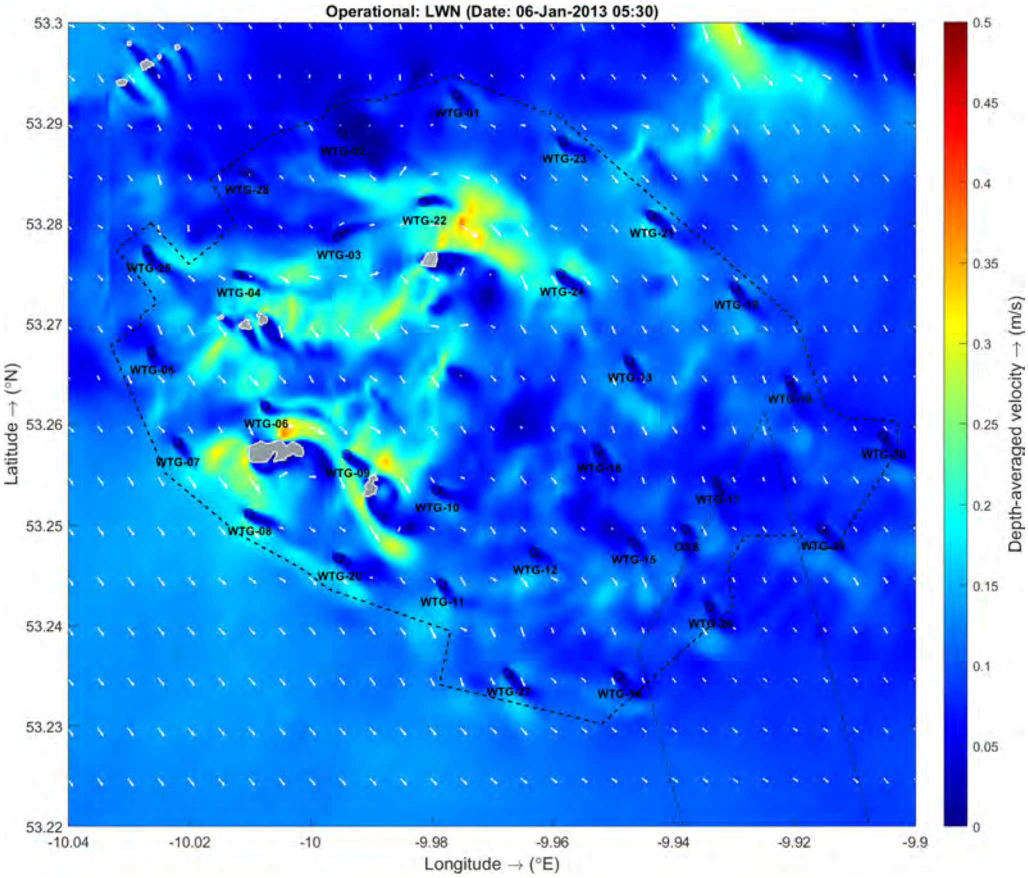

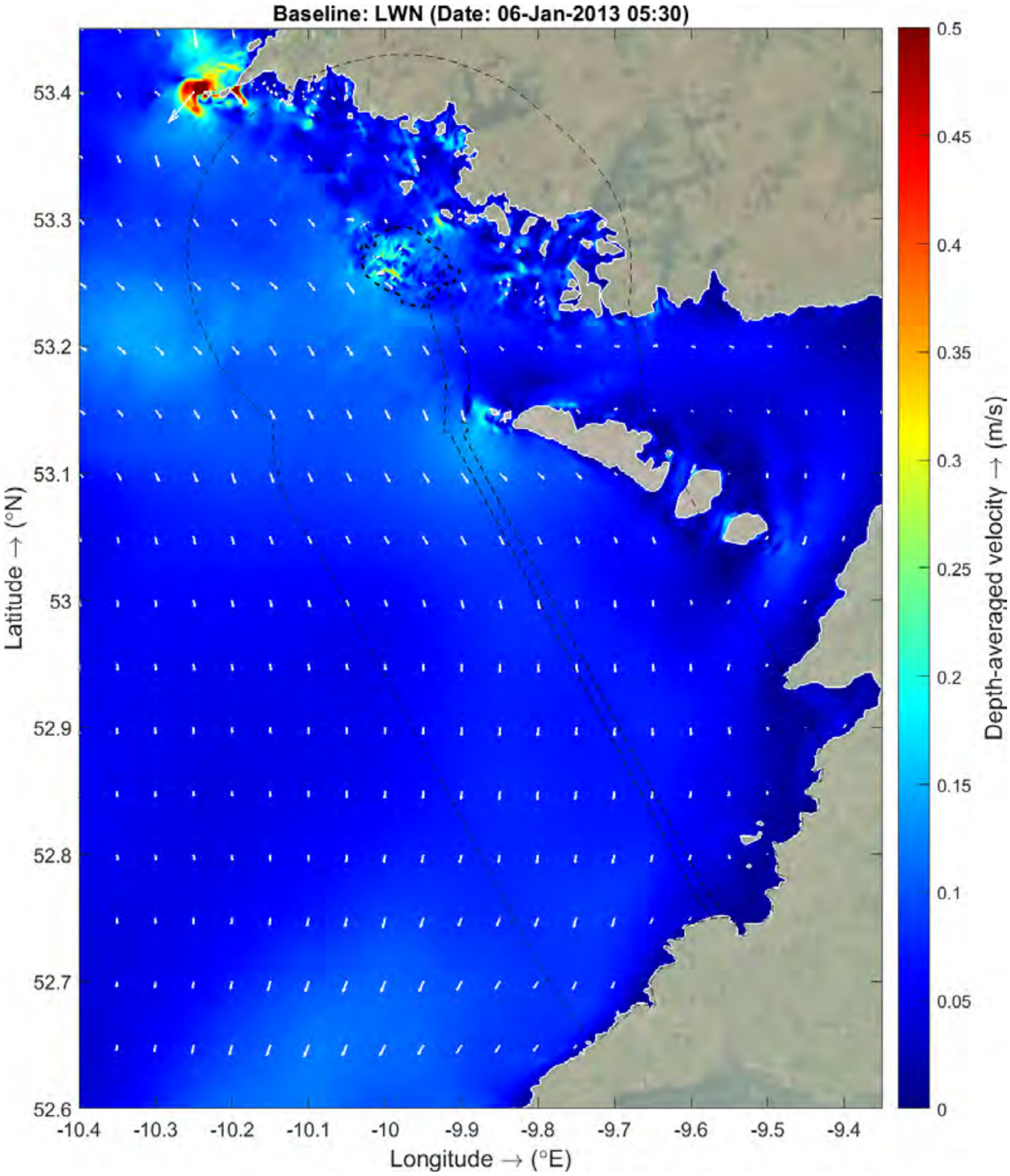

Baseline: LWN (Date: 06-Jan-2013 05:30)
53.4
53.3
53.2
53.1
53
52.9
52.8
52.7
52.6
Latitude → (°N)
-10.4
-10.3
-10.2
-10.1
-10
-9.9
-9.8
-9.7
-9.6
-9.5
-9.4
Longitude → (°E)
0.5
0.45
0.4
0.35
0.3
0.25
0.2
0.15
0.1
0.05
0
Depth-averaged velocity → (m/s)

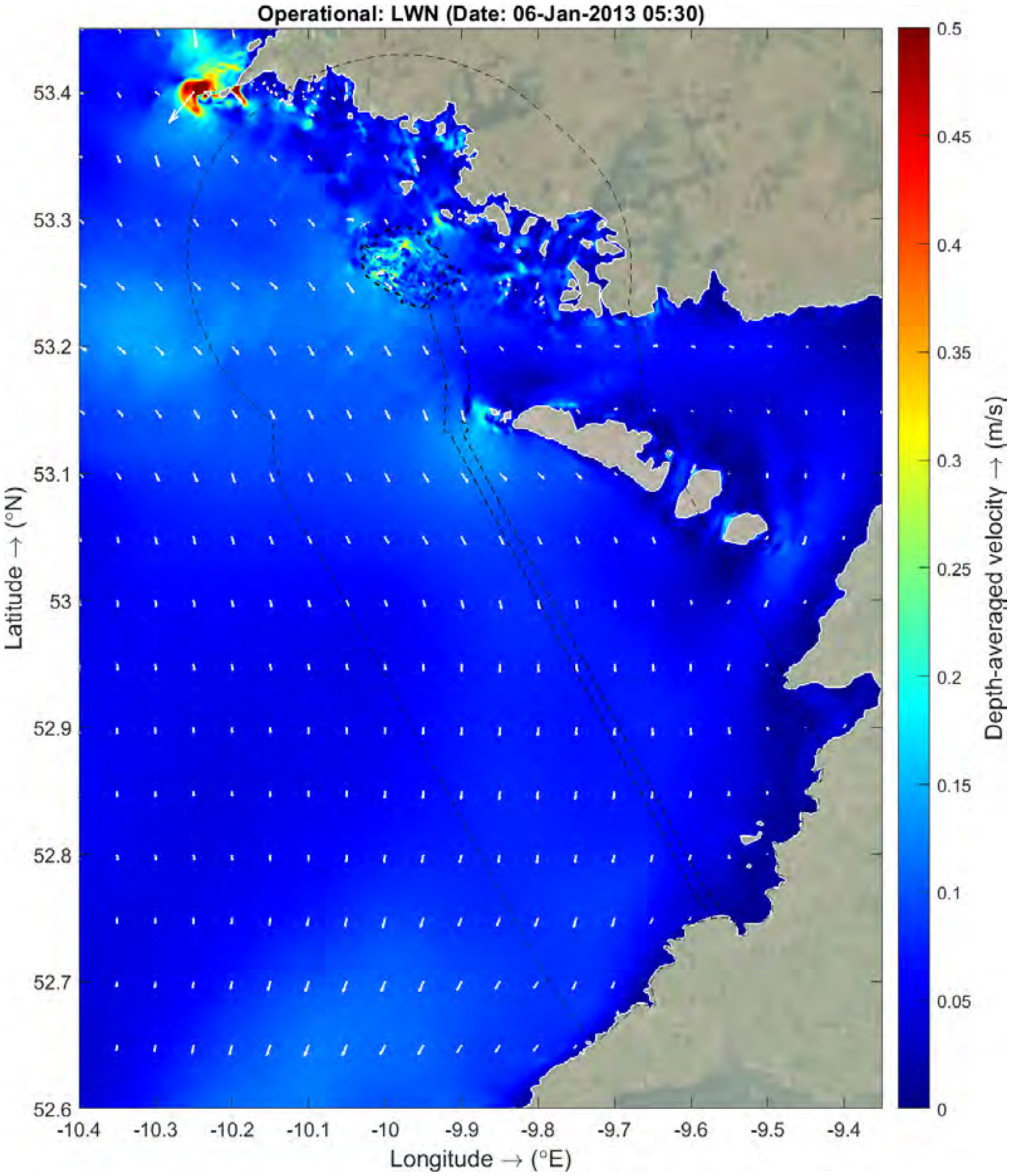
Operational: LWN (Date: 06-Jan-2013 05:30)
Latitude → (°N)
Longitude → (°E)
Depth-averaged velocity → (m/s)
53.4
53.3
53.2
53.1
53
52.9
52.8
52.7
52.6
-10.4
-10.3
-10.2
-10.1
-10
-9.9
-9.8
-9.7
-9.6
-9.5
-9.4
0.5
0.45
0.4
0.35
0.3
0.25
0.2
0.15
0.1
0.05
0

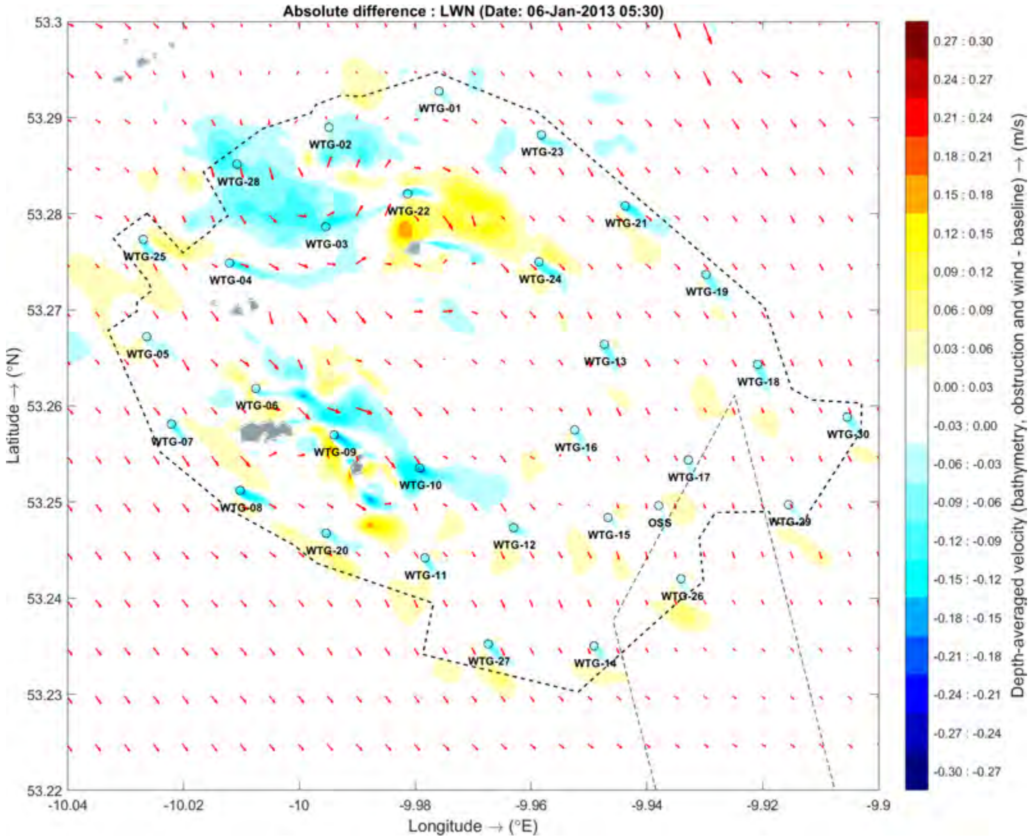
Absolute difference : LWN (Date: 06-Jan-2013 05:30)
Latitude → (°N)
Longitude → (°E)
Depth-averaged velocity (bathymetry, obstruction and wind - baseline) → (m/s)
WTG-01
WTG-02
WTG-03
WTG-04
WTG-05
WTG-06
WTG-07
WTG-08
WTG-09
WTG-10
WTG-11
WTG-12
WTG-13
WTG-14
WTG-15
WTG-16
WTG-17
WTG-18
WTG-19
WTG-20
WTG-21
WTG-22
WTG-23
WTG-24
WTG-25
WTG-26
WTG-27
WTG-28
WTG-29
WTG-30
OSS

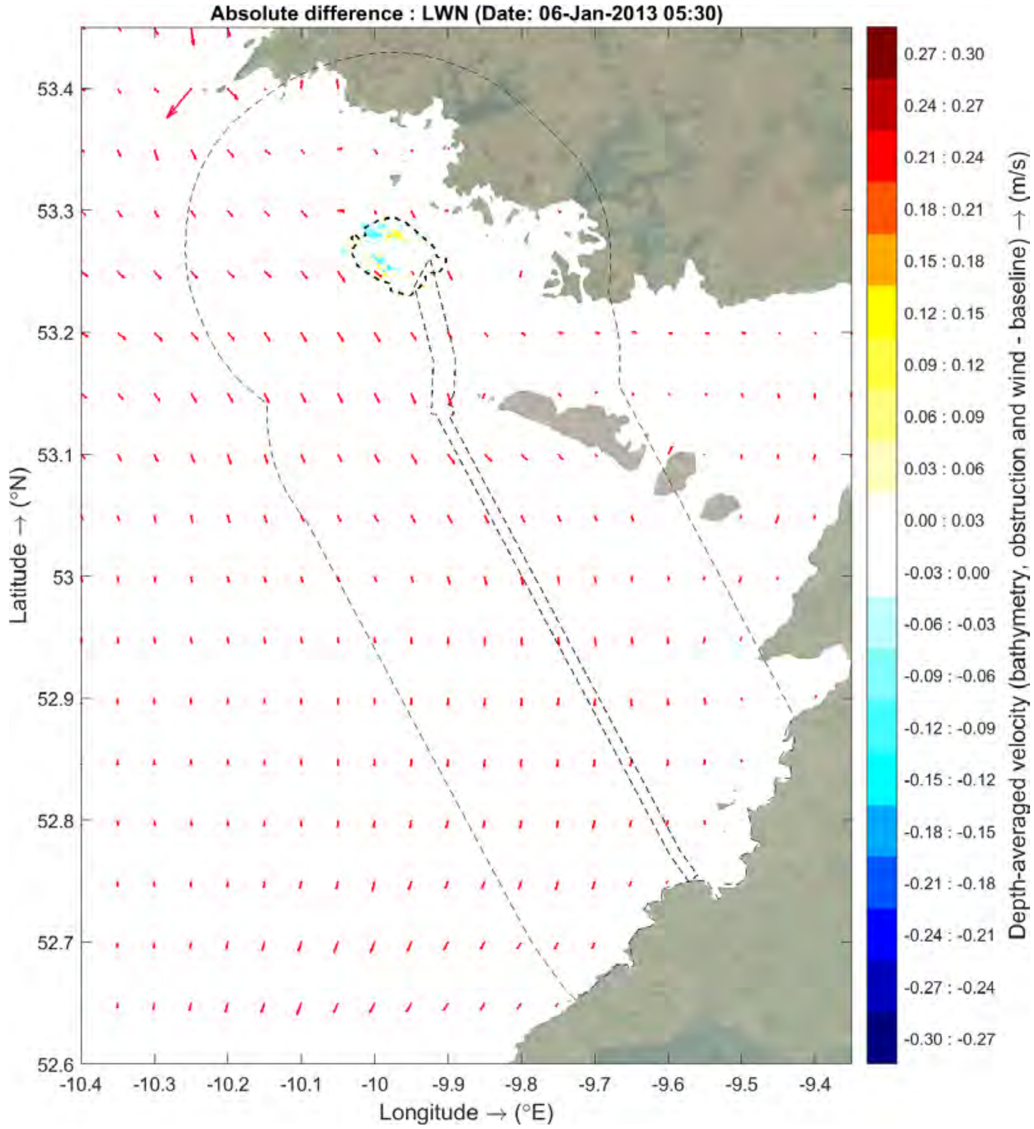
Absolute difference : LWN (Date: 06-Jan-2013 05:30)
53.4
53.3
53.2
53.1
53
52.9
52.8
52.7
52.6
Latitude → (°N)
-10.4
-10.3
-10.2
-10.1
-10
-9.9
-9.8
-9.7
-9.6
-9.5
-9.4
Longitude → (°E)
0.27 : 0.30
0.24 : 0.27
0.21 : 0.24
0.18 : 0.21
0.15 : 0.18
0.12 : 0.15
0.09 : 0.12
0.06 : 0.09
0.03 : 0.06
0.00 : 0.03
-0.03 : 0.00
-0.06 : -0.03
-0.09 : -0.06
-0.12 : -0.09
-0.15 : -0.12
-0.18 : -0.15
-0.21 : -0.18
-0.24 : -0.21
-0.27 : -0.24
-0.30 : -0.27
Depth-averaged velocity (bathymetry, obstruction and wind - baseline) → (m/s)

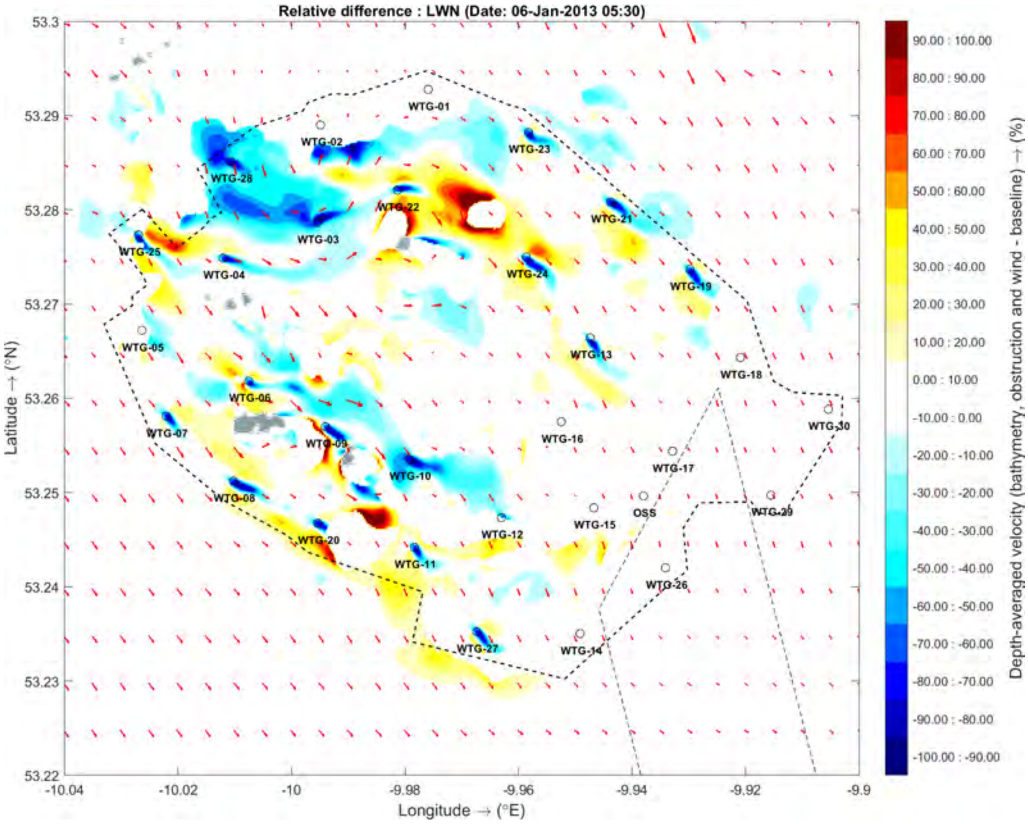
Relative difference : LWN (Date: 06-Jan-2013 05:30)
Latitude → (°N)
Longitude → (°E)
Depth-averaged velocity (bathymetry, obstruction and wind - baseline) → (%)
WTG-01
WTG-02
WTG-03
WTG-04
WTG-05
WTG-06
WTG-07
WTG-08
WTG-09
WTG-10
WTG-11
WTG-12
WTG-13
WTG-14
WTG-15
WTG-16
WTG-17
WTG-18
WTG-19
WTG-20
WTG-21
WTG-22
WTG-23
WTG-24
WTG-25
WTG-26
WTG-27
WTG-28
WTG-29
WTG-30
OSS
90.00 : 100.00
80.00 : 90.00
70.00 : 80.00
60.00 : 70.00
50.00 : 60.00
40.00 : 50.00
30.00 : 40.00
20.00 : 30.00
10.00 : 20.00
0.00 : 10.00
-10.00 : 0.00
-20.00 : -10.00
-30.00 : -20.00
-40.00 : -30.00
-50.00 : -40.00
-60.00 : -50.00
-70.00 : -60.00
-80.00 : -70.00
-90.00 : -80.00
-100.00 : -90.00

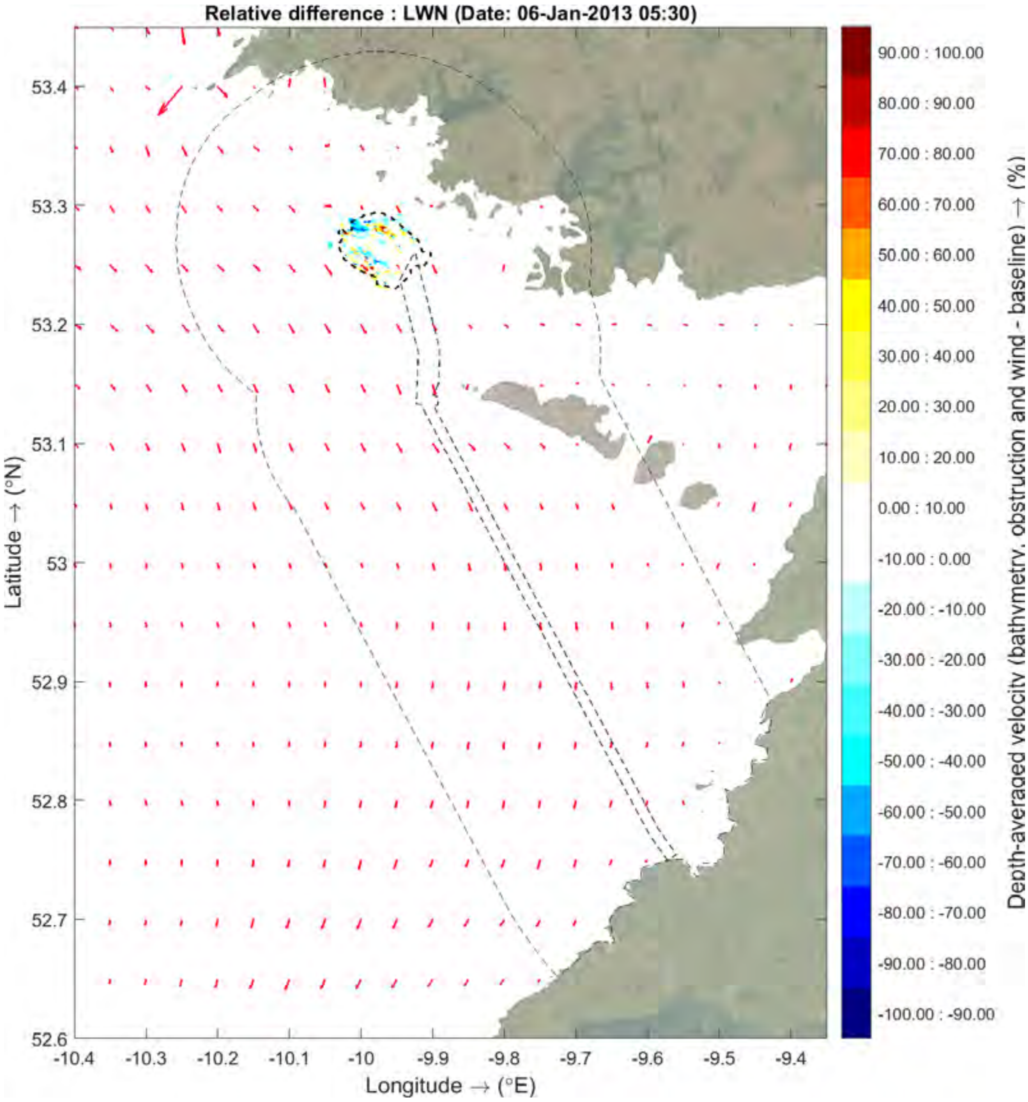
Relative difference : LWN (Date: 06-Jan-2013 05:30)
Latitude → (°N)
Longitude → (°E)
Depth-averaged velocity (bathymetry, obstruction and wind - baseline) → (%)
90.00 : 100.00
80.00 : 90.00
70.00 : 80.00
60.00 : 70.00
50.00 : 60.00
40.00 : 50.00
30.00 : 40.00
20.00 : 30.00
10.00 : 20.00
0.00 : 10.00
-10.00 : 0.00
-20.00 : -10.00
-30.00 : -20.00
-40.00 : -30.00
-50.00 : -40.00
-60.00 : -50.00
-70.00 : -60.00
-80.00 : -70.00
-90.00 : -80.00
-100.00 : -90.00

D.14 LWN water levels

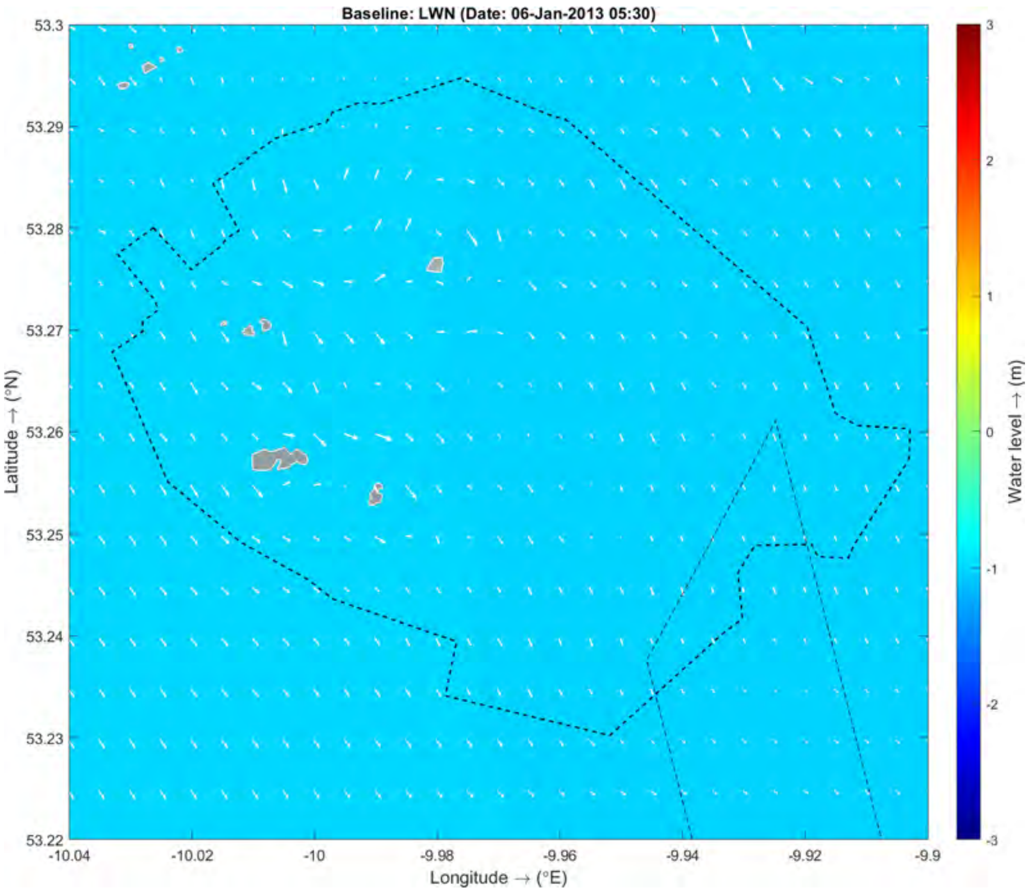

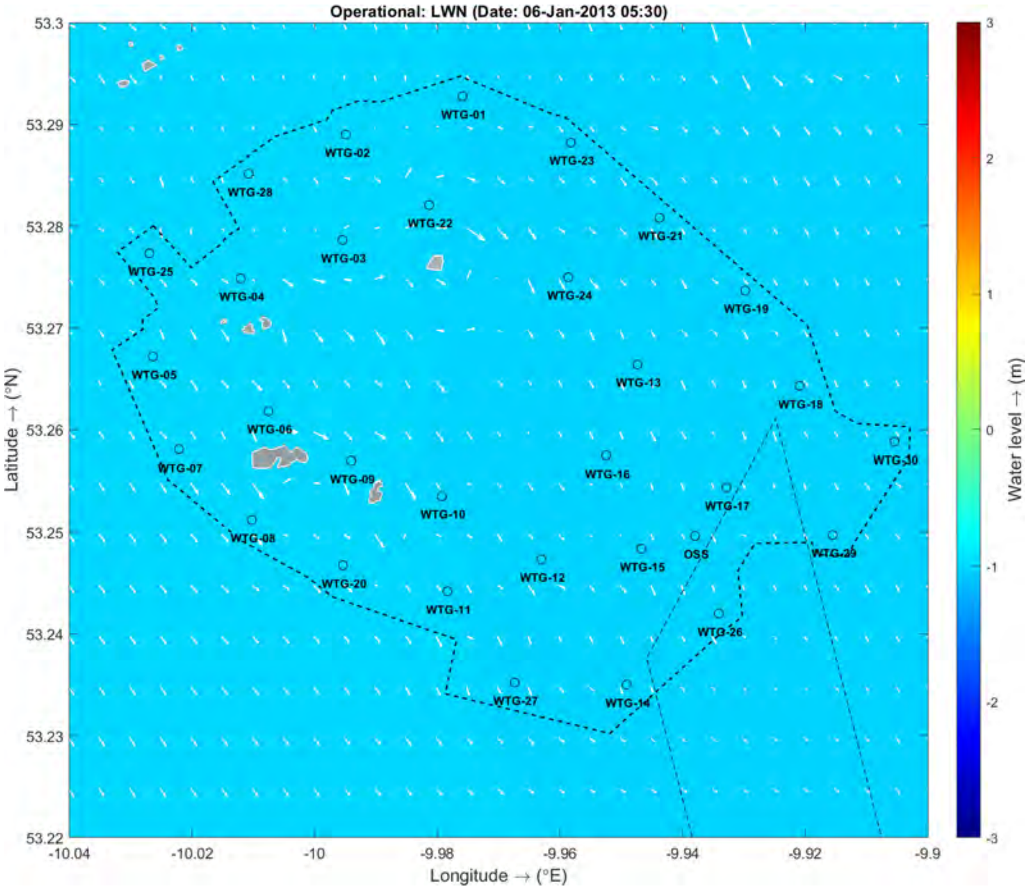
Operational: LWN (Date: 06-Jan-2013 05:30)
Latitude → (°N)
Longitude → (°E)
Water level → (m)
WTG-01
WTG-02
WTG-03
WTG-04
WTG-05
WTG-06
WTG-07
WTG-08
WTG-09
WTG-10
WTG-11
WTG-12
WTG-13
WTG-14
WTG-15
WTG-16
WTG-17
WTG-18
WTG-19
WTG-20
WTG-21
WTG-22
WTG-23
WTG-24
WTG-25
WTG-26
WTG-27
WTG-28
WTG-29
WTG-30
OSS

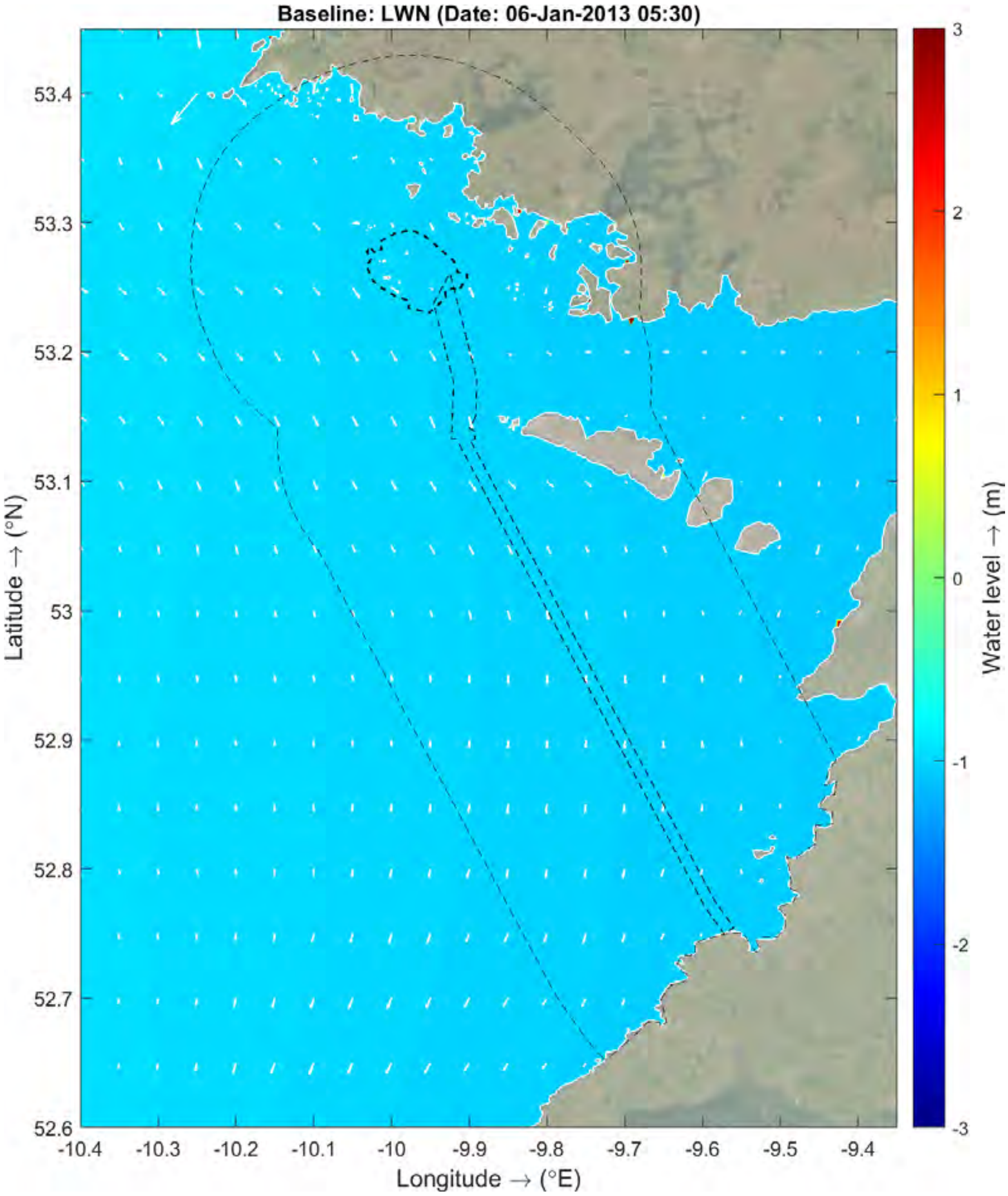

Baseline: LWN (Date: 06-Jan-2013 05:30)
53.4
53.3
53.2
53.1
53
52.9
52.8
52.7
52.6
Latitude → (°N)
-10.4
-10.3
-10.2
-10.1
-10
-9.9
-9.8
-9.7
-9.6
-9.5
-9.4
Longitude → (°E)
3
2
1
0
-1
-2
-3
Water level → (m)

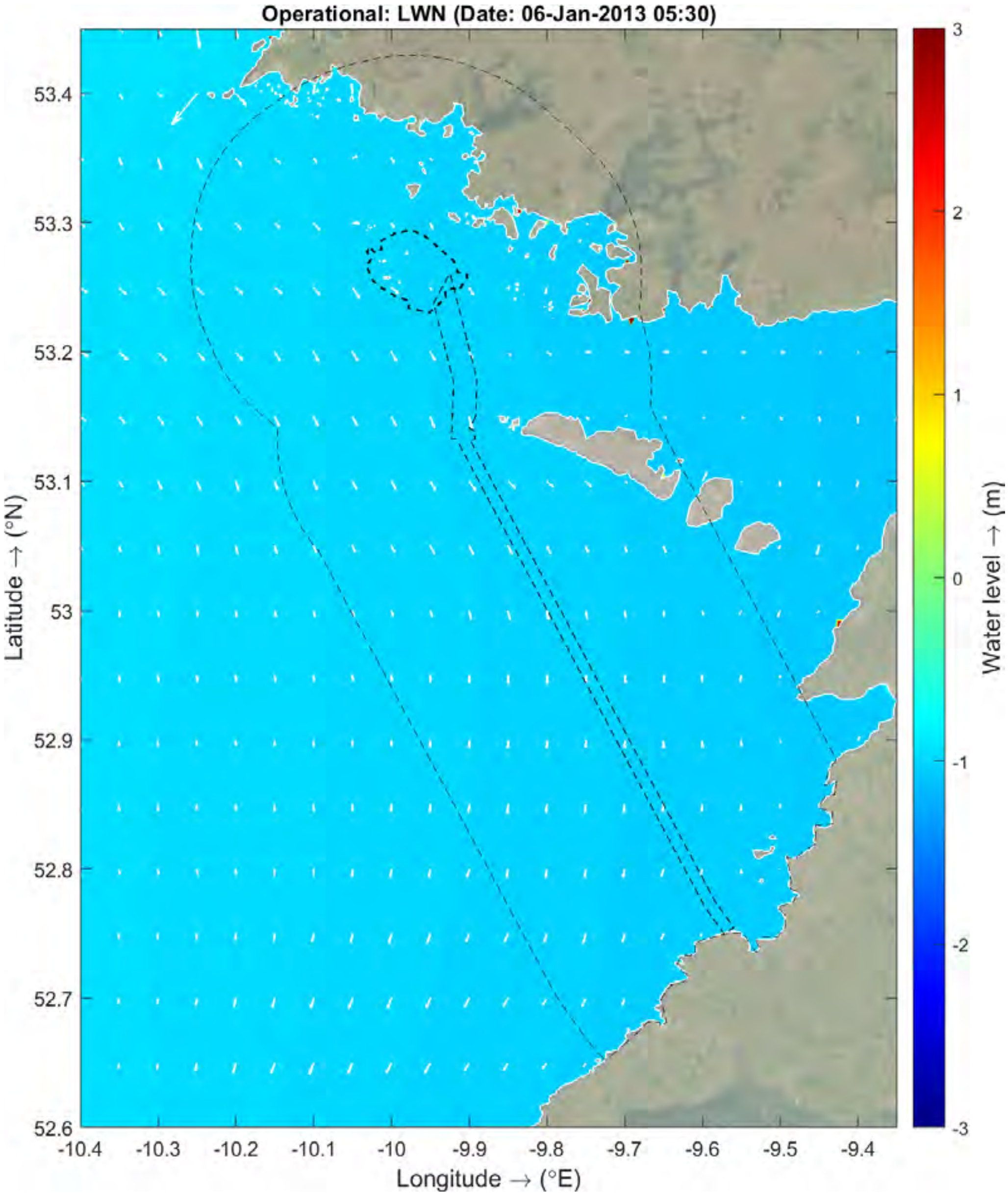
Operational: LWN (Date: 06-Jan-2013 05:30)
Latitude → (°N)
Longitude → (°E)
Water level → (m)
53.4
53.3
53.2
53.1
53
52.9
52.8
52.7
52.6
-10.4
-10.3
-10.2
-10.1
-10
-9.9
-9.8
-9.7
-9.6
-9.5
-9.4
3
2
1
0
-1
-2
-3

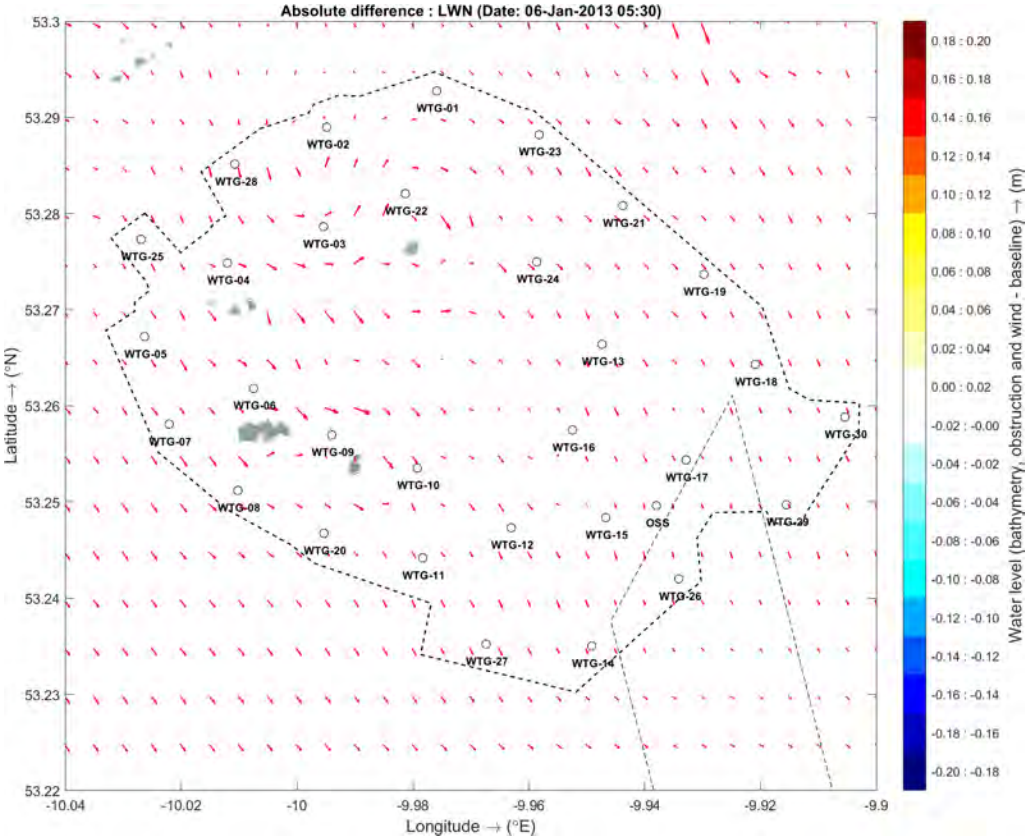
Absolute difference : LWN (Date: 06-Jan-2013 05:30)
Latitude → (°N)
Longitude → (°E)
Water level (bathymetry, obstruction and wind - baseline) → (m)
WTG-01
WTG-02
WTG-03
WTG-04
WTG-05
WTG-06
WTG-07
WTG-08
WTG-09
WTG-10
WTG-11
WTG-12
WTG-13
WTG-14
WTG-15
WTG-16
WTG-17
WTG-18
WTG-19
WTG-20
WTG-21
WTG-22
WTG-23
WTG-24
WTG-25
WTG-26
WTG-27
WTG-28
WTG-29
WTG-30
OSS
0.18 : 0.20
0.16 : 0.18
0.14 : 0.16
0.12 : 0.14
0.10 : 0.12
0.08 : 0.10
0.06 : 0.08
0.04 : 0.06
0.02 : 0.04
0.00 : 0.02
-0.02 : -0.00
-0.04 : -0.02
-0.06 : -0.04
-0.08 : -0.06
-0.10 : -0.08
-0.12 : -0.10
-0.14 : -0.12
-0.16 : -0.14
-0.18 : -0.16
-0.20 : -0.18

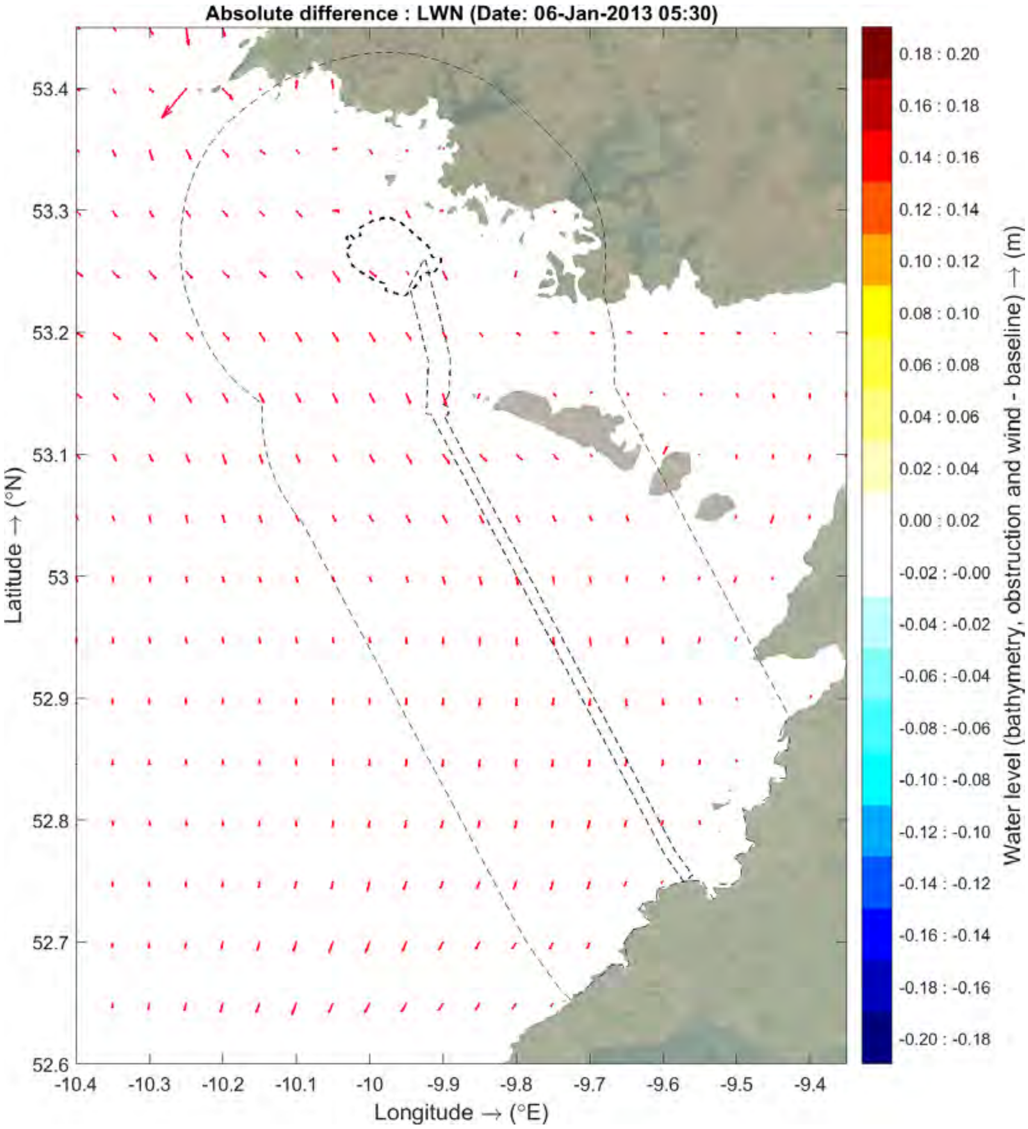

Absolute difference : LWN (Date: 06-Jan-2013 05:30)
53.4
53.3
53.2
53.1
53
52.9
52.8
52.7
52.6
Latitude → (°N)
-10.4
-10.3
-10.2
-10.1
-10
-9.9
-9.8
-9.7
-9.6
-9.5
-9.4
Longitude → (°E)
0.18 : 0.20
0.16 : 0.18
0.14 : 0.16
0.12 : 0.14
0.10 : 0.12
0.08 : 0.10
0.06 : 0.08
0.04 : 0.06
0.02 : 0.04
0.00 : 0.02
-0.02 : -0.00
-0.04 : -0.02
-0.06 : -0.04
-0.08 : -0.06
-0.10 : -0.08
-0.12 : -0.10
-0.14 : -0.12
-0.16 : -0.14
-0.18 : -0.16
-0.20 : -0.18
Water level (bathymetry, obstruction and wind - baseline) → (m)

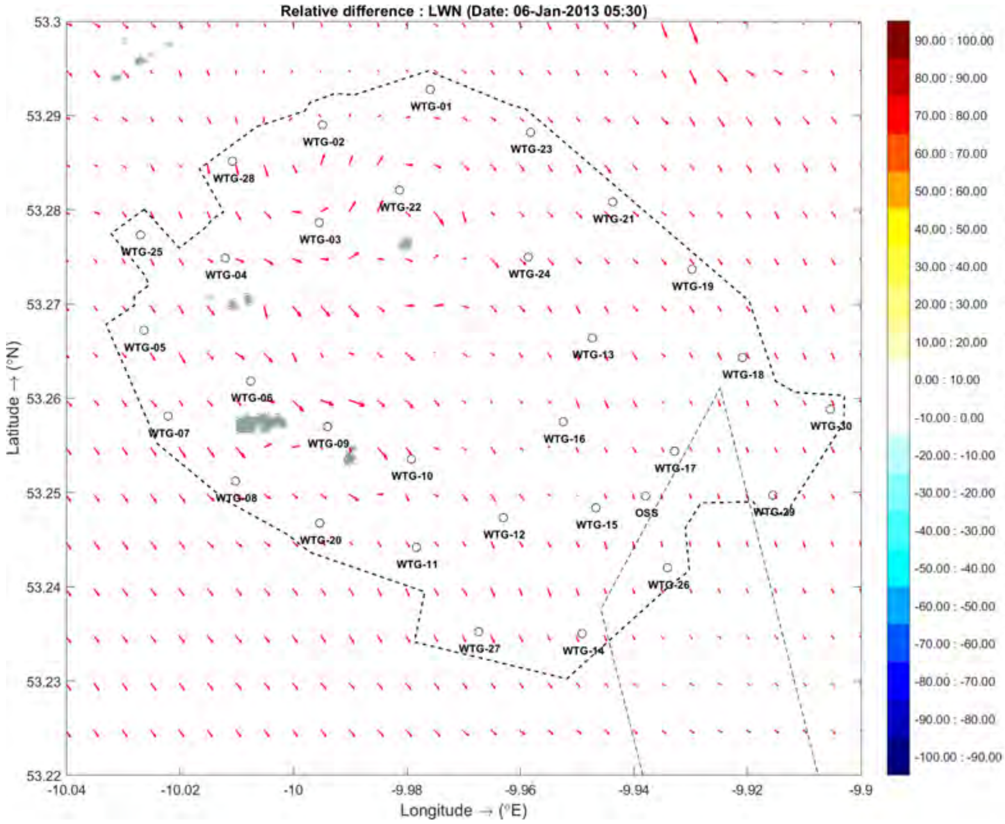

Relative difference : LWN (Date: 06-Jan-2013 05:30)
Latitude → (°N)
Longitude → (°E)
Water level (bathymetry, obstruction and wind - baseline) → (%)
90.00 : 100.00
80.00 : 90.00
70.00 : 80.00
60.00 : 70.00
50.00 : 60.00
40.00 : 50.00
30.00 : 40.00
20.00 : 30.00
10.00 : 20.00
0.00 : 10.00
-10.00 : 0.00
-20.00 : -10.00
-30.00 : -20.00
-40.00 : -30.00
-50.00 : -40.00
-60.00 : -50.00
-70.00 : -60.00
-80.00 : -70.00
-90.00 : -80.00
-100.00 : -90.00
WTG-01
WTG-02
WTG-23
WTG-28
WTG-22
WTG-21
WTG-03
WTG-25
WTG-04
WTG-24
WTG-19
WTG-05
WTG-13
WTG-18
WTG-06
WTG-30
WTG-07
WTG-09
WTG-16
WTG-17
WTG-10
WTG-08
WTG-15
OSS
WTG-29
WTG-20
WTG-12
WTG-11
WTG-26
WTG-27
WTG-14

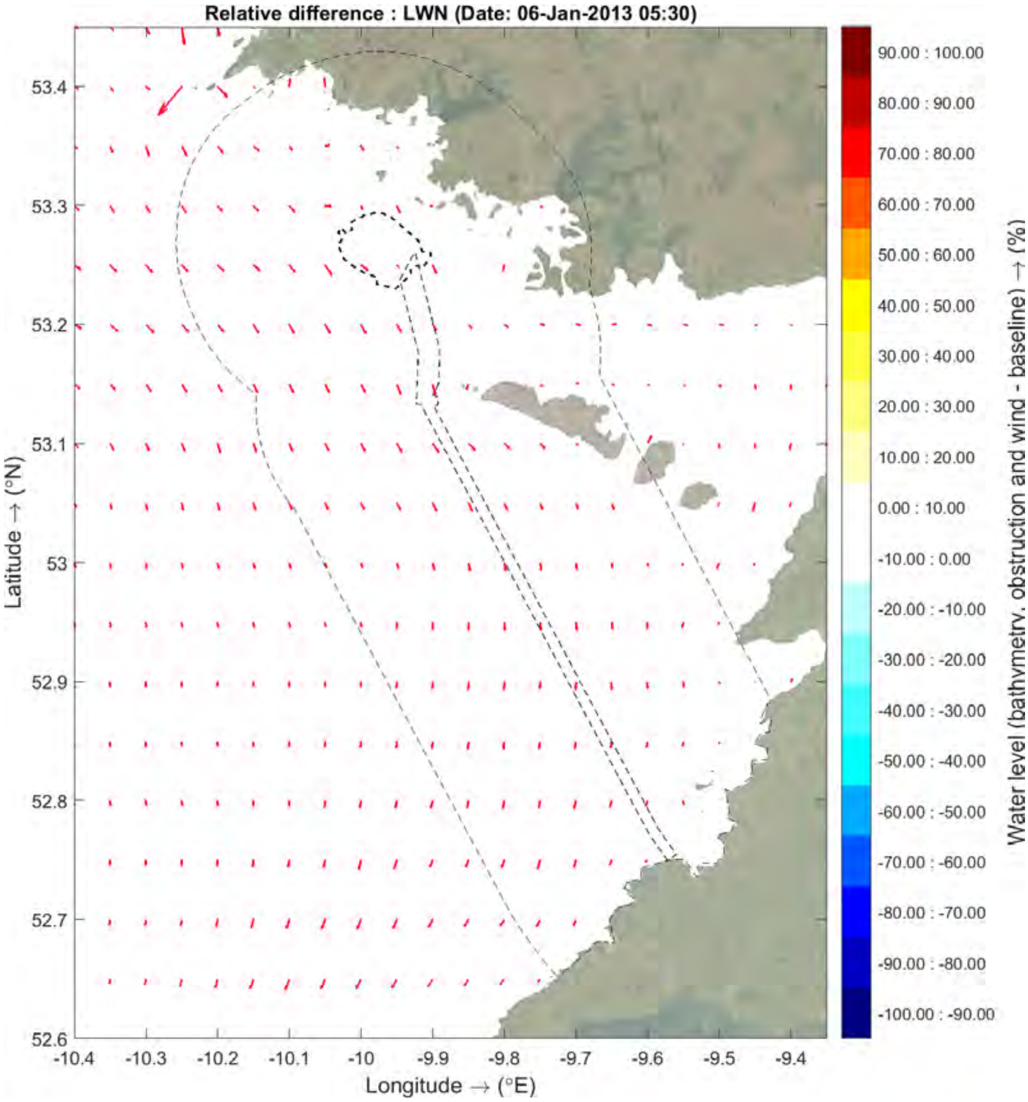
Relative difference : LWN (Date: 06-Jan-2013 05:30)
53.4
53.3
53.2
53.1
53
52.9
52.8
52.7
52.6
Latitude → (°N)
-10.4
-10.3
-10.2
-10.1
-10
-9.9
-9.8
-9.7
-9.6
-9.5
-9.4
Longitude → (°E)
90.00 : 100.00
80.00 : 90.00
70.00 : 80.00
60.00 : 70.00
50.00 : 60.00
40.00 : 50.00
30.00 : 40.00
20.00 : 30.00
10.00 : 20.00
0.00 : 10.00
-10.00 : 0.00
-20.00 : -10.00
-30.00 : -20.00
-40.00 : -30.00
-50.00 : -40.00
-60.00 : -50.00
-70.00 : -60.00
-80.00 : -70.00
-90.00 : -80.00
-100.00 : -90.00
Water level (bathymetry, obstruction and wind - baseline) → (%)

D.15 LWS currents

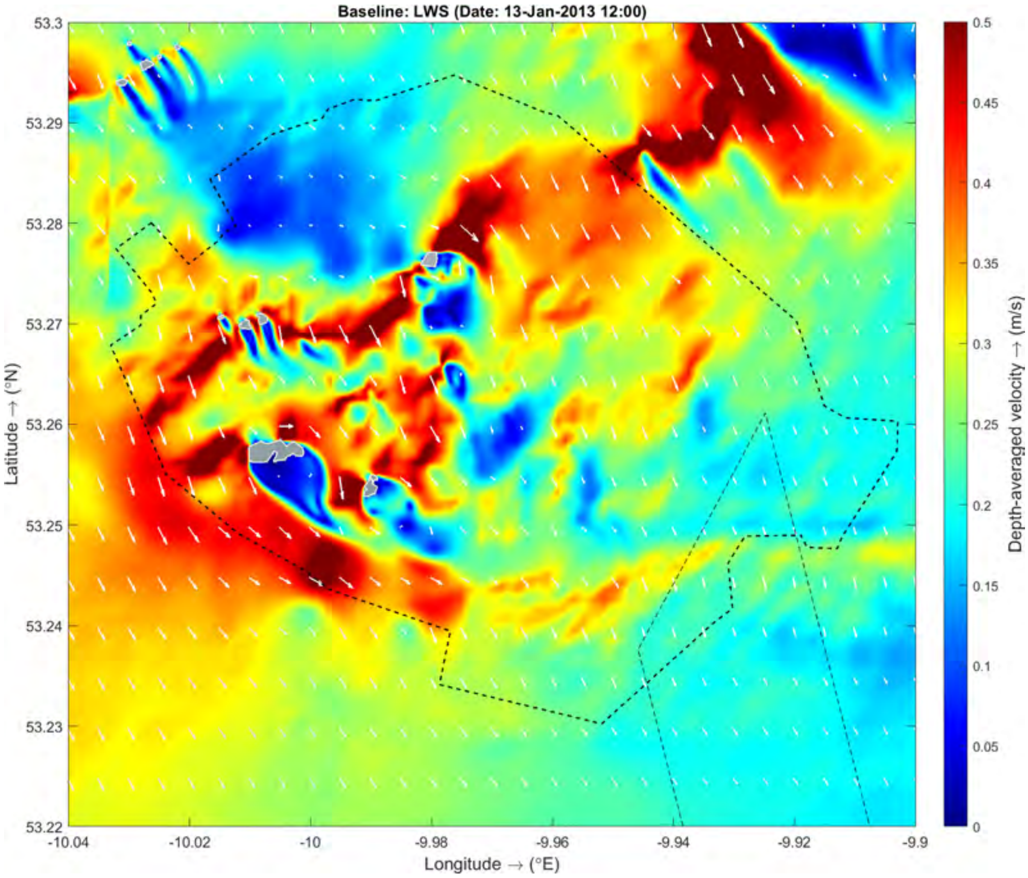

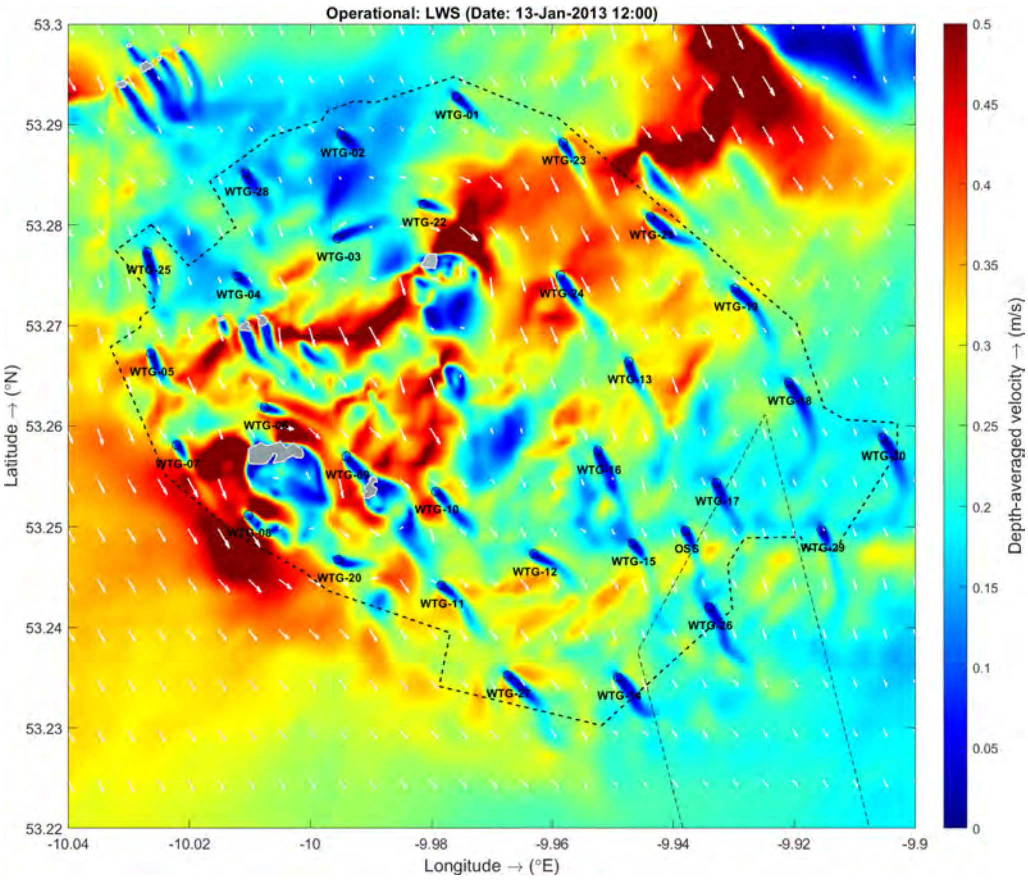

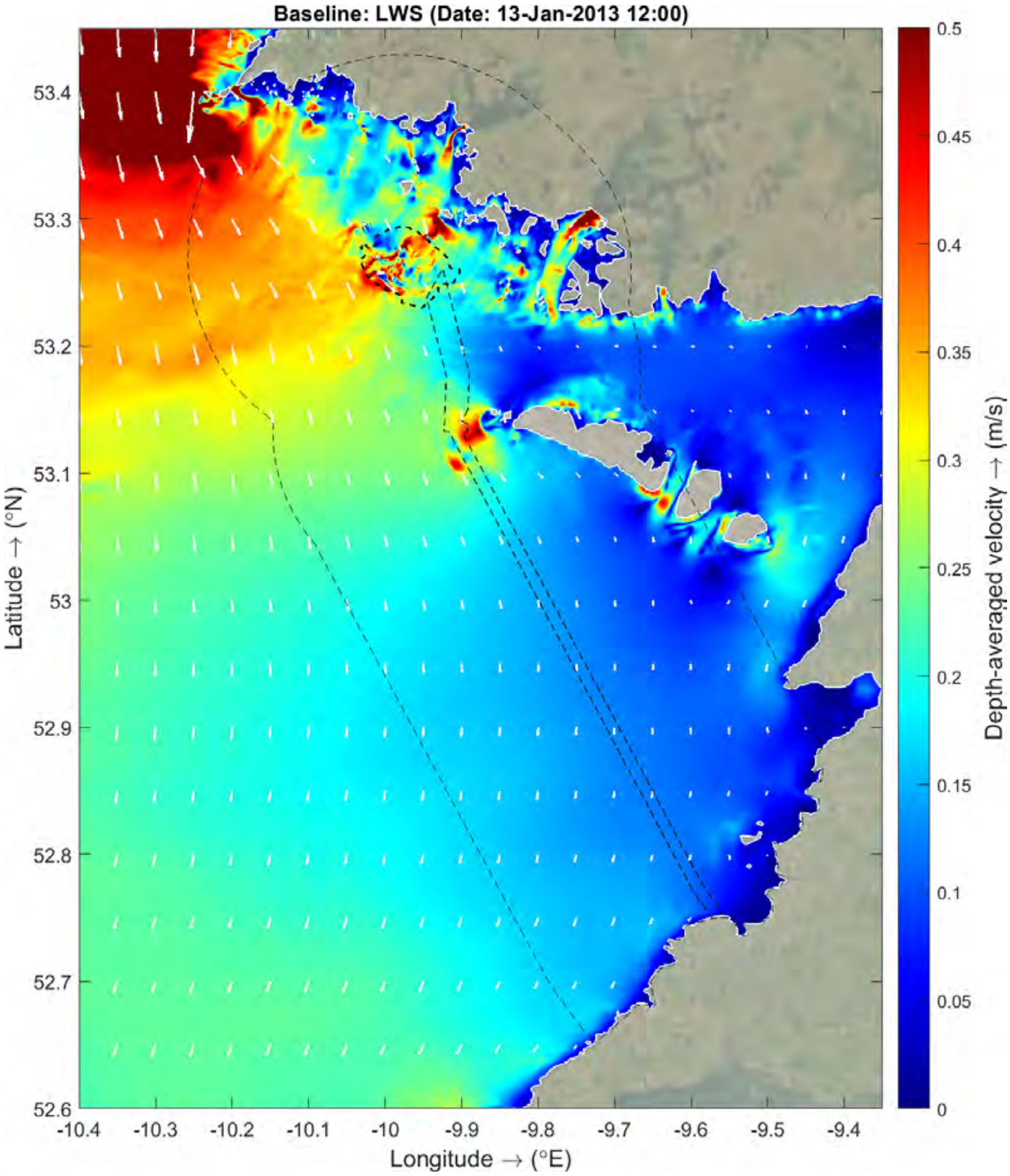
Baseline: LWS (Date: 13-Jan-2013 12:00)
Latitude → (°N)
Longitude → (°E)
Depth-averaged velocity → (m/s)
53.4
53.3
53.2
53.1
53
52.9
52.8
52.7
52.6
-10.4
-10.3
-10.2
-10.1
-10
-9.9
-9.8
-9.7
-9.6
-9.5
-9.4
0.5
0.45
0.4
0.35
0.3
0.25
0.2
0.15
0.1
0.05
0

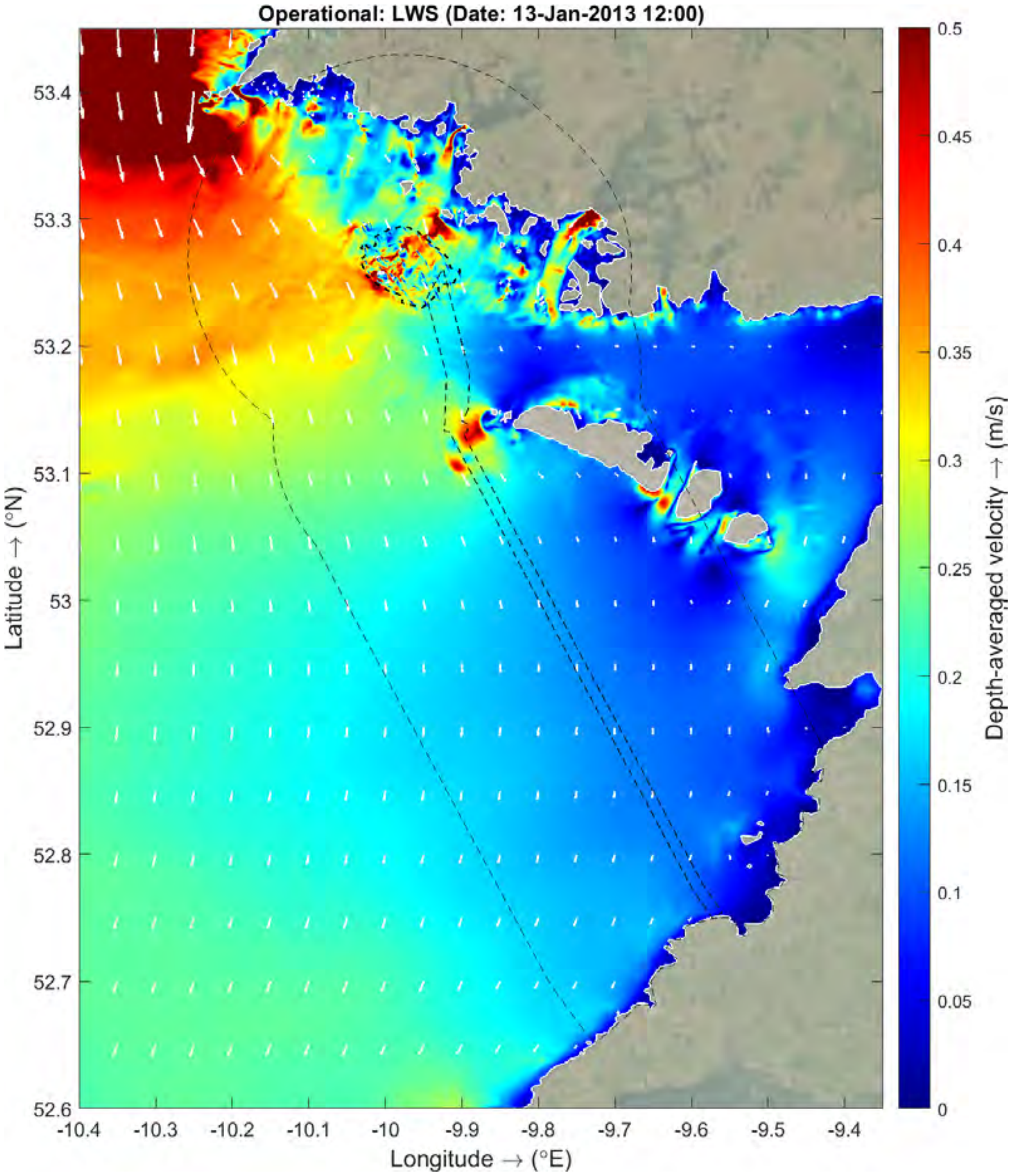
Operational: LWS (Date: 13-Jan-2013 12:00)
Latitude → (°N)
Longitude → (°E)
Depth-averaged velocity → (m/s)
53.4
53.3
53.2
53.1
53
52.9
52.8
52.7
52.6
-10.4
-10.3
-10.2
-10.1
-10
-9.9
-9.8
-9.7
-9.6
-9.5
-9.4
0.5
0.45
0.4
0.35
0.3
0.25
0.2
0.15
0.1
0.05
0

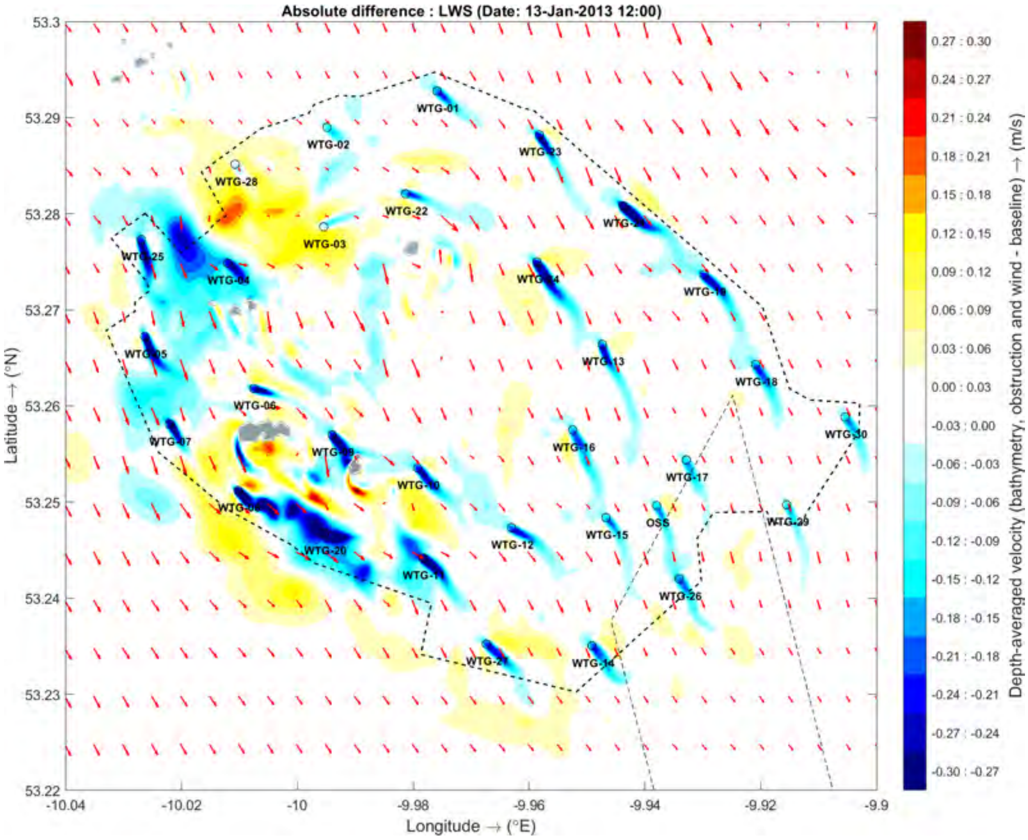
Absolute difference : LWS (Date: 13-Jan-2013 12:00)
Latitude → (°N)
Longitude → (°E)
Depth-averaged velocity (bathymetry, obstruction and wind - baseline) → (m/s)
0.27 : 0.30
0.24 : 0.27
0.21 : 0.24
0.18 : 0.21
0.15 : 0.18
0.12 : 0.15
0.09 : 0.12
0.06 : 0.09
0.03 : 0.06
0.00 : 0.03
-0.03 : 0.00
-0.06 : -0.03
-0.09 : -0.06
-0.12 : -0.09
-0.15 : -0.12
-0.18 : -0.15
-0.21 : -0.18
-0.24 : -0.21
-0.27 : -0.24
-0.30 : -0.27
WTG-01
WTG-02
WTG-03
WTG-22
WTG-28
WTG-25
WTG-05
WTG-06
WTG-07
WTG-20
WTG-12
WTG-13
WTG-15
WTG-16
WTG-17
WTG-18
WTG-26
WTG-27
WTG-30
OSS

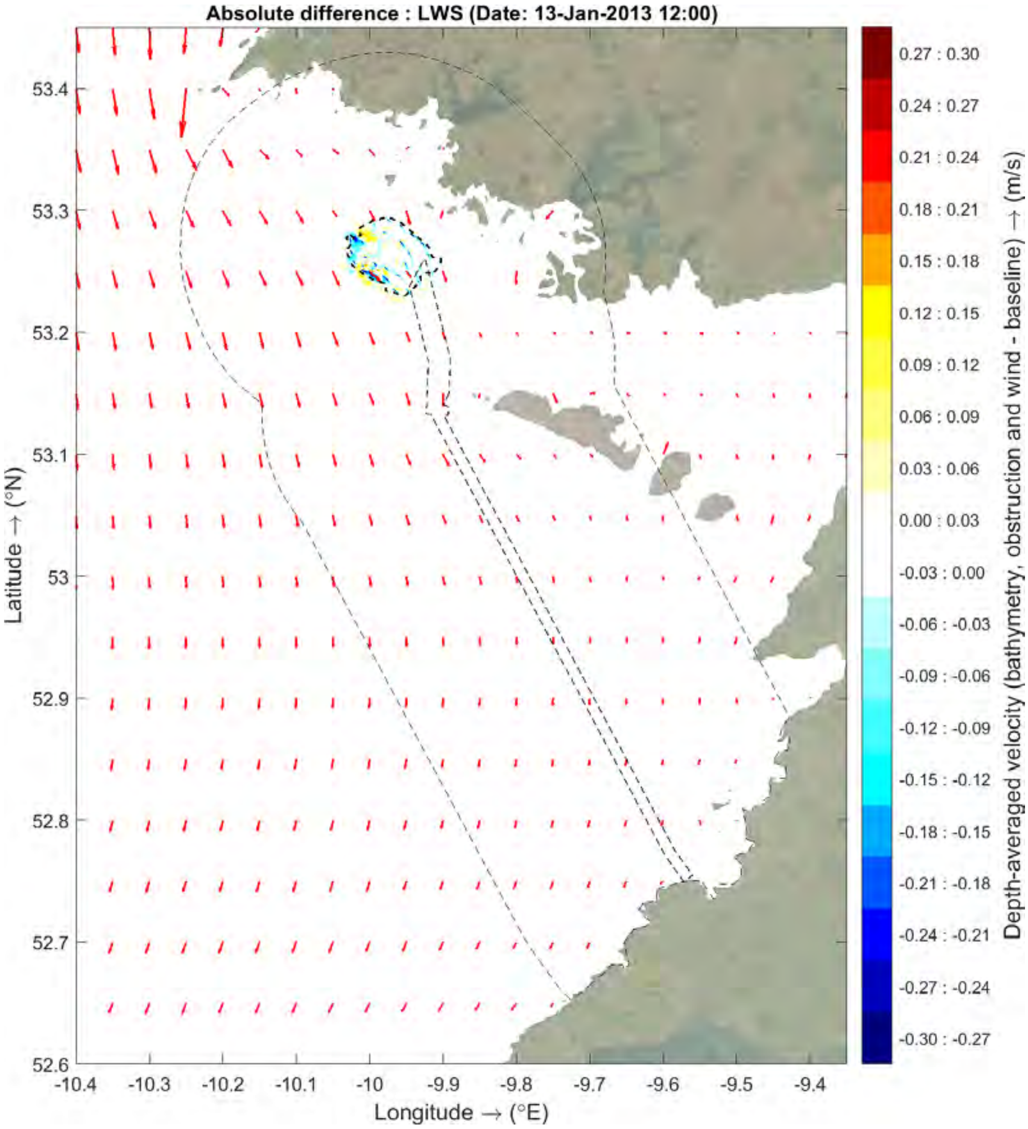

Absolute difference : LWS (Date: 13-Jan-2013 12:00)
53.4
53.3
53.2
53.1
53
52.9
52.8
52.7
52.6
Latitude → (°N)
-10.4
-10.3
-10.2
-10.1
-10
-9.9
-9.8
-9.7
-9.6
-9.5
-9.4
Longitude → (°E)
0.27 : 0.30
0.24 : 0.27
0.21 : 0.24
0.18 : 0.21
0.15 : 0.18
0.12 : 0.15
0.09 : 0.12
0.06 : 0.09
0.03 : 0.06
0.00 : 0.03
-0.03 : 0.00
-0.06 : -0.03
-0.09 : -0.06
-0.12 : -0.09
-0.15 : -0.12
-0.18 : -0.15
-0.21 : -0.18
-0.24 : -0.21
-0.27 : -0.24
-0.30 : -0.27
Depth-averaged velocity (bathymetry, obstruction and wind - baseline) → (m/s)

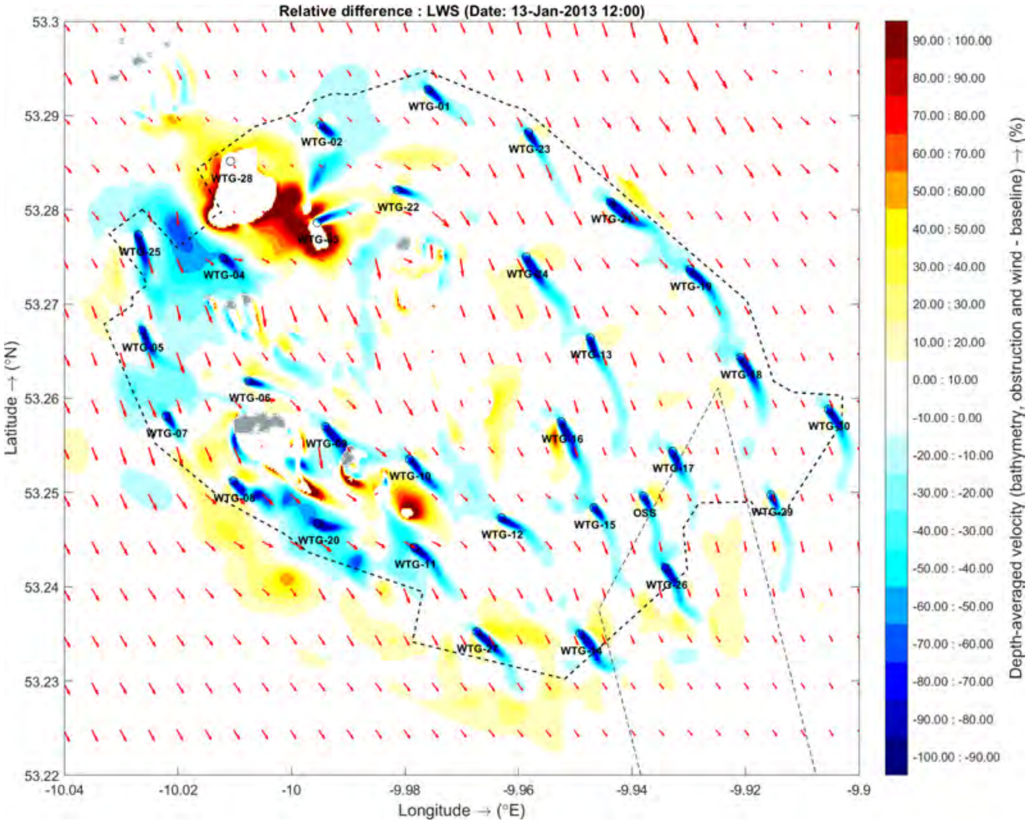
Relative difference : LWS (Date: 13-Jan-2013 12:00)
Latitude → (°N)
Longitude → (°E)
Depth-averaged velocity (bathymetry, obstruction and wind - baseline) → (%)
90.00 : 100.00
80.00 : 90.00
70.00 : 80.00
60.00 : 70.00
50.00 : 60.00
40.00 : 50.00
30.00 : 40.00
20.00 : 30.00
10.00 : 20.00
0.00 : 10.00
-10.00 : 0.00
-20.00 : -10.00
-30.00 : -20.00
-40.00 : -30.00
-50.00 : -40.00
-60.00 : -50.00
-70.00 : -60.00
-80.00 : -70.00
-90.00 : -80.00
-100.00 : -90.00
WTG-01
WTG-02
WTG-23
WTG-28
WTG-22
WTG-25
WTG-04
WTG-05
WTG-06
WTG-07
WTG-13
WTG-16
WTG-17
WTG-18
WTG-20
WTG-10
WTG-12
WTG-15
WTG-11
OSS
WTG-29
WTG-26

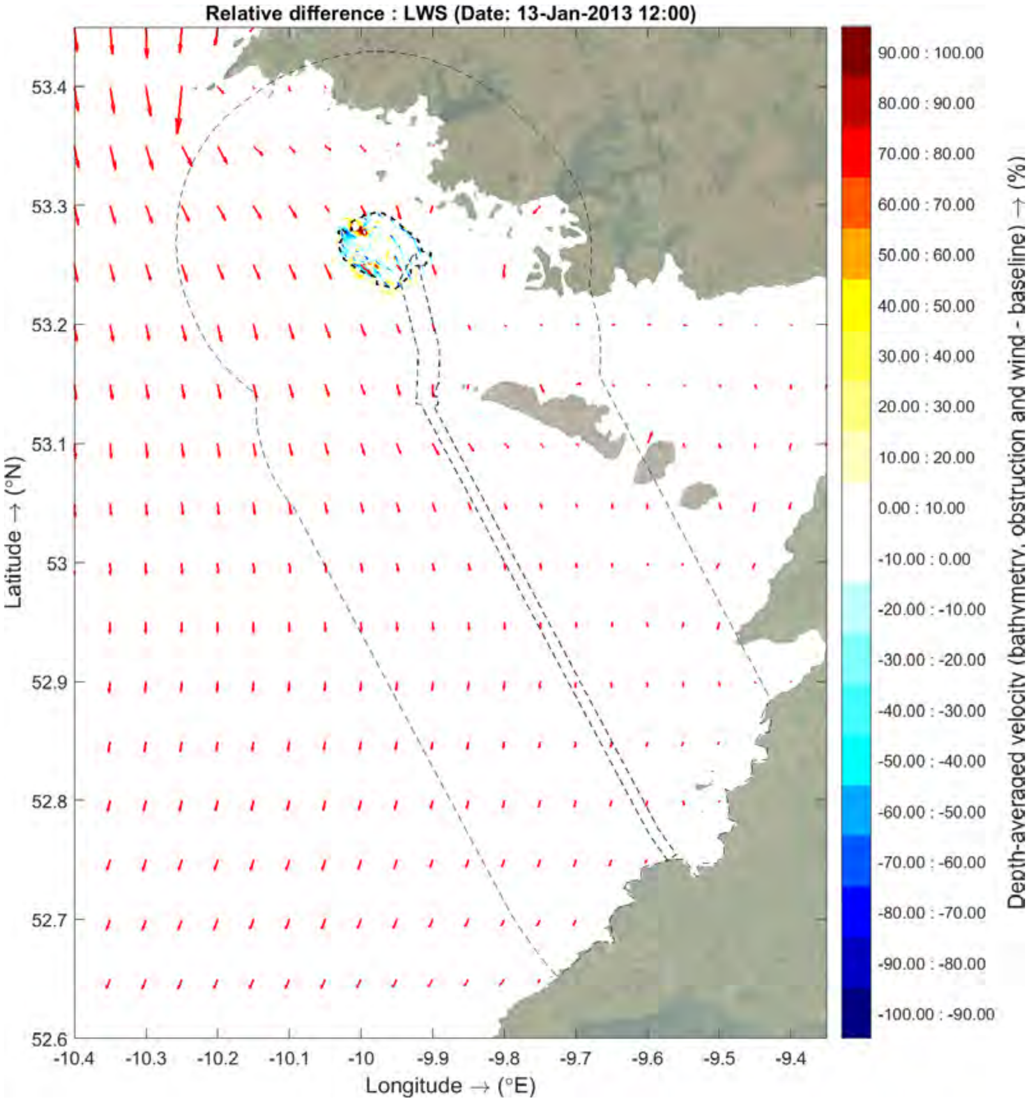
Relative difference : LWS (Date: 13-Jan-2013 12:00)
Latitude → (°N)
Longitude → (°E)
Depth-averaged velocity (bathymetry, obstruction and wind - baseline) → (%)
90.00 : 100.00
80.00 : 90.00
70.00 : 80.00
60.00 : 70.00
50.00 : 60.00
40.00 : 50.00
30.00 : 40.00
20.00 : 30.00
10.00 : 20.00
0.00 : 10.00
-10.00 : 0.00
-20.00 : -10.00
-30.00 : -20.00
-40.00 : -30.00
-50.00 : -40.00
-60.00 : -50.00
-70.00 : -60.00
-80.00 : -70.00
-90.00 : -80.00
-100.00 : -90.00

D.16 LWS water levels

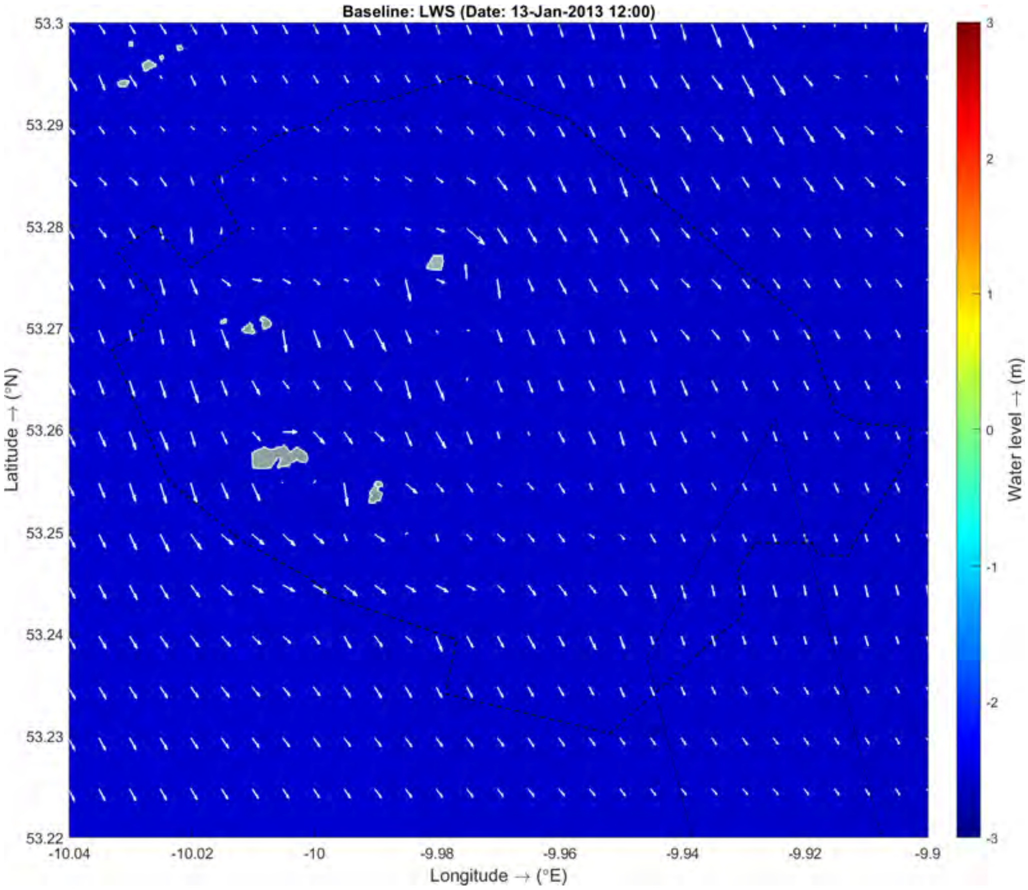

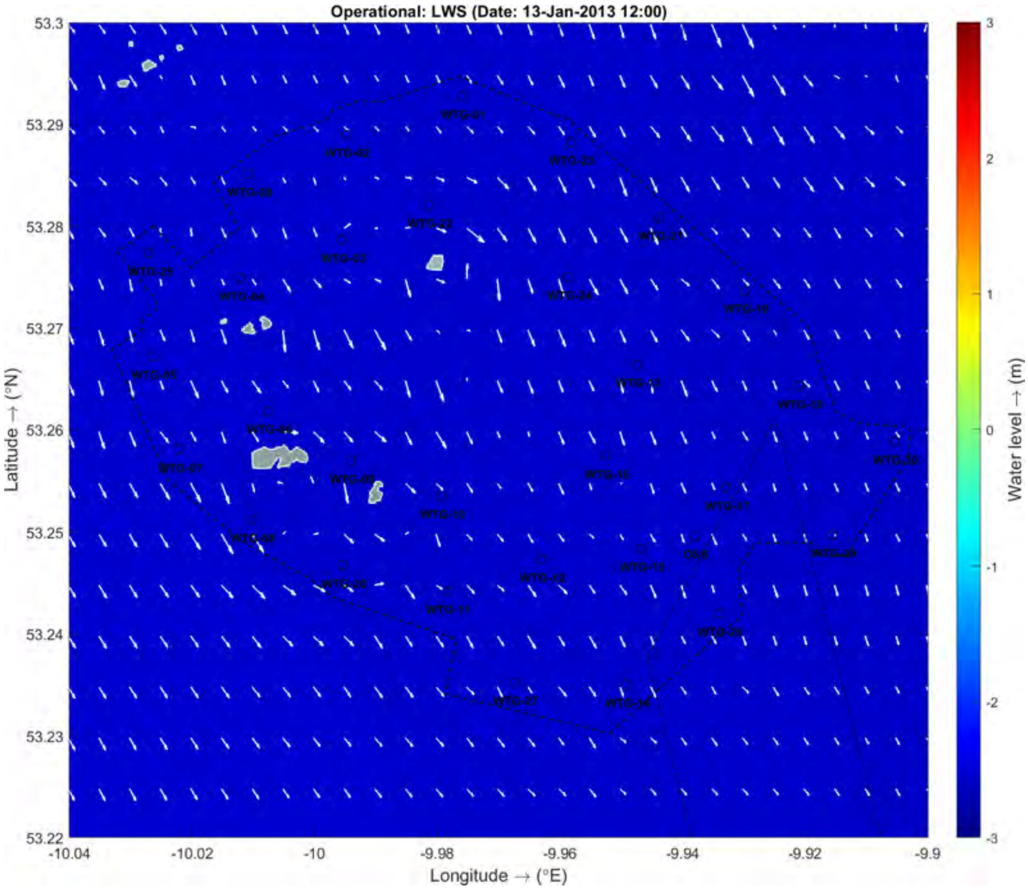
Operational: LWS (Date: 13-Jan-2013 12:00)
Latitude → (°N)
Longitude → (°E)
Water level → (m)

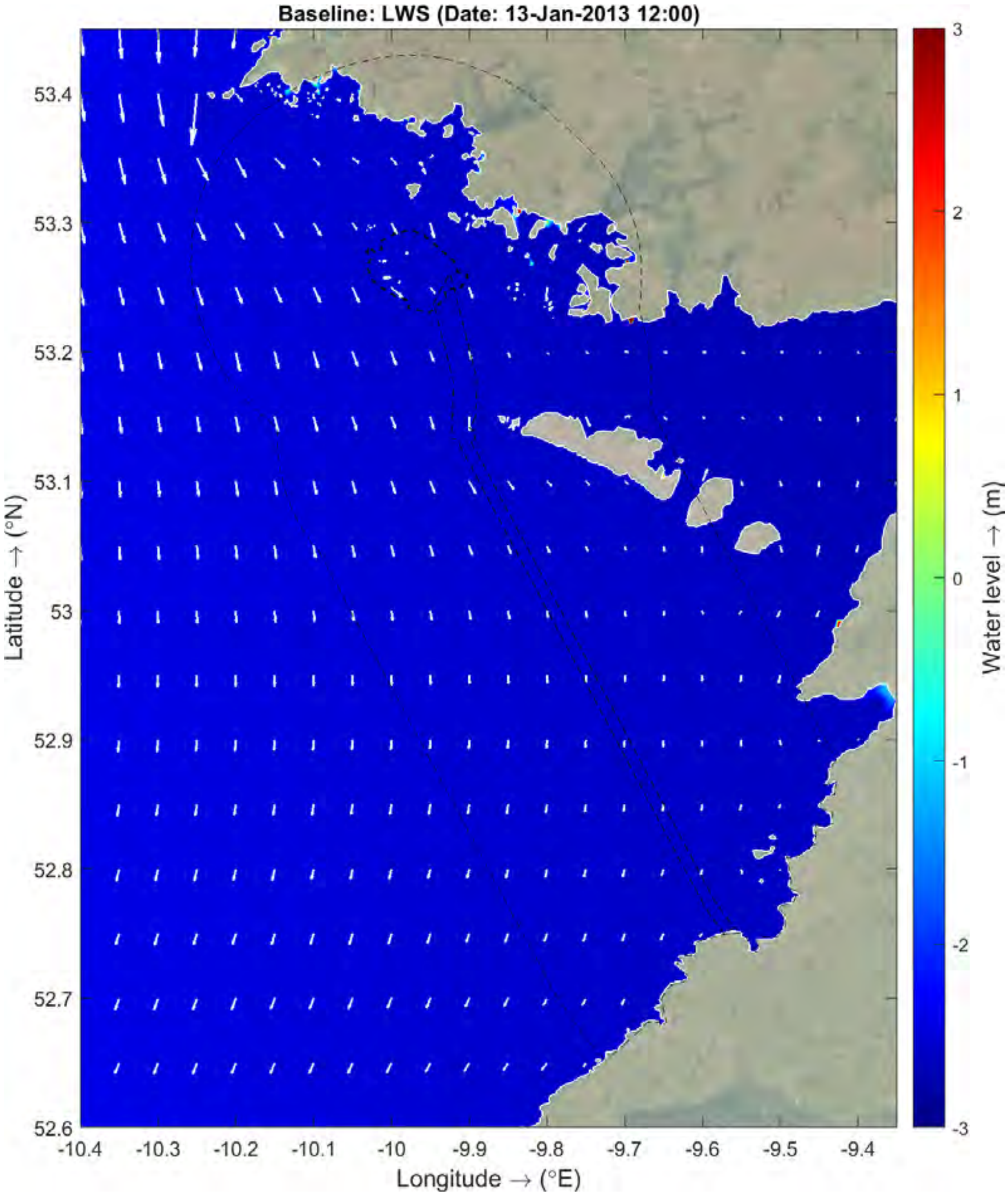
Baseline: LWS (Date: 13-Jan-2013 12:00)
Latitude → (°N)
53.4
53.3
53.2
53.1
53
52.9
52.8
52.7
52.6
-10.4
-10.3
-10.2
-10.1
-10
-9.9
-9.8
-9.7
-9.6
-9.5
-9.4
Longitude → (°E)
Water level → (m)
3
2
1
0
-1
-2
-3

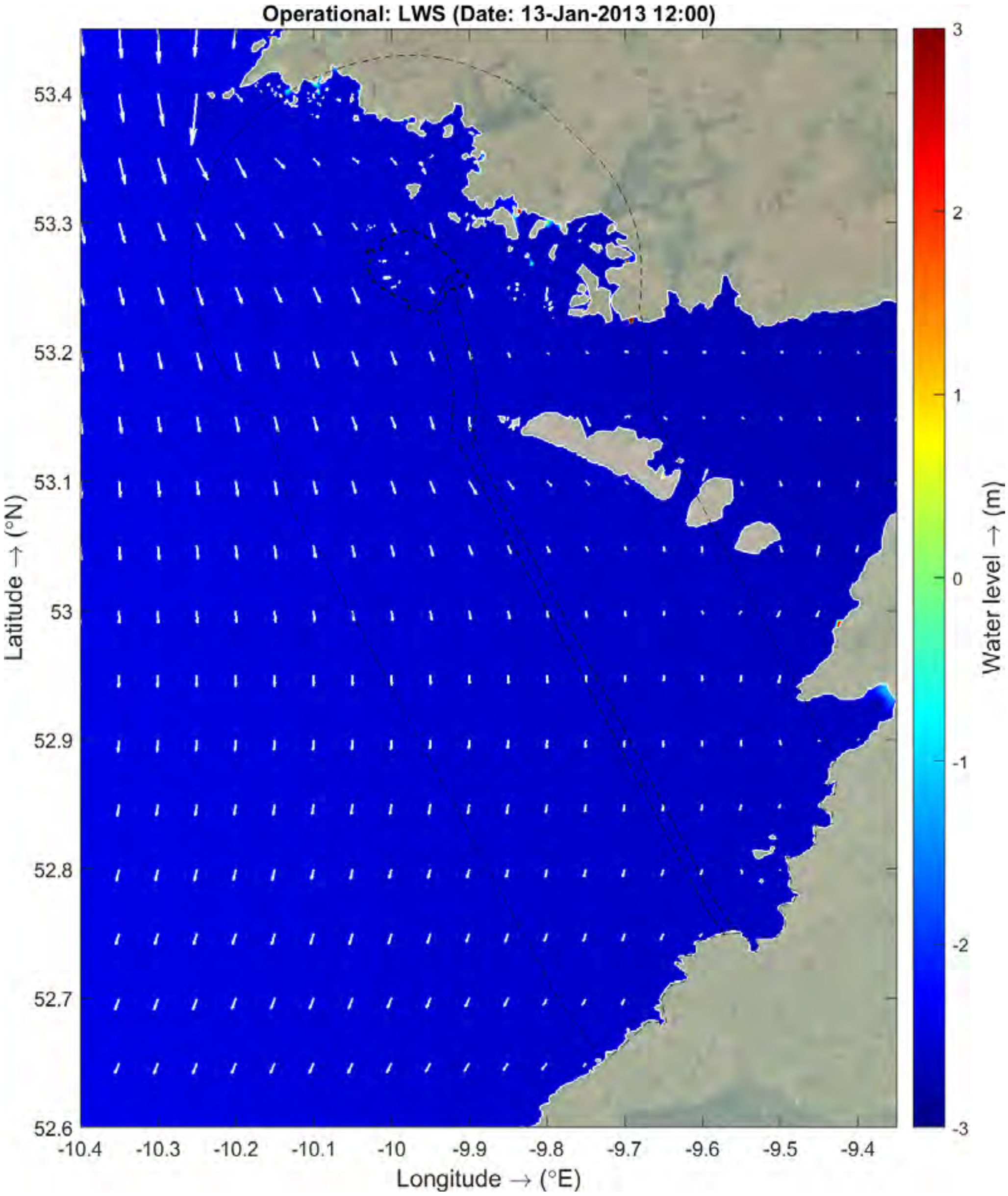
Operational: LWS (Date: 13-Jan-2013 12:00)
Latitude → (°N)
Longitude → (°E)
Water level → (m)
53.4
53.3
53.2
53.1
53
52.9
52.8
52.7
52.6
-10.4
-10.3
-10.2
-10.1
-10
-9.9
-9.8
-9.7
-9.6
-9.5
-9.4
3
2
1
0
-1
-2
-3

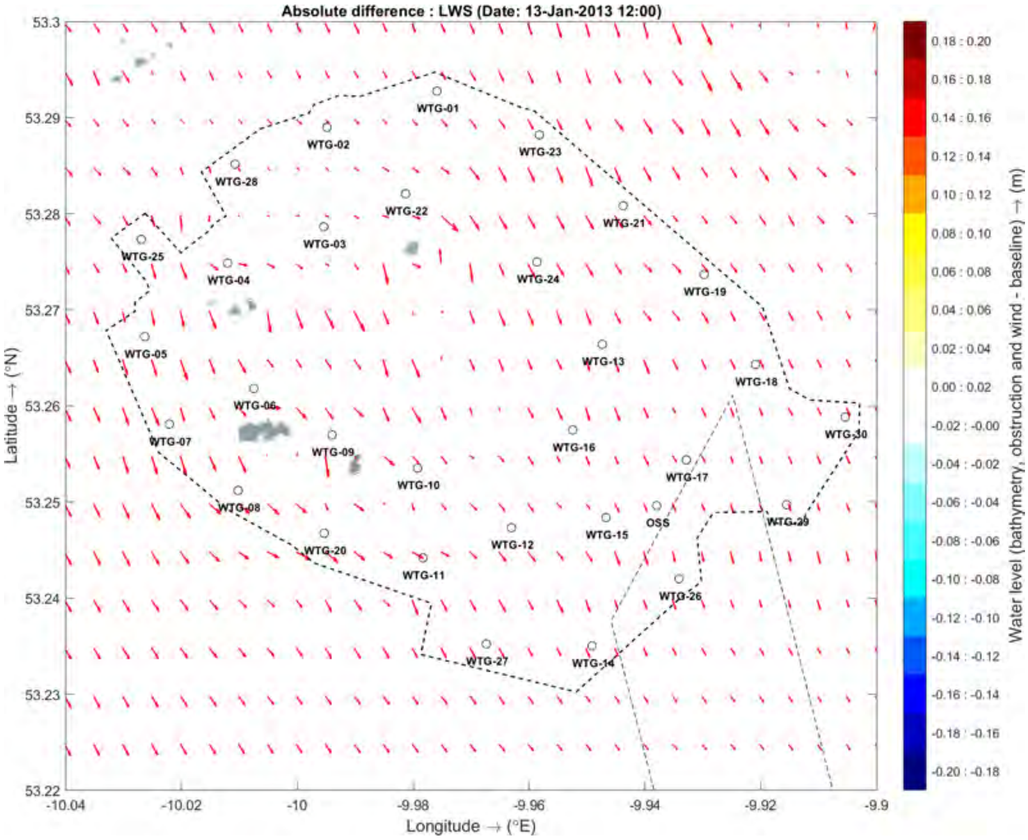
Absolute difference : LWS (Date: 13-Jan-2013 12:00)
Latitude → (°N)
Longitude → (°E)
Water level (bathymetry, obstruction and wind - baseline) → (m)
0.18 : 0.20
0.16 : 0.18
0.14 : 0.16
0.12 : 0.14
0.10 : 0.12
0.08 : 0.10
0.06 : 0.08
0.04 : 0.06
0.02 : 0.04
0.00 : 0.02
-0.02 : -0.00
-0.04 : -0.02
-0.06 : -0.04
-0.08 : -0.06
-0.10 : -0.08
-0.12 : -0.10
-0.14 : -0.12
-0.16 : -0.14
-0.18 : -0.16
-0.20 : -0.18
WTG-01
WTG-02
WTG-03
WTG-04
WTG-05
WTG-06
WTG-07
WTG-08
WTG-09
WTG-10
WTG-11
WTG-12
WTG-13
WTG-14
WTG-15
WTG-16
WTG-17
WTG-18
WTG-19
WTG-20
WTG-21
WTG-22
WTG-23
WTG-24
WTG-25
WTG-26
WTG-27
WTG-28
WTG-29
WTG-30
OSS

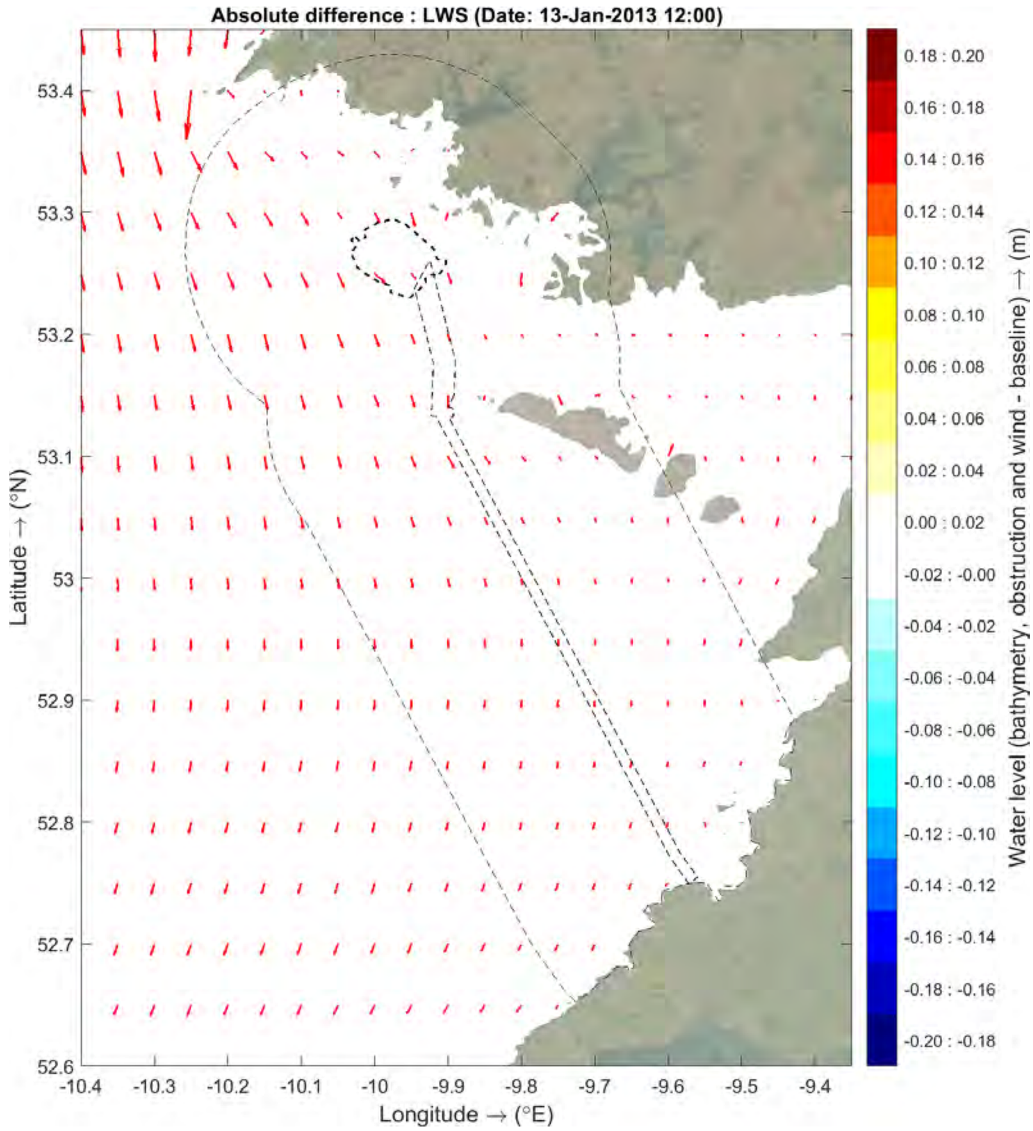
Absolute difference : LWS (Date: 13-Jan-2013 12:00)
Latitude → (°N)
Longitude → (°E)
Water level (bathymetry, obstruction and wind - baseline) → (m)
53.4
53.3
53.2
53.1
53
52.9
52.8
52.7
52.6
-10.4
-10.3
-10.2
-10.1
-10
-9.9
-9.8
-9.7
-9.6
-9.5
-9.4
0.18 : 0.20
0.16 : 0.18
0.14 : 0.16
0.12 : 0.14
0.10 : 0.12
0.08 : 0.10
0.06 : 0.08
0.04 : 0.06
0.02 : 0.04
0.00 : 0.02
-0.02 : -0.00
-0.04 : -0.02
-0.06 : -0.04
-0.08 : -0.06
-0.10 : -0.08
-0.12 : -0.10
-0.14 : -0.12
-0.16 : -0.14
-0.18 : -0.16
-0.20 : -0.18

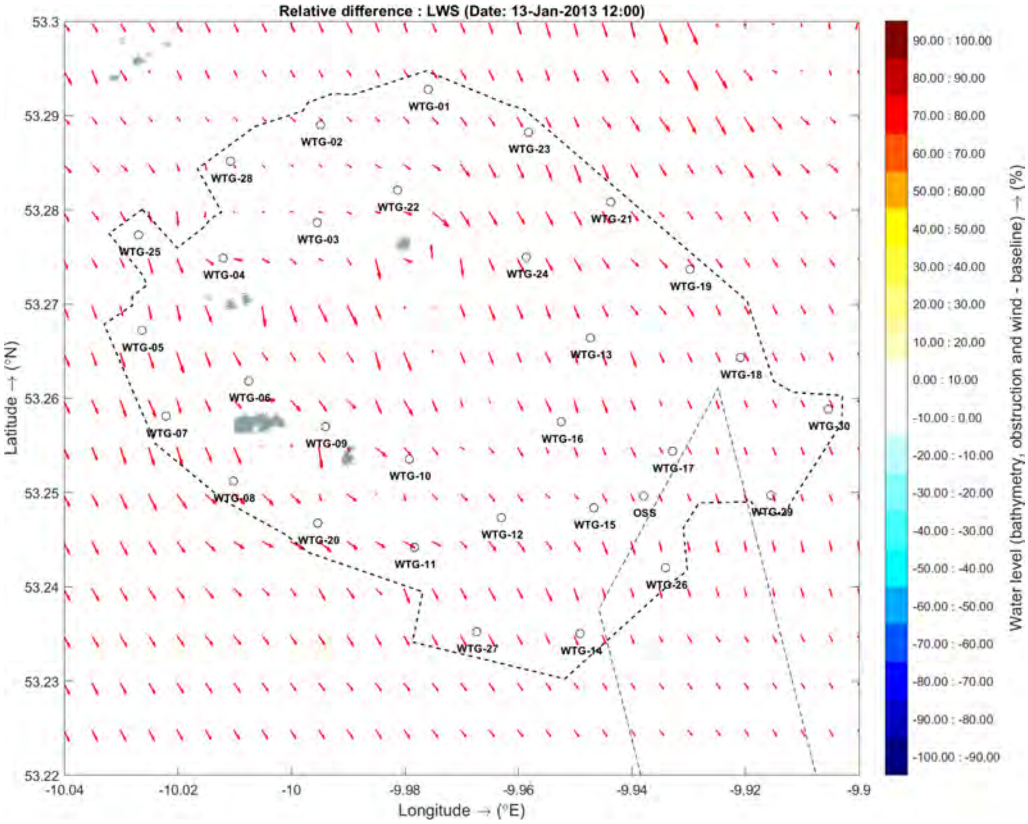
Relative difference : LWS (Date: 13-Jan-2013 12:00)
Latitude → (°N)
Longitude → (°E)
Water level (bathymetry, obstruction and wind - baseline) → (%)
90.00 : 100.00
80.00 : 90.00
70.00 : 80.00
60.00 : 70.00
50.00 : 60.00
40.00 : 50.00
30.00 : 40.00
20.00 : 30.00
10.00 : 20.00
0.00 : 10.00
-10.00 : 0.00
-20.00 : -10.00
-30.00 : -20.00
-40.00 : -30.00
-50.00 : -40.00
-60.00 : -50.00
-70.00 : -60.00
-80.00 : -70.00
-90.00 : -80.00
-100.00 : -90.00
WTG-01
WTG-02
WTG-03
WTG-04
WTG-05
WTG-06
WTG-07
WTG-08
WTG-09
WTG-10
WTG-11
WTG-12
WTG-13
WTG-14
WTG-15
WTG-16
WTG-17
WTG-18
WTG-19
WTG-20
WTG-21
WTG-22
WTG-23
WTG-24
WTG-25
WTG-26
WTG-27
WTG-28
WTG-29
WTG-30
OSS

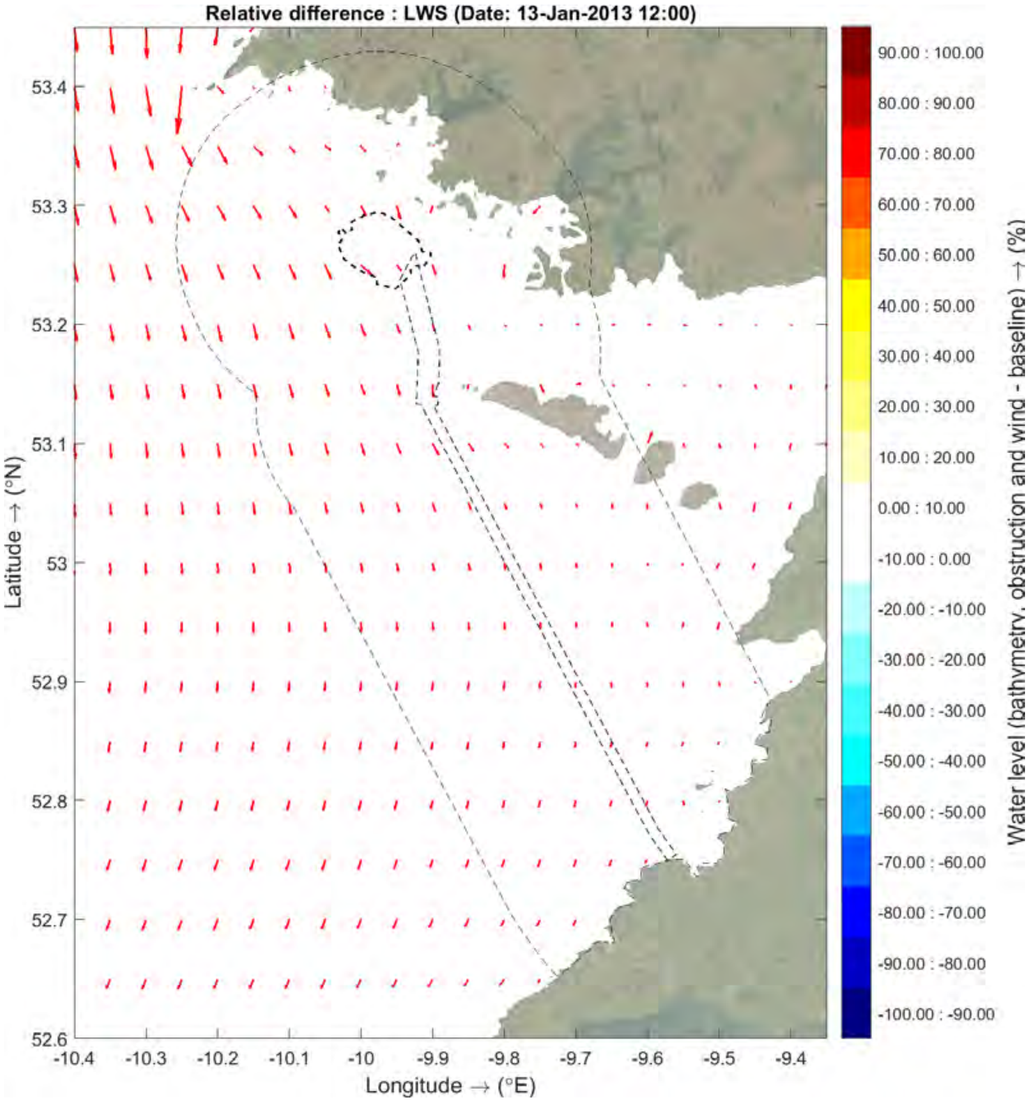
Relative difference : LWS (Date: 13-Jan-2013 12:00)
Latitude → (°N)
Longitude → (°E)
Water level (bathymetry, obstruction and wind - baseline) → (%)
90.00 : 100.00
80.00 : 90.00
70.00 : 80.00
60.00 : 70.00
50.00 : 60.00
40.00 : 50.00
30.00 : 40.00
20.00 : 30.00
10.00 : 20.00
0.00 : 10.00
-10.00 : 0.00
-20.00 : -10.00
-30.00 : -20.00
-40.00 : -30.00
-50.00 : -40.00
-60.00 : -50.00
-70.00 : -60.00
-80.00 : -70.00
-90.00 : -80.00
-100.00 : -90.00

D.17 Residuals currents

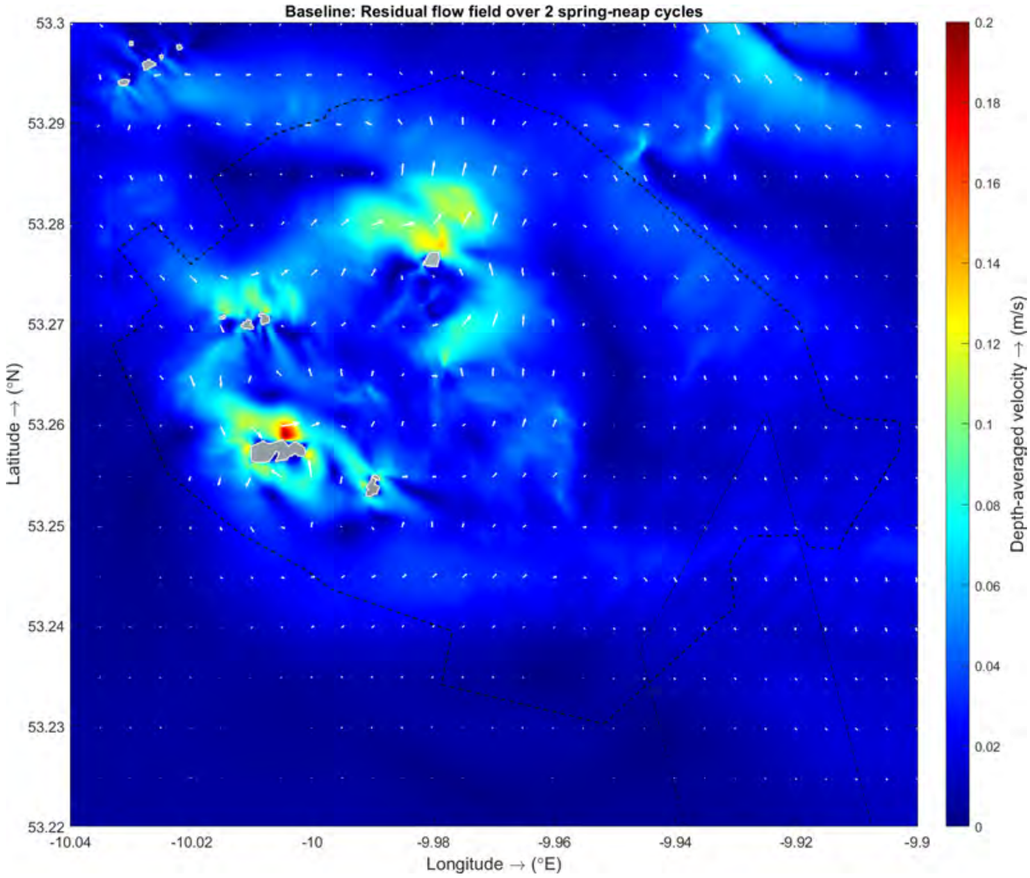

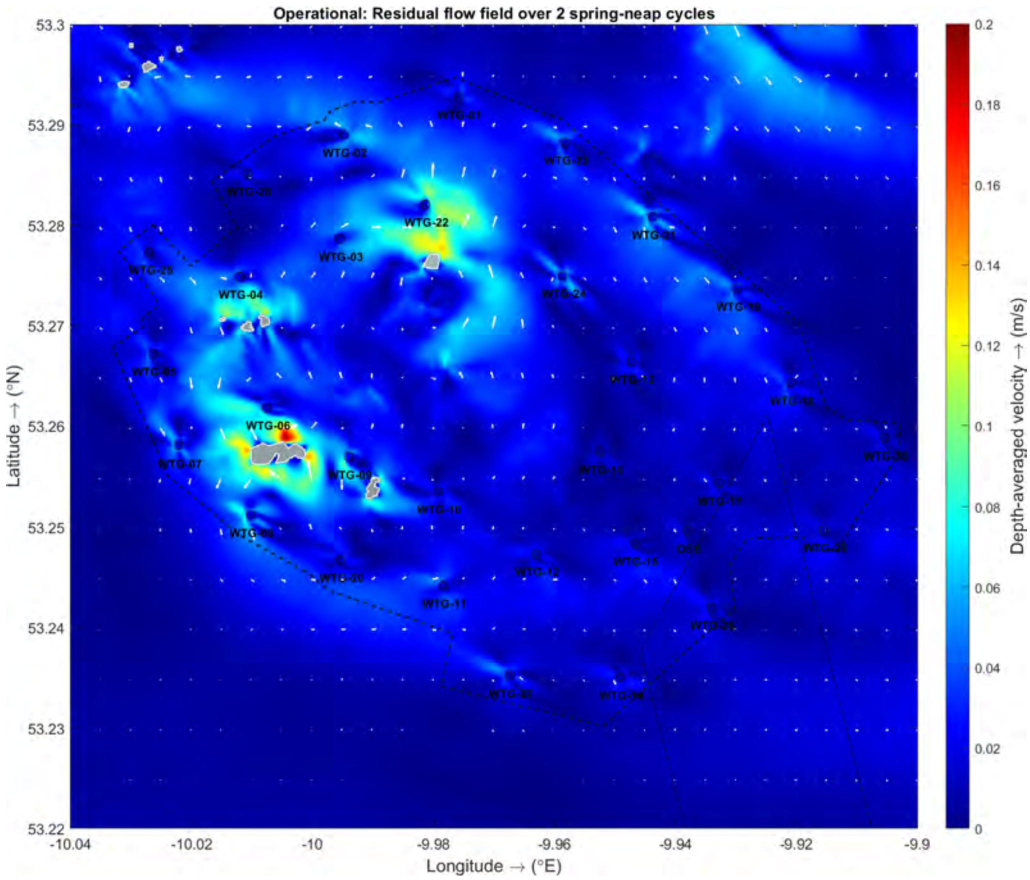

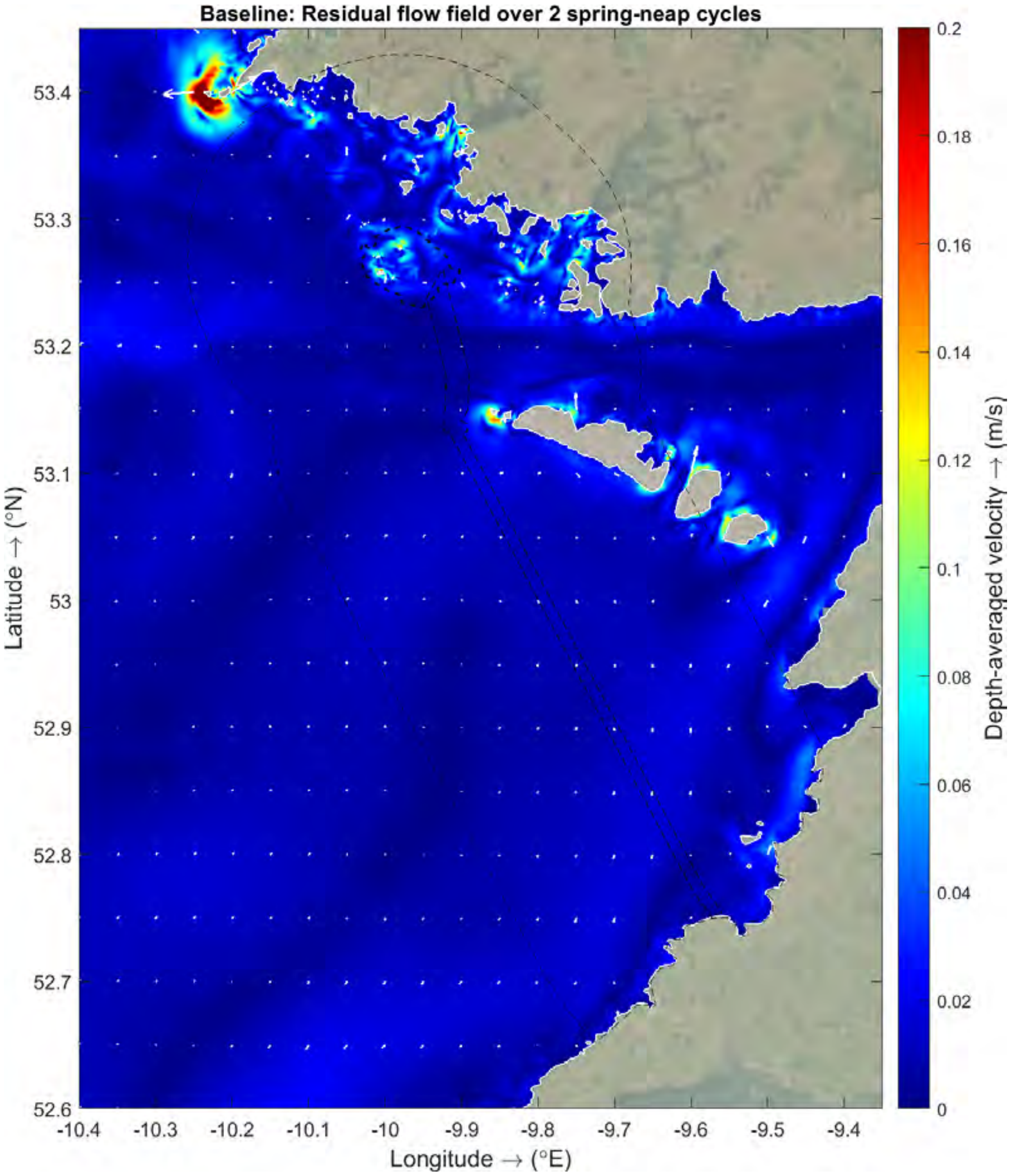
Baseline: Residual flow field over 2 spring-neap cycles
53.4
53.3
53.2
53.1
53
52.9
52.8
52.7
52.6
Latitude → (°N)
-10.4
-10.3
-10.2
-10.1
-10
-9.9
-9.8
-9.7
-9.6
-9.5
-9.4
Longitude → (°E)
0.2
0.18
0.16
0.14
0.12
0.1
0.08
0.06
0.04
0.02
0
Depth-averaged velocity → (m/s)

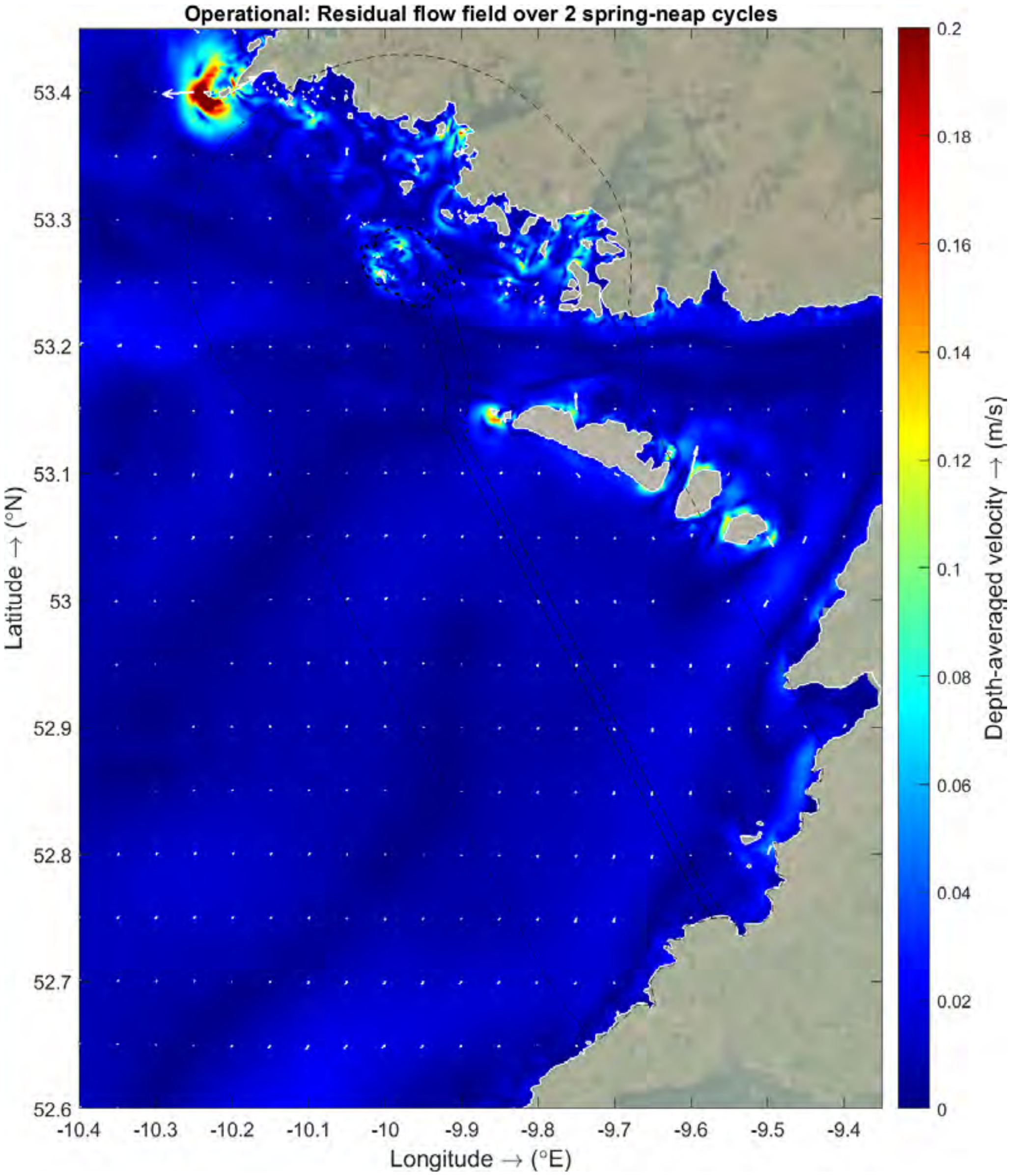
Operational: Residual flow field over 2 spring-neap cycles
53.4
53.3
53.2
53.1
53
52.9
52.8
52.7
52.6
Latitude → (°N)
-10.4
-10.3
-10.2
-10.1
-10
-9.9
-9.8
-9.7
-9.6
-9.5
-9.4
Longitude → (°E)
0.2
0.18
0.16
0.14
0.12
0.1
0.08
0.06
0.04
0.02
0
Depth-averaged velocity → (m/s)

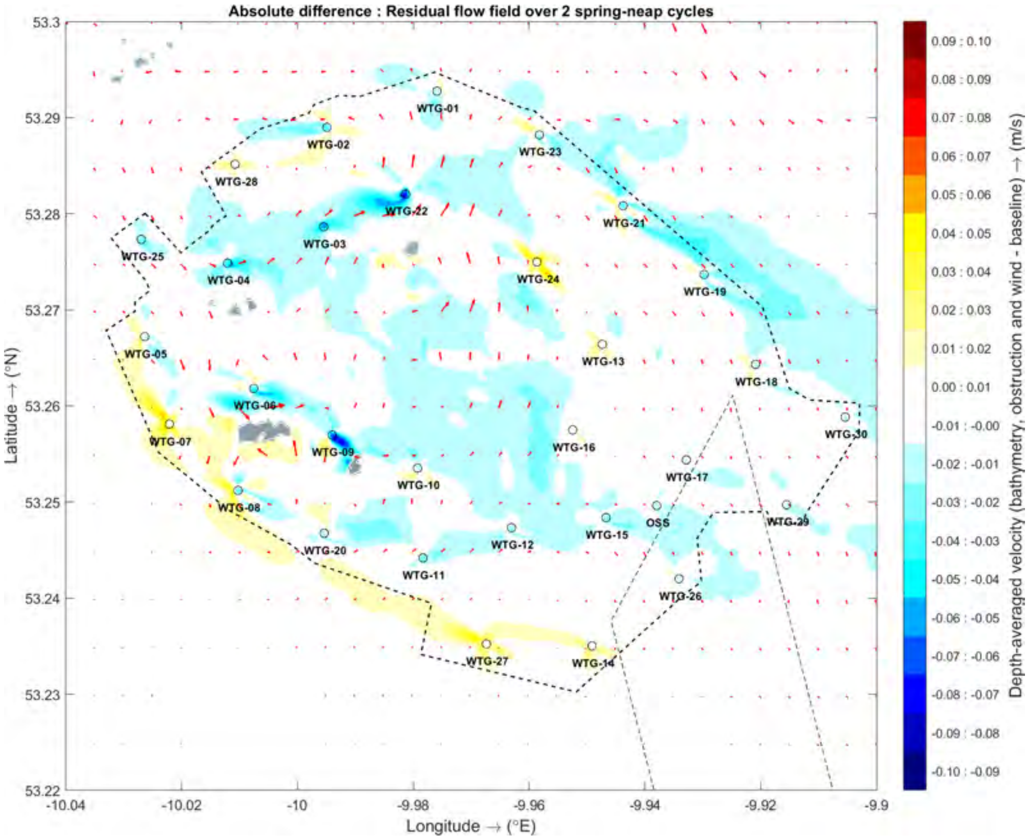
Absolute difference : Residual flow field over 2 spring-neap cycles
Latitude → (°N)
Longitude → (°E)
Depth-averaged velocity (bathymetry, obstruction and wind - baseline) → (m/s)
WTG-01
WTG-02
WTG-03
WTG-04
WTG-05
WTG-06
WTG-07
WTG-08
WTG-09
WTG-10
WTG-11
WTG-12
WTG-13
WTG-14
WTG-15
WTG-16
WTG-17
WTG-18
WTG-19
WTG-20
WTG-21
WTG-22
WTG-23
WTG-24
WTG-25
WTG-26
WTG-27
WTG-28
WTG-29
WTG-30
OSS
0.09 : 0.10
0.08 : 0.09
0.07 : 0.08
0.06 : 0.07
0.05 : 0.06
0.04 : 0.05
0.03 : 0.04
0.02 : 0.03
0.01 : 0.02
0.00 : 0.01
-0.01 : -0.00
-0.02 : -0.01
-0.03 : -0.02
-0.04 : -0.03
-0.05 : -0.04
-0.06 : -0.05
-0.07 : -0.06
-0.08 : -0.07
-0.09 : -0.08
-0.10 : -0.09

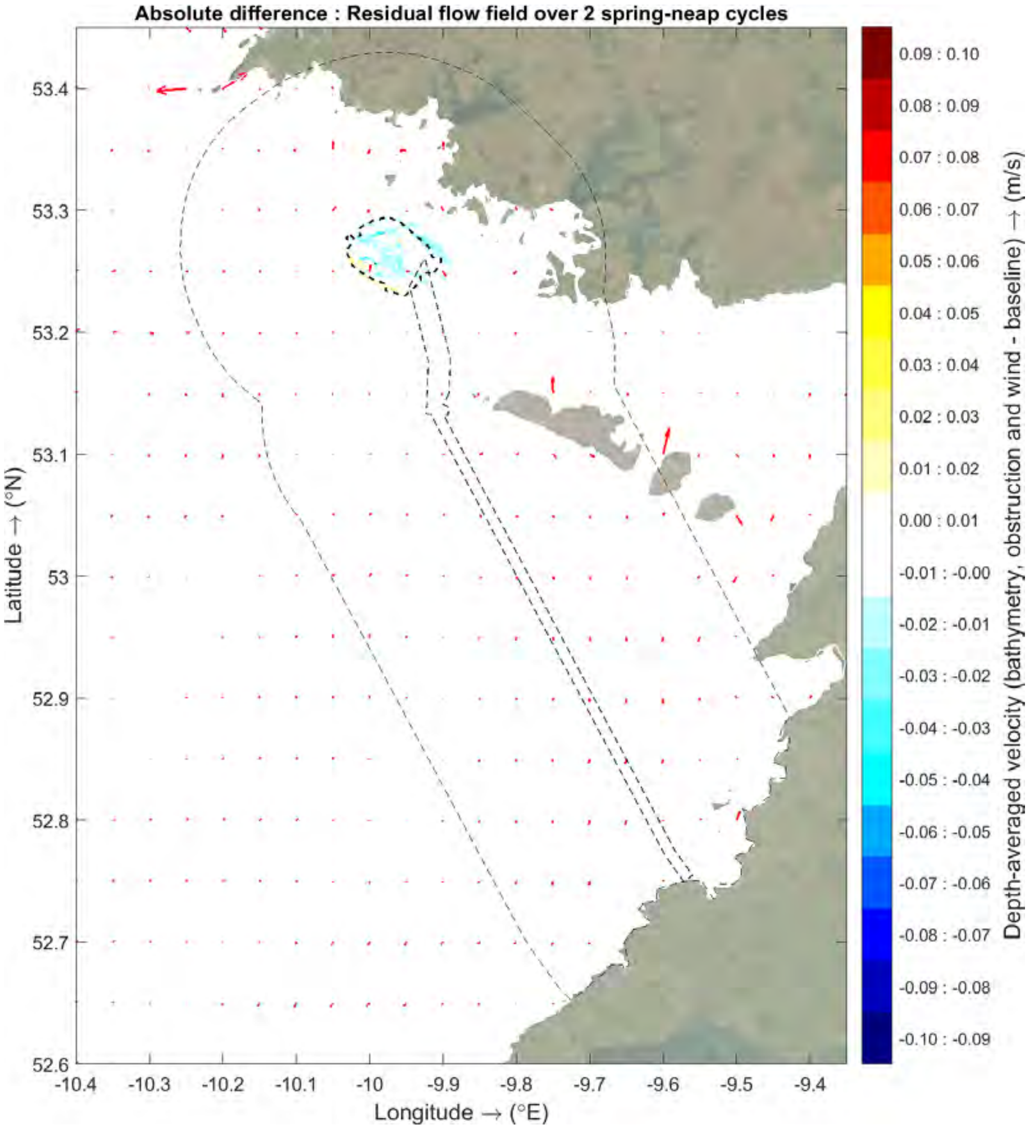
Absolute difference : Residual flow field over 2 spring-neap cycles
Latitude → (°N)
Longitude → (°E)
53.4
53.3
53.2
53.1
53
52.9
52.8
52.7
52.6
-10.4
-10.3
-10.2
-10.1
-10
-9.9
-9.8
-9.7
-9.6
-9.5
-9.4
0.09 : 0.10
0.08 : 0.09
0.07 : 0.08
0.06 : 0.07
0.05 : 0.06
0.04 : 0.05
0.03 : 0.04
0.02 : 0.03
0.01 : 0.02
0.00 : 0.01
-0.01 : -0.00
-0.02 : -0.01
-0.03 : -0.02
-0.04 : -0.03
-0.05 : -0.04
-0.06 : -0.05
-0.07 : -0.06
-0.08 : -0.07
-0.09 : -0.08
-0.10 : -0.09
Depth-averaged velocity (bathymetry, obstruction and wind - baseline) → (m/s)

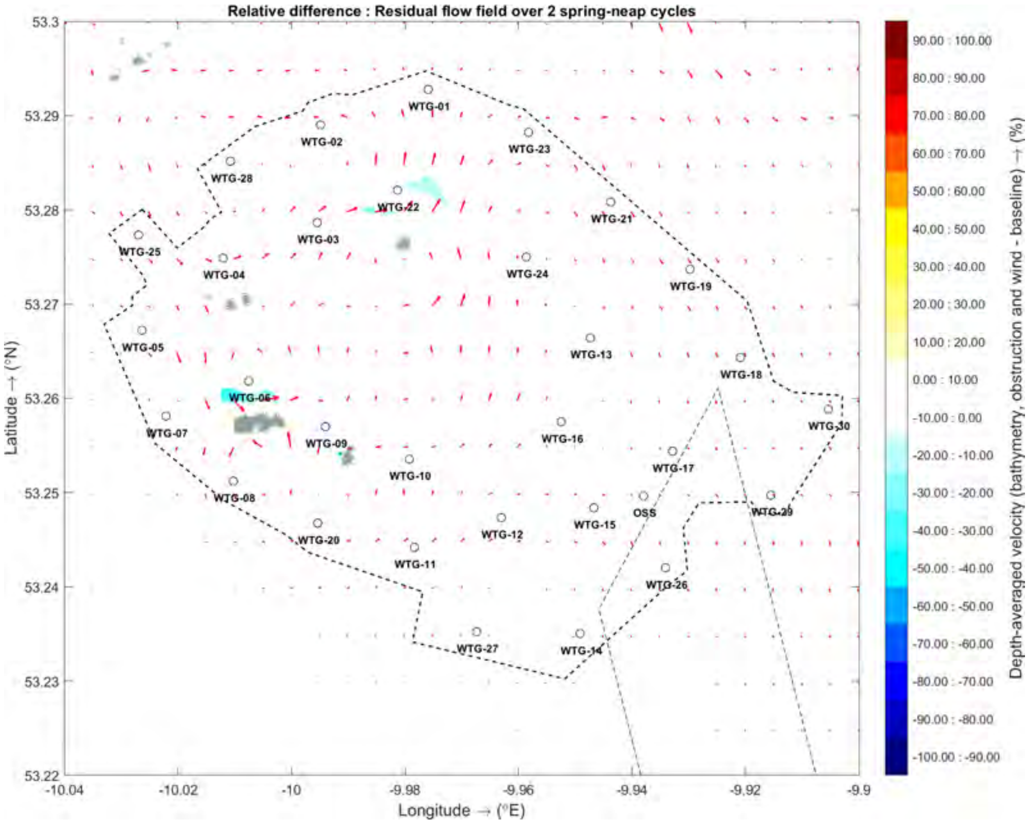
Relative difference : Residual flow field over 2 spring-neap cycles
Latitude → (°N)
Longitude → (°E)
Depth-averaged velocity (bathymetry, obstruction and wind - baseline) → (%)
WTG-01
WTG-02
WTG-03
WTG-04
WTG-05
WTG-06
WTG-07
WTG-08
WTG-09
WTG-10
WTG-11
WTG-12
WTG-13
WTG-14
WTG-15
WTG-16
WTG-17
WTG-18
WTG-19
WTG-20
WTG-21
WTG-22
WTG-23
WTG-24
WTG-25
WTG-26
WTG-27
WTG-28
WTG-29
WTG-30
OSS
90.00 : 100.00
80.00 : 90.00
70.00 : 80.00
60.00 : 70.00
50.00 : 60.00
40.00 : 50.00
30.00 : 40.00
20.00 : 30.00
10.00 : 20.00
0.00 : 10.00
-10.00 : 0.00
-20.00 : -10.00
-30.00 : -20.00
-40.00 : -30.00
-50.00 : -40.00
-60.00 : -50.00
-70.00 : -60.00
-80.00 : -70.00
-90.00 : -80.00
-100.00 : -90.00

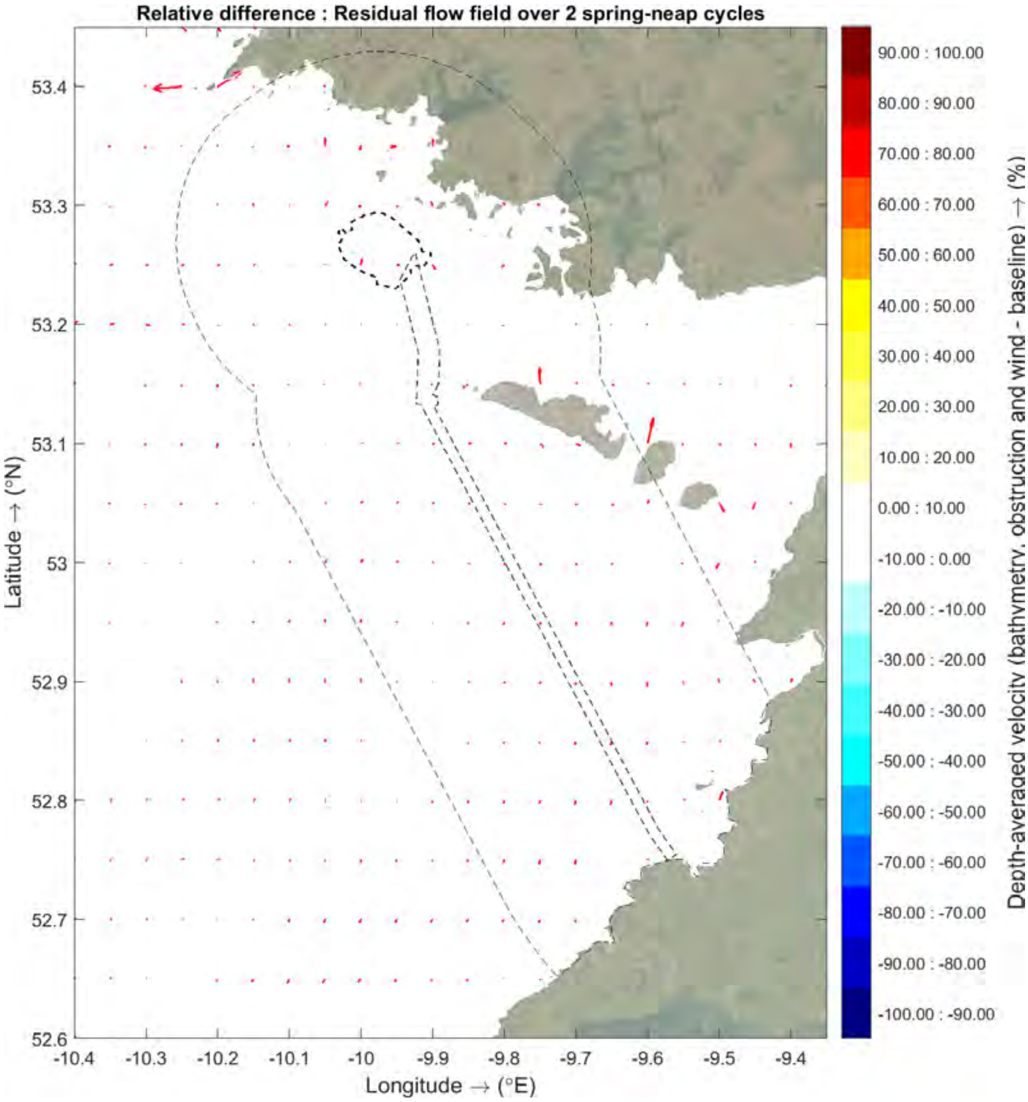
Relative difference : Residual flow field over 2 spring-neap cycles
Latitude → (°N)
Longitude → (°E)
Depth-averaged velocity (bathymetry, obstruction and wind - baseline) → (%)
90.00 : 100.00
80.00 : 90.00
70.00 : 80.00
60.00 : 70.00
50.00 : 60.00
40.00 : 50.00
30.00 : 40.00
20.00 : 30.00
10.00 : 20.00
0.00 : 10.00
-10.00 : 0.00
-20.00 : -10.00
-30.00 : -20.00
-40.00 : -30.00
-50.00 : -40.00
-60.00 : -50.00
-70.00 : -60.00
-80.00 : -70.00
-90.00 : -80.00
-100.00 : -90.00

D.18 Residuals water levels

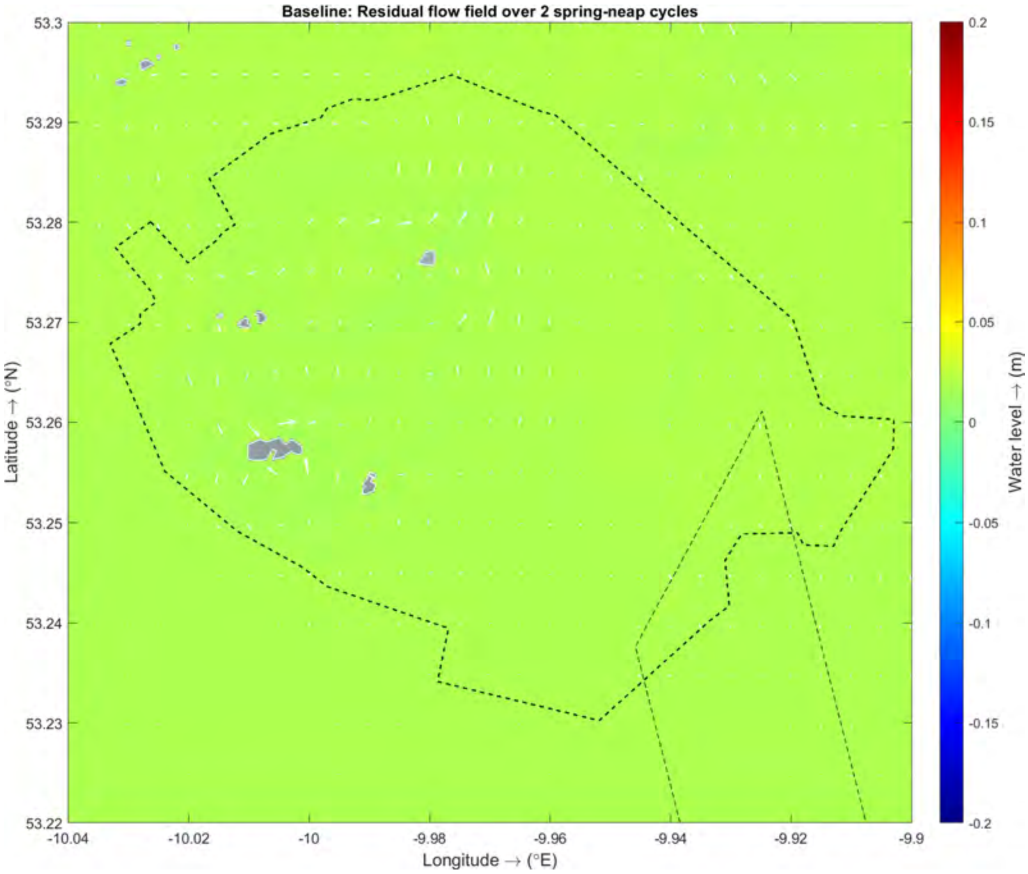

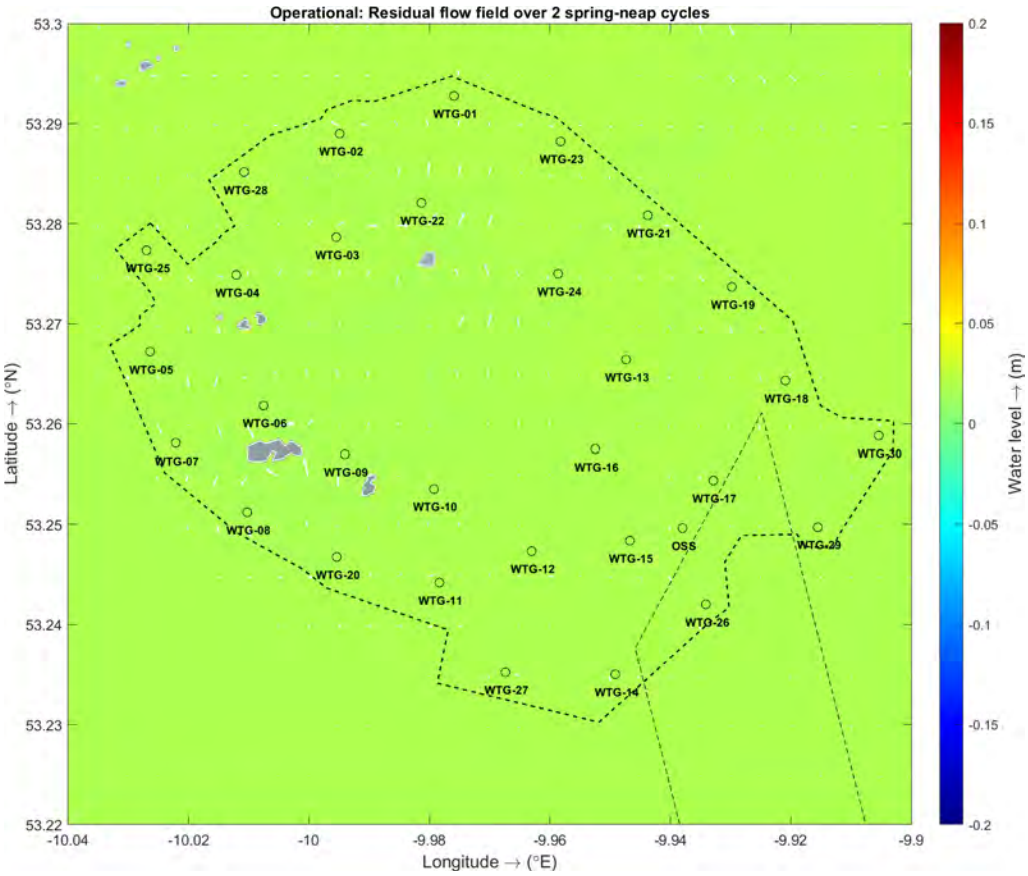

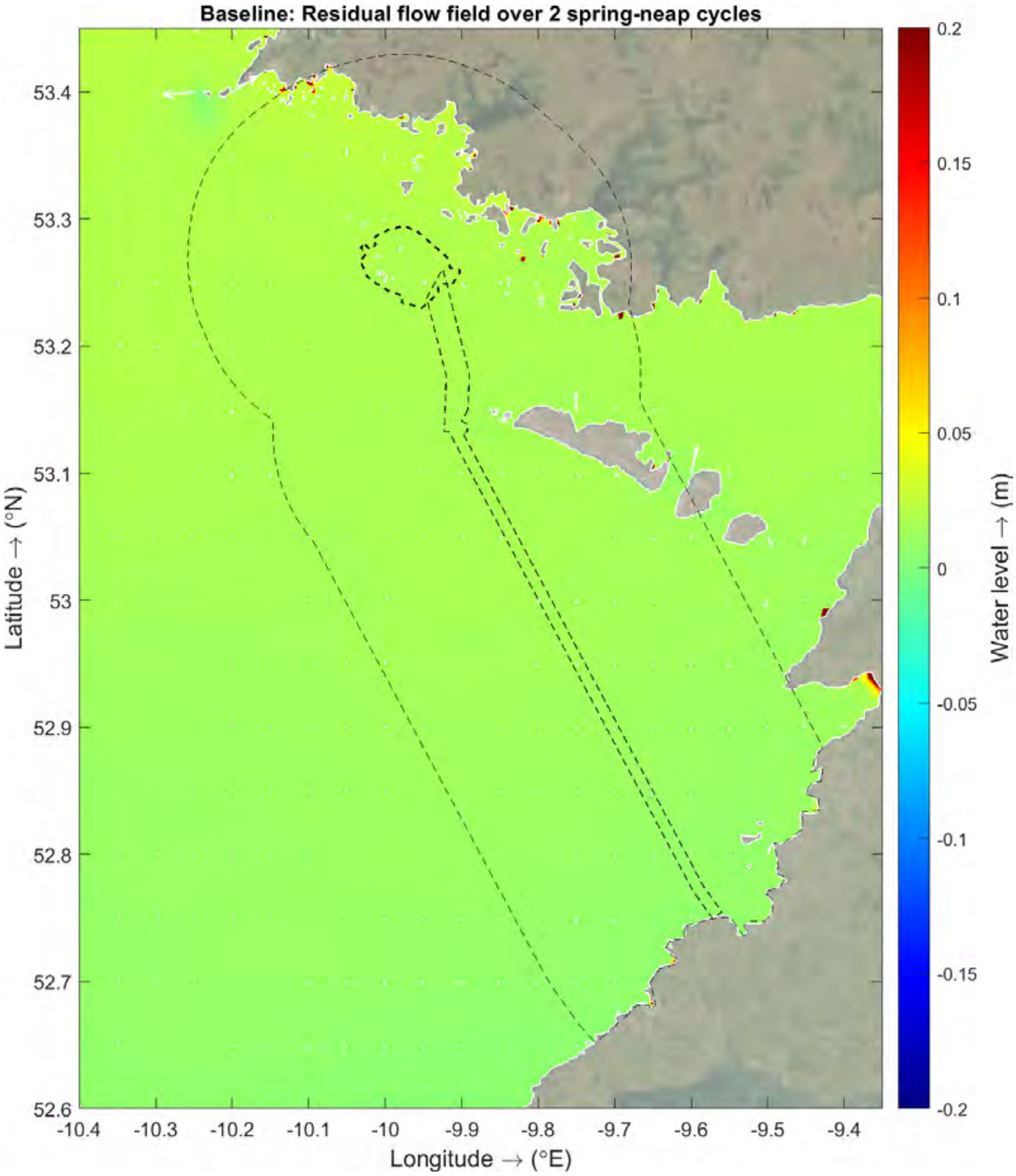
Baseline: Residual flow field over 2 spring-neap cycles
53.4
53.3
53.2
53.1
53
52.9
52.8
52.7
52.6
Latitude → (°N)
-10.4
-10.3
-10.2
-10.1
-10
-9.9
-9.8
-9.7
-9.6
-9.5
-9.4
Longitude → (°E)
0.2
0.15
0.1
0.05
0
-0.05
-0.1
-0.15
-0.2
Water level → (m)

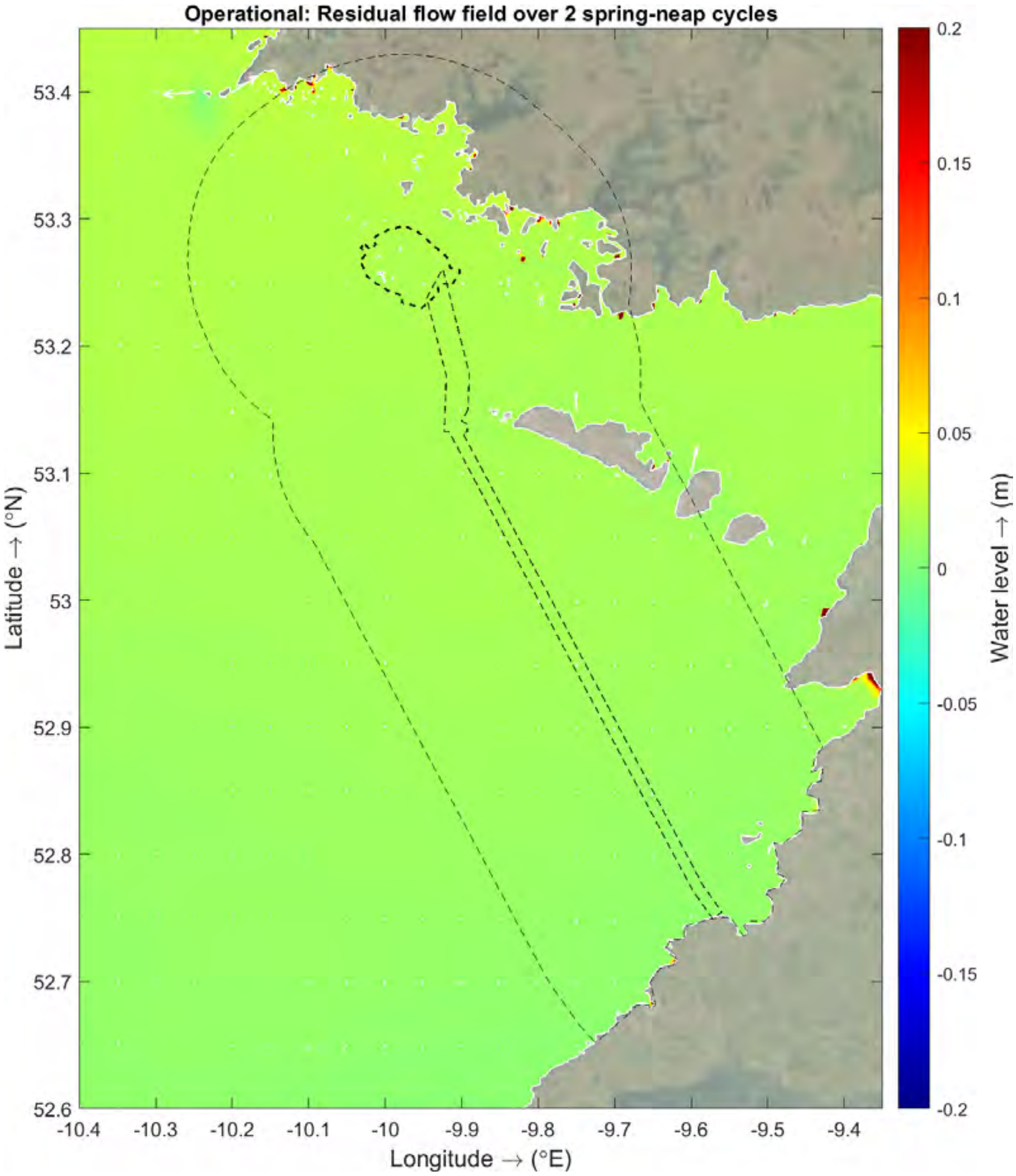
Operational: Residual flow field over 2 spring-neap cycles
53.4
53.3
53.2
53.1
53
52.9
52.8
52.7
52.6
Latitude → (°N)
-10.4
-10.3
-10.2
-10.1
-10
-9.9
-9.8
-9.7
-9.6
-9.5
-9.4
Longitude → (°E)
0.2
0.15
0.1
0.05
0
-0.05
-0.1
-0.15
-0.2
Water level → (m)

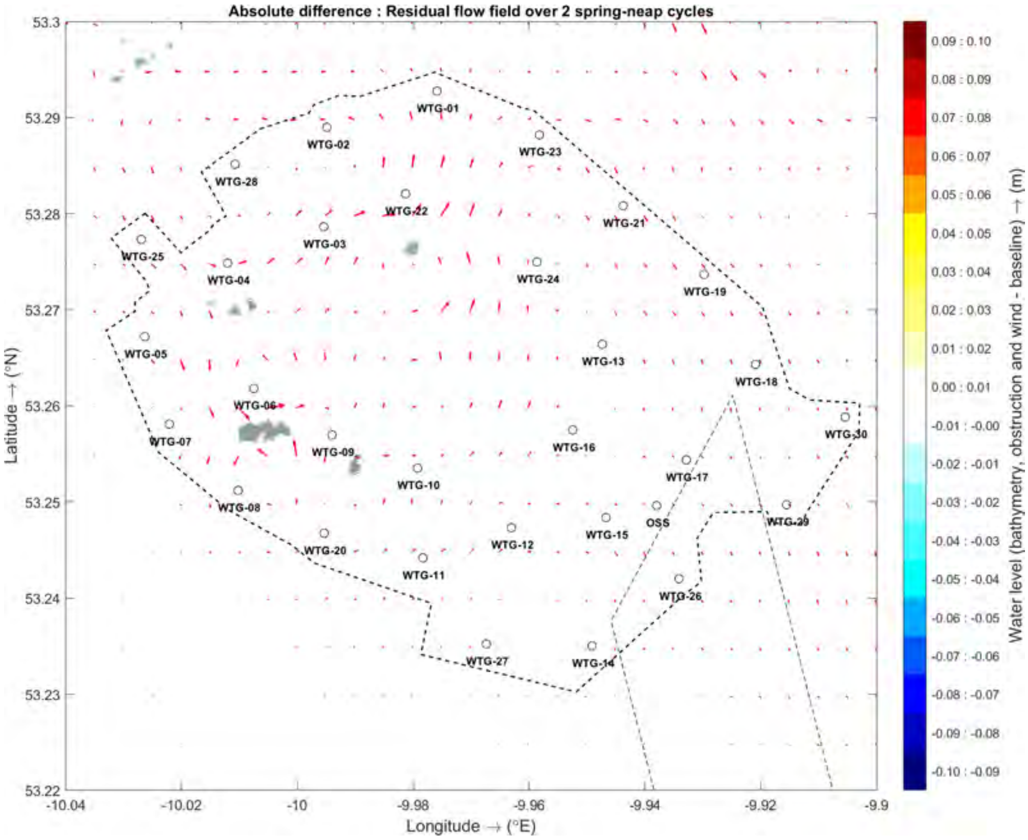
Absolute difference : Residual flow field over 2 spring-neap cycles
Latitude → (°N)
Longitude → (°E)
Water level (bathymetry, obstruction and wind - baseline) → (m)
WTG-01
WTG-02
WTG-03
WTG-04
WTG-05
WTG-06
WTG-07
WTG-08
WTG-09
WTG-10
WTG-11
WTG-12
WTG-13
WTG-14
WTG-15
WTG-16
WTG-17
WTG-18
WTG-19
WTG-20
WTG-21
WTG-22
WTG-23
WTG-24
WTG-25
WTG-26
WTG-27
WTG-28
WTG-29
WTG-30
OSS

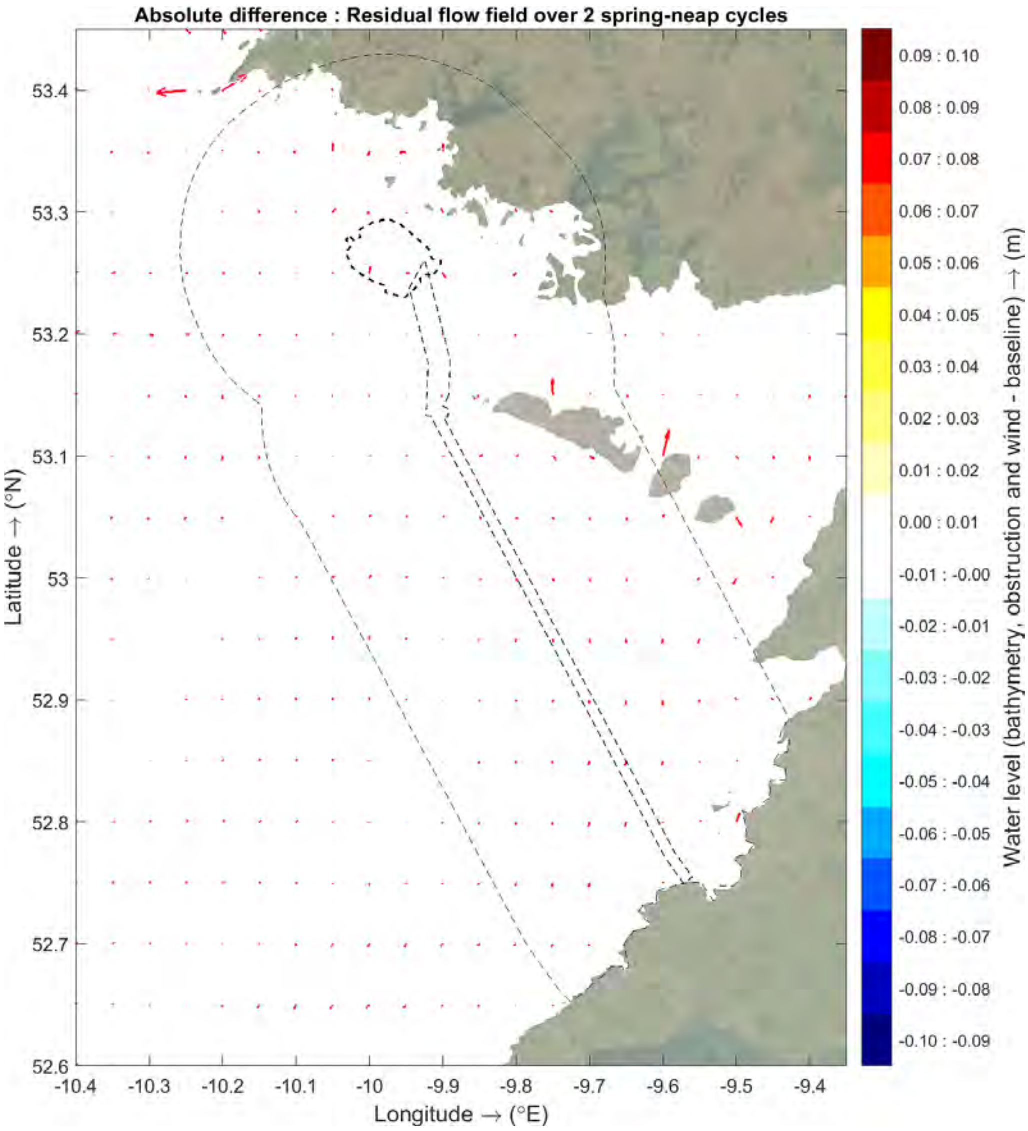
Absolute difference : Residual flow field over 2 spring-neap cycles
53.4
53.3
53.2
53.1
53
52.9
52.8
52.7
52.6
Latitude → (°N)
-10.4
-10.3
-10.2
-10.1
-10
-9.9
-9.8
-9.7
-9.6
-9.5
-9.4
Longitude → (°E)
0.09 : 0.10
0.08 : 0.09
0.07 : 0.08
0.06 : 0.07
0.05 : 0.06
0.04 : 0.05
0.03 : 0.04
0.02 : 0.03
0.01 : 0.02
0.00 : 0.01
-0.01 : -0.00
-0.02 : -0.01
-0.03 : -0.02
-0.04 : -0.03
-0.05 : -0.04
-0.06 : -0.05
-0.07 : -0.06
-0.08 : -0.07
-0.09 : -0.08
-0.10 : -0.09
Water level (bathymetry, obstruction and wind - baseline) → (m)

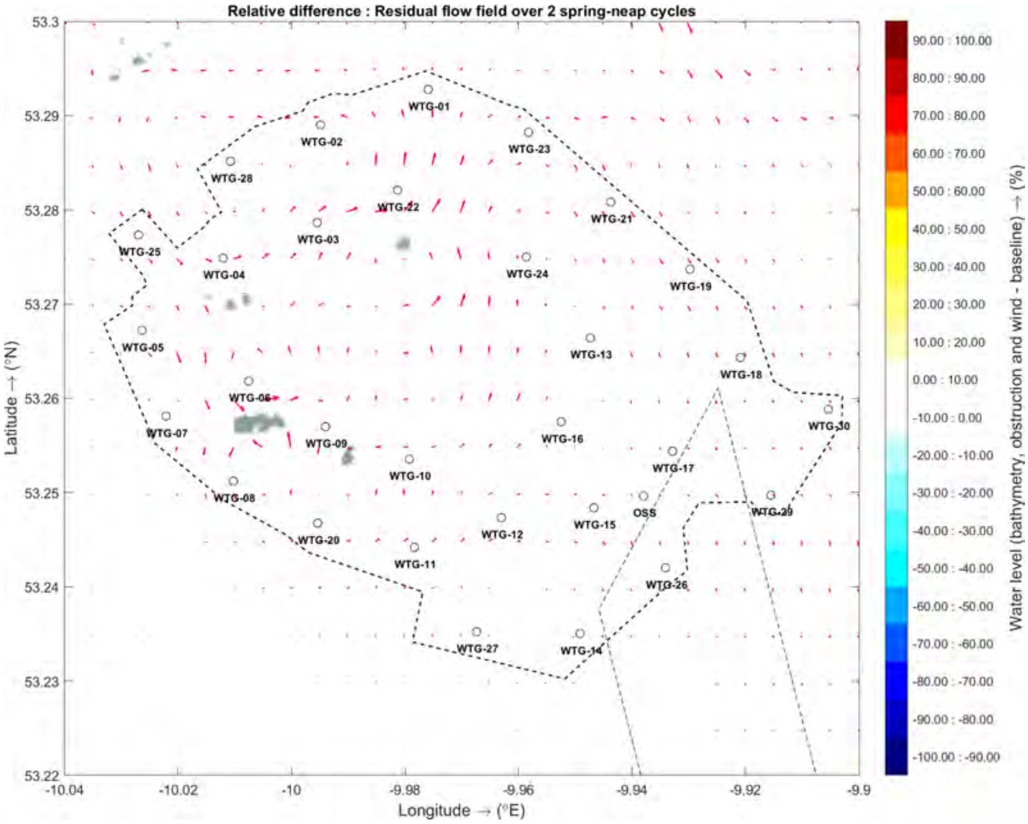
Relative difference : Residual flow field over 2 spring-neap cycles
Latitude → (°N)
Longitude → (°E)
Water level (bathymetry, obstruction and wind - baseline) → (%)
WTG-01
WTG-02
WTG-03
WTG-04
WTG-05
WTG-06
WTG-07
WTG-08
WTG-09
WTG-10
WTG-11
WTG-12
WTG-13
WTG-14
WTG-15
WTG-16
WTG-17
WTG-18
WTG-19
WTG-20
WTG-21
WTG-22
WTG-23
WTG-24
WTG-25
WTG-26
WTG-27
WTG-28
WTG-29
WTG-30
OSS
90.00 : 100.00
80.00 : 90.00
70.00 : 80.00
60.00 : 70.00
50.00 : 60.00
40.00 : 50.00
30.00 : 40.00
20.00 : 30.00
10.00 : 20.00
0.00 : 10.00
-10.00 : 0.00
-20.00 : -10.00
-30.00 : -20.00
-40.00 : -30.00
-50.00 : -40.00
-60.00 : -50.00
-70.00 : -60.00
-80.00 : -70.00
-90.00 : -80.00
-100.00 : -90.00

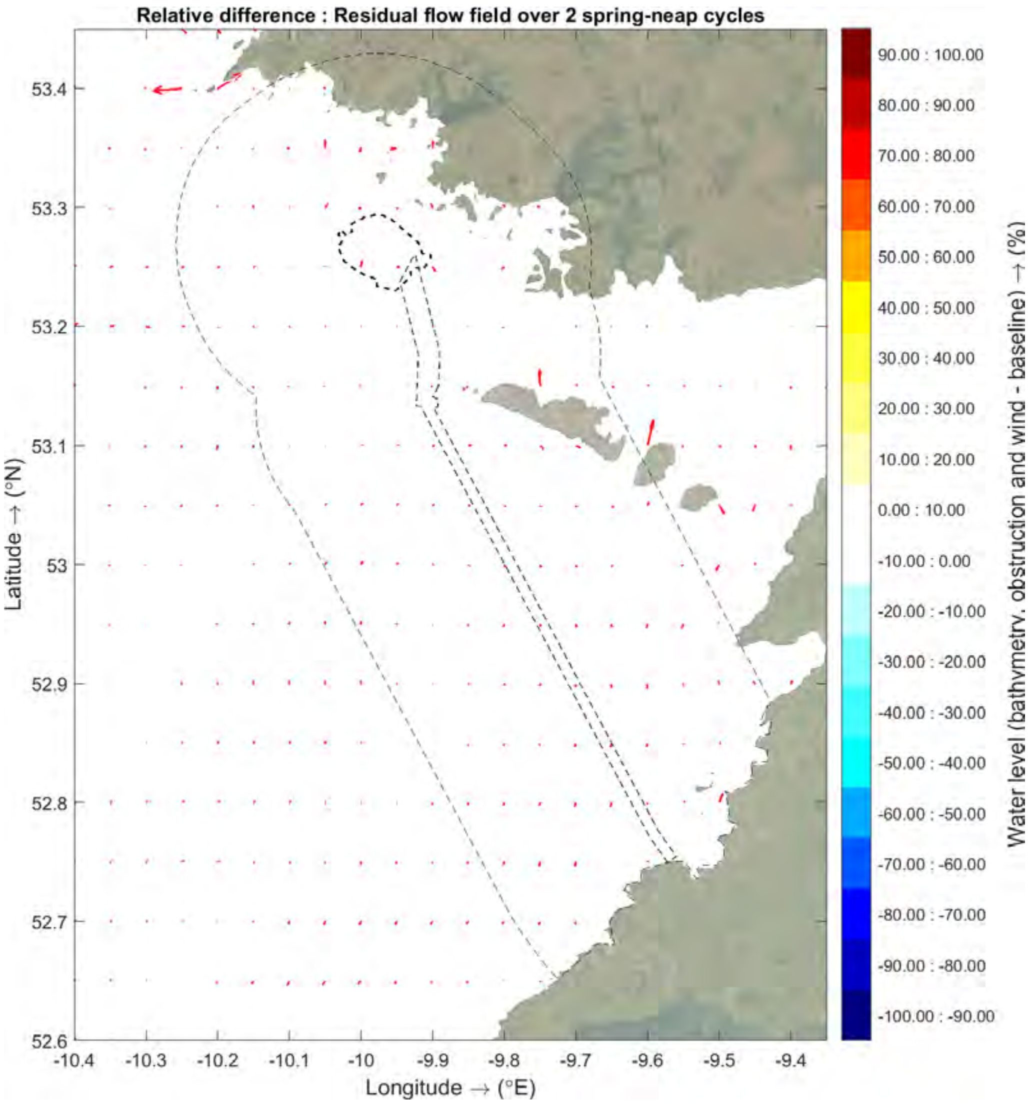
Relative difference : Residual flow field over 2 spring-neap cycles
53.4
53.3
53.2
53.1
53
52.9
52.8
52.7
52.6
Latitude → (°N)
-10.4
-10.3
-10.2
-10.1
-10
-9.9
-9.8
-9.7
-9.6
-9.5
-9.4
Longitude → (°E)
90.00 : 100.00
80.00 : 90.00
70.00 : 80.00
60.00 : 70.00
50.00 : 60.00
40.00 : 50.00
30.00 : 40.00
20.00 : 30.00
10.00 : 20.00
0.00 : 10.00
-10.00 : 0.00
-20.00 : -10.00
-30.00 : -20.00
-40.00 : -30.00
-50.00 : -40.00
-60.00 : -50.00
-70.00 : -60.00
-80.00 : -70.00
-90.00 : -80.00
-100.00 : -90.00
Water level (bathymetry, obstruction and wind - baseline) → (%)

Deltares

E Wave fields

E.1 50th percentile

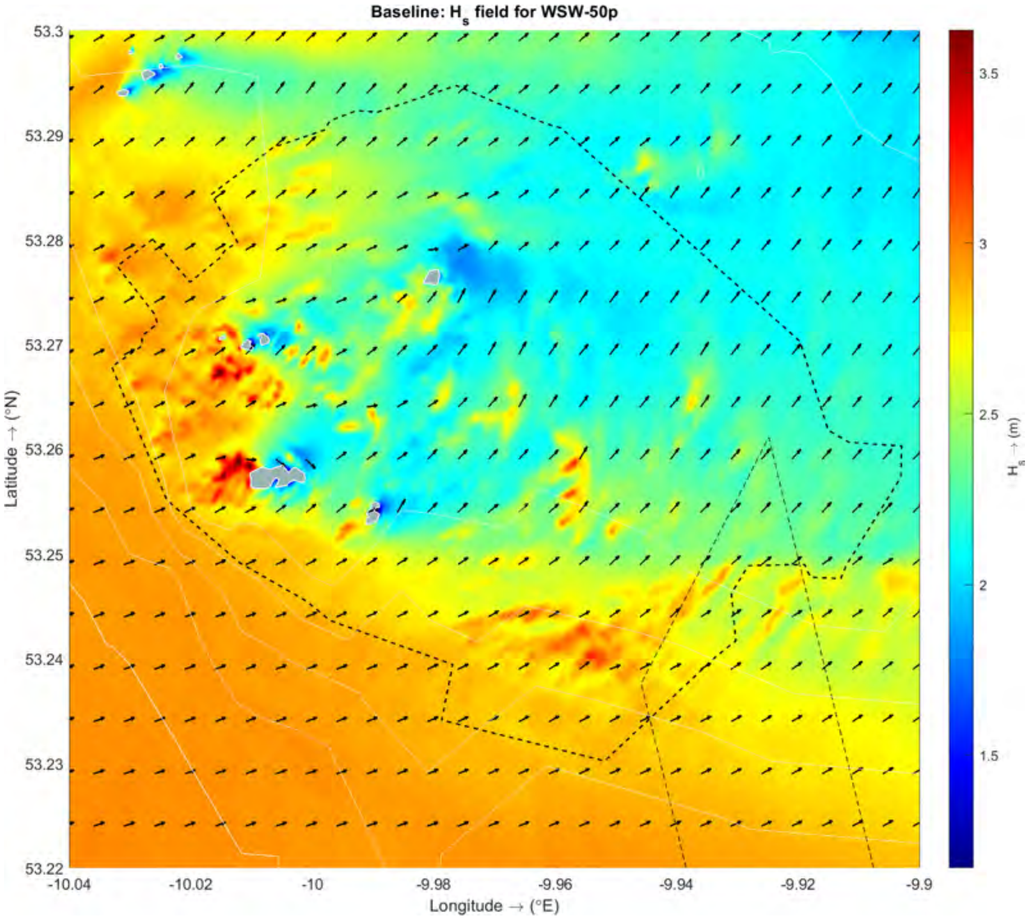

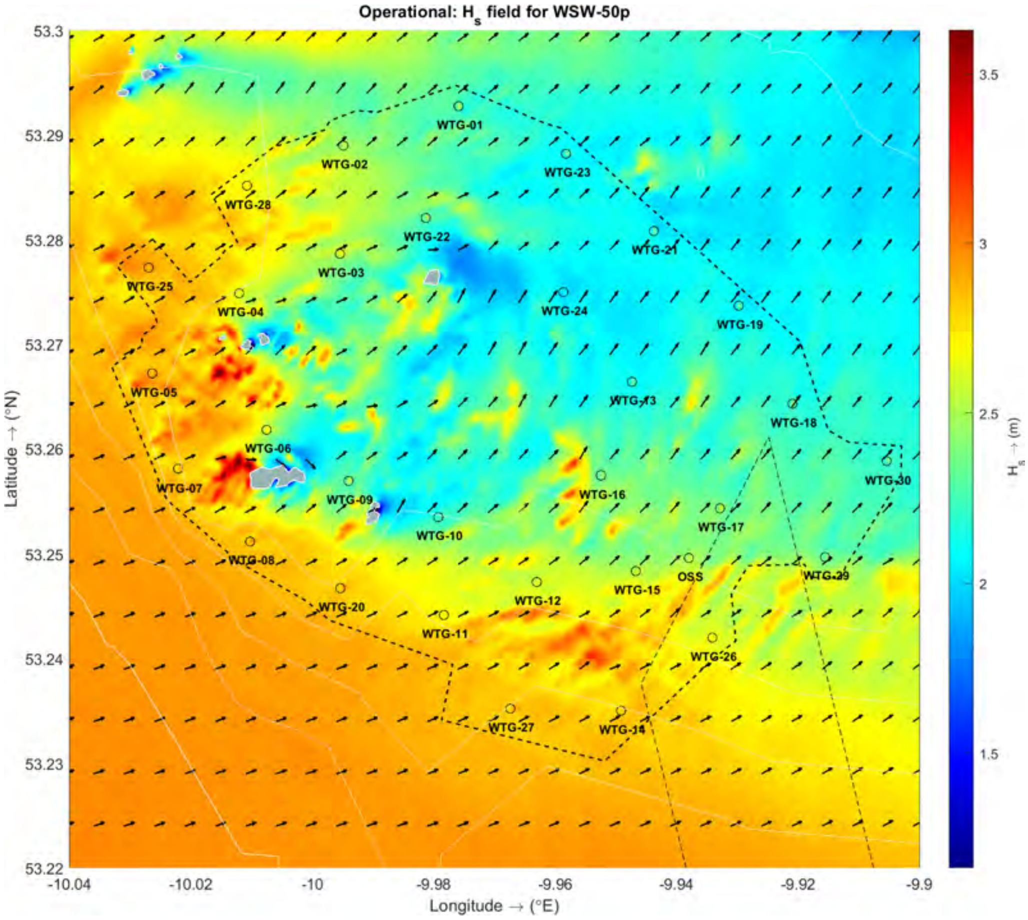
Operational: H_s field for WSW-50p
Latitude → (°N)
Longitude → (°E)
H_s → (m)

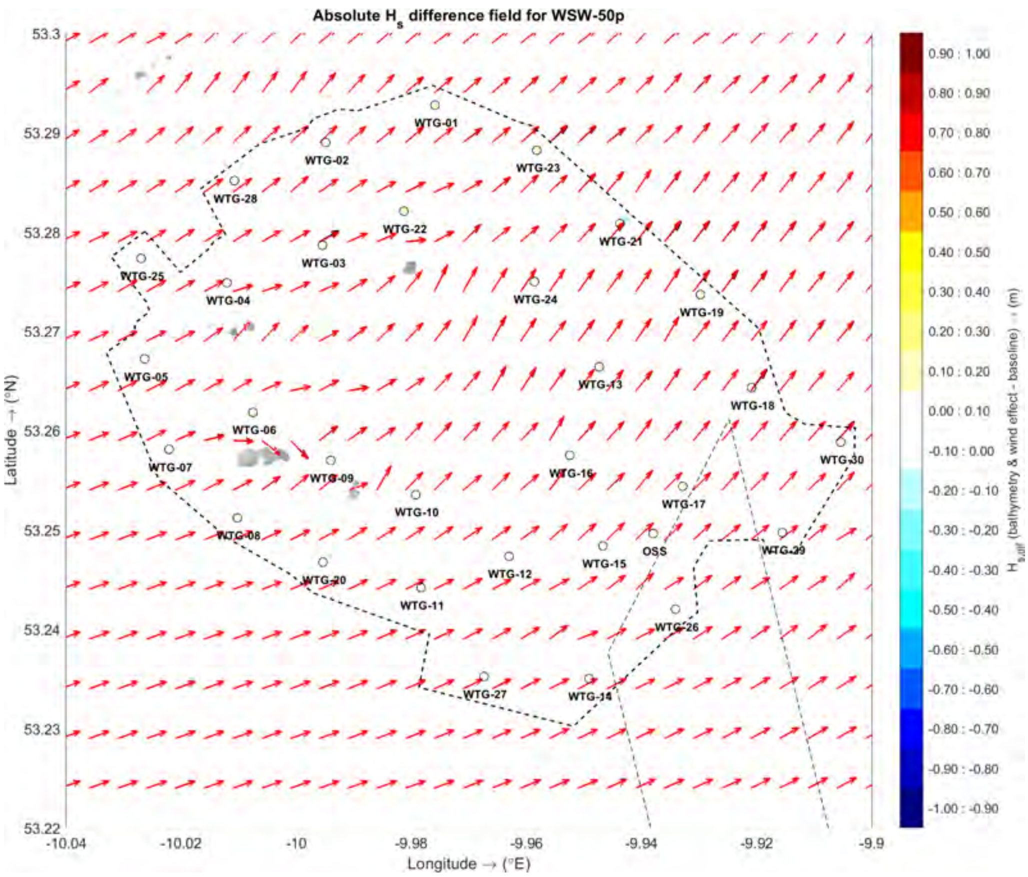
Absolute H_s difference field for WSW-50p
Latitude → (°N)
Longitude → (°E)
$H_{s,diff}$ (bathymetry & wind effect - baseline) → (m)

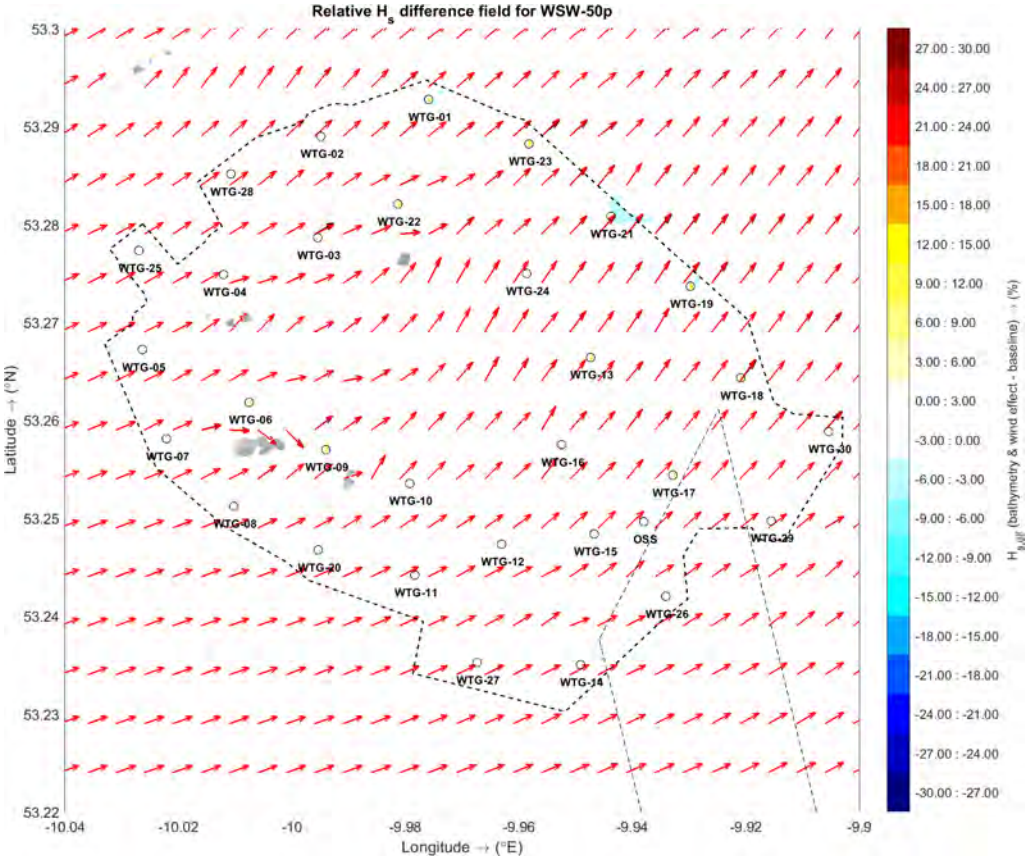
Relative H_s difference field for WSW-50p
Latitude → (°N)
Longitude → (°E)
$H_{s,diff}$ (bathymetry & wind effect - baseline) → (%)
27.00 : 30.00
24.00 : 27.00
21.00 : 24.00
18.00 : 21.00
15.00 : 18.00
12.00 : 15.00
9.00 : 12.00
6.00 : 9.00
3.00 : 6.00
0.00 : 3.00
-3.00 : 0.00
-6.00 : -3.00
-9.00 : -6.00
-12.00 : -9.00
-15.00 : -12.00
-18.00 : -15.00
-21.00 : -18.00
-24.00 : -21.00
-27.00 : -24.00
-30.00 : -27.00
WTG-01
WTG-02
WTG-03
WTG-04
WTG-05
WTG-06
WTG-07
WTG-08
WTG-09
WTG-10
WTG-11
WTG-12
WTG-13
WTG-14
WTG-15
WTG-16
WTG-17
WTG-18
WTG-19
WTG-20
WTG-21
WTG-22
WTG-23
WTG-24
WTG-25
WTG-26
WTG-27
WTG-28
WTG-29
WTG-30
OSS

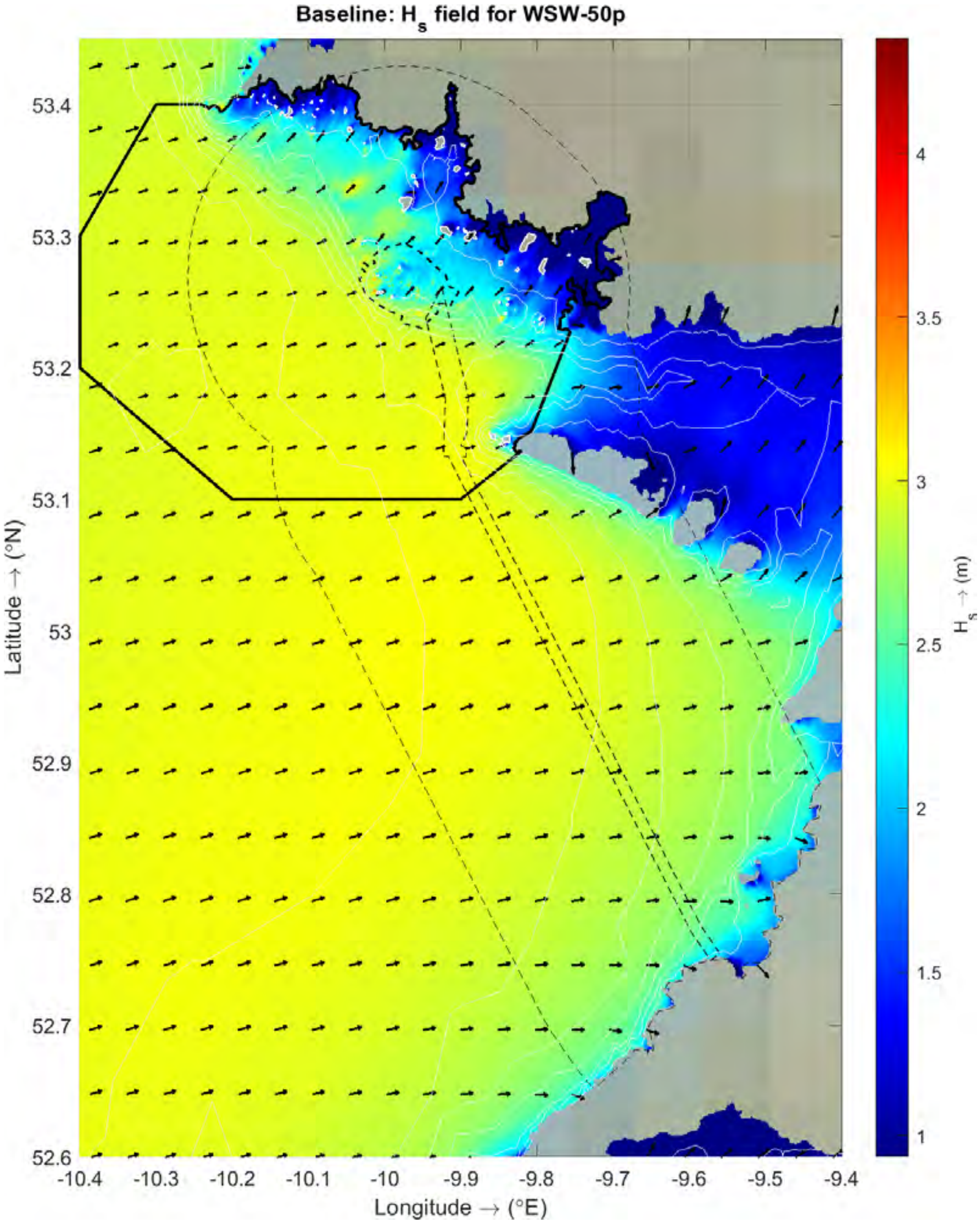
Baseline: H_s field for WSW-50p
Latitude → (°N)
Longitude → (°E)
H_s → (m)
53.4
53.3
53.2
53.1
53
52.9
52.8
52.7
52.6
-10.4
-10.3
-10.2
-10.1
-10
-9.9
-9.8
-9.7
-9.6
-9.5
-9.4
4
3.5
3
2.5
2
1.5
1

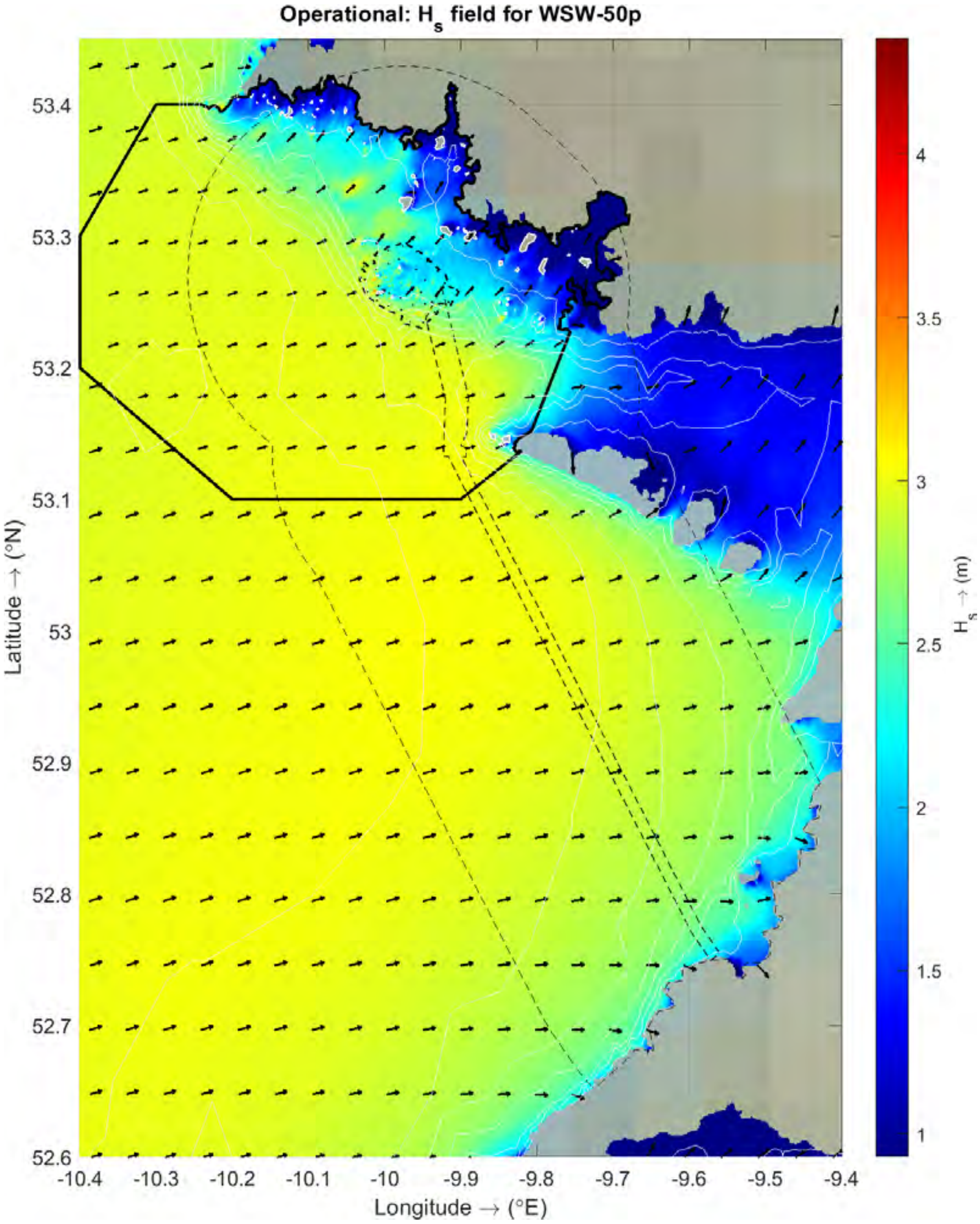
Operational: H_s field for WSW-50p
Latitude → (°N)
Longitude → (°E)
H_s → (m)
53.4
53.3
53.2
53.1
53
52.9
52.8
52.7
52.6
-10.4
-10.3
-10.2
-10.1
-10
-9.9
-9.8
-9.7
-9.6
-9.5
-9.4
4
3.5
3
2.5
2
1.5
1

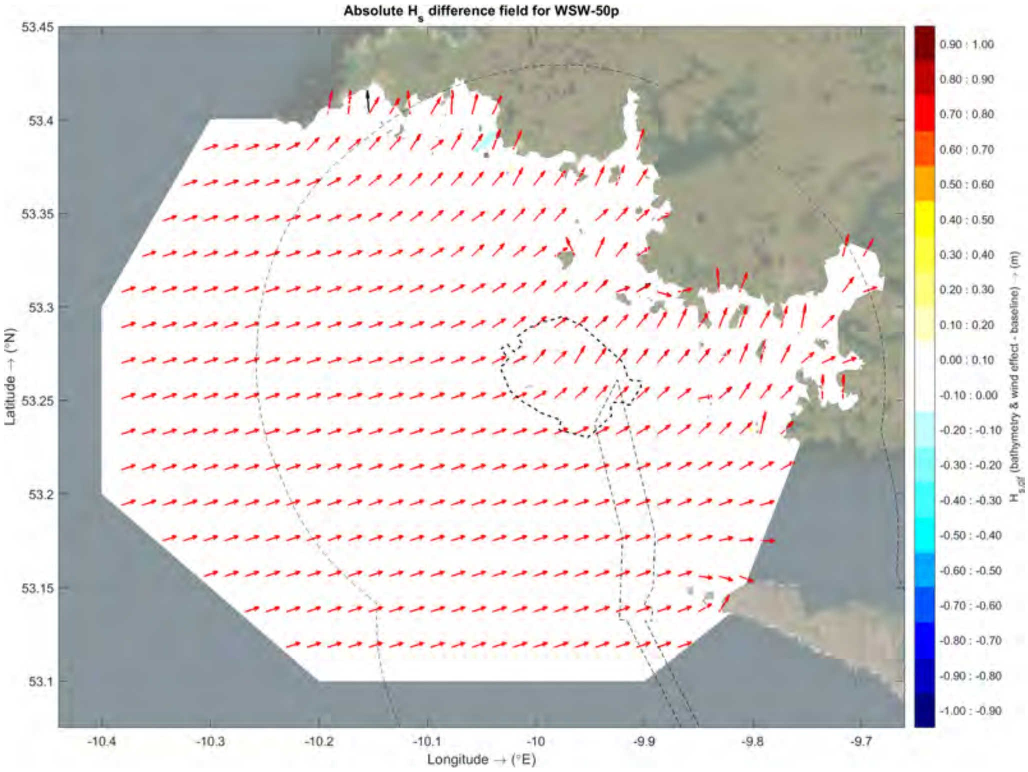
Absolute H$_s$ difference field for WSW-50p
Latitude → (°N)
Longitude → (°E)
H$_{s,dif}$ (bathymetry & wind effect - baseline) → (m)

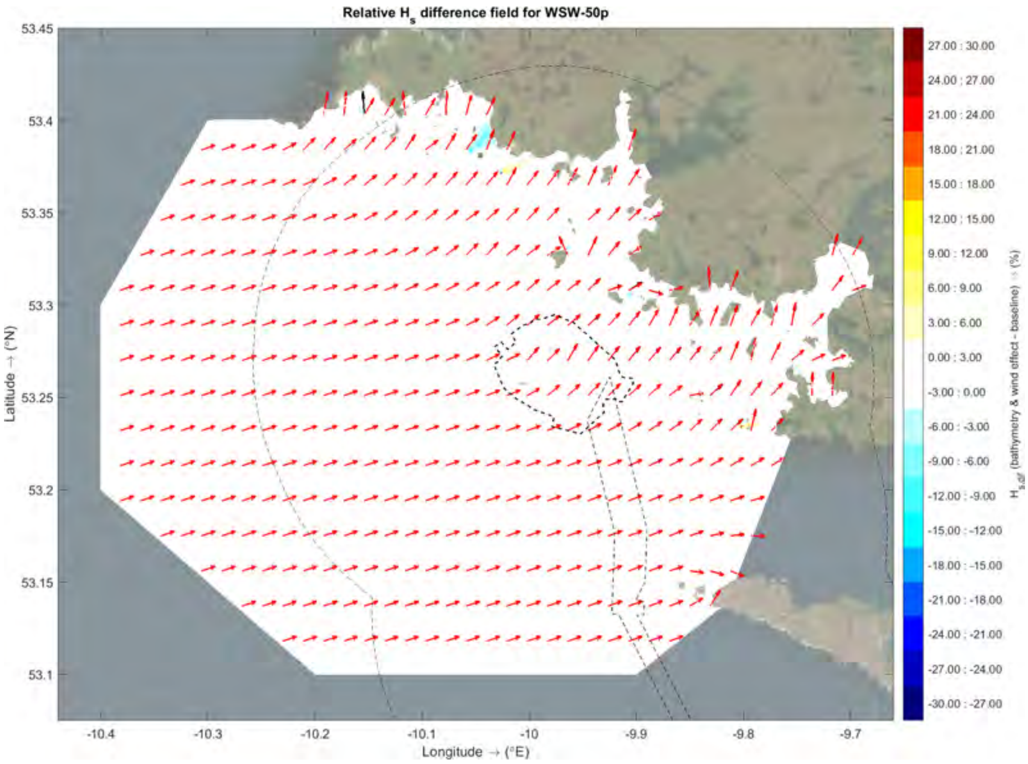
Relative H$_s$ difference field for WSW-50p
Latitude → (°N)
Longitude → (°E)
H$_{s,dif}$ (bathymetry & wind effect - baseline) → (%)

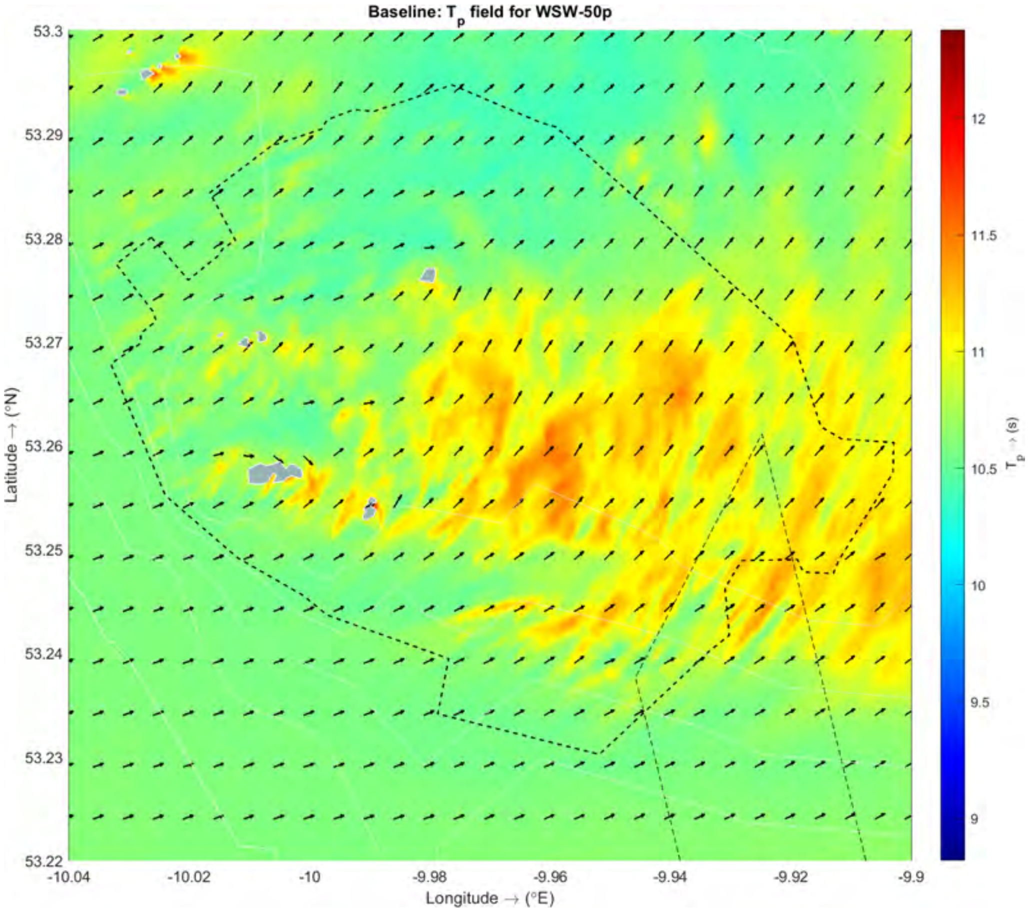
Baseline: T_p field for WSW-50p
53.3
53.29
53.28
53.27
53.26
53.25
53.24
53.23
53.22
Latitude → (°N)
-10.04
-10.02
-10
-9.98
-9.96
-9.94
-9.92
-9.9
Longitude → (°E)
12
11.5
11
10.5
10
9.5
9
T_p → (s)

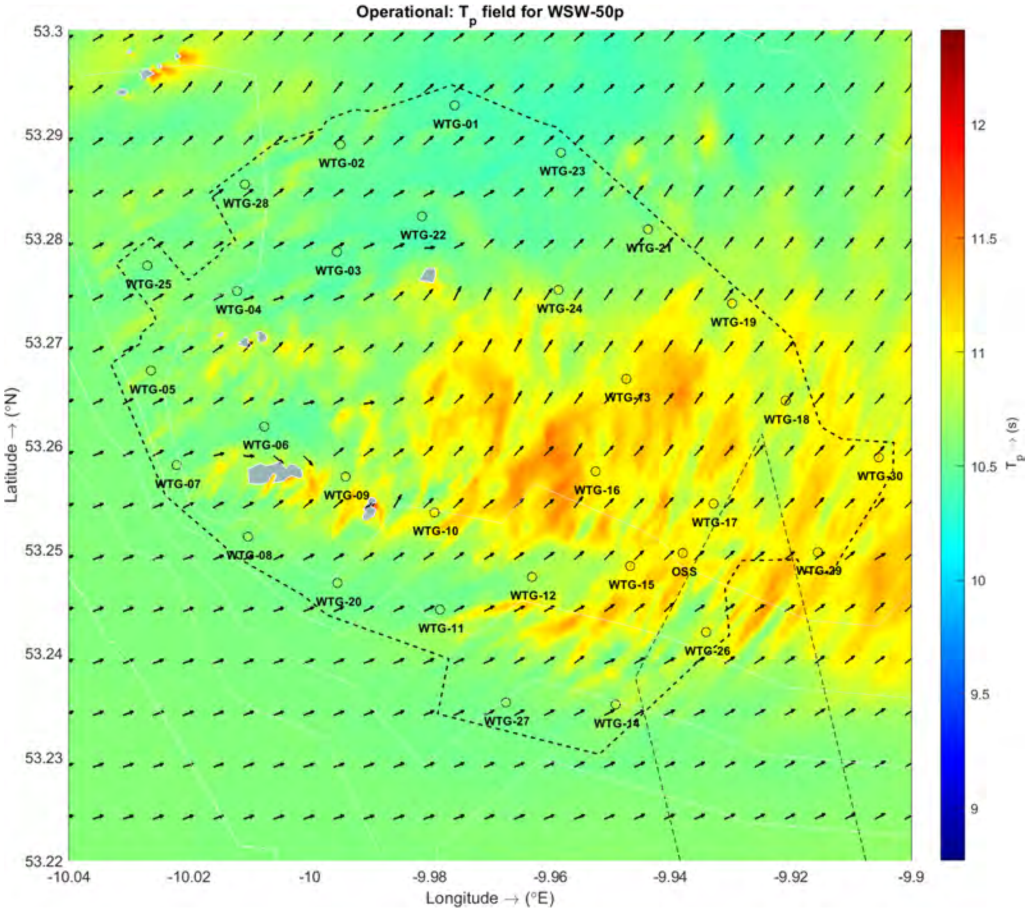
Operational: T_p field for WSW-50p
Latitude → (°N)
Longitude → (°E)
T_p → (s)
WTG-01
WTG-02
WTG-03
WTG-04
WTG-05
WTG-06
WTG-07
WTG-08
WTG-09
WTG-10
WTG-11
WTG-12
WTG-13
WTG-14
WTG-15
WTG-16
WTG-17
WTG-18
WTG-19
WTG-20
WTG-21
WTG-22
WTG-23
WTG-24
WTG-25
WTG-26
WTG-27
WTG-28
WTG-29
WTG-30
OSS

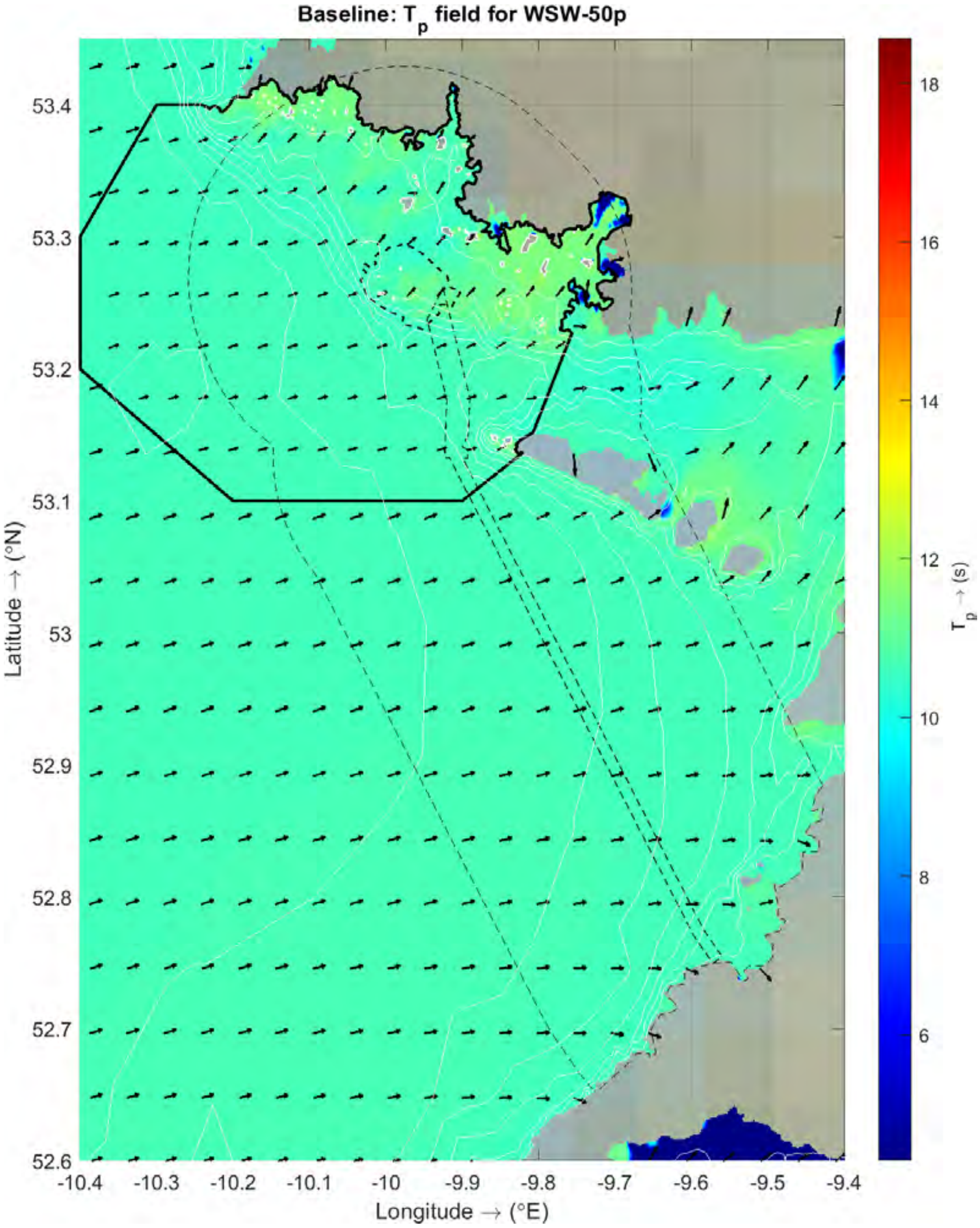
Baseline: T_p field for WSW-50p
Latitude → (°N)
53.4
53.3
53.2
53.1
53
52.9
52.8
52.7
52.6
-10.4
-10.3
-10.2
-10.1
-10
-9.9
-9.8
-9.7
-9.6
-9.5
-9.4
Longitude → (°E)
18
16
14
12
10
8
6
T_p → (s)

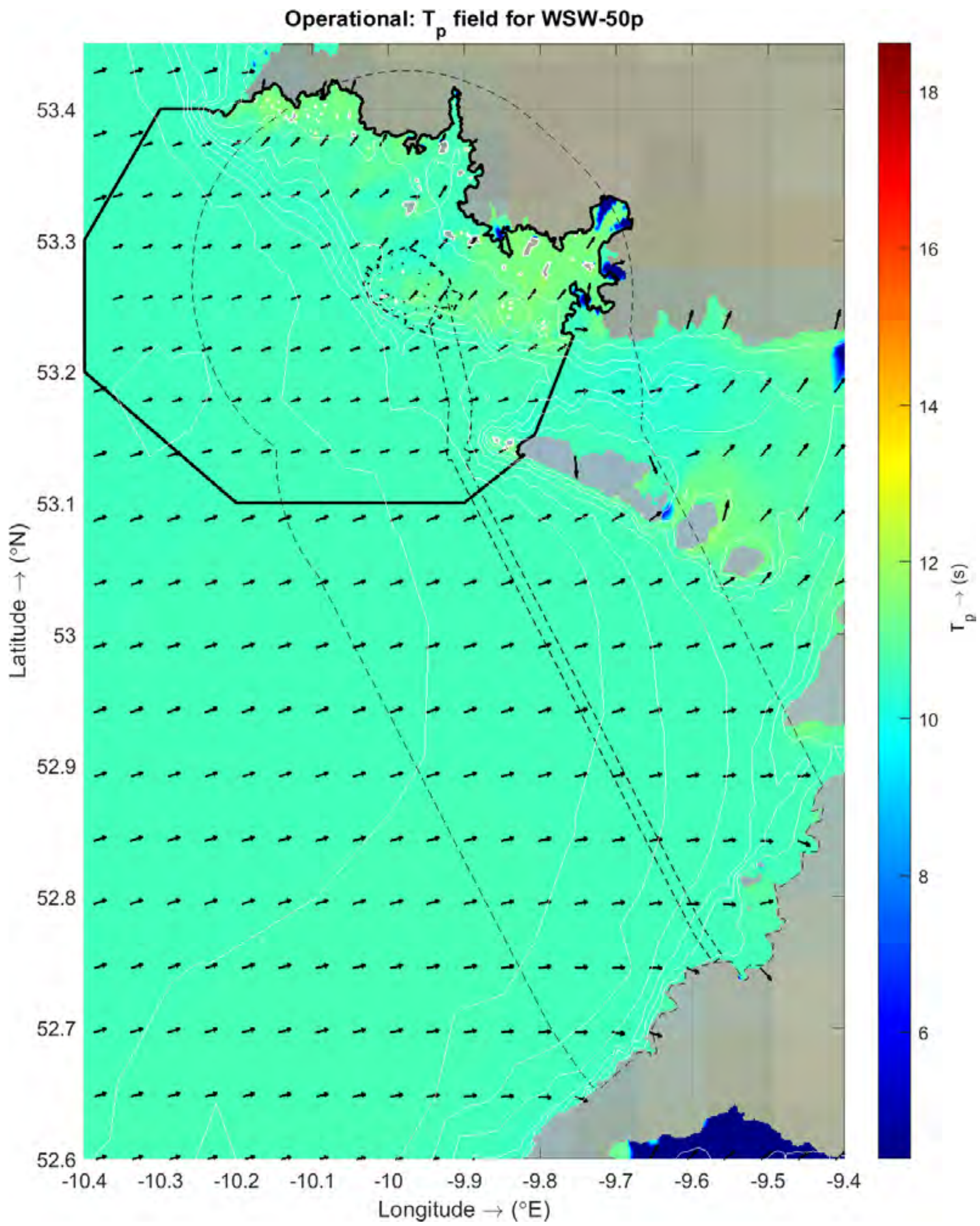

Operational: T_p field for WSW-50p
53.4
53.3
53.2
53.1
53
52.9
52.8
52.7
52.6
Latitude → (°N)
-10.4
-10.3
-10.2
-10.1
-10
-9.9
-9.8
-9.7
-9.6
-9.5
-9.4
Longitude → (°E)
18
16
14
12
10
8
6
T_p → (s)

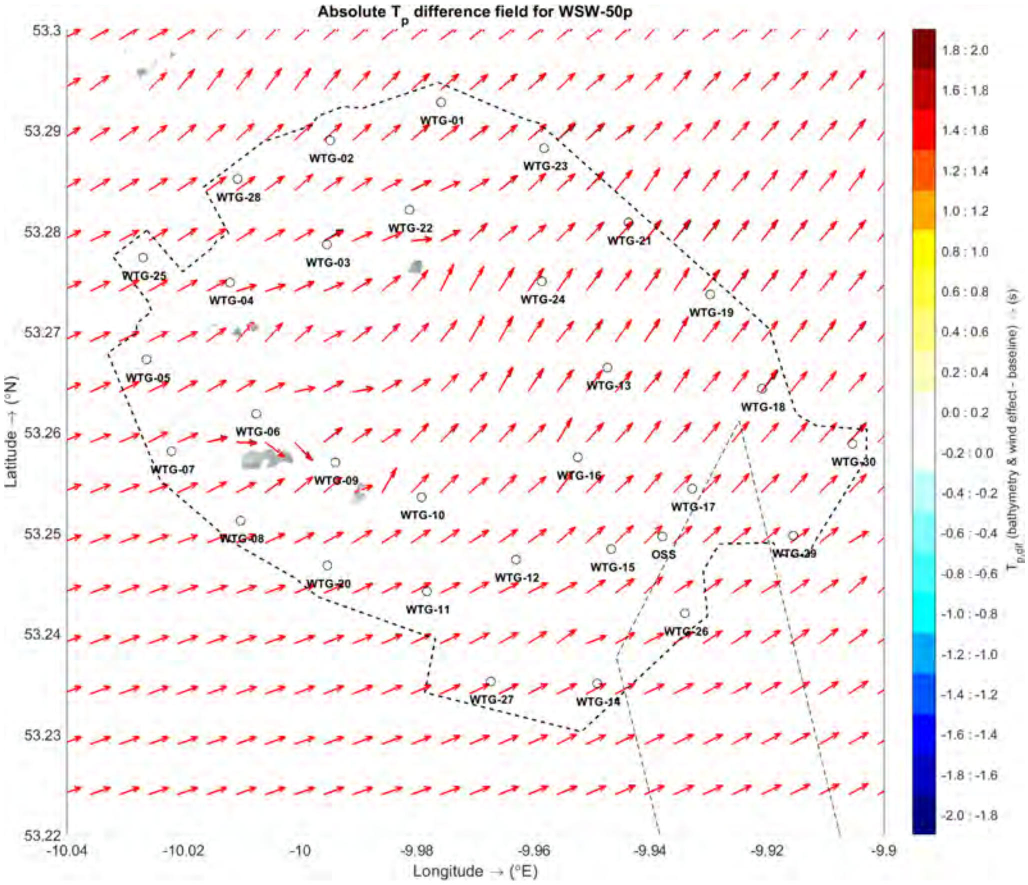

Absolute T_p difference field for WSW-50p
Latitude → (°N)
Longitude → (°E)
$T_{p,dif}$ (bathymetry & wind effect - baseline) → (s)
1.8 : 2.0
1.6 : 1.8
1.4 : 1.6
1.2 : 1.4
1.0 : 1.2
0.8 : 1.0
0.6 : 0.8
0.4 : 0.6
0.2 : 0.4
0.0 : 0.2
-0.2 : 0.0
-0.4 : -0.2
-0.6 : -0.4
-0.8 : -0.6
-1.0 : -0.8
-1.2 : -1.0
-1.4 : -1.2
-1.6 : -1.4
-1.8 : -1.6
-2.0 : -1.8

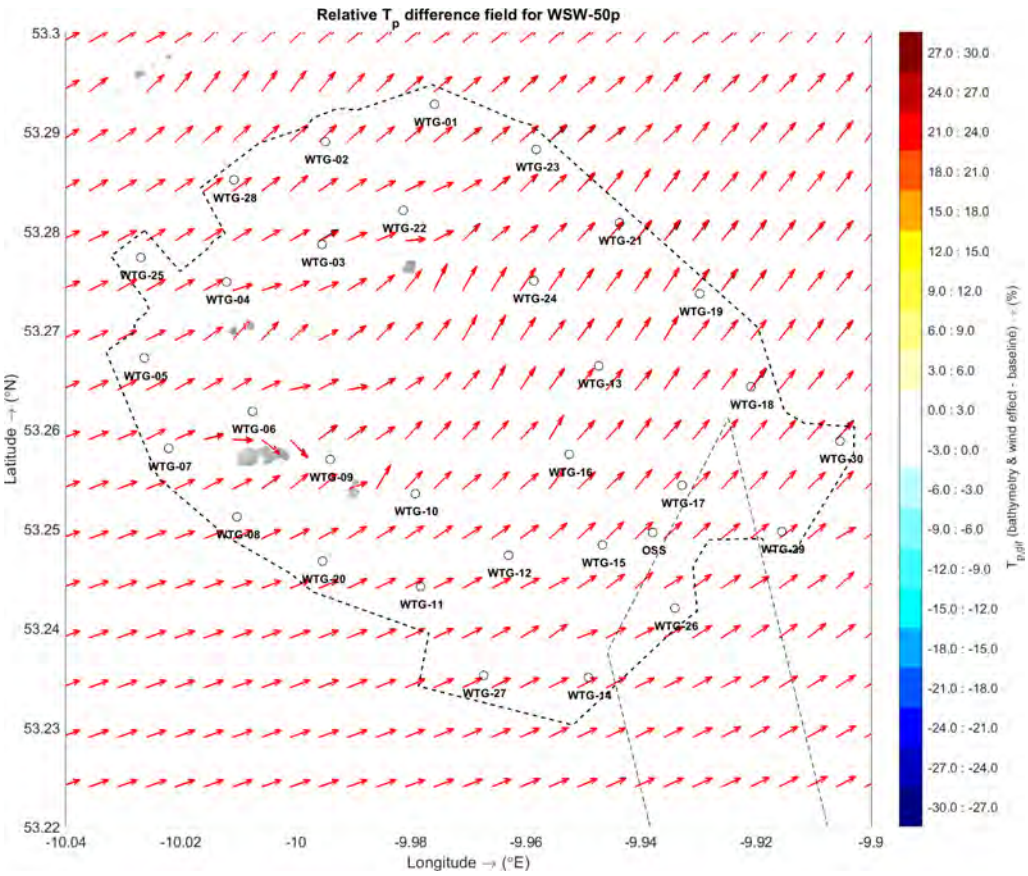

Relative T_p difference field for WSW-50p
Latitude → (°N)
Longitude → (°E)
$T_{p,dif}$ (bathymetry & wind effect - baseline) → (%)
27.0 : 30.0
24.0 : 27.0
21.0 : 24.0
18.0 : 21.0
15.0 : 18.0
12.0 : 15.0
9.0 : 12.0
6.0 : 9.0
3.0 : 6.0
0.0 : 3.0
-3.0 : 0.0
-6.0 : -3.0
-9.0 : -6.0
-12.0 : -9.0
-15.0 : -12.0
-18.0 : -15.0
-21.0 : -18.0
-24.0 : -21.0
-27.0 : -24.0
-30.0 : -27.0

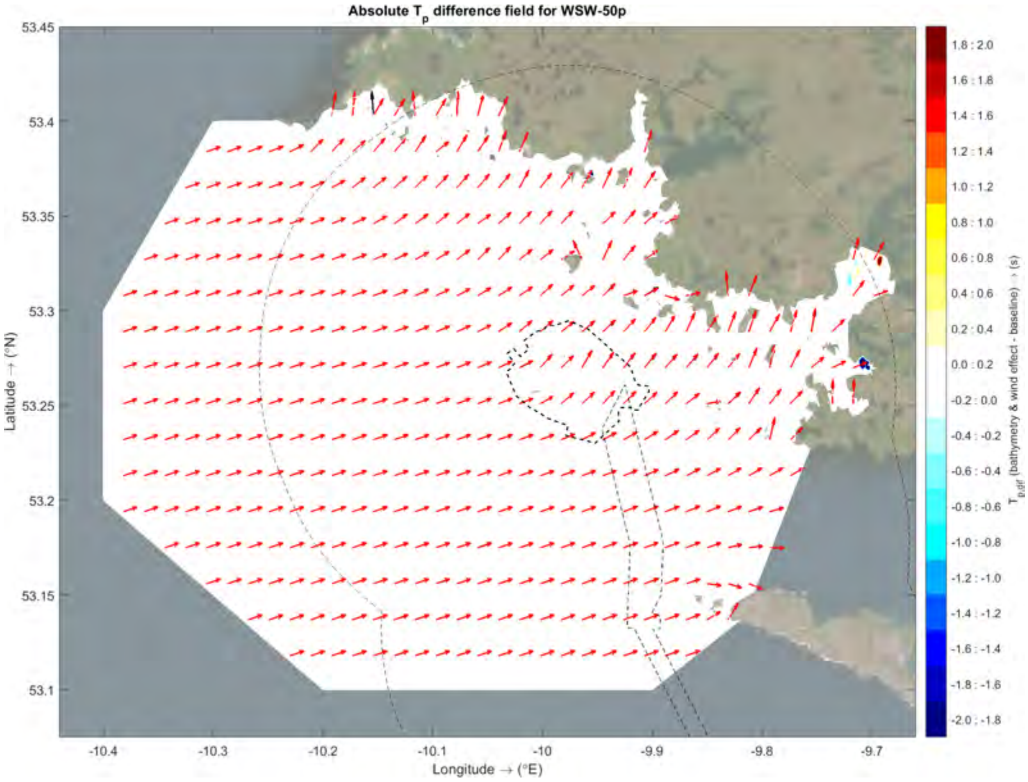
Absolute T_p difference field for WSW-50p
Latitude → (°N)
Longitude → (°E)
$T_{p,diff}$ (bathymetry & wind effect - baseline) → (s)

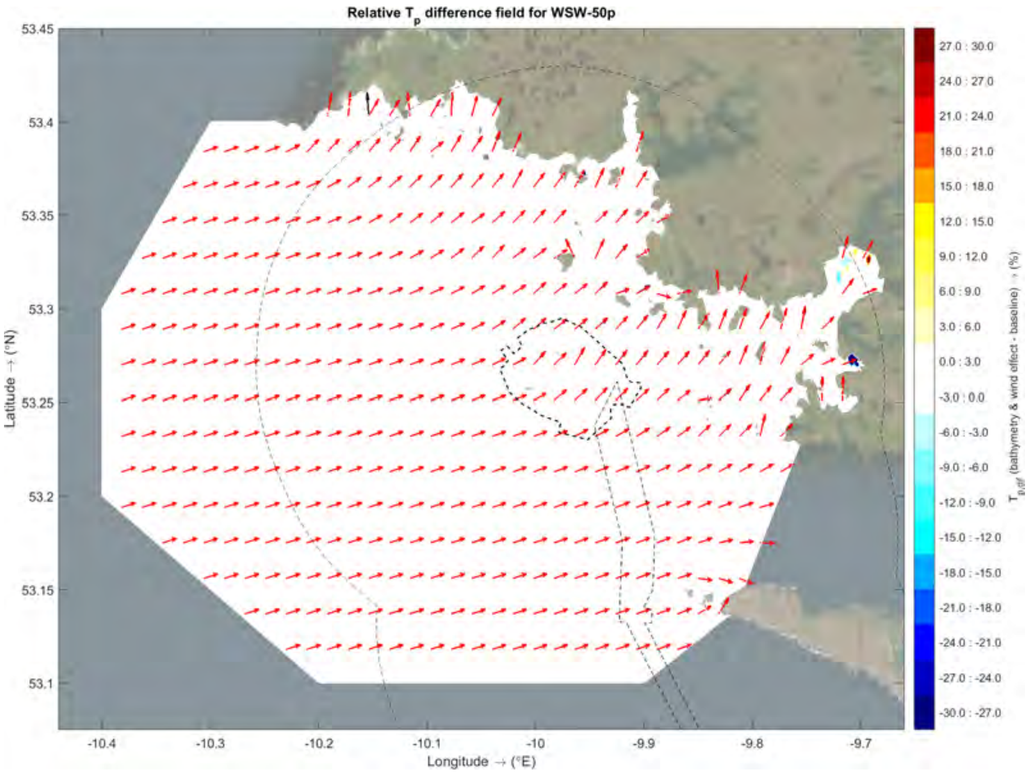
Relative T_p difference field for WSW-50p
Latitude → (°N)
Longitude → (°E)
$T_{p,diff}$ (bathymetry & wind effect - baseline) → (%)

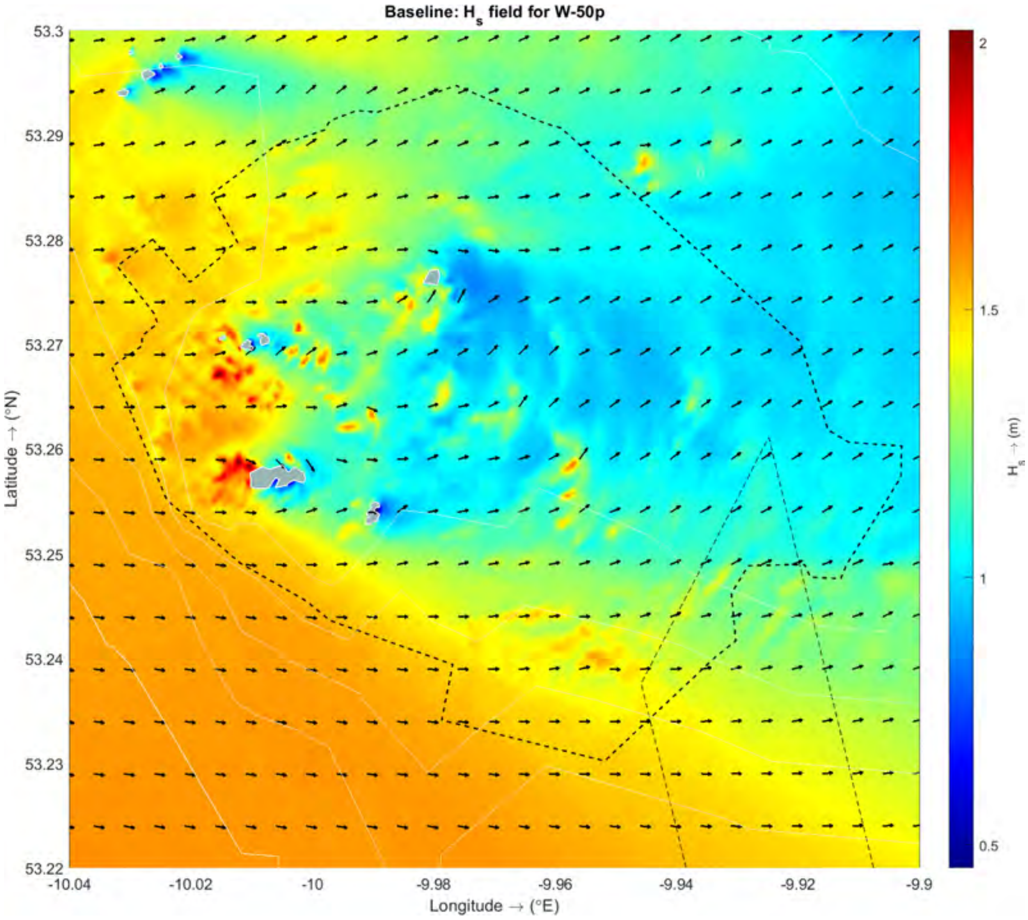
Baseline: H_s field for W-50p
53.3
53.29
53.28
53.27
53.26
53.25
53.24
53.23
53.22
Latitude → (°N)
-10.04
-10.02
-10
-9.98
-9.96
-9.94
-9.92
-9.9
Longitude → (°E)
2
1.5
1
0.5
H_s → (m)

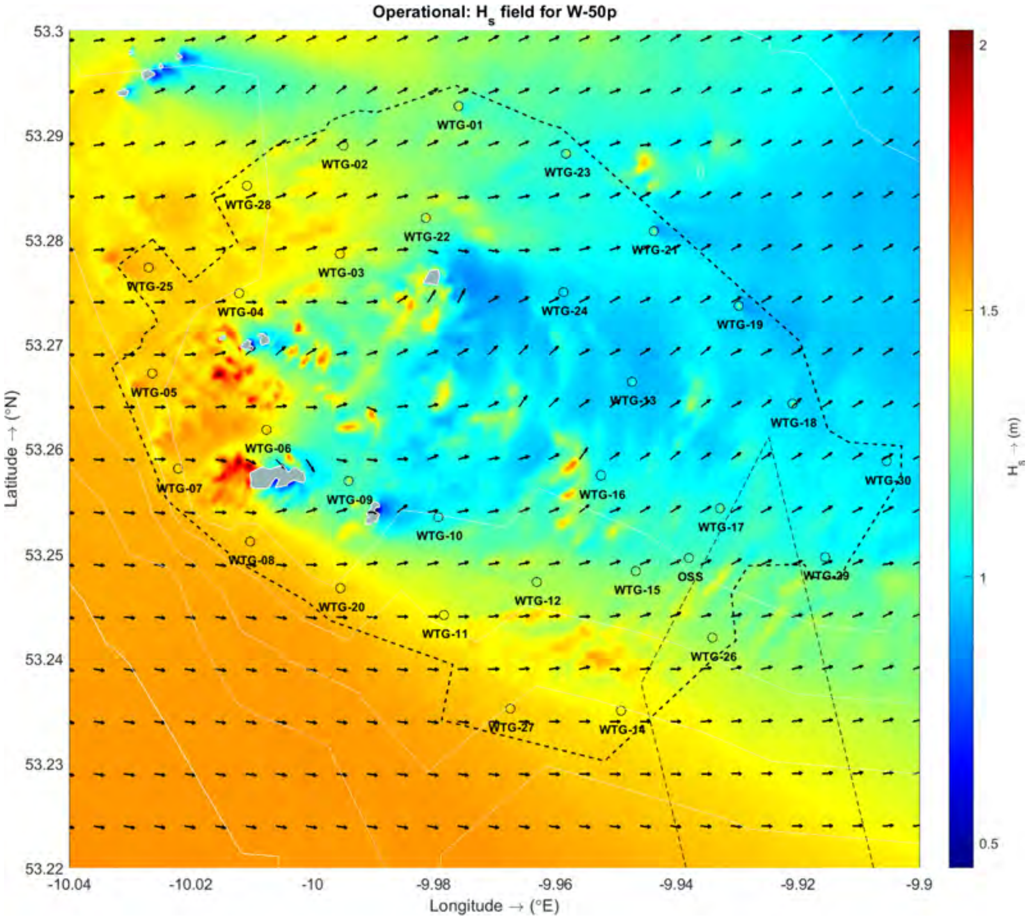
Operational: H_s field for W-50p
Latitude → (°N)
Longitude → (°E)
H_s → (m)
WTG-01
WTG-02
WTG-03
WTG-04
WTG-05
WTG-06
WTG-07
WTG-08
WTG-09
WTG-10
WTG-11
WTG-12
WTG-13
WTG-14
WTG-15
WTG-16
WTG-17
WTG-18
WTG-19
WTG-20
WTG-21
WTG-22
WTG-23
WTG-24
WTG-25
WTG-26
WTG-27
WTG-28
WTG-29
WTG-30
OSS

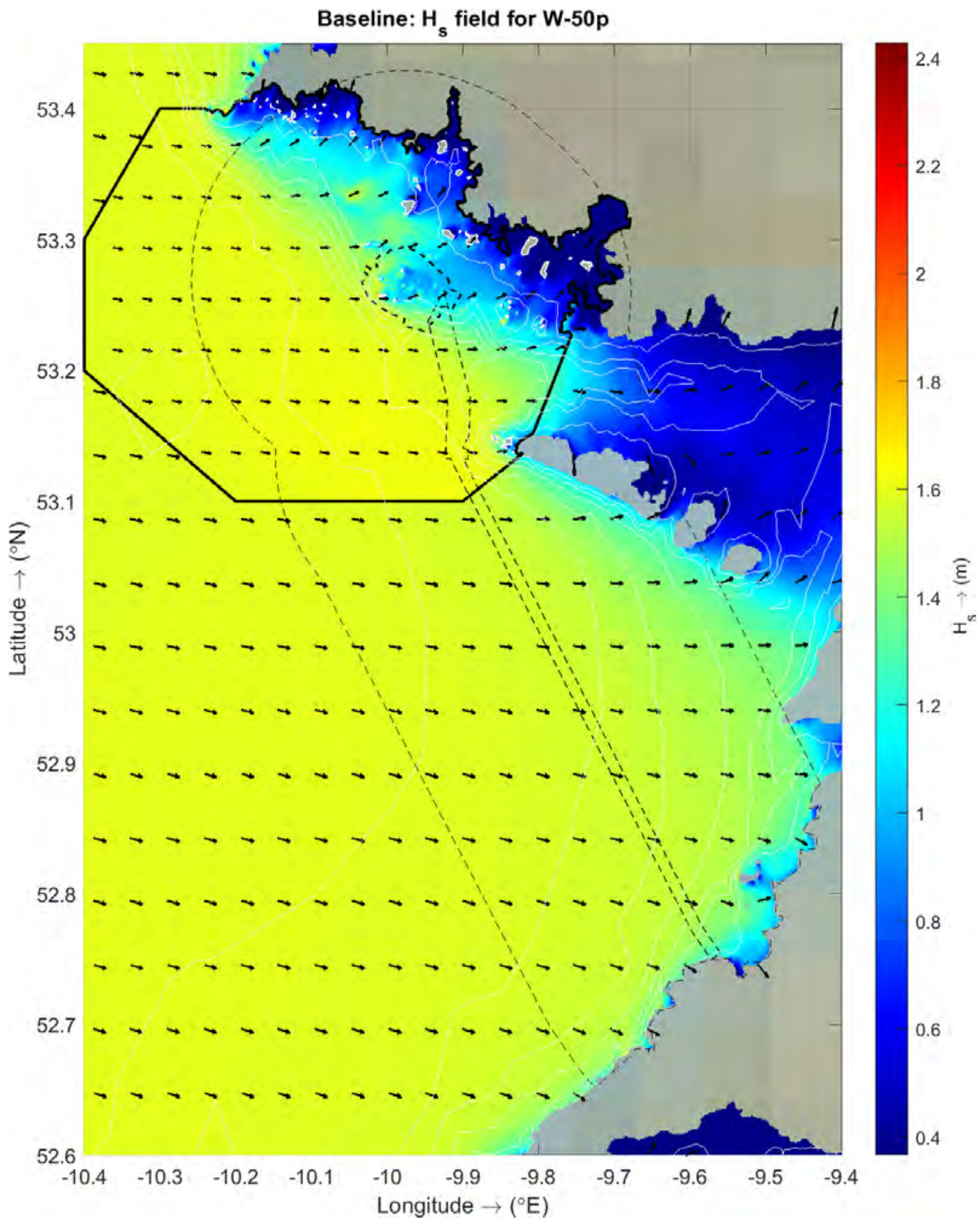
Baseline: H_s field for W-50p
53.4
53.3
53.2
53.1
53
52.9
52.8
52.7
52.6
Latitude → (°N)
-10.4
-10.3
-10.2
-10.1
-10
-9.9
-9.8
-9.7
-9.6
-9.5
-9.4
Longitude → (°E)
2.4
2.2
2
1.8
1.6
1.4
1.2
1
0.8
0.6
0.4
H_s → (m)

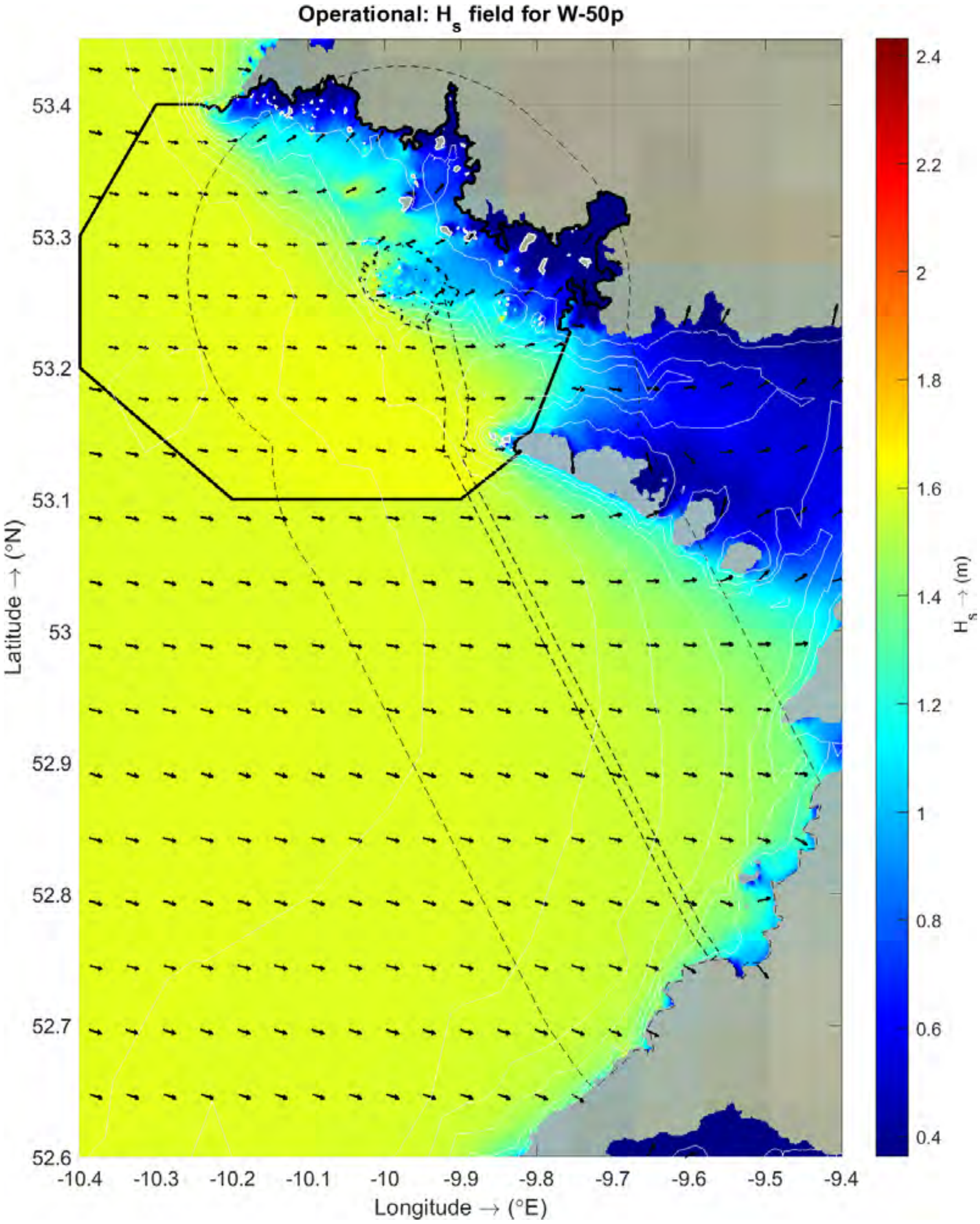
Operational: H_s field for W-50p
53.4
53.3
53.2
53.1
53
52.9
52.8
52.7
52.6
Latitude → (°N)
-10.4
-10.3
-10.2
-10.1
-10
-9.9
-9.8
-9.7
-9.6
-9.5
-9.4
Longitude → (°E)
2.4
2.2
2
1.8
1.6
1.4
1.2
1
0.8
0.6
0.4
H_s → (m)

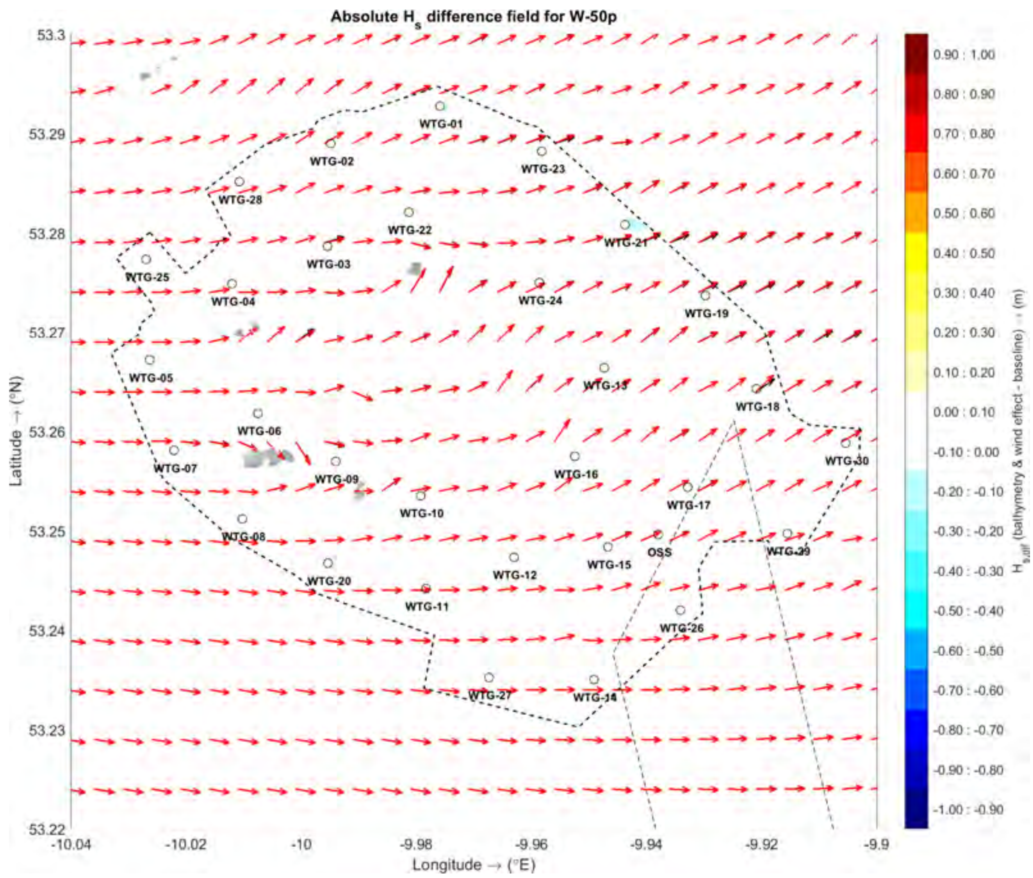
Absolute Hs difference field for W-50p
Latitude → (°N)
Longitude → (°E)
WTG-01
WTG-02
WTG-03
WTG-04
WTG-05
WTG-06
WTG-07
WTG-08
WTG-09
WTG-10
WTG-11
WTG-12
WTG-13
WTG-14
WTG-15
WTG-16
WTG-17
WTG-18
WTG-19
WTG-20
WTG-21
WTG-22
WTG-23
WTG-24
WTG-25
WTG-26
WTG-27
WTG-28
WTG-29
WTG-30
OSS
0.90 : 1.00
0.80 : 0.90
0.70 : 0.80
0.60 : 0.70
0.50 : 0.60
0.40 : 0.50
0.30 : 0.40
0.20 : 0.30
0.10 : 0.20
0.00 : 0.10
-0.10 : 0.00
-0.20 : -0.10
-0.30 : -0.20
-0.40 : -0.30
-0.50 : -0.40
-0.60 : -0.50
-0.70 : -0.60
-0.80 : -0.70
-0.90 : -0.80
-1.00 : -0.90
Hs,diff (bathymetry & wind effect - baseline) → (m)

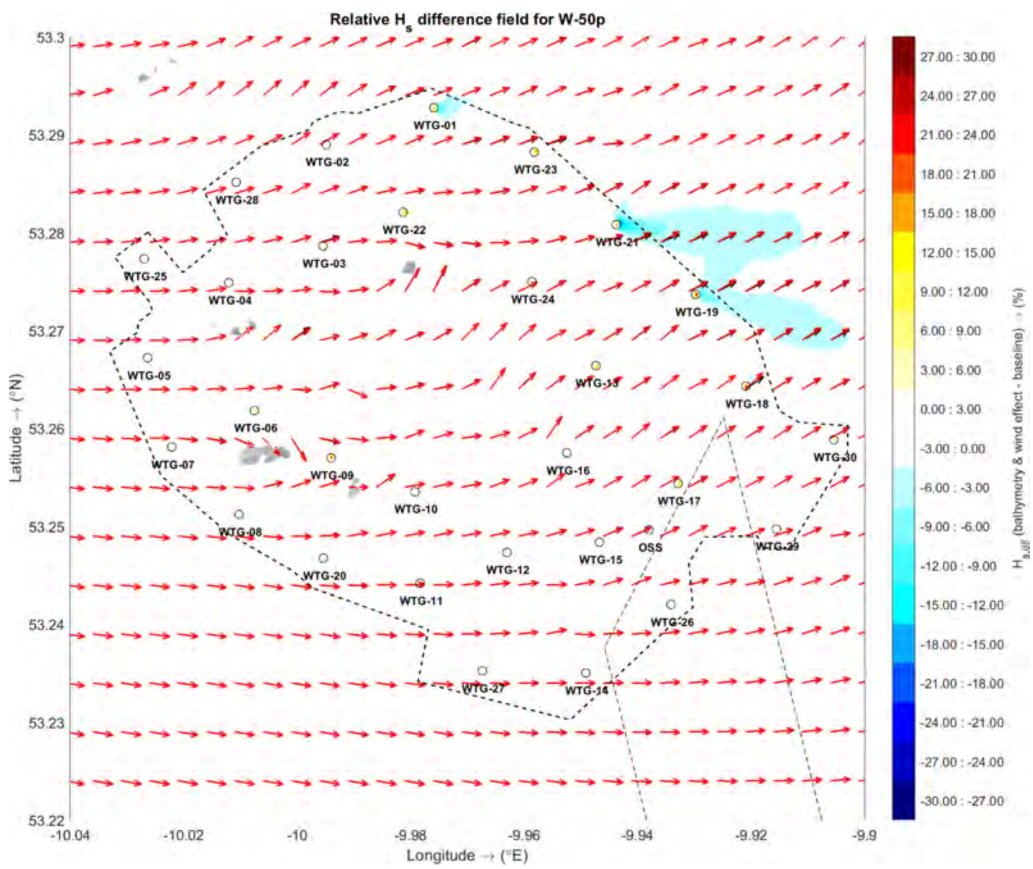
Relative Hs difference field for W-50p
Latitude → (°N)
Longitude → (°E)
27.00 : 30.00
24.00 : 27.00
21.00 : 24.00
18.00 : 21.00
15.00 : 18.00
12.00 : 15.00
9.00 : 12.00
6.00 : 9.00
3.00 : 6.00
0.00 : 3.00
-3.00 : 0.00
-6.00 : -3.00
-9.00 : -6.00
-12.00 : -9.00
-15.00 : -12.00
-18.00 : -15.00
-21.00 : -18.00
-24.00 : -21.00
-27.00 : -24.00
-30.00 : -27.00
Hs,diff (bathymetry & wind effect - baseline) → (%)

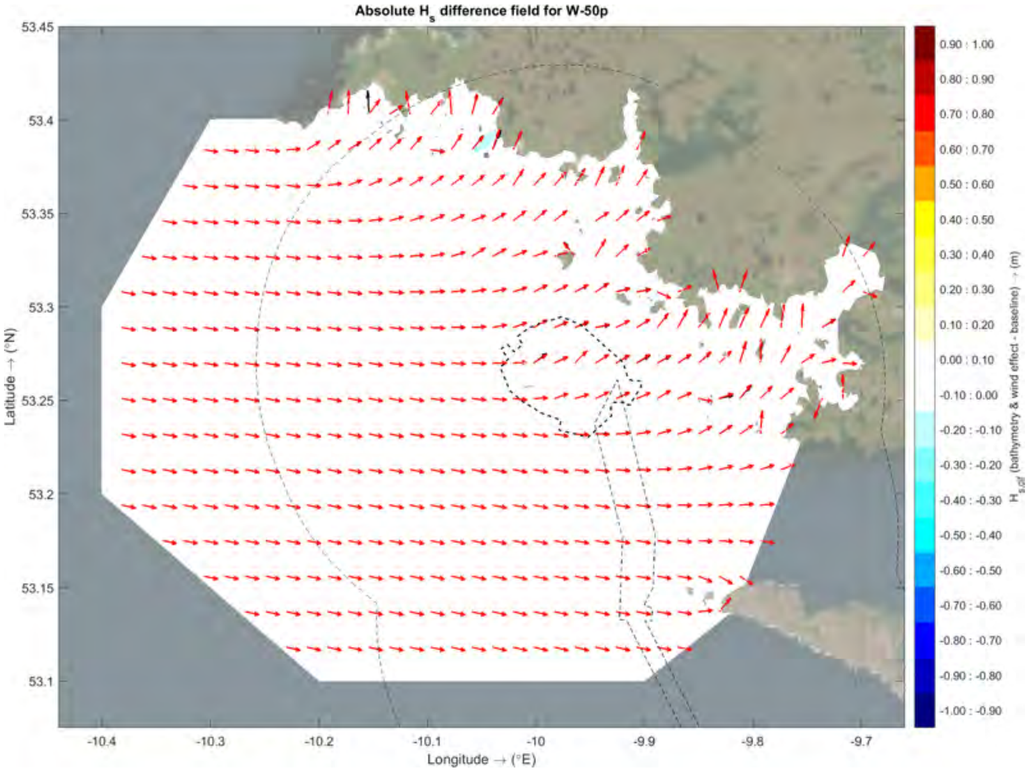
Absolute H$_s$ difference field for W-50p
Latitude → (°N)
Longitude → (°E)
H$_{s,dif}$ (bathymetry & wind effect - baseline) → (m)
0.90 : 1.00
0.80 : 0.90
0.70 : 0.80
0.60 : 0.70
0.50 : 0.60
0.40 : 0.50
0.30 : 0.40
0.20 : 0.30
0.10 : 0.20
0.00 : 0.10
-0.10 : 0.00
-0.20 : -0.10
-0.30 : -0.20
-0.40 : -0.30
-0.50 : -0.40
-0.60 : -0.50
-0.70 : -0.60
-0.80 : -0.70
-0.90 : -0.80
-1.00 : -0.90

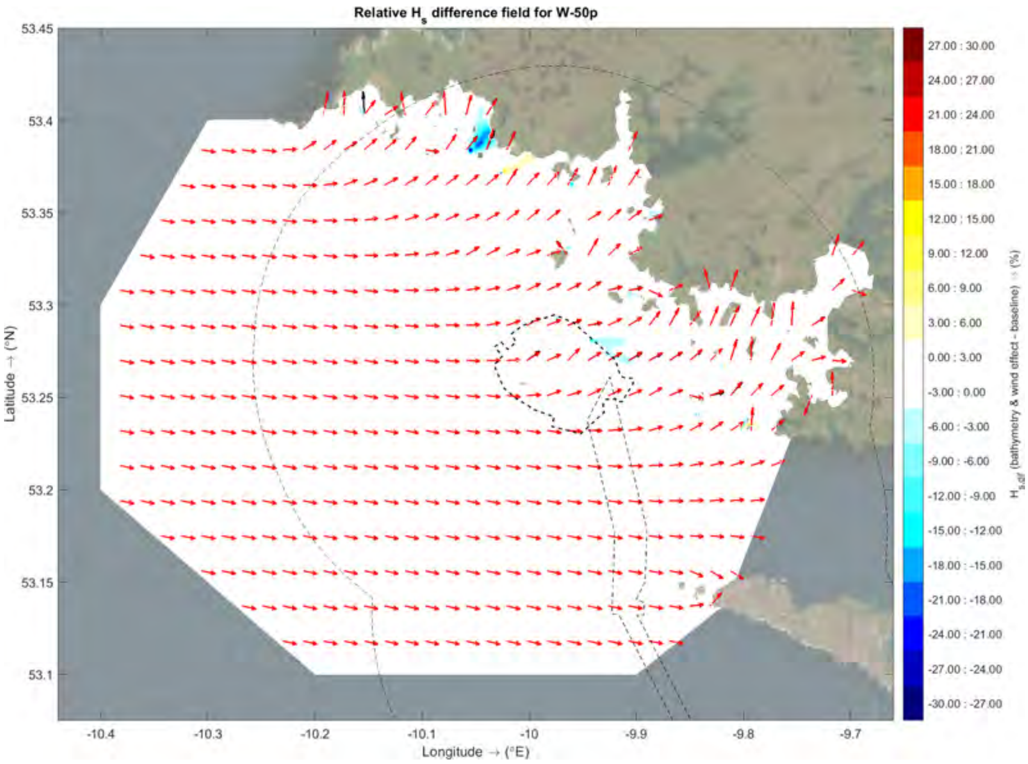
Relative H$_s$ difference field for W-50p
Latitude → (°N)
Longitude → (°E)
H$_{s,dif}$ (bathymetry & wind effect - baseline) → (%)
27.00 : 30.00
24.00 : 27.00
21.00 : 24.00
18.00 : 21.00
15.00 : 18.00
12.00 : 15.00
9.00 : 12.00
6.00 : 9.00
3.00 : 6.00
0.00 : 3.00
-3.00 : 0.00
-6.00 : -3.00
-9.00 : -6.00
-12.00 : -9.00
-15.00 : -12.00
-18.00 : -15.00
-21.00 : -18.00
-24.00 : -21.00
-27.00 : -24.00
-30.00 : -27.00

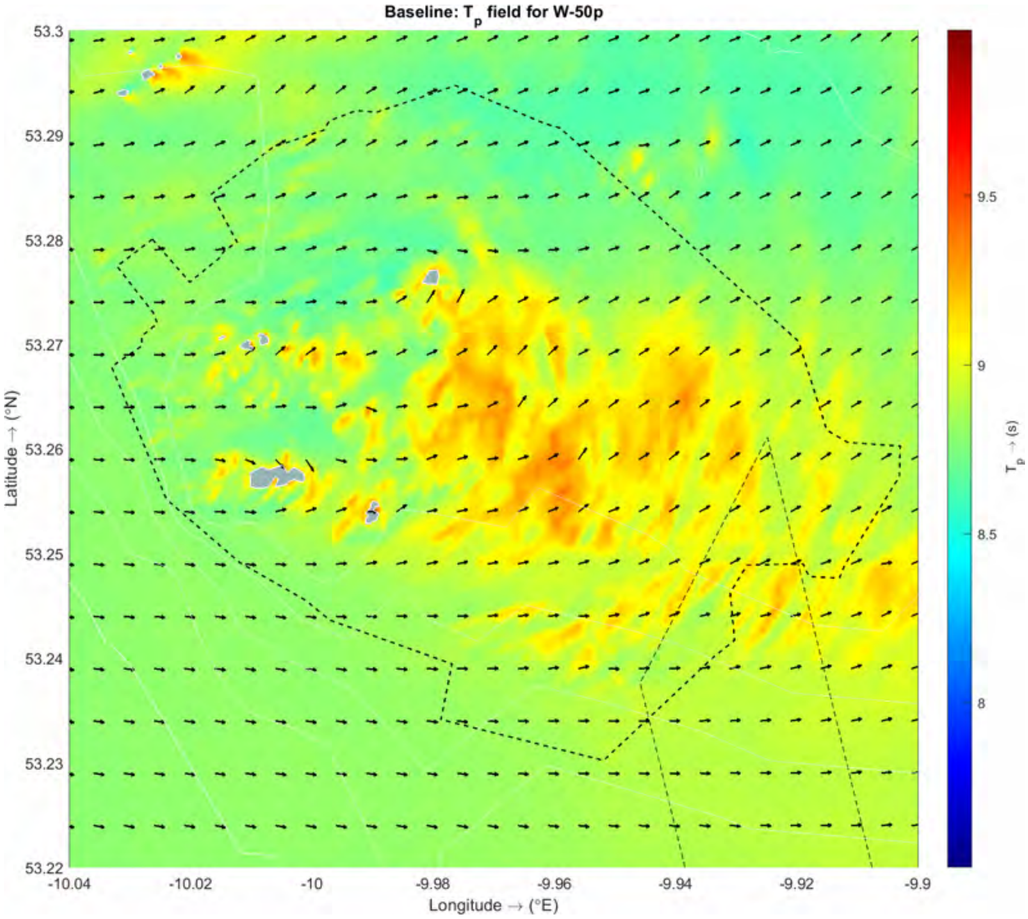
Baseline: T_p field for W-50p
53.3
53.29
53.28
53.27
53.26
53.25
53.24
53.23
53.22
Latitude → (°N)
-10.04
-10.02
-10
-9.98
-9.96
-9.94
-9.92
-9.9
Longitude → (°E)
9.5
9
8.5
8
T_p → (s)

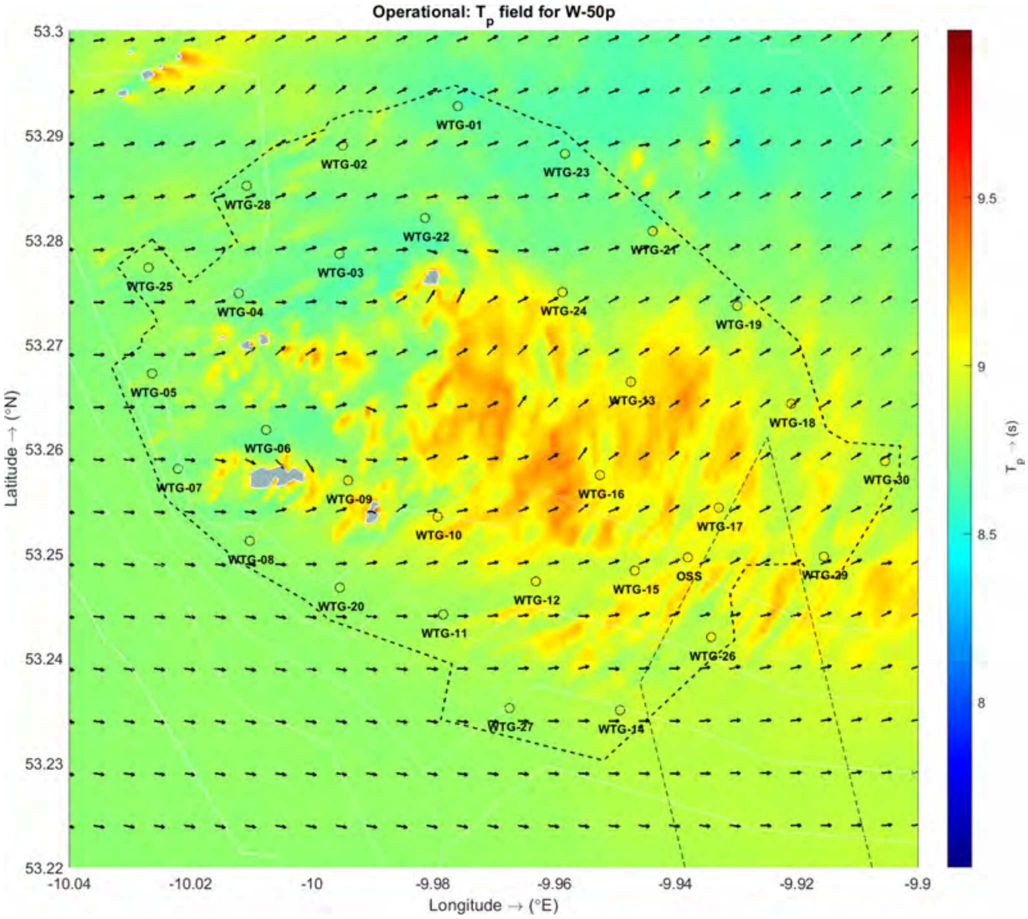
Operational: T_p field for W-50p
Latitude → (°N)
Longitude → (°E)
T_p → (s)
53.3
53.29
53.28
53.27
53.26
53.25
53.24
53.23
53.22
-10.04
-10.02
-10
-9.98
-9.96
-9.94
-9.92
-9.9
9.5
9
8.5
8
WTG-01
WTG-02
WTG-23
WTG-28
WTG-22
WTG-21
WTG-25
WTG-03
WTG-04
WTG-24
WTG-19
WTG-05
WTG-13
WTG-18
WTG-06
WTG-07
WTG-09
WTG-16
WTG-30
WTG-10
WTG-17
WTG-08
OSS
WTG-29
WTG-20
WTG-12
WTG-15
WTG-11
WTG-26
WTG-27
WTG-14

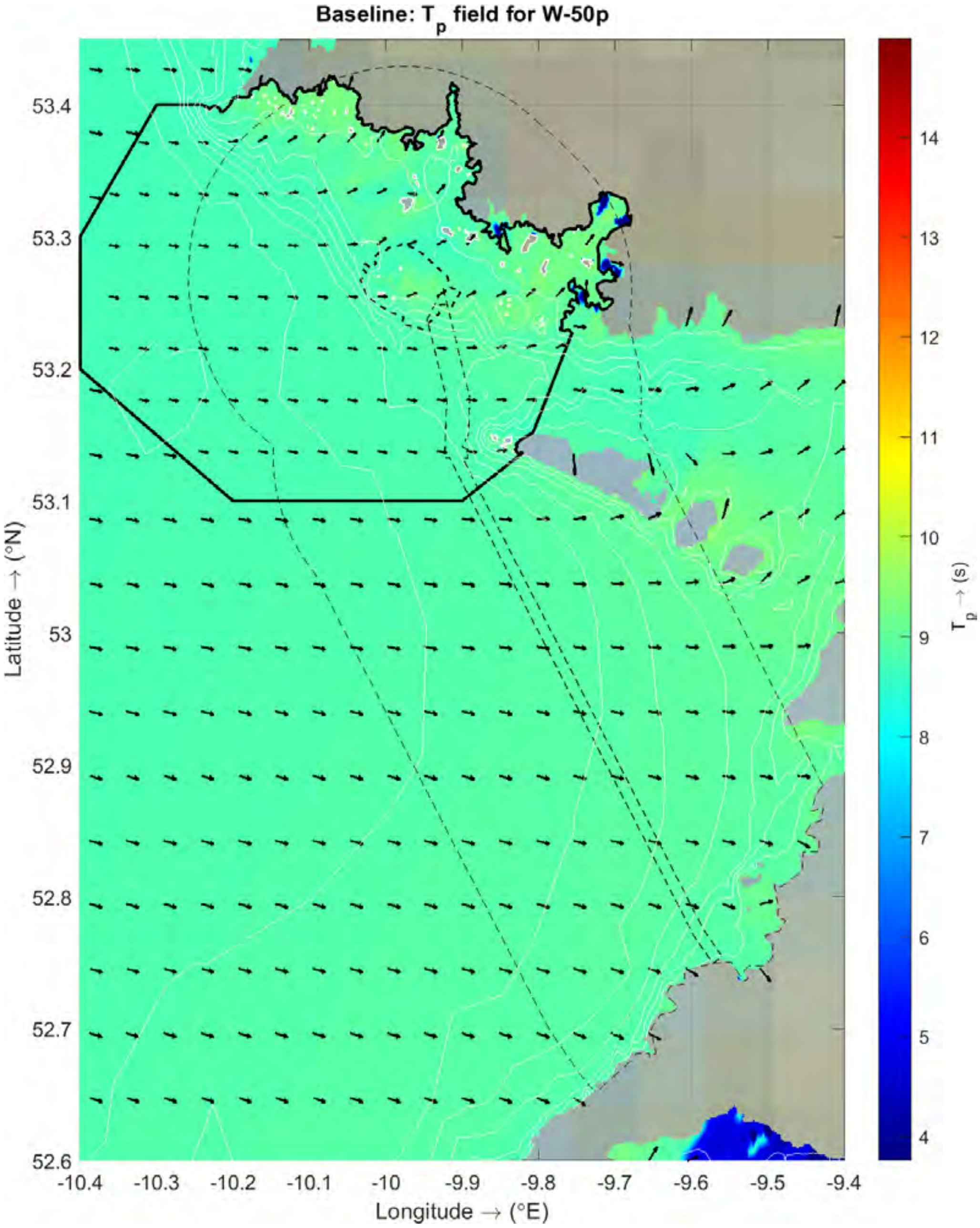
Baseline: T_p field for W-50p
53.4
53.3
53.2
53.1
53
52.9
52.8
52.7
52.6
Latitude → (°N)
-10.4
-10.3
-10.2
-10.1
-10
-9.9
-9.8
-9.7
-9.6
-9.5
-9.4
Longitude → (°E)
14
13
12
11
10
9
8
7
6
5
4
T_p → (s)

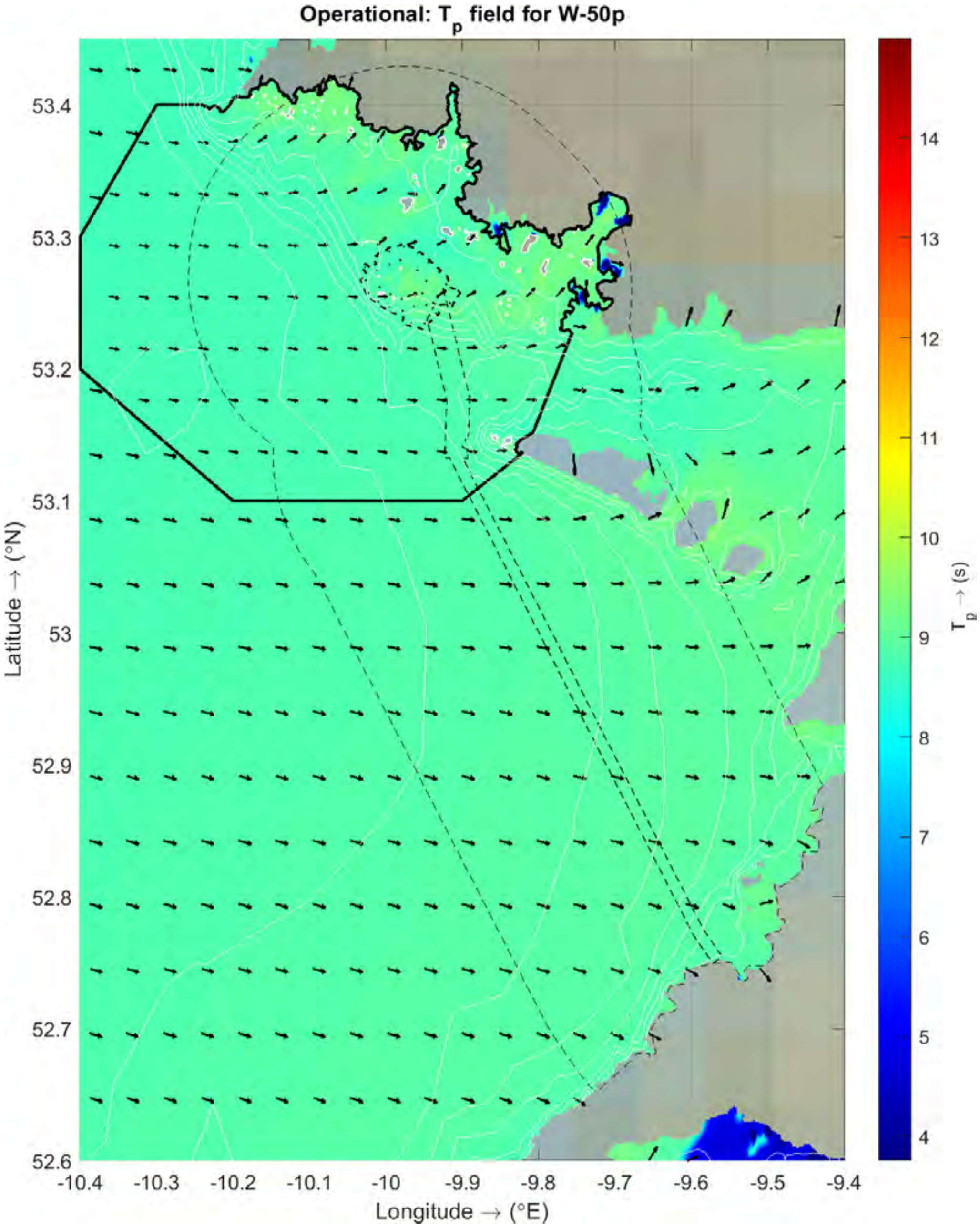
Operational: T_p field for W-50p
Latitude → (°N)
Longitude → (°E)
T_p → (s)
53.4
53.3
53.2
53.1
53
52.9
52.8
52.7
52.6
-10.4
-10.3
-10.2
-10.1
-10
-9.9
-9.8
-9.7
-9.6
-9.5
-9.4
14
13
12
11
10
9
8
7
6
5
4

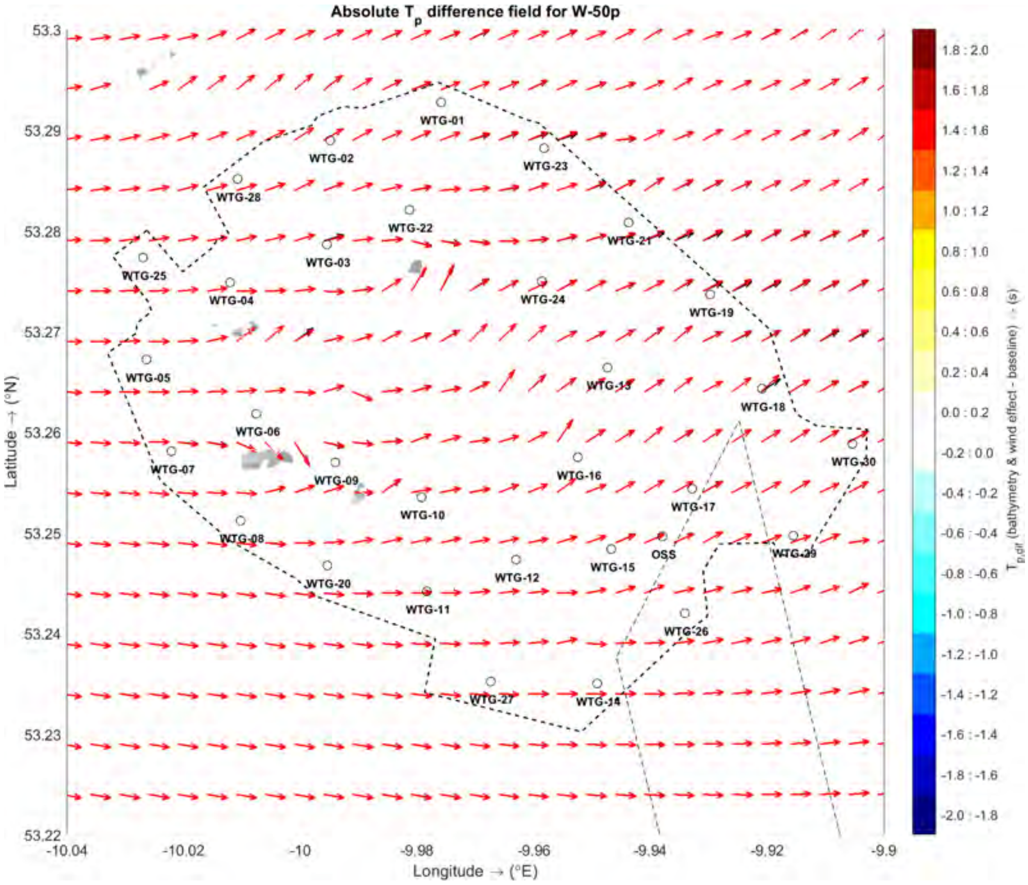

Absolute T_p difference field for W-50p
Latitude → (°N)
Longitude → (°E)
$T_{p,dif}$ (bathymetry & wind effect - baseline) → (s)
1.8 : 2.0
1.6 : 1.8
1.4 : 1.6
1.2 : 1.4
1.0 : 1.2
0.8 : 1.0
0.6 : 0.8
0.4 : 0.6
0.2 : 0.4
0.0 : 0.2
-0.2 : 0.0
-0.4 : -0.2
-0.6 : -0.4
-0.8 : -0.6
-1.0 : -0.8
-1.2 : -1.0
-1.4 : -1.2
-1.6 : -1.4
-1.8 : -1.6
-2.0 : -1.8
WTG-01
WTG-02
WTG-03
WTG-04
WTG-05
WTG-06
WTG-07
WTG-08
WTG-09
WTG-10
WTG-11
WTG-12
WTG-13
WTG-14
WTG-15
WTG-16
WTG-17
WTG-18
WTG-19
WTG-20
WTG-21
WTG-22
WTG-23
WTG-24
WTG-25
WTG-26
WTG-27
WTG-28
WTG-29
WTG-30
OSS

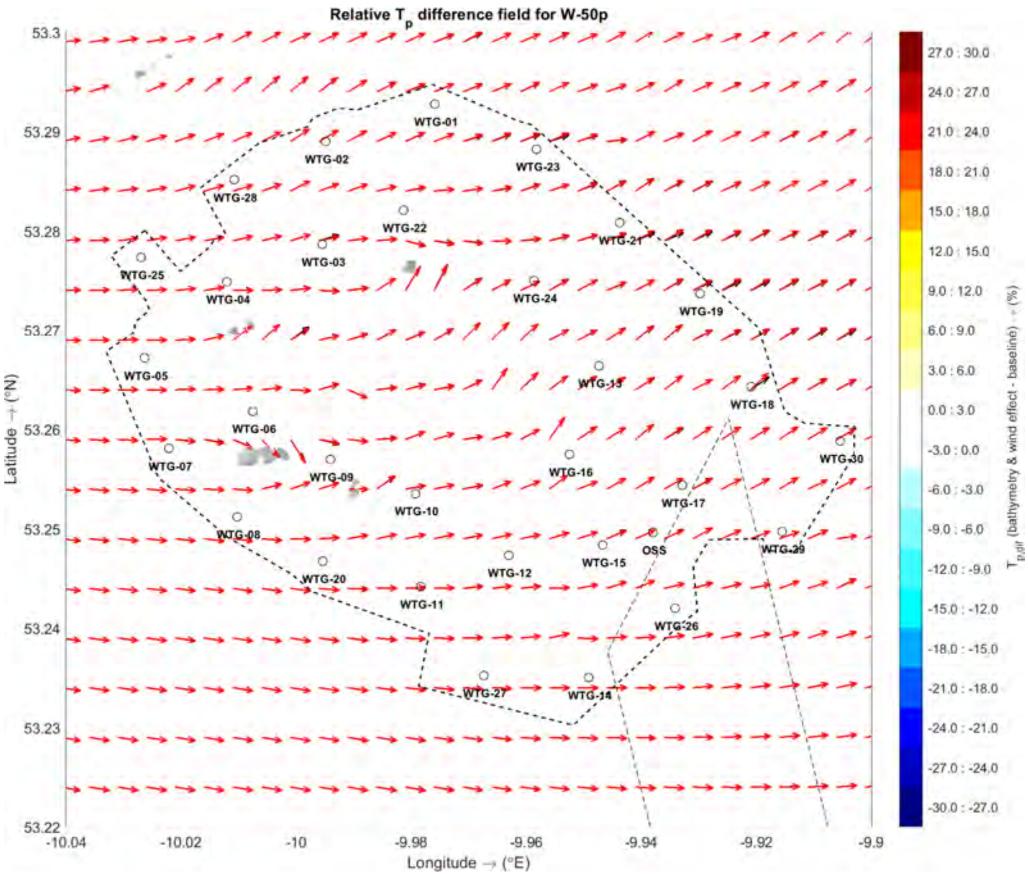

Relative T_p difference field for W-50p
Latitude → (°N)
Longitude → (°E)
$T_{p,dif}$ (bathymetry & wind effect - baseline) → (%)
27.0 : 30.0
24.0 : 27.0
21.0 : 24.0
18.0 : 21.0
15.0 : 18.0
12.0 : 15.0
9.0 : 12.0
6.0 : 9.0
3.0 : 6.0
0.0 : 3.0
-3.0 : 0.0
-6.0 : -3.0
-9.0 : -6.0
-12.0 : -9.0
-15.0 : -12.0
-18.0 : -15.0
-21.0 : -18.0
-24.0 : -21.0
-27.0 : -24.0
-30.0 : -27.0

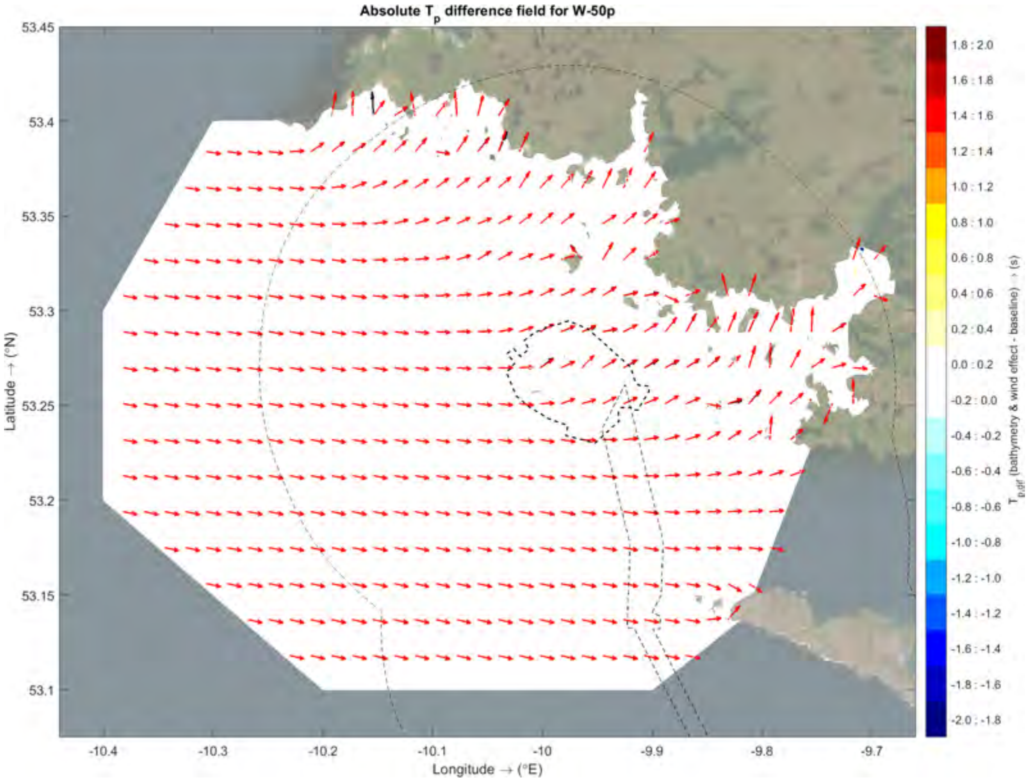
Absolute T_p difference field for W-50p
Latitude → (°N)
Longitude → (°E)
$T_{p,diff}$ (bathymetry & wind effect - baseline) → (s)
1.8 : 2.0
1.6 : 1.8
1.4 : 1.6
1.2 : 1.4
1.0 : 1.2
0.8 : 1.0
0.6 : 0.8
0.4 : 0.6
0.2 : 0.4
0.0 : 0.2
-0.2 : 0.0
-0.4 : -0.2
-0.6 : -0.4
-0.8 : -0.6
-1.0 : -0.8
-1.2 : -1.0
-1.4 : -1.2
-1.6 : -1.4
-1.8 : -1.6
-2.0 : -1.8

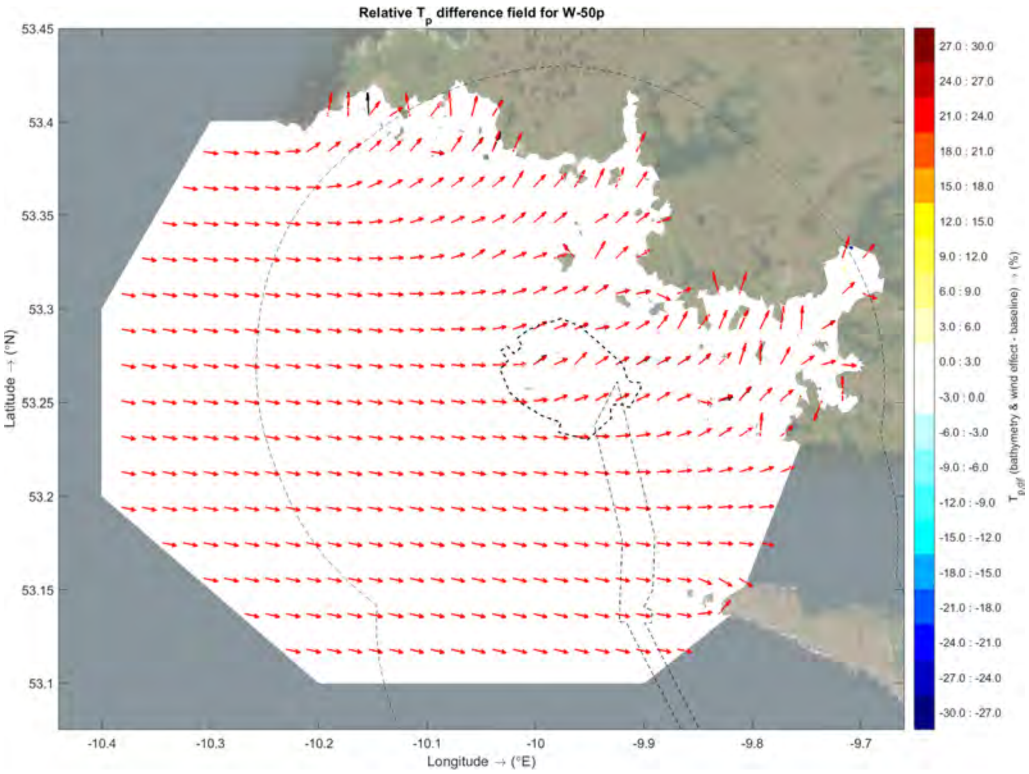
Relative T_p difference field for W-50p
Latitude → (°N)
Longitude → (°E)
$T_{p,diff}$ (bathymetry & wind effect - baseline) → (%)
27.0 : 30.0
24.0 : 27.0
21.0 : 24.0
18.0 : 21.0
15.0 : 18.0
12.0 : 15.0
9.0 : 12.0
6.0 : 9.0
3.0 : 6.0
0.0 : 3.0
-3.0 : 0.0
-6.0 : -3.0
-9.0 : -6.0
-12.0 : -9.0
-15.0 : -12.0
-18.0 : -15.0
-21.0 : -18.0
-24.0 : -21.0
-27.0 : -24.0
-30.0 : -27.0

E.2 90th percentile

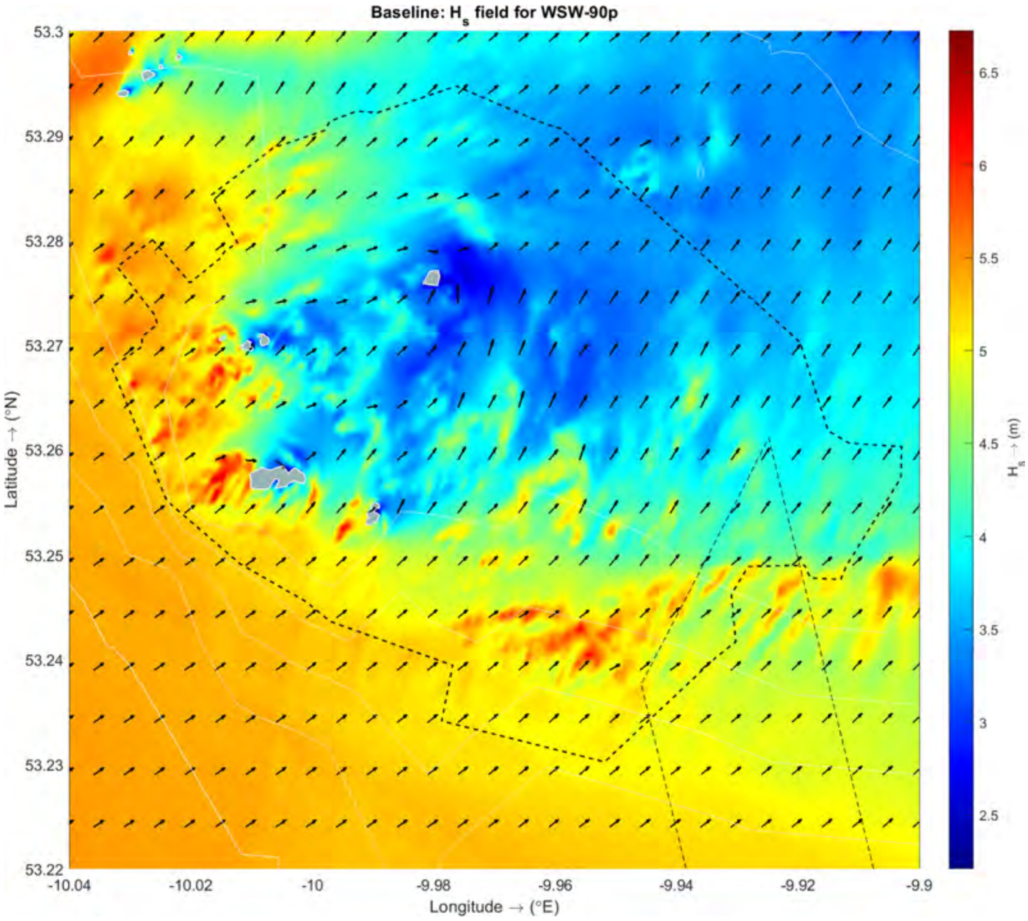

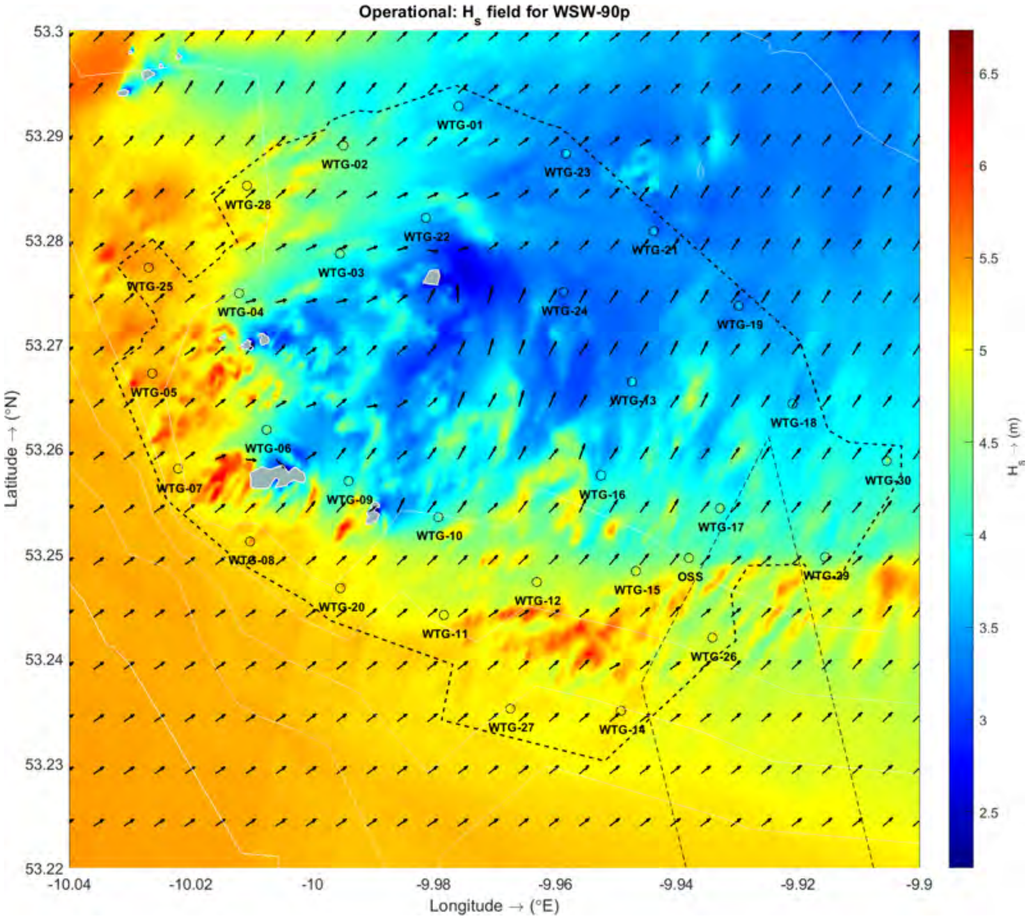

Operational: Hs field for WSW-90p
WTG-01
WTG-02
WTG-23
WTG-28
WTG-22
WTG-21
WTG-03
WTG-25
WTG-04
WTG-24
WTG-19
WTG-05
WTG-13
WTG-18
WTG-06
WTG-30
WTG-07
WTG-16
WTG-09
WTG-17
WTG-10
WTG-08
OSS
WTG-29
WTG-15
WTG-20
WTG-12
WTG-11
WTG-26
WTG-27
WTG-14
Latitude → (°N)
Longitude → (°E)
Hs → (m)

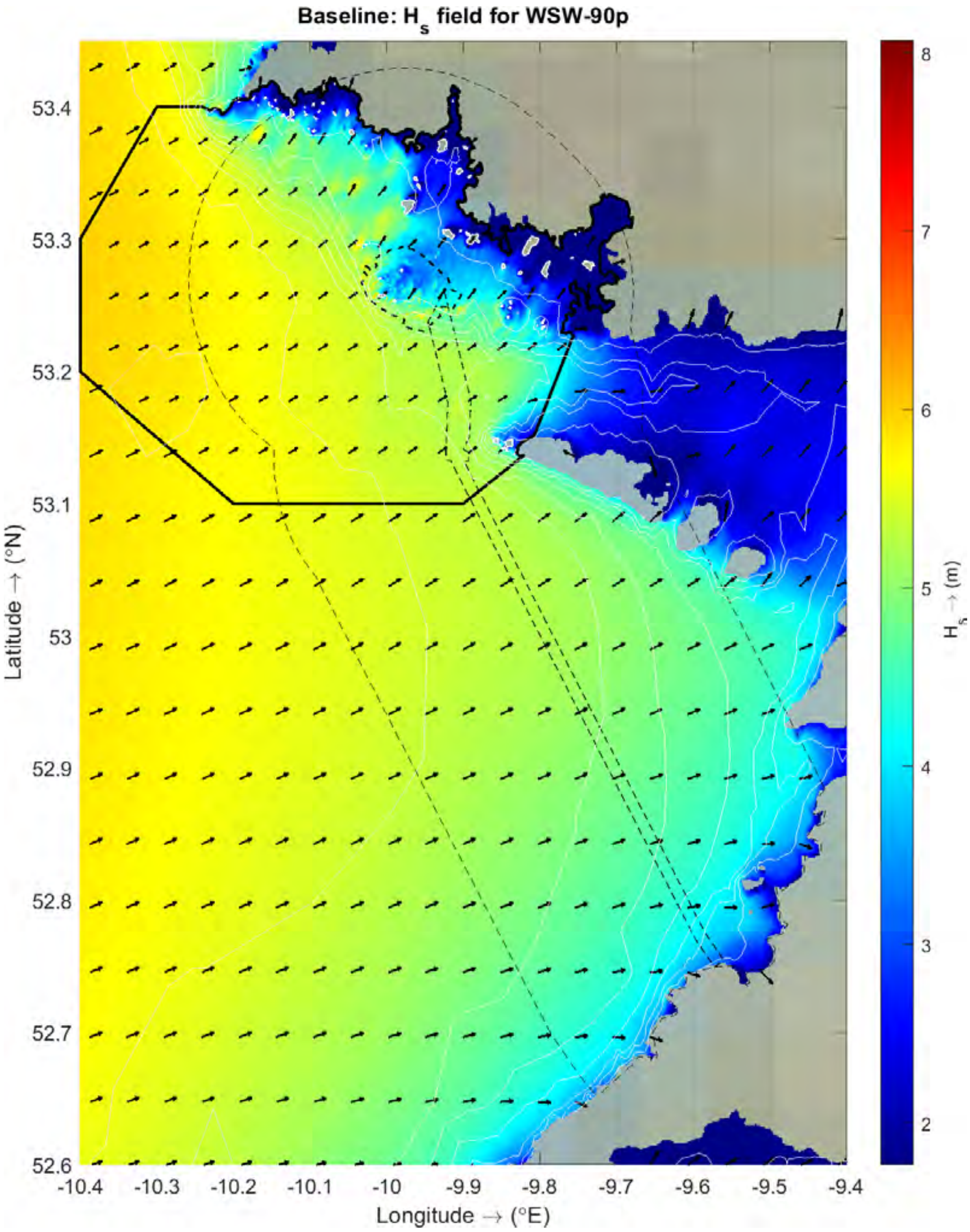
Baseline: H
s
field for WSW-90p
53.4
53.3
53.2
53.1
53
52.9
52.8
52.7
52.6
Latitude → (°N)
-10.4
-10.3
-10.2
-10.1
-10
-9.9
-9.8
-9.7
-9.6
-9.5
-9.4
Longitude → (°E)
8
7
6
5
4
3
2
H
s
→ (m)

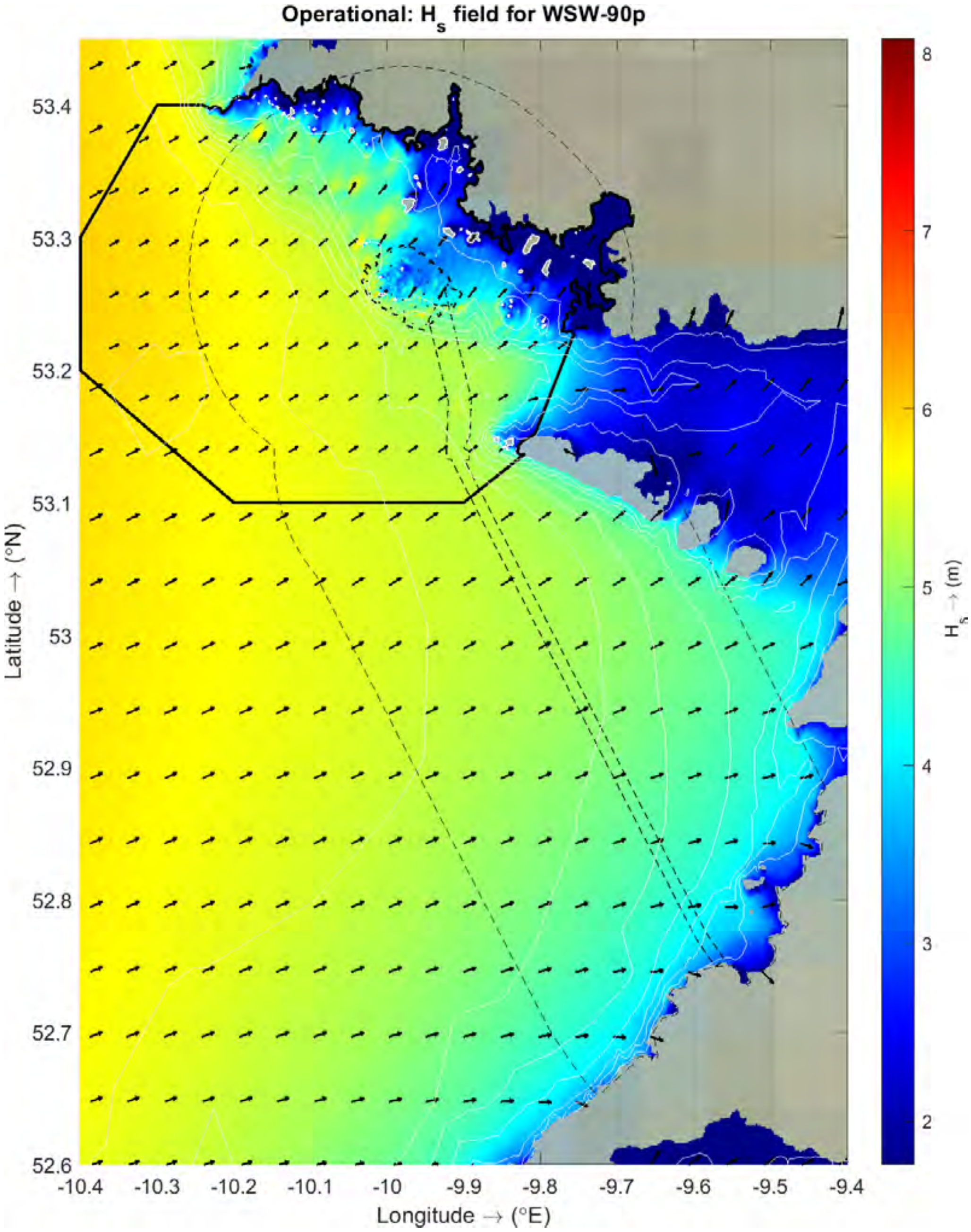
Operational: H_s field for WSW-90p
Latitude → (°N)
Longitude → (°E)
H_s → (m)
53.4
53.3
53.2
53.1
53
52.9
52.8
52.7
52.6
-10.4
-10.3
-10.2
-10.1
-10
-9.9
-9.8
-9.7
-9.6
-9.5
-9.4
8
7
6
5
4
3
2

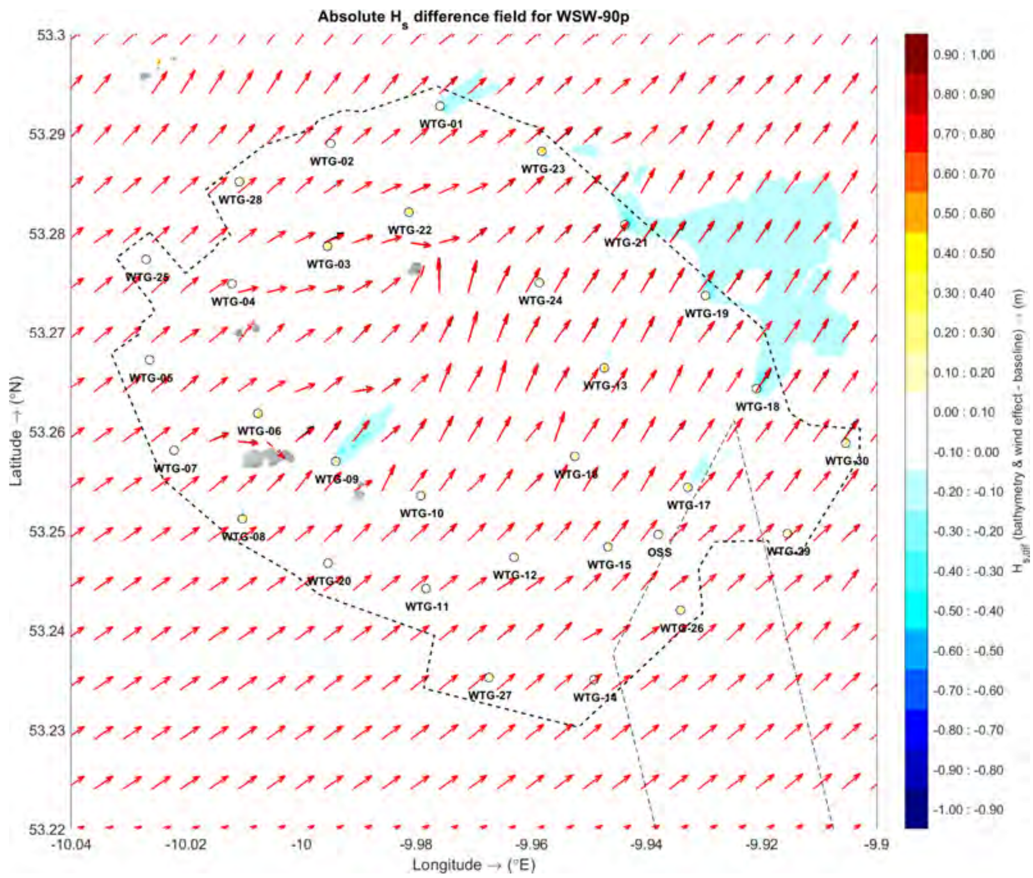
Absolute H_s difference field for WSW-90p
Latitude → (°N)
Longitude → (°E)
$H_{s,diff}$ (bathymetry & wind effect - baseline) → (m)
0.90 : 1.00
0.80 : 0.90
0.70 : 0.80
0.60 : 0.70
0.50 : 0.60
0.40 : 0.50
0.30 : 0.40
0.20 : 0.30
0.10 : 0.20
0.00 : 0.10
-0.10 : 0.00
-0.20 : -0.10
-0.30 : -0.20
-0.40 : -0.30
-0.50 : -0.40
-0.60 : -0.50
-0.70 : -0.60
-0.80 : -0.70
-0.90 : -0.80
-1.00 : -0.90
OSS

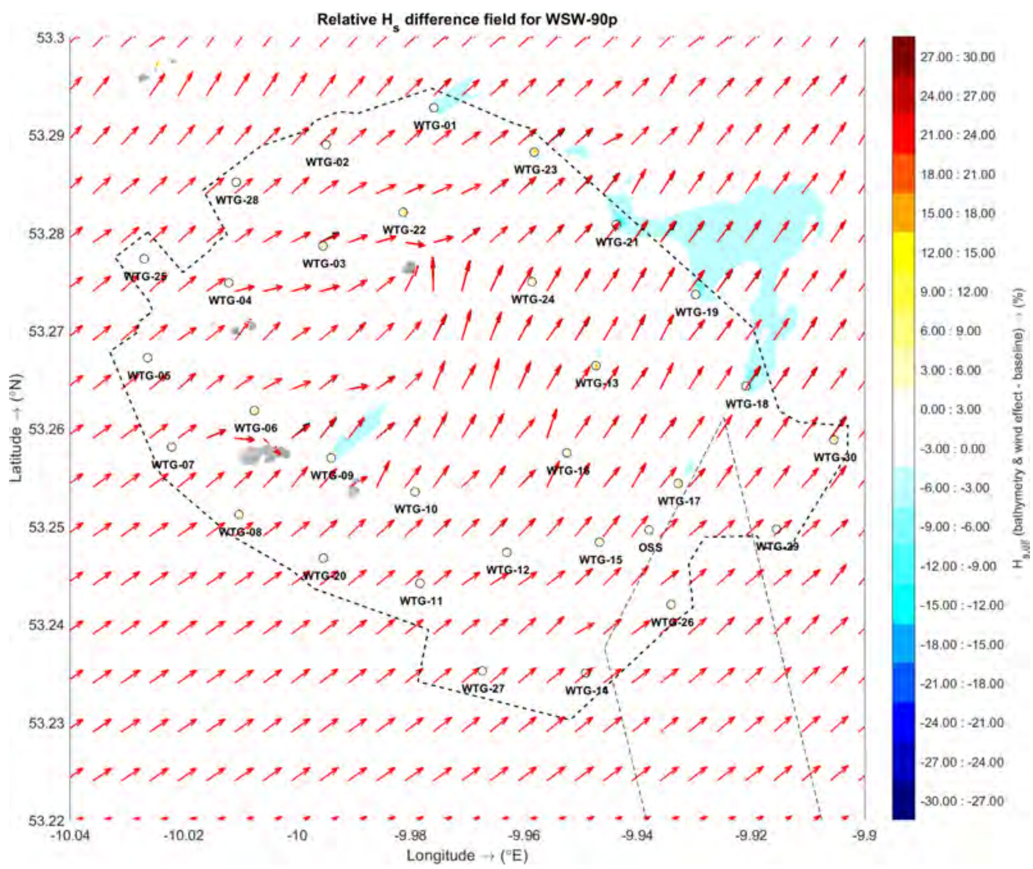
Relative H_s difference field for WSW-90p
Latitude → (°N)
Longitude → (°E)
$H_{s,diff}$ (bathymetry & wind effect - baseline) → (%)
27.00 : 30.00
24.00 : 27.00
21.00 : 24.00
18.00 : 21.00
15.00 : 18.00
12.00 : 15.00
9.00 : 12.00
6.00 : 9.00
3.00 : 6.00
0.00 : 3.00
-3.00 : 0.00
-6.00 : -3.00
-9.00 : -6.00
-12.00 : -9.00
-15.00 : -12.00
-18.00 : -15.00
-21.00 : -18.00
-24.00 : -21.00
-27.00 : -24.00
-30.00 : -27.00
OSS

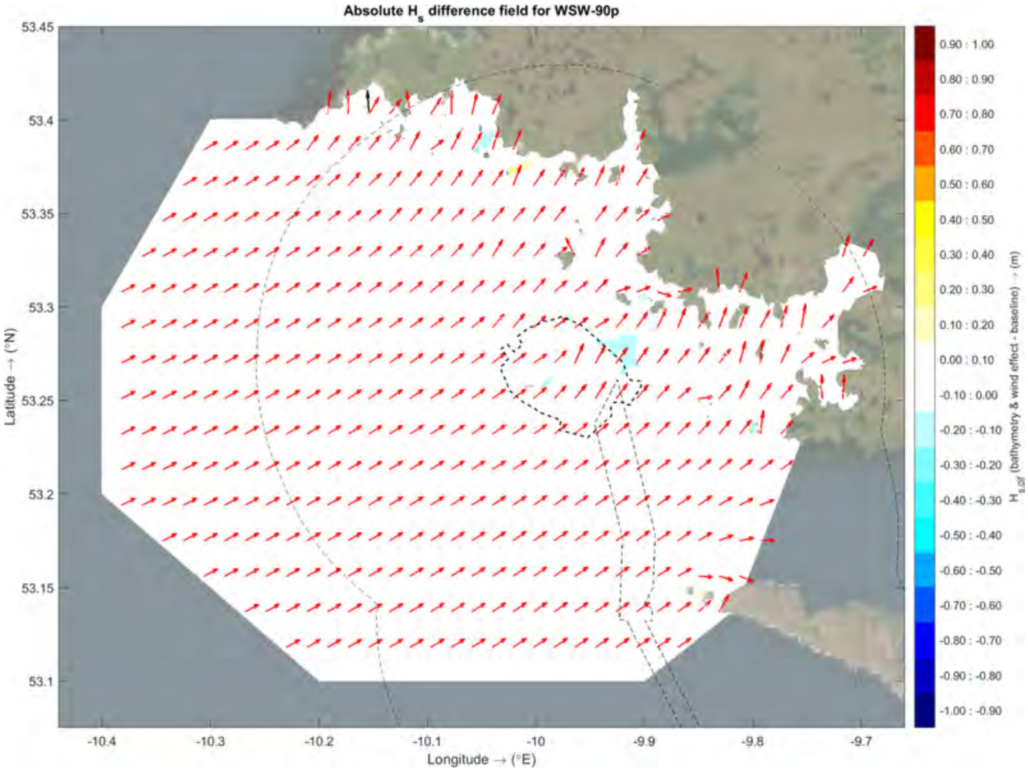
Absolute H_s difference field for WSW-90p
Latitude → (°N)
Longitude → (°E)
$H_{s,dif}$ (bathymetry & wind effect - baseline) → (m)
0.90 : 1.00
0.80 : 0.90
0.70 : 0.80
0.60 : 0.70
0.50 : 0.60
0.40 : 0.50
0.30 : 0.40
0.20 : 0.30
0.10 : 0.20
0.00 : 0.10
-0.10 : 0.00
-0.20 : -0.10
-0.30 : -0.20
-0.40 : -0.30
-0.50 : -0.40
-0.60 : -0.50
-0.70 : -0.60
-0.80 : -0.70
-0.90 : -0.80
-1.00 : -0.90

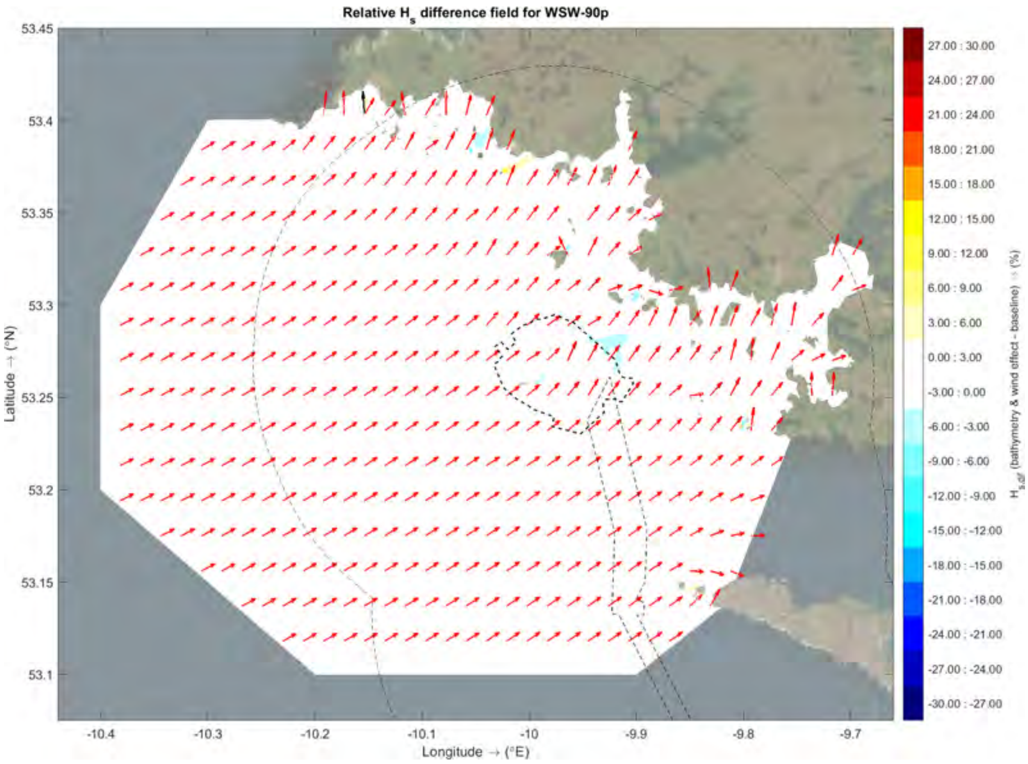
Relative H_s difference field for WSW-90p
Latitude → (°N)
Longitude → (°E)
$H_{s,dif}$ (bathymetry & wind effect - baseline) → (%)
27.00 : 30.00
24.00 : 27.00
21.00 : 24.00
18.00 : 21.00
15.00 : 18.00
12.00 : 15.00
9.00 : 12.00
6.00 : 9.00
3.00 : 6.00
0.00 : 3.00
-3.00 : 0.00
-6.00 : -3.00
-9.00 : -6.00
-12.00 : -9.00
-15.00 : -12.00
-18.00 : -15.00
-21.00 : -18.00
-24.00 : -21.00
-27.00 : -24.00
-30.00 : -27.00

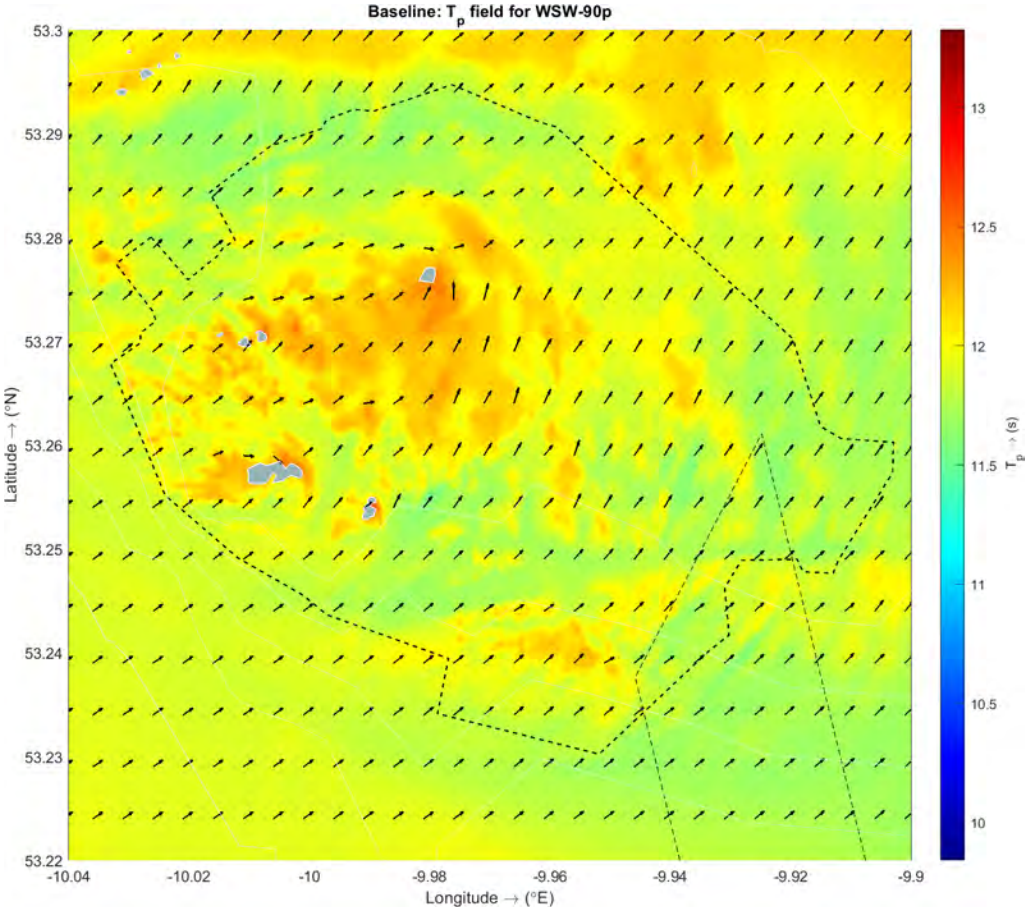
Baseline: T_p field for WSW-90p
53.3
53.29
53.28
53.27
53.26
53.25
53.24
53.23
53.22
Latitude → (°N)
-10.04
-10.02
-10
-9.98
-9.96
-9.94
-9.92
-9.9
Longitude → (°E)
13
12.5
12
11.5
11
10.5
10
T_p → (s)

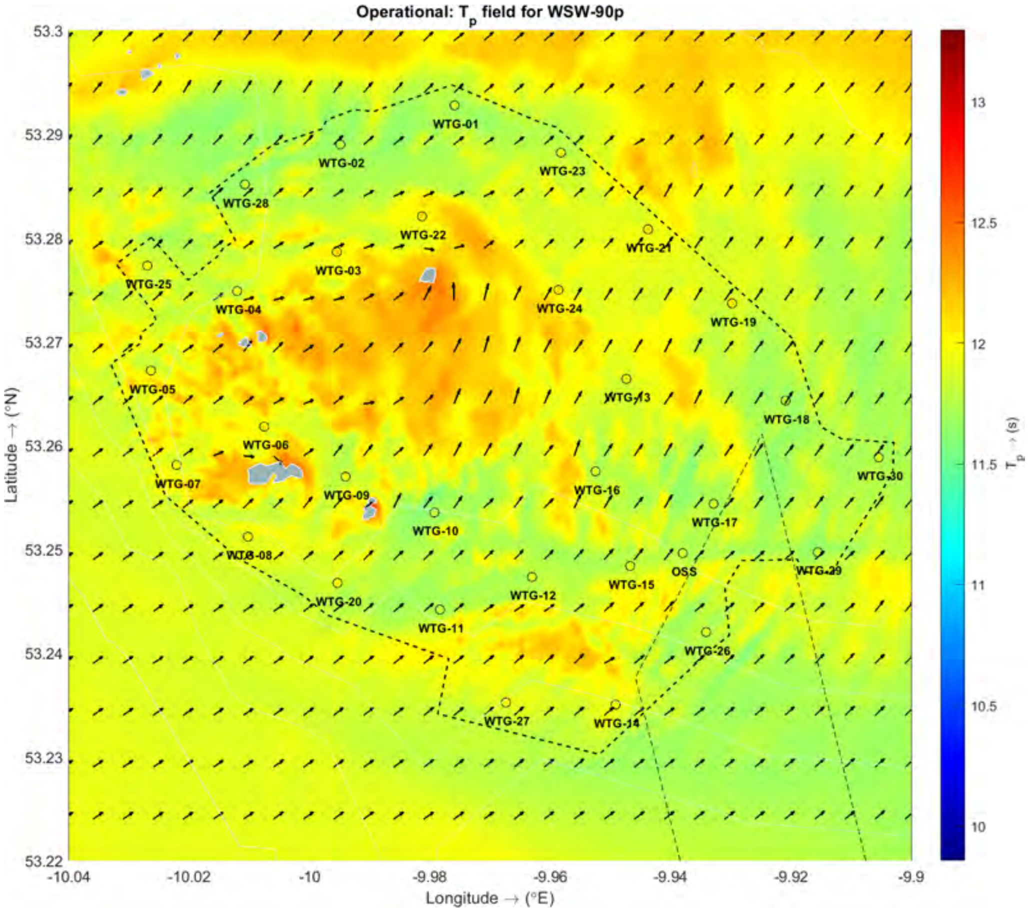
Operational: T_p field for WSW-90p
Latitude → (°N)
Longitude → (°E)
T_p → (s)
53.3
53.29
53.28
53.27
53.26
53.25
53.24
53.23
53.22
-10.04
-10.02
-10
-9.98
-9.96
-9.94
-9.92
-9.9
13
12.5
12
11.5
11
10.5
10
WTG-01
WTG-02
WTG-03
WTG-04
WTG-05
WTG-06
WTG-07
WTG-08
WTG-09
WTG-10
WTG-11
WTG-12
WTG-13
WTG-14
WTG-15
WTG-16
WTG-17
WTG-18
WTG-19
WTG-20
WTG-21
WTG-22
WTG-23
WTG-24
WTG-25
WTG-26
WTG-27
WTG-28
WTG-29
WTG-30
OSS

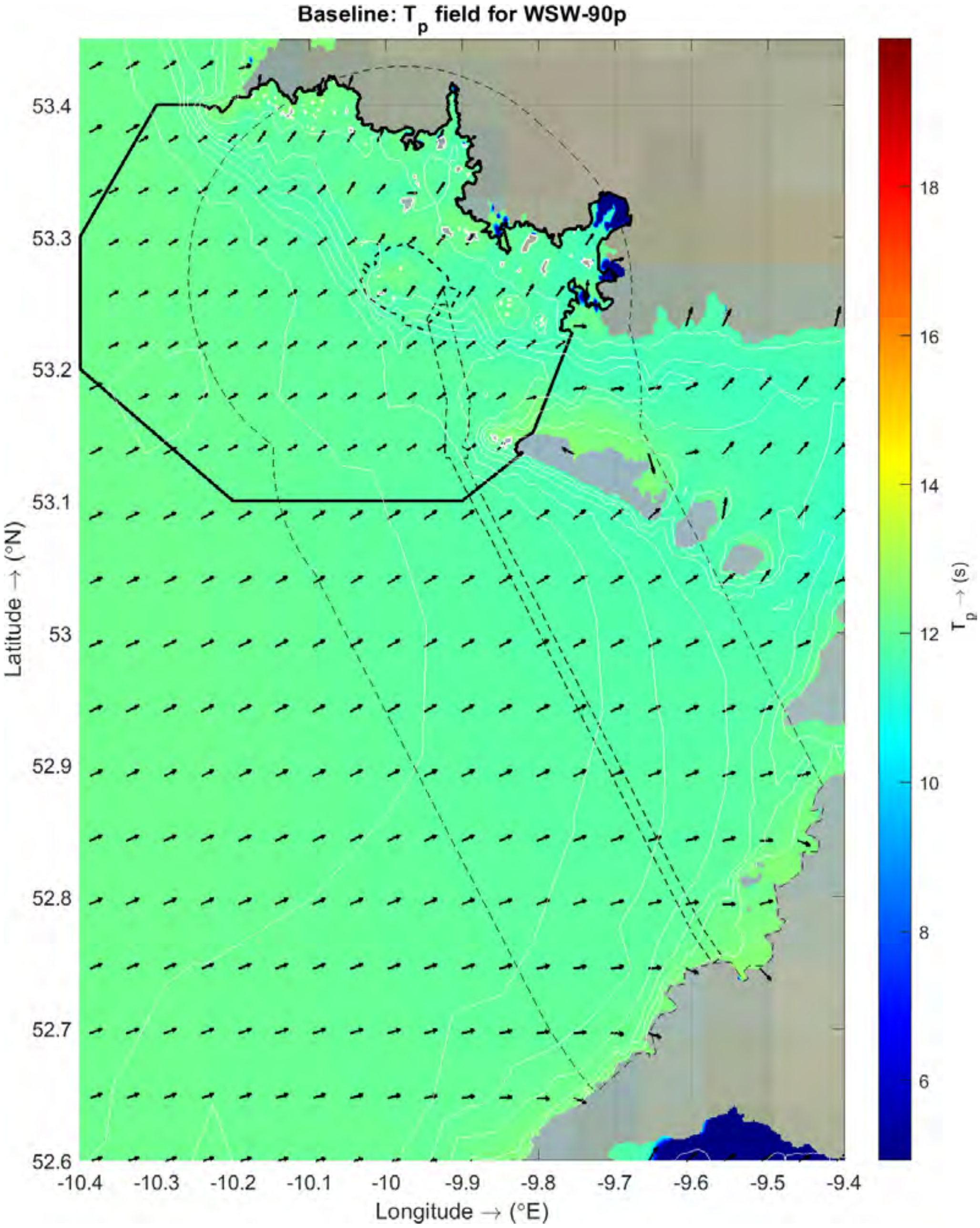
Baseline: T_p field for WSW-90p
53.4
53.3
53.2
53.1
53
52.9
52.8
52.7
52.6
Latitude → (°N)
-10.4
-10.3
-10.2
-10.1
-10
-9.9
-9.8
-9.7
-9.6
-9.5
-9.4
Longitude → (°E)
18
16
14
12
10
8
6
T_p → (s)

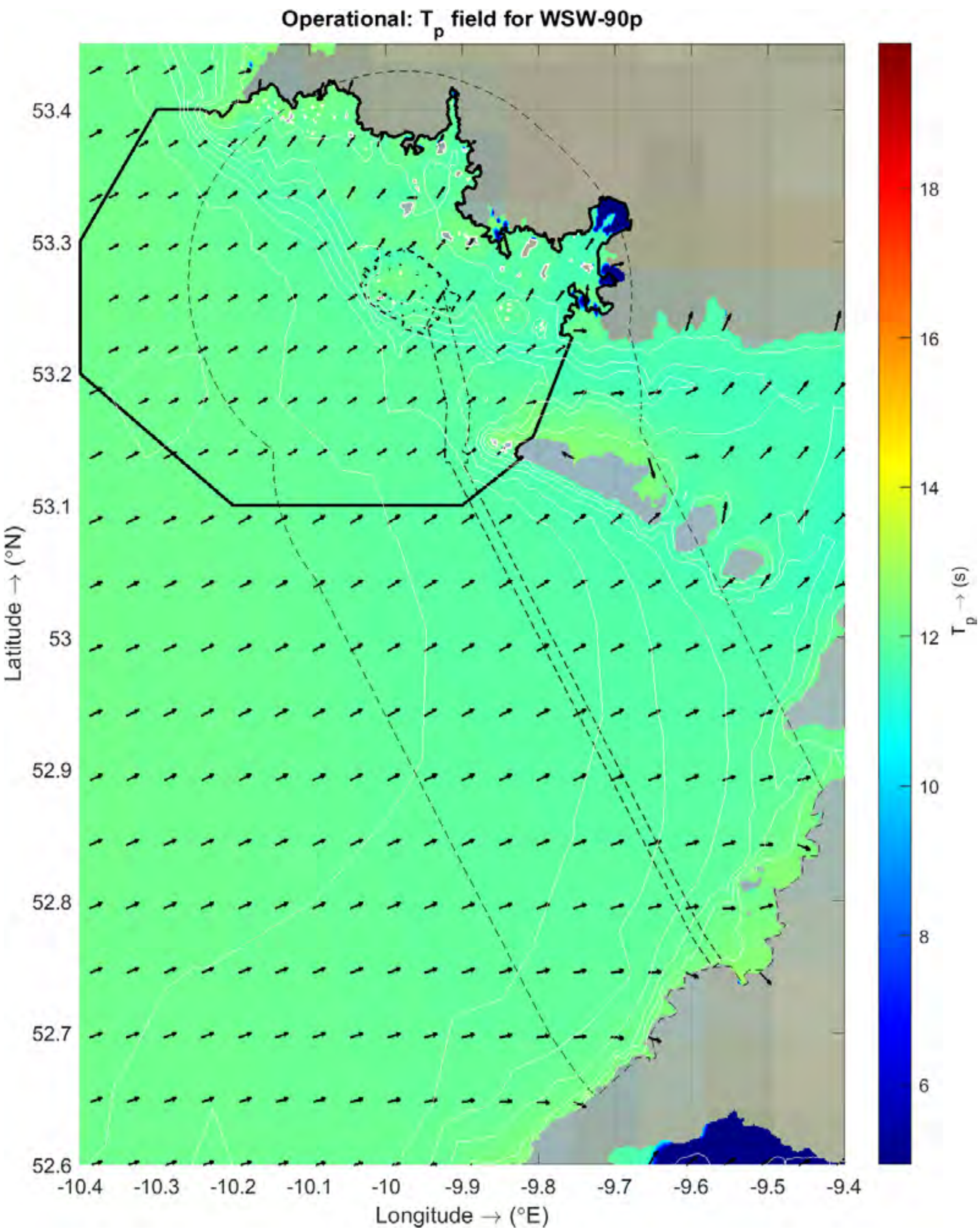

Operational: T_p field for WSW-90p
53.4
53.3
53.2
53.1
53
52.9
52.8
52.7
52.6
Latitude → (°N)
-10.4
-10.3
-10.2
-10.1
-10
-9.9
-9.8
-9.7
-9.6
-9.5
-9.4
Longitude → (°E)
18
16
14
12
10
8
6
T_p → (s)

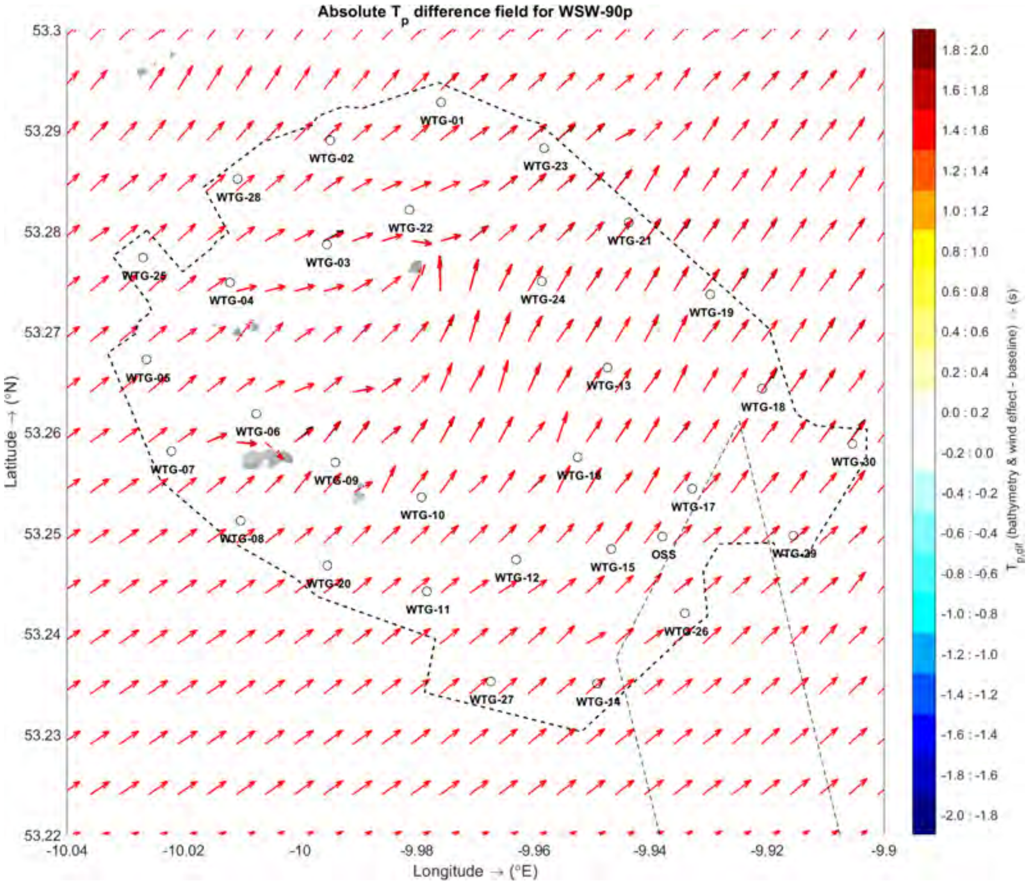
Absolute T_p difference field for WSW-90p
Latitude → (°N)
Longitude → (°E)
$T_{p,dif}$ (bathymetry & wind effect - baseline) → (s)
WTG-01
WTG-02
WTG-03
WTG-04
WTG-05
WTG-06
WTG-07
WTG-08
WTG-09
WTG-10
WTG-11
WTG-12
WTG-13
WTG-14
WTG-15
WTG-16
WTG-17
WTG-18
WTG-19
WTG-20
WTG-21
WTG-22
WTG-23
WTG-24
WTG-25
WTG-26
WTG-27
WTG-28
WTG-29
WTG-30
OSS

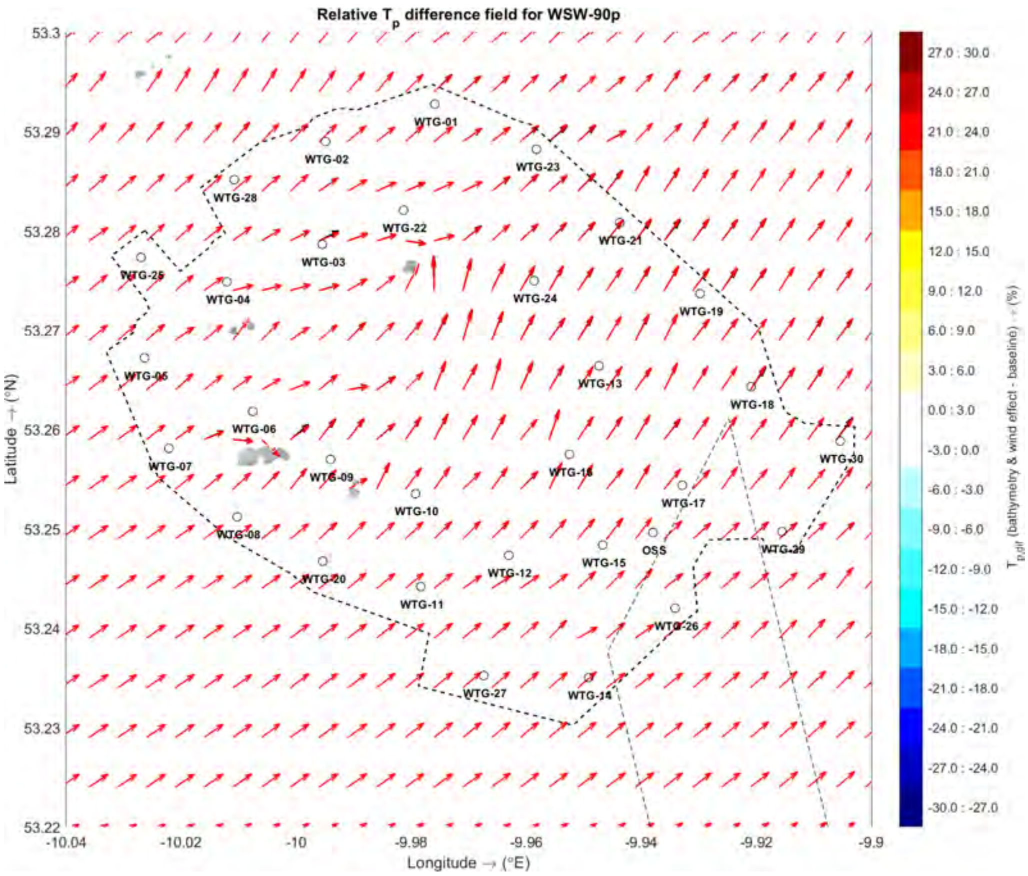
Relative T_p difference field for WSW-90p
Latitude → (°N)
Longitude → (°E)
$T_{p,dif}$ (bathymetry & wind effect - baseline) → (%)

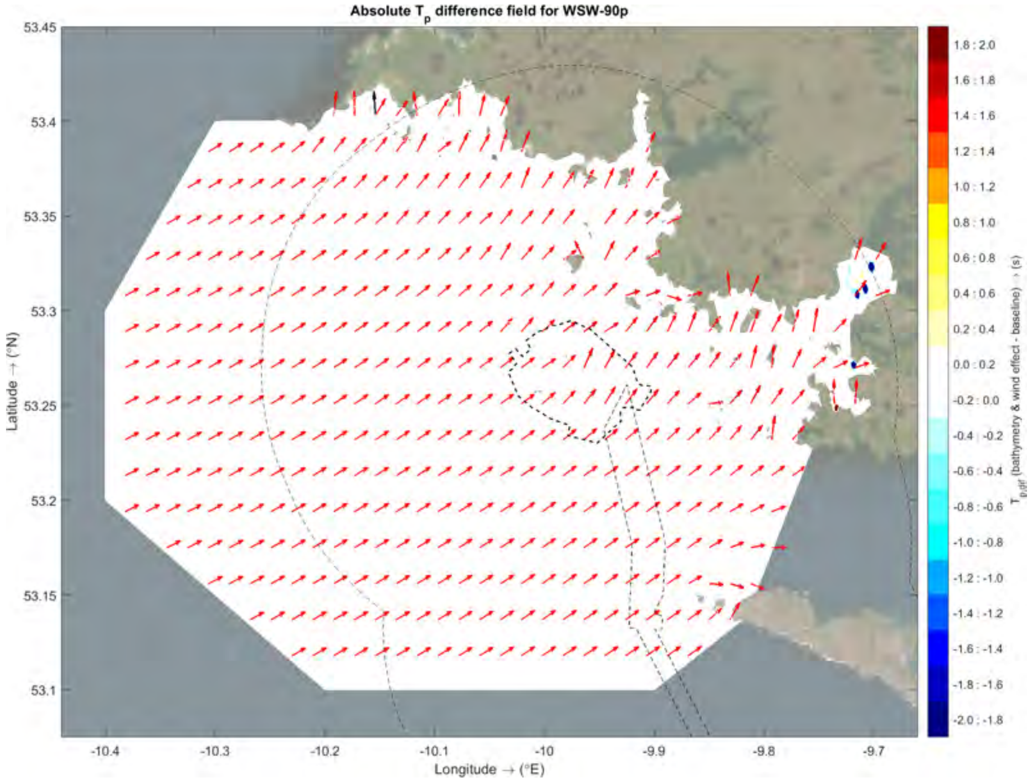
Absolute T_p difference field for WSW-90p
Latitude → (°N)
Longitude → (°E)
$T_{p,diff}$ (bathymetry & wind effect - baseline) → (s)

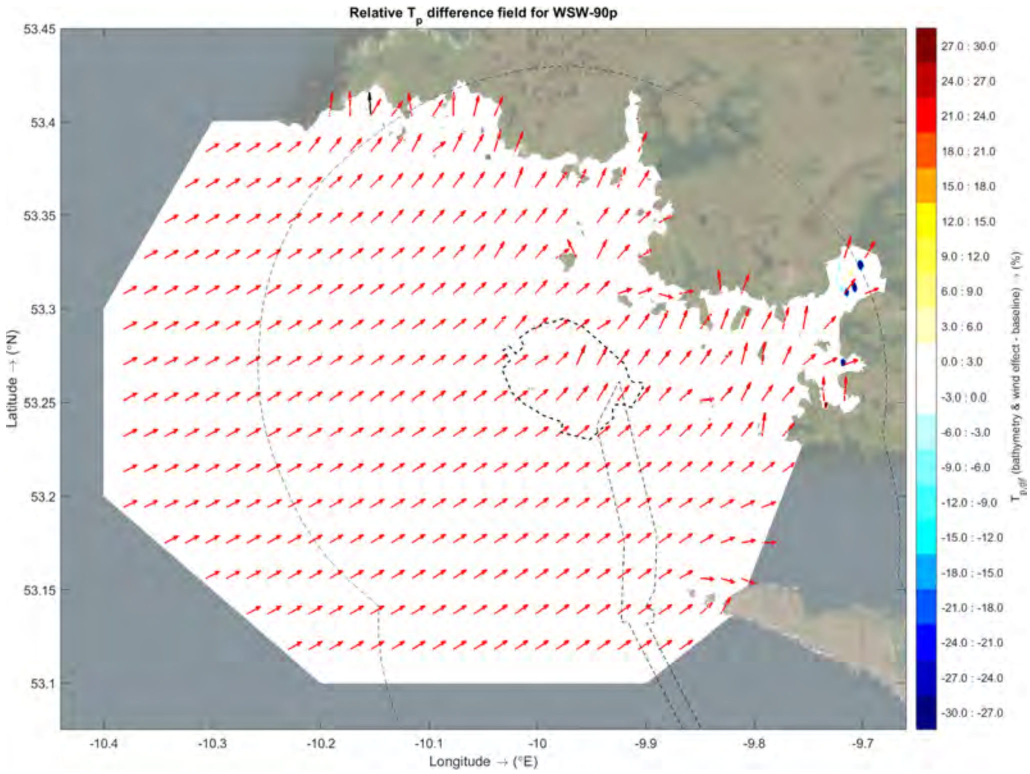
Relative T_p difference field for WSW-90p
Latitude → (°N)
Longitude → (°E)
$T_{p,diff}$ (bathymetry & wind effect - baseline) → (%)

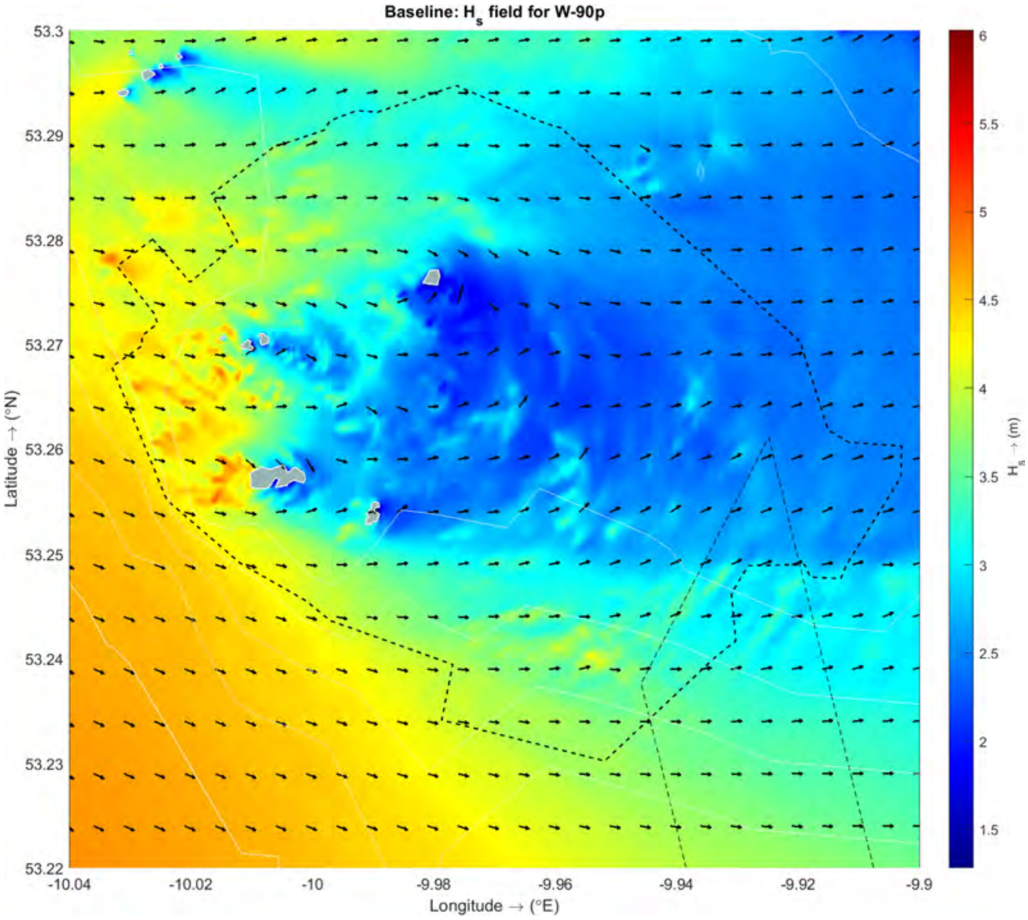

Baseline: H_s field for W-90p
Latitude → (°N)
Longitude → (°E)
H_s → (m)
53.3
53.29
53.28
53.27
53.26
53.25
53.24
53.23
53.22
-10.04
-10.02
-10
-9.98
-9.96
-9.94
-9.92
-9.9
6
5.5
5
4.5
4
3.5
3
2.5
2
1.5

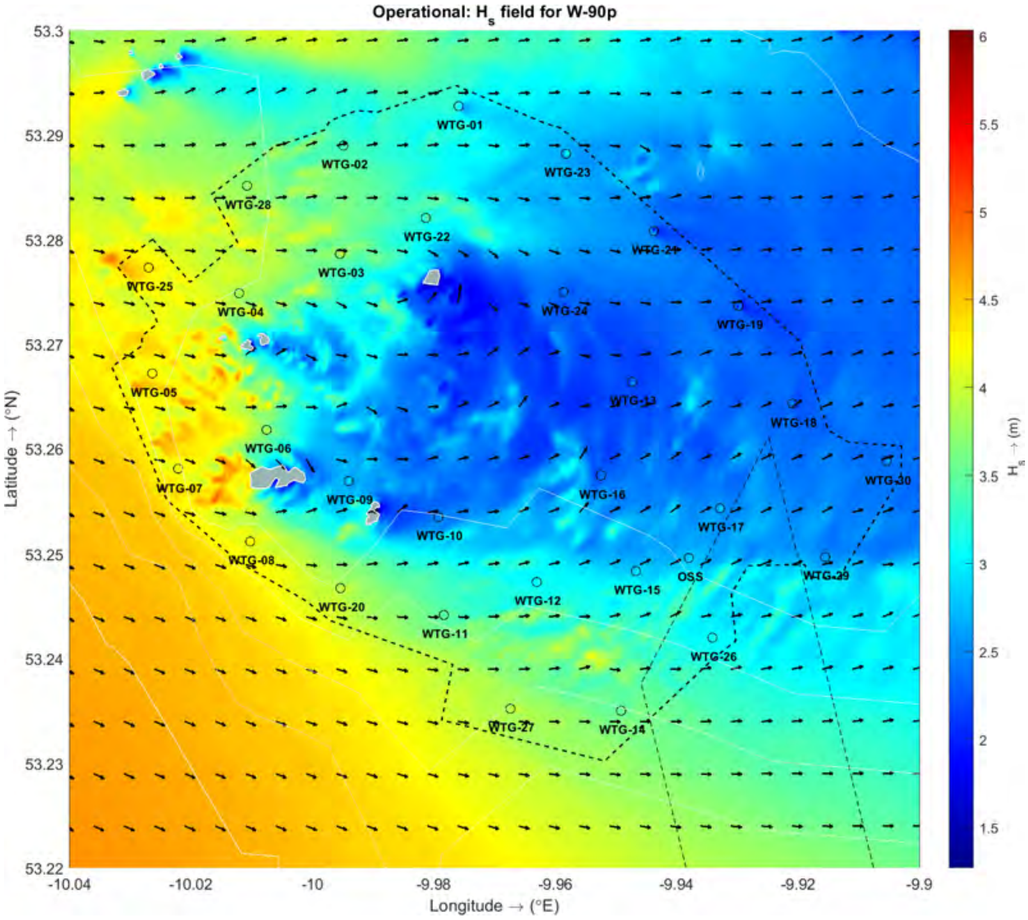
Operational: H_s field for W-90p
WTG-01
WTG-02
WTG-03
WTG-04
WTG-05
WTG-06
WTG-07
WTG-08
WTG-09
WTG-10
WTG-11
WTG-12
WTG-13
WTG-14
WTG-15
WTG-16
WTG-17
WTG-18
WTG-19
WTG-20
WTG-21
WTG-22
WTG-23
WTG-24
WTG-25
WTG-26
WTG-27
WTG-28
WTG-29
WTG-30
OSS
Latitude → (°N)
Longitude → (°E)
H_s → (m)

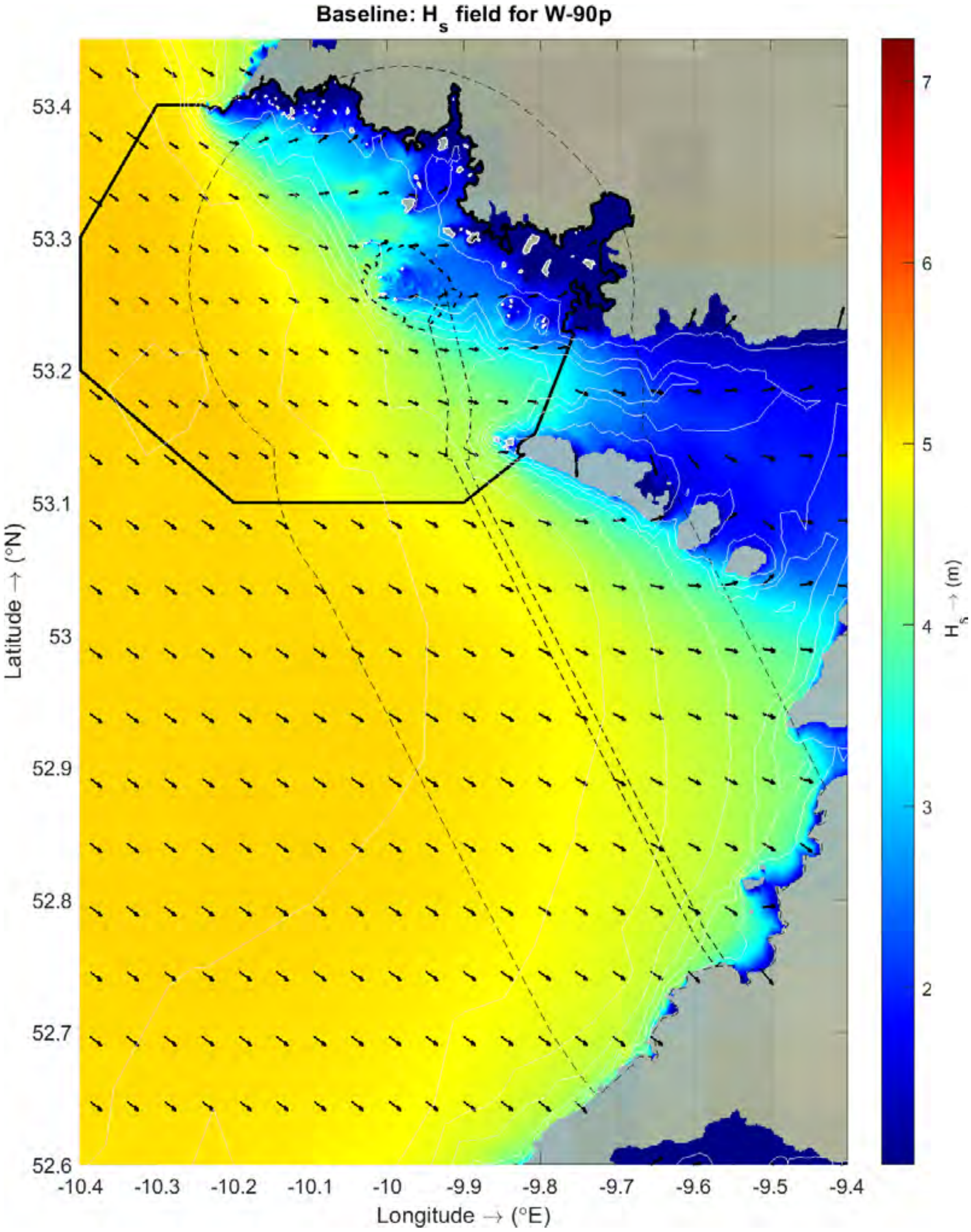
Baseline: H_s field for W-90p
53.4
53.3
53.2
53.1
53
52.9
52.8
52.7
52.6
Latitude → (°N)
-10.4
-10.3
-10.2
-10.1
-10
-9.9
-9.8
-9.7
-9.6
-9.5
-9.4
Longitude → (°E)
7
6
5
4
3
2
H_s → (m)

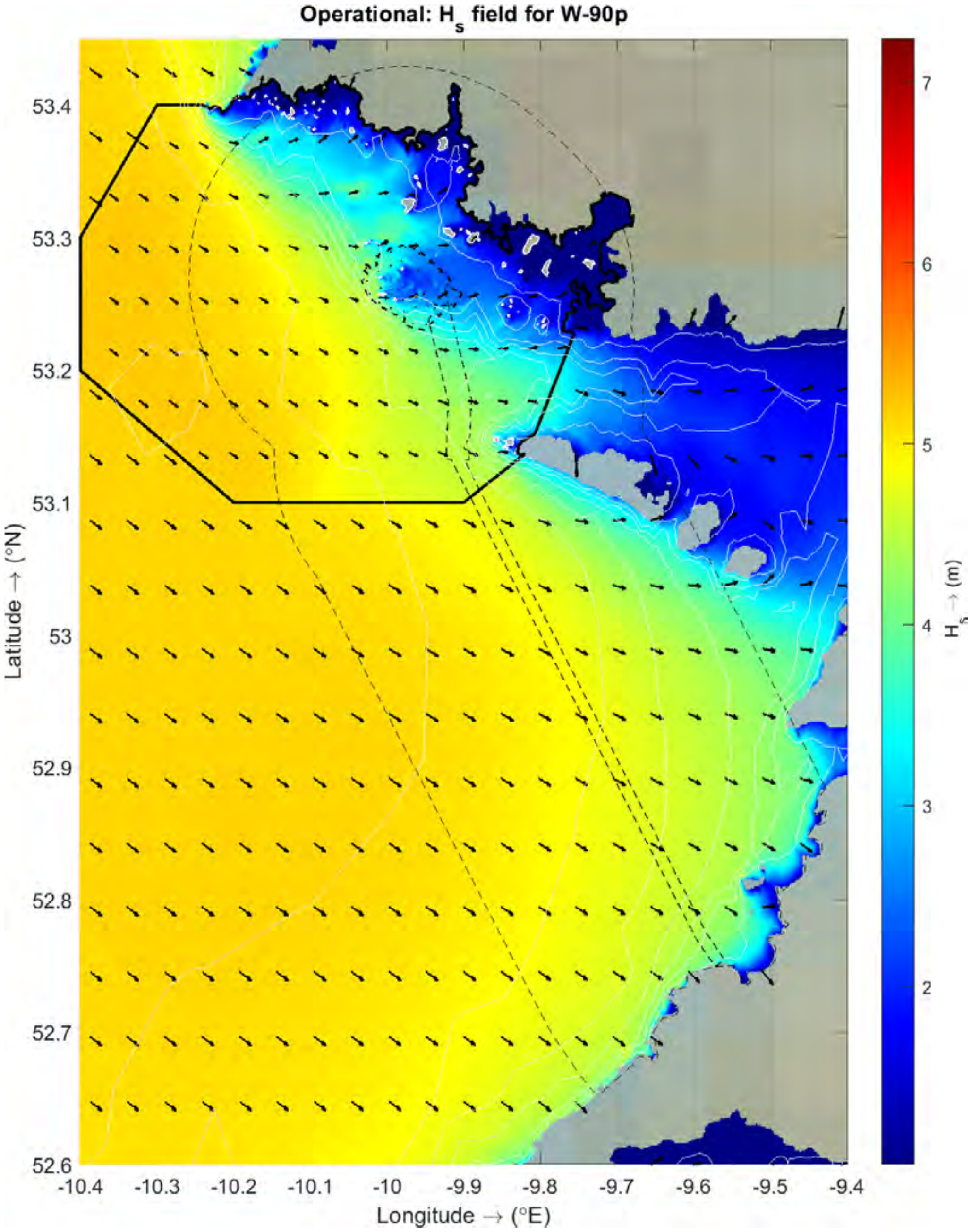

Operational: Hs field for W-90p
53.4
53.3
53.2
53.1
53
52.9
52.8
52.7
52.6
Latitude → (°N)
-10.4
-10.3
-10.2
-10.1
-10
-9.9
-9.8
-9.7
-9.6
-9.5
-9.4
Longitude → (°E)
7
6
5
4
3
2
Hs → (m)

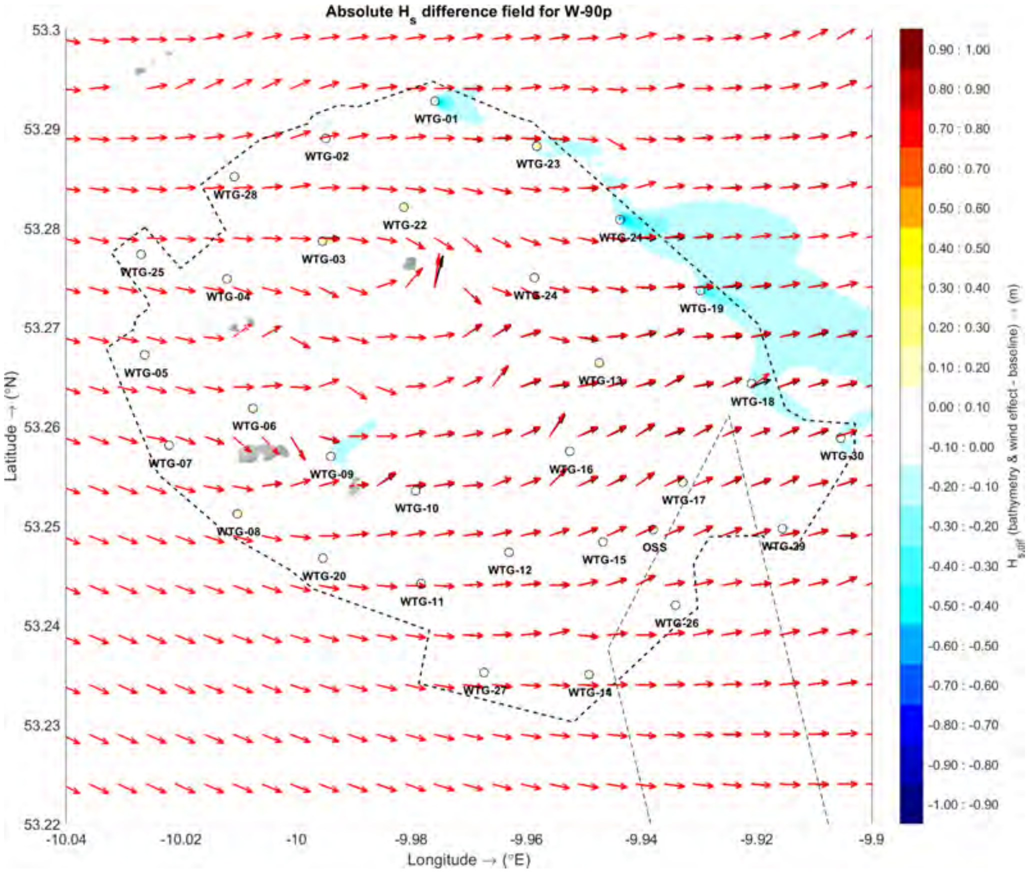
Absolute H_s difference field for W-90p
Latitude → (°N)
Longitude → (°E)
$H_{s,diff}$ (bathymetry & wind effect - baseline) → (m)
0.90 : 1.00
0.80 : 0.90
0.70 : 0.80
0.60 : 0.70
0.50 : 0.60
0.40 : 0.50
0.30 : 0.40
0.20 : 0.30
0.10 : 0.20
0.00 : 0.10
-0.10 : 0.00
-0.20 : -0.10
-0.30 : -0.20
-0.40 : -0.30
-0.50 : -0.40
-0.60 : -0.50
-0.70 : -0.60
-0.80 : -0.70
-0.90 : -0.80
-1.00 : -0.90
WTG-01
WTG-02
WTG-03
WTG-04
WTG-05
WTG-06
WTG-07
WTG-08
WTG-09
WTG-10
WTG-11
WTG-12
WTG-13
WTG-14
WTG-15
WTG-16
WTG-17
WTG-18
WTG-19
WTG-20
WTG-21
WTG-22
WTG-23
WTG-24
WTG-25
WTG-26
WTG-27
WTG-28
WTG-29
WTG-30
OSS

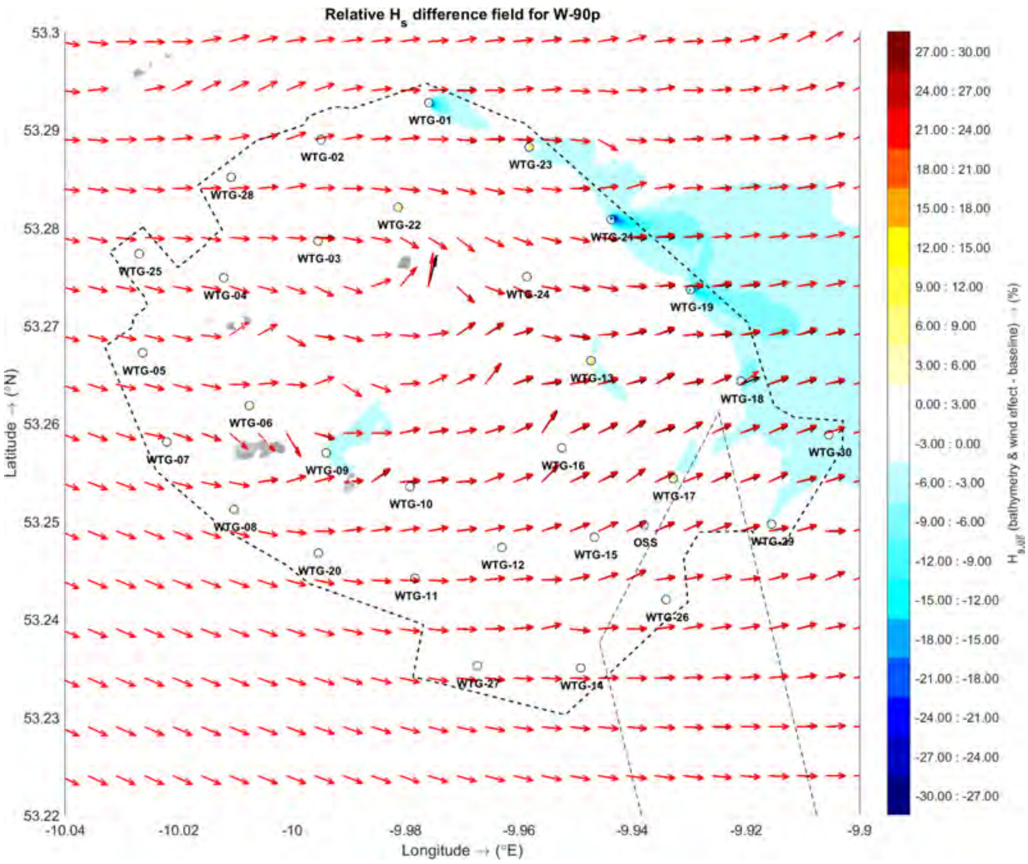
Relative H_s difference field for W-90p
Latitude → (°N)
Longitude → (°E)
$H_{s,diff}$ (bathymetry & wind effect - baseline) → (%)
27.00 : 30.00
24.00 : 27.00
21.00 : 24.00
18.00 : 21.00
15.00 : 18.00
12.00 : 15.00
9.00 : 12.00
6.00 : 9.00
3.00 : 6.00
0.00 : 3.00
-3.00 : 0.00
-6.00 : -3.00
-9.00 : -6.00
-12.00 : -9.00
-15.00 : -12.00
-18.00 : -15.00
-21.00 : -18.00
-24.00 : -21.00
-27.00 : -24.00
-30.00 : -27.00

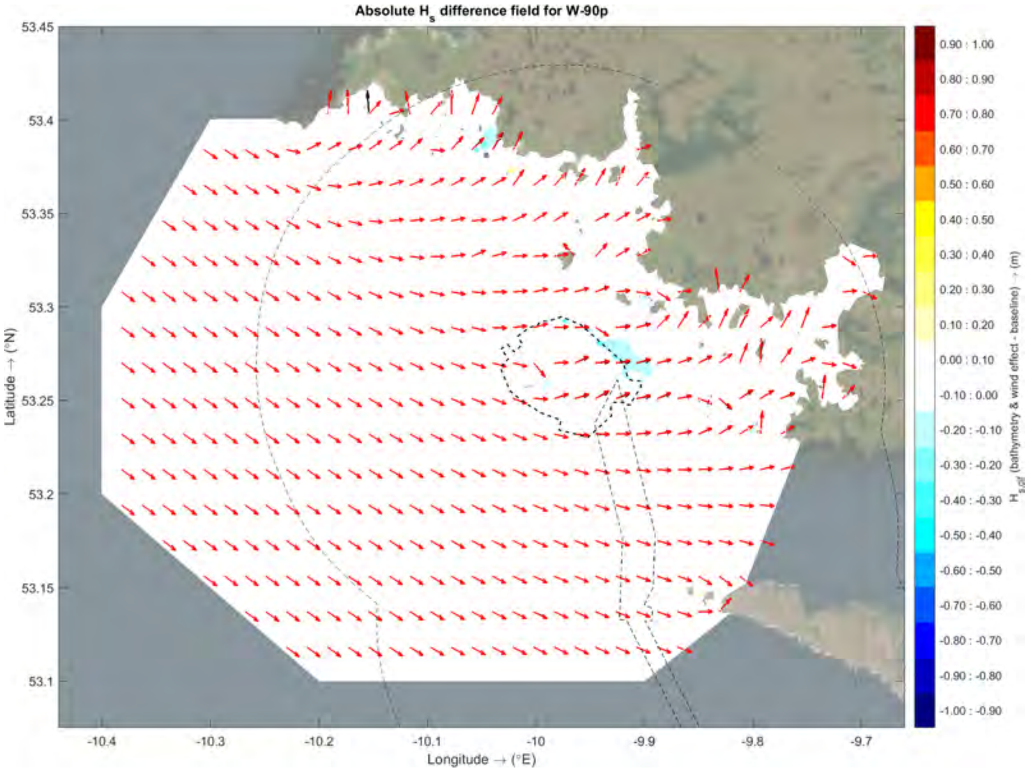
Absolute Hs difference field for W-90p
Latitude → (°N)
Longitude → (°E)
Hs,dif (bathymetry & wind effect - baseline) → (m)
0.90 : 1.00
0.80 : 0.90
0.70 : 0.80
0.60 : 0.70
0.50 : 0.60
0.40 : 0.50
0.30 : 0.40
0.20 : 0.30
0.10 : 0.20
0.00 : 0.10
-0.10 : 0.00
-0.20 : -0.10
-0.30 : -0.20
-0.40 : -0.30
-0.50 : -0.40
-0.60 : -0.50
-0.70 : -0.60
-0.80 : -0.70
-0.90 : -0.80
-1.00 : -0.90

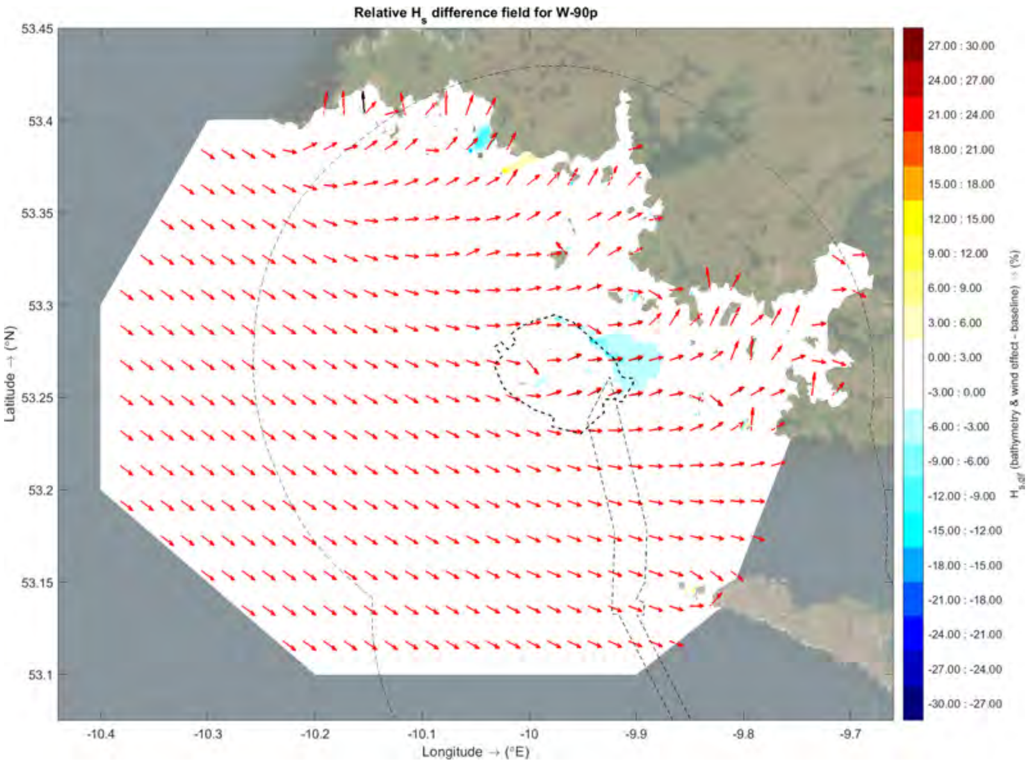
Relative Hs difference field for W-90p
Latitude → (°N)
Longitude → (°E)
Hs,dif (bathymetry & wind effect - baseline) → (%)
27.00 : 30.00
24.00 : 27.00
21.00 : 24.00
18.00 : 21.00
15.00 : 18.00
12.00 : 15.00
9.00 : 12.00
6.00 : 9.00
3.00 : 6.00
0.00 : 3.00
-3.00 : 0.00
-6.00 : -3.00
-9.00 : -6.00
-12.00 : -9.00
-15.00 : -12.00
-18.00 : -15.00
-21.00 : -18.00
-24.00 : -21.00
-27.00 : -24.00
-30.00 : -27.00

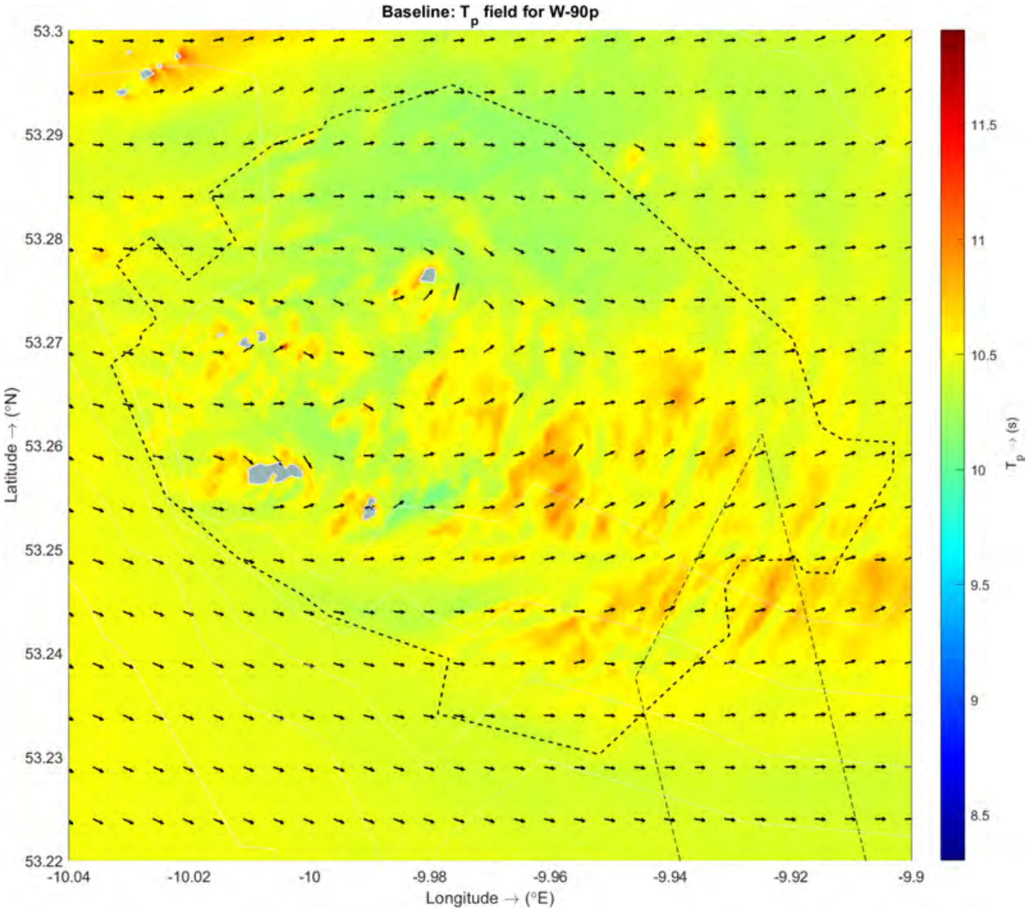
Baseline: T_p field for W-90p
Latitude → (°N)
Longitude → (°E)
T_p → (s)
53.3
53.29
53.28
53.27
53.26
53.25
53.24
53.23
53.22
-10.04
-10.02
-10
-9.98
-9.96
-9.94
-9.92
-9.9
11.5
11
10.5
10
9.5
9
8.5

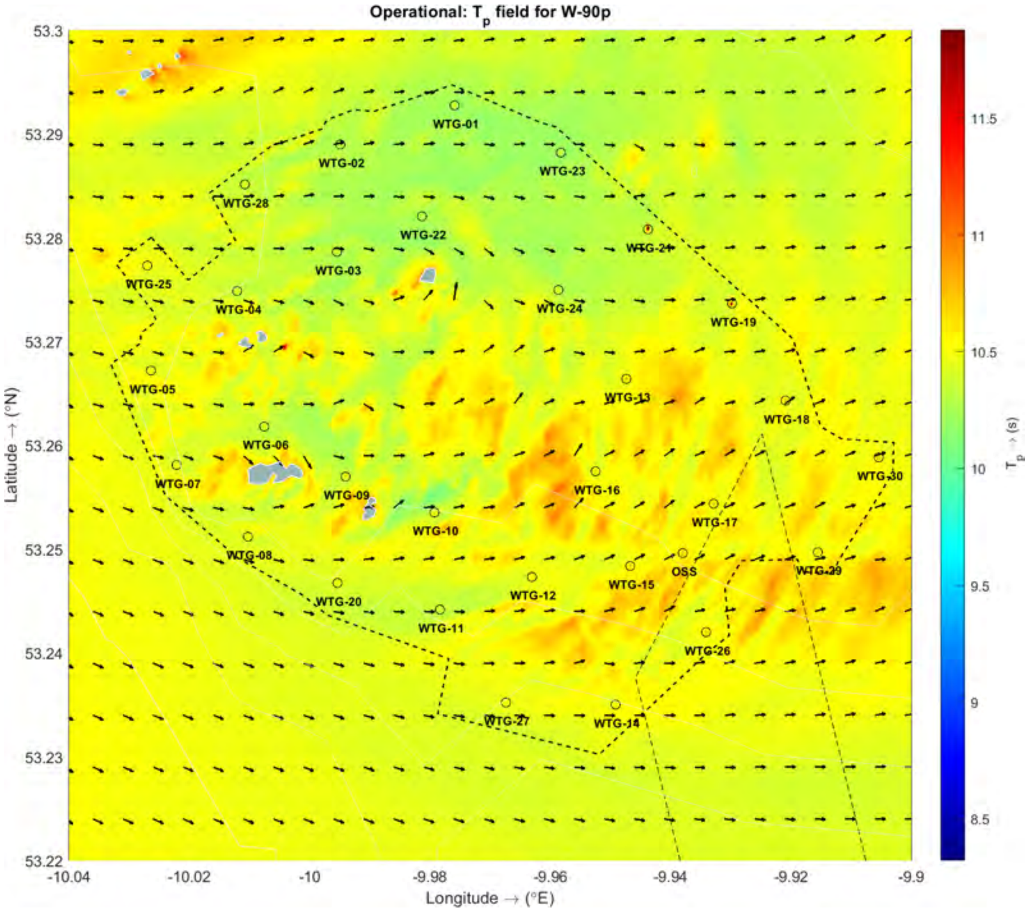
Operational: T_p field for W-90p
WTG-01
WTG-02
WTG-23
WTG-28
WTG-22
WTG-21
WTG-03
WTG-25
WTG-04
WTG-24
WTG-19
WTG-05
WTG-13
WTG-18
WTG-06
WTG-07
WTG-09
WTG-16
WTG-30
WTG-17
WTG-10
WTG-08
OSS
WTG-29
WTG-15
WTG-20
WTG-12
WTG-11
WTG-26
WTG-27
WTG-14
Latitude → (°N)
Longitude → (°E)
T_p → (s)

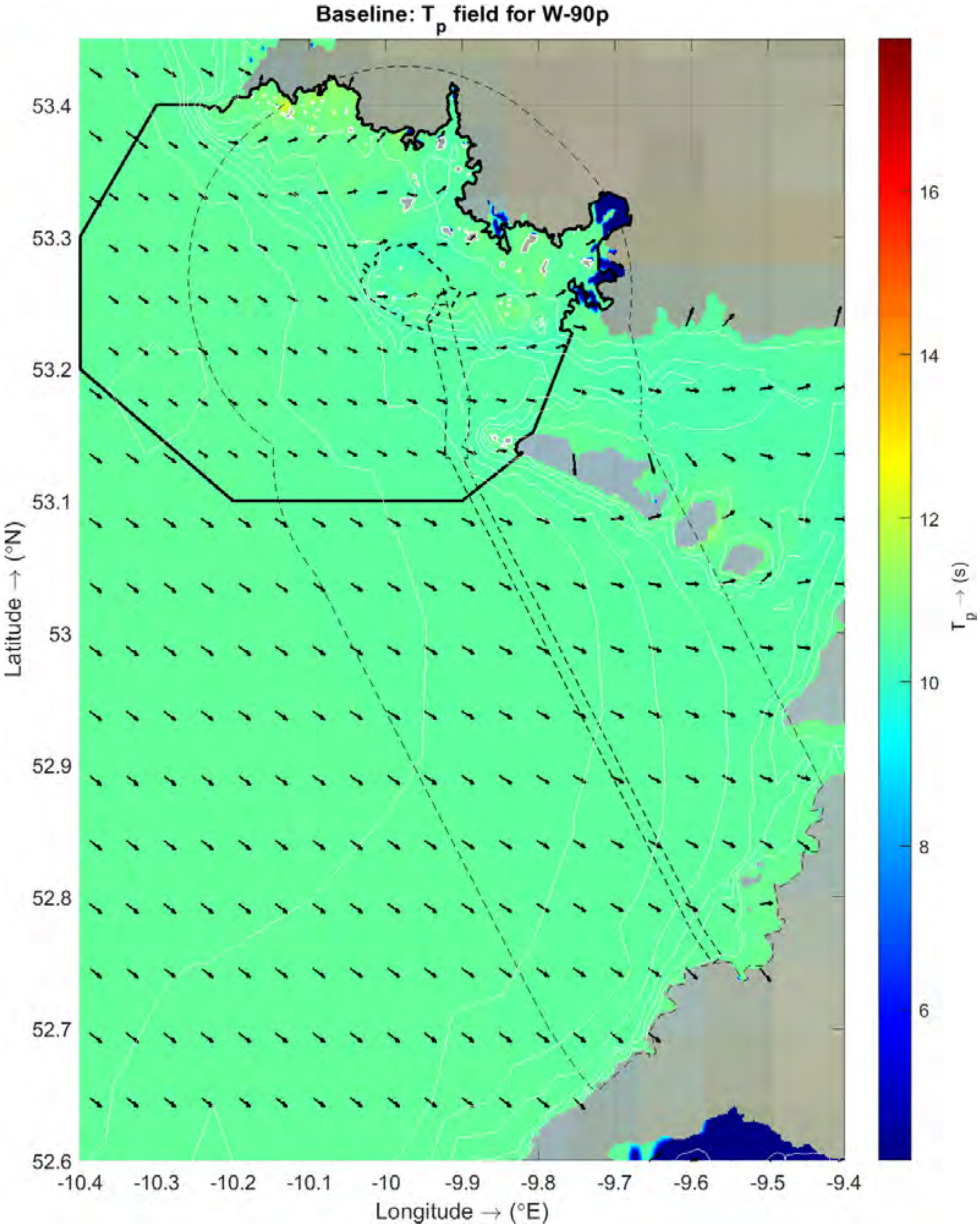
Baseline: T_p field for W-90p
53.4
53.3
53.2
53.1
53
52.9
52.8
52.7
52.6
Latitude → (°N)
-10.4
-10.3
-10.2
-10.1
-10
-9.9
-9.8
-9.7
-9.6
-9.5
-9.4
Longitude → (°E)
16
14
12
10
8
6
T_p → (s)

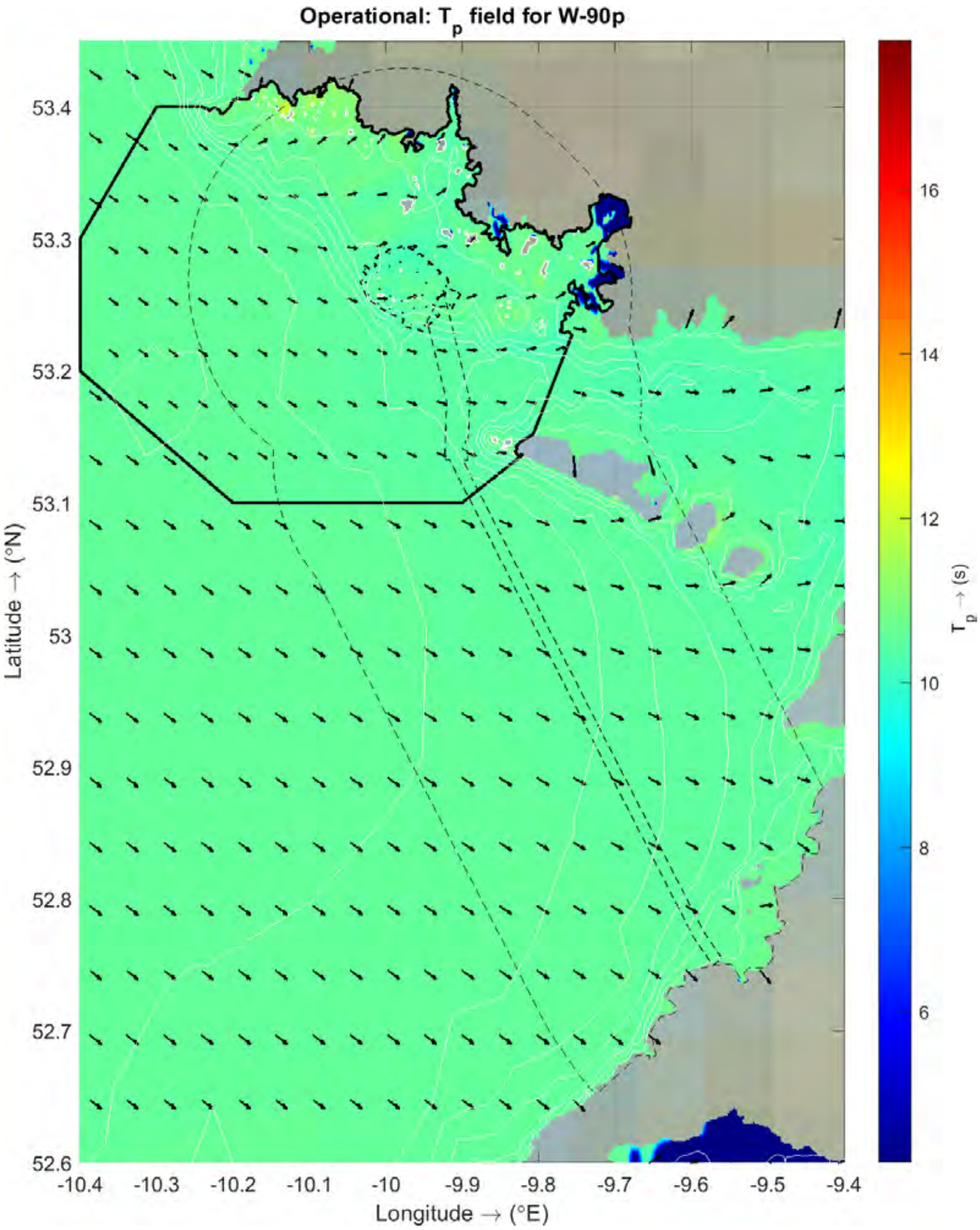
Operational: T_p field for W-90p
53.4
53.3
53.2
53.1
53
52.9
52.8
52.7
52.6
Latitude → (°N)
-10.4
-10.3
-10.2
-10.1
-10
-9.9
-9.8
-9.7
-9.6
-9.5
-9.4
Longitude → (°E)
16
14
12
10
8
6
T_p → (s)

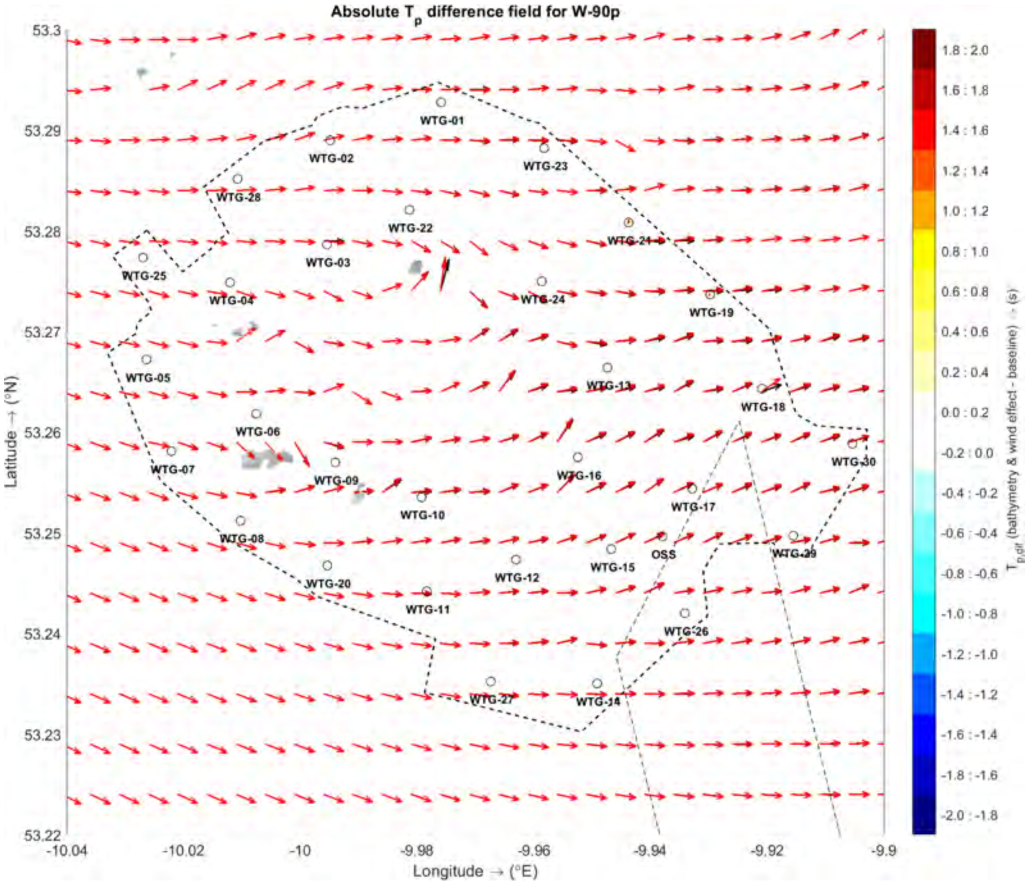
Absolute T_p difference field for W-90p
Latitude → (°N)
Longitude → (°E)
$T_{p,dif}$ (bathymetry & wind effect - baseline) → (s)
1.8 : 2.0
1.6 : 1.8
1.4 : 1.6
1.2 : 1.4
1.0 : 1.2
0.8 : 1.0
0.6 : 0.8
0.4 : 0.6
0.2 : 0.4
0.0 : 0.2
-0.2 : 0.0
-0.4 : -0.2
-0.6 : -0.4
-0.8 : -0.6
-1.0 : -0.8
-1.2 : -1.0
-1.4 : -1.2
-1.6 : -1.4
-1.8 : -1.6
-2.0 : -1.8

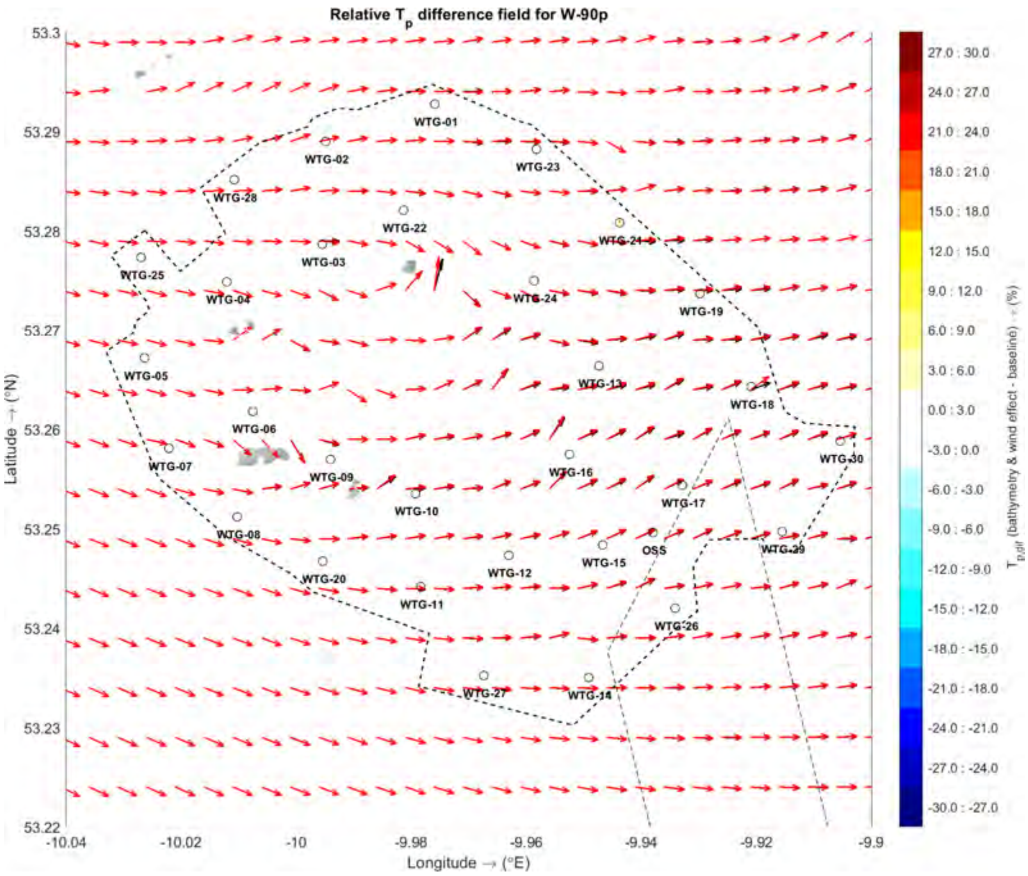
Relative T_p difference field for W-90p
Latitude → (°N)
Longitude → (°E)
$T_{p,dif}$ (bathymetry & wind effect - baseline) → (%)
27.0 : 30.0
24.0 : 27.0
21.0 : 24.0
18.0 : 21.0
15.0 : 18.0
12.0 : 15.0
9.0 : 12.0
6.0 : 9.0
3.0 : 6.0
0.0 : 3.0
-3.0 : 0.0
-6.0 : -3.0
-9.0 : -6.0
-12.0 : -9.0
-15.0 : -12.0
-18.0 : -15.0
-21.0 : -18.0
-24.0 : -21.0
-27.0 : -24.0
-30.0 : -27.0

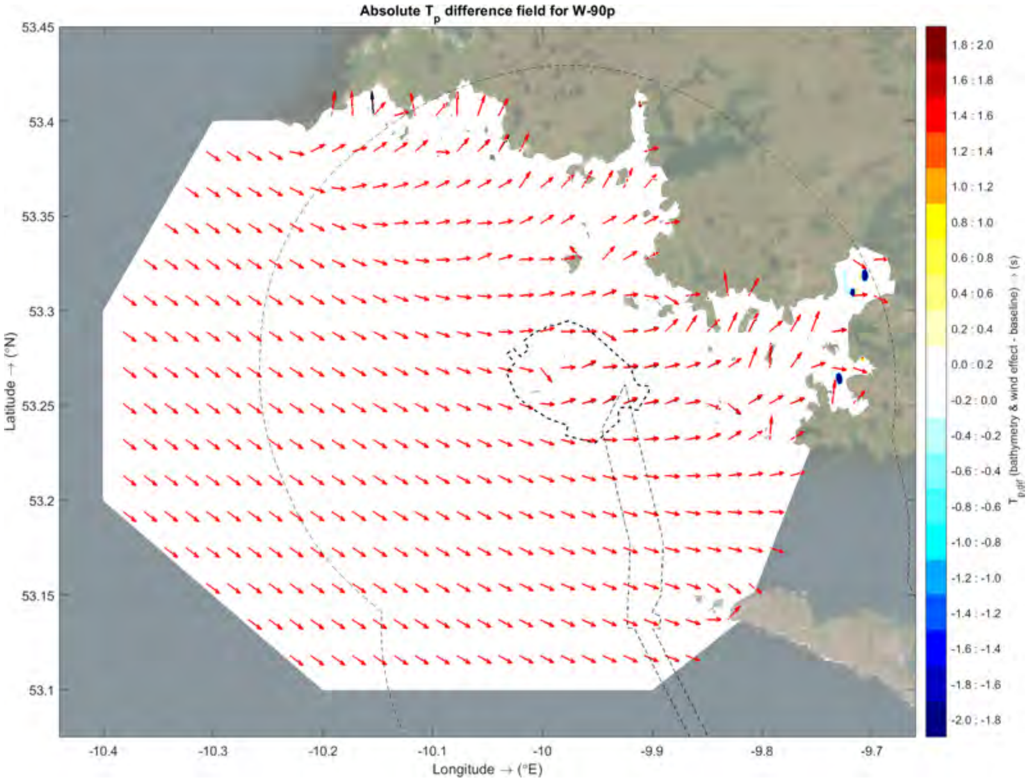
Absolute T_p difference field for W-90p
Latitude → (°N)
Longitude → (°E)
$T_{p,diff}$ (bathymetry & wind effect - baseline) → (s)
1.8 : 2.0
1.6 : 1.8
1.4 : 1.6
1.2 : 1.4
1.0 : 1.2
0.8 : 1.0
0.6 : 0.8
0.4 : 0.6
0.2 : 0.4
0.0 : 0.2
-0.2 : 0.0
-0.4 : -0.2
-0.6 : -0.4
-0.8 : -0.6
-1.0 : -0.8
-1.2 : -1.0
-1.4 : -1.2
-1.6 : -1.4
-1.8 : -1.6
-2.0 : -1.8

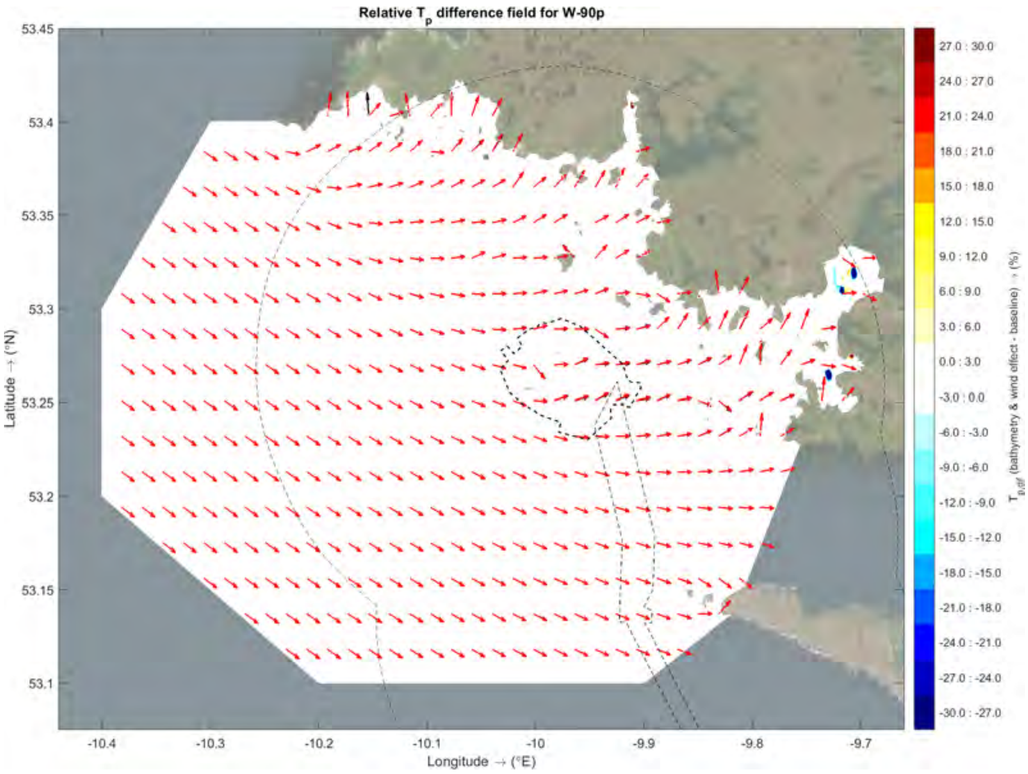
Relative T_p difference field for W-90p
Latitude → (°N)
Longitude → (°E)
$T_{p,diff}$ (bathymetry & wind effect - baseline) → (%)
27.0 : 30.0
24.0 : 27.0
21.0 : 24.0
18.0 : 21.0
15.0 : 18.0
12.0 : 15.0
9.0 : 12.0
6.0 : 9.0
3.0 : 6.0
0.0 : 3.0
-3.0 : 0.0
-6.0 : -3.0
-9.0 : -6.0
-12.0 : -9.0
-15.0 : -12.0
-18.0 : -15.0
-21.0 : -18.0
-24.0 : -21.0
-27.0 : -24.0
-30.0 : -27.0

E.3 1-yr RP

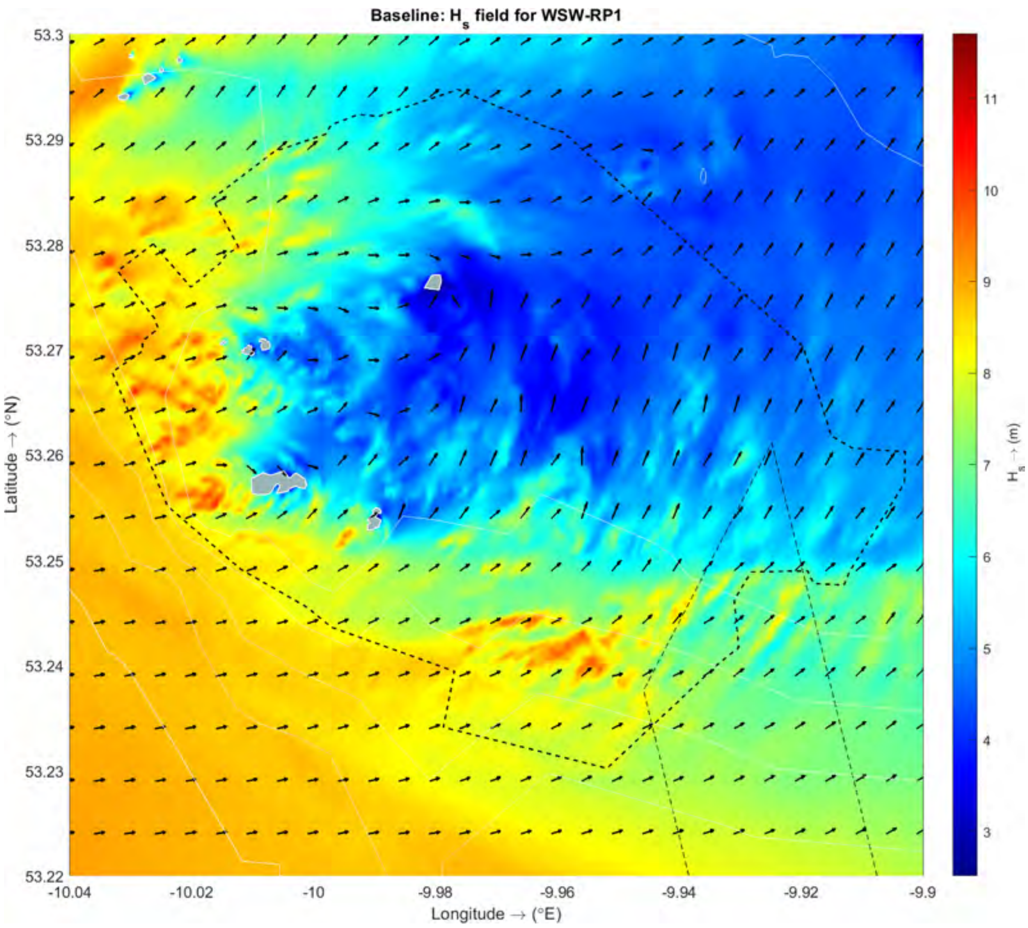

Baseline: H_s field for WSW-RP1
53.3
53.29
53.28
53.27
53.26
53.25
53.24
53.23
53.22
Latitude → (°N)
-10.04
-10.02
-10
-9.98
-9.96
-9.94
-9.92
-9.9
Longitude → (°E)
11
10
9
8
7
6
5
4
3
H_s → (m)

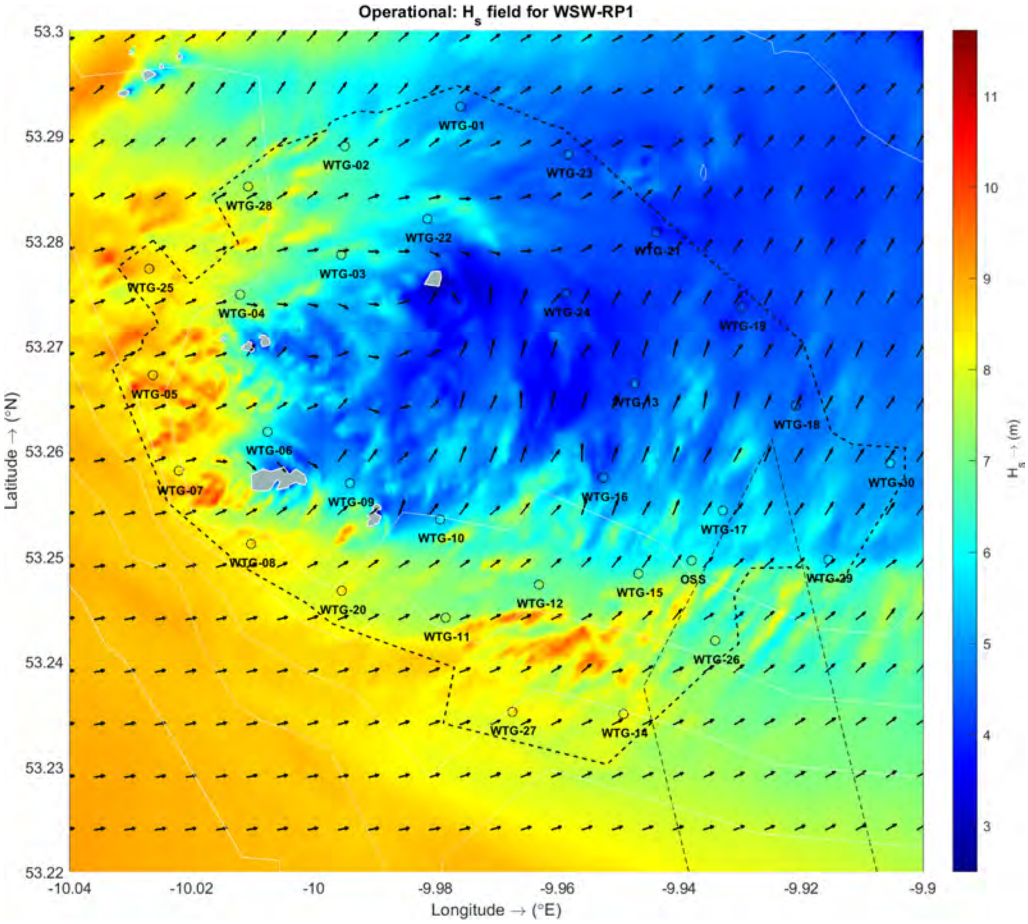

Operational: H_s field for WSW-RP1
Latitude → (°N)
Longitude → (°E)
H_s → (m)
53.3
53.29
53.28
53.27
53.26
53.25
53.24
53.23
53.22
-10.04
-10.02
-10
-9.98
-9.96
-9.94
-9.92
-9.9
11
10
9
8
7
6
5
4
3
WTG-01
WTG-02
WTG-03
WTG-04
WTG-05
WTG-06
WTG-07
WTG-08
WTG-09
WTG-10
WTG-11
WTG-12
WTG-13
WTG-14
WTG-15
WTG-16
WTG-17
WTG-18
WTG-19
WTG-20
WTG-21
WTG-22
WTG-23
WTG-24
WTG-25
WTG-26
WTG-27
WTG-28
WTG-29
WTG-30
OSS

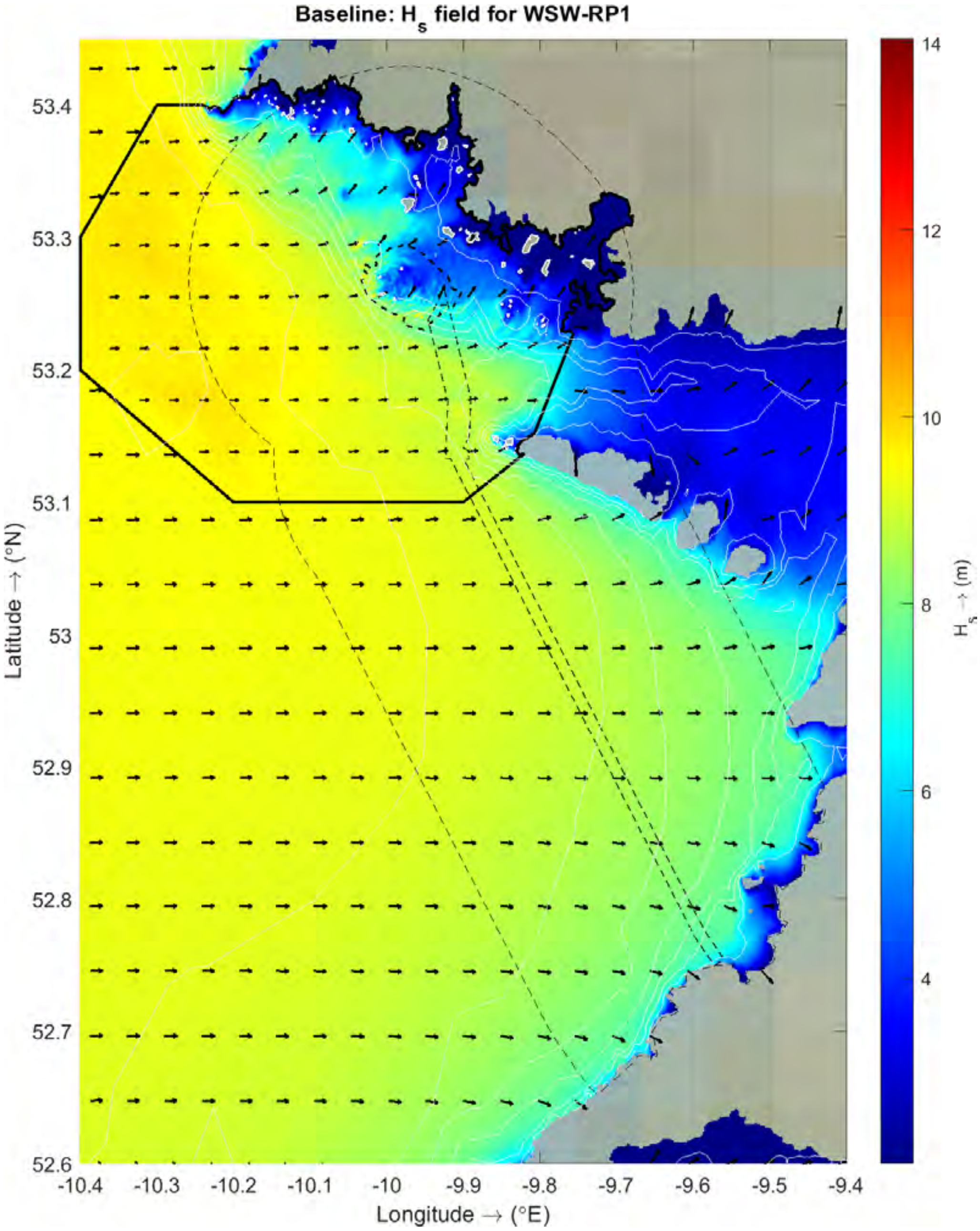
Baseline: H_s field for WSW-RP1
Latitude → (°N)
Longitude → (°E)
H_s → (m)
53.4
53.3
53.2
53.1
53
52.9
52.8
52.7
52.6
-10.4
-10.3
-10.2
-10.1
-10
-9.9
-9.8
-9.7
-9.6
-9.5
-9.4
14
12
10
8
6
4

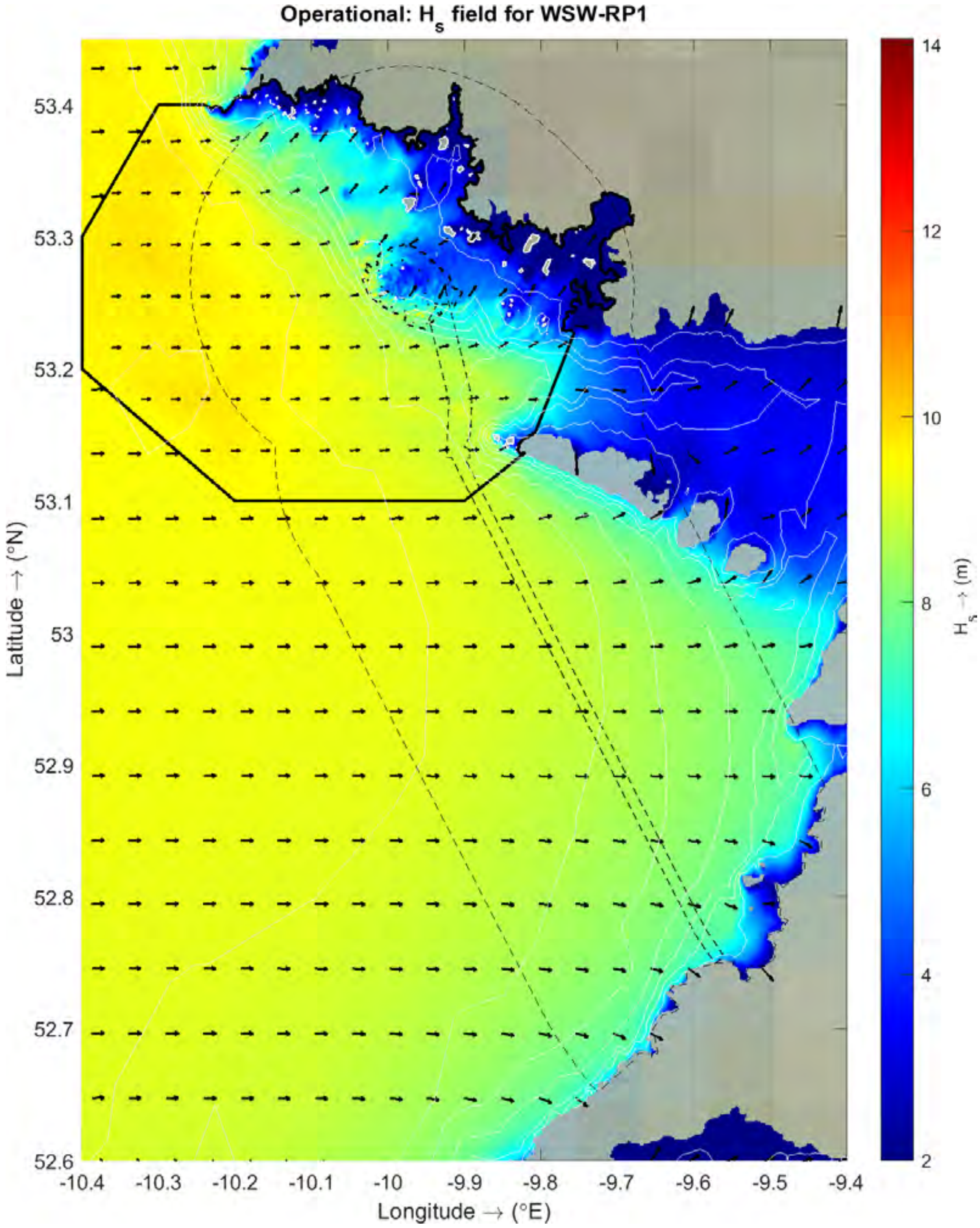
Operational: H_s field for WSW-RP1
53.4
53.3
53.2
53.1
53
52.9
52.8
52.7
52.6
Latitude → (°N)
-10.4
-10.3
-10.2
-10.1
-10
-9.9
-9.8
-9.7
-9.6
-9.5
-9.4
Longitude → (°E)
14
12
10
8
6
4
2
H_s → (m)

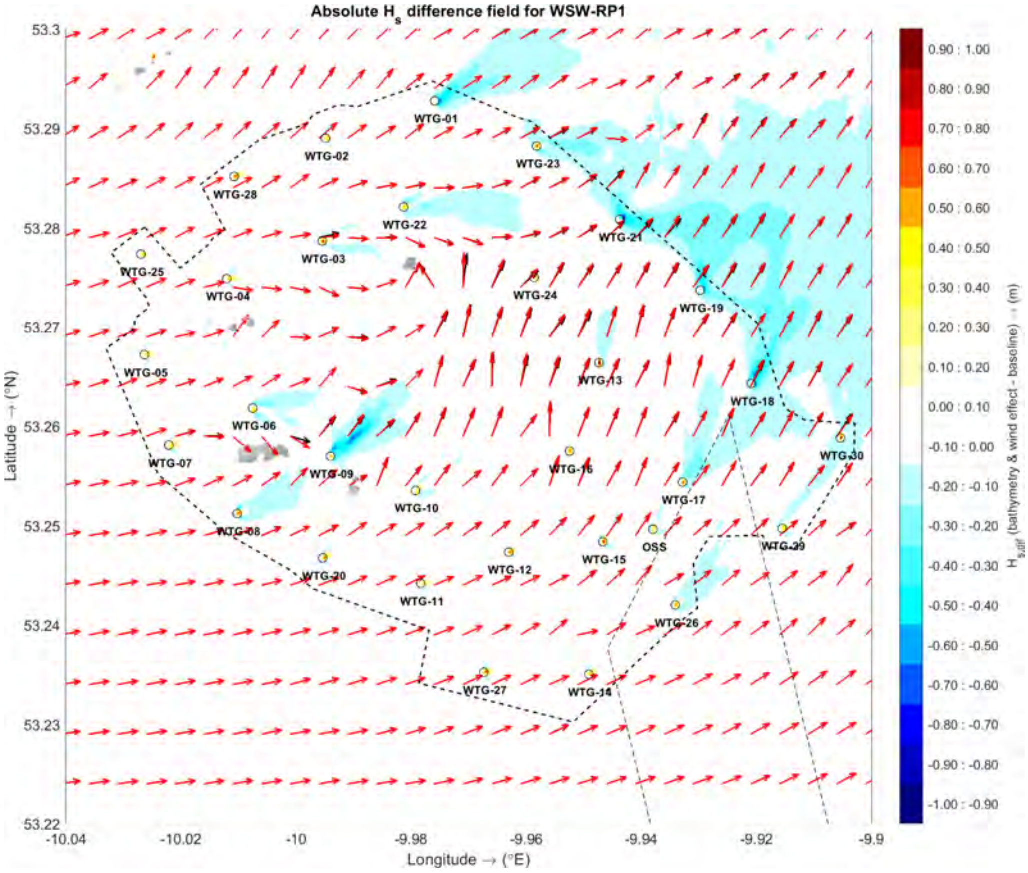
Absolute H_s difference field for WSW-RP1
Latitude → (°N)
Longitude → (°E)
$H_{s,diff}$ (bathymetry & wind effect - baseline) → (m)
0.90 : 1.00
0.80 : 0.90
0.70 : 0.80
0.60 : 0.70
0.50 : 0.60
0.40 : 0.50
0.30 : 0.40
0.20 : 0.30
0.10 : 0.20
0.00 : 0.10
-0.10 : 0.00
-0.20 : -0.10
-0.30 : -0.20
-0.40 : -0.30
-0.50 : -0.40
-0.60 : -0.50
-0.70 : -0.60
-0.80 : -0.70
-0.90 : -0.80
-1.00 : -0.90
WTG-01
WTG-02
WTG-03
WTG-04
WTG-05
WTG-06
WTG-07
WTG-08
WTG-09
WTG-10
WTG-11
WTG-12
WTG-13
WTG-14
WTG-15
WTG-16
WTG-17
WTG-18
WTG-19
WTG-20
WTG-21
WTG-22
WTG-23
WTG-24
WTG-25
WTG-26
WTG-27
WTG-28
WTG-29
WTG-30
OSS

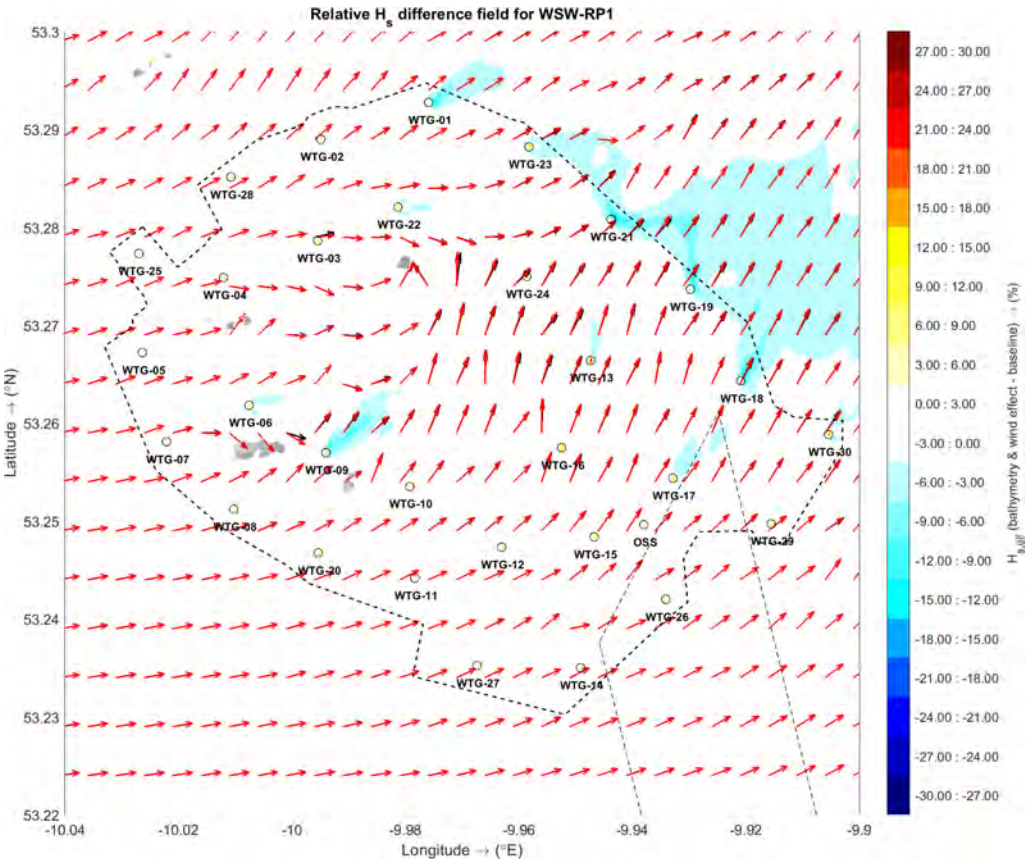
Relative H_s difference field for WSW-RP1
Latitude → (°N)
Longitude → (°E)
$H_{s,diff}$ (bathymetry & wind effect - baseline) → (%)
27.00 : 30.00
24.00 : 27.00
21.00 : 24.00
18.00 : 21.00
15.00 : 18.00
12.00 : 15.00
9.00 : 12.00
6.00 : 9.00
3.00 : 6.00
0.00 : 3.00
-3.00 : 0.00
-6.00 : -3.00
-9.00 : -6.00
-12.00 : -9.00
-15.00 : -12.00
-18.00 : -15.00
-21.00 : -18.00
-24.00 : -21.00
-27.00 : -24.00
-30.00 : -27.00

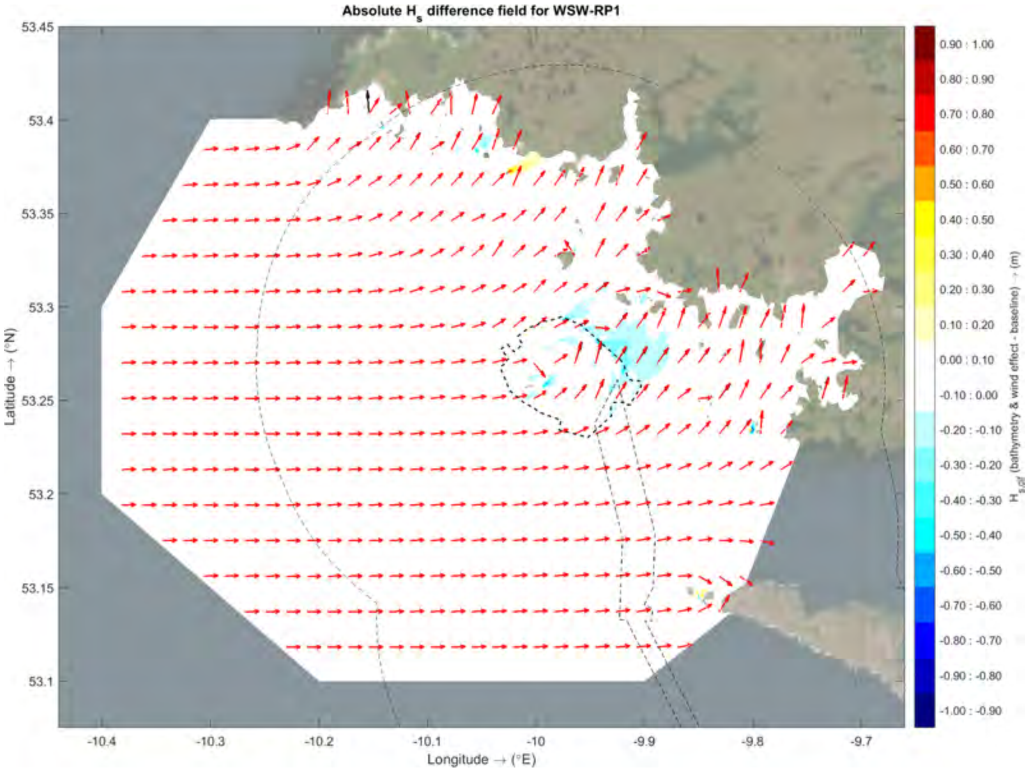
Absolute Hs difference field for WSW-RP1
Latitude → (°N)
Longitude → (°E)
Hs,of (bathymetry & wind effect - baseline) → (m)
0.90 : 1.00
0.80 : 0.90
0.70 : 0.80
0.60 : 0.70
0.50 : 0.60
0.40 : 0.50
0.30 : 0.40
0.20 : 0.30
0.10 : 0.20
0.00 : 0.10
-0.10 : 0.00
-0.20 : -0.10
-0.30 : -0.20
-0.40 : -0.30
-0.50 : -0.40
-0.60 : -0.50
-0.70 : -0.60
-0.80 : -0.70
-0.90 : -0.80
-1.00 : -0.90

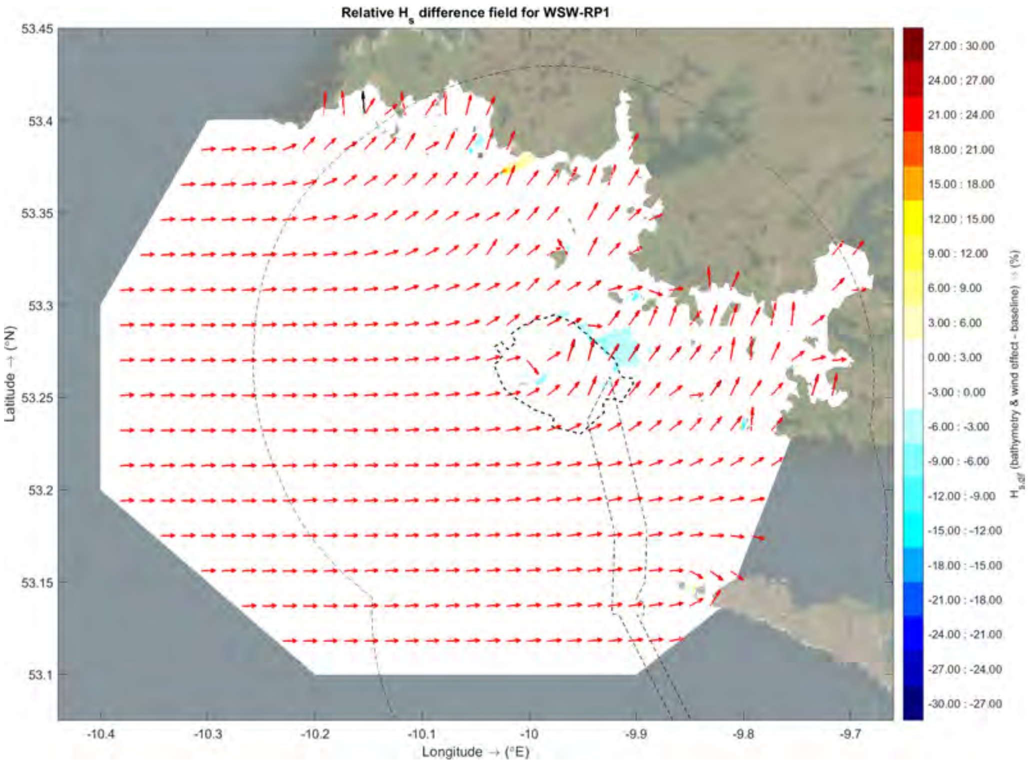
Relative Hs difference field for WSW-RP1
Latitude → (°N)
Longitude → (°E)
Hs,of (bathymetry & wind effect - baseline) → (%)
27.00 : 30.00
24.00 : 27.00
21.00 : 24.00
18.00 : 21.00
15.00 : 18.00
12.00 : 15.00
9.00 : 12.00
6.00 : 9.00
3.00 : 6.00
0.00 : 3.00
-3.00 : 0.00
-6.00 : -3.00
-9.00 : -6.00
-12.00 : -9.00
-15.00 : -12.00
-18.00 : -15.00
-21.00 : -18.00
-24.00 : -21.00
-27.00 : -24.00
-30.00 : -27.00

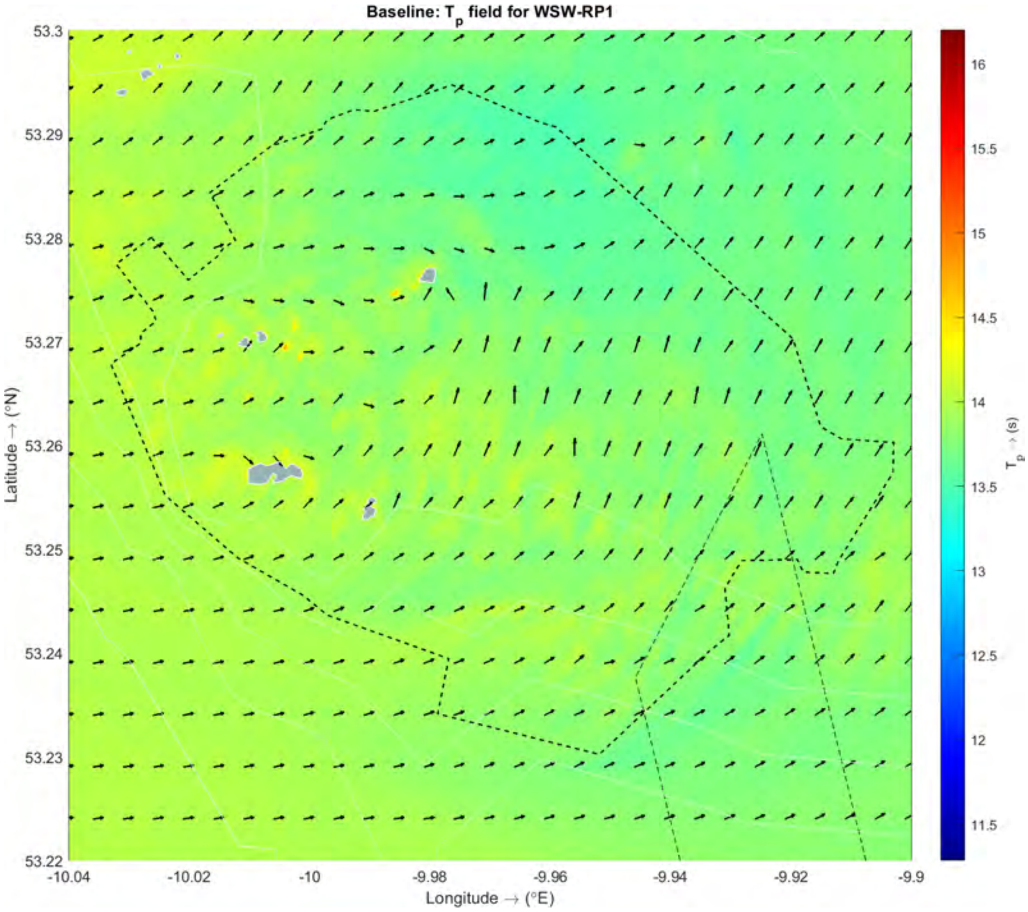
Baseline: T_p field for WSW-RP1
53.3
53.29
53.28
53.27
53.26
53.25
53.24
53.23
53.22
Latitude → (°N)
-10.04
-10.02
-10
-9.98
-9.96
-9.94
-9.92
-9.9
Longitude → (°E)
16
15.5
15
14.5
14
13.5
13
12.5
12
11.5
T_p → (s)

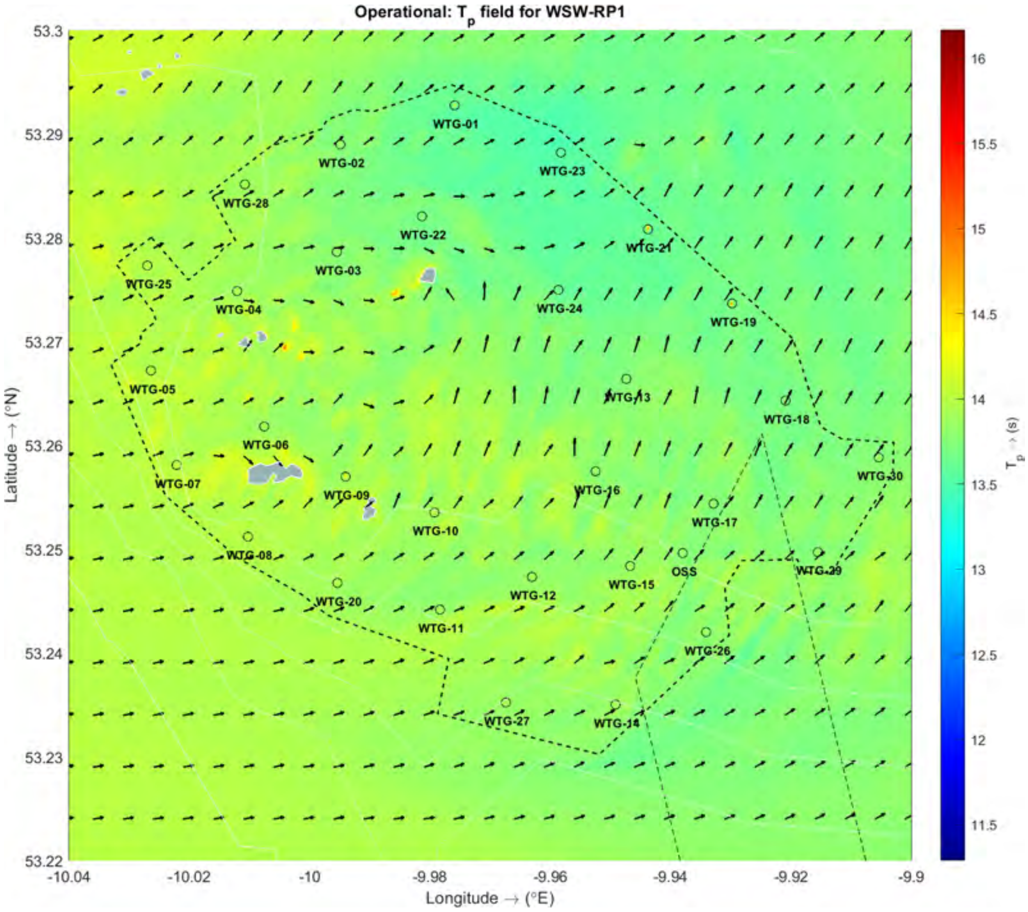

Operational: T_p field for WSW-RP1
Latitude → (°N)
Longitude → (°E)
T_p → (s)
WTG-01
WTG-02
WTG-03
WTG-04
WTG-05
WTG-06
WTG-07
WTG-08
WTG-09
WTG-10
WTG-11
WTG-12
WTG-13
WTG-14
WTG-15
WTG-16
WTG-17
WTG-18
WTG-19
WTG-20
WTG-21
WTG-22
WTG-23
WTG-24
WTG-25
WTG-26
WTG-27
WTG-28
WTG-29
WTG-30
OSS

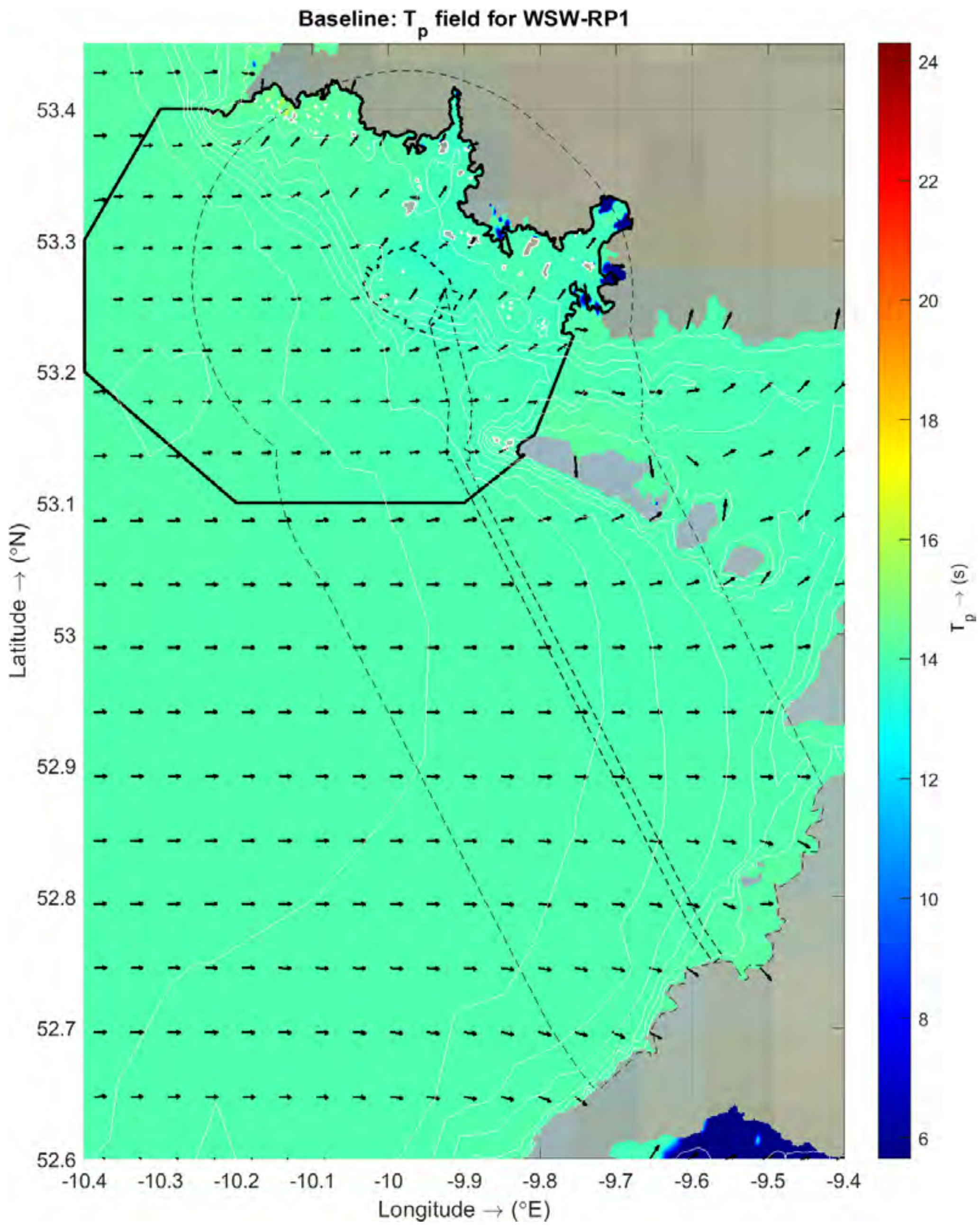
Baseline: T_p field for WSW-RP1
Latitude → (°N)
53.4
53.3
53.2
53.1
53
52.9
52.8
52.7
52.6
-10.4
-10.3
-10.2
-10.1
-10
-9.9
-9.8
-9.7
-9.6
-9.5
-9.4
Longitude → (°E)
T_p → (s)
24
22
20
18
16
14
12
10
8
6

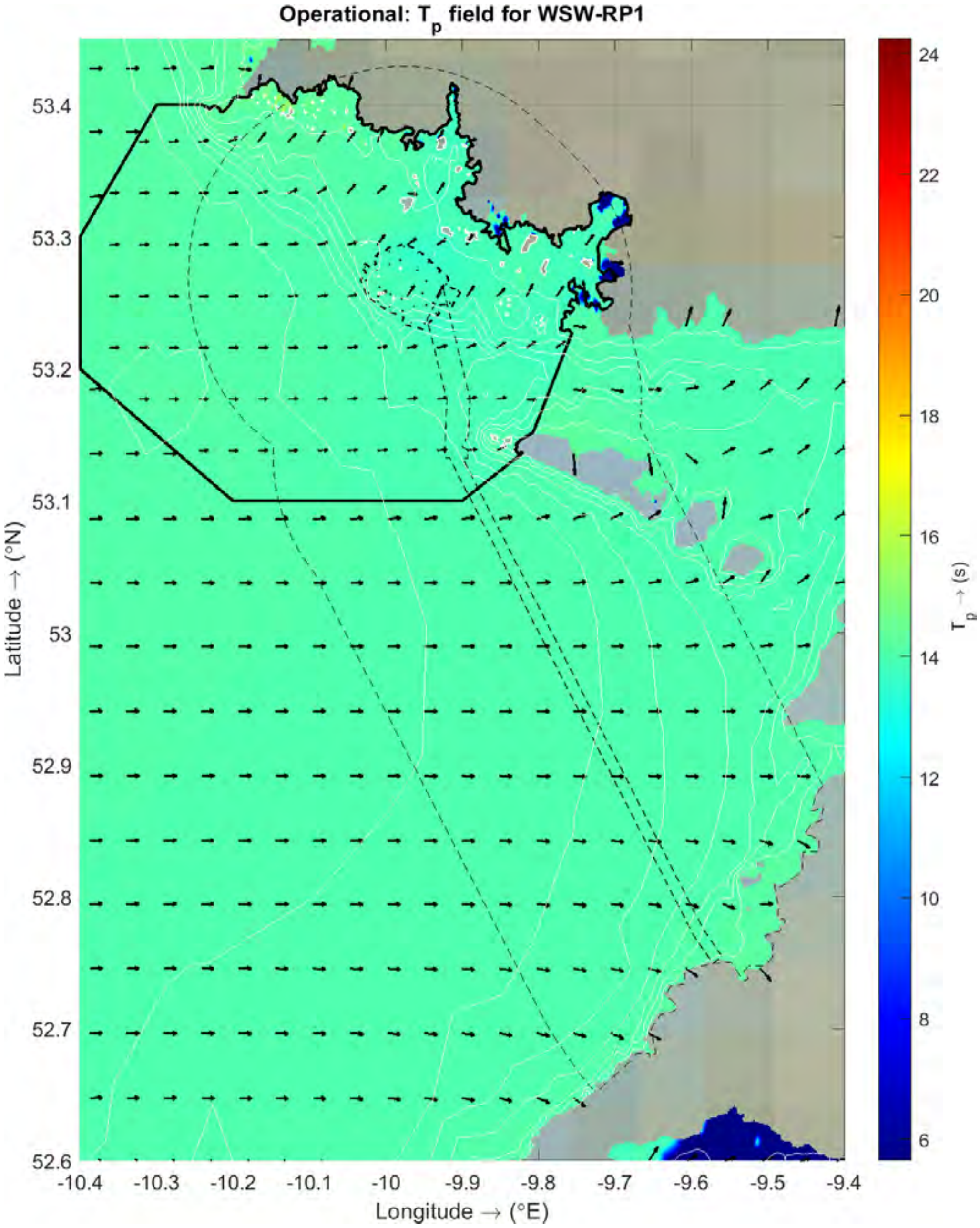
Operational: T_p field for WSW-RP1
Latitude → (°N)
53.4
53.3
53.2
53.1
53
52.9
52.8
52.7
52.6
-10.4
-10.3
-10.2
-10.1
-10
-9.9
-9.8
-9.7
-9.6
-9.5
-9.4
Longitude → (°E)
24
22
20
18
16
14
12
10
8
6
T_p → (s)

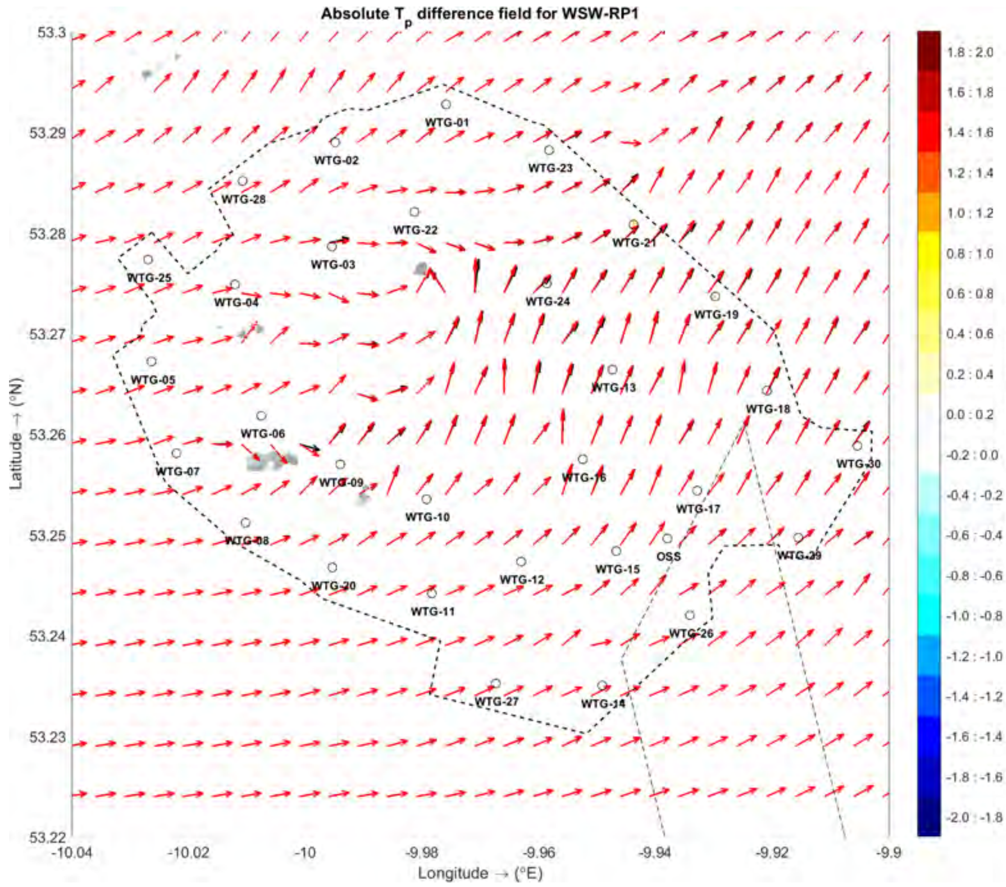
Absolute T_p difference field for WSW-RP1
Latitude → (°N)
Longitude → (°E)
$T_{p,dif}$ (bathymetry & wind effect - baseline) → (s)
WTG-01
WTG-02
WTG-03
WTG-04
WTG-05
WTG-06
WTG-07
WTG-08
WTG-09
WTG-10
WTG-11
WTG-12
WTG-13
WTG-14
WTG-15
WTG-16
WTG-17
WTG-18
WTG-19
WTG-20
WTG-21
WTG-22
WTG-23
WTG-24
WTG-25
WTG-26
WTG-27
WTG-28
WTG-29
WTG-30
OSS
1.8 : 2.0
1.6 : 1.8
1.4 : 1.6
1.2 : 1.4
1.0 : 1.2
0.8 : 1.0
0.6 : 0.8
0.4 : 0.6
0.2 : 0.4
0.0 : 0.2
-0.2 : 0.0
-0.4 : -0.2
-0.6 : -0.4
-0.8 : -0.6
-1.0 : -0.8
-1.2 : -1.0
-1.4 : -1.2
-1.6 : -1.4
-1.8 : -1.6
-2.0 : -1.8

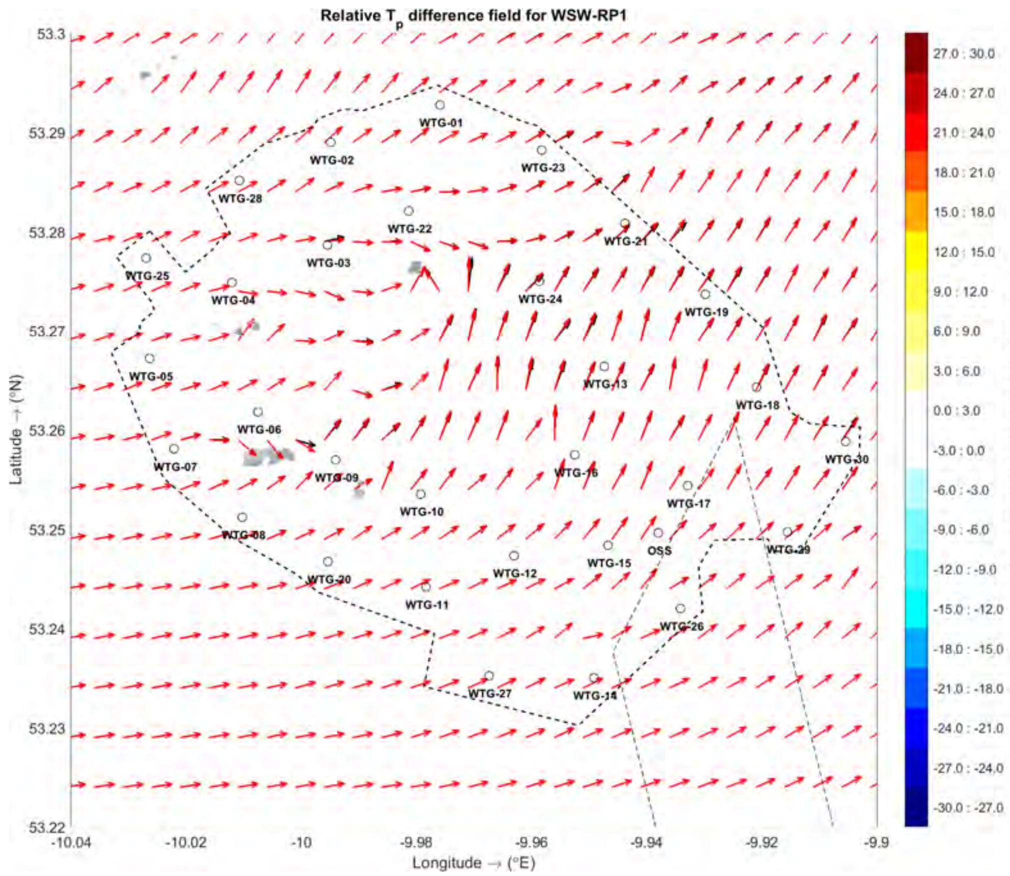
Relative T_p difference field for WSW-RP1
Latitude → (°N)
Longitude → (°E)
$T_{p,dif}$ (bathymetry & wind effect - baseline) → (%)
27.0 : 30.0
24.0 : 27.0
21.0 : 24.0
18.0 : 21.0
15.0 : 18.0
12.0 : 15.0
9.0 : 12.0
6.0 : 9.0
3.0 : 6.0
0.0 : 3.0
-3.0 : 0.0
-6.0 : -3.0
-9.0 : -6.0
-12.0 : -9.0
-15.0 : -12.0
-18.0 : -15.0
-21.0 : -18.0
-24.0 : -21.0
-27.0 : -24.0
-30.0 : -27.0

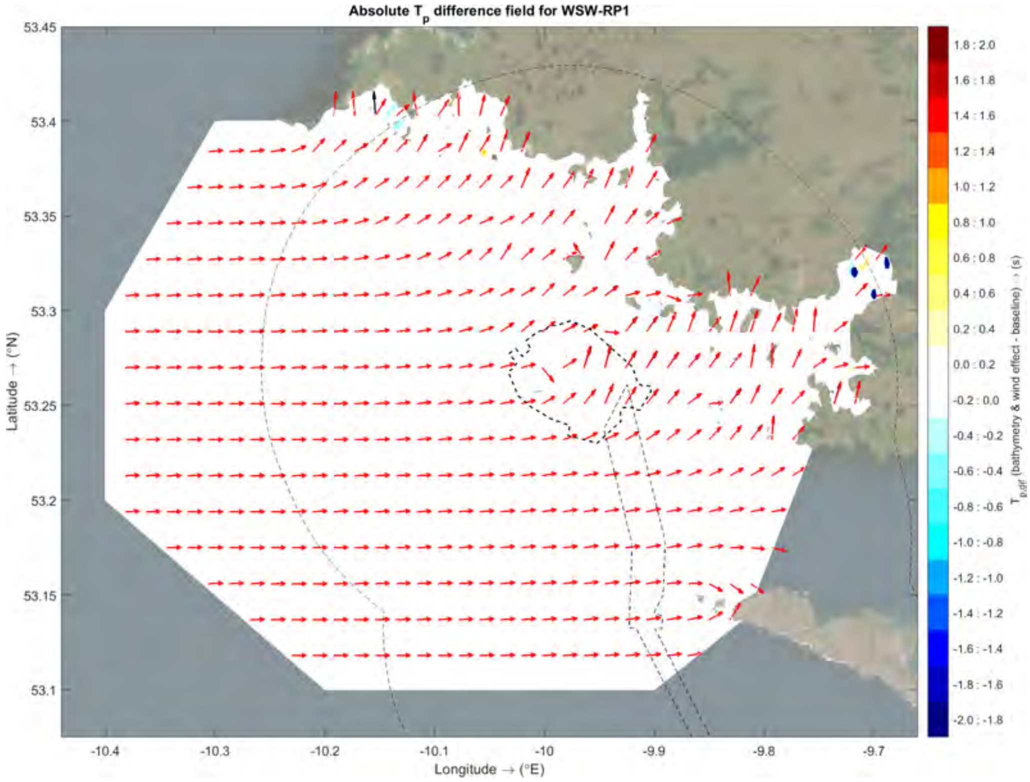
Absolute Tp difference field for WSW-RP1
Latitude → (°N)
Longitude → (°E)
53.45
53.4
53.35
53.3
53.25
53.2
53.15
53.1
-10.4
-10.3
-10.2
-10.1
-10
-9.9
-9.8
-9.7
1.8 : 2.0
1.6 : 1.8
1.4 : 1.6
1.2 : 1.4
1.0 : 1.2
0.8 : 1.0
0.6 : 0.8
0.4 : 0.6
0.2 : 0.4
0.0 : 0.2
-0.2 : 0.0
-0.4 : -0.2
-0.6 : -0.4
-0.8 : -0.6
-1.0 : -0.8
-1.2 : -1.0
-1.4 : -1.2
-1.6 : -1.4
-1.8 : -1.6
-2.0 : -1.8
Tp,diff (bathymetry & wind effect - baseline) → (s)

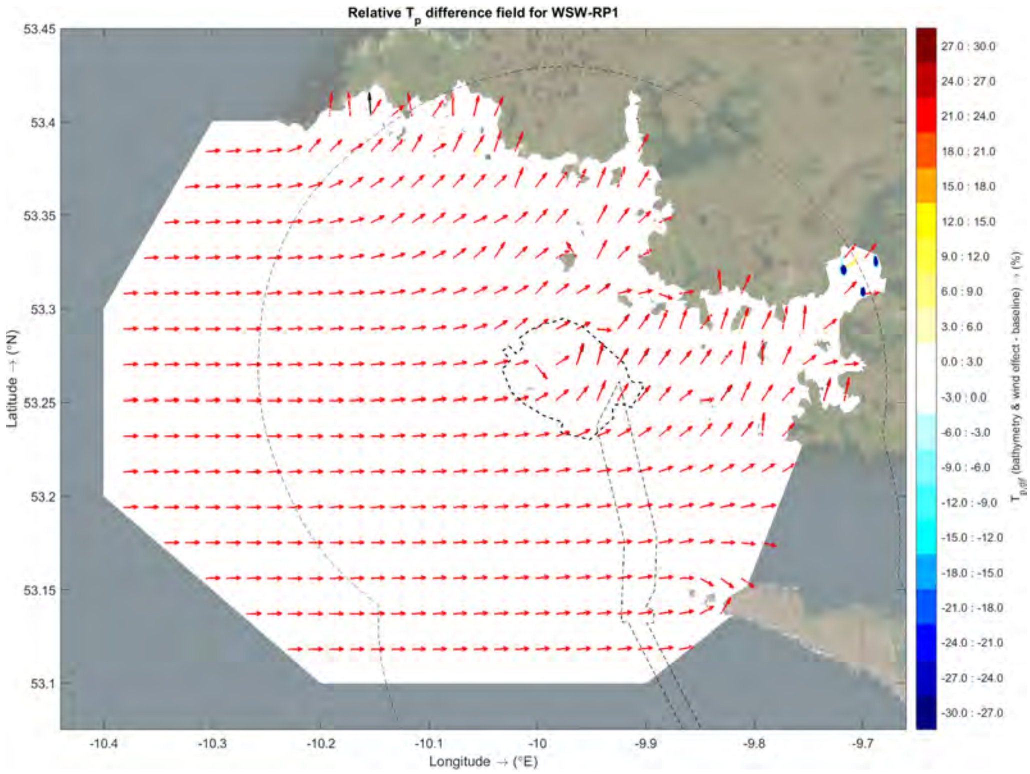
Relative Tp difference field for WSW-RP1
Latitude → (°N)
Longitude → (°E)
53.45
53.4
53.35
53.3
53.25
53.2
53.15
53.1
-10.4
-10.3
-10.2
-10.1
-10
-9.9
-9.8
-9.7
27.0 : 30.0
24.0 : 27.0
21.0 : 24.0
18.0 : 21.0
15.0 : 18.0
12.0 : 15.0
9.0 : 12.0
6.0 : 9.0
3.0 : 6.0
0.0 : 3.0
-3.0 : 0.0
-6.0 : -3.0
-9.0 : -6.0
-12.0 : -9.0
-15.0 : -12.0
-18.0 : -15.0
-21.0 : -18.0
-24.0 : -21.0
-27.0 : -24.0
-30.0 : -27.0
Tp,diff (bathymetry & wind effect - baseline) → (%)

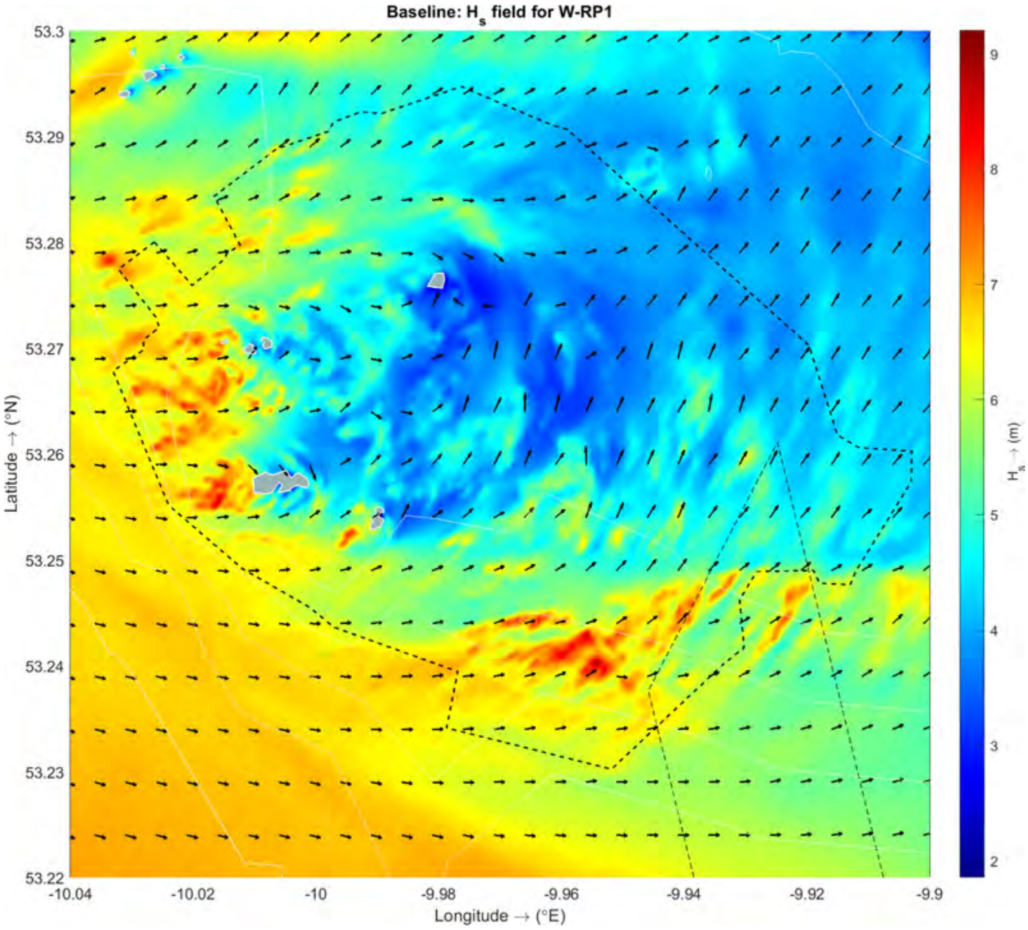
Baseline: H_s field for W-RP1
Latitude → (°N)
Longitude → (°E)
H_s → (m)
53.3
53.29
53.28
53.27
53.26
53.25
53.24
53.23
53.22
-10.04
-10.02
-10
-9.98
-9.96
-9.94
-9.92
-9.9
9
8
7
6
5
4
3
2

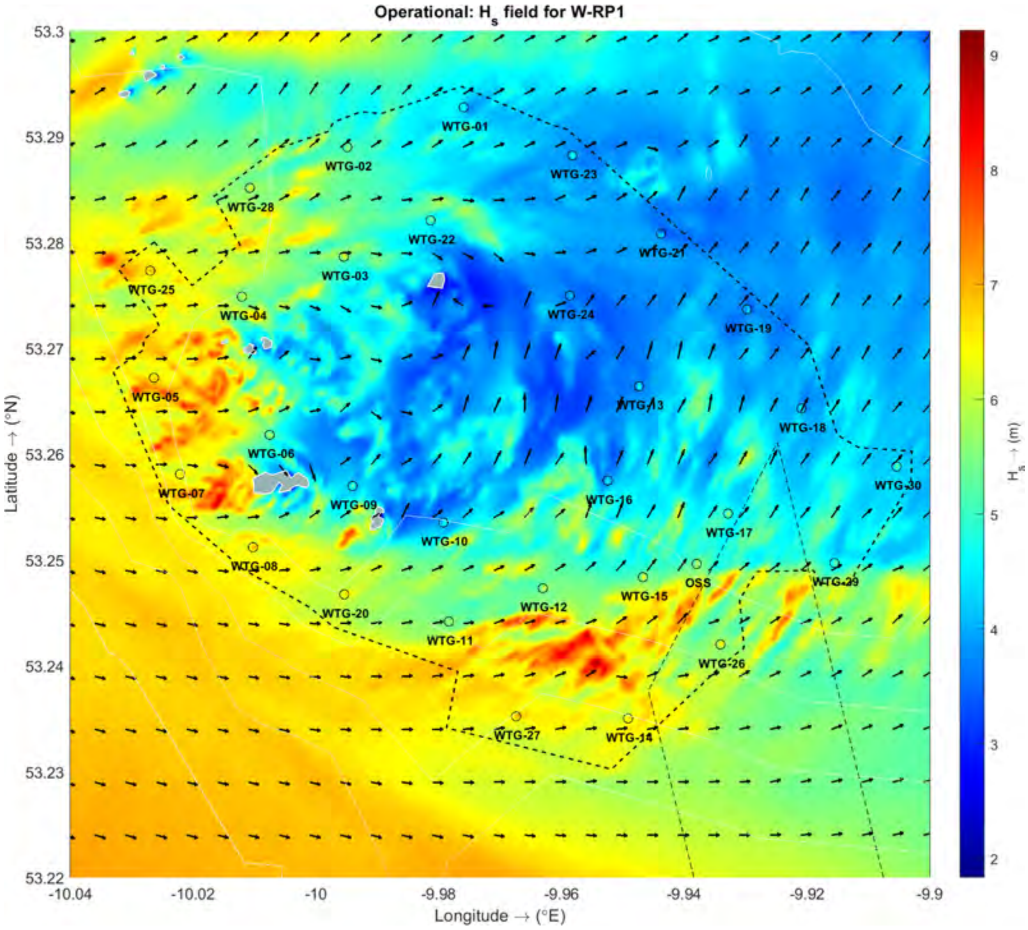

Operational: H_s field for W-RP1
Latitude → (°N)
Longitude → (°E)
H_s → (m)
WTG-01
WTG-02
WTG-03
WTG-04
WTG-05
WTG-06
WTG-07
WTG-08
WTG-09
WTG-10
WTG-11
WTG-12
WTG-13
WTG-14
WTG-15
WTG-16
WTG-17
WTG-18
WTG-19
WTG-20
WTG-21
WTG-22
WTG-23
WTG-24
WTG-25
WTG-26
WTG-27
WTG-28
WTG-29
WTG-30
OSS

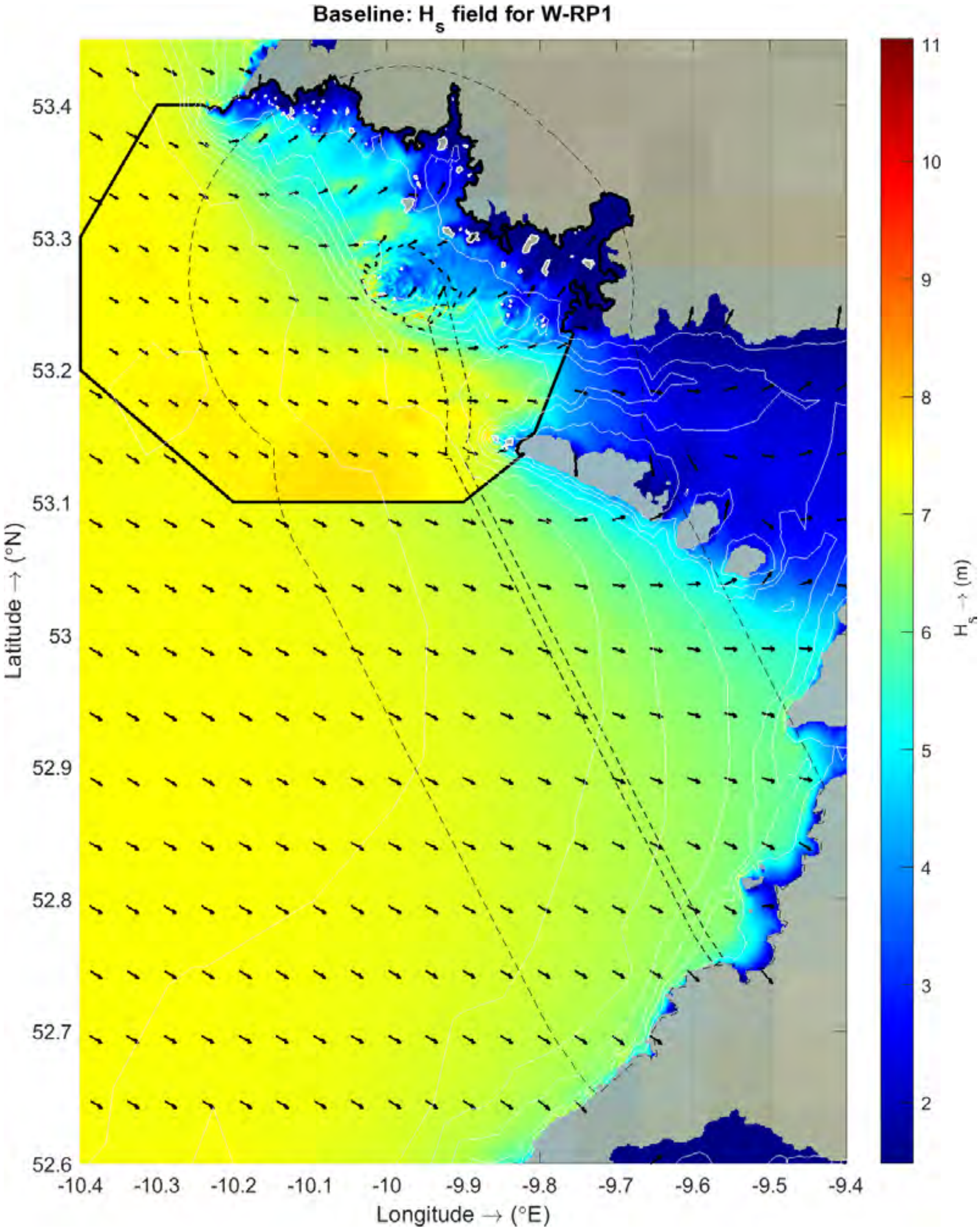
Baseline: H_s field for W-RP1
Latitude → (°N)
53.4
53.3
53.2
53.1
53
52.9
52.8
52.7
52.6
-10.4
-10.3
-10.2
-10.1
-10
-9.9
-9.8
-9.7
-9.6
-9.5
-9.4
Longitude → (°E)
H_s → (m)
11
10
9
8
7
6
5
4
3
2

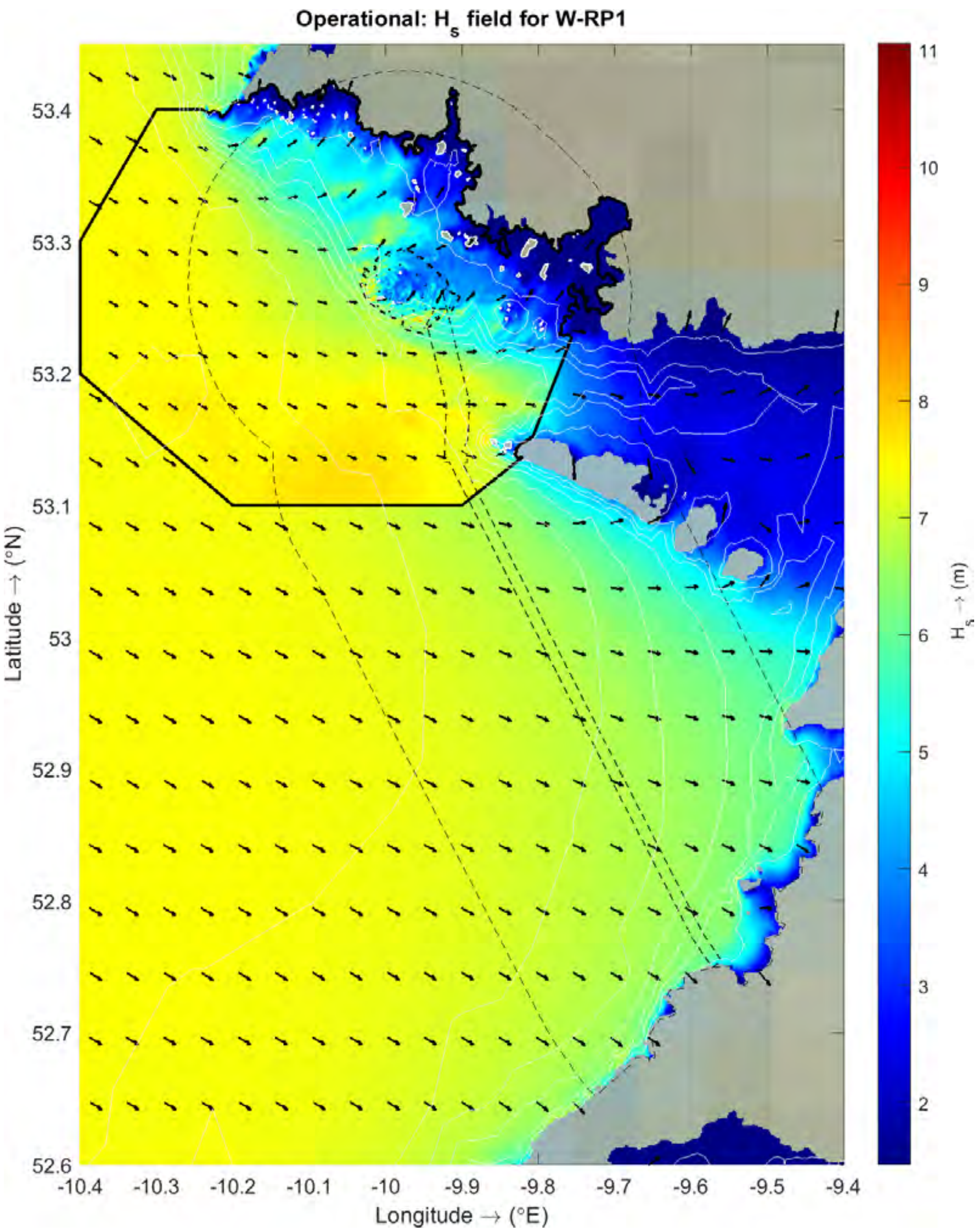
Operational: H_s field for W-RP1
53.4
53.3
53.2
53.1
53
52.9
52.8
52.7
52.6
Latitude → (°N)
-10.4
-10.3
-10.2
-10.1
-10
-9.9
-9.8
-9.7
-9.6
-9.5
-9.4
Longitude → (°E)
11
10
9
8
7
6
5
4
3
2
H_s → (m)

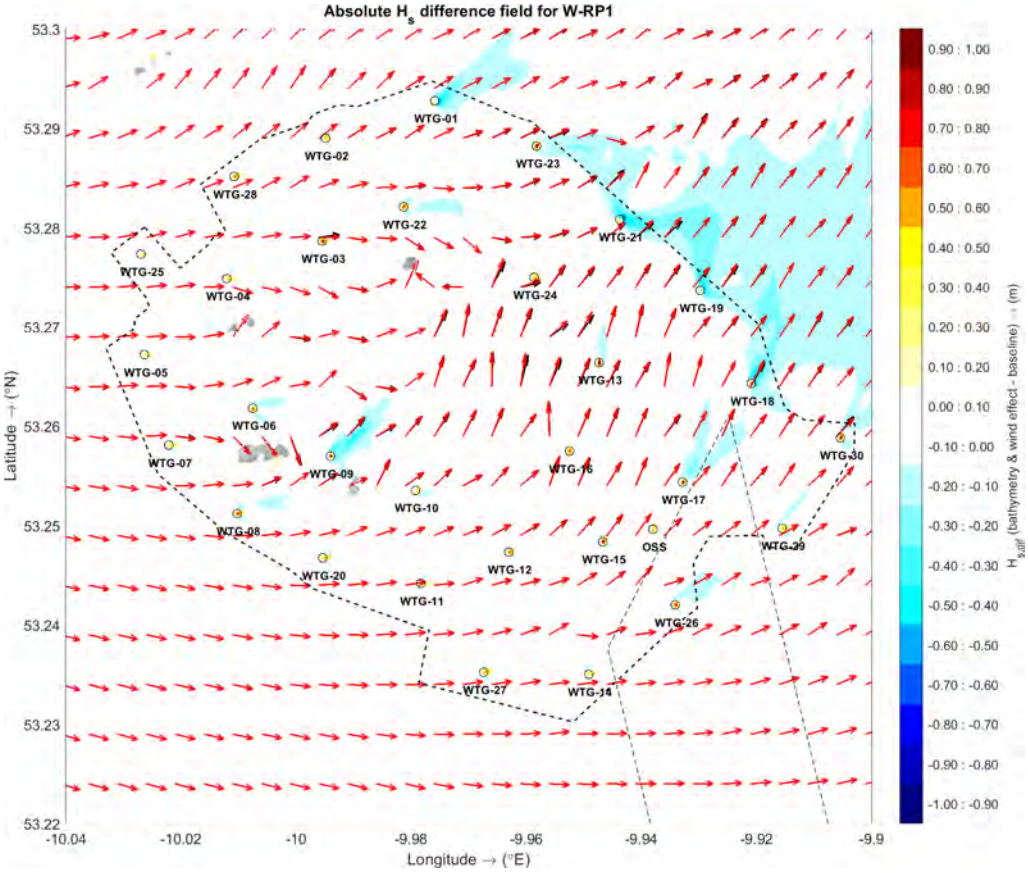
Absolute Hs difference field for W-RP1
Latitude → (°N)
Longitude → (°E)
Hs,diff (bathymetry & wind effect - baseline) → (m)
0.90 : 1.00
0.80 : 0.90
0.70 : 0.80
0.60 : 0.70
0.50 : 0.60
0.40 : 0.50
0.30 : 0.40
0.20 : 0.30
0.10 : 0.20
0.00 : 0.10
-0.10 : 0.00
-0.20 : -0.10
-0.30 : -0.20
-0.40 : -0.30
-0.50 : -0.40
-0.60 : -0.50
-0.70 : -0.60
-0.80 : -0.70
-0.90 : -0.80
-1.00 : -0.90

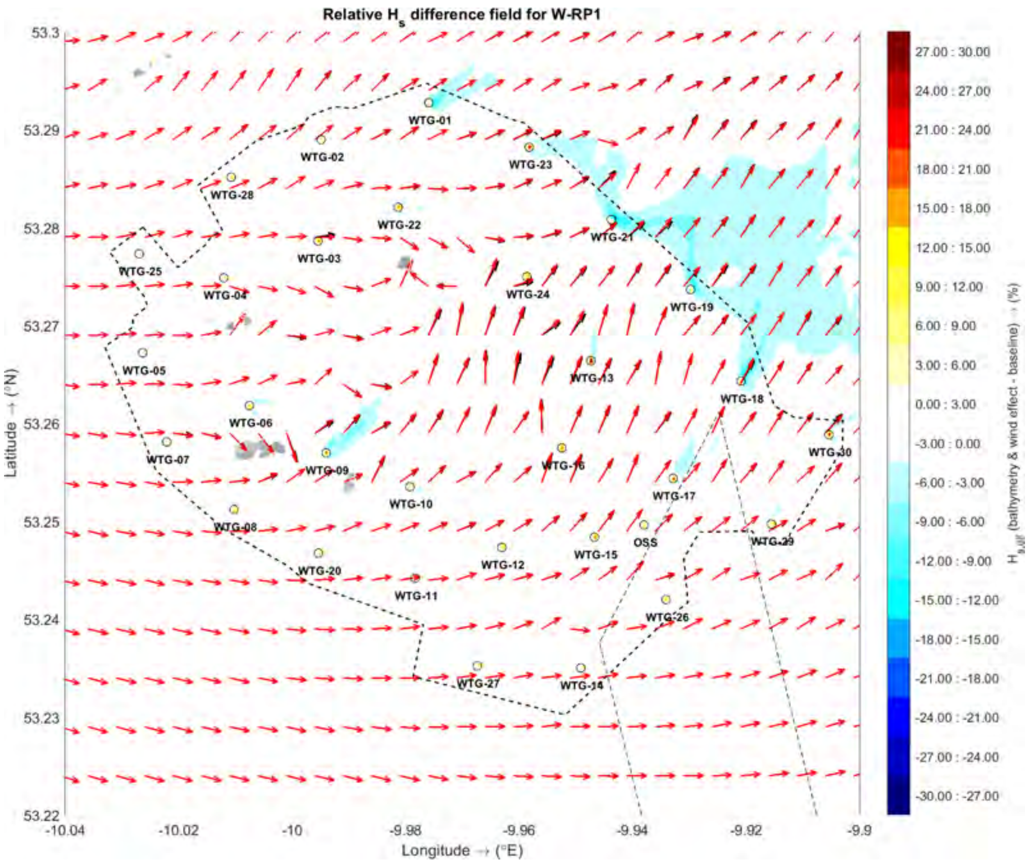
Relative Hs difference field for W-RP1
Latitude → (°N)
Longitude → (°E)
Hs,diff (bathymetry & wind effect - baseline) → (%)
27.00 : 30.00
24.00 : 27.00
21.00 : 24.00
18.00 : 21.00
15.00 : 18.00
12.00 : 15.00
9.00 : 12.00
6.00 : 9.00
3.00 : 6.00
0.00 : 3.00
-3.00 : 0.00
-6.00 : -3.00
-9.00 : -6.00
-12.00 : -9.00
-15.00 : -12.00
-18.00 : -15.00
-21.00 : -18.00
-24.00 : -21.00
-27.00 : -24.00
-30.00 : -27.00

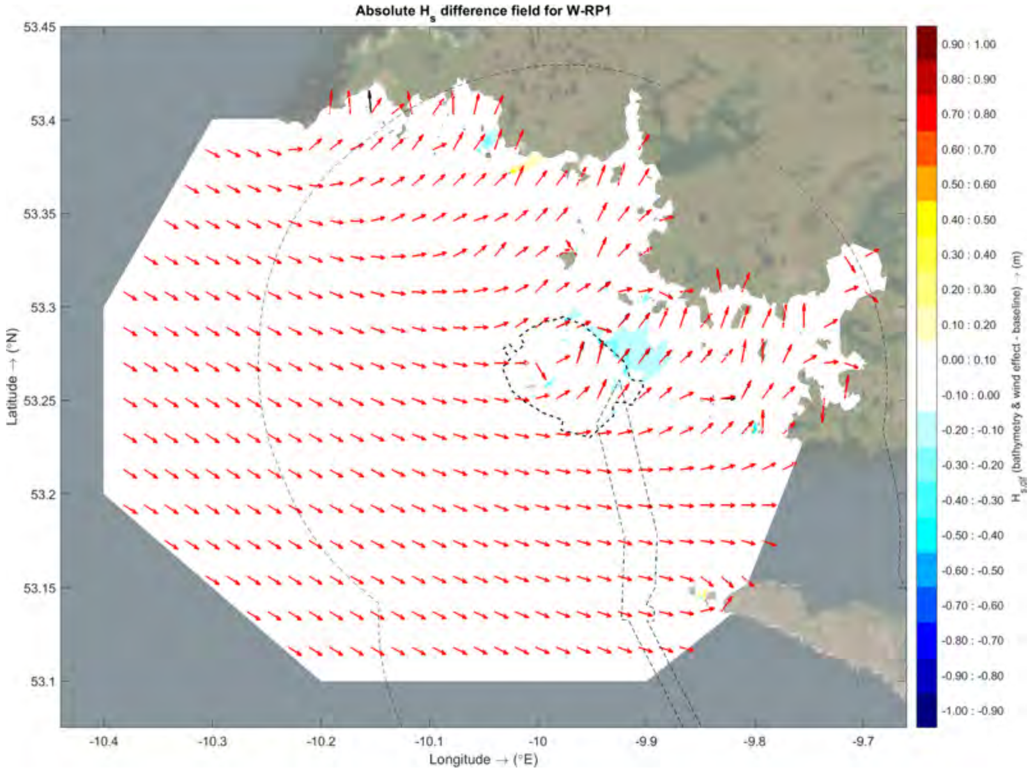
Absolute Hs difference field for W-RP1
Latitude → (°N)
Longitude → (°E)
53.45
53.4
53.35
53.3
53.25
53.2
53.15
53.1
-10.4
-10.3
-10.2
-10.1
-10
-9.9
-9.8
-9.7
0.90 : 1.00
0.80 : 0.90
0.70 : 0.80
0.60 : 0.70
0.50 : 0.60
0.40 : 0.50
0.30 : 0.40
0.20 : 0.30
0.10 : 0.20
0.00 : 0.10
-0.10 : 0.00
-0.20 : -0.10
-0.30 : -0.20
-0.40 : -0.30
-0.50 : -0.40
-0.60 : -0.50
-0.70 : -0.60
-0.80 : -0.70
-0.90 : -0.80
-1.00 : -0.90
Hs,dif (bathymetry & wind effect - baseline) → (m)

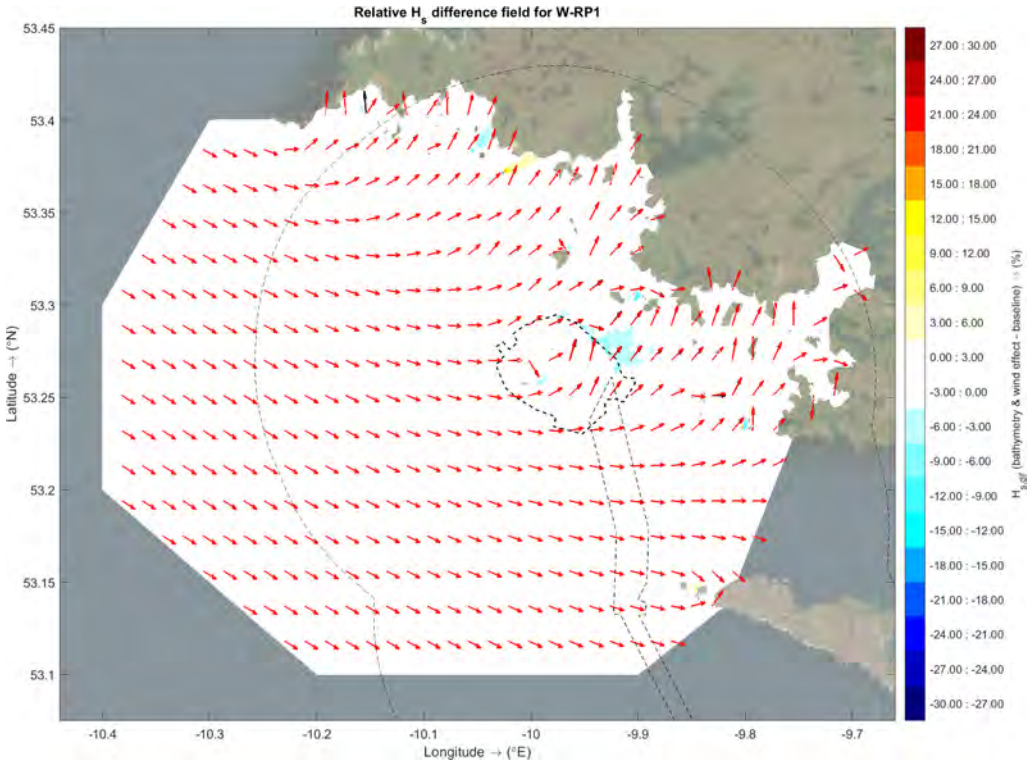
Relative Hs difference field for W-RP1
Latitude → (°N)
Longitude → (°E)
53.45
53.4
53.35
53.3
53.25
53.2
53.15
53.1
-10.4
-10.3
-10.2
-10.1
-10
-9.9
-9.8
-9.7
27.00 : 30.00
24.00 : 27.00
21.00 : 24.00
18.00 : 21.00
15.00 : 18.00
12.00 : 15.00
9.00 : 12.00
6.00 : 9.00
3.00 : 6.00
0.00 : 3.00
-3.00 : 0.00
-6.00 : -3.00
-9.00 : -6.00
-12.00 : -9.00
-15.00 : -12.00
-18.00 : -15.00
-21.00 : -18.00
-24.00 : -21.00
-27.00 : -24.00
-30.00 : -27.00
Hs,dif (bathymetry & wind effect - baseline) → (%)

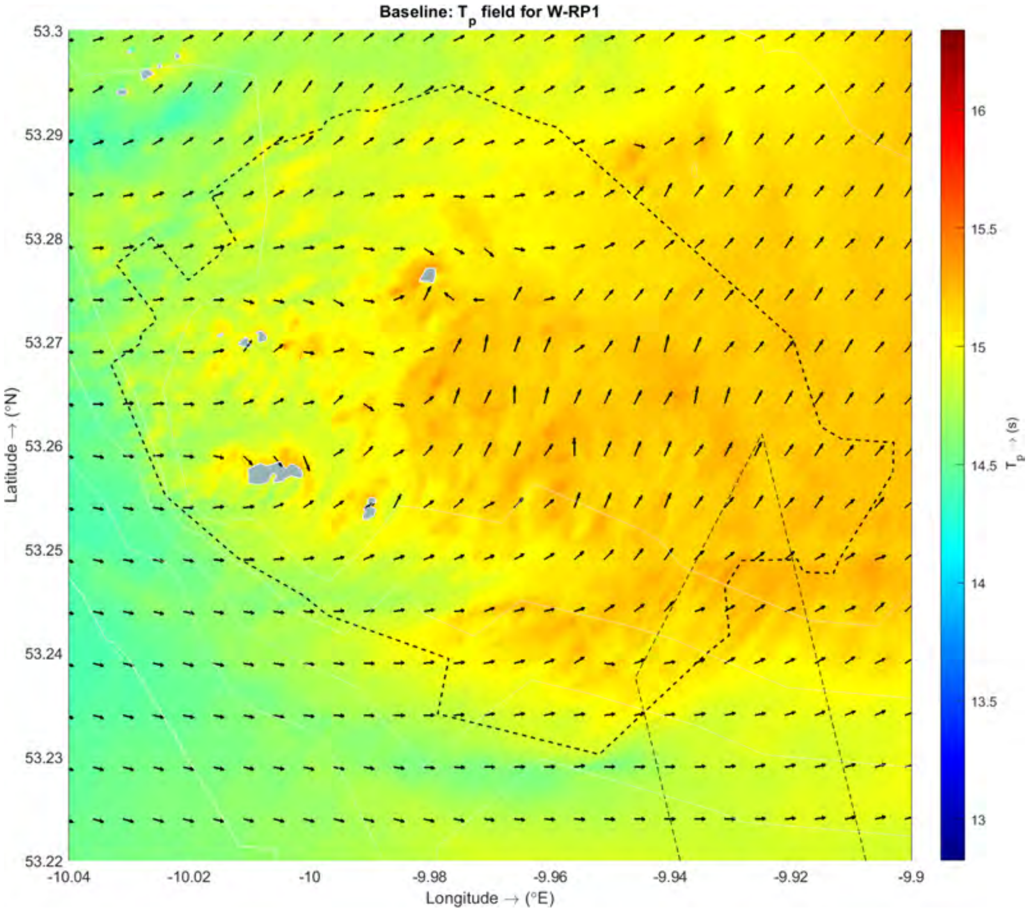
Baseline: T_p field for W-RP1
Latitude → (°N)
Longitude → (°E)
T_p → (s)
53.3
53.29
53.28
53.27
53.26
53.25
53.24
53.23
53.22
-10.04
-10.02
-10
-9.98
-9.96
-9.94
-9.92
-9.9
16
15.5
15
14.5
14
13.5
13

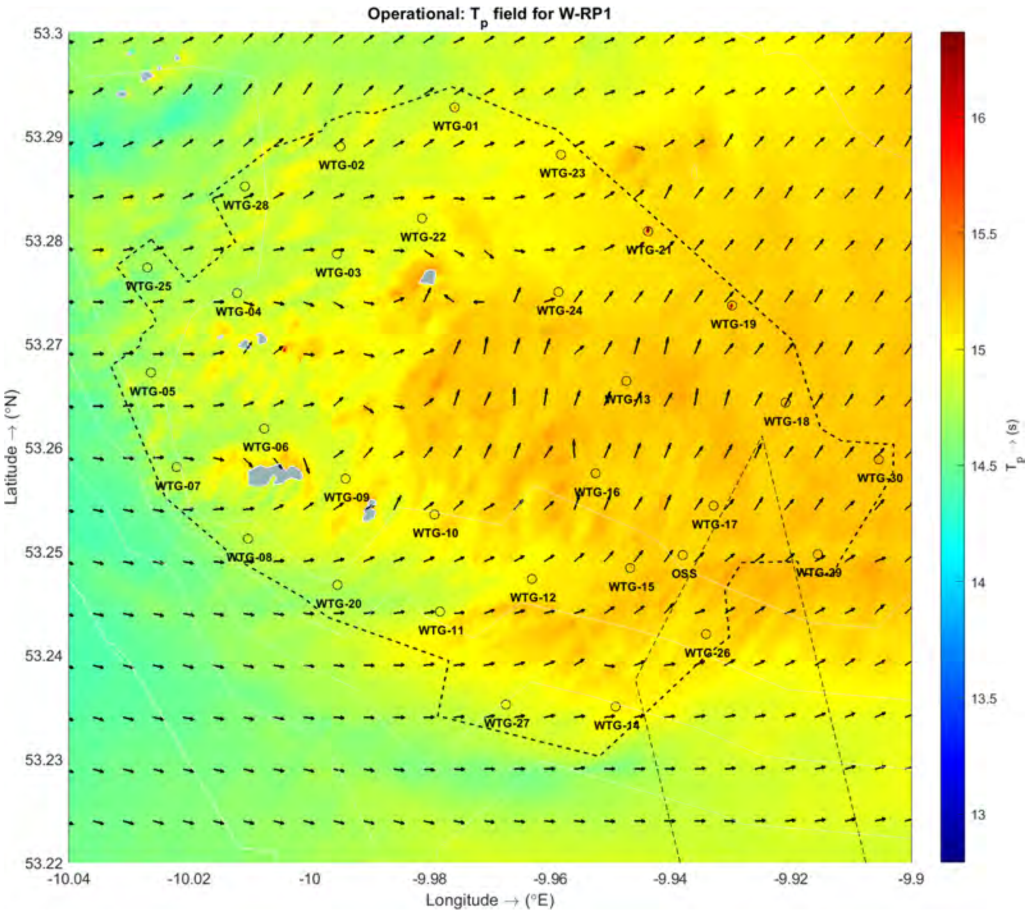

Operational: T_p field for W-RP1
Latitude → (°N)
Longitude → (°E)
T_p → (s)
WTG-01
WTG-02
WTG-03
WTG-04
WTG-05
WTG-06
WTG-07
WTG-08
WTG-09
WTG-10
WTG-11
WTG-12
WTG-13
WTG-14
WTG-15
WTG-16
WTG-17
WTG-18
WTG-19
WTG-20
WTG-21
WTG-22
WTG-23
WTG-24
WTG-25
WTG-26
WTG-27
WTG-28
WTG-29
WTG-30
OSS

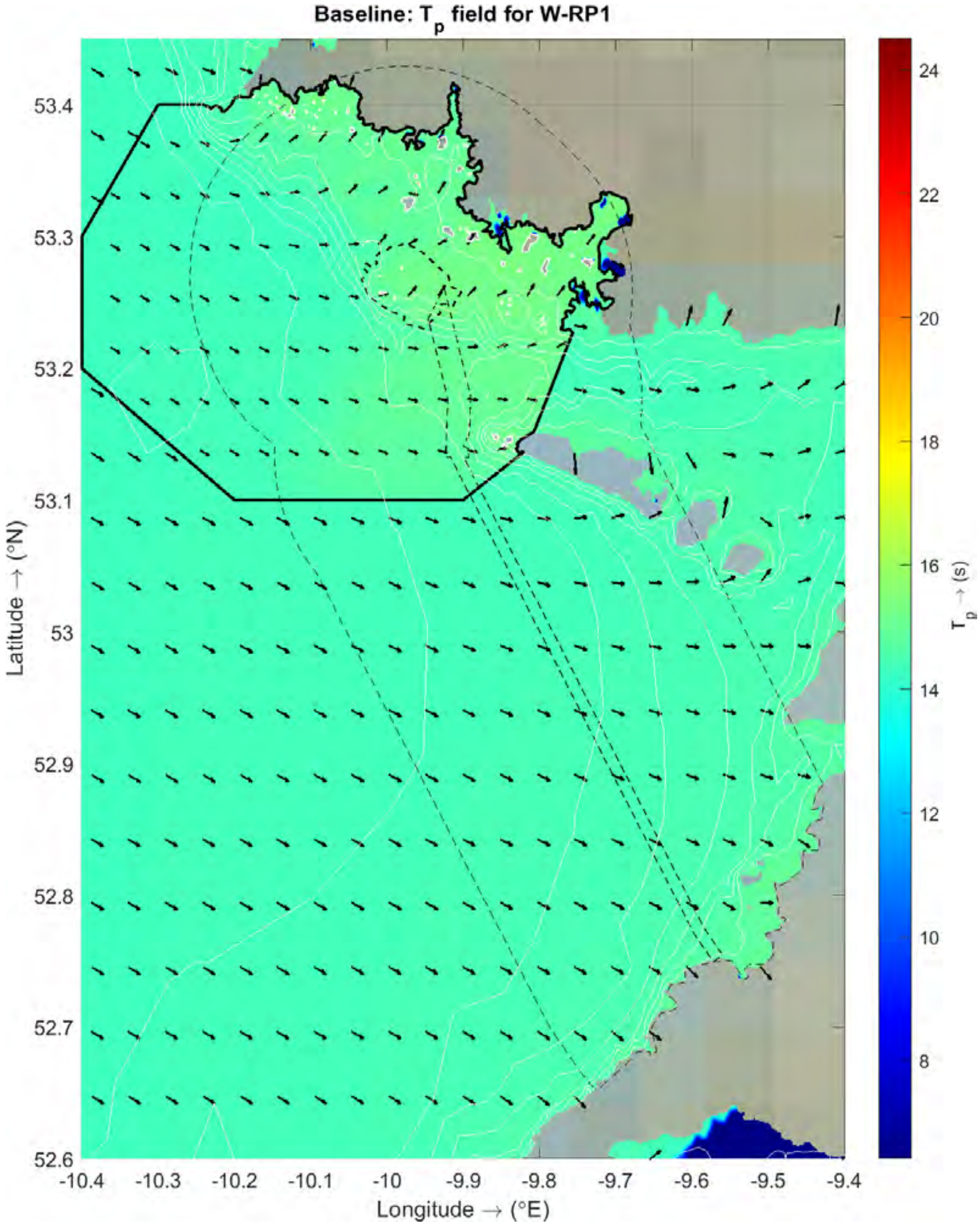
Baseline: T_p field for W-RP1
53.4
53.3
53.2
53.1
53
52.9
52.8
52.7
52.6
Latitude → (°N)
-10.4
-10.3
-10.2
-10.1
-10
-9.9
-9.8
-9.7
-9.6
-9.5
-9.4
Longitude → (°E)
24
22
20
18
16
14
12
10
8
T_p → (s)

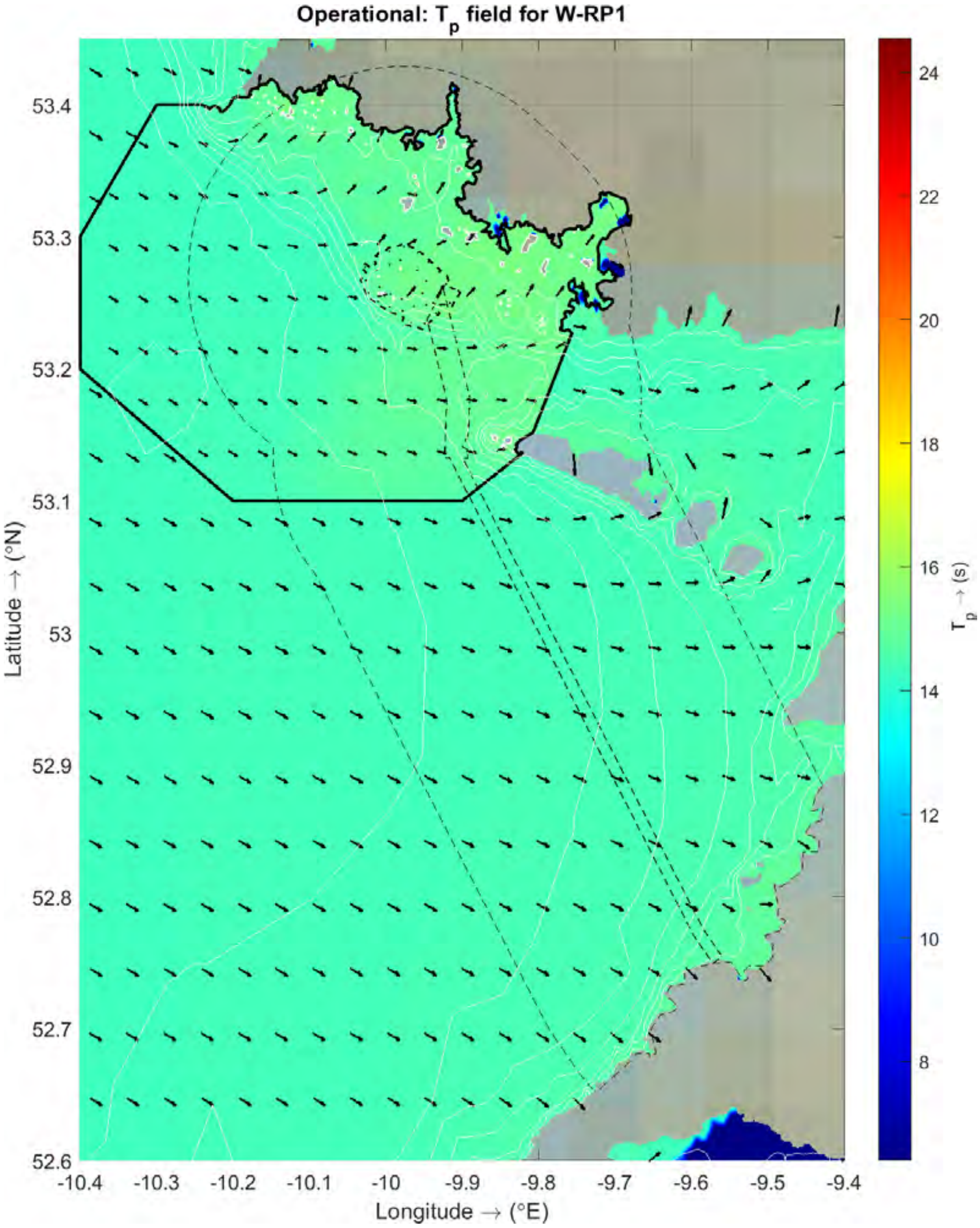
Operational: T_p field for W-RP1
53.4
53.3
53.2
53.1
53
52.9
52.8
52.7
52.6
Latitude → (°N)
-10.4
-10.3
-10.2
-10.1
-10
-9.9
-9.8
-9.7
-9.6
-9.5
-9.4
Longitude → (°E)
24
22
20
18
16
14
12
10
8
T_p → (s)

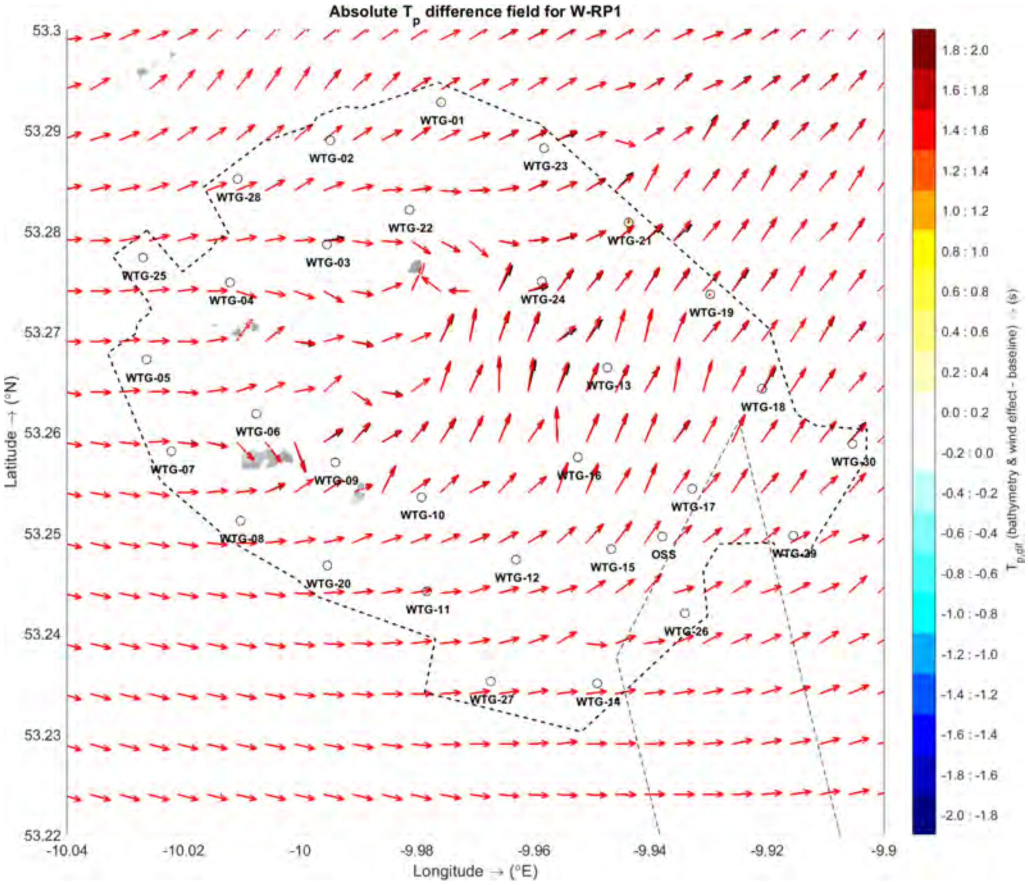
Absolute T_p difference field for W-RP1
Latitude → (°N)
Longitude → (°E)
$T_{p,dif}$ (bathymetry & wind effect - baseline) → (s)
WTG-01
WTG-02
WTG-03
WTG-04
WTG-05
WTG-06
WTG-07
WTG-08
WTG-09
WTG-10
WTG-11
WTG-12
WTG-13
WTG-14
WTG-15
WTG-16
WTG-17
WTG-18
WTG-19
WTG-20
WTG-21
WTG-22
WTG-23
WTG-24
WTG-25
WTG-26
WTG-27
WTG-28
WTG-29
WTG-30
OSS
1.8 : 2.0
1.6 : 1.8
1.4 : 1.6
1.2 : 1.4
1.0 : 1.2
0.8 : 1.0
0.6 : 0.8
0.4 : 0.6
0.2 : 0.4
0.0 : 0.2
-0.2 : 0.0
-0.4 : -0.2
-0.6 : -0.4
-0.8 : -0.6
-1.0 : -0.8
-1.2 : -1.0
-1.4 : -1.2
-1.6 : -1.4
-1.8 : -1.6
-2.0 : -1.8

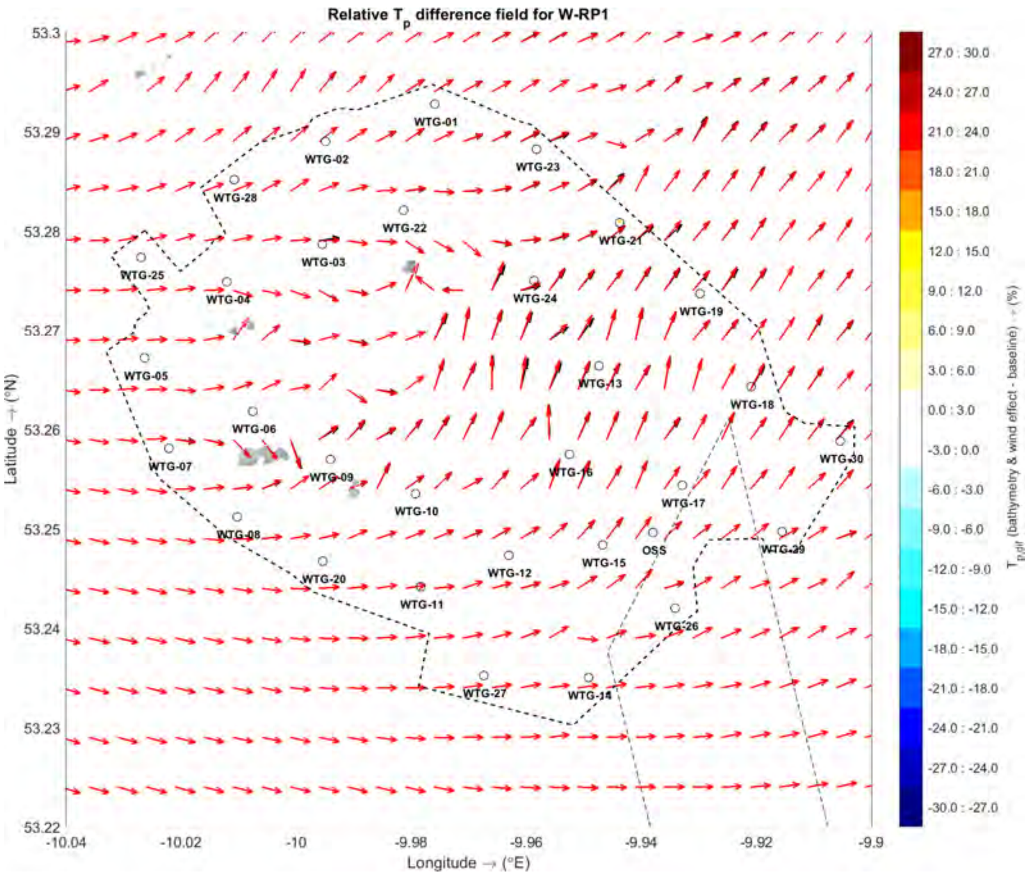
Relative T_p difference field for W-RP1
Latitude → (°N)
Longitude → (°E)
$T_{p,dif}$ (bathymetry & wind effect - baseline) → (%)
27.0 : 30.0
24.0 : 27.0
21.0 : 24.0
18.0 : 21.0
15.0 : 18.0
12.0 : 15.0
9.0 : 12.0
6.0 : 9.0
3.0 : 6.0
0.0 : 3.0
-3.0 : 0.0
-6.0 : -3.0
-9.0 : -6.0
-12.0 : -9.0
-15.0 : -12.0
-18.0 : -15.0
-21.0 : -18.0
-24.0 : -21.0
-27.0 : -24.0
-30.0 : -27.0

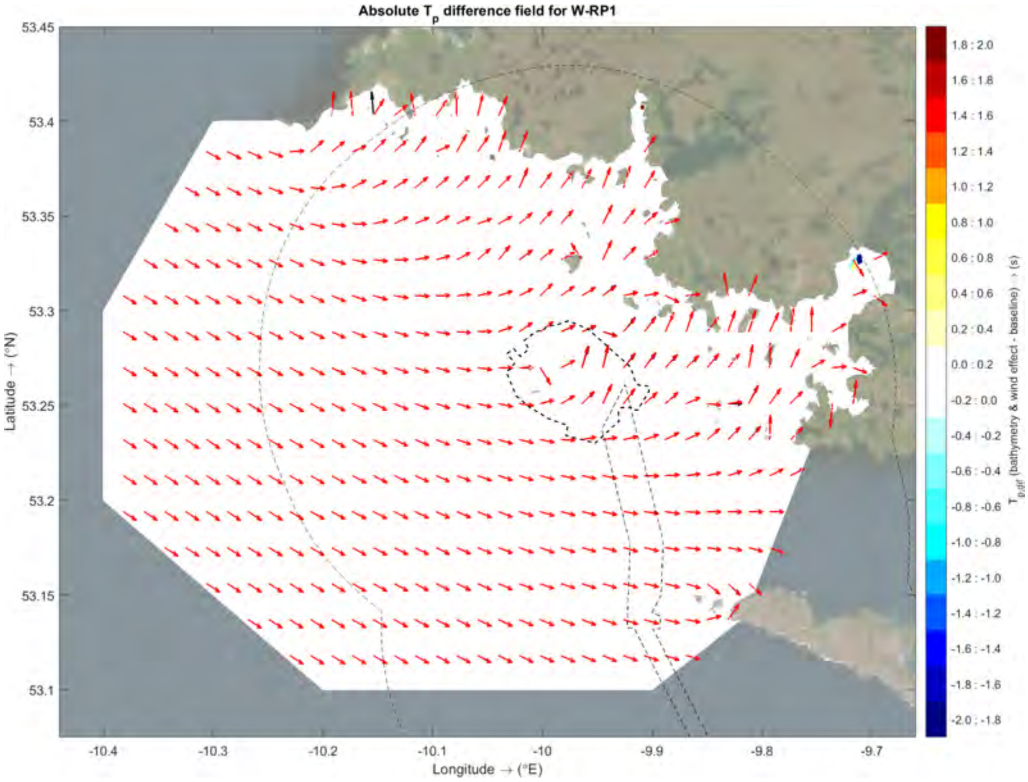
Absolute T_p difference field for W-RP1
Latitude → (°N)
Longitude → (°E)
T_p,dif (bathymetry & wind effect - baseline) → (s)
1.8 : 2.0
1.6 : 1.8
1.4 : 1.6
1.2 : 1.4
1.0 : 1.2
0.8 : 1.0
0.6 : 0.8
0.4 : 0.6
0.2 : 0.4
0.0 : 0.2
-0.2 : 0.0
-0.4 : -0.2
-0.6 : -0.4
-0.8 : -0.6
-1.0 : -0.8
-1.2 : -1.0
-1.4 : -1.2
-1.6 : -1.4
-1.8 : -1.6
-2.0 : -1.8

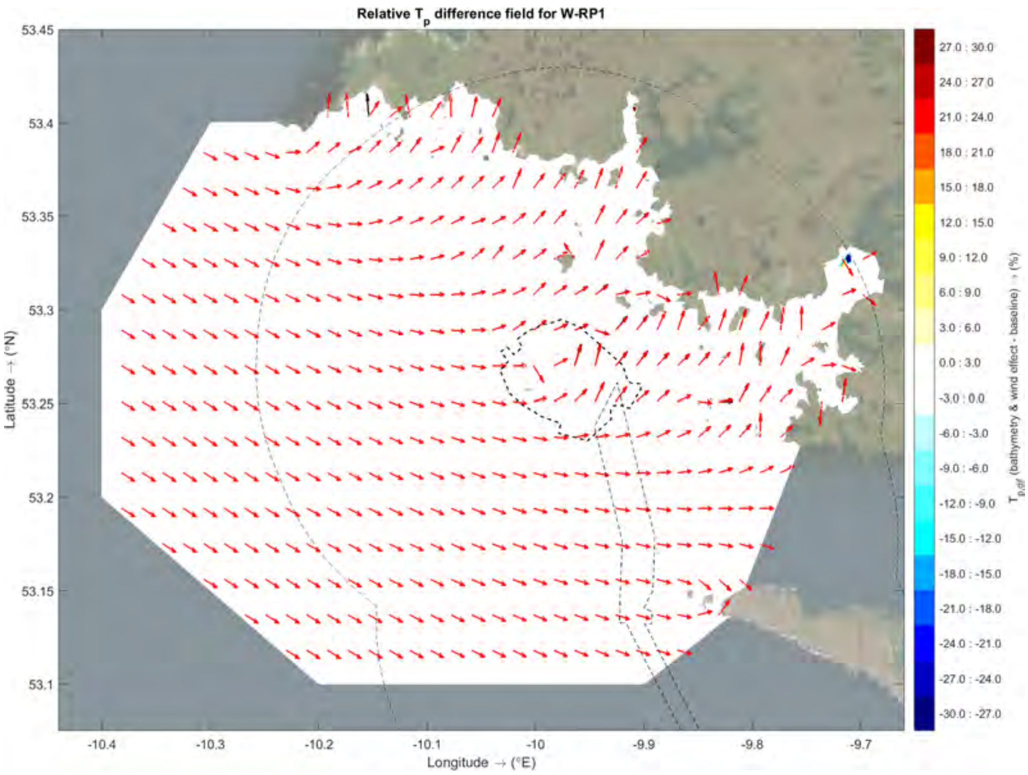
Relative T_p difference field for W-RP1
Latitude → (°N)
Longitude → (°E)
T_p,dif (bathymetry & wind effect - baseline) → (%)
27.0 : 30.0
24.0 : 27.0
21.0 : 24.0
18.0 : 21.0
15.0 : 18.0
12.0 : 15.0
9.0 : 12.0
6.0 : 9.0
3.0 : 6.0
0.0 : 3.0
-3.0 : 0.0
-6.0 : -3.0
-9.0 : -6.0
-12.0 : -9.0
-15.0 : -12.0
-18.0 : -15.0
-21.0 : -18.0
-24.0 : -21.0
-27.0 : -24.0
-30.0 : -27.0

E.4 5-yr RP

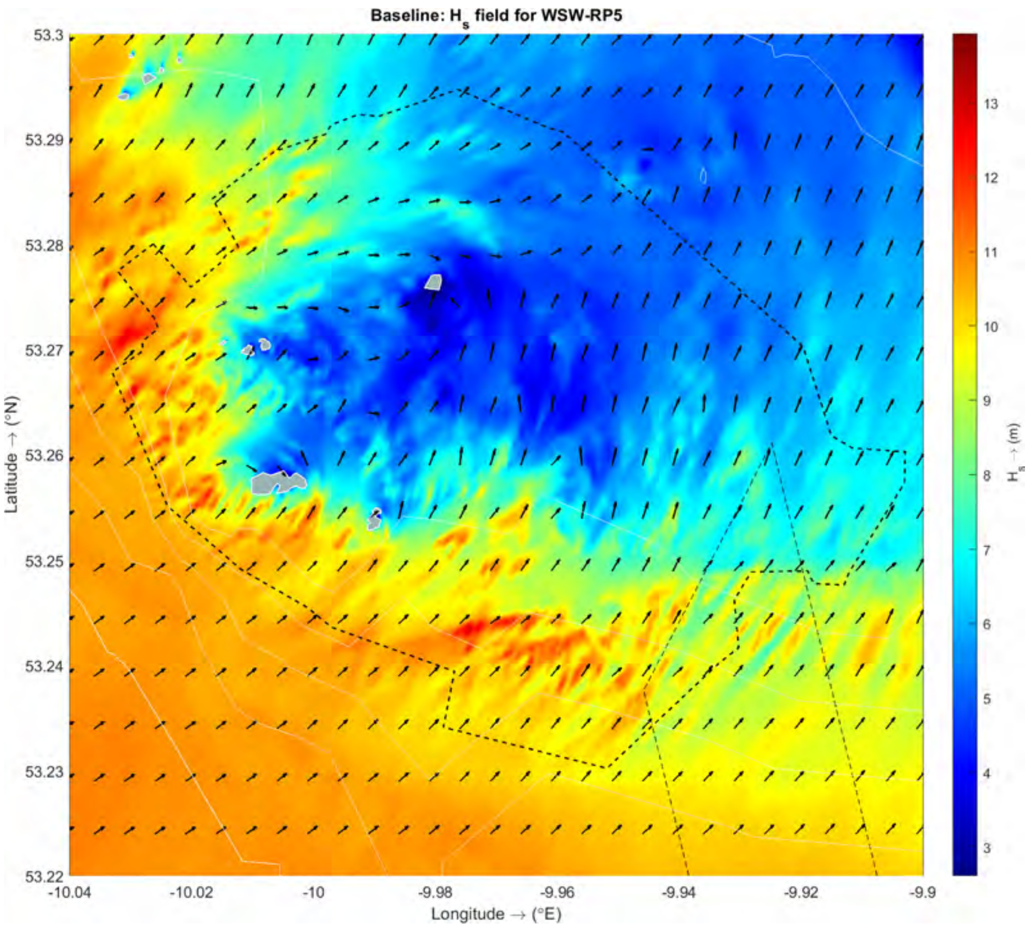

Baseline: H_s field for WSW-RP5
53.3
53.29
53.28
53.27
53.26
53.25
53.24
53.23
53.22
Latitude → (°N)
-10.04
-10.02
-10
-9.98
-9.96
-9.94
-9.92
-9.9
Longitude → (°E)
13
12
11
10
9
8
7
6
5
4
3
H_s → (m)

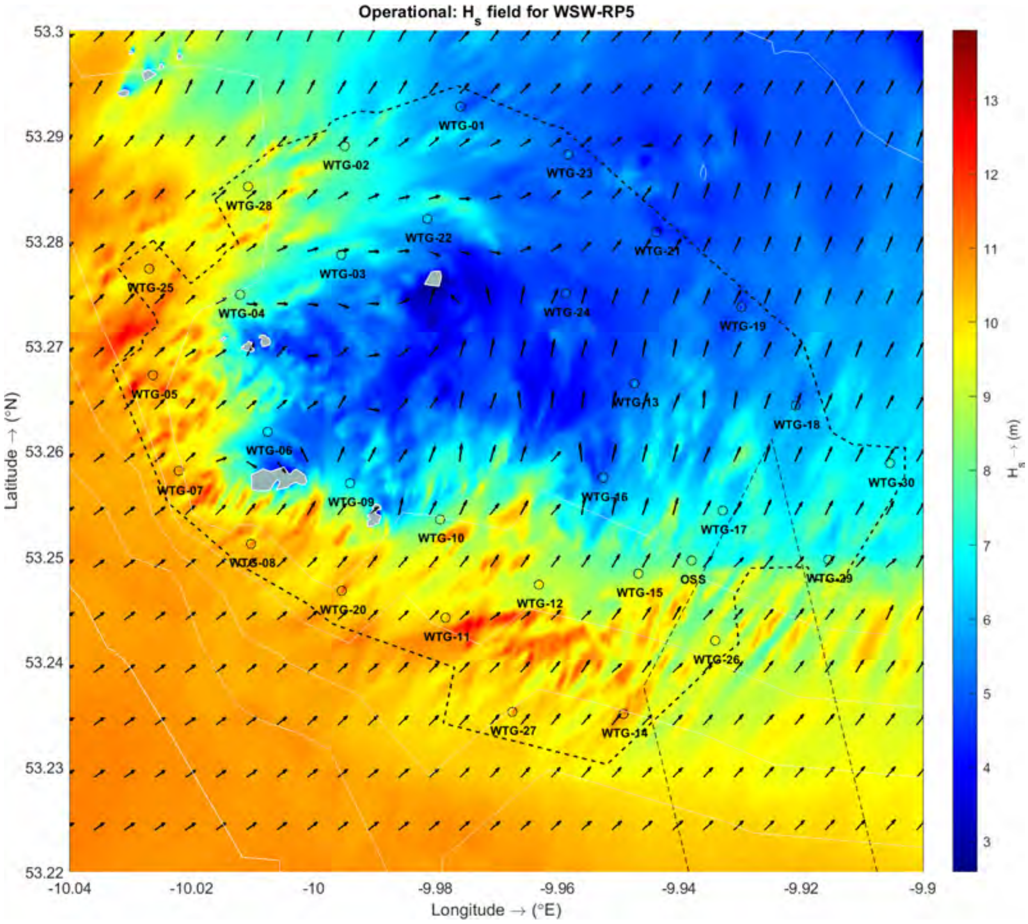
Operational: H_s field for WSW-RP5
Latitude → (°N)
Longitude → (°E)
H_s → (m)
WTG-01
WTG-02
WTG-03
WTG-04
WTG-05
WTG-06
WTG-07
WTG-08
WTG-09
WTG-10
WTG-11
WTG-12
WTG-13
WTG-14
WTG-15
WTG-16
WTG-17
WTG-18
WTG-19
WTG-20
WTG-21
WTG-22
WTG-23
WTG-24
WTG-25
WTG-26
WTG-27
WTG-28
WTG-29
WTG-30
OSS

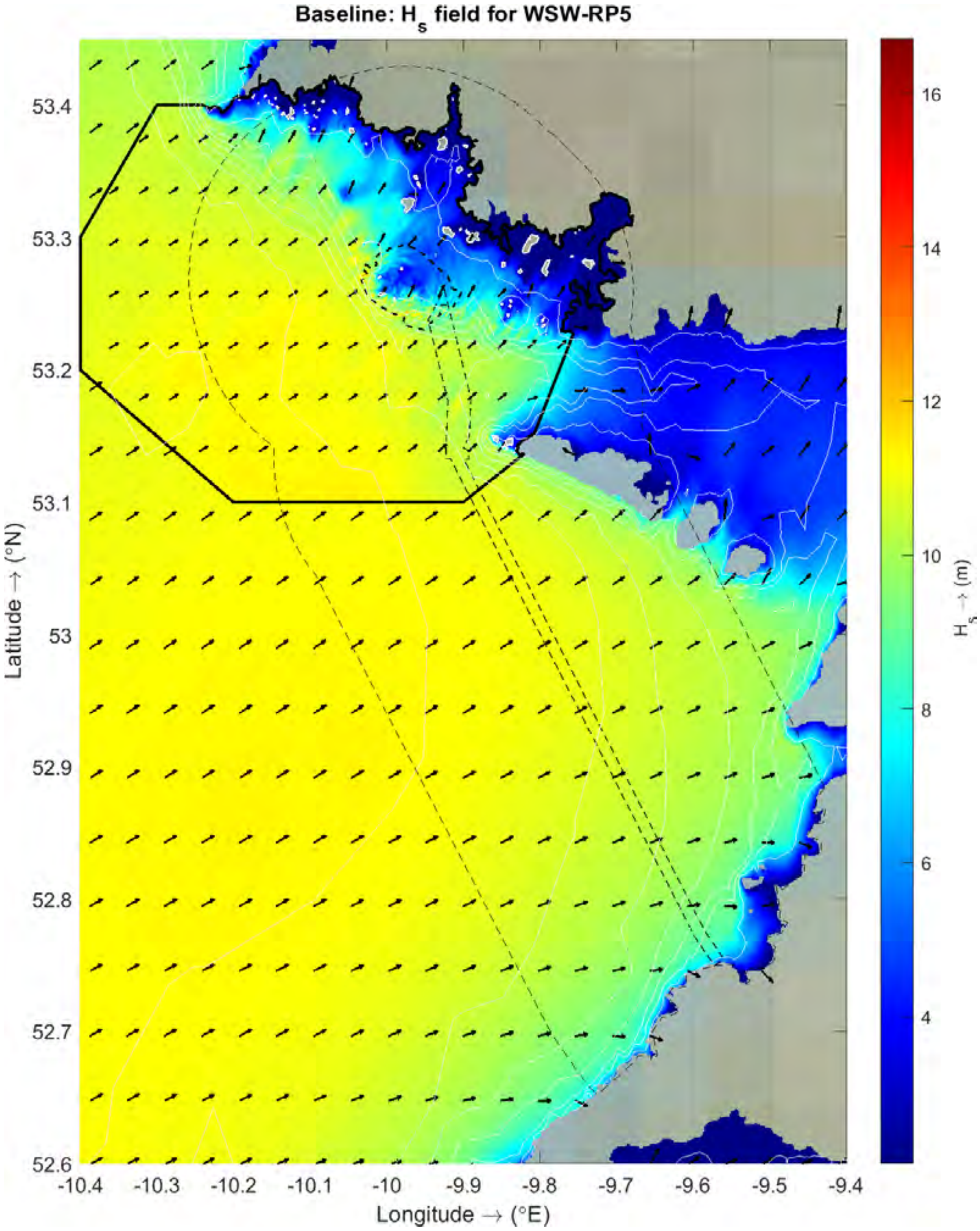
Baseline: H_s field for WSW-RP5
53.4
53.3
53.2
53.1
53
52.9
52.8
52.7
52.6
Latitude → (°N)
-10.4
-10.3
-10.2
-10.1
-10
-9.9
-9.8
-9.7
-9.6
-9.5
-9.4
Longitude → (°E)
16
14
12
10
8
6
4
H_s → (m)

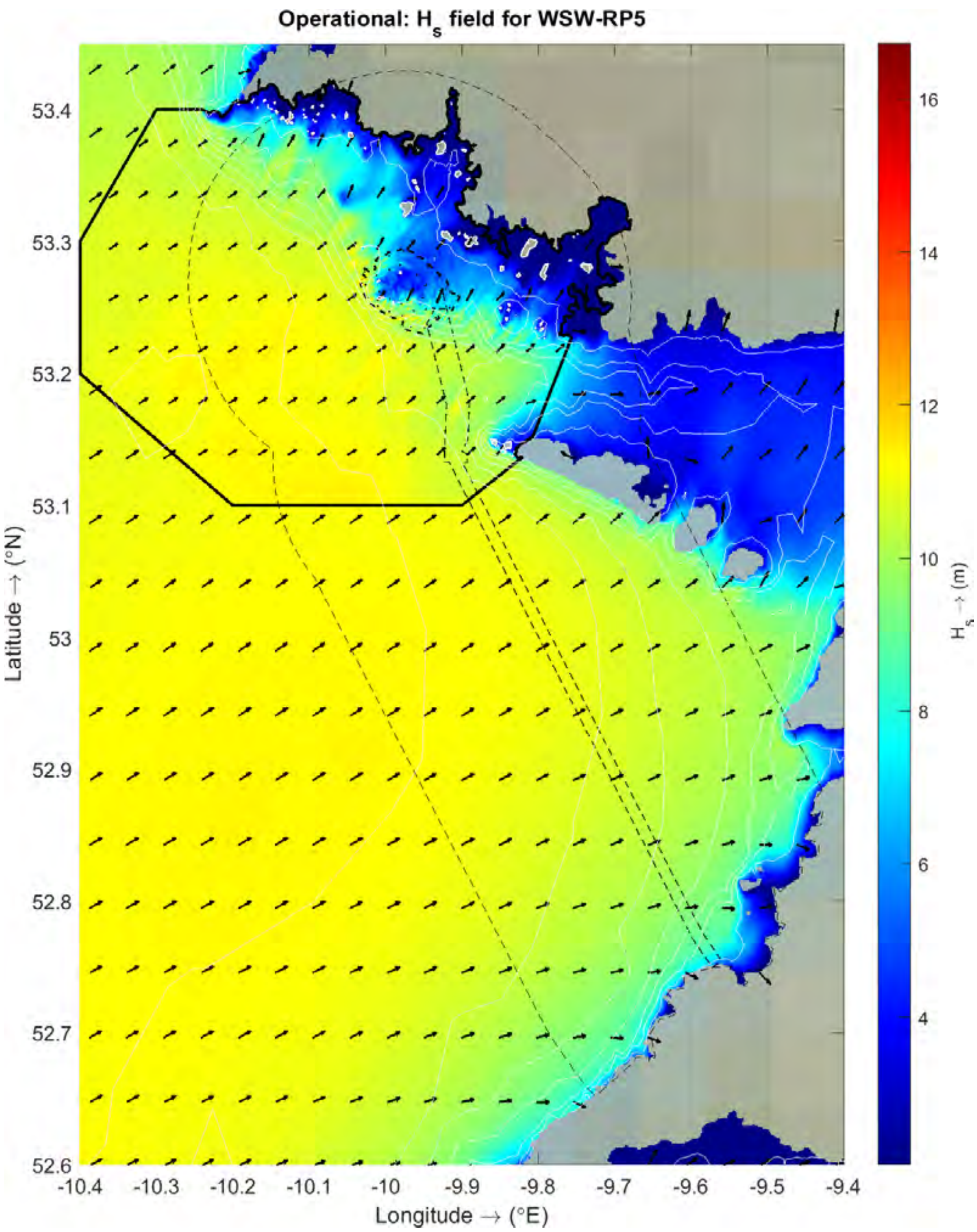
Operational: Hs field for WSW-RP5
53.4
53.3
53.2
53.1
53
52.9
52.8
52.7
52.6
Latitude → (°N)
-10.4
-10.3
-10.2
-10.1
-10
-9.9
-9.8
-9.7
-9.6
-9.5
-9.4
Longitude → (°E)
16
14
12
10
8
6
4
Hs → (m)

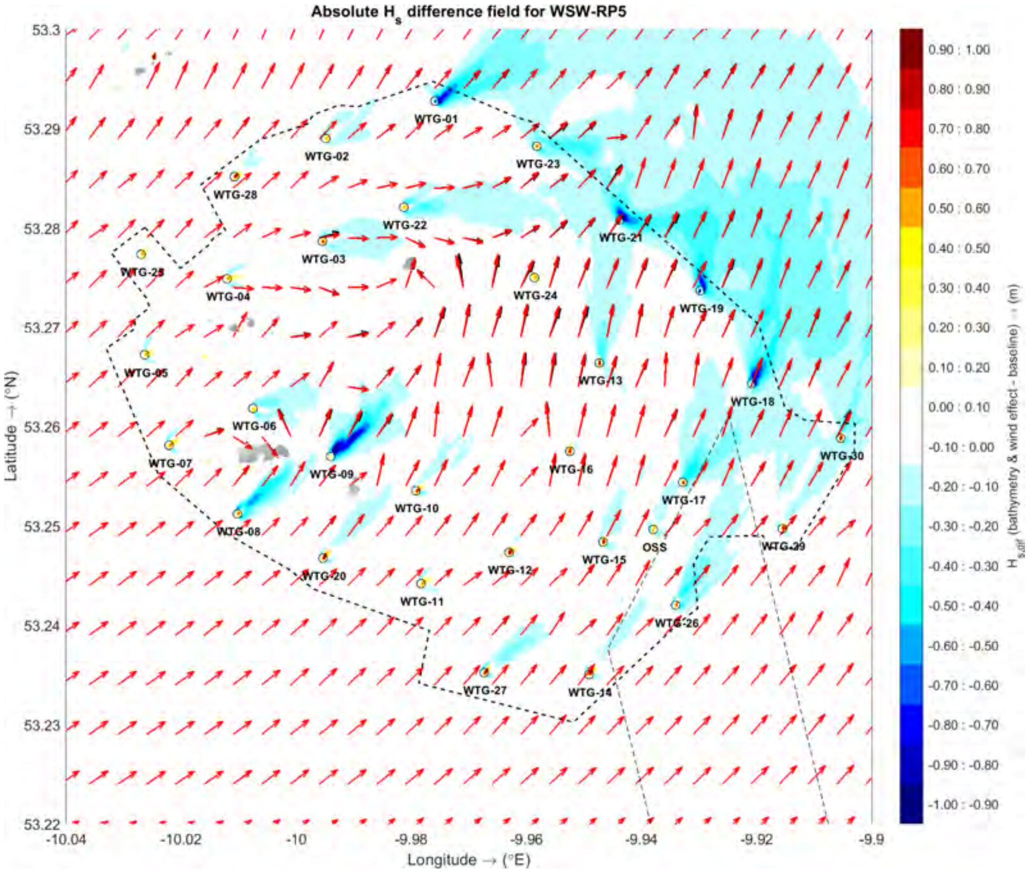
Absolute H_s difference field for WSW-RP5
Latitude → (°N)
Longitude → (°E)
WTG-01
WTG-02
WTG-03
WTG-04
WTG-05
WTG-06
WTG-07
WTG-08
WTG-09
WTG-10
WTG-11
WTG-12
WTG-13
WTG-14
WTG-15
WTG-16
WTG-17
WTG-18
WTG-19
WTG-20
WTG-21
WTG-22
WTG-23
WTG-24
WTG-25
WTG-26
WTG-27
WTG-28
WTG-29
WTG-30
OSS
H_s,diff (bathymetry & wind effect - baseline) → (m)

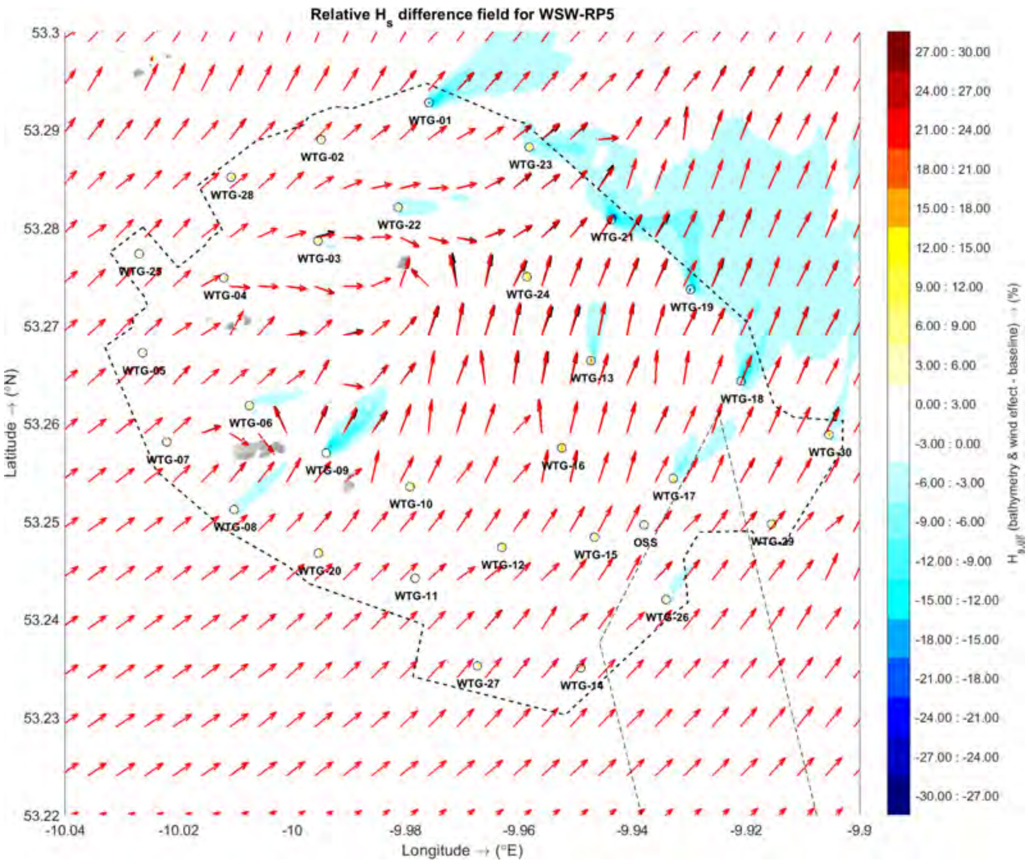
Relative H_s difference field for WSW-RP5
Latitude → (°N)
Longitude → (°E)
H_s,diff (bathymetry & wind effect - baseline) → (%)

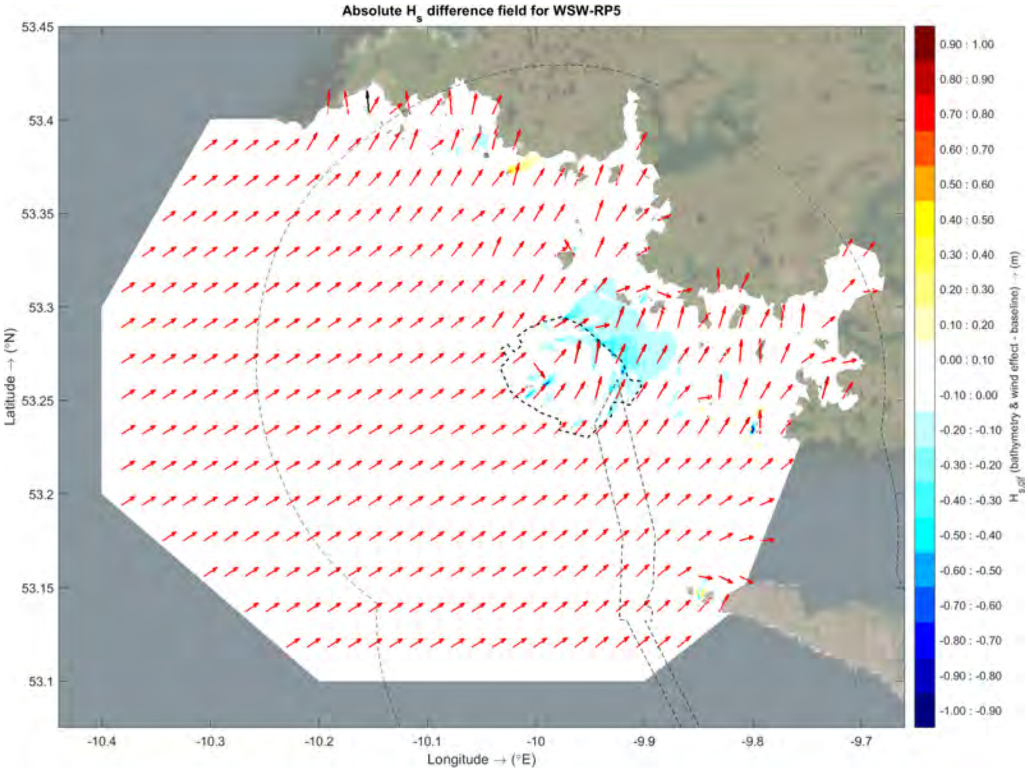
Absolute Hs difference field for WSW-RP5
Latitude → (°N)
Longitude → (°E)
Hs,dif (bathymetry & wind effect - baseline) → (m)

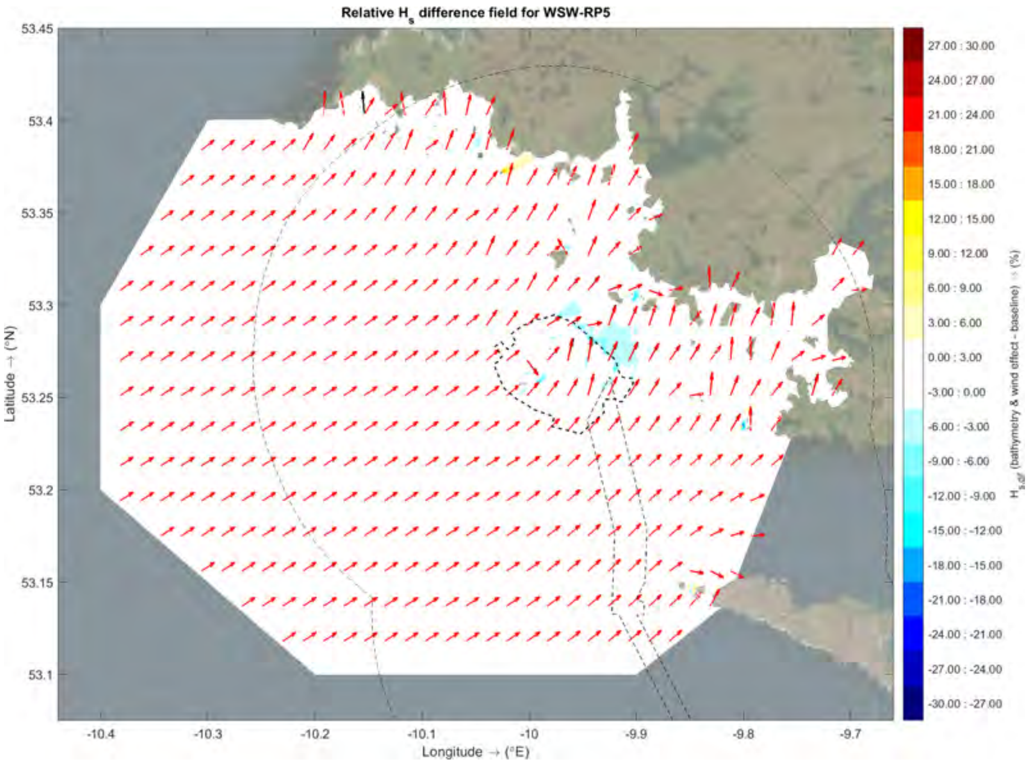
Relative Hs difference field for WSW-RP5
Latitude → (°N)
Longitude → (°E)
Hs,dif (bathymetry & wind effect - baseline) → (%)

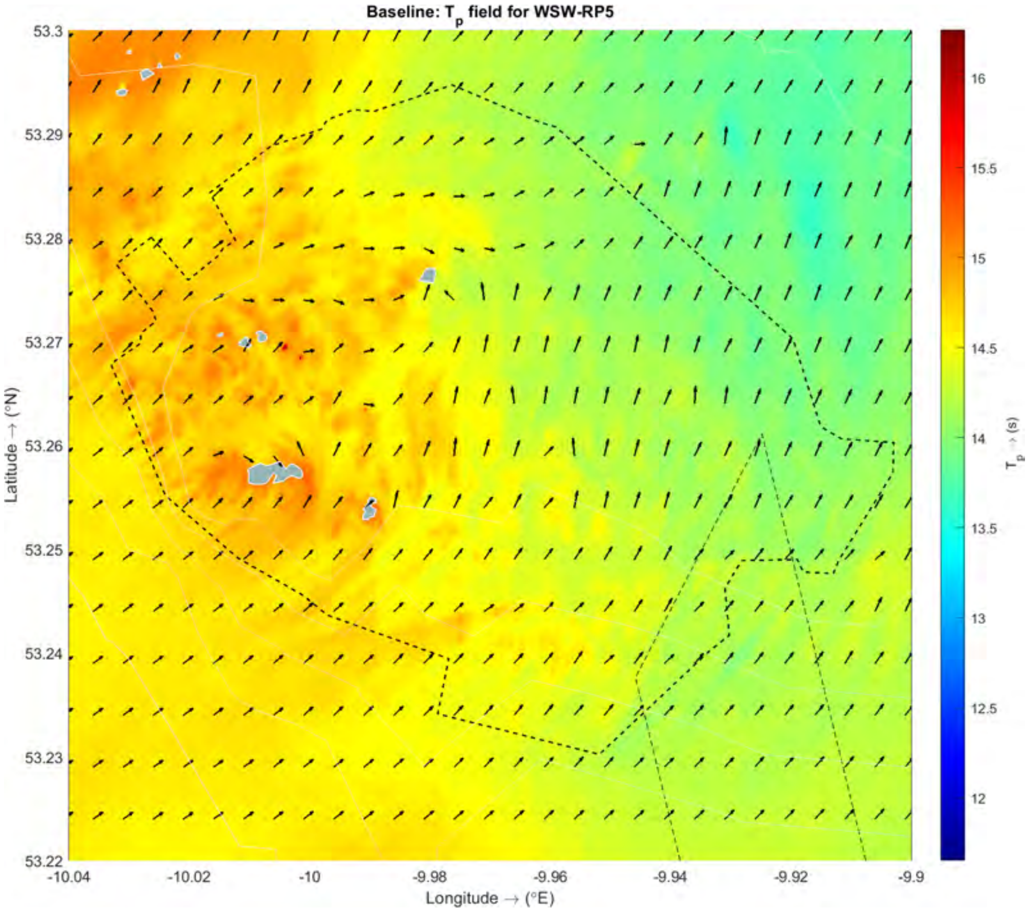
Baseline: T_p field for WSW-RP5
53.3
53.29
53.28
53.27
53.26
53.25
53.24
53.23
53.22
Latitude → (°N)
-10.04
-10.02
-10
-9.98
-9.96
-9.94
-9.92
-9.9
Longitude → (°E)
16
15.5
15
14.5
14
13.5
13
12.5
12
T_p → (s)

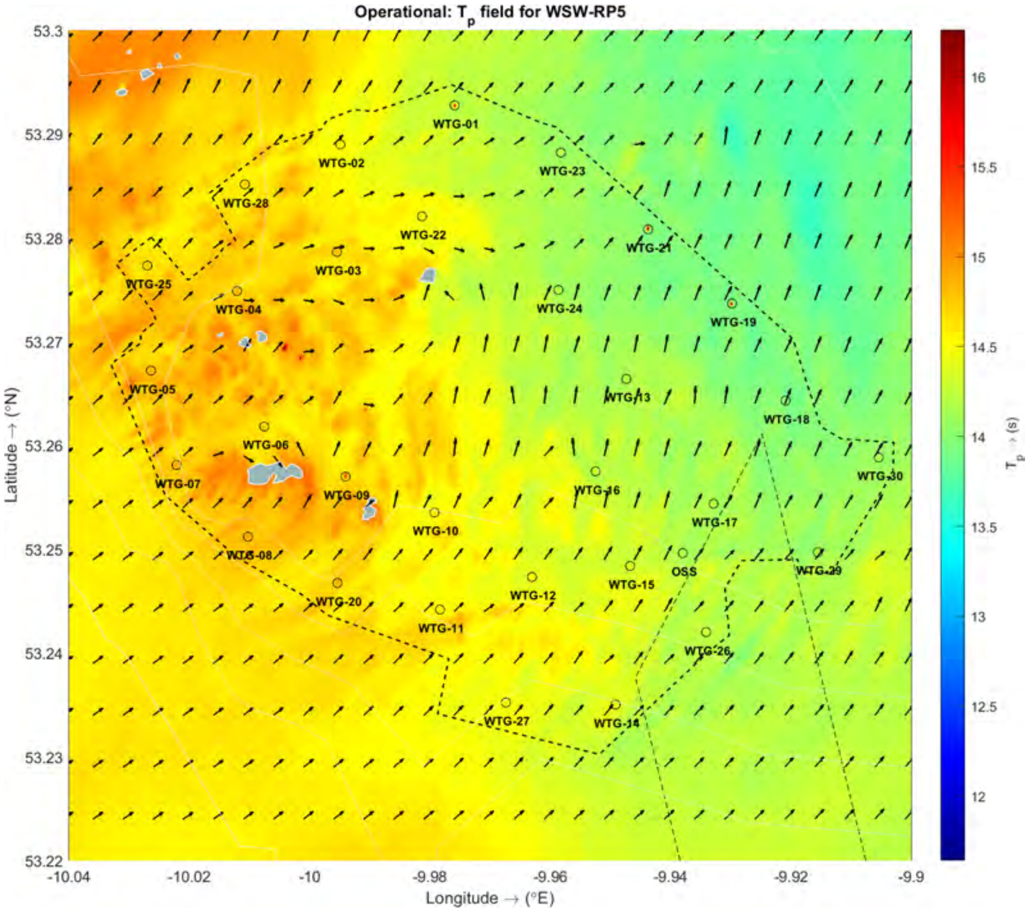
Operational: T_p field for WSW-RP5
Latitude → (°N)
Longitude → (°E)
T_p → (s)
WTG-01
WTG-02
WTG-03
WTG-04
WTG-05
WTG-06
WTG-07
WTG-08
WTG-09
WTG-10
WTG-11
WTG-12
WTG-13
WTG-14
WTG-15
WTG-16
WTG-17
WTG-18
WTG-19
WTG-20
WTG-21
WTG-22
WTG-23
WTG-24
WTG-25
WTG-26
WTG-27
WTG-28
WTG-29
WTG-30
OSS

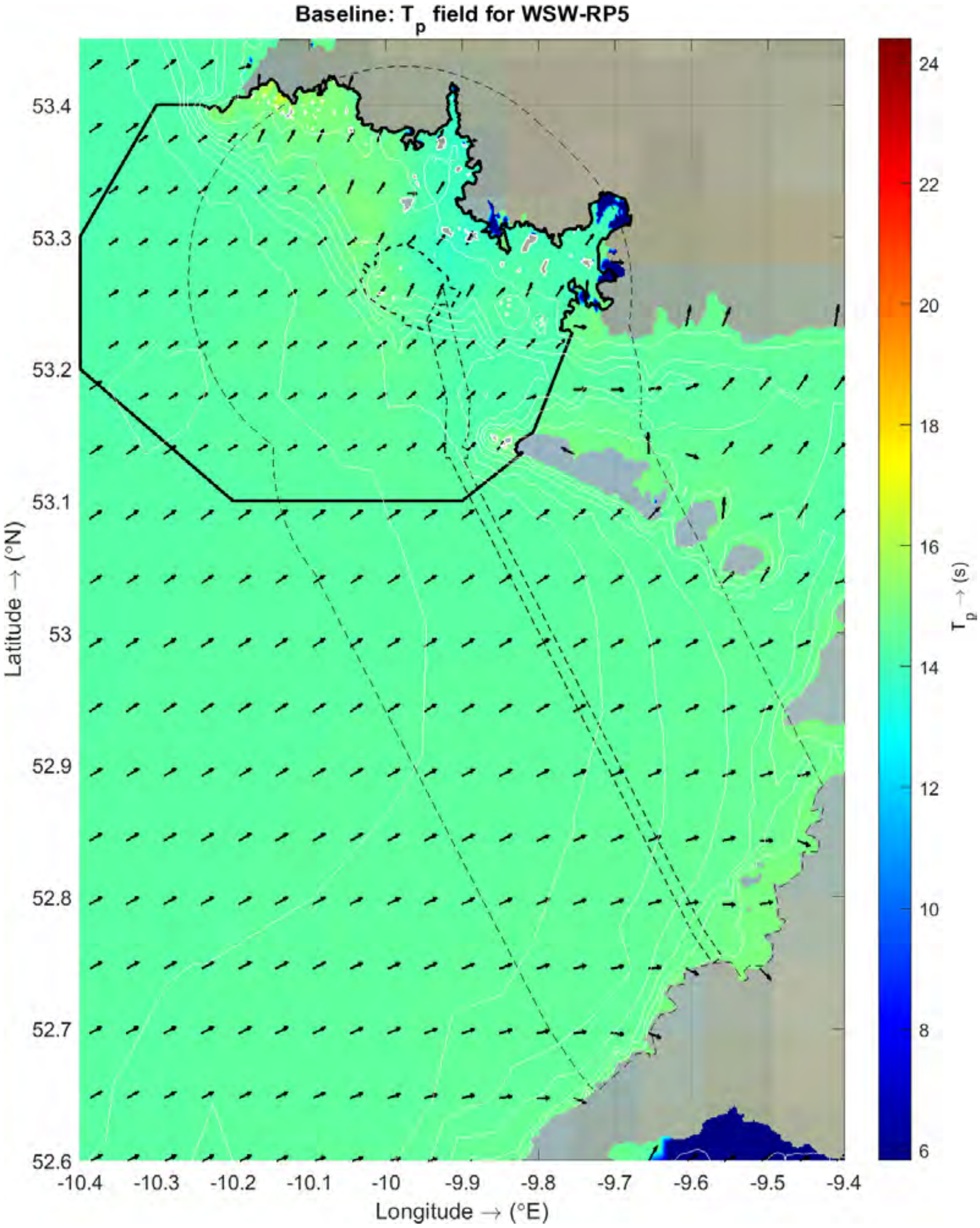
Baseline: T_p field for WSW-RP5
Latitude → (°N)
Longitude → (°E)
T_p → (s)
53.4
53.3
53.2
53.1
53
52.9
52.8
52.7
52.6
-10.4
-10.3
-10.2
-10.1
-10
-9.9
-9.8
-9.7
-9.6
-9.5
-9.4
24
22
20
18
16
14
12
10
8
6

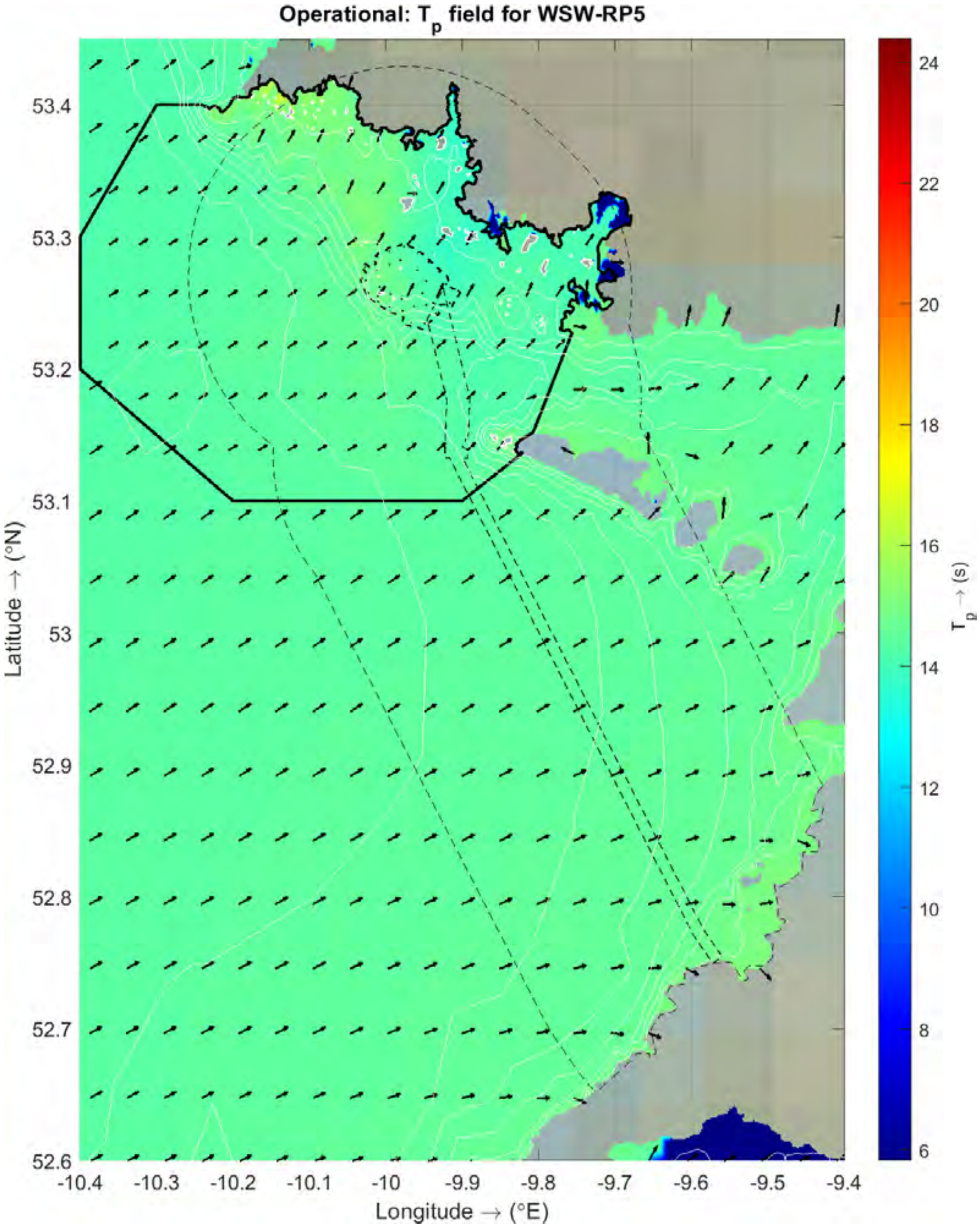

Operational: T_p field for WSW-RP5
Latitude → (°N)
Longitude → (°E)
T_p → (s)
53.4
53.3
53.2
53.1
53
52.9
52.8
52.7
52.6
-10.4
-10.3
-10.2
-10.1
-10
-9.9
-9.8
-9.7
-9.6
-9.5
-9.4
24
22
20
18
16
14
12
10
8
6

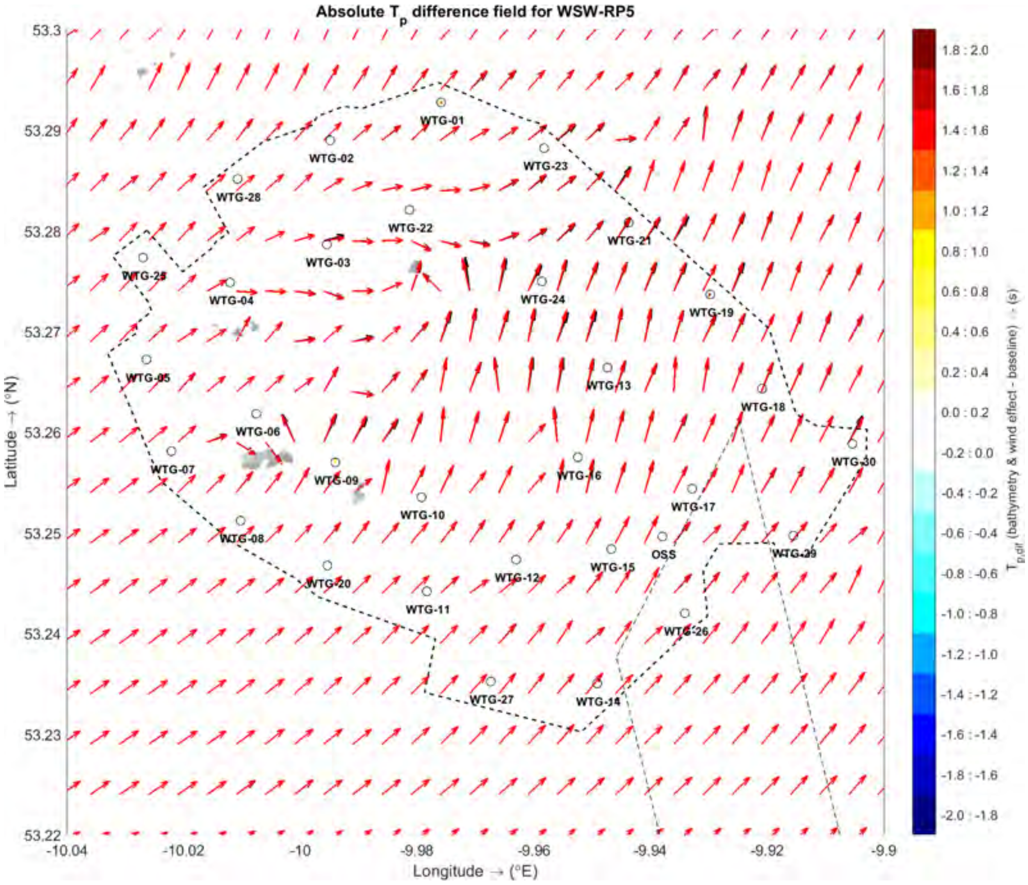
Absolute T_p difference field for WSW-RP5
Latitude → (°N)
Longitude → (°E)
$T_{p,dif}$ (bathymetry & wind effect - baseline) → (s)
1.8 : 2.0
1.6 : 1.8
1.4 : 1.6
1.2 : 1.4
1.0 : 1.2
0.8 : 1.0
0.6 : 0.8
0.4 : 0.6
0.2 : 0.4
0.0 : 0.2
-0.2 : 0.0
-0.4 : -0.2
-0.6 : -0.4
-0.8 : -0.6
-1.0 : -0.8
-1.2 : -1.0
-1.4 : -1.2
-1.6 : -1.4
-1.8 : -1.6
-2.0 : -1.8
WTG-01
WTG-02
WTG-03
WTG-04
WTG-05
WTG-06
WTG-07
WTG-08
WTG-09
WTG-10
WTG-11
WTG-12
WTG-13
WTG-14
WTG-15
WTG-16
WTG-17
WTG-18
WTG-19
WTG-20
WTG-21
WTG-22
WTG-23
WTG-24
WTG-25
WTG-26
WTG-27
WTG-28
WTG-29
WTG-30
OSS

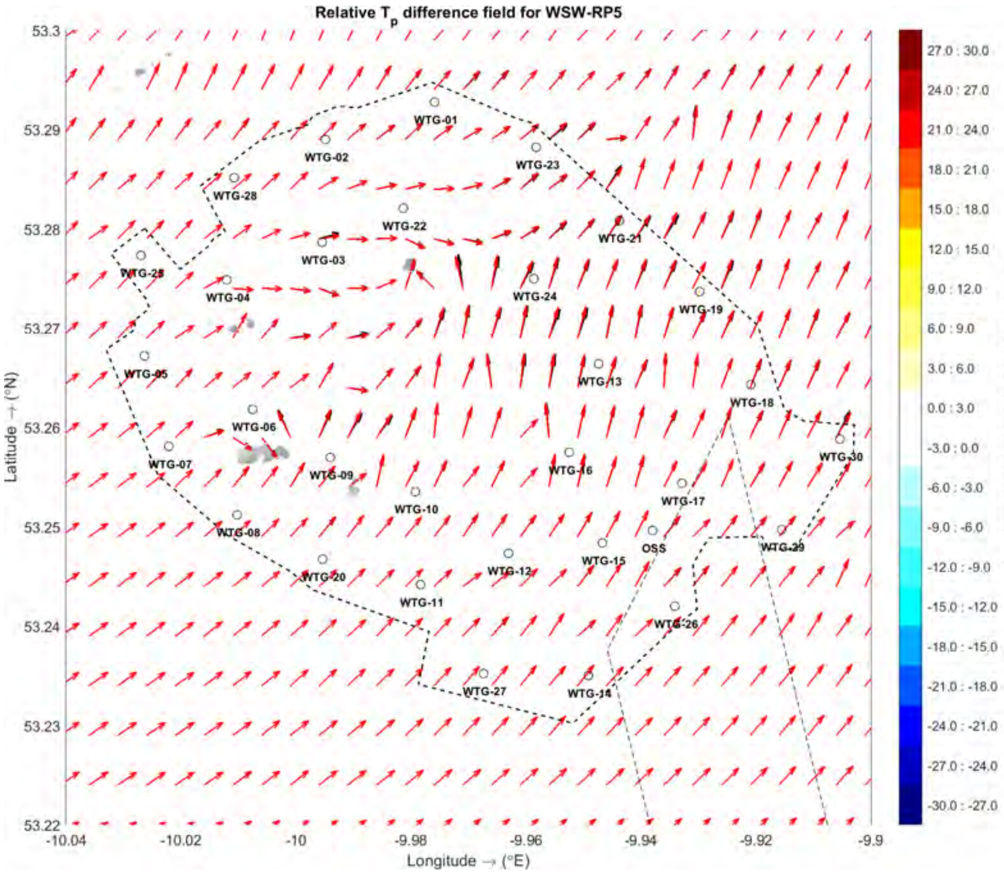
Relative T_p difference field for WSW-RP5
Latitude → (°N)
Longitude → (°E)
$T_{p,dif}$ (bathymetry & wind effect - baseline) → (%)
27.0 : 30.0
24.0 : 27.0
21.0 : 24.0
18.0 : 21.0
15.0 : 18.0
12.0 : 15.0
9.0 : 12.0
6.0 : 9.0
3.0 : 6.0
0.0 : 3.0
-3.0 : 0.0
-6.0 : -3.0
-9.0 : -6.0
-12.0 : -9.0
-15.0 : -12.0
-18.0 : -15.0
-21.0 : -18.0
-24.0 : -21.0
-27.0 : -24.0
-30.0 : -27.0
OSS

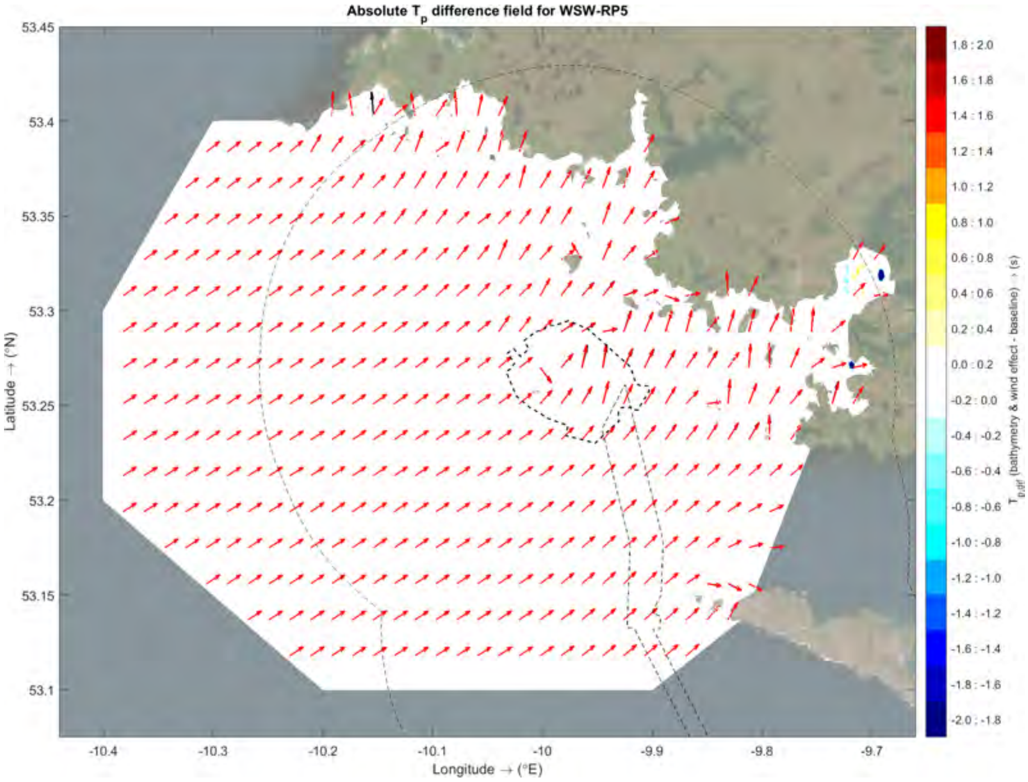
Absolute T_p difference field for WSW-RP5
Latitude → (°N)
Longitude → (°E)
$T_{p,diff}$ (bathymetry & wind effect - baseline) → (s)

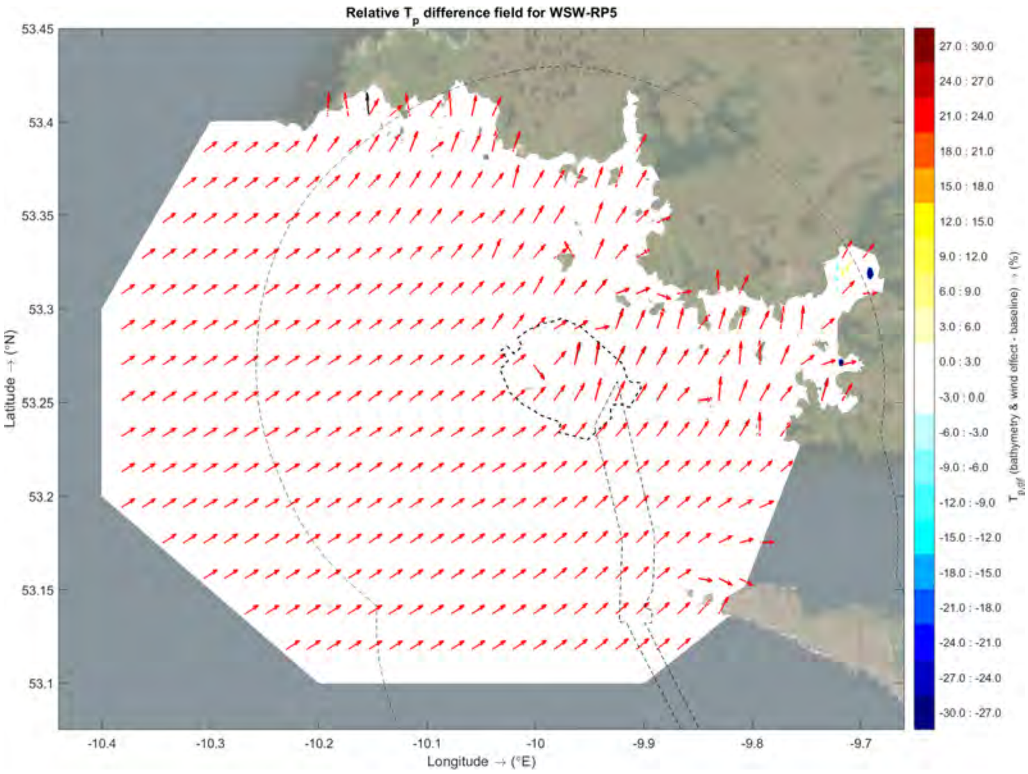
Relative T_p difference field for WSW-RP5
Latitude → (°N)
Longitude → (°E)
$T_{p,diff}$ (bathymetry & wind effect - baseline) → (%)

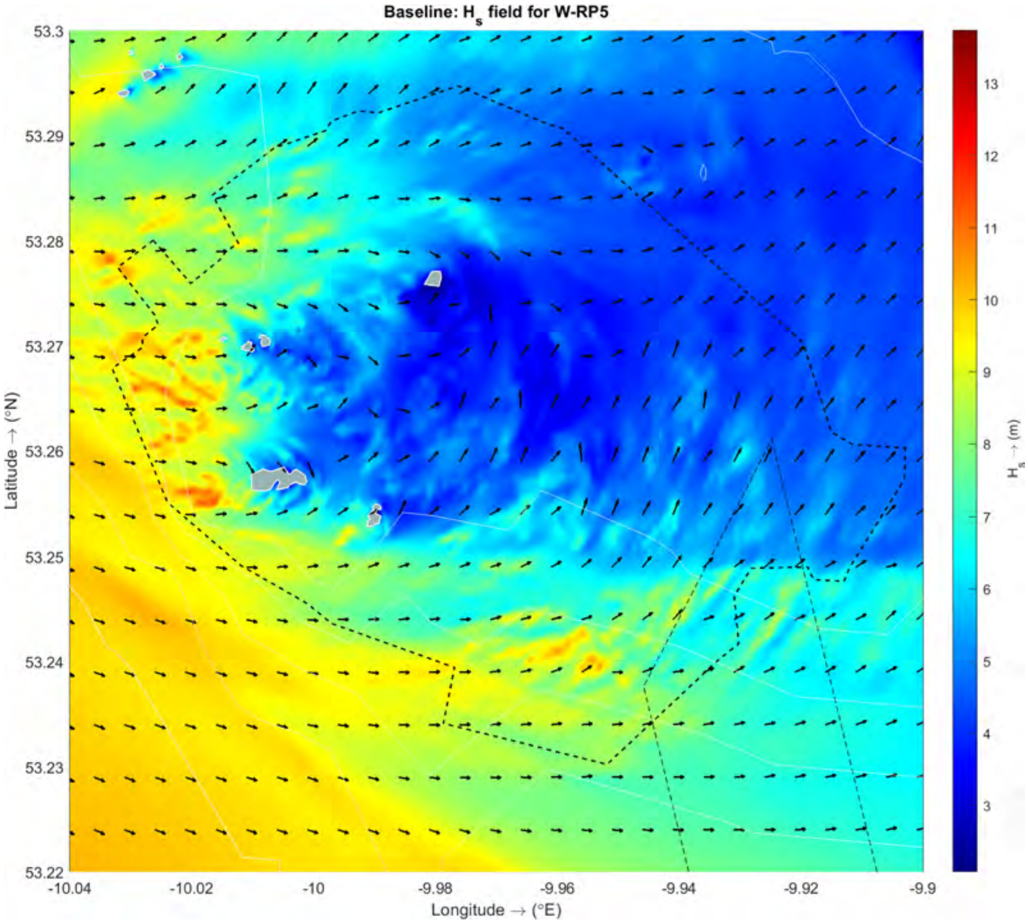
Baseline: H_s field for W-RP5
53.3
53.29
53.28
53.27
53.26
53.25
53.24
53.23
53.22
Latitude → (°N)
-10.04
-10.02
-10
-9.98
-9.96
-9.94
-9.92
-9.9
Longitude → (°E)
13
12
11
10
9
8
7
6
5
4
3
H_s → (m)

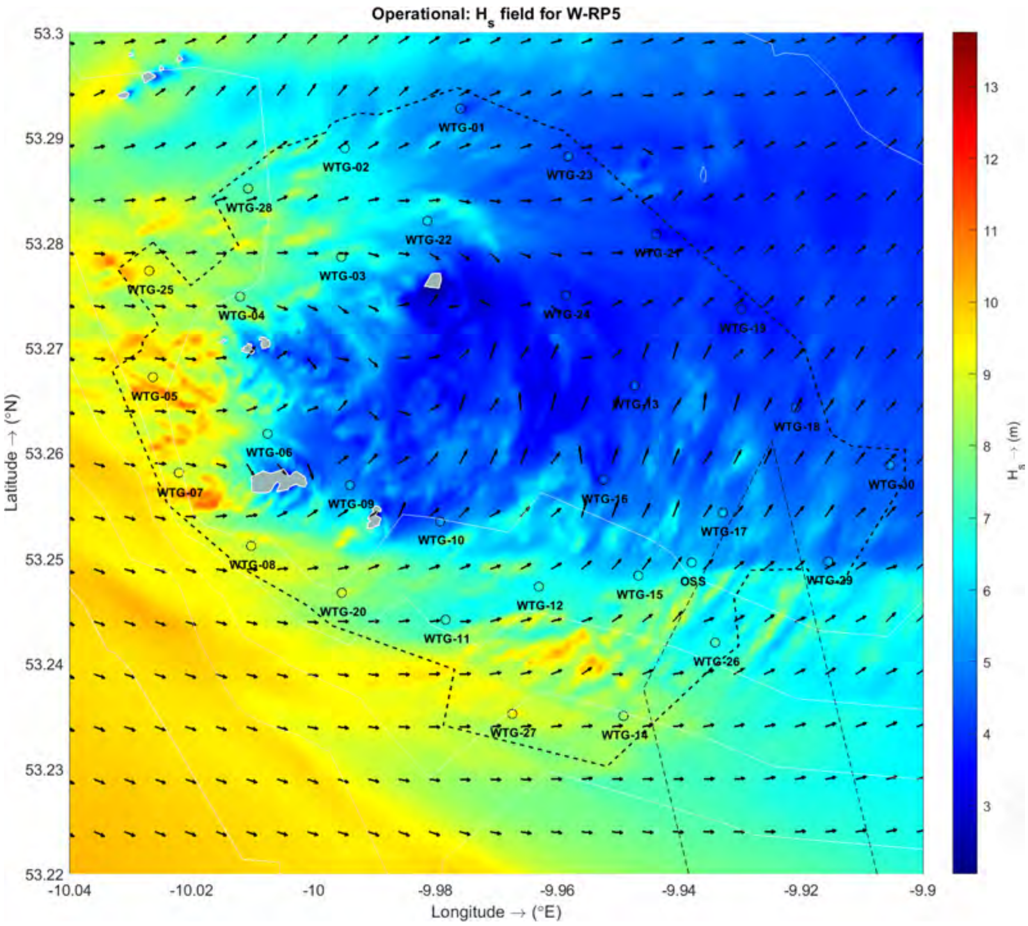
Operational: H_s field for W-RP5
Latitude → (°N)
Longitude → (°E)
H_s → (m)
WTG-01
WTG-02
WTG-03
WTG-04
WTG-05
WTG-06
WTG-07
WTG-08
WTG-09
WTG-10
WTG-11
WTG-12
WTG-13
WTG-14
WTG-15
WTG-16
WTG-17
WTG-18
WTG-19
WTG-20
WTG-21
WTG-22
WTG-23
WTG-24
WTG-25
WTG-26
WTG-27
WTG-28
WTG-29
WTG-30
OSS

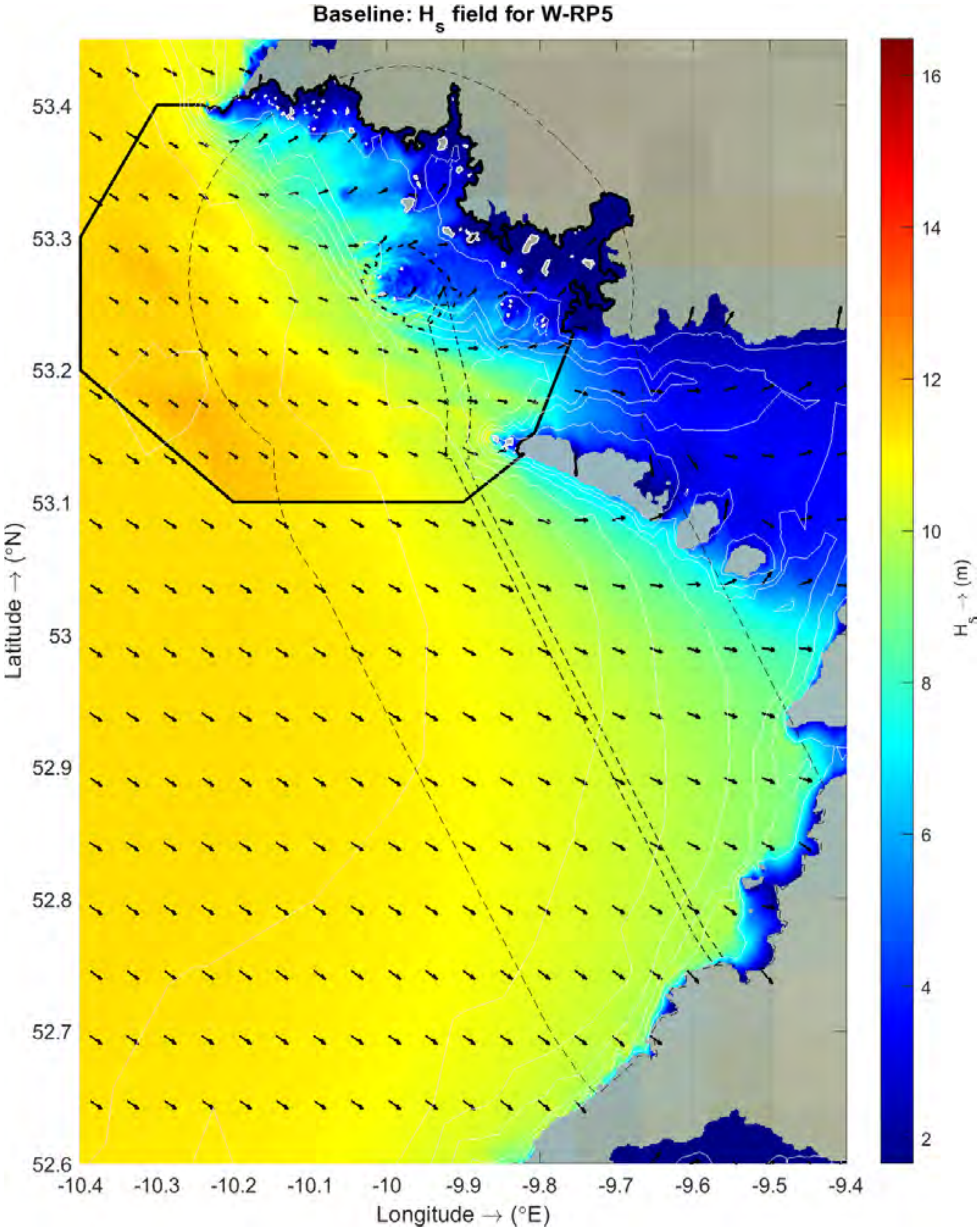

Baseline: H_s field for W-RP5
Latitude → (°N)
Longitude → (°E)
H_s → (m)
53.4
53.3
53.2
53.1
53
52.9
52.8
52.7
52.6
-10.4
-10.3
-10.2
-10.1
-10
-9.9
-9.8
-9.7
-9.6
-9.5
-9.4
16
14
12
10
8
6
4
2

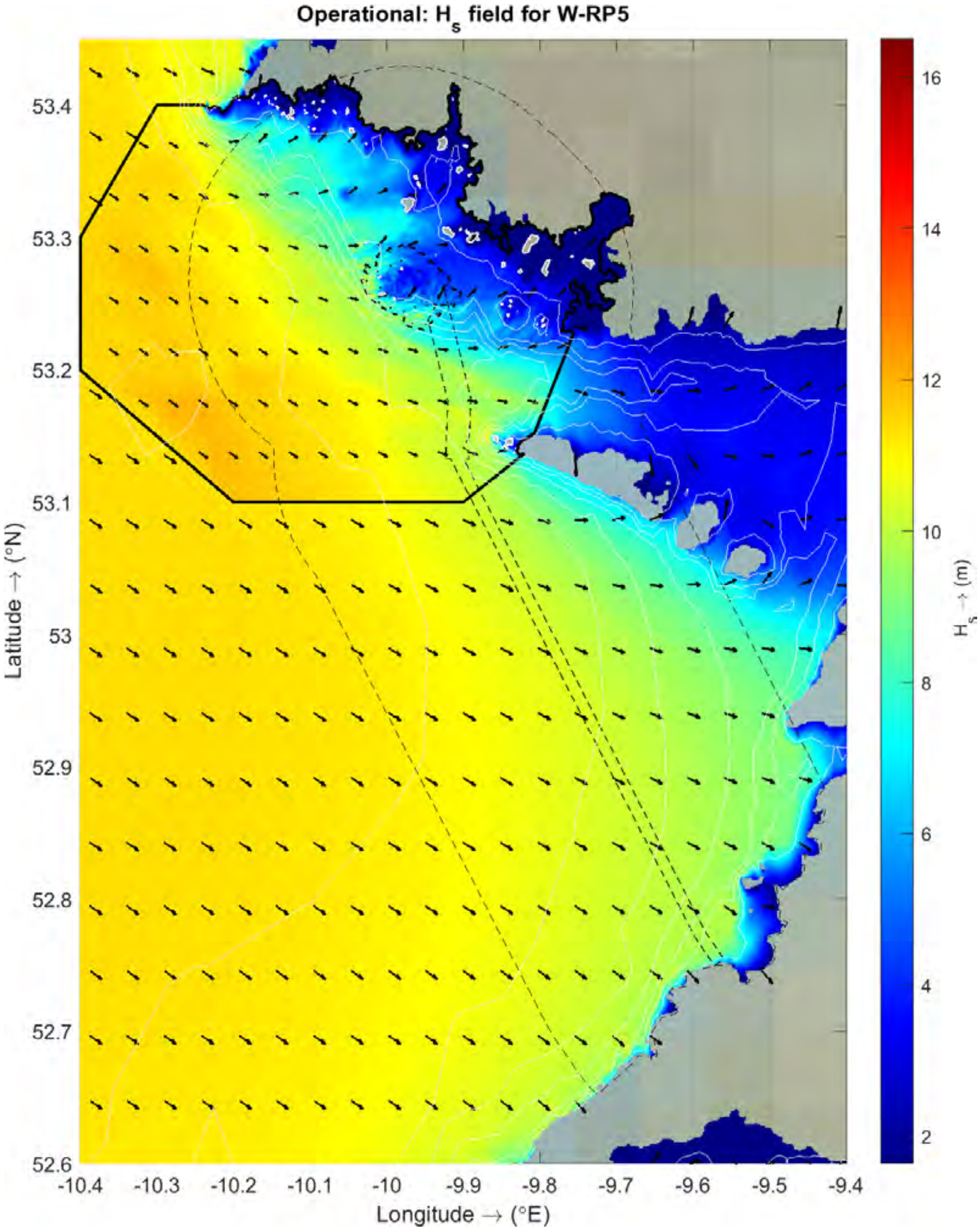
Operational: H_s field for W-RP5
53.4
53.3
53.2
53.1
53
52.9
52.8
52.7
52.6
Latitude → (°N)
-10.4
-10.3
-10.2
-10.1
-10
-9.9
-9.8
-9.7
-9.6
-9.5
-9.4
Longitude → (°E)
16
14
12
10
8
6
4
2
H_s → (m)

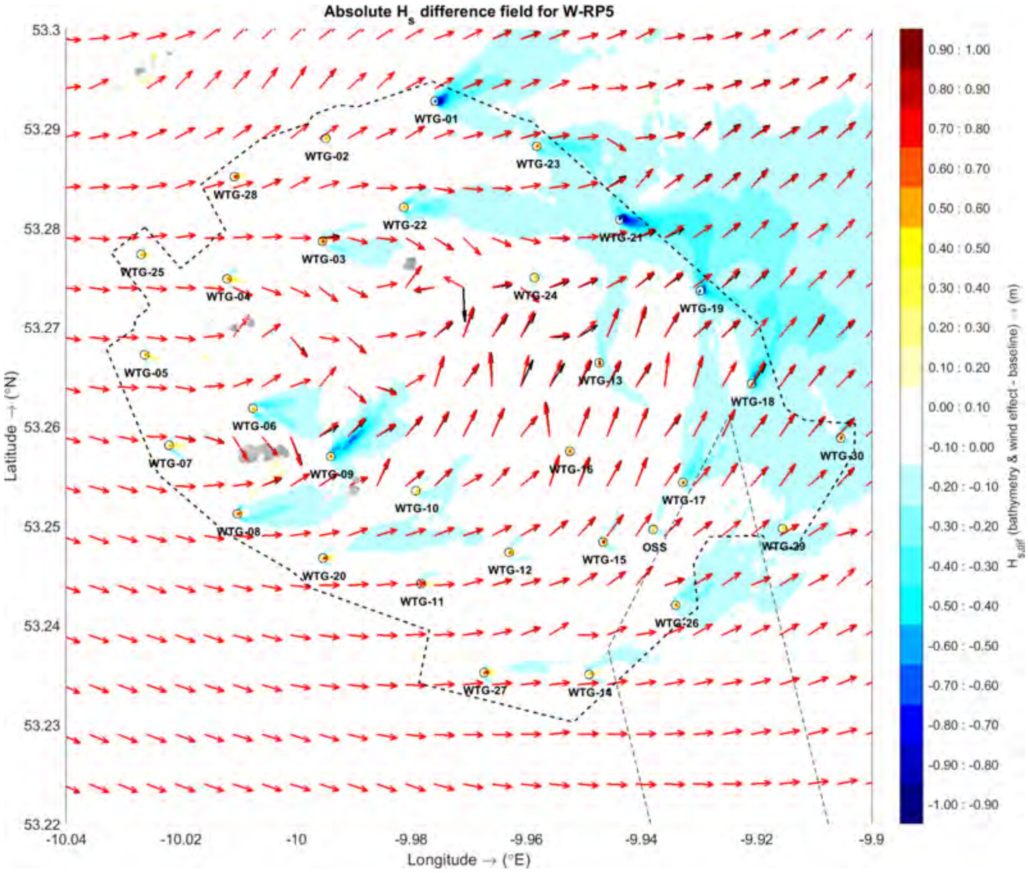
Absolute H_s difference field for W-RP5
Latitude → (°N)
Longitude → (°E)
$H_{s,diff}$ (bathymetry & wind effect - baseline) → (m)
0.90 : 1.00
0.80 : 0.90
0.70 : 0.80
0.60 : 0.70
0.50 : 0.60
0.40 : 0.50
0.30 : 0.40
0.20 : 0.30
0.10 : 0.20
0.00 : 0.10
-0.10 : 0.00
-0.20 : -0.10
-0.30 : -0.20
-0.40 : -0.30
-0.50 : -0.40
-0.60 : -0.50
-0.70 : -0.60
-0.80 : -0.70
-0.90 : -0.80
-1.00 : -0.90
WTG-01
WTG-02
WTG-03
WTG-04
WTG-05
WTG-06
WTG-07
WTG-08
WTG-09
WTG-10
WTG-11
WTG-12
WTG-13
WTG-14
WTG-15
WTG-16
WTG-17
WTG-18
WTG-19
WTG-20
WTG-21
WTG-22
WTG-23
WTG-24
WTG-25
WTG-26
WTG-27
WTG-28
WTG-29
WTG-30
OSS

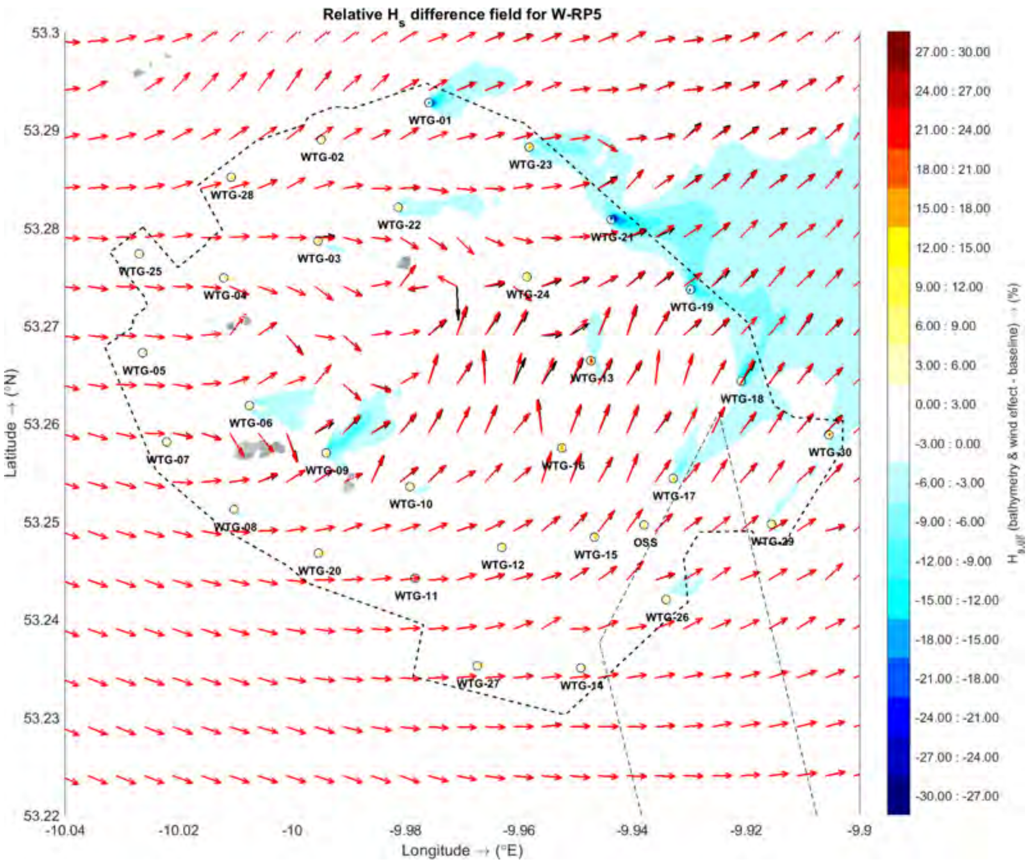
Relative H_s difference field for W-RP5
Latitude → (°N)
Longitude → (°E)
$H_{s,diff}$ (bathymetry & wind effect - baseline) → (%)
27.00 : 30.00
24.00 : 27.00
21.00 : 24.00
18.00 : 21.00
15.00 : 18.00
12.00 : 15.00
9.00 : 12.00
6.00 : 9.00
3.00 : 6.00
0.00 : 3.00
-3.00 : 0.00
-6.00 : -3.00
-9.00 : -6.00
-12.00 : -9.00
-15.00 : -12.00
-18.00 : -15.00
-21.00 : -18.00
-24.00 : -21.00
-27.00 : -24.00
-30.00 : -27.00
OSS

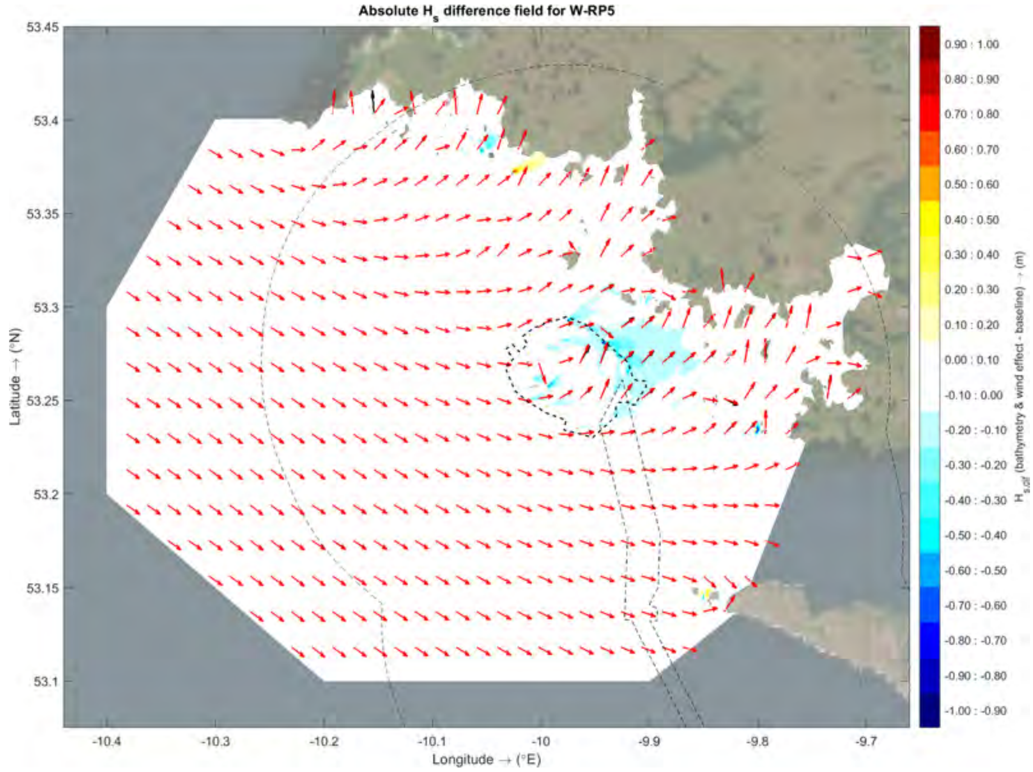
Absolute H_s difference field for W-RP5
Latitude → (°N)
Longitude → (°E)
$H_{s,dif}$ (bathymetry & wind effect - baseline) → (m)
0.90 : 1.00
0.80 : 0.90
0.70 : 0.80
0.60 : 0.70
0.50 : 0.60
0.40 : 0.50
0.30 : 0.40
0.20 : 0.30
0.10 : 0.20
0.00 : 0.10
-0.10 : 0.00
-0.20 : -0.10
-0.30 : -0.20
-0.40 : -0.30
-0.50 : -0.40
-0.60 : -0.50
-0.70 : -0.60
-0.80 : -0.70
-0.90 : -0.80
-1.00 : -0.90

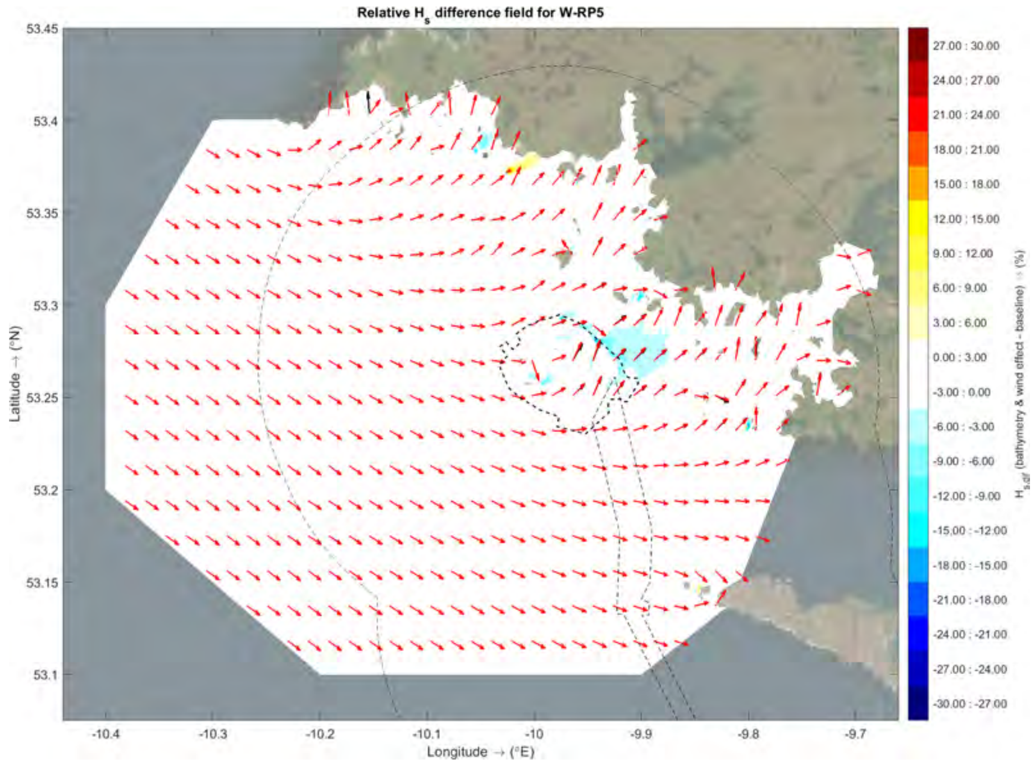
Relative H_s difference field for W-RP5
Latitude → (°N)
Longitude → (°E)
$H_{s,dif}$ (bathymetry & wind effect - baseline) → (%)
27.00 : 30.00
24.00 : 27.00
21.00 : 24.00
18.00 : 21.00
15.00 : 18.00
12.00 : 15.00
9.00 : 12.00
6.00 : 9.00
3.00 : 6.00
0.00 : 3.00
-3.00 : 0.00
-6.00 : -3.00
-9.00 : -6.00
-12.00 : -9.00
-15.00 : -12.00
-18.00 : -15.00
-21.00 : -18.00
-24.00 : -21.00
-27.00 : -24.00
-30.00 : -27.00

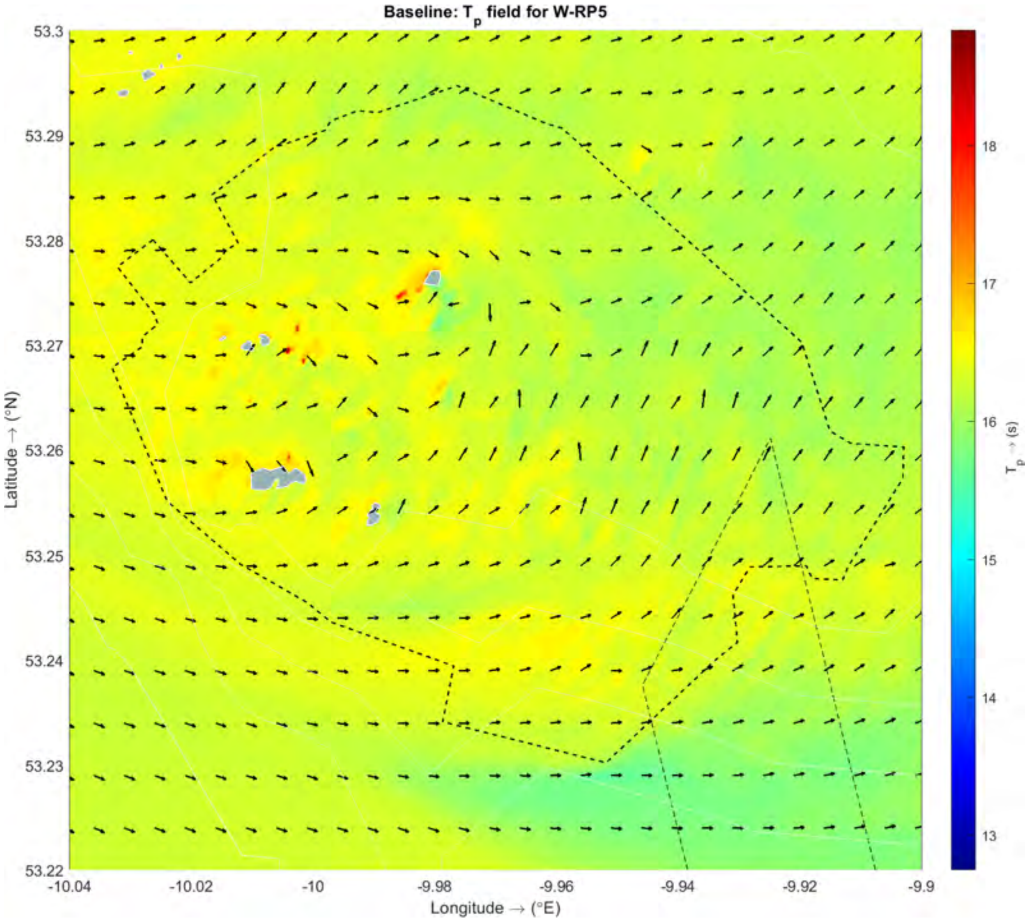
Baseline: T_p field for W-RP5
Latitude → (°N)
Longitude → (°E)
T_p → (s)
53.3
53.29
53.28
53.27
53.26
53.25
53.24
53.23
53.22
-10.04
-10.02
-10
-9.98
-9.96
-9.94
-9.92
-9.9
18
17
16
15
14
13

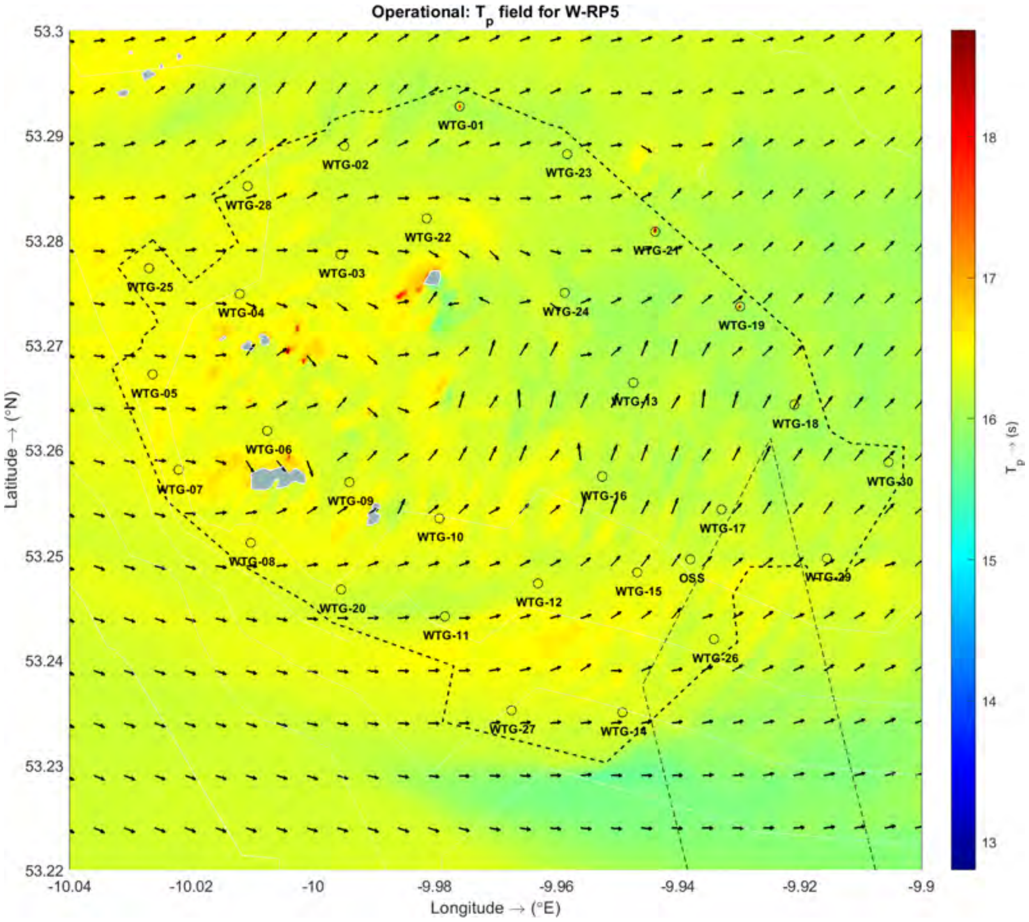
Operational: T_p field for W-RP5
Latitude → (°N)
Longitude → (°E)
T_p → (s)
53.3
53.29
53.28
53.27
53.26
53.25
53.24
53.23
53.22
-10.04
-10.02
-10
-9.98
-9.96
-9.94
-9.92
-9.9
13
14
15
16
17
18
WTG-01
WTG-02
WTG-03
WTG-04
WTG-05
WTG-06
WTG-07
WTG-08
WTG-09
WTG-10
WTG-11
WTG-12
WTG-13
WTG-14
WTG-15
WTG-16
WTG-17
WTG-18
WTG-19
WTG-20
WTG-21
WTG-22
WTG-23
WTG-24
WTG-25
WTG-26
WTG-27
WTG-28
WTG-29
WTG-30
OSS

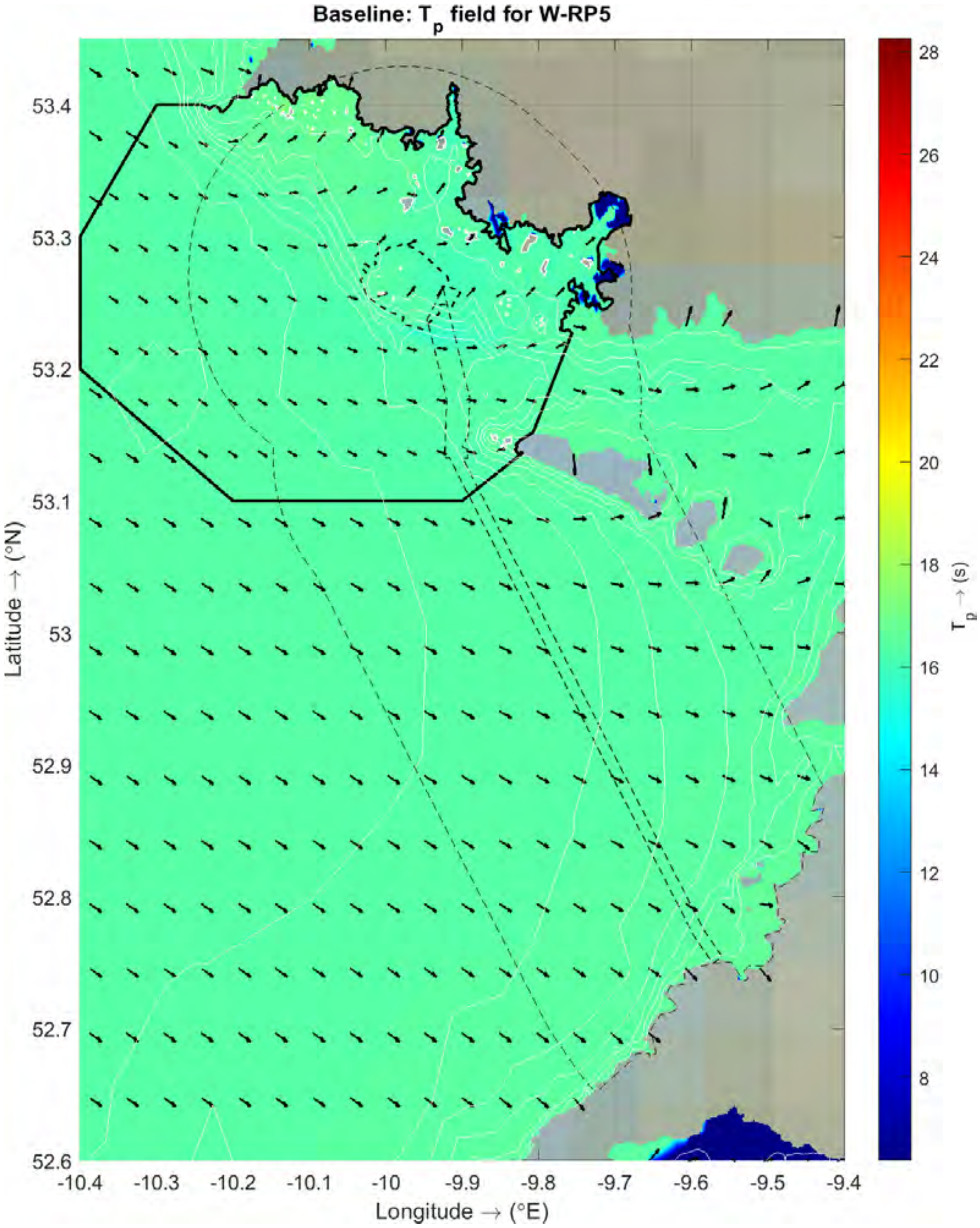
Baseline: T_p field for W-RP5
53.4
53.3
53.2
53.1
53
52.9
52.8
52.7
52.6
Latitude → (°N)
-10.4
-10.3
-10.2
-10.1
-10
-9.9
-9.8
-9.7
-9.6
-9.5
-9.4
Longitude → (°E)
28
26
24
22
20
18
16
14
12
10
8
T_p → (s)

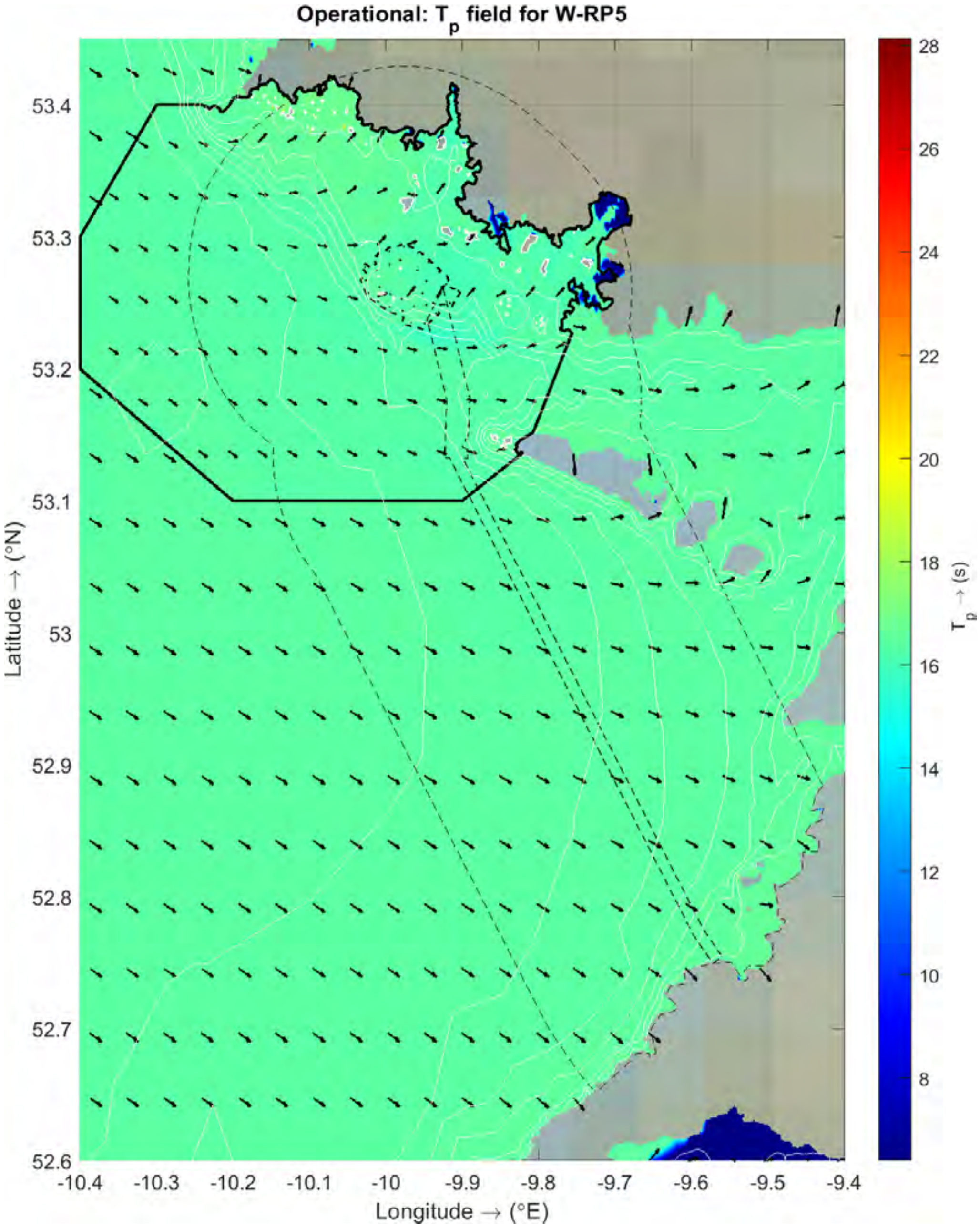
Operational: T_p field for W-RP5
53.4
53.3
53.2
53.1
53
52.9
52.8
52.7
52.6
Latitude → (°N)
-10.4
-10.3
-10.2
-10.1
-10
-9.9
-9.8
-9.7
-9.6
-9.5
-9.4
Longitude → (°E)
28
26
24
22
20
18
16
14
12
10
8
T_p → (s)

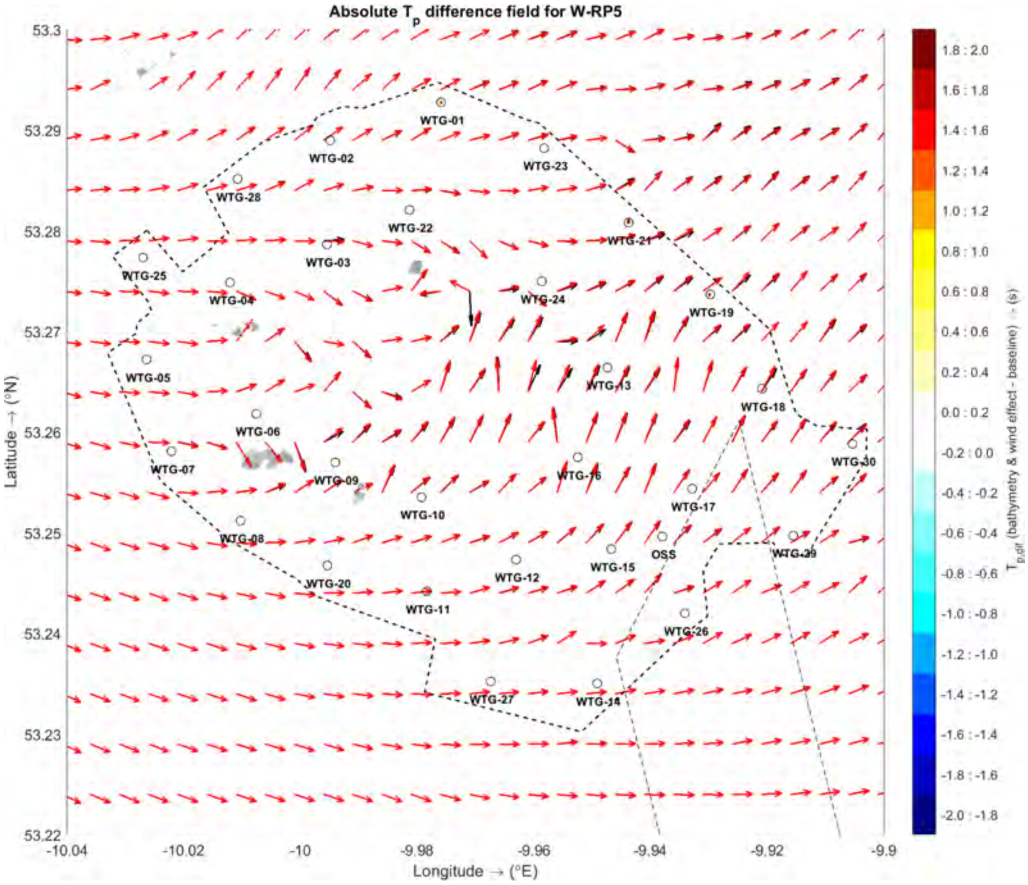
Absolute T_p difference field for W-RP5
Latitude → (°N)
Longitude → (°E)
$T_{p,dif}$ (bathymetry & wind effect - baseline) → (s)
WTG-01
WTG-02
WTG-03
WTG-04
WTG-05
WTG-06
WTG-07
WTG-08
WTG-09
WTG-10
WTG-11
WTG-12
WTG-13
WTG-14
WTG-15
WTG-16
WTG-17
WTG-18
WTG-19
WTG-20
WTG-21
WTG-22
WTG-23
WTG-24
WTG-25
WTG-26
WTG-27
WTG-28
WTG-29
WTG-30
OSS

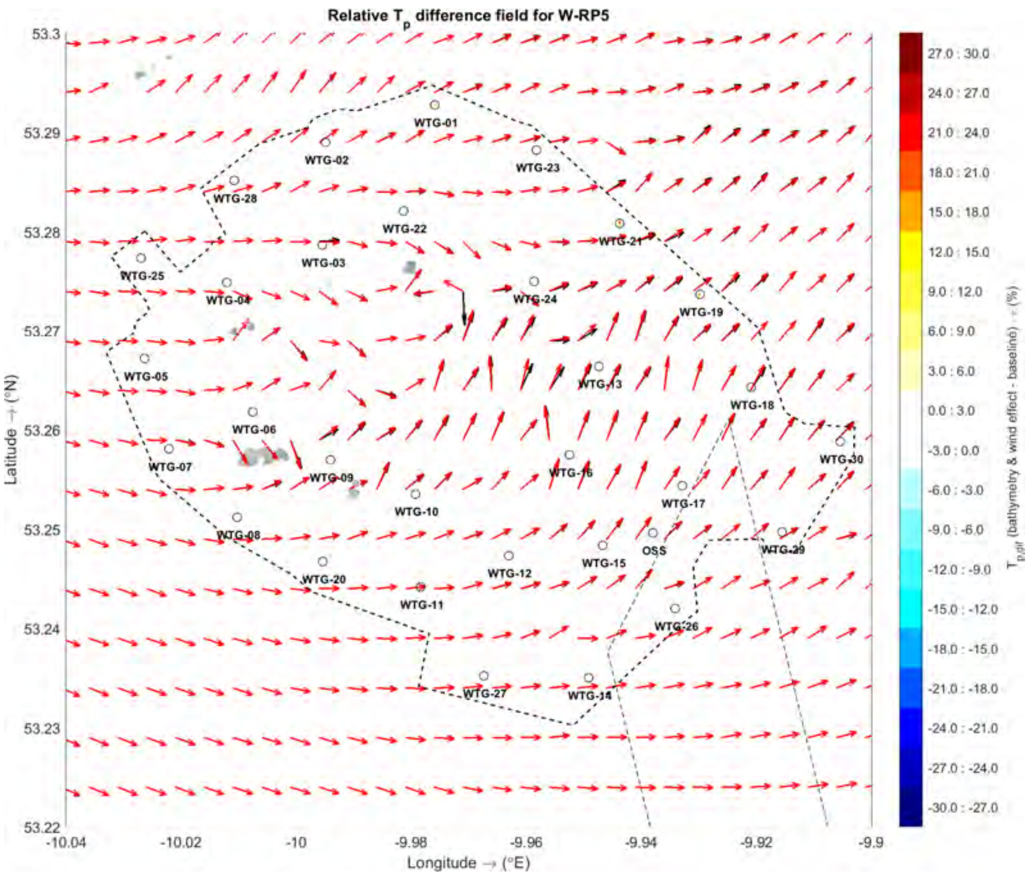
Relative T_p difference field for W-RP5
Latitude → (°N)
Longitude → (°E)
$T_{p,dif}$ (bathymetry & wind effect - baseline) → (%)

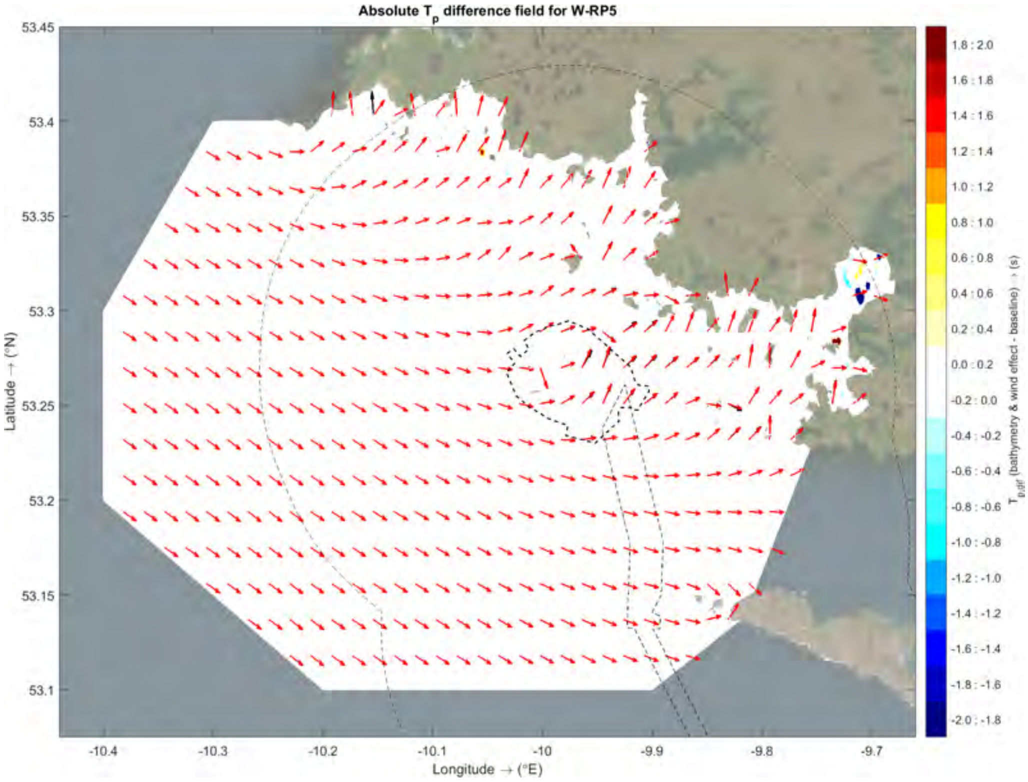
Absolute T_p difference field for W-RP5
Latitude → (°N)
Longitude → (°E)
T_p,diff (bathymetry & wind effect - baseline) → (s)
1.8 : 2.0
1.6 : 1.8
1.4 : 1.6
1.2 : 1.4
1.0 : 1.2
0.8 : 1.0
0.6 : 0.8
0.4 : 0.6
0.2 : 0.4
0.0 : 0.2
-0.2 : 0.0
-0.4 : -0.2
-0.6 : -0.4
-0.8 : -0.6
-1.0 : -0.8
-1.2 : -1.0
-1.4 : -1.2
-1.6 : -1.4
-1.8 : -1.6
-2.0 : -1.8

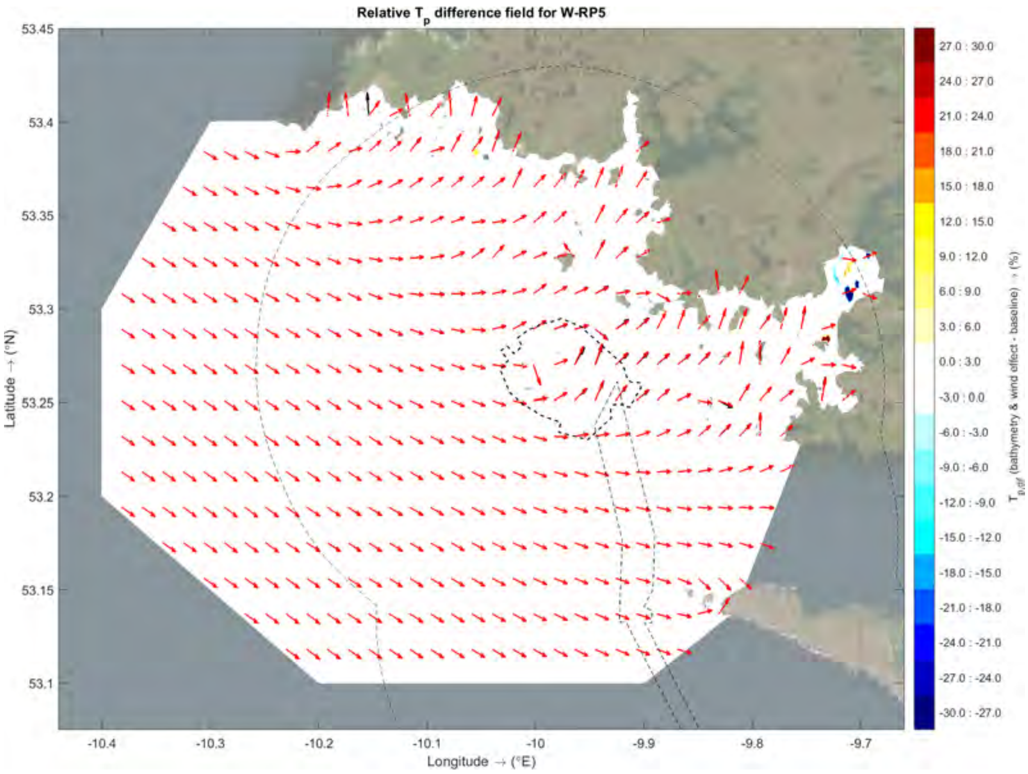
Relative T_p difference field for W-RP5
Latitude → (°N)
Longitude → (°E)
T_p,diff (bathymetry & wind effect - baseline) → (%)
27.0 : 30.0
24.0 : 27.0
21.0 : 24.0
18.0 : 21.0
15.0 : 18.0
12.0 : 15.0
9.0 : 12.0
6.0 : 9.0
3.0 : 6.0
0.0 : 3.0
-3.0 : 0.0
-6.0 : -3.0
-9.0 : -6.0
-12.0 : -9.0
-15.0 : -12.0
-18.0 : -15.0
-21.0 : -18.0
-24.0 : -21.0
-27.0 : -24.0
-30.0 : -27.0

E.5 10-yr RP

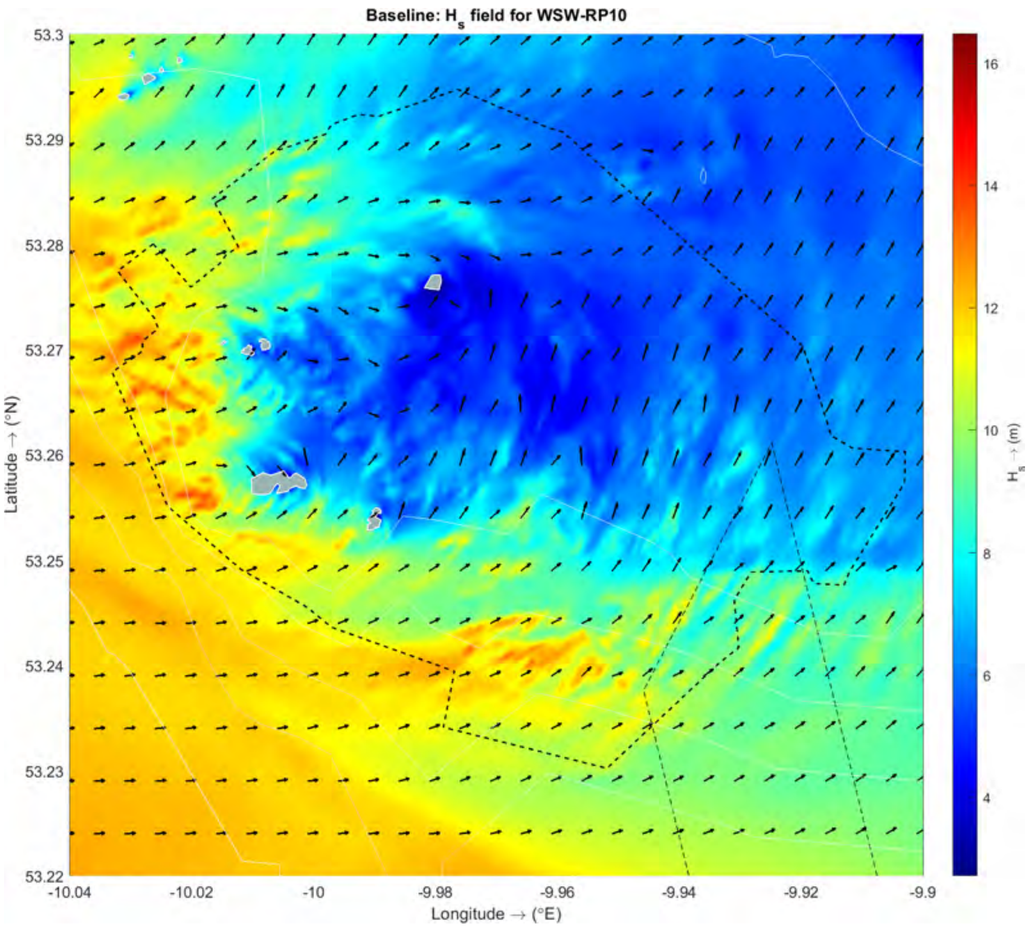

Baseline: H_s field for WSW-RP10
53.3
53.29
53.28
53.27
53.26
53.25
53.24
53.23
53.22
Latitude → (°N)
-10.04
-10.02
-10
-9.98
-9.96
-9.94
-9.92
-9.9
Longitude → (°E)
16
14
12
10
8
6
4
H_s → (m)

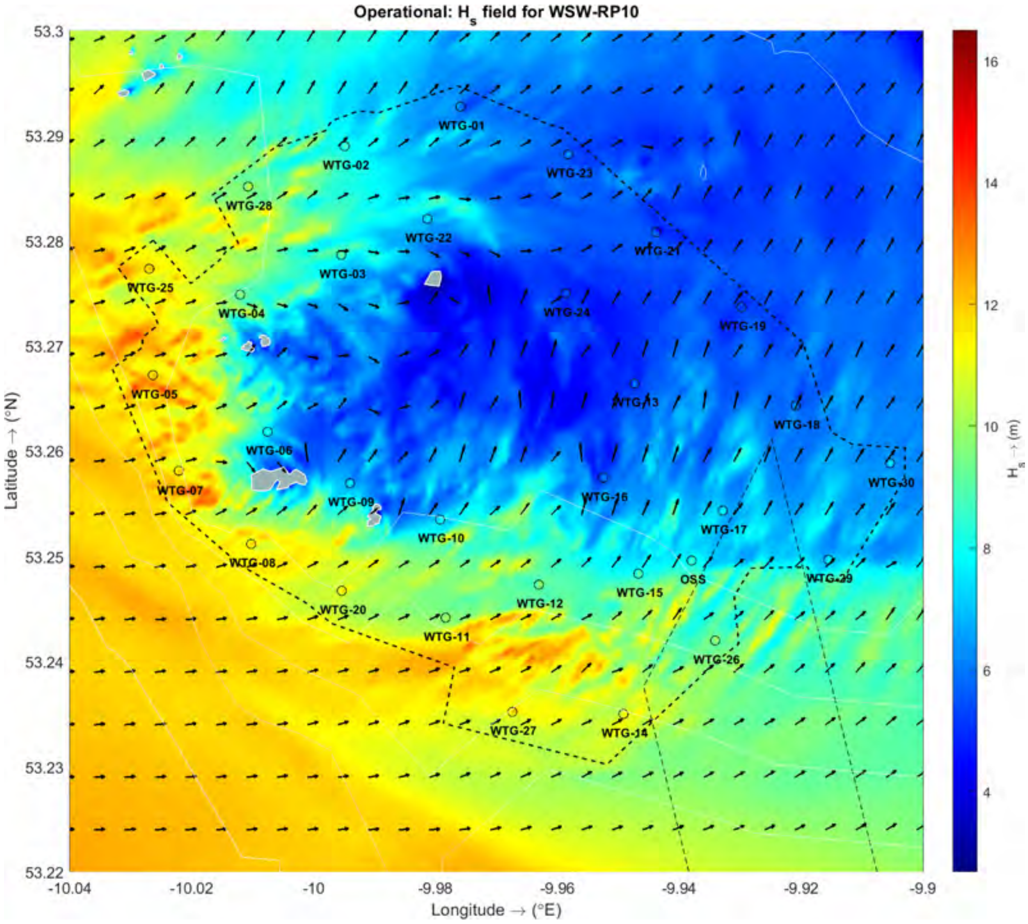

Operational: H_s field for WSW-RP10
Latitude → (°N)
Longitude → (°E)
H_s → (m)
WTG-01
WTG-02
WTG-03
WTG-04
WTG-05
WTG-06
WTG-07
WTG-08
WTG-09
WTG-10
WTG-11
WTG-12
WTG-13
WTG-14
WTG-15
WTG-16
WTG-17
WTG-18
WTG-19
WTG-20
WTG-21
WTG-22
WTG-23
WTG-24
WTG-25
WTG-26
WTG-27
WTG-28
WTG-29
WTG-30
OSS

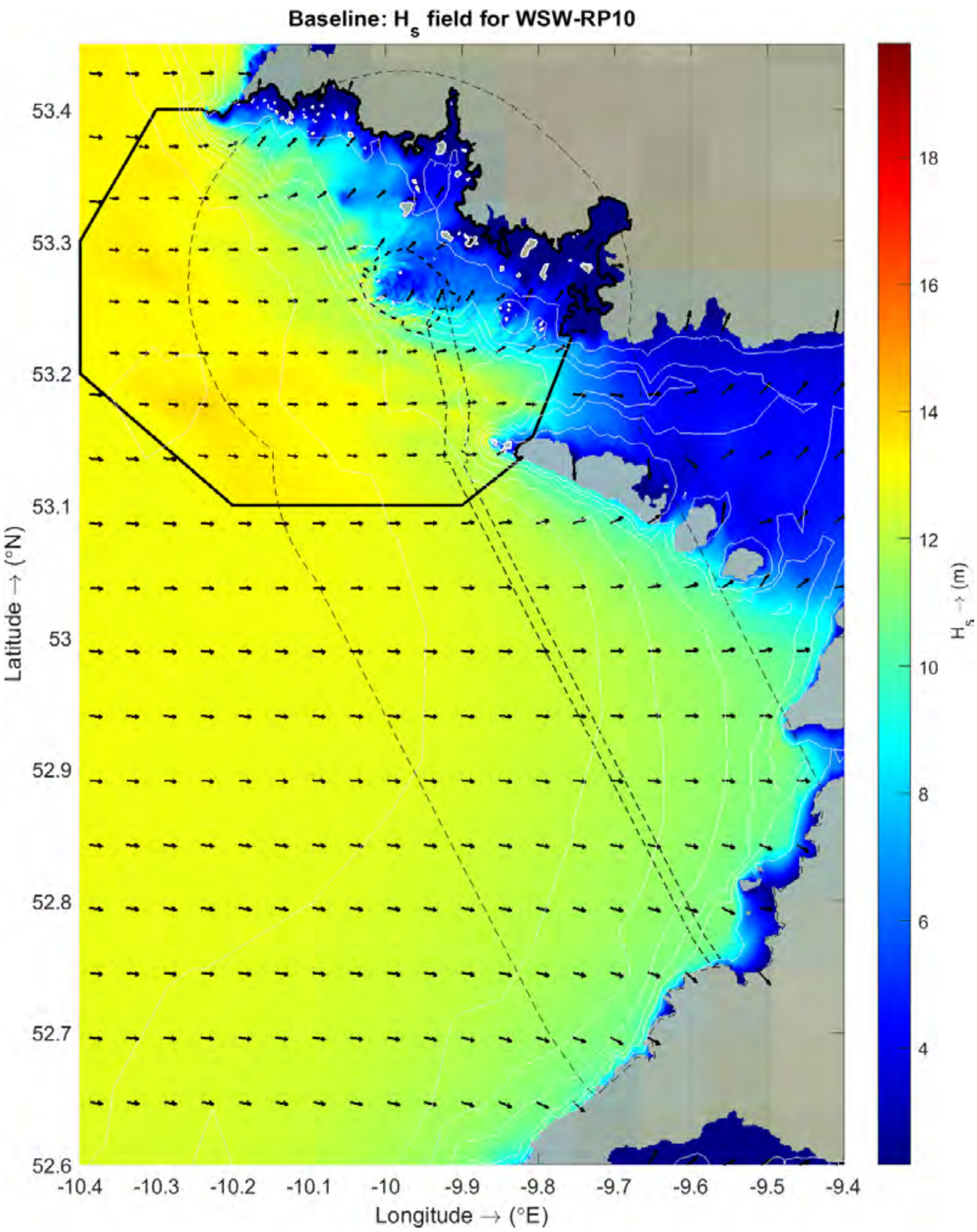
Baseline: H_s field for WSW-RP10
Latitude → (°N)
Longitude → (°E)
H_s → (m)
53.4
53.3
53.2
53.1
53
52.9
52.8
52.7
52.6
-10.4
-10.3
-10.2
-10.1
-10
-9.9
-9.8
-9.7
-9.6
-9.5
-9.4
18
16
14
12
10
8
6
4

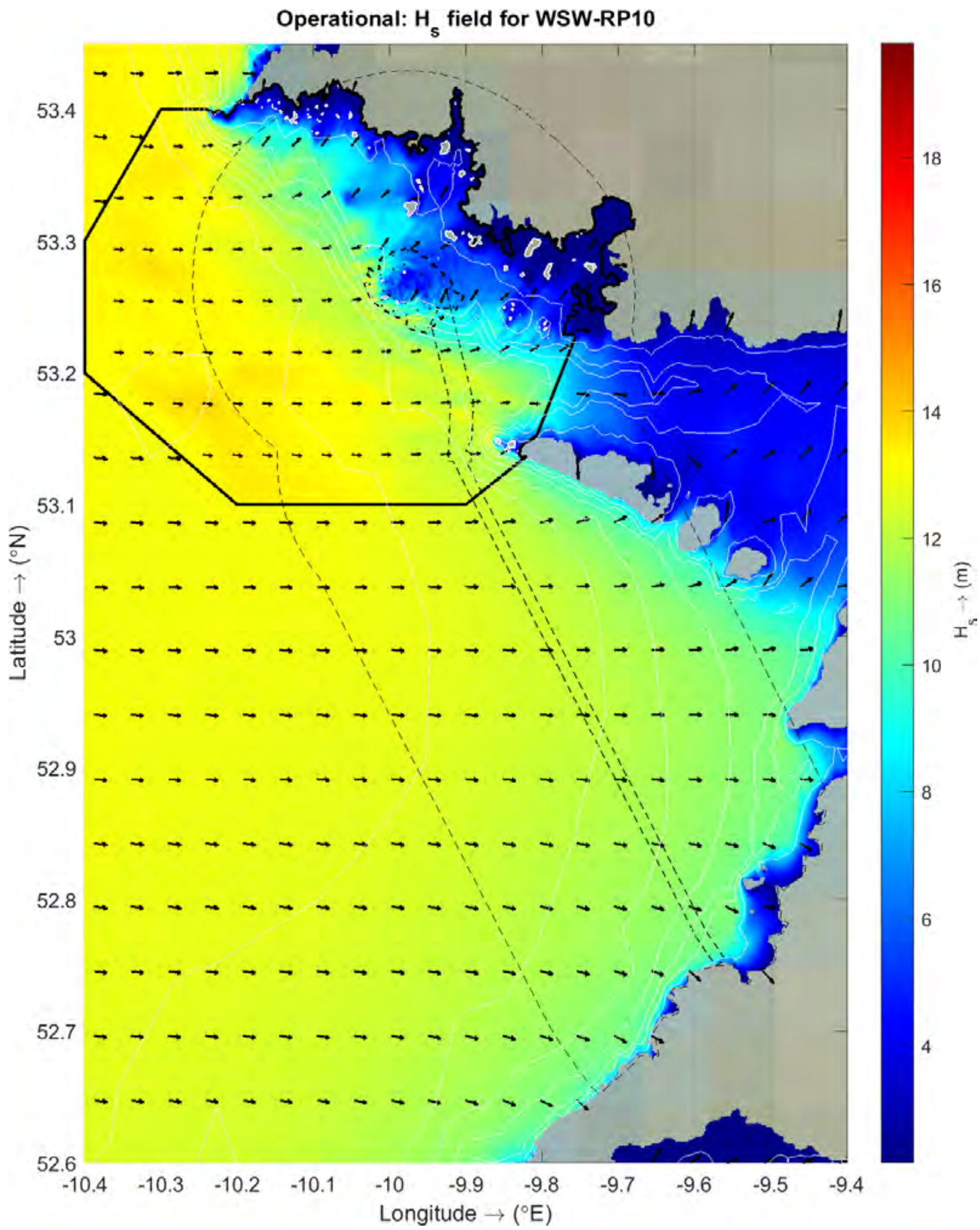
Operational: H_s field for WSW-RP10
Latitude → (°N)
Longitude → (°E)
H_s → (m)
53.4
53.3
53.2
53.1
53
52.9
52.8
52.7
52.6
-10.4
-10.3
-10.2
-10.1
-10
-9.9
-9.8
-9.7
-9.6
-9.5
-9.4
18
16
14
12
10
8
6
4

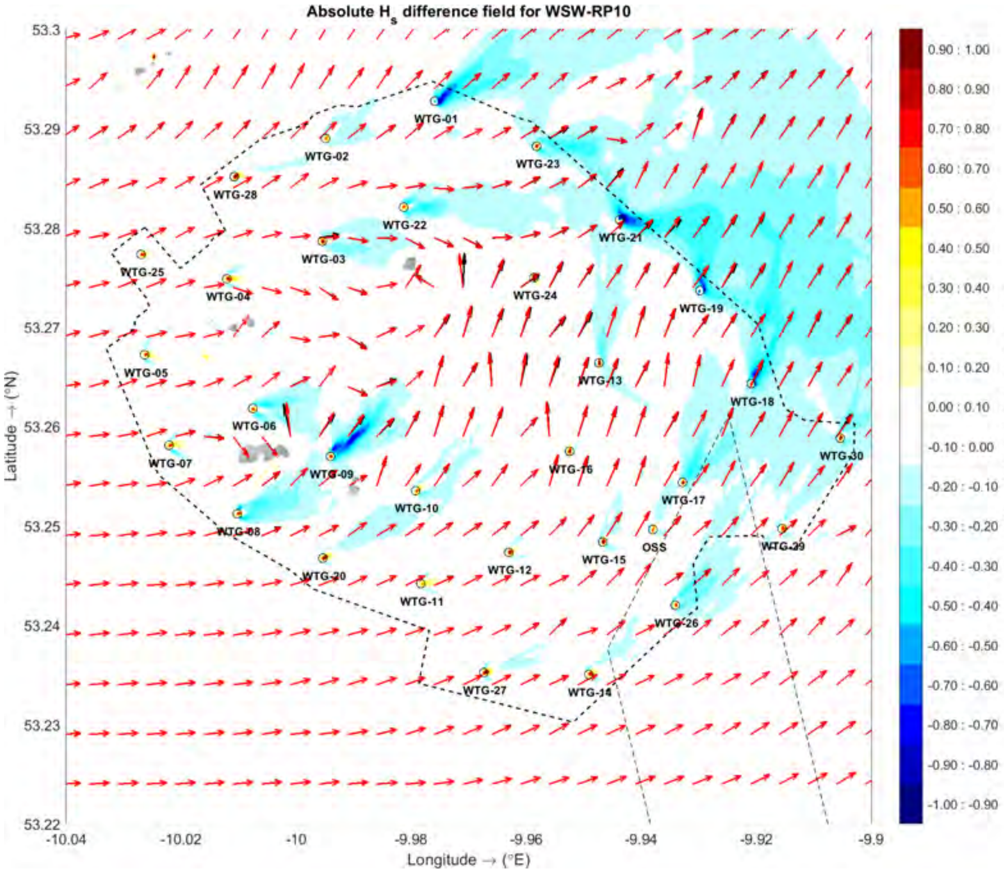
Absolute H_s difference field for WSW-RP10
Latitude → (°N)
Longitude → (°E)
H_s,diff (bathymetry & wind effect - baseline) → (m)
WTG-01
WTG-02
WTG-03
WTG-04
WTG-05
WTG-06
WTG-07
WTG-08
WTG-09
WTG-10
WTG-11
WTG-12
WTG-13
WTG-14
WTG-15
WTG-16
WTG-17
WTG-18
WTG-19
WTG-20
WTG-21
WTG-22
WTG-23
WTG-24
WTG-25
WTG-26
WTG-27
WTG-28
WTG-29
WTG-30
OSS
0.90 : 1.00
0.80 : 0.90
0.70 : 0.80
0.60 : 0.70
0.50 : 0.60
0.40 : 0.50
0.30 : 0.40
0.20 : 0.30
0.10 : 0.20
0.00 : 0.10
-0.10 : 0.00
-0.20 : -0.10
-0.30 : -0.20
-0.40 : -0.30
-0.50 : -0.40
-0.60 : -0.50
-0.70 : -0.60
-0.80 : -0.70
-0.90 : -0.80
-1.00 : -0.90

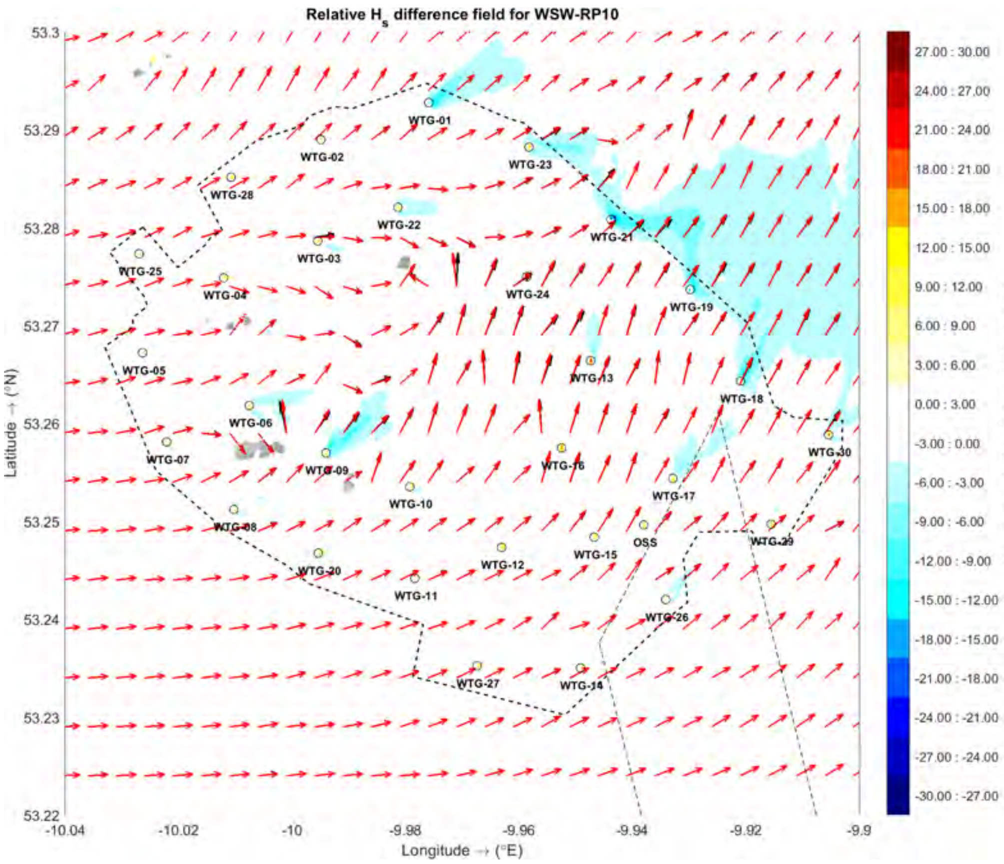
Relative H_s difference field for WSW-RP10
Latitude → (°N)
Longitude → (°E)
H_s,diff (bathymetry & wind effect - baseline) → (%)
27.00 : 30.00
24.00 : 27.00
21.00 : 24.00
18.00 : 21.00
15.00 : 18.00
12.00 : 15.00
9.00 : 12.00
6.00 : 9.00
3.00 : 6.00
0.00 : 3.00
-3.00 : 0.00
-6.00 : -3.00
-9.00 : -6.00
-12.00 : -9.00
-15.00 : -12.00
-18.00 : -15.00
-21.00 : -18.00
-24.00 : -21.00
-27.00 : -24.00
-30.00 : -27.00

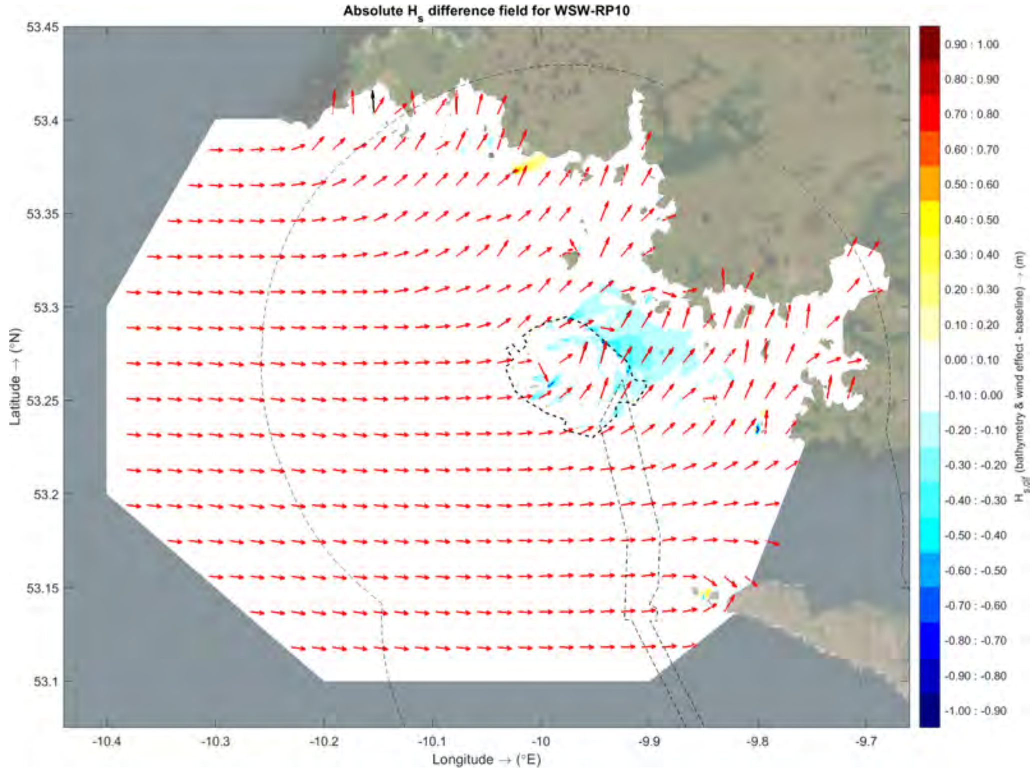

Absolute H_s difference field for WSW-RP10
Latitude → (°N)
Longitude → (°E)
$H_{s,dif}$ (bathymetry & wind effect - baseline) → (m)

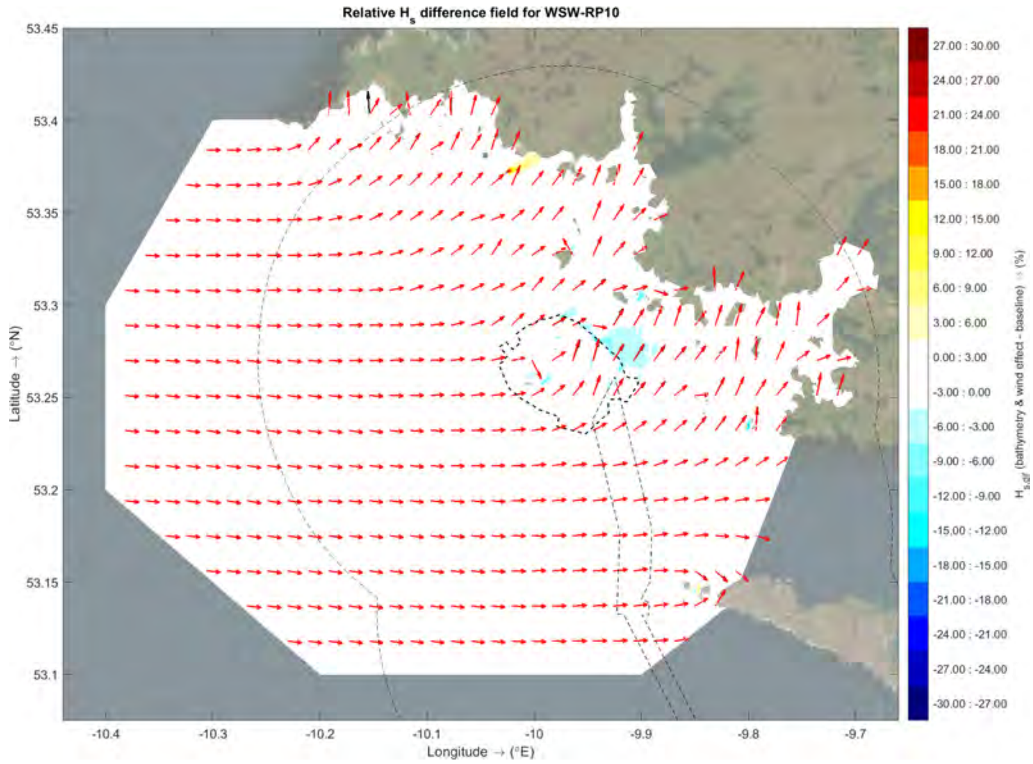

Relative H_s difference field for WSW-RP10
Latitude → (°N)
Longitude → (°E)
$H_{s,dif}$ (bathymetry & wind effect - baseline) → (%)

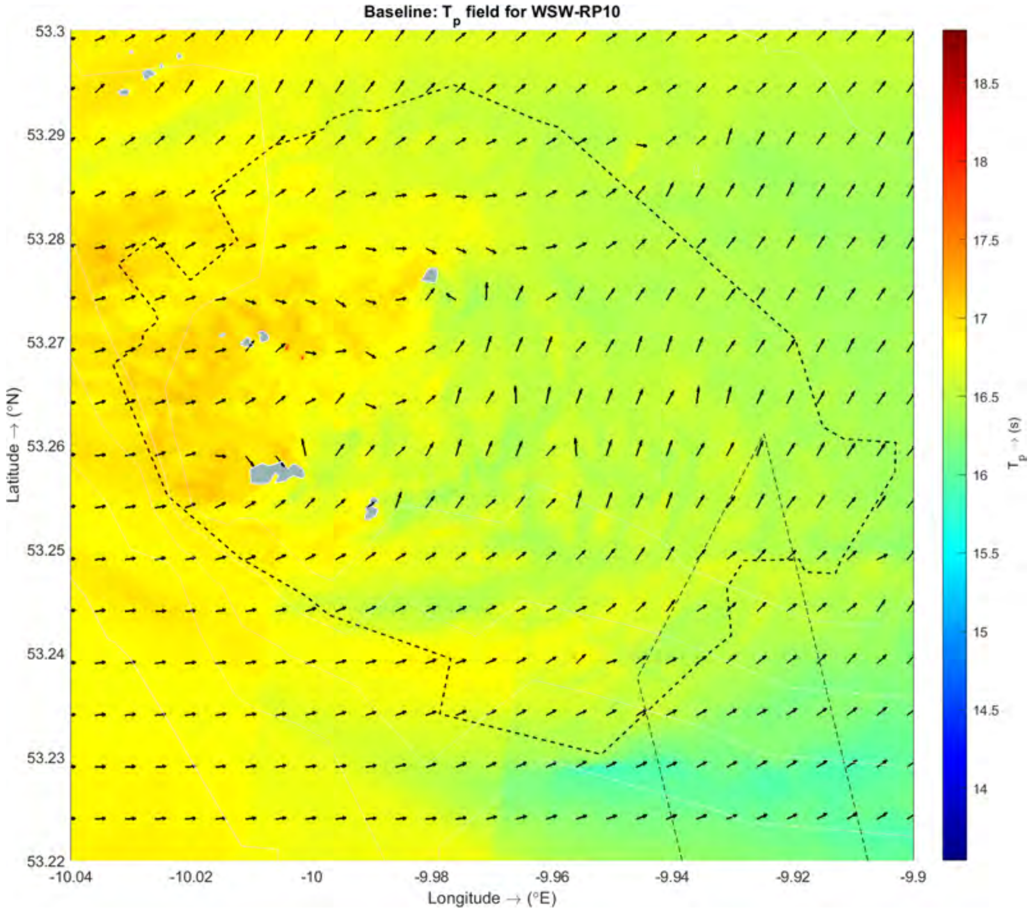
Baseline: T_p field for WSW-RP10
53.3
53.29
53.28
53.27
53.26
53.25
53.24
53.23
53.22
Latitude → (°N)
-10.04
-10.02
-10
-9.98
-9.96
-9.94
-9.92
-9.9
Longitude → (°E)
18.5
18
17.5
17
16.5
16
15.5
15
14.5
14
T_p → (s)

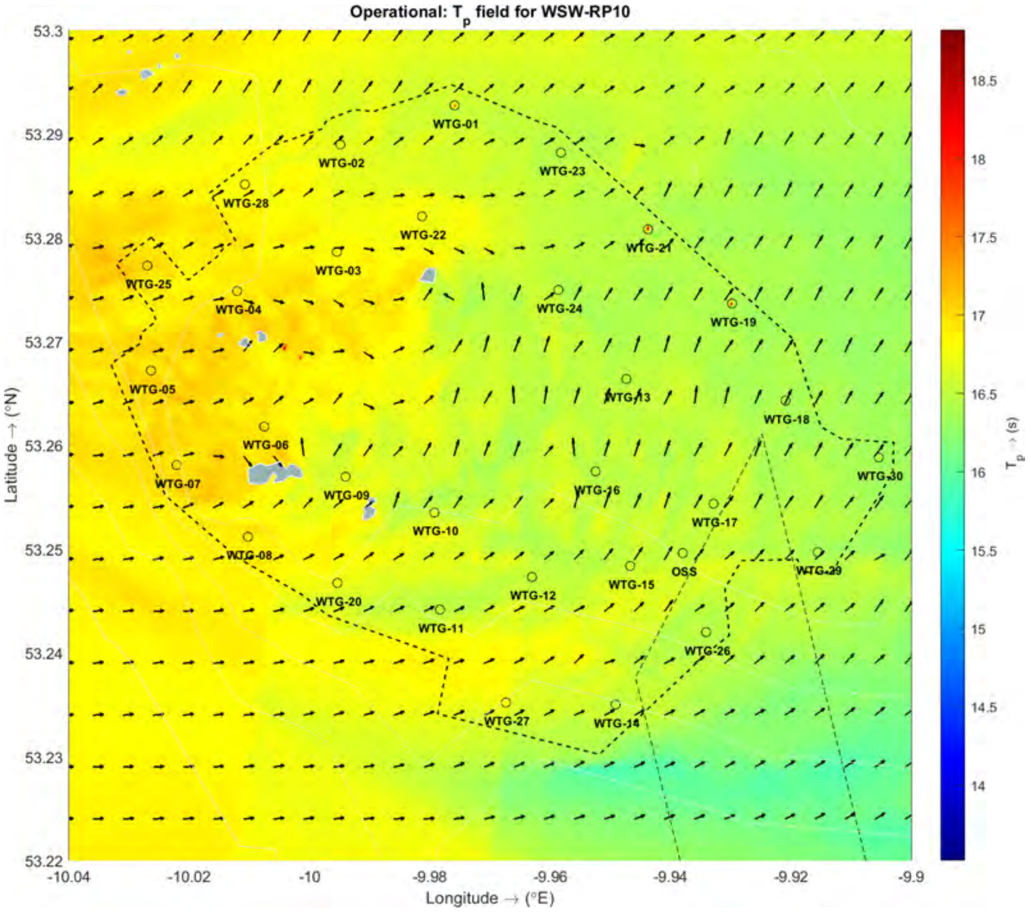
Operational: T_p field for WSW-RP10
Latitude → (°N)
Longitude → (°E)
T_p → (s)
WTG-01
WTG-02
WTG-03
WTG-04
WTG-05
WTG-06
WTG-07
WTG-08
WTG-09
WTG-10
WTG-11
WTG-12
WTG-13
WTG-14
WTG-15
WTG-16
WTG-17
WTG-18
WTG-19
WTG-20
WTG-21
WTG-22
WTG-23
WTG-24
WTG-25
WTG-26
WTG-27
WTG-28
WTG-29
WTG-30
OSS

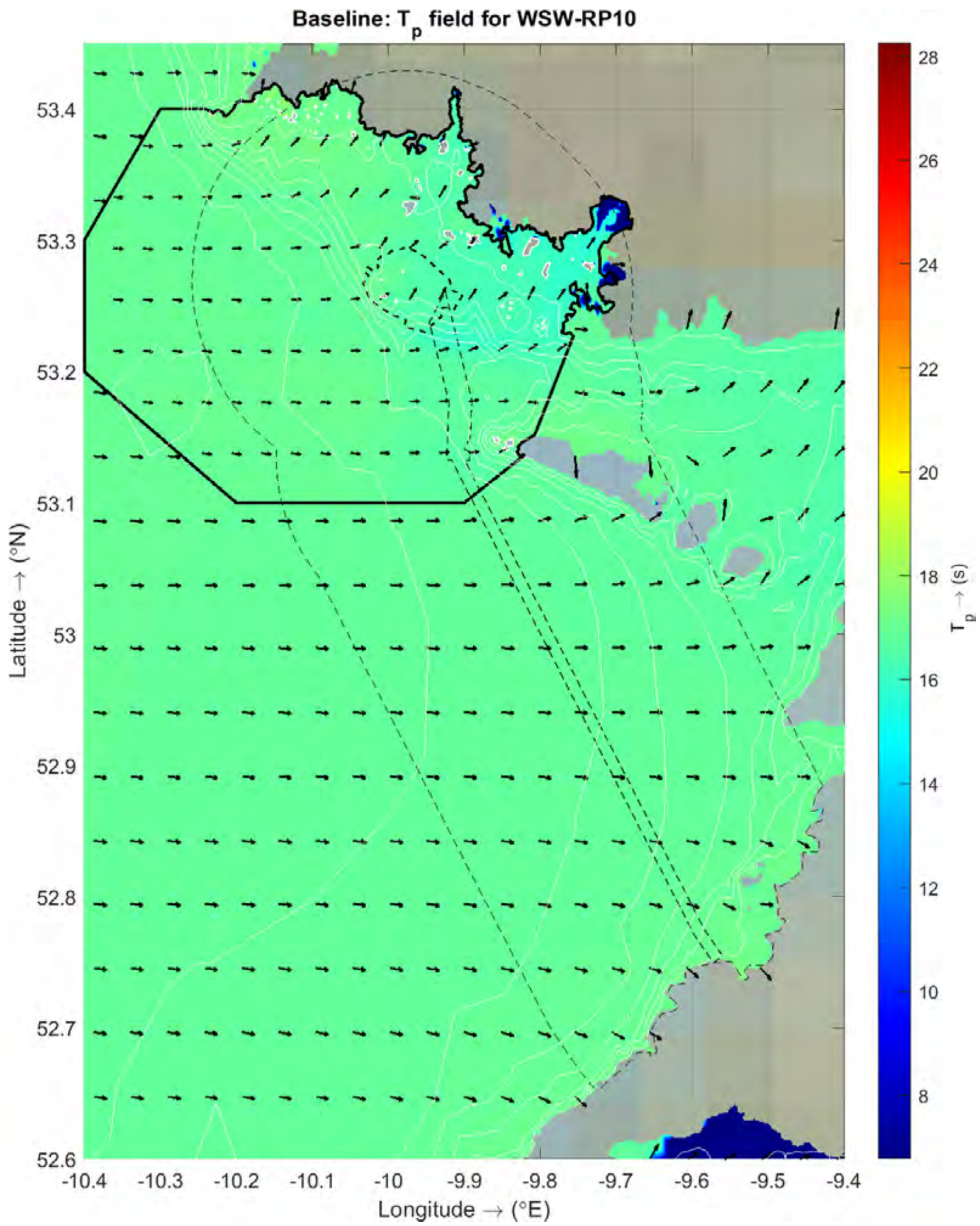

Baseline: T_p field for WSW-RP10
Latitude → (°N)
Longitude → (°E)
T_p → (s)
53.4
53.3
53.2
53.1
53
52.9
52.8
52.7
52.6
-10.4
-10.3
-10.2
-10.1
-10
-9.9
-9.8
-9.7
-9.6
-9.5
-9.4
28
26
24
22
20
18
16
14
12
10
8

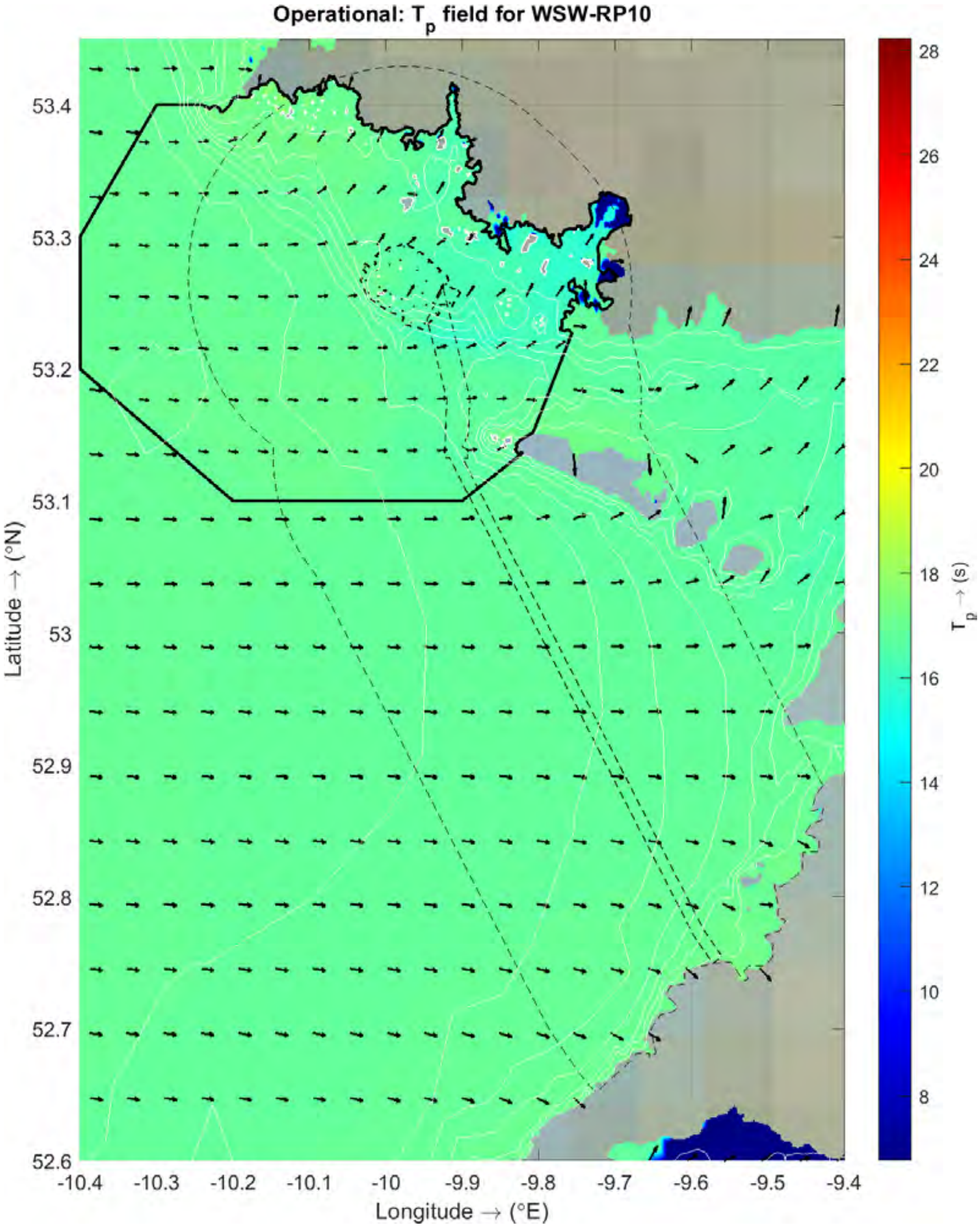
Operational: T_p field for WSW-RP10
53.4
53.3
53.2
53.1
53
52.9
52.8
52.7
52.6
Latitude → (°N)
-10.4
-10.3
-10.2
-10.1
-10
-9.9
-9.8
-9.7
-9.6
-9.5
-9.4
Longitude → (°E)
28
26
24
22
20
18
16
14
12
10
8
T_p → (s)

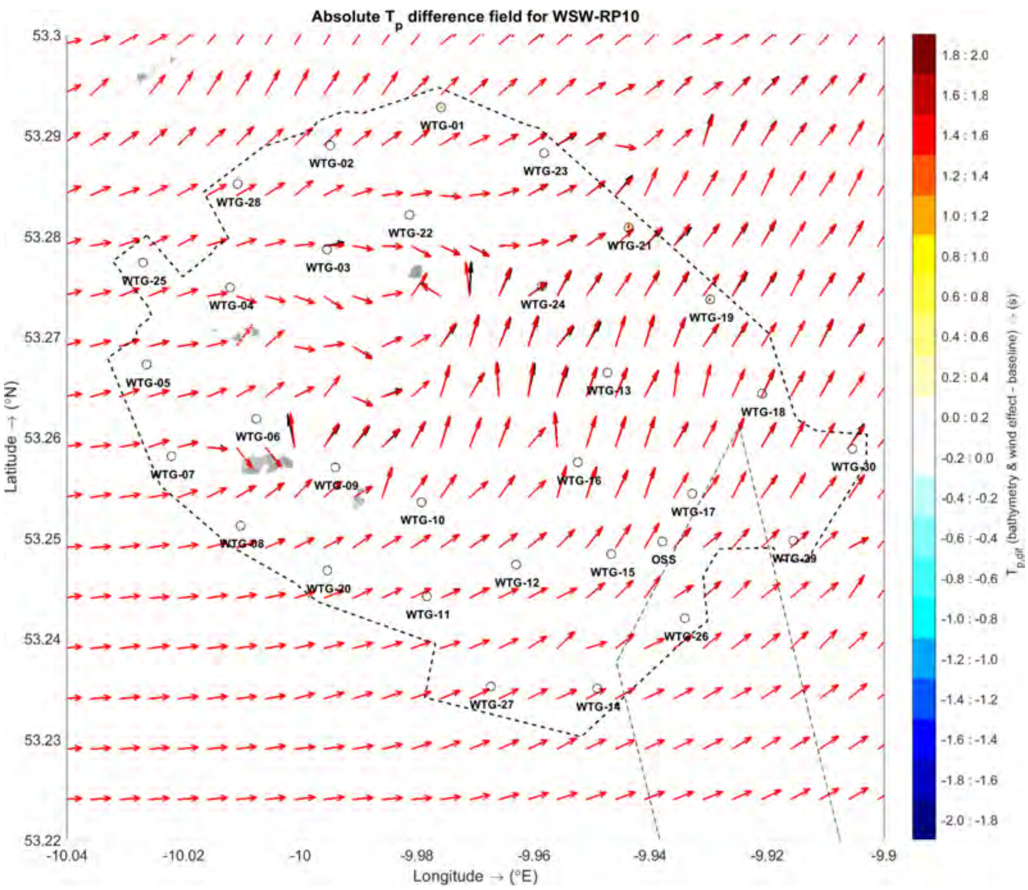
Absolute T_p difference field for WSW-RP10
Latitude → (°N)
Longitude → (°E)
$T_{p,dif}$ (bathymetry & wind effect - baseline) → (s)
1.8 : 2.0
1.6 : 1.8
1.4 : 1.6
1.2 : 1.4
1.0 : 1.2
0.8 : 1.0
0.6 : 0.8
0.4 : 0.6
0.2 : 0.4
0.0 : 0.2
-0.2 : 0.0
-0.4 : -0.2
-0.6 : -0.4
-0.8 : -0.6
-1.0 : -0.8
-1.2 : -1.0
-1.4 : -1.2
-1.6 : -1.4
-1.8 : -1.6
-2.0 : -1.8

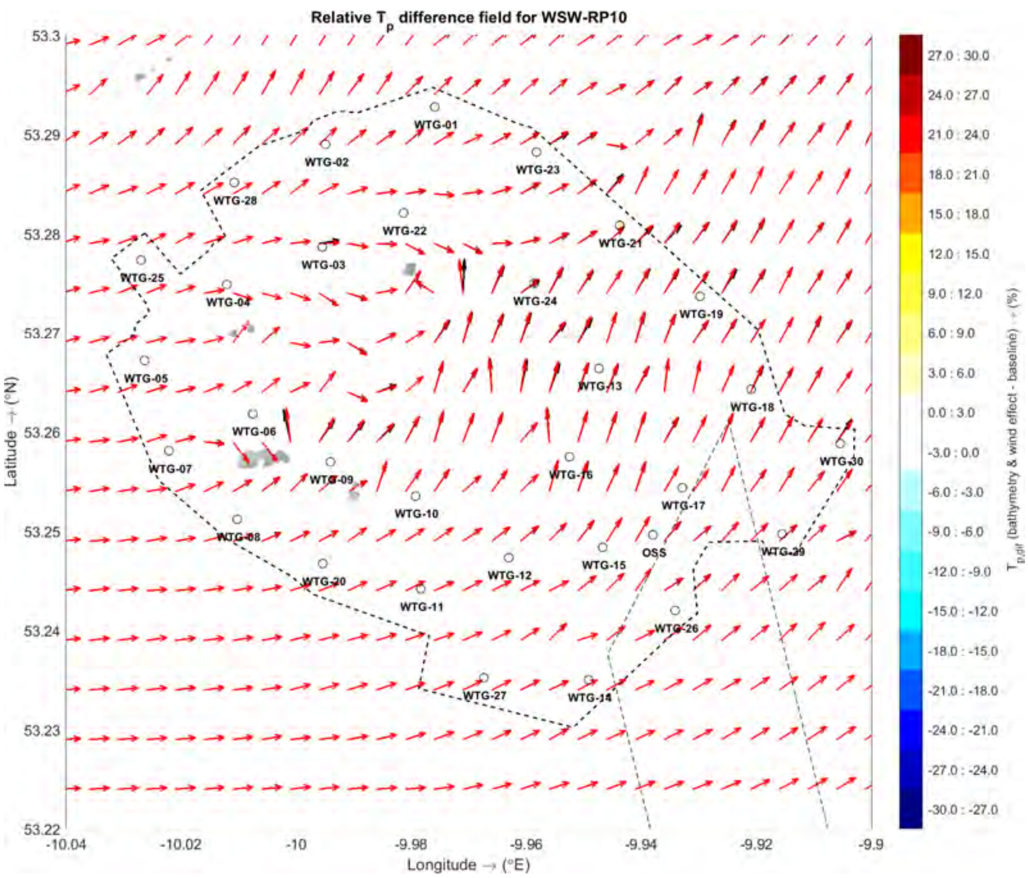
Relative T_p difference field for WSW-RP10
Latitude → (°N)
Longitude → (°E)
$T_{p,dif}$ (bathymetry & wind effect - baseline) → (%)
27.0 : 30.0
24.0 : 27.0
21.0 : 24.0
18.0 : 21.0
15.0 : 18.0
12.0 : 15.0
9.0 : 12.0
6.0 : 9.0
3.0 : 6.0
0.0 : 3.0
-3.0 : 0.0
-6.0 : -3.0
-9.0 : -6.0
-12.0 : -9.0
-15.0 : -12.0
-18.0 : -15.0
-21.0 : -18.0
-24.0 : -21.0
-27.0 : -24.0
-30.0 : -27.0

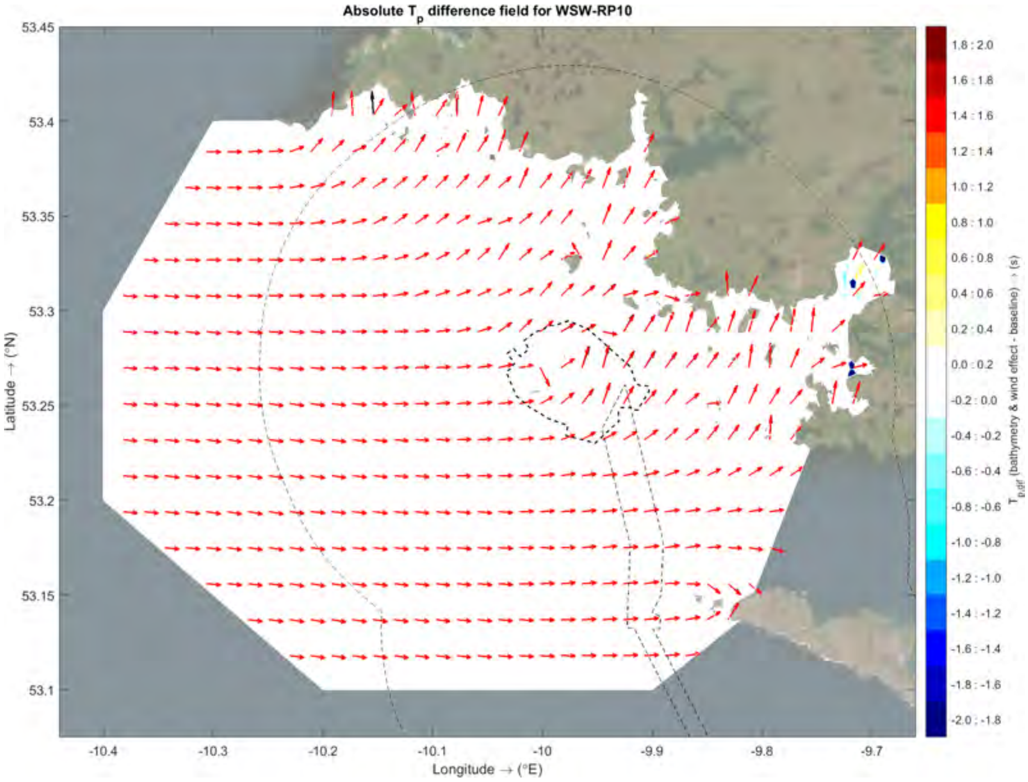

Absolute T_p difference field for WSW-RP10
Latitude → (°N)
Longitude → (°E)
$T_{p,diff}$ (bathymetry & wind effect - baseline) → (s)

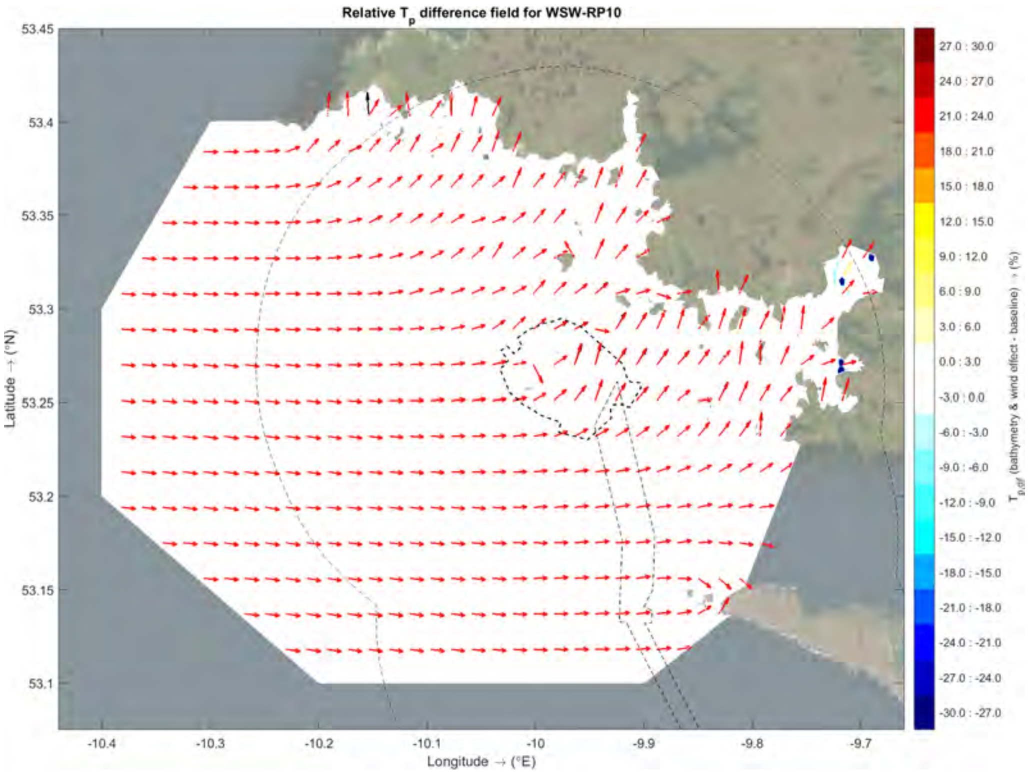

Relative T_p difference field for WSW-RP10
Latitude → (°N)
Longitude → (°E)
$T_{p,diff}$ (bathymetry & wind effect - baseline) → (%)

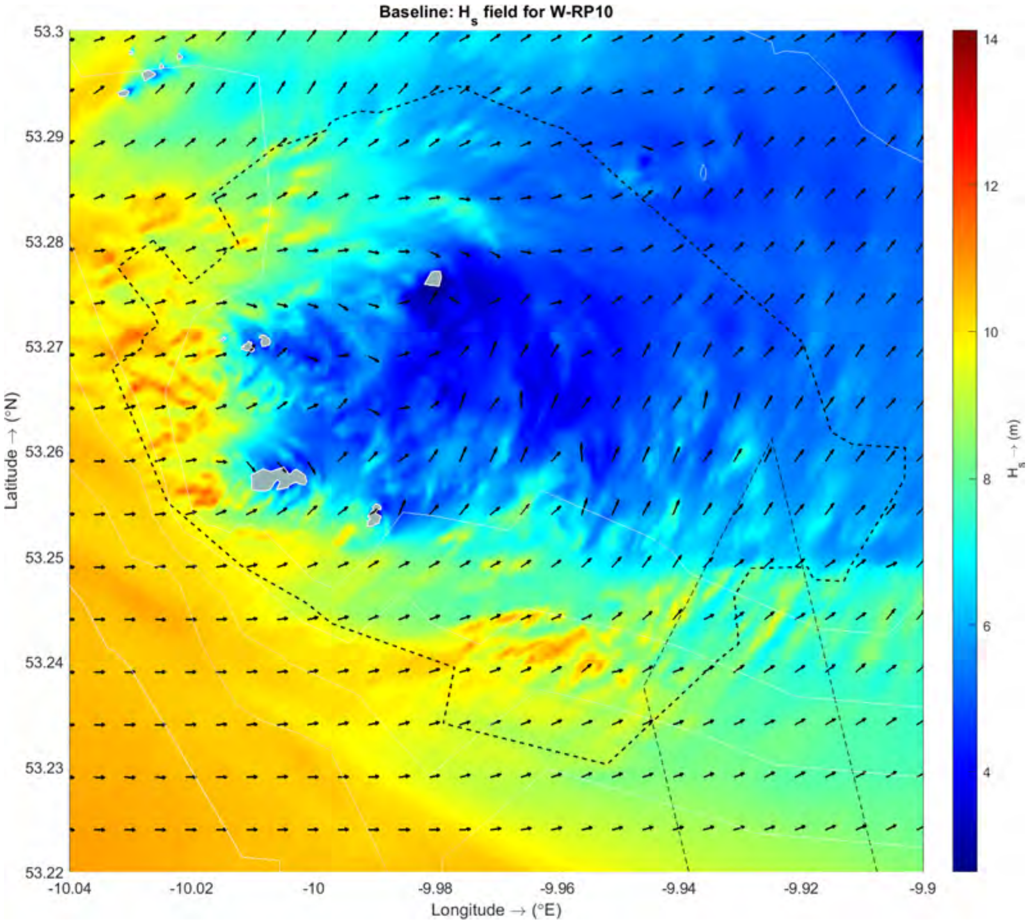
Baseline: H_s field for W-RP10
53.3
53.29
53.28
53.27
53.26
53.25
53.24
53.23
53.22
Latitude → (°N)
-10.04
-10.02
-10
-9.98
-9.96
-9.94
-9.92
-9.9
Longitude → (°E)
14
12
10
8
6
4
H_s → (m)

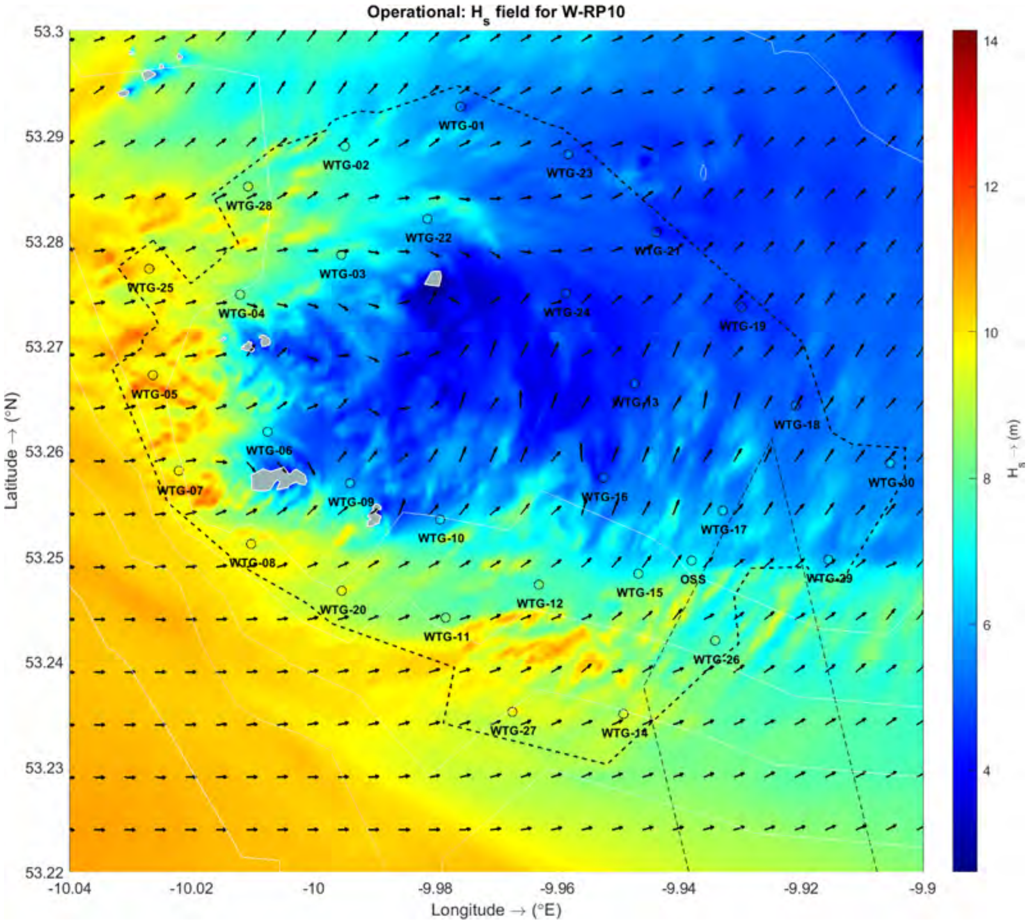
Operational: H_s field for W-RP10
Latitude → (°N)
Longitude → (°E)
H_s → (m)
WTG-01
WTG-02
WTG-03
WTG-04
WTG-05
WTG-06
WTG-07
WTG-08
WTG-09
WTG-10
WTG-11
WTG-12
WTG-13
WTG-14
WTG-15
WTG-16
WTG-17
WTG-18
WTG-19
WTG-20
WTG-21
WTG-22
WTG-23
WTG-24
WTG-25
WTG-26
WTG-27
WTG-28
WTG-29
WTG-30
OSS

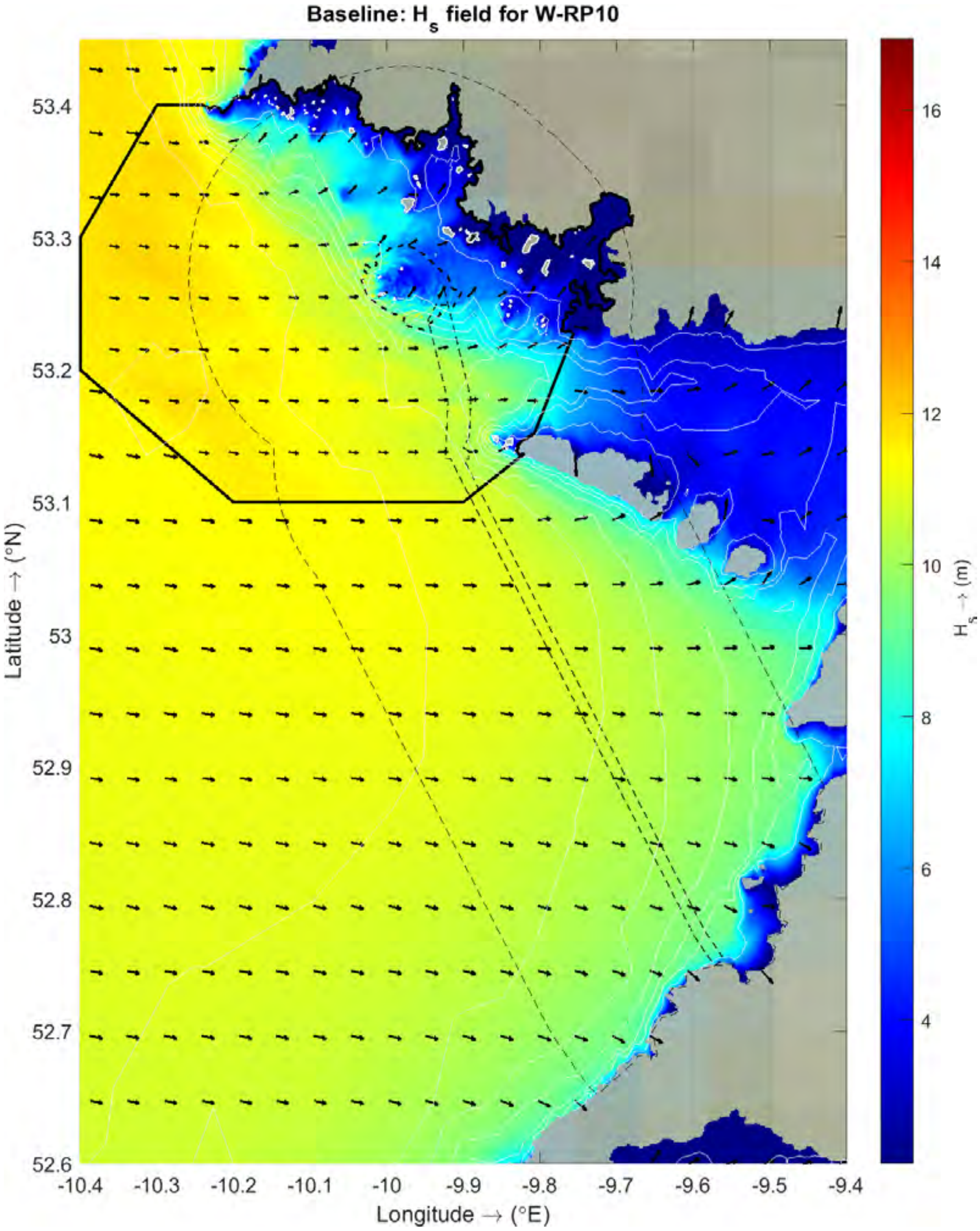
Baseline: H_s field for W-RP10
Latitude → (°N)
Longitude → (°E)
H_s → (m)
53.4
53.3
53.2
53.1
53
52.9
52.8
52.7
52.6
-10.4
-10.3
-10.2
-10.1
-10
-9.9
-9.8
-9.7
-9.6
-9.5
-9.4
16
14
12
10
8
6
4

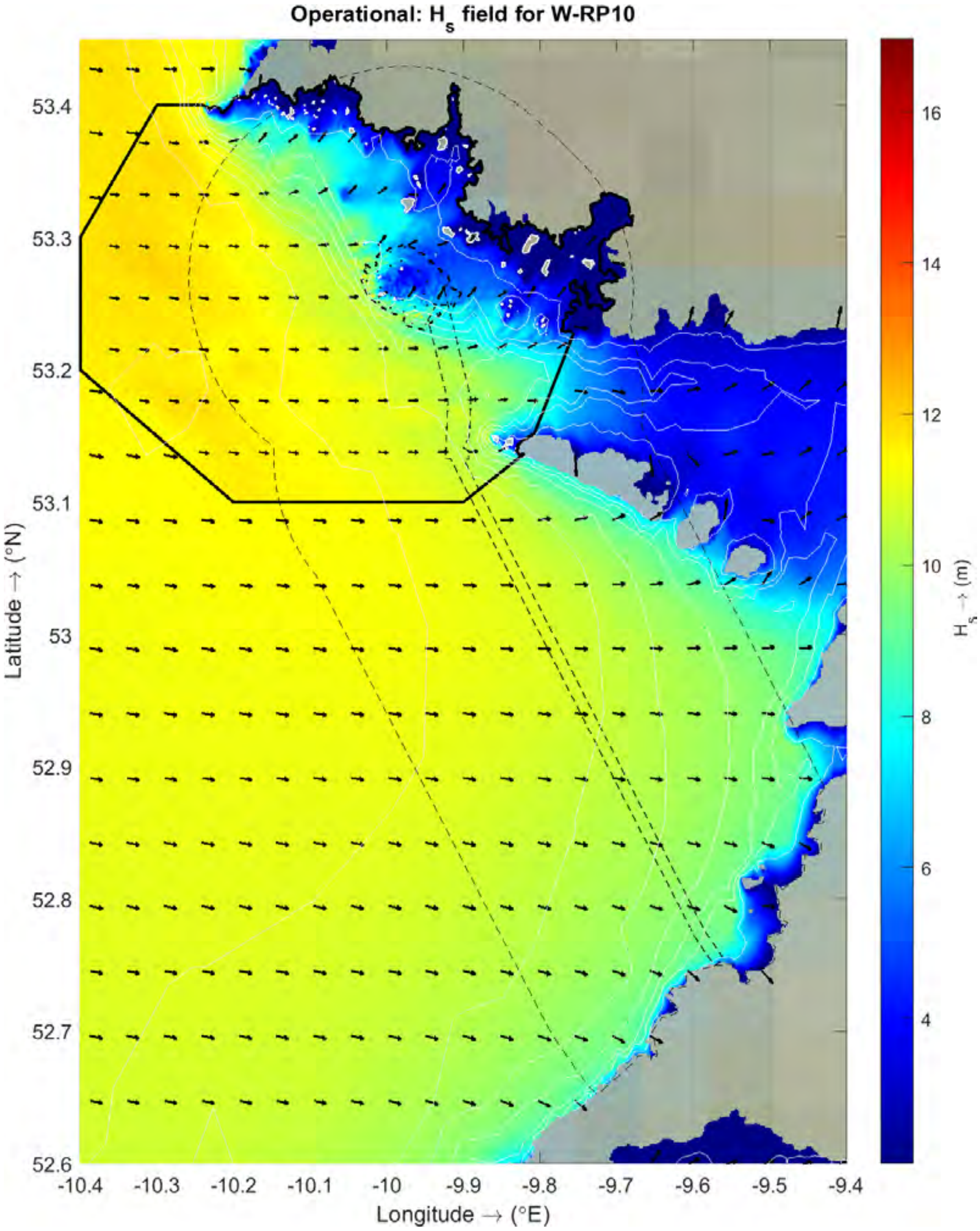
Operational: H_s field for W-RP10
Latitude → (°N)
Longitude → (°E)
H_s → (m)
53.4
53.3
53.2
53.1
53
52.9
52.8
52.7
52.6
-10.4
-10.3
-10.2
-10.1
-10
-9.9
-9.8
-9.7
-9.6
-9.5
-9.4
16
14
12
10
8
6
4

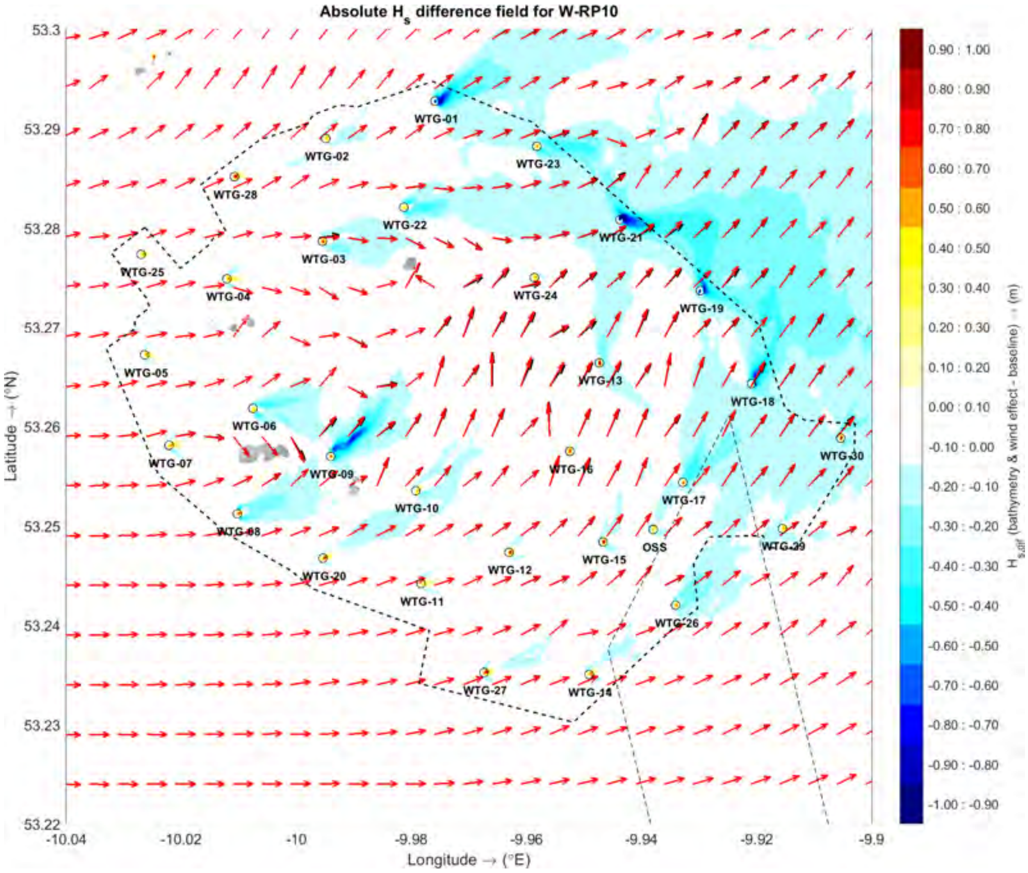
Absolute Hs difference field for W-RP10
Latitude → (°N)
Longitude → (°E)
Hs,diff (bathymetry & wind effect - baseline) → (m)
0.90 : 1.00
0.80 : 0.90
0.70 : 0.80
0.60 : 0.70
0.50 : 0.60
0.40 : 0.50
0.30 : 0.40
0.20 : 0.30
0.10 : 0.20
0.00 : 0.10
-0.10 : 0.00
-0.20 : -0.10
-0.30 : -0.20
-0.40 : -0.30
-0.50 : -0.40
-0.60 : -0.50
-0.70 : -0.60
-0.80 : -0.70
-0.90 : -0.80
-1.00 : -0.90
WTG-01
WTG-02
WTG-03
WTG-04
WTG-05
WTG-06
WTG-07
WTG-08
WTG-09
WTG-10
WTG-11
WTG-12
WTG-13
WTG-14
WTG-15
WTG-16
WTG-17
WTG-18
WTG-19
WTG-20
WTG-21
WTG-22
WTG-23
WTG-24
WTG-25
WTG-26
WTG-27
WTG-28
WTG-29
WTG-30
OSS

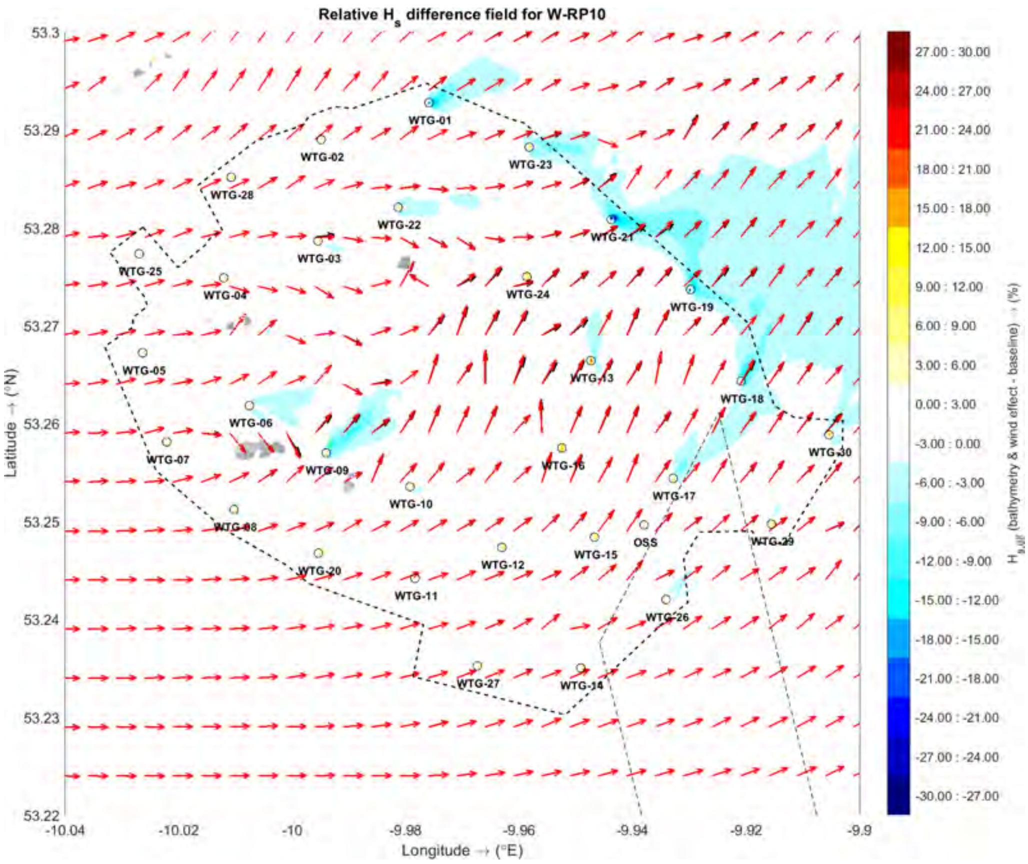
Relative Hs difference field for W-RP10
Latitude → (°N)
Longitude → (°E)
Hs,diff (bathymetry & wind effect - baseline) → (%)
27.00 : 30.00
24.00 : 27.00
21.00 : 24.00
18.00 : 21.00
15.00 : 18.00
12.00 : 15.00
9.00 : 12.00
6.00 : 9.00
3.00 : 6.00
0.00 : 3.00
-3.00 : 0.00
-6.00 : -3.00
-9.00 : -6.00
-12.00 : -9.00
-15.00 : -12.00
-18.00 : -15.00
-21.00 : -18.00
-24.00 : -21.00
-27.00 : -24.00
-30.00 : -27.00

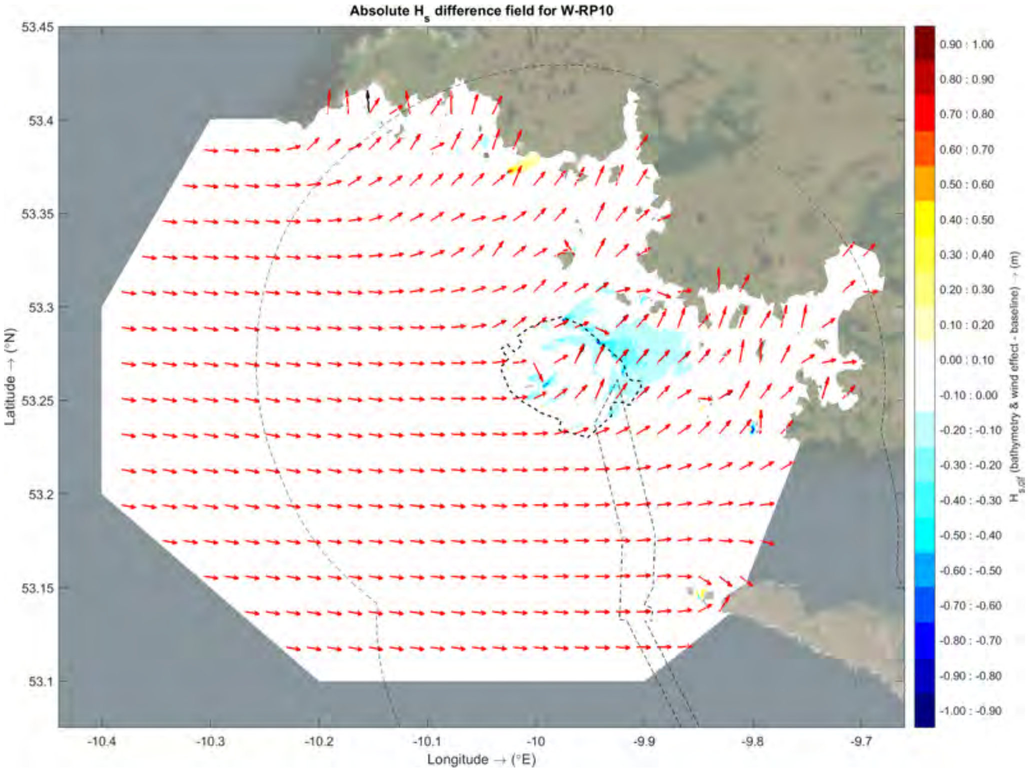

Absolute H_s difference field for W-RP10
Latitude → (°N)
Longitude → (°E)
$H_{s,dif}$ (bathymetry & wind effect - baseline) → (m)
0.90 : 1.00
0.80 : 0.90
0.70 : 0.80
0.60 : 0.70
0.50 : 0.60
0.40 : 0.50
0.30 : 0.40
0.20 : 0.30
0.10 : 0.20
0.00 : 0.10
-0.10 : 0.00
-0.20 : -0.10
-0.30 : -0.20
-0.40 : -0.30
-0.50 : -0.40
-0.60 : -0.50
-0.70 : -0.60
-0.80 : -0.70
-0.90 : -0.80
-1.00 : -0.90

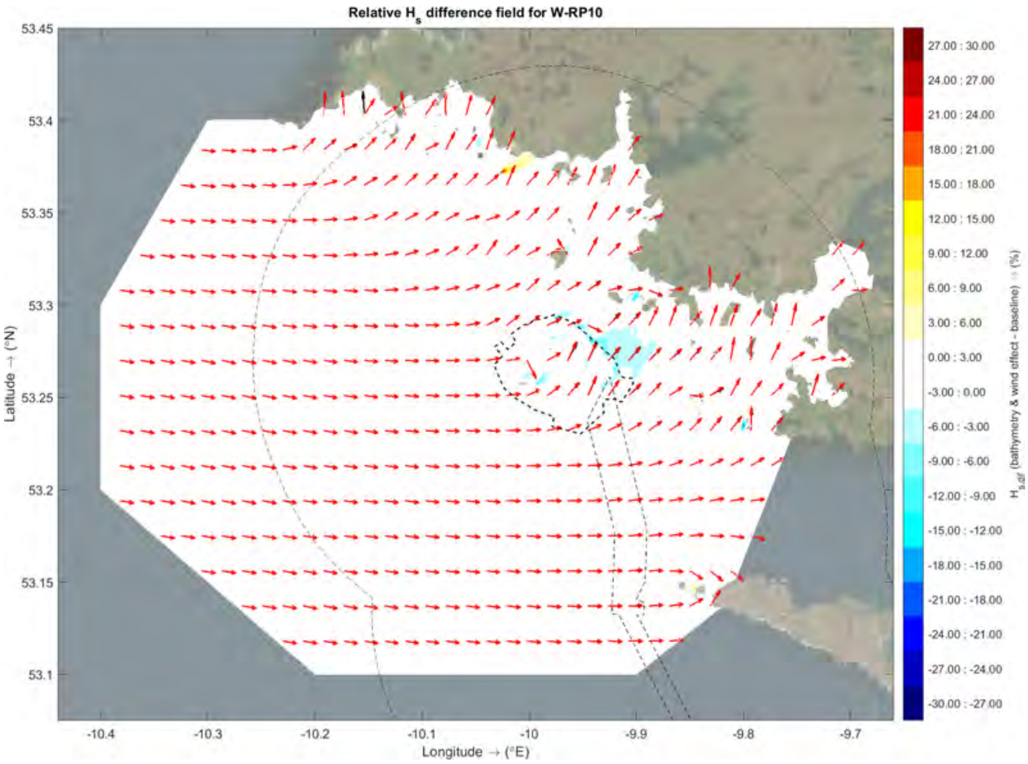

Relative H_s difference field for W-RP10
Latitude → (°N)
Longitude → (°E)
$H_{s,dif}$ (bathymetry & wind effect - baseline) → (%)
27.00 : 30.00
24.00 : 27.00
21.00 : 24.00
18.00 : 21.00
15.00 : 18.00
12.00 : 15.00
9.00 : 12.00
6.00 : 9.00
3.00 : 6.00
0.00 : 3.00
-3.00 : 0.00
-6.00 : -3.00
-9.00 : -6.00
-12.00 : -9.00
-15.00 : -12.00
-18.00 : -15.00
-21.00 : -18.00
-24.00 : -21.00
-27.00 : -24.00
-30.00 : -27.00

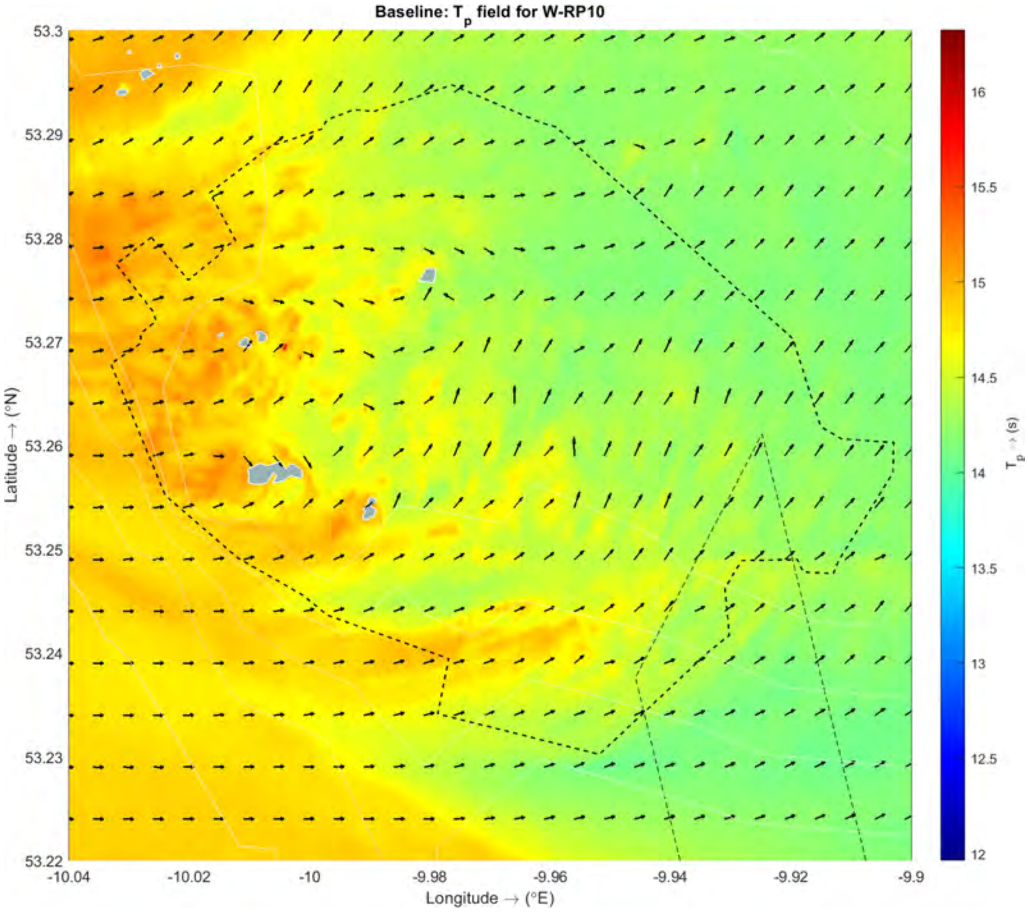
Baseline: T_p field for W-RP10
53.3
53.29
53.28
53.27
53.26
53.25
53.24
53.23
53.22
Latitude → (°N)
-10.04
-10.02
-10
-9.98
-9.96
-9.94
-9.92
-9.9
Longitude → (°E)
16
15.5
15
14.5
14
13.5
13
12.5
12
T_p → (s)

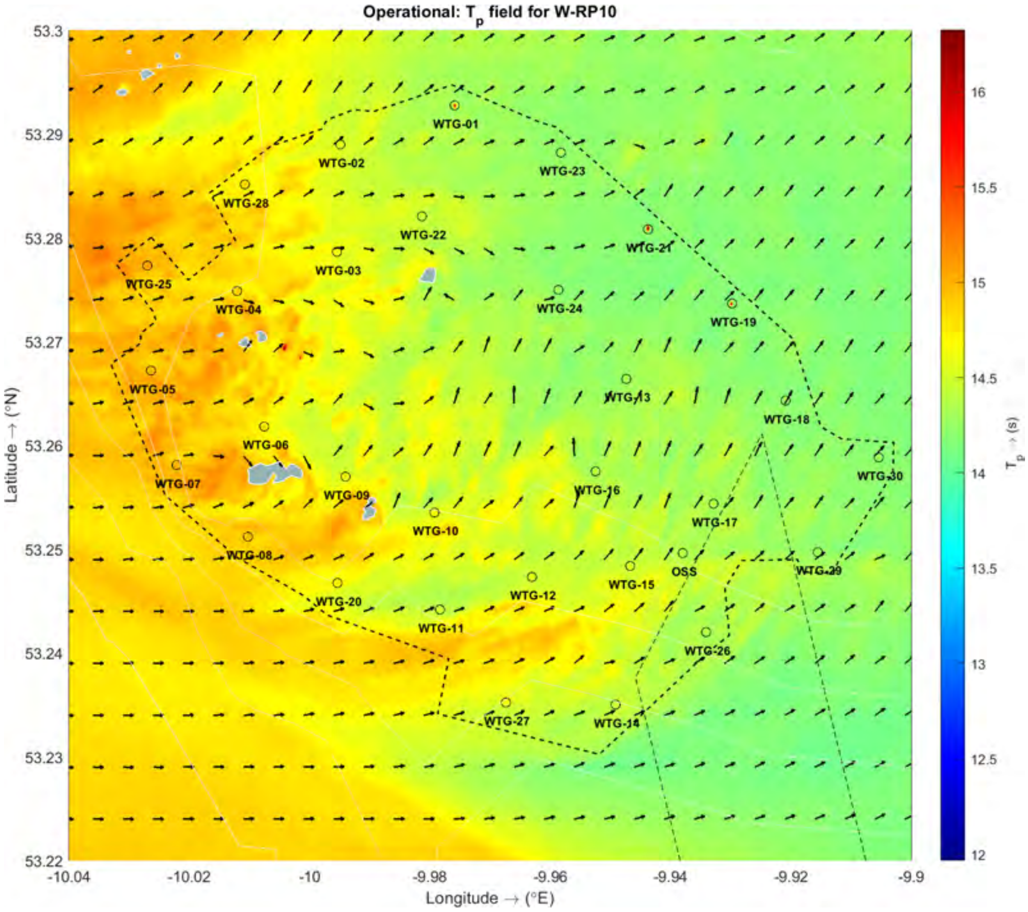

Operational: T_p field for W-RP10
Latitude → (°N)
Longitude → (°E)
T_p → (s)
WTG-01
WTG-02
WTG-03
WTG-04
WTG-05
WTG-06
WTG-07
WTG-08
WTG-09
WTG-10
WTG-11
WTG-12
WTG-13
WTG-14
WTG-15
WTG-16
WTG-17
WTG-18
WTG-19
WTG-20
WTG-21
WTG-22
WTG-23
WTG-24
WTG-25
WTG-26
WTG-27
WTG-28
WTG-29
WTG-30
OSS

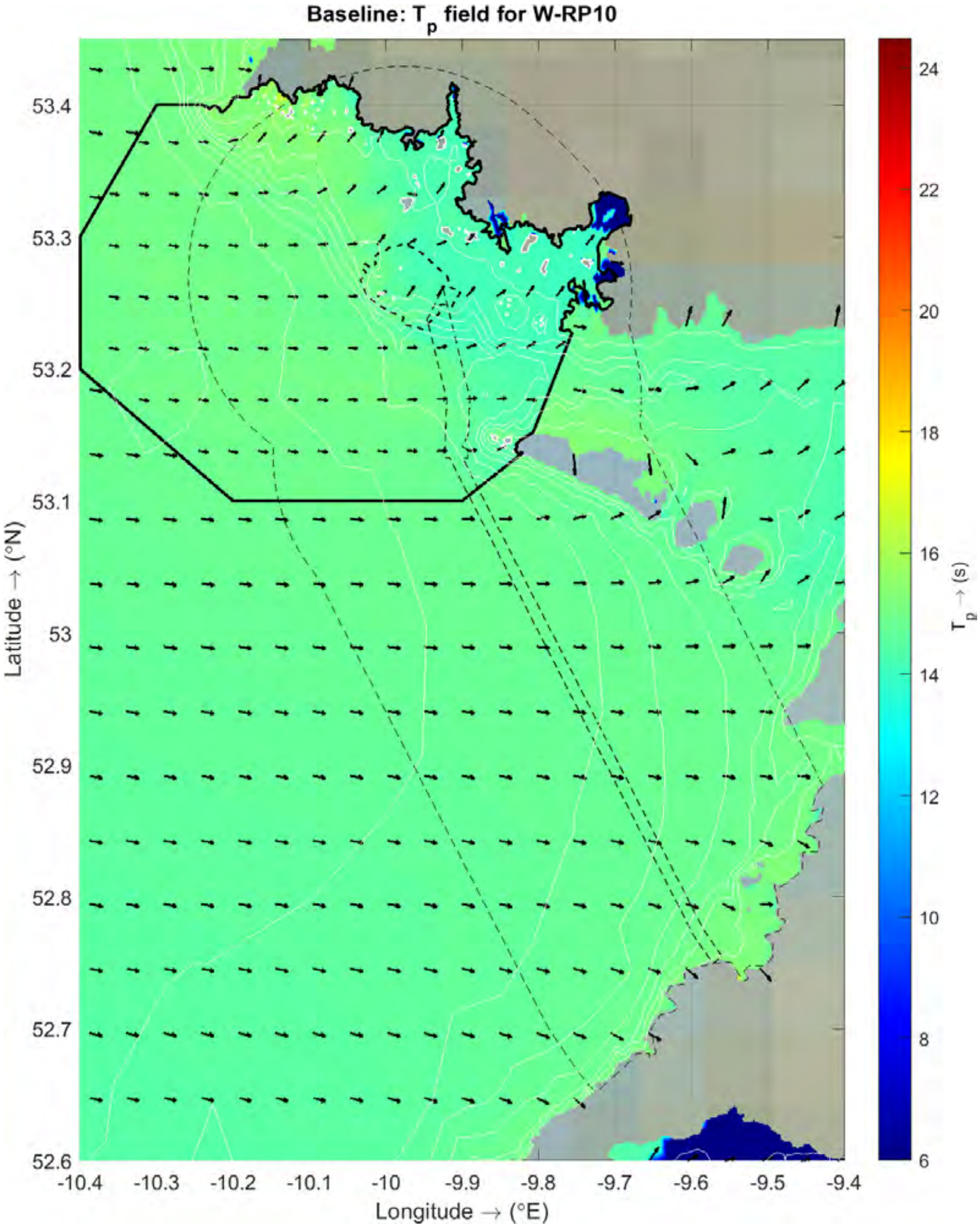
Baseline: T p field for W-RP10
53.4
53.3
53.2
53.1
53
52.9
52.8
52.7
52.6
Latitude → (°N)
-10.4
-10.3
-10.2
-10.1
-10
-9.9
-9.8
-9.7
-9.6
-9.5
-9.4
Longitude → (°E)
24
22
20
18
16
14
12
10
8
6
T p → (s)

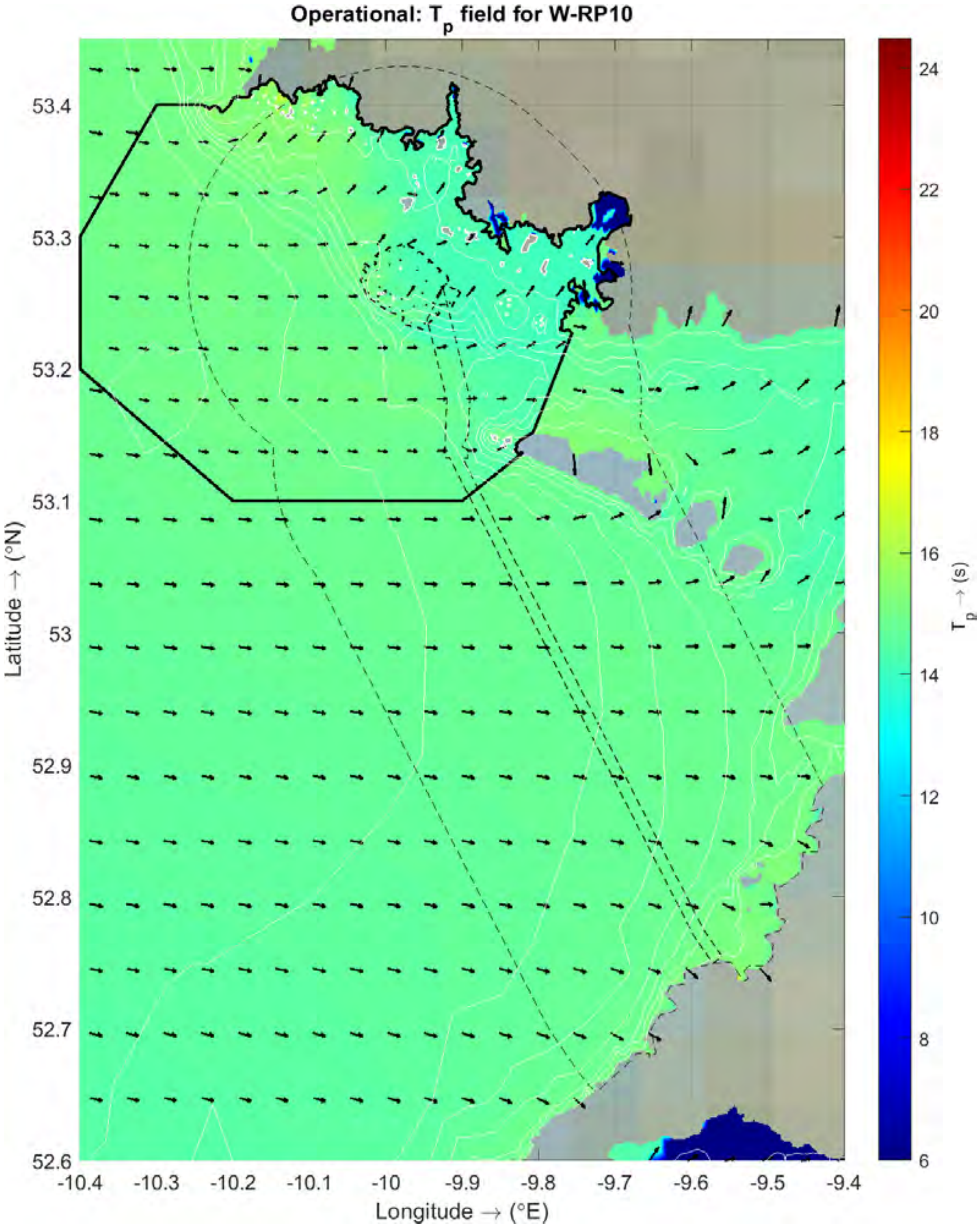
Operational: T_p field for W-RP10
53.4
53.3
53.2
53.1
53
52.9
52.8
52.7
52.6
Latitude → (°N)
-10.4
-10.3
-10.2
-10.1
-10
-9.9
-9.8
-9.7
-9.6
-9.5
-9.4
Longitude → (°E)
24
22
20
18
16
14
12
10
8
6
T_p → (s)

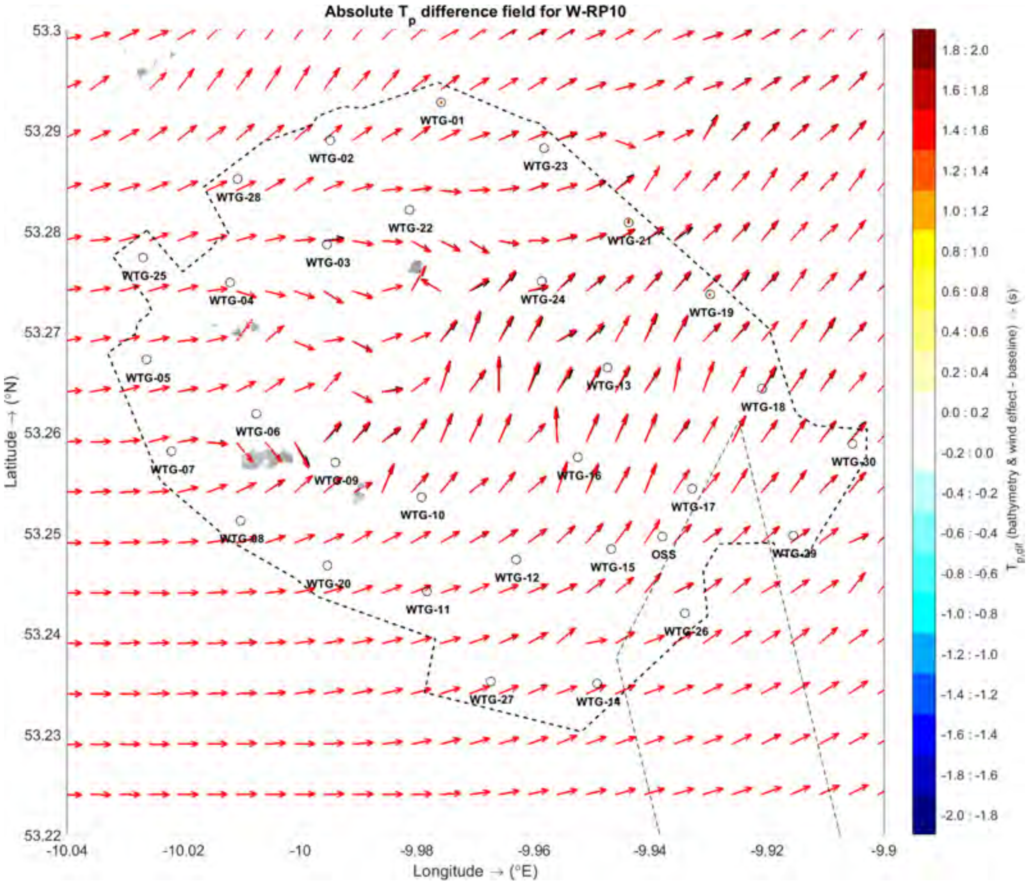
Absolute T_p difference field for W-RP10
Latitude → (°N)
Longitude → (°E)
$T_{p,dif}$ (bathymetry & wind effect - baseline) → (s)
1.8 : 2.0
1.6 : 1.8
1.4 : 1.6
1.2 : 1.4
1.0 : 1.2
0.8 : 1.0
0.6 : 0.8
0.4 : 0.6
0.2 : 0.4
0.0 : 0.2
-0.2 : 0.0
-0.4 : -0.2
-0.6 : -0.4
-0.8 : -0.6
-1.0 : -0.8
-1.2 : -1.0
-1.4 : -1.2
-1.6 : -1.4
-1.8 : -1.6
-2.0 : -1.8
OSS

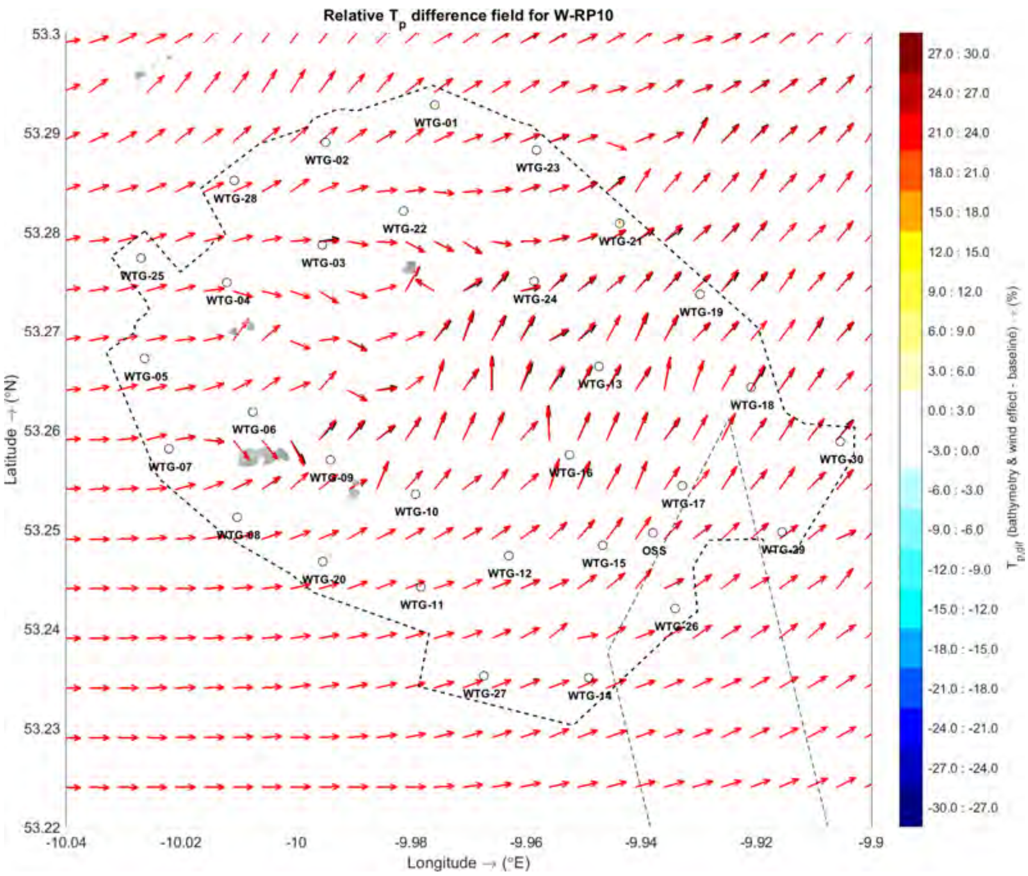
Relative T_p difference field for W-RP10
Latitude → (°N)
Longitude → (°E)
$T_{p,dif}$ (bathymetry & wind effect - baseline) → (%)
27.0 : 30.0
24.0 : 27.0
21.0 : 24.0
18.0 : 21.0
15.0 : 18.0
12.0 : 15.0
9.0 : 12.0
6.0 : 9.0
3.0 : 6.0
0.0 : 3.0
-3.0 : 0.0
-6.0 : -3.0
-9.0 : -6.0
-12.0 : -9.0
-15.0 : -12.0
-18.0 : -15.0
-21.0 : -18.0
-24.0 : -21.0
-27.0 : -24.0
-30.0 : -27.0
OSS

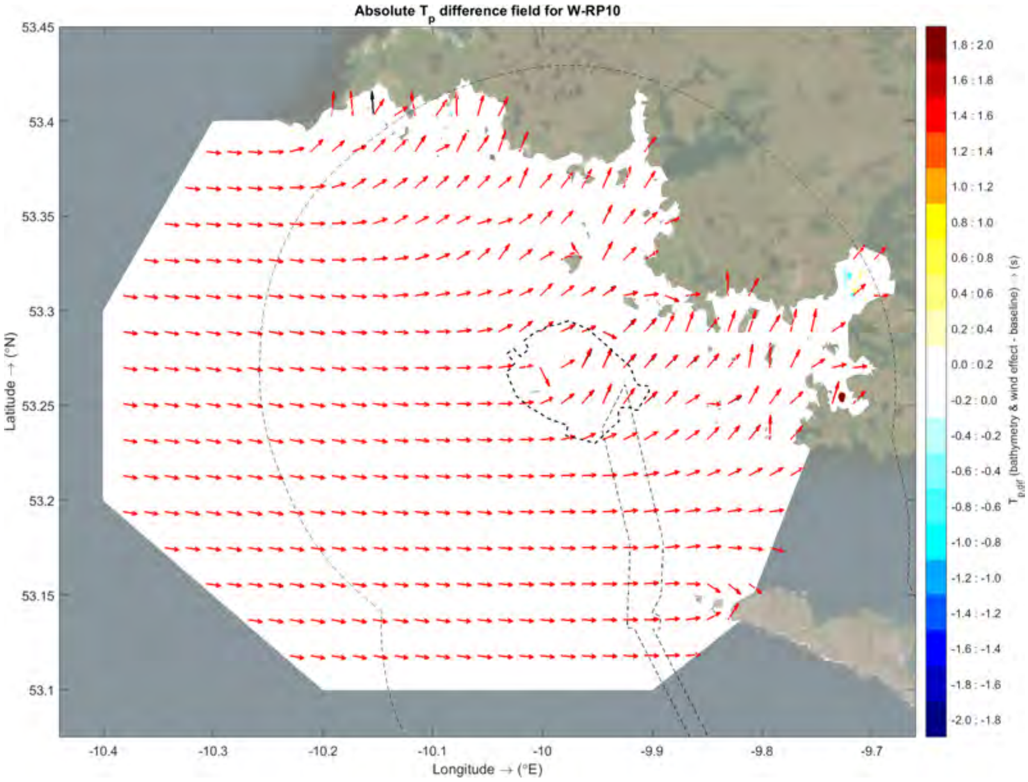
Absolute T_p difference field for W-RP10
Latitude → (°N)
Longitude → (°E)
$T_{p,diff}$ (bathymetry & wind effect - baseline) → (s)
1.8 : 2.0
1.6 : 1.8
1.4 : 1.6
1.2 : 1.4
1.0 : 1.2
0.8 : 1.0
0.6 : 0.8
0.4 : 0.6
0.2 : 0.4
0.0 : 0.2
-0.2 : 0.0
-0.4 : -0.2
-0.6 : -0.4
-0.8 : -0.6
-1.0 : -0.8
-1.2 : -1.0
-1.4 : -1.2
-1.6 : -1.4
-1.8 : -1.6
-2.0 : -1.8

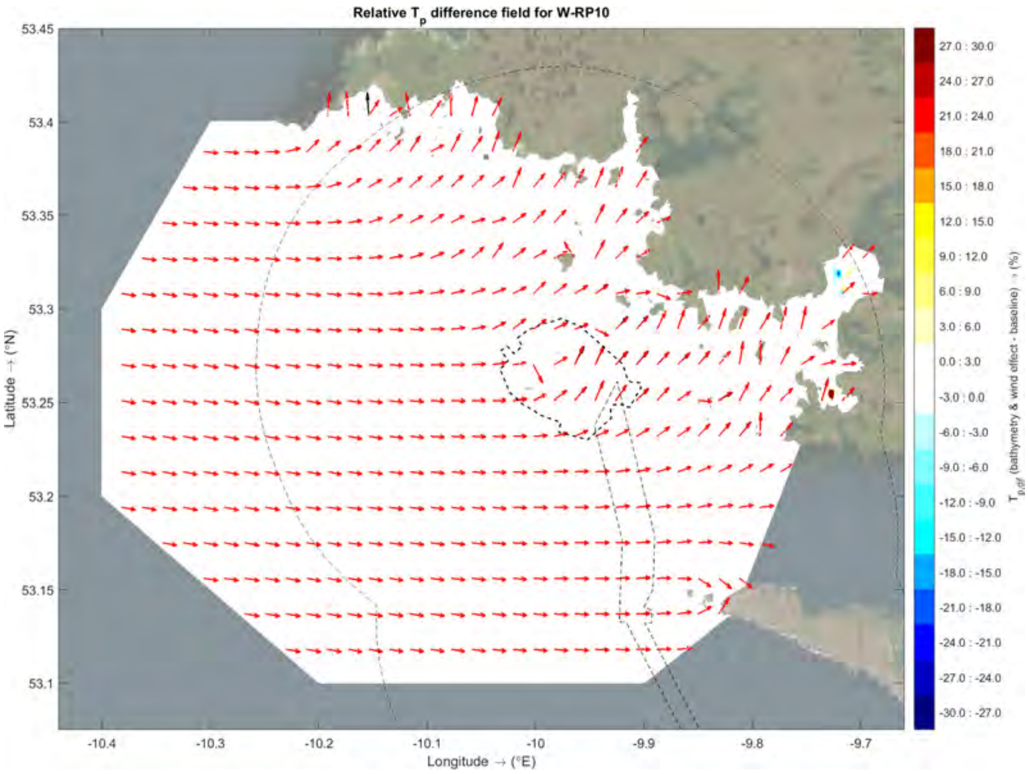
Relative T_p difference field for W-RP10
Latitude → (°N)
Longitude → (°E)
$T_{p,diff}$ (bathymetry & wind effect - baseline) → (%)
27.0 : 30.0
24.0 : 27.0
21.0 : 24.0
18.0 : 21.0
15.0 : 18.0
12.0 : 15.0
9.0 : 12.0
6.0 : 9.0
3.0 : 6.0
0.0 : 3.0
-3.0 : 0.0
-6.0 : -3.0
-9.0 : -6.0
-12.0 : -9.0
-15.0 : -12.0
-18.0 : -15.0
-21.0 : -18.0
-24.0 : -21.0
-27.0 : -24.0
-30.0 : -27.0

E.6 50-yr RP

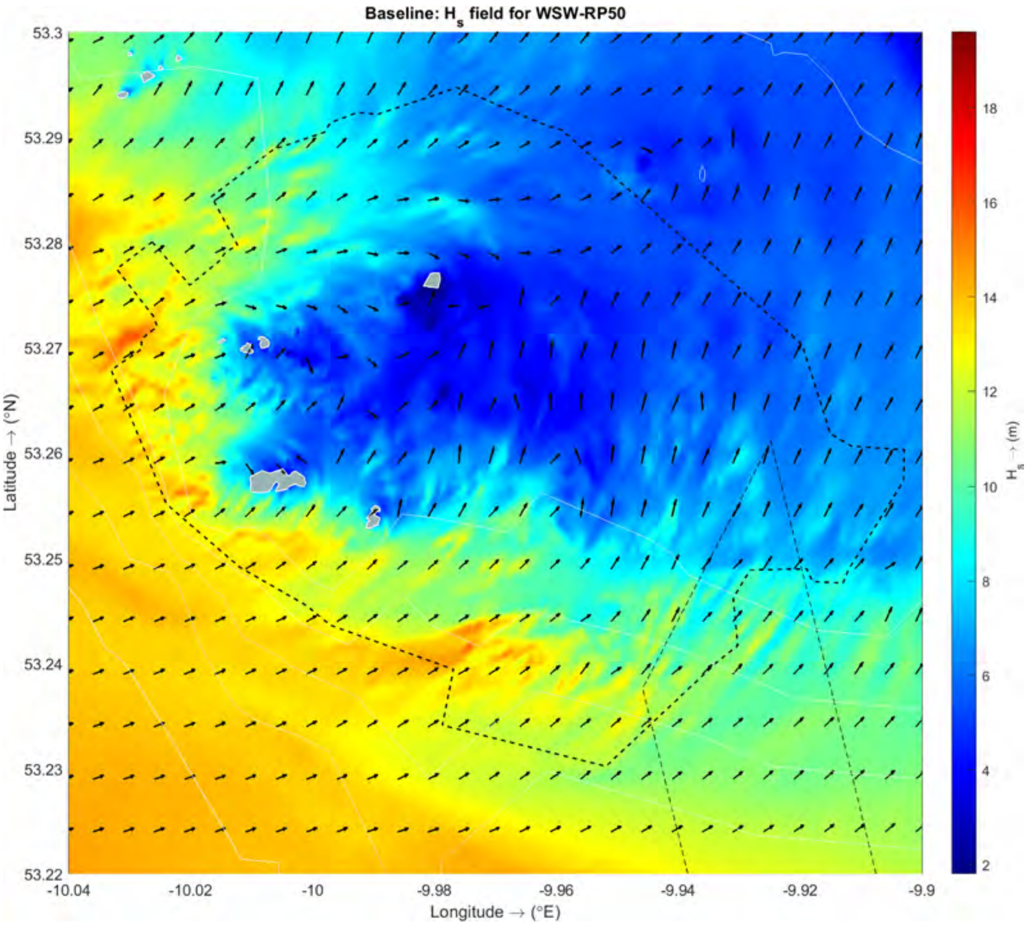

Baseline: H_s field for WSW-RP50
Latitude → (°N)
Longitude → (°E)
H_s → (m)
53.3
53.29
53.28
53.27
53.26
53.25
53.24
53.23
53.22
-10.04
-10.02
-10
-9.98
-9.96
-9.94
-9.92
-9.9
18
16
14
12
10
8
6
4
2

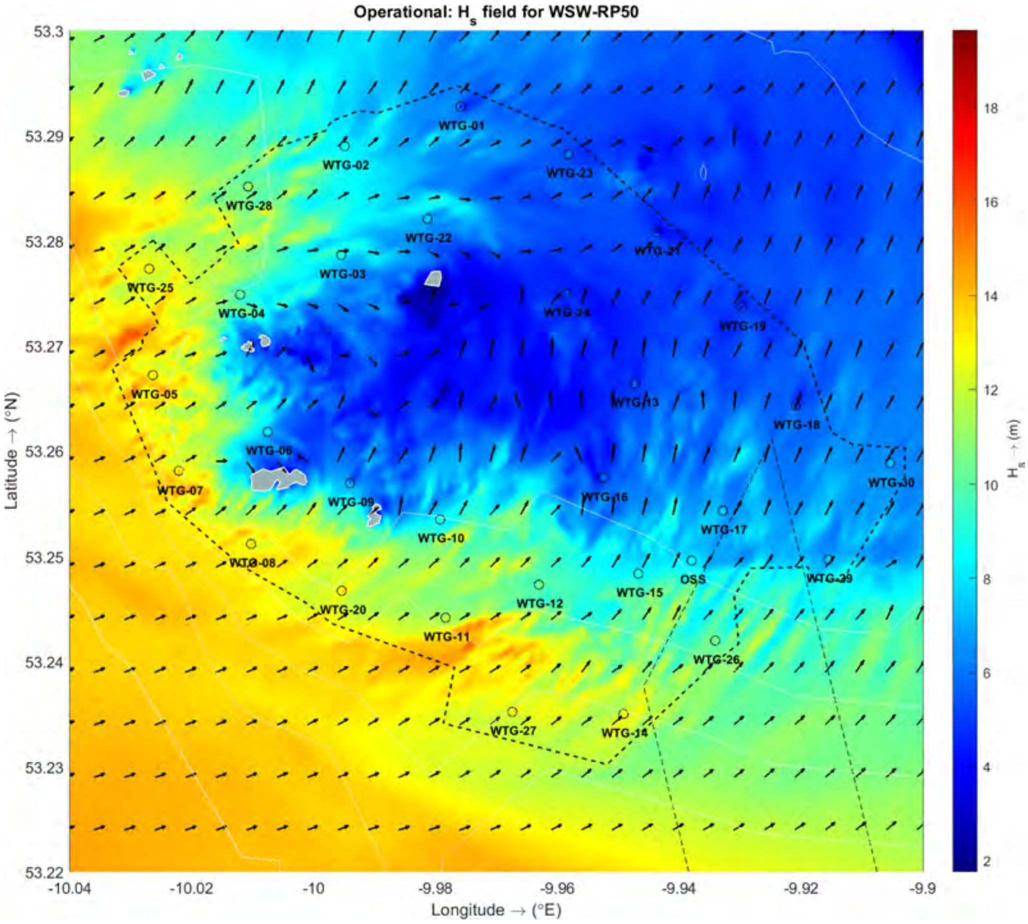
Operational: H_s field for WSW-RP50
WTG-01
WTG-02
WTG-23
WTG-28
WTG-22
WTG-21
WTG-25
WTG-03
WTG-04
WTG-24
WTG-19
WTG-05
WTG-13
WTG-18
WTG-06
WTG-07
WTG-16
WTG-30
WTG-09
WTG-17
WTG-10
WTG-08
OSS
WTG-29
WTG-15
WTG-12
WTG-20
WTG-11
WTG-26
WTG-27
WTG-14
Latitude → (°N)
Longitude → (°E)
H_s → (m)

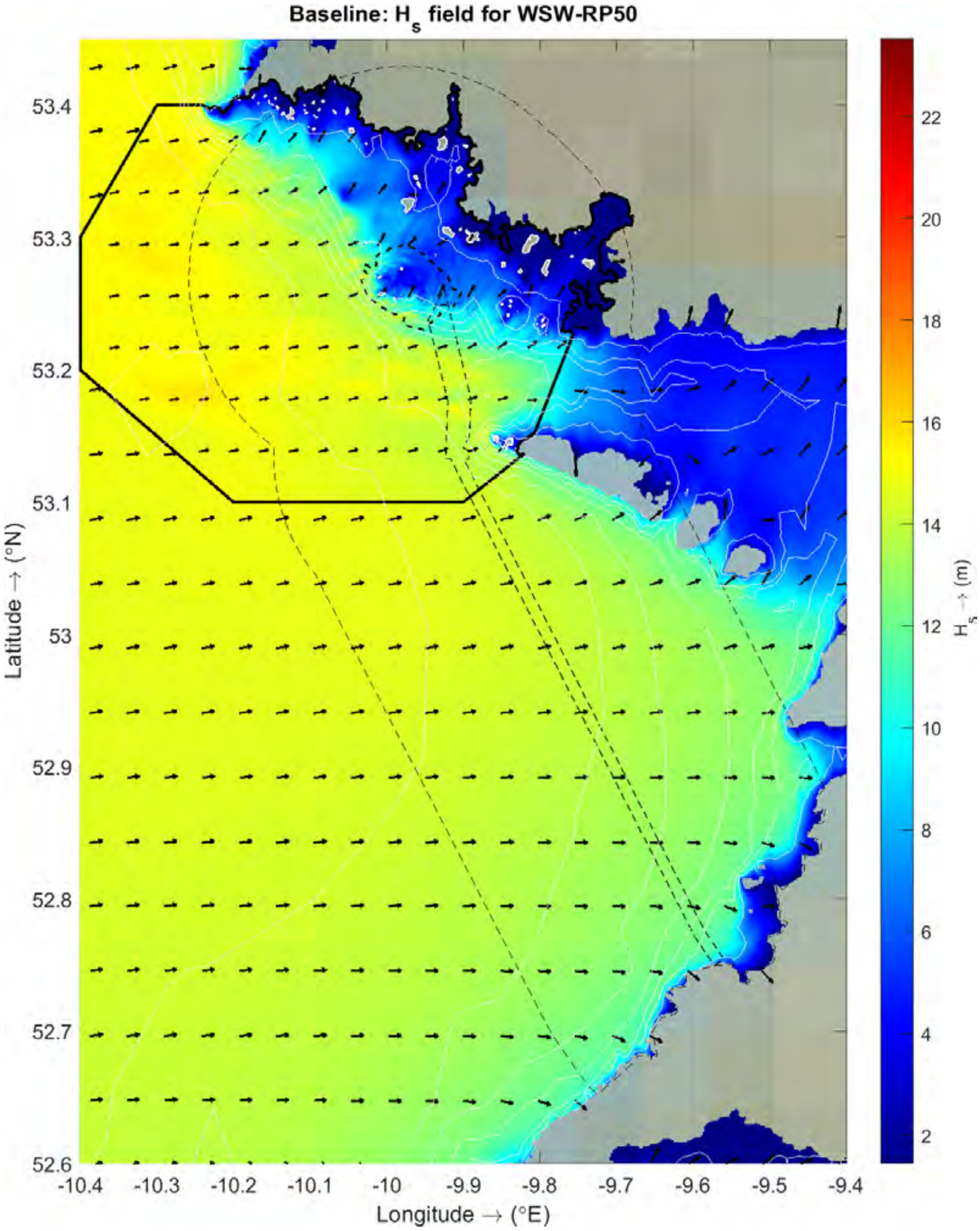
Baseline: H_s field for WSW-RP50
Latitude → (°N)
Longitude → (°E)
H_s → (m)
53.4
53.3
53.2
53.1
53
52.9
52.8
52.7
52.6
-10.4
-10.3
-10.2
-10.1
-10
-9.9
-9.8
-9.7
-9.6
-9.5
-9.4
22
20
18
16
14
12
10
8
6
4
2

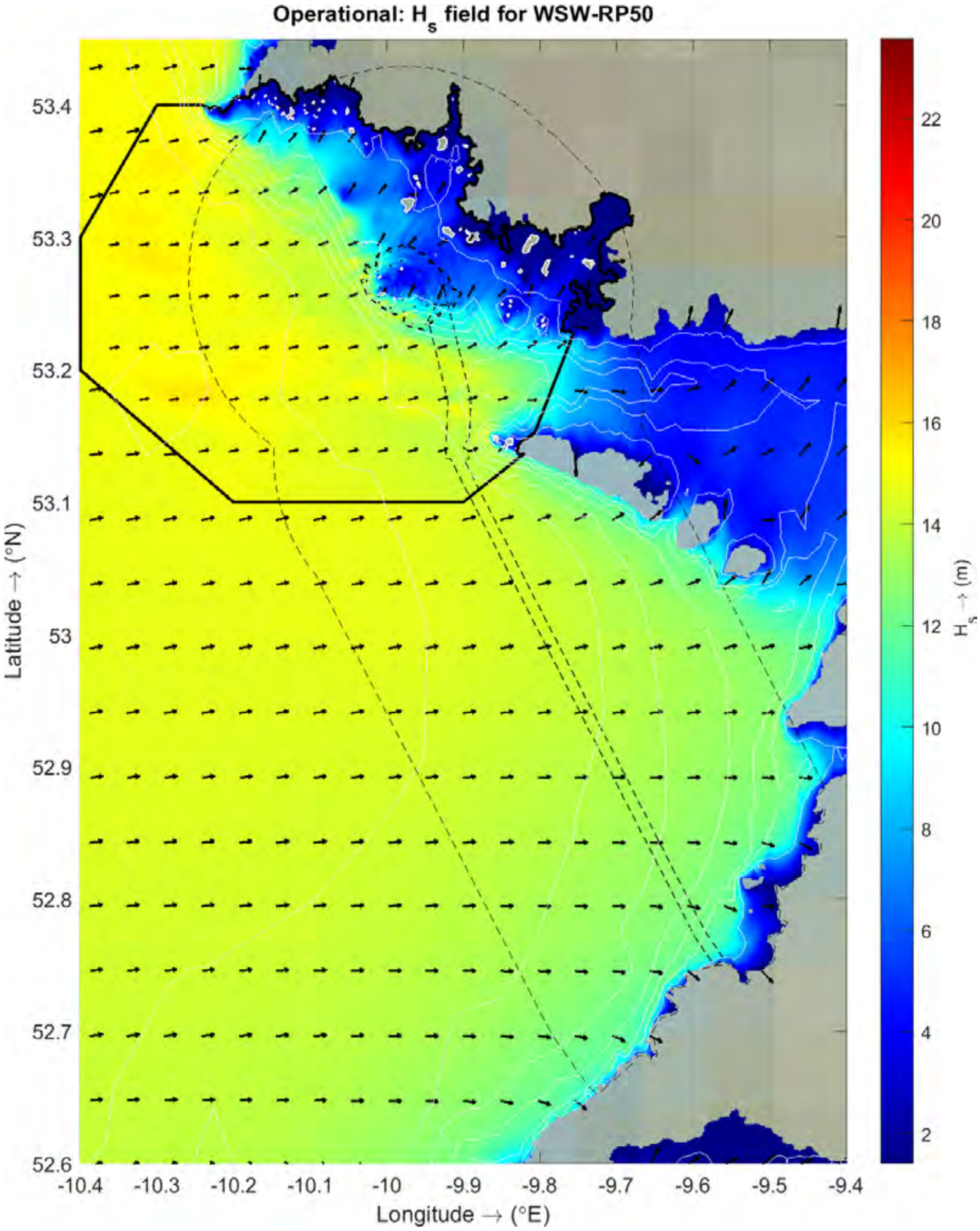
Operational: H_s field for WSW-RP50
53.4
53.3
53.2
53.1
53
52.9
52.8
52.7
52.6
Latitude → (°N)
-10.4
-10.3
-10.2
-10.1
-10
-9.9
-9.8
-9.7
-9.6
-9.5
-9.4
Longitude → (°E)
22
20
18
16
14
12
10
8
6
4
2
H_s → (m)

Deltares

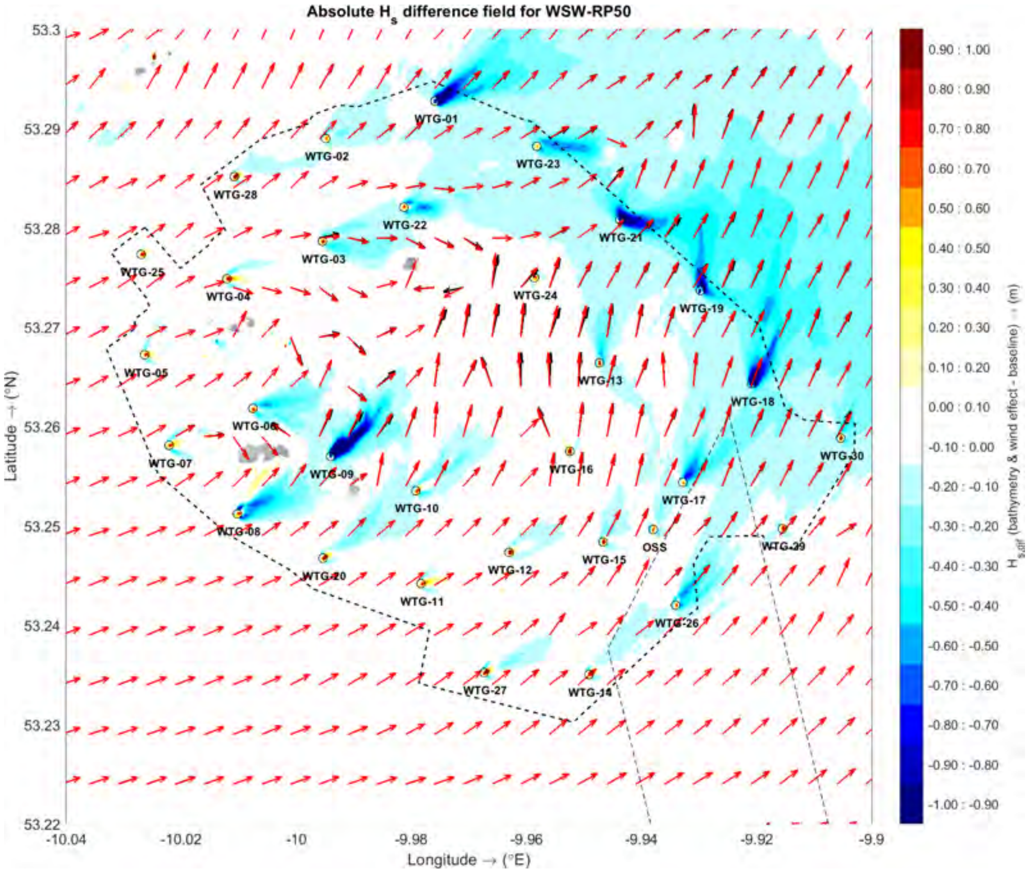
Absolute H$_s$ difference field for WSW-RP50
Latitude → (°N)
Longitude → (°E)
H$_{s,dif}$ (bathymetry & wind effect - baseline) → (m)
0.90 : 1.00
0.80 : 0.90
0.70 : 0.80
0.60 : 0.70
0.50 : 0.60
0.40 : 0.50
0.30 : 0.40
0.20 : 0.30
0.10 : 0.20
0.00 : 0.10
-0.10 : 0.00
-0.20 : -0.10
-0.30 : -0.20
-0.40 : -0.30
-0.50 : -0.40
-0.60 : -0.50
-0.70 : -0.60
-0.80 : -0.70
-0.90 : -0.80
-1.00 : -0.90
WTG-01
WTG-02
WTG-03
WTG-04
WTG-05
WTG-06
WTG-07
WTG-08
WTG-09
WTG-10
WTG-11
WTG-12
WTG-13
WTG-14
WTG-15
WTG-16
WTG-17
WTG-18
WTG-19
WTG-20
WTG-21
WTG-22
WTG-23
WTG-24
WTG-25
WTG-26
WTG-27
WTG-28
WTG-29
WTG-30
OSS
53.3
53.29
53.28
53.27
53.26
53.25
53.24
53.23
53.22
-10.04
-10.02
-10
-9.98
-9.96
-9.94
-9.92
-9.9

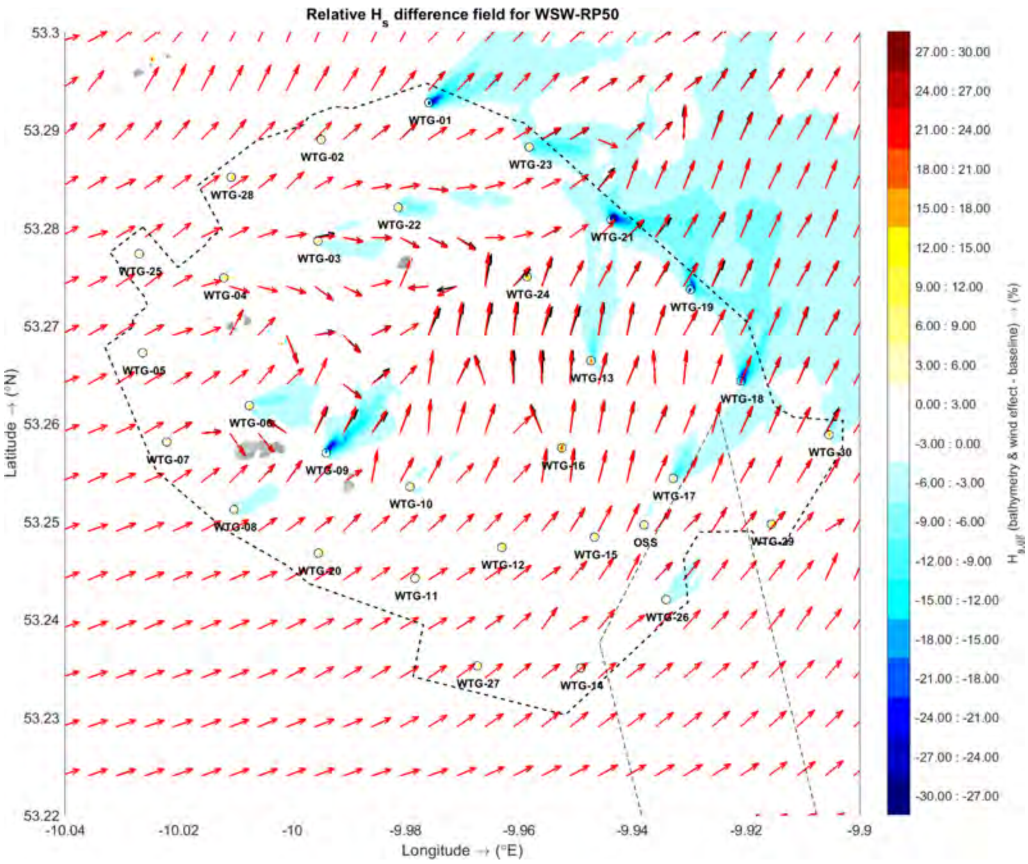
Relative H$_s$ difference field for WSW-RP50
Latitude → (°N)
Longitude → (°E)
H$_{s,dif}$ (bathymetry & wind effect - baseline) → (%)
27.00 : 30.00
24.00 : 27.00
21.00 : 24.00
18.00 : 21.00
15.00 : 18.00
12.00 : 15.00
9.00 : 12.00
6.00 : 9.00
3.00 : 6.00
0.00 : 3.00
-3.00 : 0.00
-6.00 : -3.00
-9.00 : -6.00
-12.00 : -9.00
-15.00 : -12.00
-18.00 : -15.00
-21.00 : -18.00
-24.00 : -21.00
-27.00 : -24.00
-30.00 : -27.00
WTG-01
WTG-02
WTG-03
WTG-04
WTG-05
WTG-06
WTG-07
WTG-08
WTG-09
WTG-10
WTG-11
WTG-12
WTG-13
WTG-14
WTG-15
WTG-16
WTG-17
WTG-18
WTG-19
WTG-20
WTG-21
WTG-22
WTG-23
WTG-24
WTG-25
WTG-26
WTG-27
WTG-28
WTG-29
WTG-30
OSS
53.3
53.29
53.28
53.27
53.26
53.25
53.24
53.23
53.22
-10.04
-10.02
-10
-9.98
-9.96
-9.94
-9.92
-9.9

Deltares

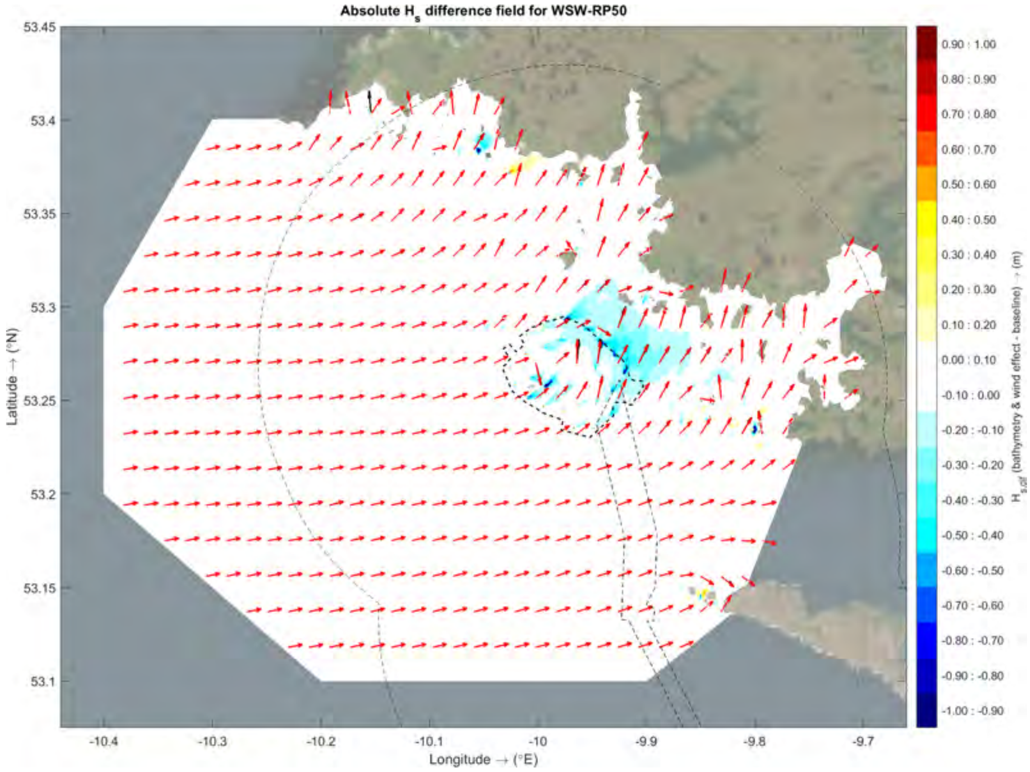
Absolute H$_s$ difference field for WSW-RP50
Latitude → (°N)
Longitude → (°E)
H$_{s,dif}$ (bathymetry & wind effect - baseline) → (m)

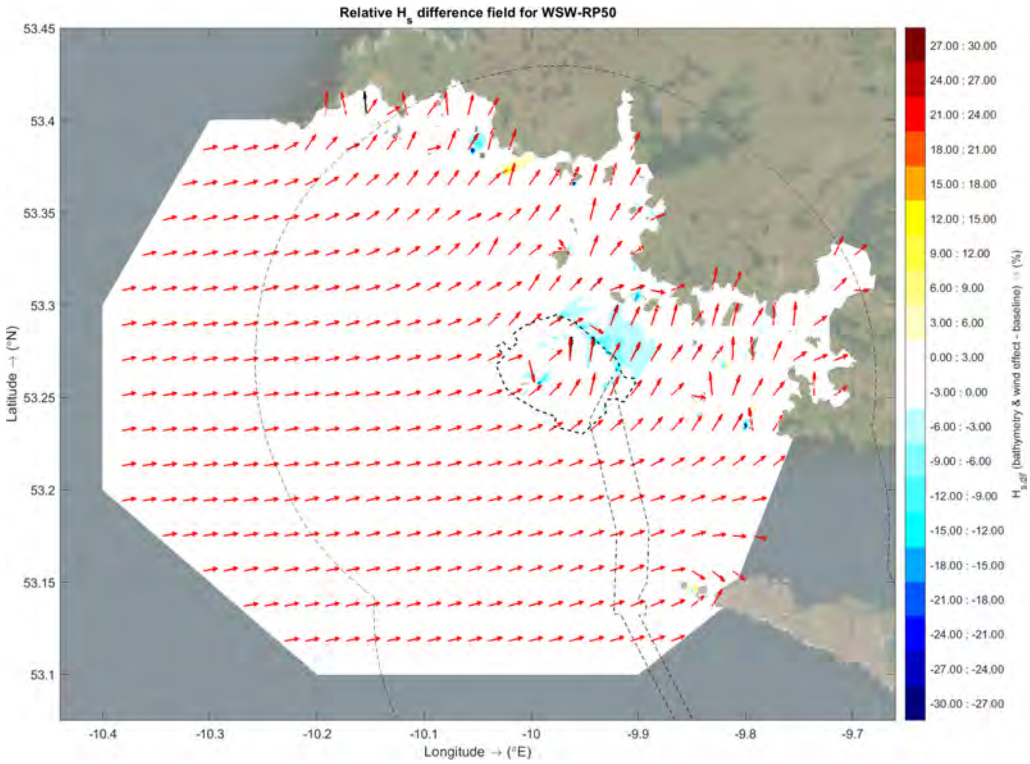
Relative H$_s$ difference field for WSW-RP50
Latitude → (°N)
Longitude → (°E)
H$_{s,dif}$ (bathymetry & wind effect - baseline) → (%)

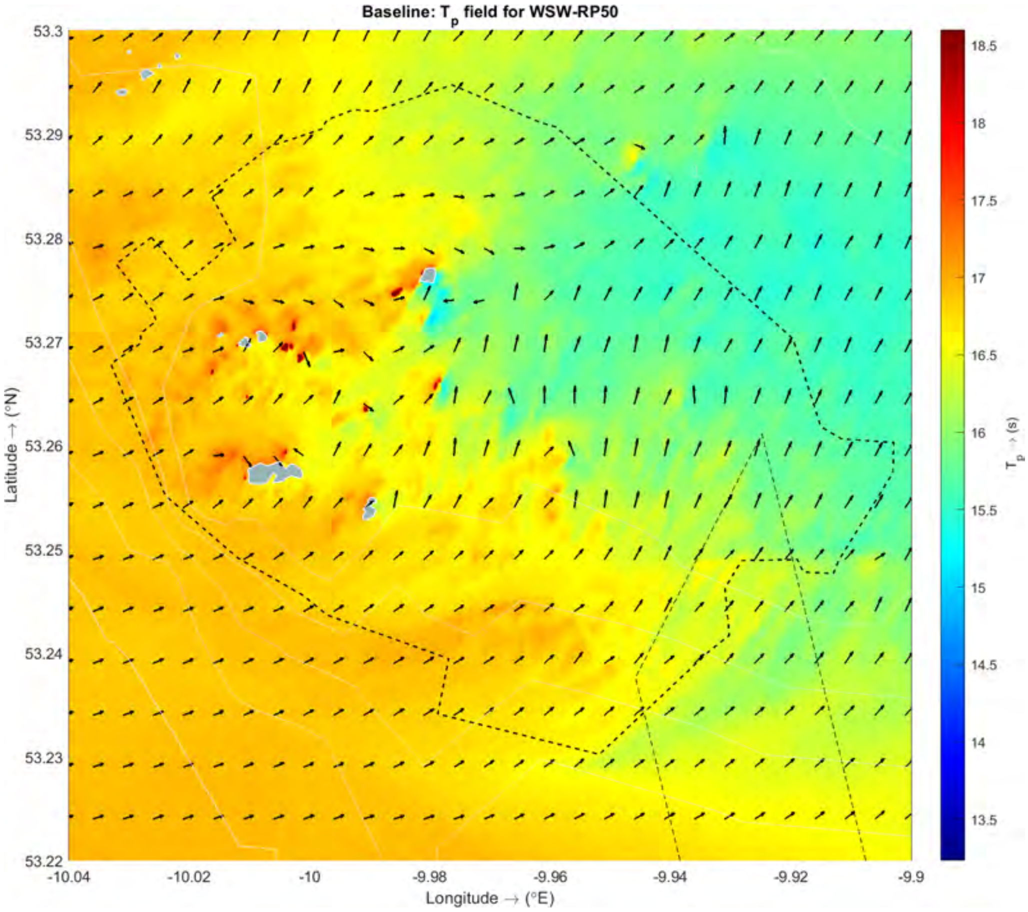
Baseline: T_p field for WSW-RP50
Latitude → (°N)
Longitude → (°E)
T_p → (s)
53.3
53.29
53.28
53.27
53.26
53.25
53.24
53.23
53.22
-10.04
-10.02
-10
-9.98
-9.96
-9.94
-9.92
-9.9
18.5
18
17.5
17
16.5
16
15.5
15
14.5
14
13.5

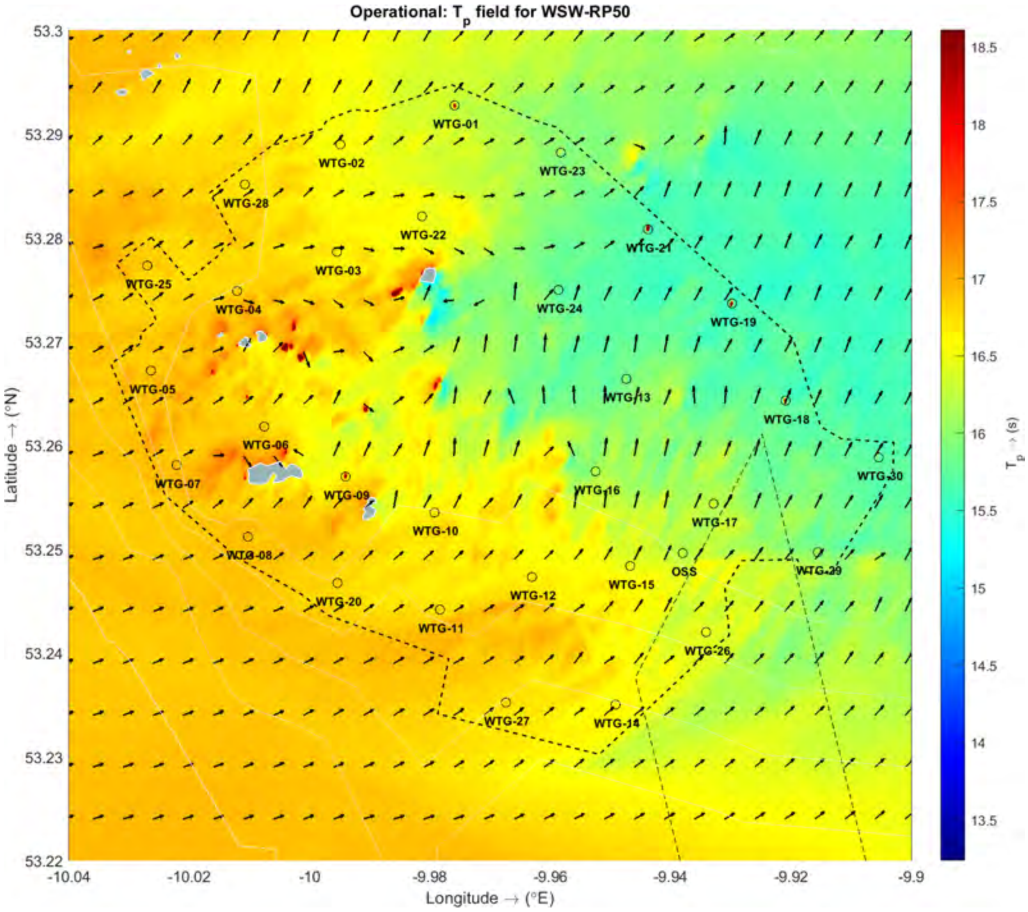
Operational: T_p field for WSW-RP50
Latitude → (°N)
Longitude → (°E)
T_p → (s)
WTG-01
WTG-02
WTG-03
WTG-04
WTG-05
WTG-06
WTG-07
WTG-08
WTG-09
WTG-10
WTG-11
WTG-12
WTG-13
WTG-14
WTG-15
WTG-16
WTG-17
WTG-18
WTG-19
WTG-20
WTG-21
WTG-22
WTG-23
WTG-24
WTG-25
WTG-26
WTG-27
WTG-28
WTG-29
WTG-30
OSS

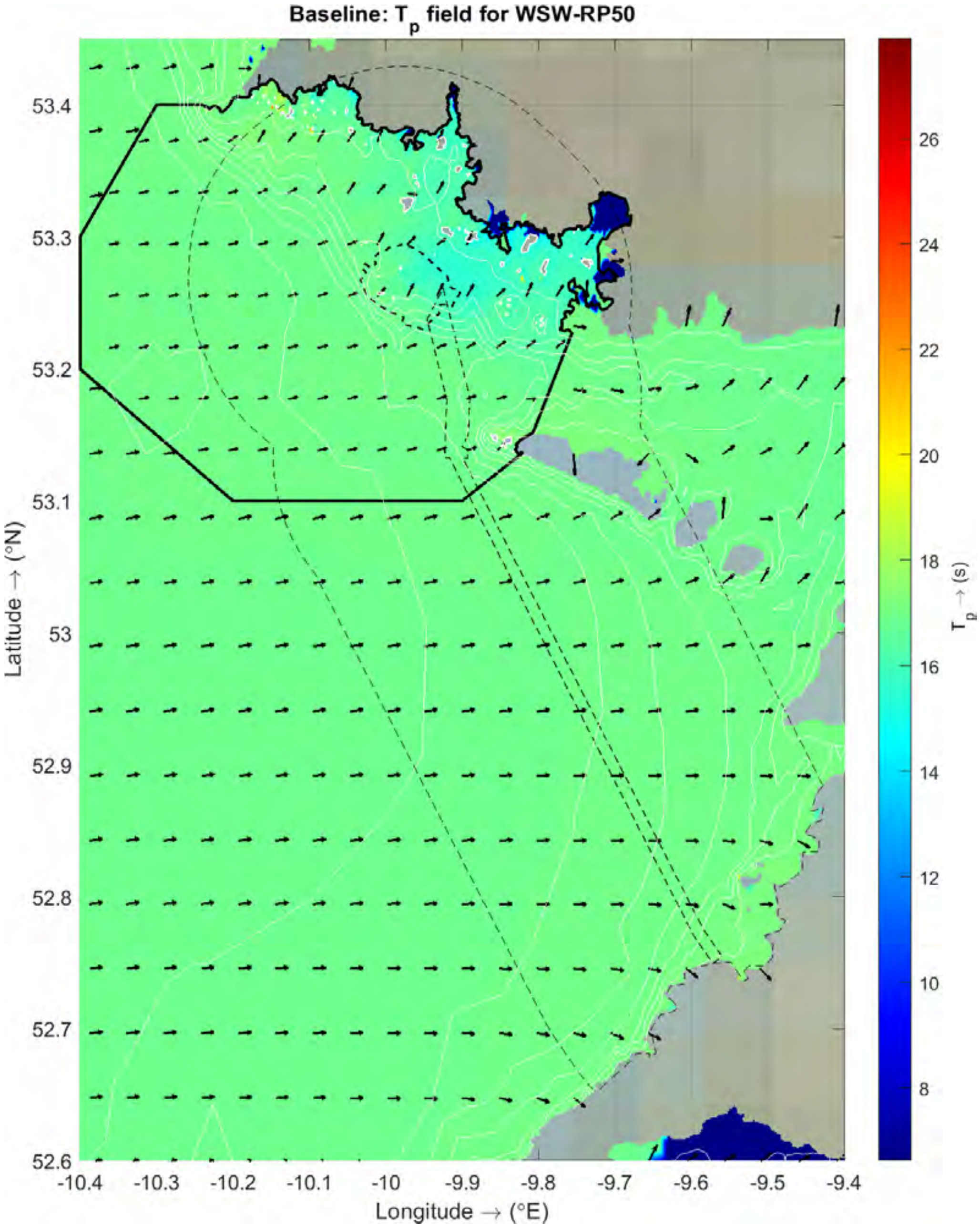
Baseline: T p field for WSW-RP50
53.4
53.3
53.2
53.1
53
52.9
52.8
52.7
52.6
Latitude → (°N)
-10.4
-10.3
-10.2
-10.1
-10
-9.9
-9.8
-9.7
-9.6
-9.5
-9.4
Longitude → (°E)
26
24
22
20
18
16
14
12
10
8
T p → (s)

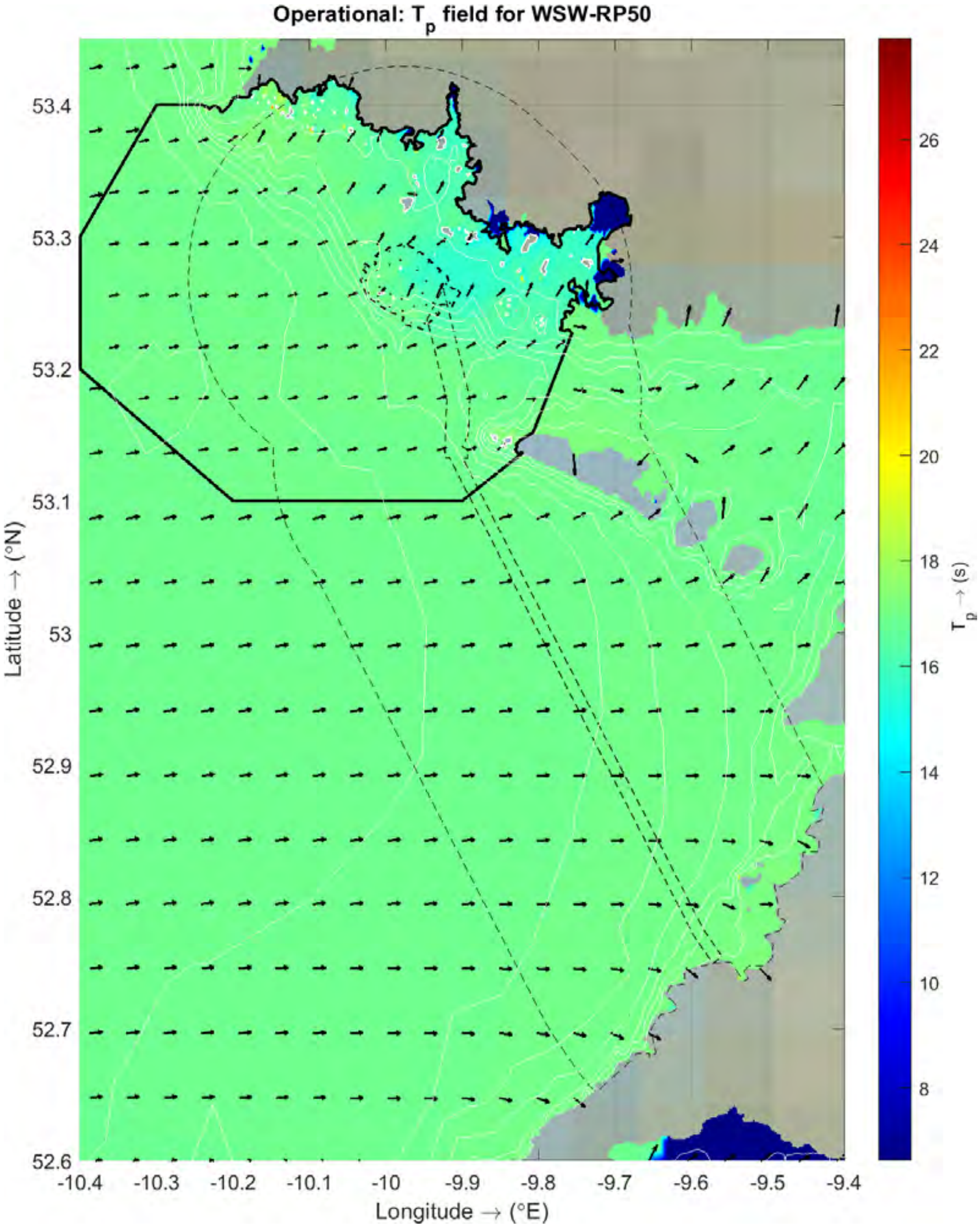

Operational: T_p field for WSW-RP50
53.4
53.3
53.2
53.1
53
52.9
52.8
52.7
52.6
Latitude → (°N)
-10.4
-10.3
-10.2
-10.1
-10
-9.9
-9.8
-9.7
-9.6
-9.5
-9.4
Longitude → (°E)
26
24
22
20
18
16
14
12
10
8
T_p → (s)

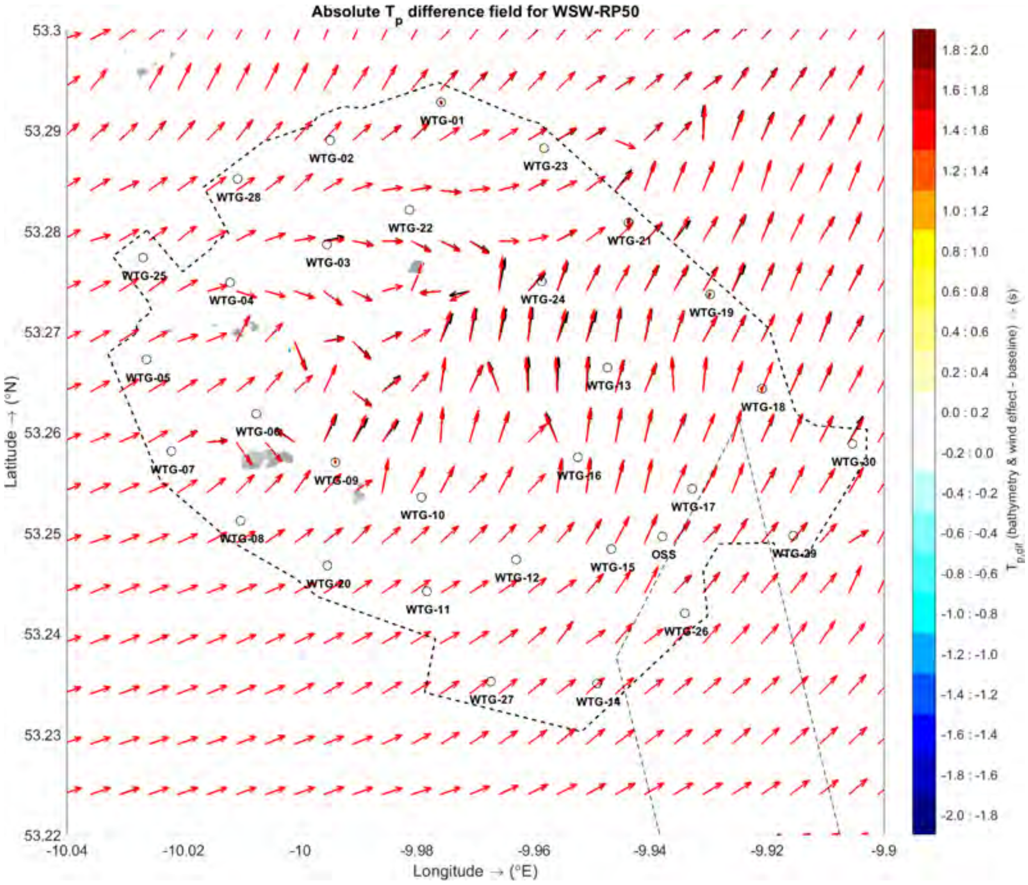
Absolute T_p difference field for WSW-RP50
Latitude → (°N)
Longitude → (°E)
$T_{p,dif}$ (bathymetry & wind effect - baseline) → (s)
1.8 : 2.0
1.6 : 1.8
1.4 : 1.6
1.2 : 1.4
1.0 : 1.2
0.8 : 1.0
0.6 : 0.8
0.4 : 0.6
0.2 : 0.4
0.0 : 0.2
-0.2 : 0.0
-0.4 : -0.2
-0.6 : -0.4
-0.8 : -0.6
-1.0 : -0.8
-1.2 : -1.0
-1.4 : -1.2
-1.6 : -1.4
-1.8 : -1.6
-2.0 : -1.8

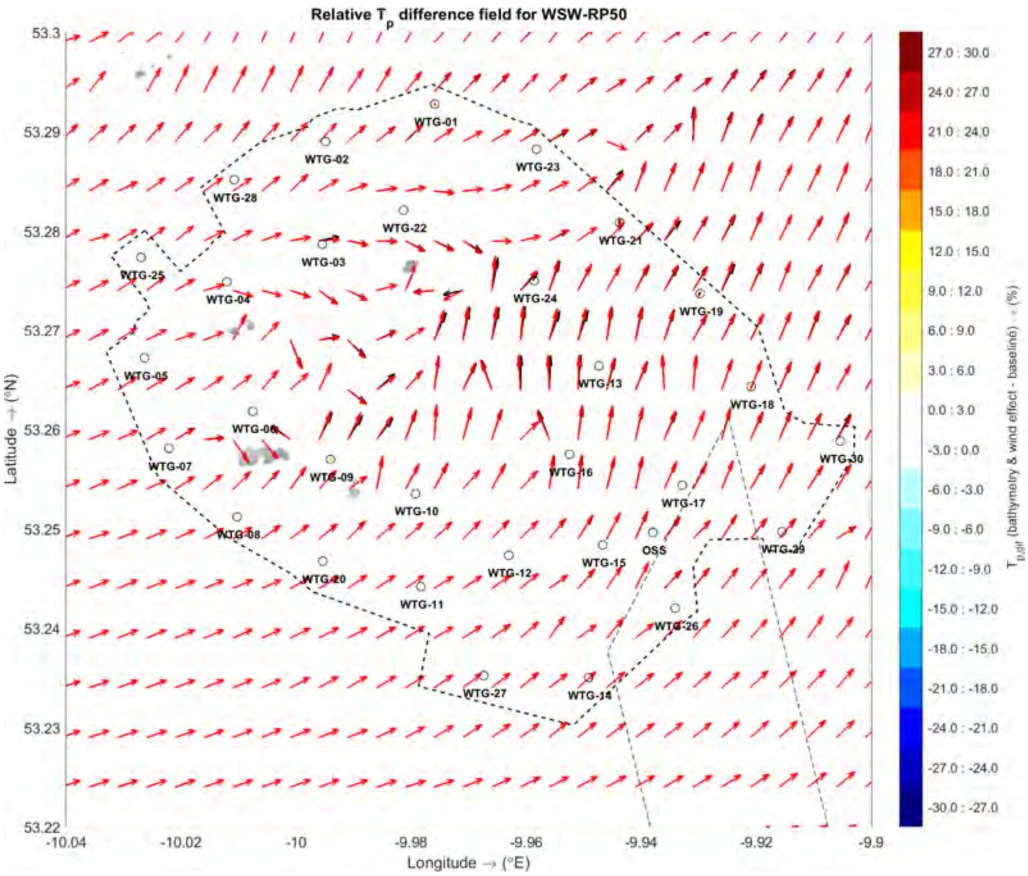
Relative T_p difference field for WSW-RP50
Latitude → (°N)
Longitude → (°E)
$T_{p,dif}$ (bathymetry & wind effect - baseline) → (%)
27.0 : 30.0
24.0 : 27.0
21.0 : 24.0
18.0 : 21.0
15.0 : 18.0
12.0 : 15.0
9.0 : 12.0
6.0 : 9.0
3.0 : 6.0
0.0 : 3.0
-3.0 : 0.0
-6.0 : -3.0
-9.0 : -6.0
-12.0 : -9.0
-15.0 : -12.0
-18.0 : -15.0
-21.0 : -18.0
-24.0 : -21.0
-27.0 : -24.0
-30.0 : -27.0

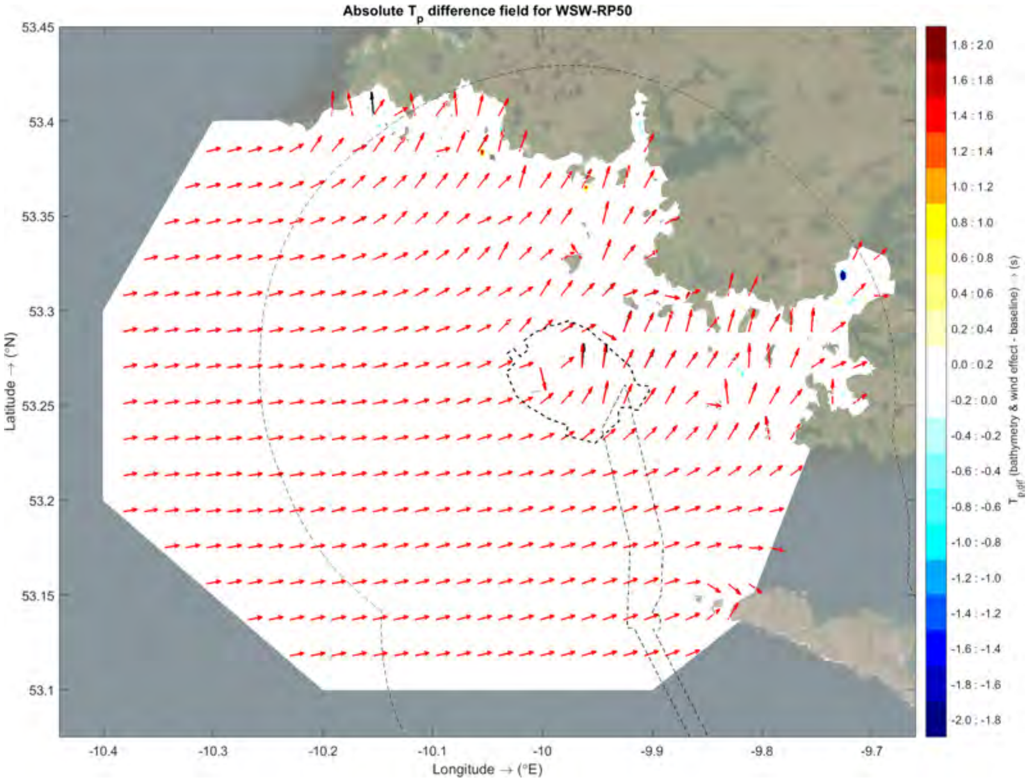
Absolute T_p difference field for WSW-RP50
Latitude → (°N)
Longitude → (°E)
$T_{p,diff}$ (bathymetry & wind effect - baseline) → (s)
1.8 : 2.0
1.6 : 1.8
1.4 : 1.6
1.2 : 1.4
1.0 : 1.2
0.8 : 1.0
0.6 : 0.8
0.4 : 0.6
0.2 : 0.4
0.0 : 0.2
-0.2 : 0.0
-0.4 : -0.2
-0.6 : -0.4
-0.8 : -0.6
-1.0 : -0.8
-1.2 : -1.0
-1.4 : -1.2
-1.6 : -1.4
-1.8 : -1.6
-2.0 : -1.8

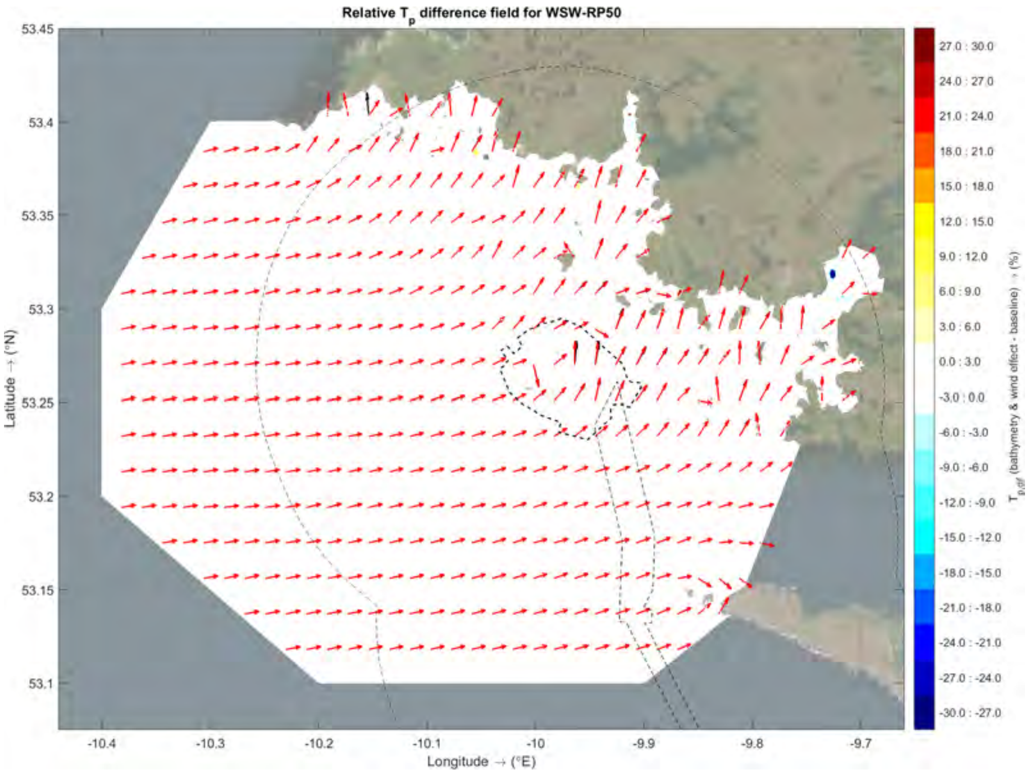
Relative T_p difference field for WSW-RP50
Latitude → (°N)
Longitude → (°E)
$T_{p,diff}$ (bathymetry & wind effect - baseline) → (%)
27.0 : 30.0
24.0 : 27.0
21.0 : 24.0
18.0 : 21.0
15.0 : 18.0
12.0 : 15.0
9.0 : 12.0
6.0 : 9.0
3.0 : 6.0
0.0 : 3.0
-3.0 : 0.0
-6.0 : -3.0
-9.0 : -6.0
-12.0 : -9.0
-15.0 : -12.0
-18.0 : -15.0
-21.0 : -18.0
-24.0 : -21.0
-27.0 : -24.0
-30.0 : -27.0

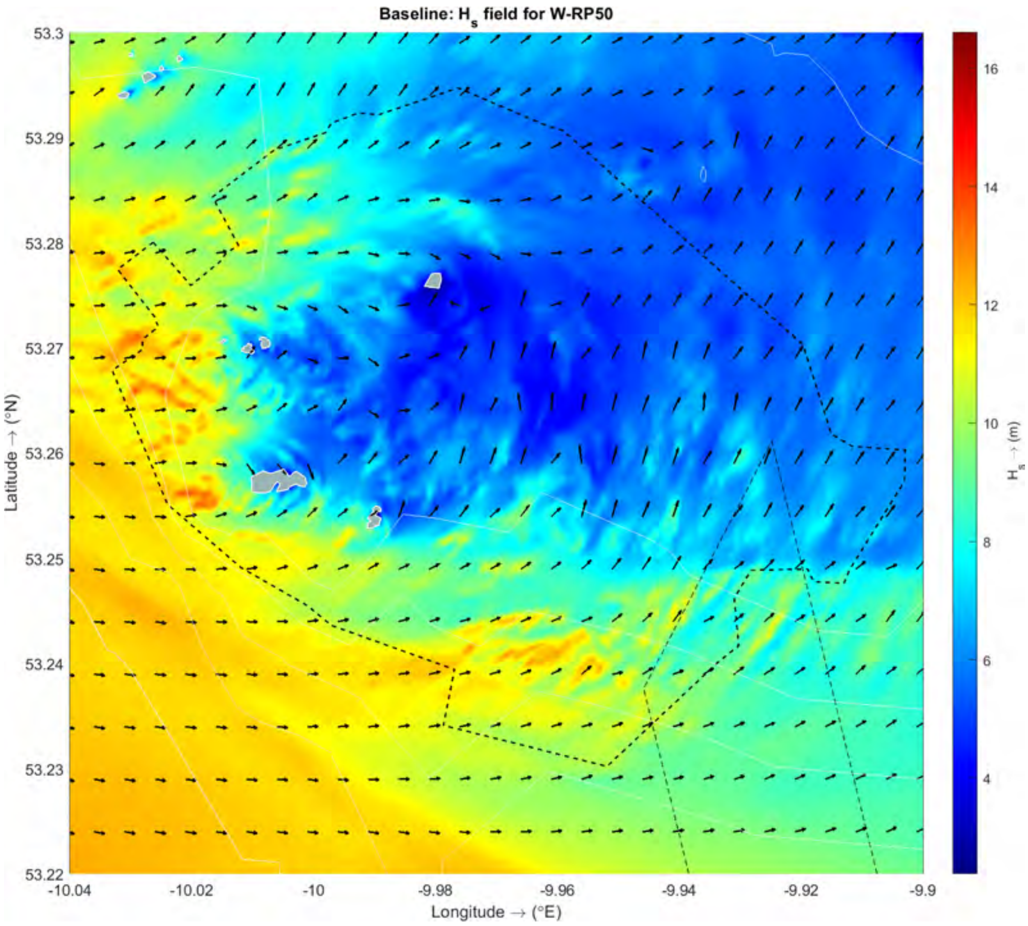
Baseline: H_s field for W-RP50
Latitude → (°N)
53.3
53.29
53.28
53.27
53.26
53.25
53.24
53.23
53.22
-10.04
-10.02
-10
-9.98
-9.96
-9.94
-9.92
-9.9
Longitude → (°E)
16
14
12
10
8
6
4
H_s → (m)

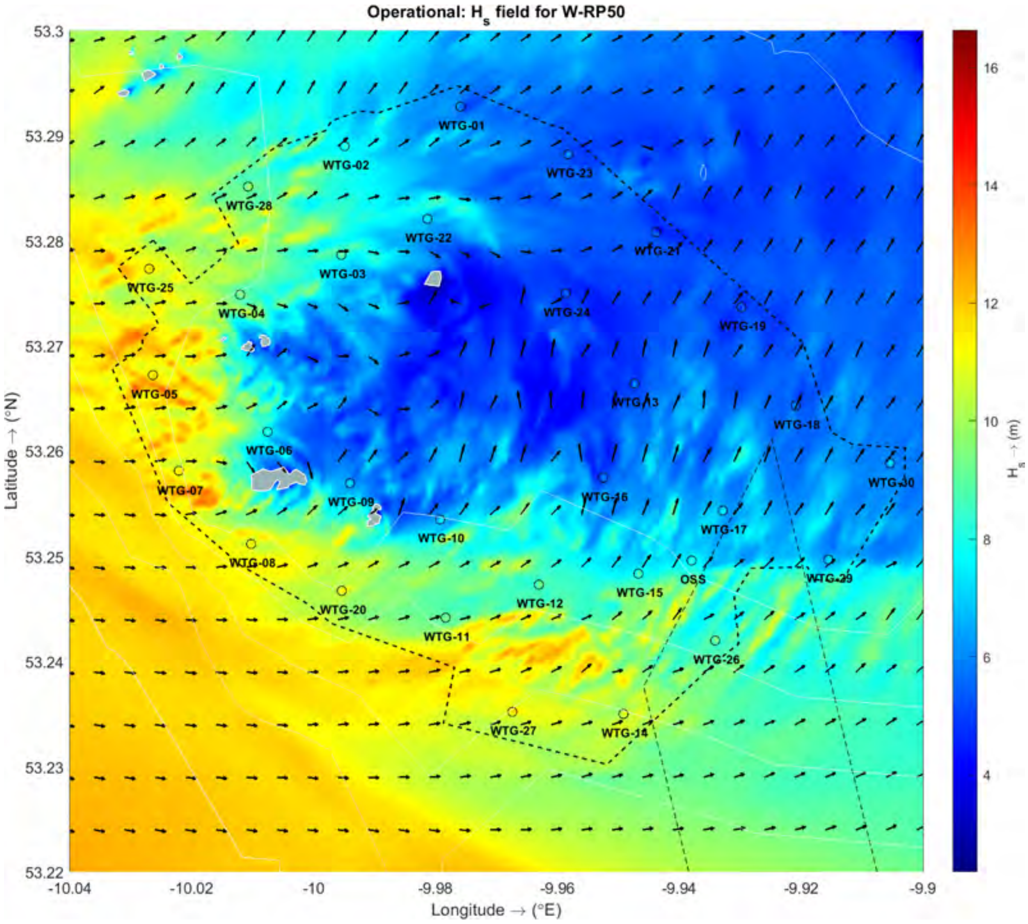
Operational: H_s field for W-RP50
Latitude → (°N)
Longitude → (°E)
H_s → (m)
WTG-01
WTG-02
WTG-03
WTG-04
WTG-05
WTG-06
WTG-07
WTG-08
WTG-09
WTG-10
WTG-11
WTG-12
WTG-13
WTG-14
WTG-15
WTG-16
WTG-17
WTG-18
WTG-19
WTG-20
WTG-21
WTG-22
WTG-23
WTG-24
WTG-25
WTG-26
WTG-27
WTG-28
WTG-29
WTG-30
OSS

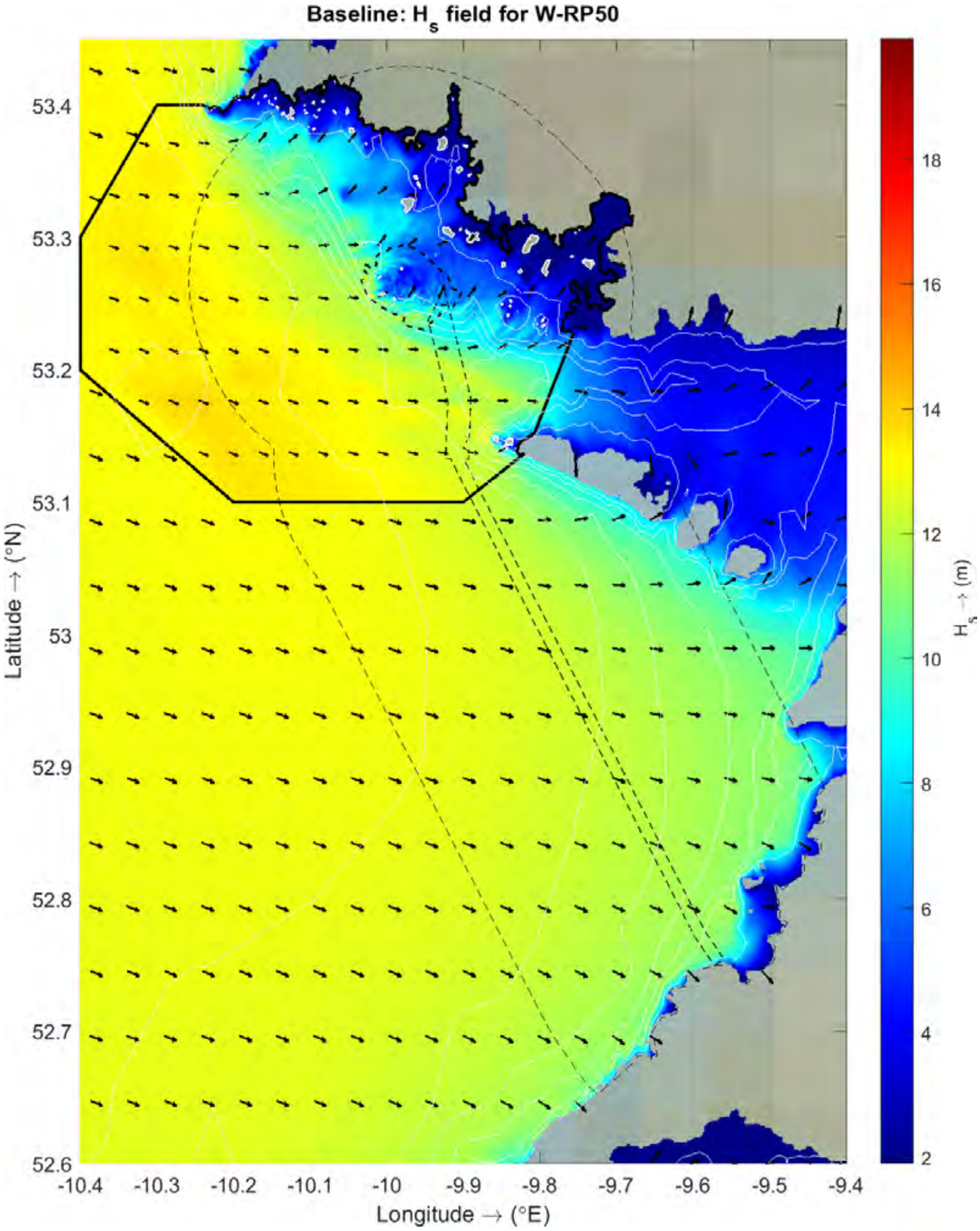
Baseline: H_s field for W-RP50
Latitude → (°N)
53.4
53.3
53.2
53.1
53
52.9
52.8
52.7
52.6
-10.4
-10.3
-10.2
-10.1
-10
-9.9
-9.8
-9.7
-9.6
-9.5
-9.4
Longitude → (°E)
H_s → (m)
18
16
14
12
10
8
6
4
2

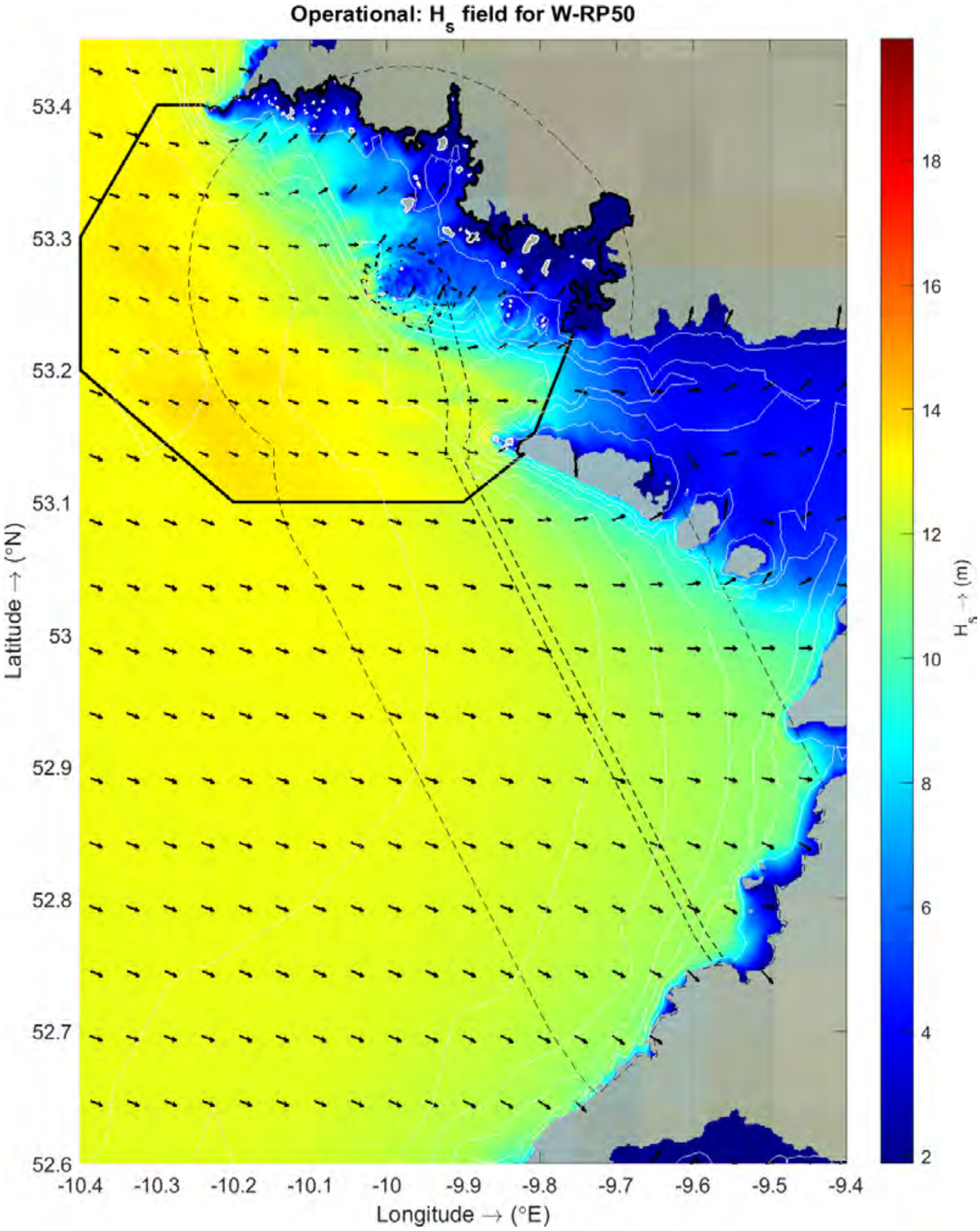
Operational: H_s field for W-RP50
53.4
53.3
53.2
53.1
53
52.9
52.8
52.7
52.6
Latitude → (°N)
-10.4
-10.3
-10.2
-10.1
-10
-9.9
-9.8
-9.7
-9.6
-9.5
-9.4
Longitude → (°E)
18
16
14
12
10
8
6
4
2
H_s → (m)

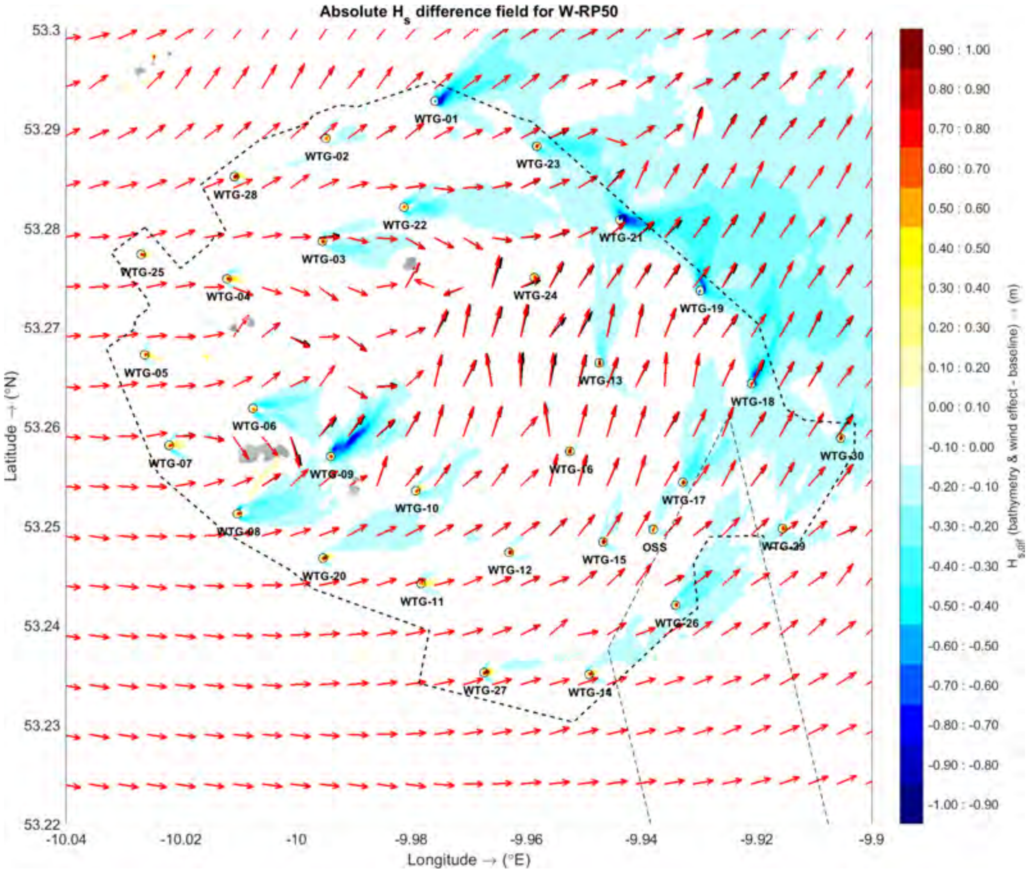

Absolute H$_s$ difference field for W-RP50
Latitude → (°N)
Longitude → (°E)
H$_{s,dif}$ (bathymetry & wind effect - baseline) → (m)
WTG-01
WTG-02
WTG-03
WTG-04
WTG-05
WTG-06
WTG-07
WTG-08
WTG-09
WTG-10
WTG-11
WTG-12
WTG-13
WTG-14
WTG-15
WTG-16
WTG-17
WTG-18
WTG-19
WTG-20
WTG-21
WTG-22
WTG-23
WTG-24
WTG-25
WTG-26
WTG-27
WTG-28
WTG-29
WTG-30
OSS
0.90 : 1.00
0.80 : 0.90
0.70 : 0.80
0.60 : 0.70
0.50 : 0.60
0.40 : 0.50
0.30 : 0.40
0.20 : 0.30
0.10 : 0.20
0.00 : 0.10
-0.10 : 0.00
-0.20 : -0.10
-0.30 : -0.20
-0.40 : -0.30
-0.50 : -0.40
-0.60 : -0.50
-0.70 : -0.60
-0.80 : -0.70
-0.90 : -0.80
-1.00 : -0.90

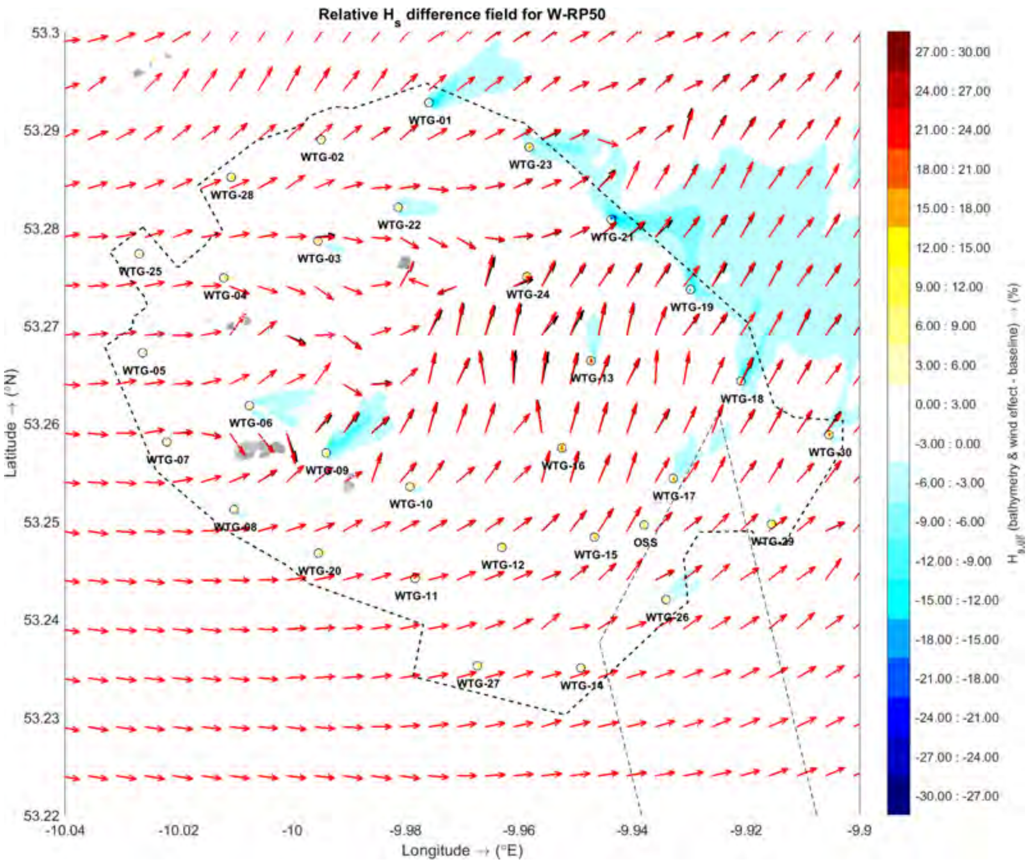

Relative H$_s$ difference field for W-RP50
Latitude → (°N)
Longitude → (°E)
H$_{s,dif}$ (bathymetry & wind effect - baseline) → (%)
27.00 : 30.00
24.00 : 27.00
21.00 : 24.00
18.00 : 21.00
15.00 : 18.00
12.00 : 15.00
9.00 : 12.00
6.00 : 9.00
3.00 : 6.00
0.00 : 3.00
-3.00 : 0.00
-6.00 : -3.00
-9.00 : -6.00
-12.00 : -9.00
-15.00 : -12.00
-18.00 : -15.00
-21.00 : -18.00
-24.00 : -21.00
-27.00 : -24.00
-30.00 : -27.00

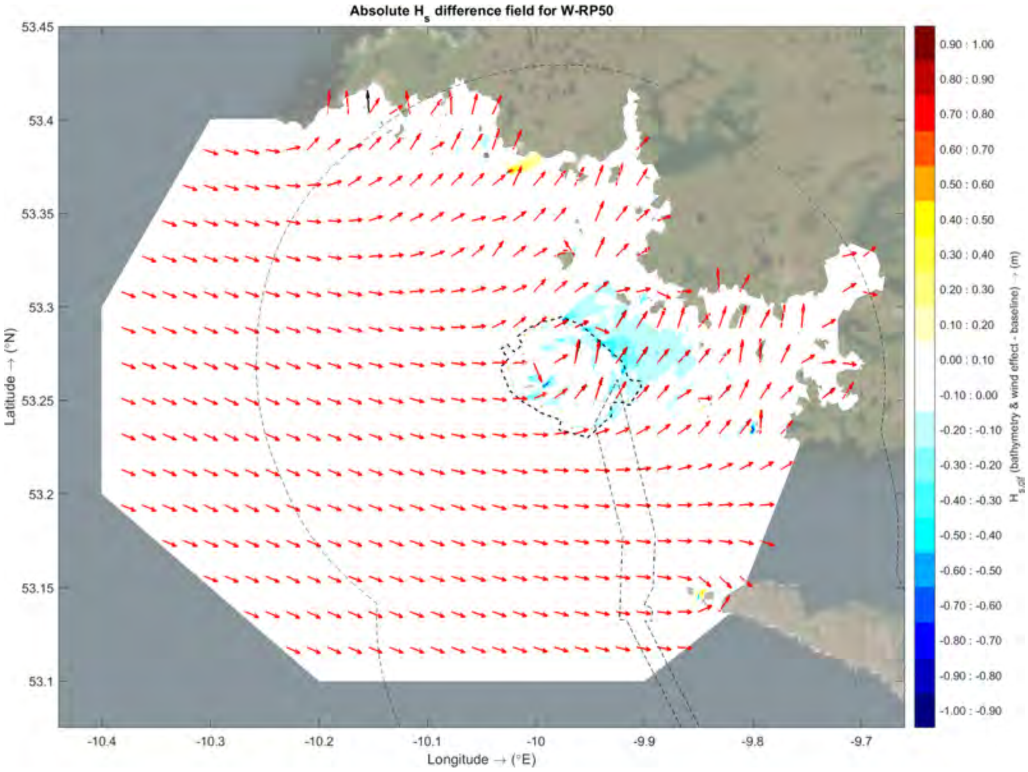
Absolute Hs difference field for W-RP50
53.45
53.4
53.35
53.3
53.25
53.2
53.15
53.1
Latitude → (°N)
-10.4
-10.3
-10.2
-10.1
-10
-9.9
-9.8
-9.7
Longitude → (°E)
0.90 : 1.00
0.80 : 0.90
0.70 : 0.80
0.60 : 0.70
0.50 : 0.60
0.40 : 0.50
0.30 : 0.40
0.20 : 0.30
0.10 : 0.20
0.00 : 0.10
-0.10 : 0.00
-0.20 : -0.10
-0.30 : -0.20
-0.40 : -0.30
-0.50 : -0.40
-0.60 : -0.50
-0.70 : -0.60
-0.80 : -0.70
-0.90 : -0.80
-1.00 : -0.90
Hs,dif (bathymetry & wind effect - baseline) → (m)

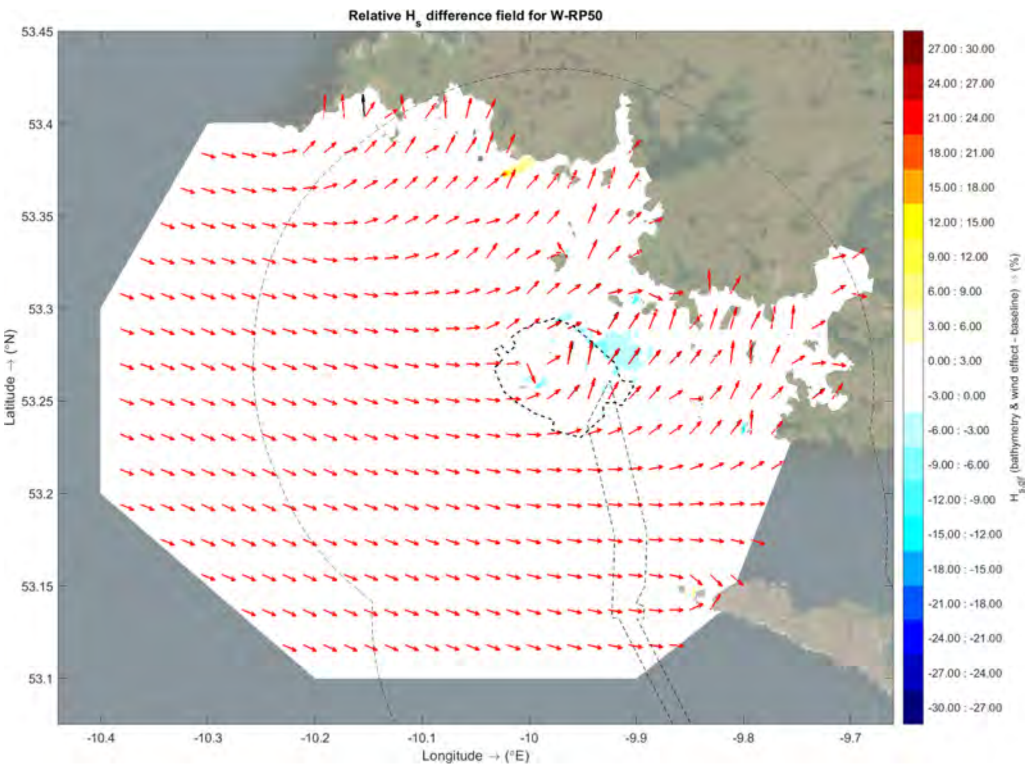
Relative Hs difference field for W-RP50
53.45
53.4
53.35
53.3
53.25
53.2
53.15
53.1
Latitude → (°N)
-10.4
-10.3
-10.2
-10.1
-10
-9.9
-9.8
-9.7
Longitude → (°E)
27.00 : 30.00
24.00 : 27.00
21.00 : 24.00
18.00 : 21.00
15.00 : 18.00
12.00 : 15.00
9.00 : 12.00
6.00 : 9.00
3.00 : 6.00
0.00 : 3.00
-3.00 : 0.00
-6.00 : -3.00
-9.00 : -6.00
-12.00 : -9.00
-15.00 : -12.00
-18.00 : -15.00
-21.00 : -18.00
-24.00 : -21.00
-27.00 : -24.00
-30.00 : -27.00
Hs,dif (bathymetry & wind effect - baseline) → (%)

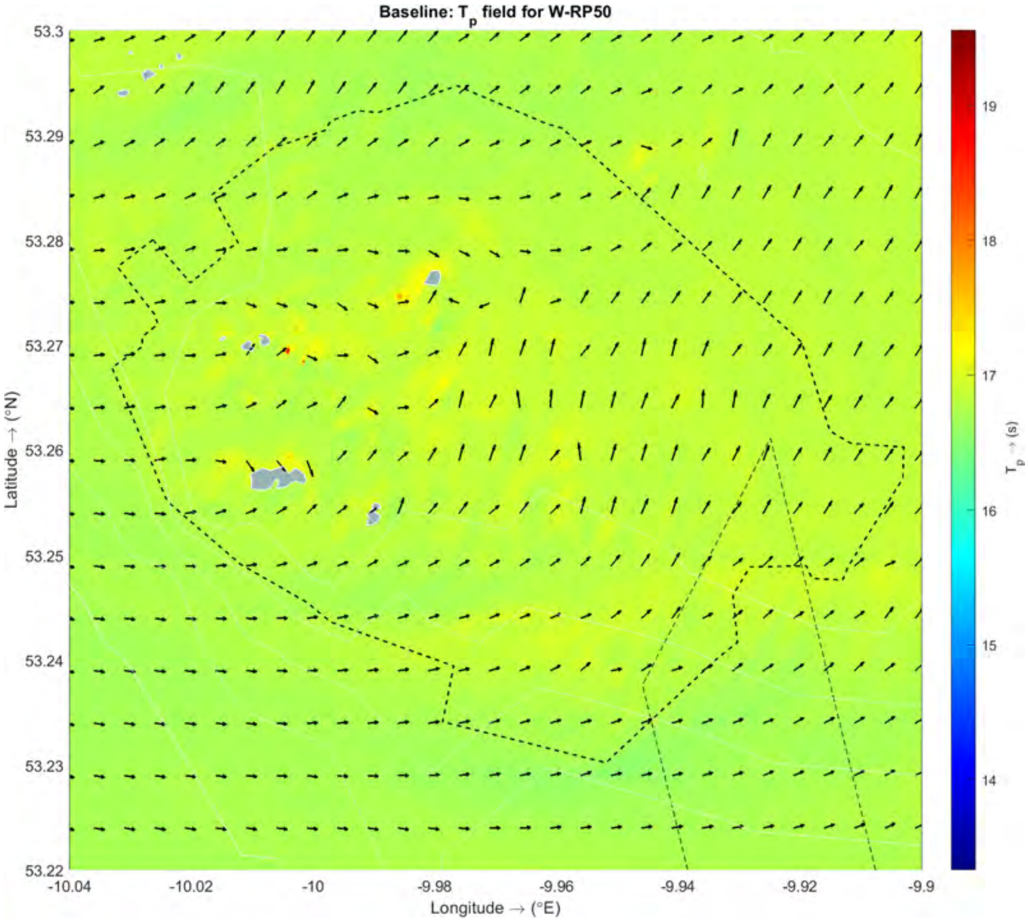
Baseline: T_p field for W-RP50
53.3
53.29
53.28
53.27
53.26
53.25
53.24
53.23
53.22
Latitude → (°N)
-10.04
-10.02
-10
-9.98
-9.96
-9.94
-9.92
-9.9
Longitude → (°E)
19
18
17
16
15
14
T_p → (s)

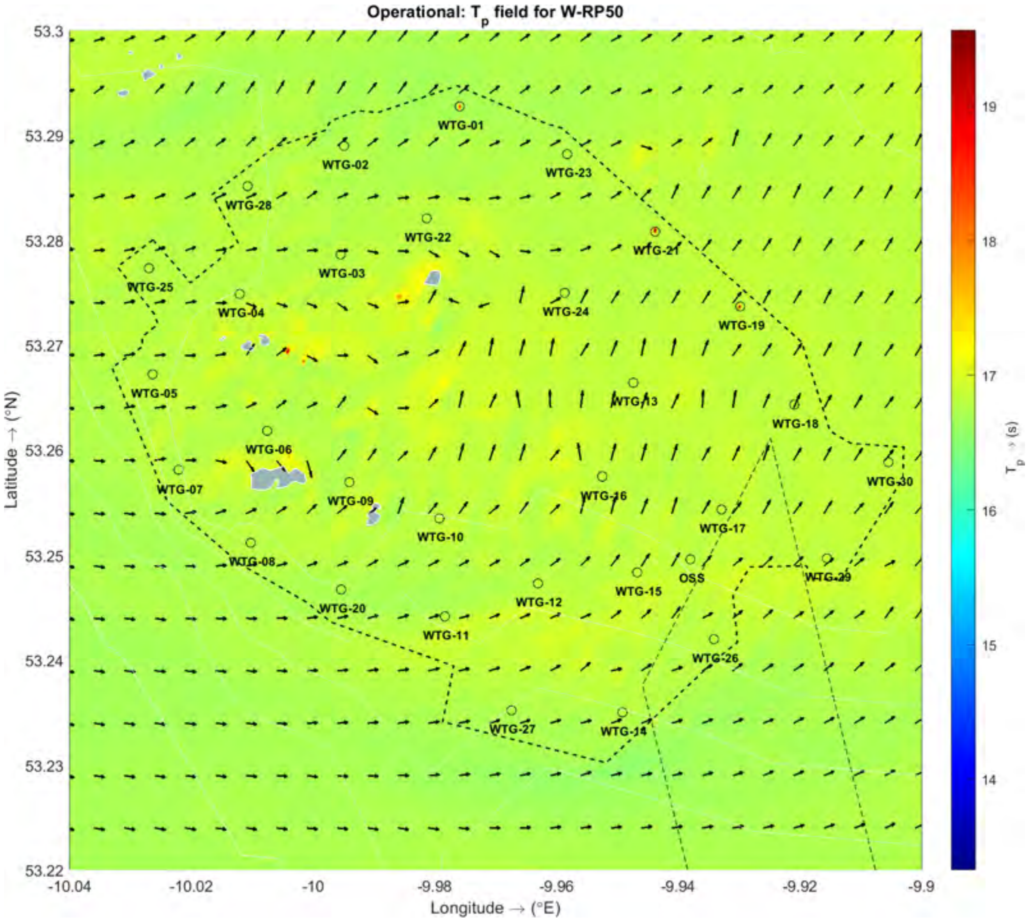

Operational: T_p field for W-RP50
Latitude → (°N)
Longitude → (°E)
T_p → (s)
WTG-01
WTG-02
WTG-03
WTG-04
WTG-05
WTG-06
WTG-07
WTG-08
WTG-09
WTG-10
WTG-11
WTG-12
WTG-13
WTG-14
WTG-15
WTG-16
WTG-17
WTG-18
WTG-19
WTG-20
WTG-21
WTG-22
WTG-23
WTG-24
WTG-25
WTG-26
WTG-27
WTG-28
WTG-29
WTG-30
OSS

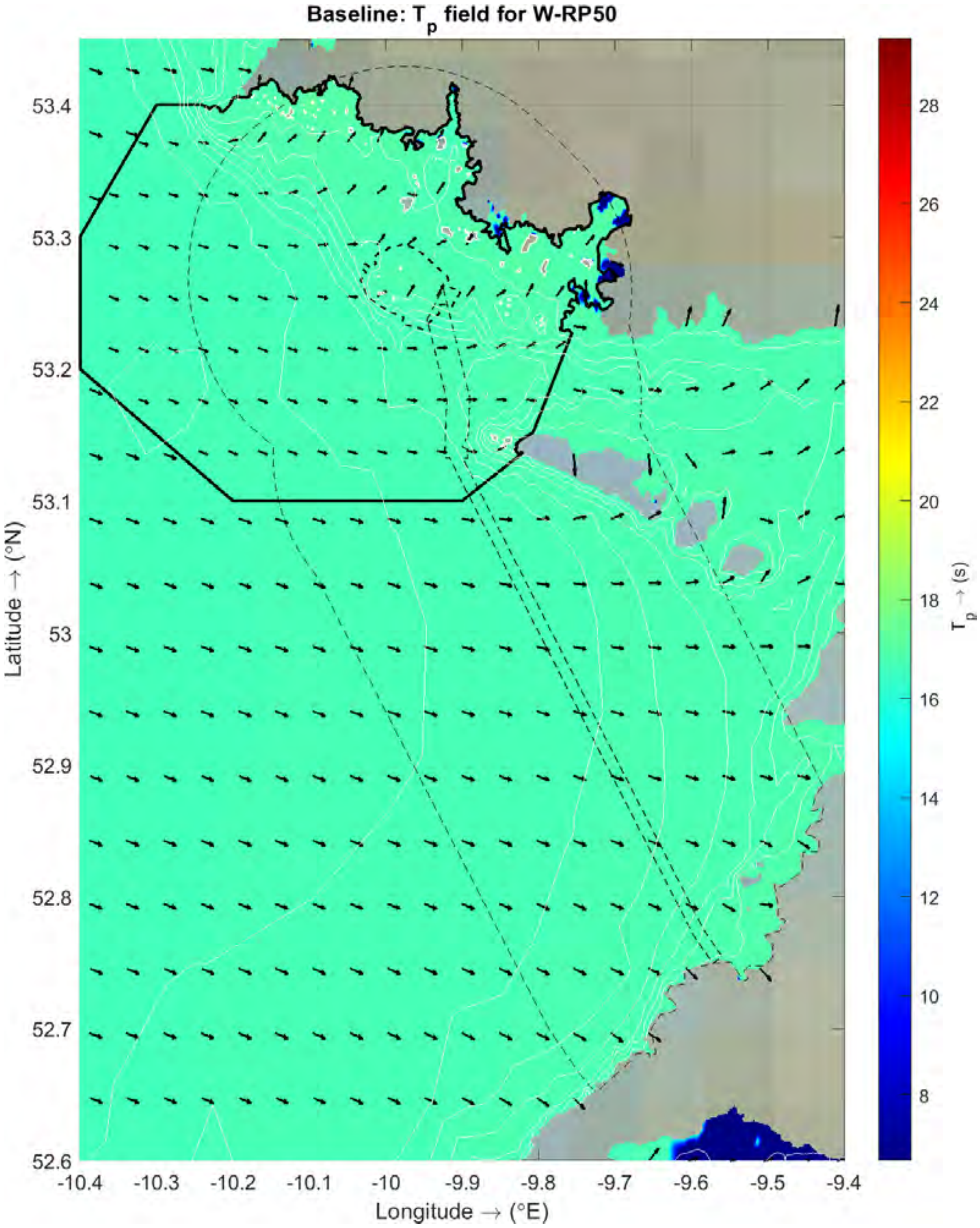

Baseline: T_p field for W-RP50
53.4
53.3
53.2
53.1
53
52.9
52.8
52.7
52.6
Latitude → (°N)
-10.4
-10.3
-10.2
-10.1
-10
-9.9
-9.8
-9.7
-9.6
-9.5
-9.4
Longitude → (°E)
28
26
24
22
20
18
16
14
12
10
8
T_p → (s)

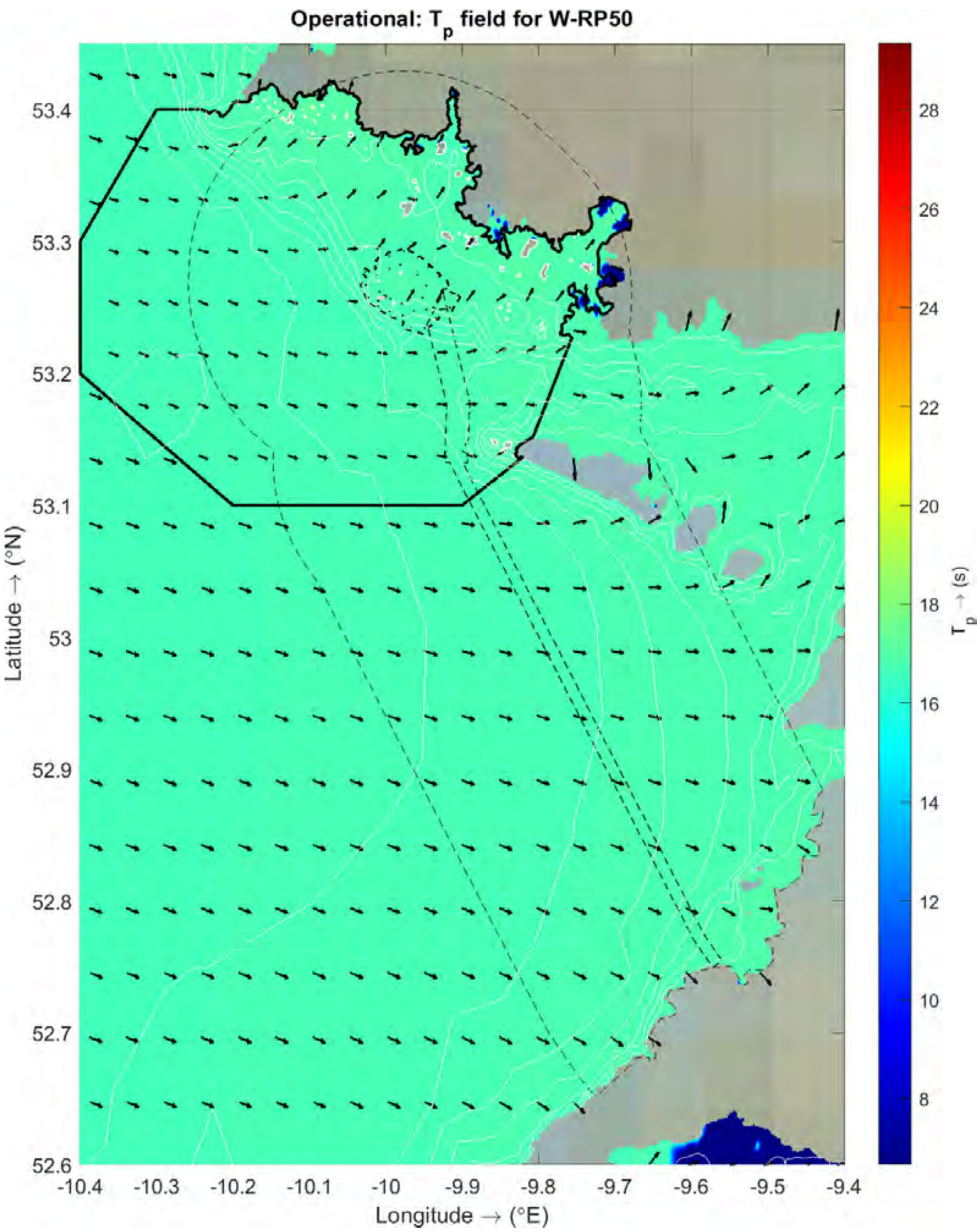
Operational: T_p field for W-RP50
53.4
53.3
53.2
53.1
53
52.9
52.8
52.7
52.6
Latitude → (°N)
-10.4
-10.3
-10.2
-10.1
-10
-9.9
-9.8
-9.7
-9.6
-9.5
-9.4
Longitude → (°E)
28
26
24
22
20
18
16
14
12
10
8
T_p → (s)

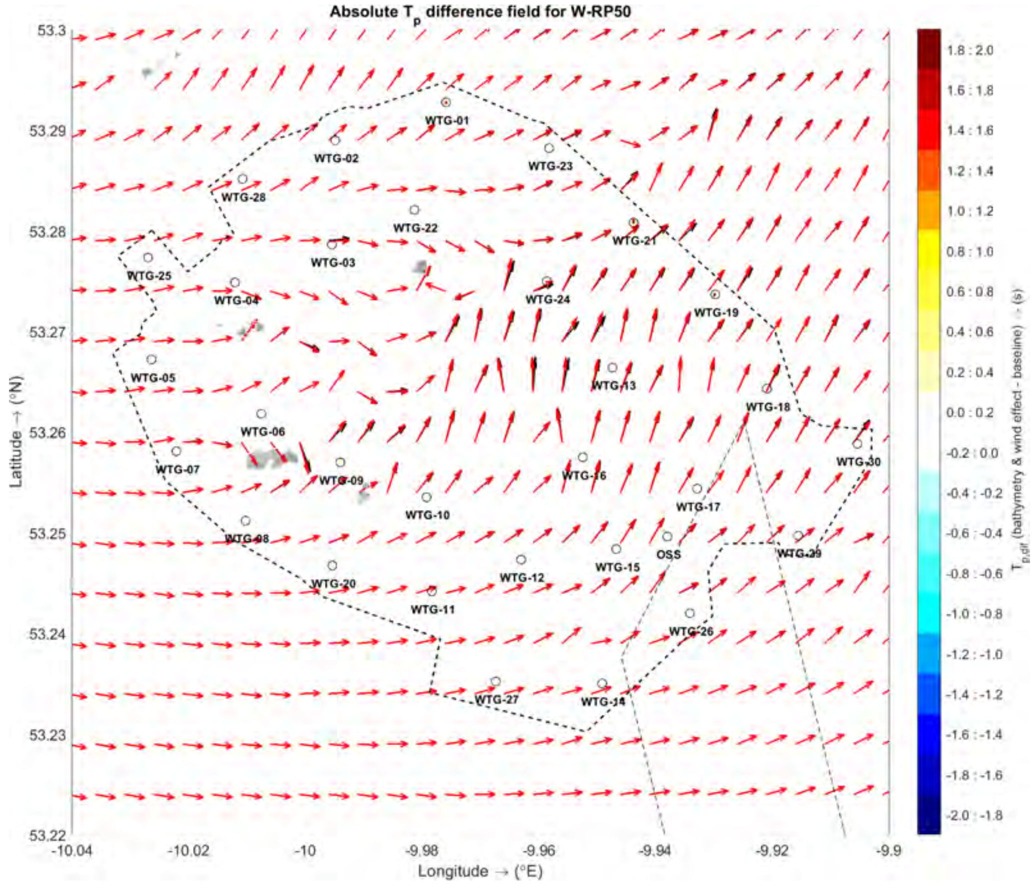

Absolute T_p difference field for W-RP50
Latitude → (°N)
Longitude → (°E)
$T_{p,dif}$ (bathymetry & wind effect - baseline) → (s)

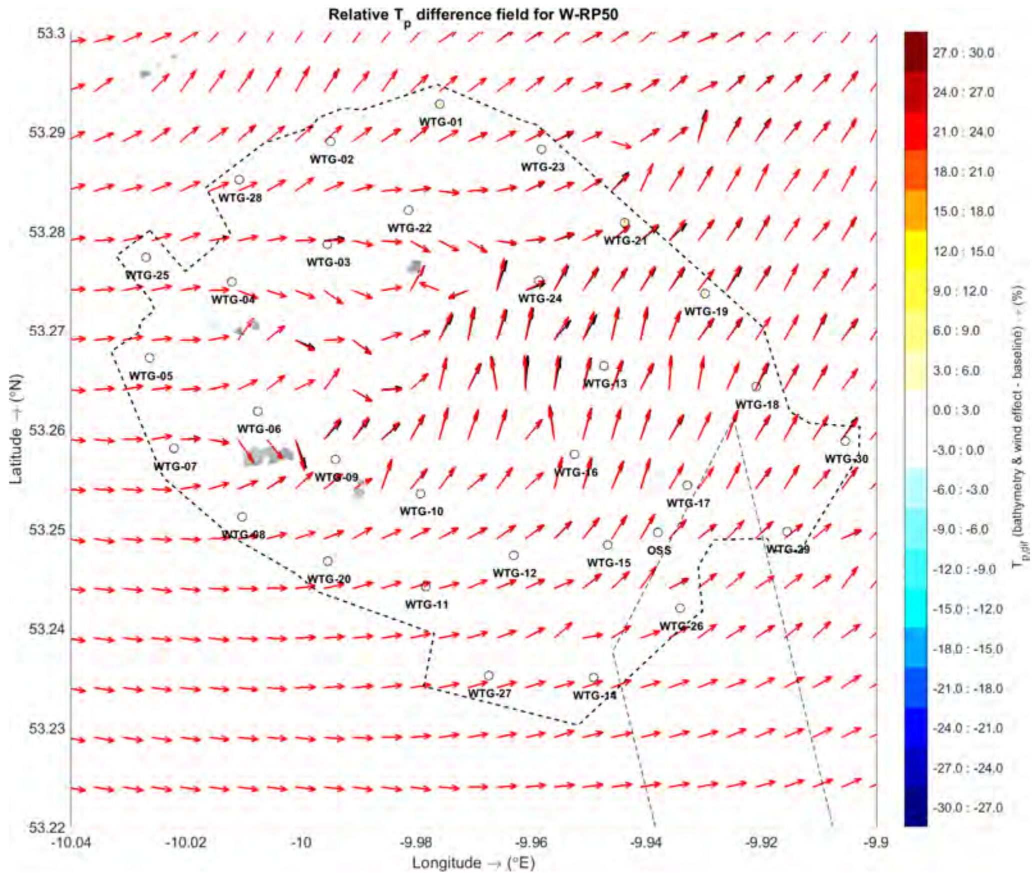

Relative T_p difference field for W-RP50
Latitude → (°N)
Longitude → (°E)
$T_{p,dif}$ (bathymetry & wind effect - baseline) → (%)

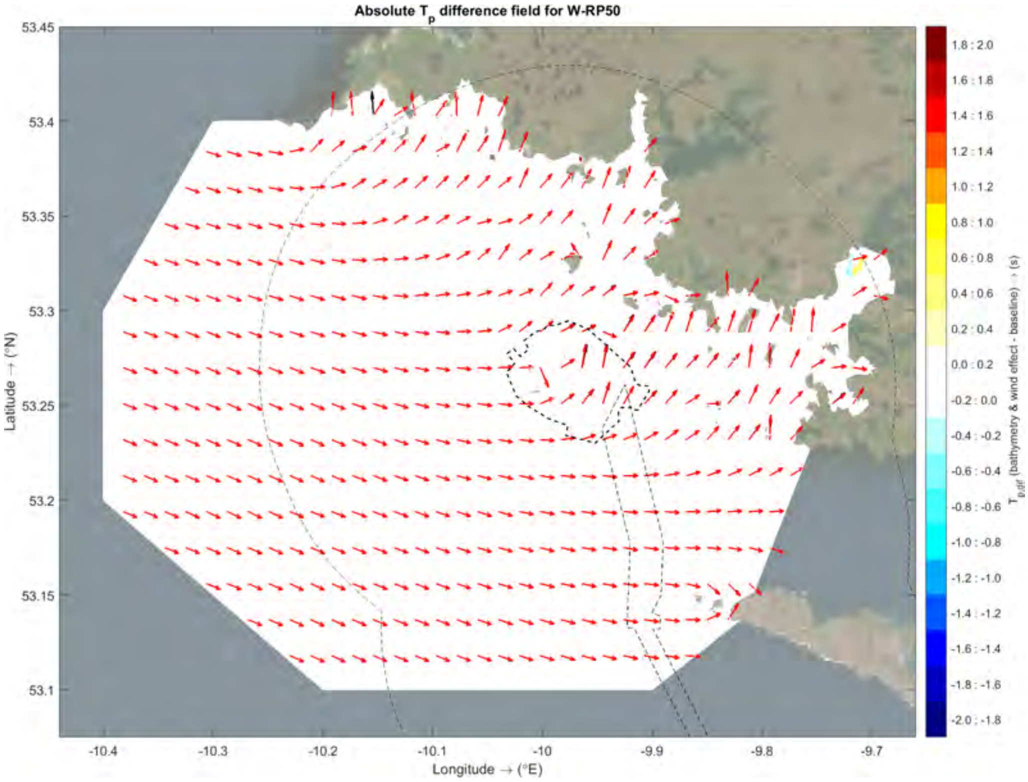
Absolute T_p difference field for W-RP50
Latitude → (°N)
Longitude → (°E)
$T_{p,diff}$ (bathymetry & wind effect - baseline) → (s)

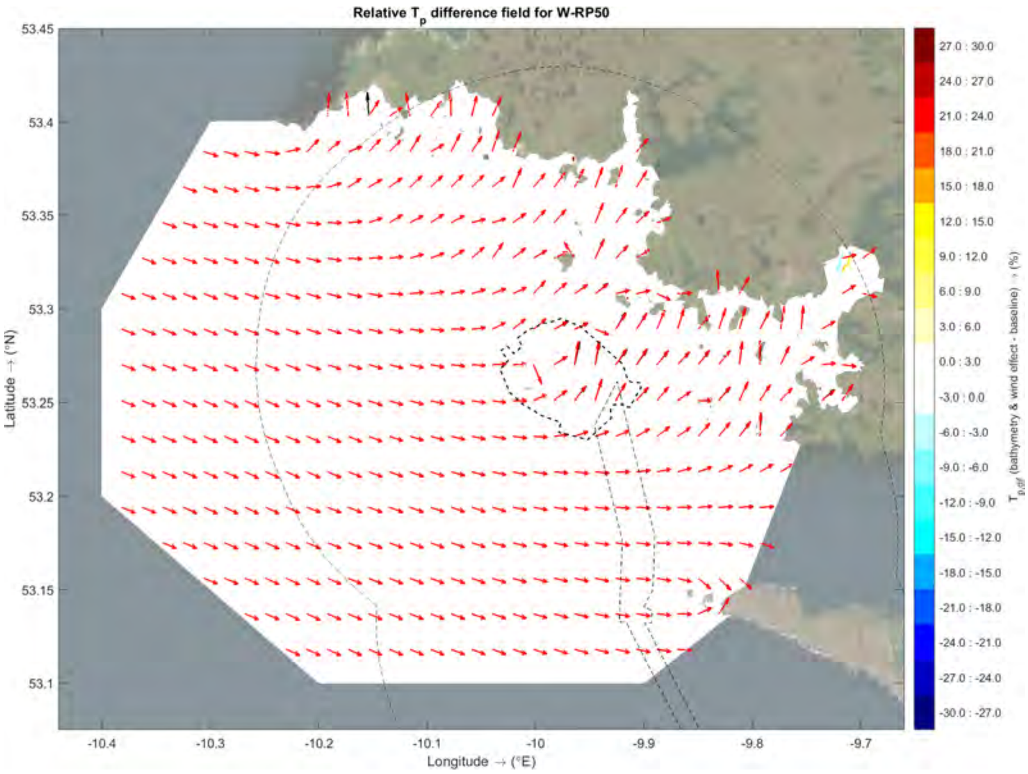
Relative T_p difference field for W-RP50
Latitude → (°N)
Longitude → (°E)
$T_{p,diff}$ (bathymetry & wind effect - baseline) → (%)

Deltares is an independent institute for applied research in the field of water and subsurface. Throughout the world, we work on smart solutions for people, environment and society.

Deltares

www.deltares.nl